The development of a novel 3D migration assay to study the effects of cell signalling and microenvironment on the migratory behaviour of colorectal cancer

ADAMS, ROSIE,LOUISE

Durham University

School of Biological and Biomedical Sciences

The development of a novel 3D migration assay to study the effects of cell signalling and microenvironment on the migratory behaviour of colorectal cancer

Rosie Louise Adams

September 2014

A thesis submitted for the degree of Doctor of Philosophy

Declaration

The work described herein was carried out in the Department of Chemistry, or the School of Biological and Biomedical Sciences, University of Durham between October 2010 and September 2014. All of the work is my own, except where specifically stated otherwise. No part has previously been submitted for a degree at this or any other university.

Statement of Copyright

Abstract

Colorectal cancer is one of the mostly commonly diagnosed cancers for both men and women in the UK, with a poor survival rate compared to other Western countries and other commonly diagnosed cancer types. Part of the reason for poor prognosis for patients is the diagnosis of the disease at an advanced stage of progression, which has been shown to have a severe impact on patient survival rates. Due to this, the signalling events surrounding the adoption of an invasive phenotype may provide the opportunity to develop therapies to limit the spread of tumours from their original site and improve patient prognosis.

It has previously been highlighted that the culture of cells in standard two-dimensional (2D) induces alterations to gene expression via the imposition of a microenvironment which does not reflect the microenvironment experienced by cancer cells *in vivo*. This limits the accuracy of data obtained using 2D migration assays and can help to account for the failure of some anti-migratory compounds to be effective in *in vivo* or clinical screening, after showing promise in conventional cell culture tests.

This project has aimed to develop a novel three-dimensional (3D) migration assay based on Alvetex® technology, which provides a more biologically relevant microenvironment *in vitro*, to investigate the role of cell signalling and microenvironment in determining the migratory behaviour of colorectal cancer cells. Through extensive optimisation, the 3D culture of two colorectal cancer cell lines, SW480 and SW620, was established to allow for the assessment of cell migration via histological processing, in addition to the assessment of other behavioural traits via the use of commercial biochemical assays.

Modulation of both the Wnt and Insulin-like Growth Factor (IGF)-I signalling pathways via small molecule inhibitors and exogenous protein application has highlighted compounds which alter the migratory behaviour of the colorectal cancer cell lines, results which were not reflected in counterpart 2D scratch wound assays. This underlines the need to use culturing techniques which better reflect the biological system in question, as the anti-migratory applications of these compounds have the potential to be missed if subjected to 2D screening only.

The biological relevance of the model developed here was also increased by altering the culture microenvironment by the addition of extracellular matrix (ECM) coatings or co-culture, demonstrating that this model can be adapted to recreate a variety of microenvironments depending on the aims of the research undertaken.

Together, the data presented in this thesis demonstrates the suitability of this novel culture system to assess the migratory behaviour of colorectal cancer cells *in vitro*, with the possibility of the adaption of this system to assess the behaviour of other cancer types.

Acknowledgments

I would like to start by acknowledging the Grevillea Trust, BBSRC and Reinnervate Limited for providing the funding for this project.

I would like to thank my primary supervisor Professor Stefan Przyborski for his support and encouragement over the last four years. I would also like to thank various members of his lab group, especially Bridie Murray, Eleanor Knight and Rachel Lopez-Real, for assistance with protocols and getting me started off on the project.

I would like to thank my second supervisor Professor Chris Hutchison for his input into the project, in addition to Pam Ritchie and Clare Foster for guidance on the culturing of the colorectal cancer cell lines and Katherine O'Mahony for help in sourcing the antibodies used in this project.

Outside of those lab groups I would also like to thank James Carthew for his invaluable help with Western blotting and Dr Shane Richards for his guidance on statistics.

I would like to thanks the members of office 234 and lab 4, both past and present, for making the experience an enjoyable one, particularly those of you that were there to keep me company during early starts and late nights in the lab.

Beyond the university, I would like to thank Matt Cashmore, Caroline Walters, Beth Richards and David Griffith for being a fantastic pub quiz team and giving me an excuse to forget about the thesis for a few hours a week.

I would also like to thank Mum, Dad, Jack and the rest of my family for supporting me during the past four years and being understanding when I haven't been in touch for a while. Finally, I would like to thank Robbie Glendinning for his patience in putting up with me for the past few years and his words of encouragement.

Publications arising from this work:

Papers

Adams RL, Knight EG, Hutchison CJ and Przyborski SA (2014, in preparation) Development and Application of a Novel Three Dimensional Culture Model to Study the Migration of Colorectal Cancer Cells

Published Abstracts:

Adams R (2013) Developing a novel 3D model to study colon cancer cell invasion. Cancer Research In: Proceedings of the 104th Annual Meeting of the American Association for Cancer Research; 2013 Apr 6-10; Washington, DC. Philadelphia (PA): AACR; Cancer Res 2013;73(8 Suppl):Abstract nr 3845.

Adams RL and Przyborski SA (2012) Developing a novel 3D migration model to study colon cancer cell invasion. European Cells and Materials Vol. 23. Suppl. 4, 2012 (page 92)

Oral Presentations

Adams RL, Hutchison CJ and Przyborski SA (2012) Developing a novel 3D migration model to study colon cancer cell invasion. CCPD Collaborative Network Early Stage Researcher's Forum, Nottingham, UK

Adams RL, Hutchison CJ and Przyborski SA (2012) Developing a novel 3D migration model to study colon cancer cell invasion. North East Post Graduate Conference, Newcastle, UK

Poster Presentations:

Adams RL, Hutchison CJ and Przyborski SA (2013) Investigating Colorectal Cancer Cell Migration and the Role of Wnt Signalling in a Novel 3D Micro-environment Model. BACR Tumour Microenvironment Meeting, Bristol, UK

Adams RL, Hutchison CJ and Przyborski SA (2013) A 3D model to study the role of the Wnt signalling pathway in colon cancer cell invasion. Advances in In-Vitro Cell and Tissue Culture and 5th Annual Quasi-Vivo® User Group Meeting, Liverpool, UK

Adams RL, Hutchison CJ and Przyborski SA (2012) Developing a Novel 3D Model to Study Colon Cancer Cell Invasion. TCES Annual Conference, Liverpool, UK

Adams RL, Hutchison CJ and Przyborski SA (2012) Studying cancer cell invasion using a novel 3D cell migration model. 2nd Year Postgraduate Poster Presentation, Durham, UK

Table of Contents

Table of Figures

Table of Tables

Abbreviations

%	…	percentage
5-FU	…	5-fluorouracil
ACM	…	artifical cell mass
ADAMTS	…	MMP-related disintegrin and metalloproteinase with thrombospondin motifs
AETI	…	alveolar epithelial type I
AETII	…	alveolar epithelial type II
AJCC	…	American Joint Committee on Cancer
AML	…	acute myeloid leukaemia
Ang-1	…	angiopoietin 1
AP	…	Alkaline phosphatase
APS	…	Ammonium Persulfate
BAPN	…	β-aminopropionitrile
bFGF	…	basic fibroblast growth factor
BSA	…	Bovine Albumin
CAF	…	cancer associated fibroblast
CAF-LM	…	CAFs obtained from liver metastases
CAF-PT	…	CAFs obtained from primary tumours
CAM	…	chorioallantoic membrane
CD-DST	…	collagen gel droplet embedded culture drug sensitivity test
CIMP	…	CpG island methylator phenotype
CIN	…	chromosomal instability
CP	…	carcinoma percentage
CSF-1	…	colony-stimulating factor-1
CSK	…	C-terminal Src kinase
CTx	…	C-terminal telopeptide of type I collagen
-Da	…	dalton
DAB	…	3,3' Diaminobenzidine
dH_2O	...	distilled water
Dkk1	...	Dickkopf
DMBA	…	7,12-dimethylbenz(α)anthracene
DMEM	…	Dulbecco's Modified Eagle Medium
DMSO	…	Dimethyl Sulfoxide
dnIGF-IR	…	dominant negative IGF-IR
dnTCF-4	…	dominant negative TCF-4
DOX	…	Doxorubicin
EB	…	embryoid body
ECM	…	extracellular matrix
EDTA	…	Versene
EGF	…	epidermal growth factor
EHS	…	Engelbreth-Holm-Swarm
ELISA	…	enzyme-linked immunosorbent assay
EMT	…	epithelial-mesenchymal transition
FAK	…	focal adhesion kinase

FAP	…	familial adenomatous polyposis
FAP-α	…	fibroblast activation protein-α
FBS	…	Foetal Bovine Serum
FHL2	…	four and a half LIM domain protein-2
FITC	…	Fluorescein Isothiocyanate
-g	…	gram
GAG	…	glucosaminoglycan
GFP	…	green fluorescent protein
GH	…	growth hormone
GSK-3β	...	glycogen synthase kinase 3 beta
Gy	…	gray
HDACi	…	histone deactylase inhibitor
HGF/SF	…	hepatocyte growth factor/scatter factor
HIF	…	hypoxia-inducible factor
HNPCC	…	Hereditary nonpolyposis colorectal cancer
HPSC	…	human pancreatic stellate cell
HRP	…	horseradish peroxidase
IGF-I	…	insulin-like growth factor-I
IGF-IR	…	IGF-I receptor
IL-1β	…	interleukin-1β
IRS-1	…	insulin response substrate-1
IWR	…	inhibitor of Wnt response
-l	…	litre
LID	…	liver-specific IGF-I deficient
LOH	…	loss of heterozygosity
LOX	…	lysyl oxidase
LTB	…	Escherichia coli heat-labile enterotoxin
k-	...	kilo
m-	…	milli
-m	…	metre
-M	…	molar
MEC	…	mammary epithelial cells
MET	…	mesenchymal-epithelial transition
MLCK	…	myosin light chain kinase
MMP	…	matrix metalloproteinase
MSI	…	microsatellite instability
MT1-MMP	…	membrane type-1 MMP
MTT	…	Thiazolyl Blue Tetrazolium Bromide
n-	…	nano
^{o}C	…	degrees Celsius
PA	…	polyacrylamide
PAA	…	Protogel Acrylamide
PARsylation	…	poly-ADP-ribosylation
PBS	…	Phosphate Buffered Solution
PCNA	…	proliferating cell nuclear antigen

PCR	…	polymerase chain reaction
PDGF	…	platelet-derived growth factor
PFA	…	Paraformaldehyde
PI3K	…	phosphatidylinositol 3-kinase
PICP	…	carboxyterminal propetide of type I collagen
PKB	…	protein kinase B
PolyHEMA	…	poly-2-hydroxyethylmetacrylate
PVDF	…	Polyvinylidene Difluoride
PyVT	…	polyoma middle-T
ROCK	…	Rho-kinase
rpm	…	rotations per minute
RPTPα	…	receptor-type tyrosine-protein phosphatase alpha
SAGE	…	serial analysis of gene expression
SAIN	…	Shc and IRS-1 NPXY binding
SCC	…	squamous cell carcinoma
SDF-1	…	stromal cell-derived factor-1
SDS	…	Sodium Dodecyl Sulphate
SEER	…	Surveillance, Epidemiology and End Results
SFA	…	surface fibroblast antigen
SMM	…	smooth muscle myosin
STC-1	…	stanniocalcin-1
SV40 TAg tsA58	…	temperature sensitive simian virus 40 large tumour antigen
TACS	…	tumour-associated collagen signature
T_c	…	cytotoxic T-cell
TCF-4	...	transcription factor 4
TCSF	…	tumour cell-derived collagenase-stimulatory factor
TEMED	…	Tetramethylethylenediamine
TGALN	…	transgelin
TGFβ	…	transforming growth factor β
TIMP	…	tissue inhibitor of metalloproteinase
TLR-4	…	toll-like receptor 4
TNKS	…	tankyrase
Treg	…	regulatory T-cell
UICC	…	Union for International Cancer Control
uPA	…	urokinase plasminogen activator
uPAR	…	uPA receptor
V	…	volts
v/v	…	volume per volume
VEGF	…	vascular endothelial growth factor
VEGFR-2	…	VEGF receptor 2
w/v	…	weight per volume
α-SMA	…	α-smooth muscle actin
µ-	…	micro

1 Introduction

1.1 Cancer is a leading cause of death in the UK

The incidence of cancer has been steadily rising in the UK, with 431 new cases per 100,000 men and 375 new cases per 100,000 women diagnosed in the period 2008-10, compared to 403 and 343 new cases per 100,000 in 2001-03 respectively [1]. The mortality rates for cancer have not followed this trend, with 204 deaths per 100,000 men and 149 deaths per 100,000 women recorded in 2008-10, down from 299 and 161 deaths per 100,000 in 2001-03 respectively [1]. Despite this decrease in mortality, cancer is currently the largest percentage cause of deaths in England and Wales, with 29% of all registered deaths in 2012 attributed to this disease group [2].

As cancer describes a collection of diseases arising from many tissues in the body, it cannot be attributed to changes to a single protein or pathway and there has been much discussion in the literature to define the unifying properties of cancers in general. Certain gross properties of the disease have been identified for many years, such as the stages of spread of the tumours throughout the body [3]. In addition to this, general mechanisms for tumour progression have been identified, from the hijacking of the wound healing mechanisms in the body to produce stroma to maintain tumour growth [4] to the genetic changes occurring in key oncogenes and genes linked to specific cancer types [5].

Two landmark reviews by Hanahan and Weinberg, the first in 2000 [6] and a follow up in 2011 [7], have gone a long way to outline a framework in which the development of tumours are viewed. In these articles, they outlined a total of eight 'hallmarks of cancer', six initial ones, namely the sustainment of proliferative signalling, resistance of cell death, evasion of growth suppressors, enablement of replicative immortality, induction of angiogenesis and activation of invasion and metastasis, and two emerging hallmarks, the deregulation of cellular energetics and evasion of immune destruction. When these are considered along with the two enabling characteristics of tumour promoting inflammation and genome instability and mutation, they provide a description of the behaviour of the cells of tumours when taken as a whole, and are not to be taken as the characteristics of all cells within tumours at all times [8].

The Hanahan and Weinberg articles [6, 7] also stress the complex signalling interactions which occur within tumours and the multicellular nature of the tumour microenvironment, with hallmarks arising from the perturbation of a variety of pathways and interactions between cell types.

1.2 Colorectal cancer is the fourth most common cancer in the UK

1.2.1 Colorectal cancer prevalence and survival

Colorectal cancer was the fourth most commonly diagnosed in England in 2011, after breast, prostate and lung, accounting for 12.4% of the total cancer diagnoses [9]. Both the one-year and five-year survival rates for this cancer are slowly increasing, with 77.1% of men and 73.1% of women diagnosed with colon cancer in 2011 surviving past one year, compared to 66.0% and

62.6% survival for men and women, respectively, diagnosed with colon cancer in 1996 [10]. Additionally, 53.4% of men and 52.3% of women diagnosed with colon cancer in 2006 survived past five years, compared to 45.2% and 44.4% survival for men and women, respectively, diagnosed with colon cancer in 1996 [10].

While this improvement in patient survival is a good sign, the UK still trails behind many of its Western neighbours. An analysis of the five-year survival rates for patients diagnosed with colorectal cancer in nine European countries and seven states in the USA in the period 1996-98 demonstrated that most of these obtained a survival rate of 45% or greater, with only Poland falling below 40%, with a European average of 50% and a USA average of 58% survival, which out performs the 44.8% attained by England for the same time period [11]. Additionally, a comparison of the one-year survival rates for colon cancer in Australia, Canada, Denmark, Norway, Sweden and the UK for patients diagnosed in 2000-07 demonstrated that the UK attained the lowest survival rate out of these countries and this was maintained when a variety of staging methods were applied to the patients [12].

With this poorer performance in terms of colorectal cancer survival, studies have been undertaken to assess the impact that additional factors play in the patient outcomes. A study looking at colorectal cancer patients in the North East of England found that deprivation increased the odds of a patient receiving a diagnosis of a stage IV tumour and decreased the odds of them receiving any treatment for their cancer, with this being more marked for colon cancer than rectal cancer, while amount of travel required to receive appropriate healthcare was not a factor [13]. A further study covering the whole of England also found that deprivation increased the mortality of patients within 12 months of diagnosis and this increase was also seen in patients presenting as an emergency case or failing to obtain resection surgery as treatment [14].

1.2.2 Types of colorectal cancer

As with many other types of cancer, colorectal cancer can arise as sporadic cases, due to inherited susceptibility or as a result of a specific hereditary disease, with inherited genetic factors responsible for up to 35% of colorectal cancer cases [15]. The mutations which occur in the development of the disease can be broadly divided into two groups, resulting in cancers with microsatellite instability (MSI) or chromosomal instability (CIN) [16], in addition to demonstration of the CpG Island Methylator Phenotype (CIMP) on tumour suppressor genes in ~40% of colorectal cancers [17]. With these, tumours can be classified into one of five subtypes via their molecular fingerprint [18], with the subtypes defined as: Type 1 (CIMP-high/MSI-high/BRAF mutation), Type 2 (CIMP-high/MSI-low or microsatellite stable (MSS)/BRAF mutation), Type 3 (CIMP-low/MSS or MSI-low/KRAS mutation), Type 4 (CIMP-negative/MSS) and Type 5 (CIMP-negative/MSI-high).

1.2.2.1 MSI pathway

The MSI pathway arises from mutations to DNA mismatch repair genes and this pathway is thought to be the underlying cause of ~15% of colorectal cancer cases [19, 20]. While the mutations to mismatch repair genes are the driving force behind this type of carcinogenesis, MSI tumours have been found to contain a number of mutations to the Wnt signalling pathway [21], a key component of the proposed adenoma-carcinoma progression of colorectal cancer. Within this group of

colorectal cancers, there is the most common form of hereditary colorectal cancer, Hereditary Non-Polyposis Colorectal Cancer (HNPCC, also referred to as Lynch syndrome), which accounts for 3% of diagnosed colorectal cancer cases [22]. This autosomal dominant disease increases the expected lifetime risk of developing colorectal cancer to 50-80% [23], with mutations found in the mismatch repair genes *MLH1* [24], *MSH2* [24], *PMS1* [25], *PMS2* [25] and *MSH6* [26].

1.2.2.2 CIN pathway

The CIN pathway accounts for the remaining 85% of cases not accounted for by the MSI pathway [27], with structural changes seen to many chromosomes [28]. The group of CIN tumours contains the subset of tumours, less than 1% of the total number of cases [22], formed as a result of the autosomal dominant disease familial adenomatous polyposis (FAP), which results in a 100% risk of developing colorectal over the average lifetime of patients [23]. The genetic cause of this disease was initially narrowed down to a gene found on chromosome 5 [29, 30], with the identification of the *adenomatous polyposis coli* (*APC*) gene as the one responsible for FAP coming in 1991 [31-34].

1.2.2.3 The adenoma-carcinoma progression of colorectal cancer

Despite the different pathways in colorectal cancer development, there appears to be a sequence of key genes which are mutated at various points within the progression of this type of cancer. This adenoma-carcinoma progression was first proposed by Fearon and Vogelstein in 1990 [35] and has since been reported and refined by other parties [36-38] to incorporate ongoing research, such as the contribution of loss of heterozygosity (LOH) mutations to carcinogenesis [39]. The most recent adaption of this pathway was presented in Pinto and Clevers in 2005 [40] and is reproduced in Figure 1.1. This pathway demonstrates that major components of the Wnt signalling pathway are found at the beginning of this progression and that mutations to these genes are critical for the development of colorectal cancers.

1.2.3 Risk factors for colorectal cancer

While genetic factors can play a large role in determining the risk an individual faces for developing colorectal cancer over their lifetime, it has also been shown that lifestyle may affect the occurrence of the disease. Many of these are linked to the dietary behaviour of patients, with those adopting a ‘healthy’ eating pattern with lower meat and increased fruit and vegetable consumption found to have a lower risk of developing colorectal cancer [41]. There is also a link between dietary diseases and colorectal cancer incidence, with links found between increased body-mass index, a sign of obesity, [42] and diabetes [43]. In addition to these risk factors, a clear correlation has been demonstrated between smoking [44] or alcohol consumption [45] and the incidence of colorectal cancer.

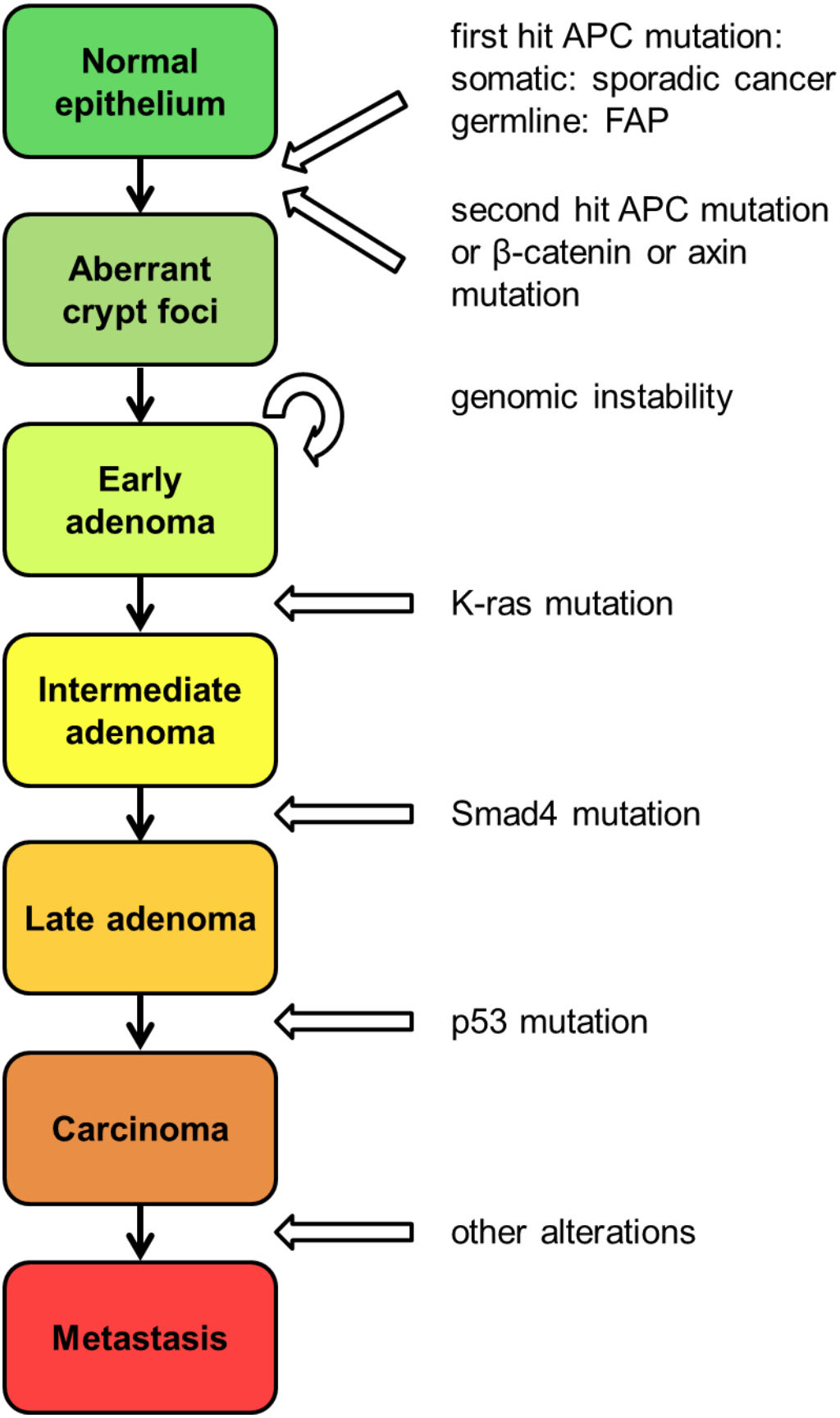

Figure 1.1: The adenoma-carcinoma progression of colorectal cancer. The initiation and development of colorectal cancer depends on a defined sequence of genetic mutations, adapted from Pinto and Clevers (2005) [40]. First hit mutations occur to key proteins in the Wnt signalling pathway to initiate tumour growth via aberrant crypt foci, while further mutations to known oncogenes further the progression of the disease to a carcinoma with metastatic growth.

1.2.4 Staging of colorectal cancer

The stage at which a cancer is diagnosed has large implications for the treatment of the disease and the overall patient prognosis. There are currently two major systems of colorectal cancer staging in use, the Dukes system which was first proposed in 1932 [46] and the American Joint Committee on Cancer (AJCC)/Union for International Cancer Control (UICC) system which was introduced in 1977 [47]. These systems use different criteria for determining the stage of a colorectal cancer tumour and are both used in the current literature. Many colorectal cancer cell lines were isolated and cultured prior to the introduction of the AJCC/UICC staging system and so are given with their Dukes classification, an example being the eleven cell lines established by Leibovitz *et al* in 1976 [48], while more recent work involving patient samples tends to use the AJCC/UICC system, such as the 2001 paper by Chan *et al* [49].

1.2.4.1 Dukes staging

The Dukes staging system was initially proposed for rectal cancer [46] and defined three stages of the disease based on the spread of the tumour through the rectum as follows:

A. Growth limited to the wall of the rectum;

B. Extension of growth to extra rectal tissues, but no metastases in regional lymph nodes;

C. Metastases in regional lymph nodes.

These classifications based on the penetration of the tumour through the tissue layers of the rectum, as illustrated in Figure 1.2A, were also seen to have prognostic value, as those patients which were determined to have later stages of the disease had a lower probability of surviving for 3 years after excision of the rectum.

This system was then adapted by two papers in 1949, the first by Kirklin *et al* [50] proposed both the extension of the Dukes system to the classification of colon cancer and altered the layer of tissue penetration required to meet the criteria for each stage. Stage A tumours were defined as those confined to the mucosa; B_1 tumours as those extending into, but not through, the muscularis propria; B_2 tumours as those which had extended through the muscularis propria and stage C tumours as those stage B tumours which also had lymph node involvement. Meanwhile, separately, Dukes proposed a subdivision of stage C rectal tumours into C_1 tumours where the lymph node involvement is limited to the regional lymph nodes and C_2 tumours where distant lymph nodes were also involved [51]. These two proposals were combined by Astler and Coller in 1954 [52] who also demonstrated that these adaptions to the initial staging system proposed in 1932 were also sufficient to provide clear prognostic indicators for colorectal cancer patients, as the 5-year survival for patients was decreased in those patients diagnosed with later stages of the disease and this observation was separately reported for rectal cancer by Dukes and Bussey in 1958 [53].

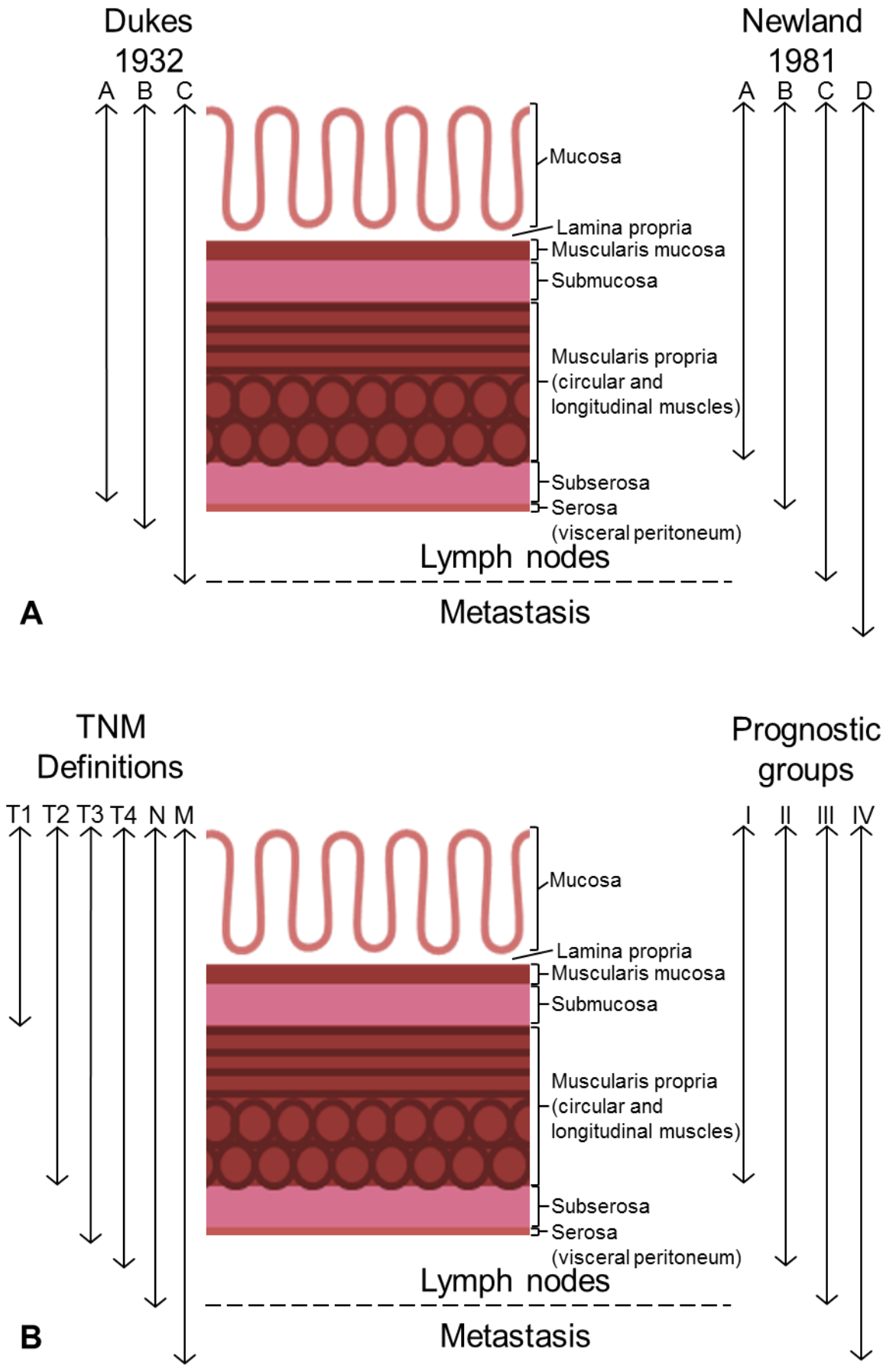

Figure 1.2: The staging of colorectal cancer is dependent on the spread of the tumour. The extent of primary tumour spread through the tissue layers of the colon, image adapted from Ovalle and Nahirney (2008) [54], is used to determine the stage of colorectal cancer under A: the Dukes' staging system, with the initial Duke's (1932) [46] definitions on the left and the latest Newland et al. (1981) [57] definitions on the right, and B: the AJCC/UICC staging system, Edge et al (2011) [47], with the TNM definitions on the left and the prognostic groups on the right.

The fourth stage was first introduced in 1967 by Turnbull et al [55], which defined stage D tumours as those which had metastasised to the liver, lung or bone or had grown and invaded either the abdominal wall or adjacent organs. A method of defining tumours which had grown and become adherent to adjacent structures was also proposed by Gunderson and Sosin in 1974 [56] where the stages of B_3 and C_3 were proposed to defined those tumours in the absence and presence of lymph node involvement respectively. The proposals of Kirklin *et al*, Astler and Coller and Gunderson and Sosin have been grouped together to form the Modified Astler-Coller system for the classification of colorectal cancers.

The final adaption to the Dukes staging system was proposed in 1981 by Newland *et al* [57] which subdivided the stage A tumours into A_1 tumours limited to the mucosa, A_2 tumours which had extended into the submucosa and A_3 tumours which had extended into the muscularis propria. In line which these changes, B_1 tumours were also redefined to include tumours which had spread beyond the muscularis propria and B_2 tumours as those involving the serosa. Stage D tumours were also subdivided into D_1 tumours where the primary tumour was remaining after surgical resection and D_2 tumours which were present with distant metastases. The system defined here is also illustrated in Figure 1.2A and it is clear that over the various changes to the Dukes system, the extent of tumour spread in stage A and B tumours is smaller in later versions and the later versions have added in a method of defining colorectal cancer cases where distant metastases are present.

While the staging of colorectal cancer via the Dukes' system provides a progression for the spread of the tumour from the healthy colonic epithelium (Figure 1.3A) to the initial spread of the tumour mass (Figure 1.3B) and beyond, the tissue organisation of cancers within each staging group can vary. Whilst pathology of Dukes' Stage B and C tumours demonstrate that both contain epithelial (arrows, Figure 1.3C-F) and stromal cells (arrowheads, Figure 1.3C-F), with the epithelial cells forming disrupted crypt structures, the proportion of these cell types can vary between patients, which has implication for patient prognosis [58].

Throughout the different versions of the Dukes' staging system it has maintained its function as a prognostic tool as those patients diagnosed with later stages of the disease are seen to have lower survival rates. This is reflected in the latest released data for colorectal cancer cases in England by the National Cancer Intelligence Network [59]. This data shows that the 5-year survival rates for patients diagnosed between 1996 and 2002 were 93.2, 77.0, 47.7 and 6.6% for patients diagnosed with Dukes stage A through D respectively.

However, due to the large number of alterations made to the Dukes system over the years and the lack of clarity in reporting which variant of the Dukes system a research group has employed, there can be discrepancies in the staging of tumours between different research groups. This was demonstrated by Raraty and Winstanley in 1998 [60] where pathology reports for 14 cases of colorectal cancer were distributed to 9 consultants for them to stage. The 9 consultants only reached a consensus on 6 of the 14 cases, with a split of 5:4 seen in one of the cases. This demonstrates that without a clear indication of which version of the Dukes system is employed at the point of diagnosis, the patient could receive an altered diagnosis which could affect the treatment options available and the overall patient prognosis.

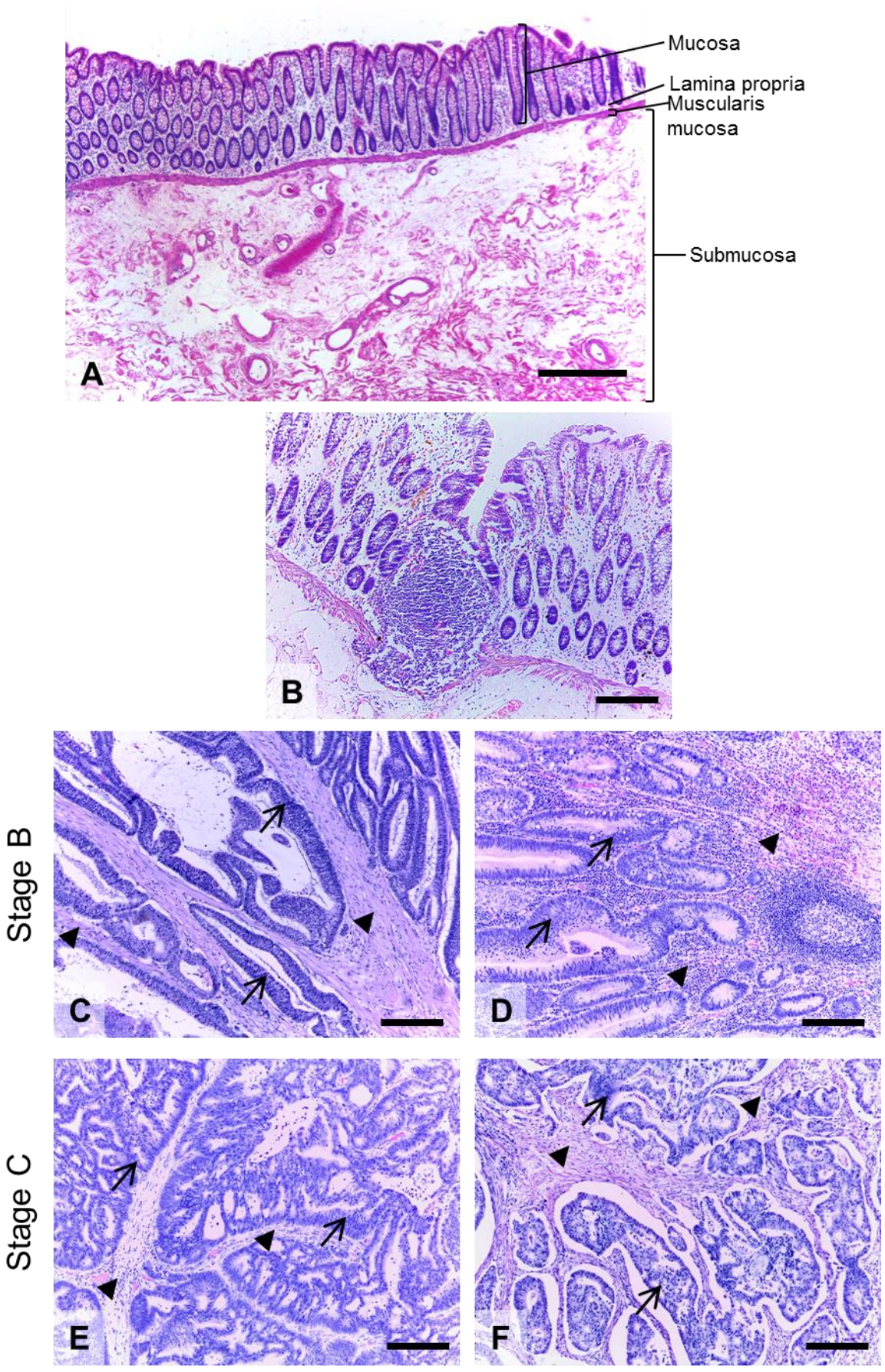

Figure 1.3: Colorectal cancer disrupts the normal organisation of the healthy colon. A: the tissue layers of the healthy colon are clearly seen in histological samples and B: tumour growths disrupt these organised tissue layers. Examples of pathological samples from C and D: Dukes' Stage B and E and F: Dukes' Stage C tumours demonstrating the disrupted organisation of the tissue in addition to the varying level of carcinoma (arrows) and stromal (arrowheads) involvement in the tumours. Scale bars = 500μm for image A and 200μm for images B-F.

1.2.4.2 AJCC/UICC staging

The AJCC/UICC staging system is currently on its 7th edition, with updated staging criteria released every 4-7 years [47]. This system stages cancers based on scoring the extent of the primary tumour (T), the spread of the tumour to localised lymph nodes (N) and the absence or presence of distant metastases, including non-regional lymph node involvement, (M). Together the TNM scores are used to define the anatomic stage or prognostic group of the cancer. The general definitions for the TNM scores can be applied to all solid cancer types, with more specific definitions given for each cancer type. The current, 7th edition, TNM score definitions for colorectal cancer are given in Figure 1.4A and illustrated in Figure 1.2B and these demonstrate the progress of the primary tumour through the layers of the colon or rectum as the disease progresses. The individual TNM scores are then used to grade the cancer from stage I through to stage IV and are given in Figure 1.4B and illustrated in Figure 1.2B, with subdivisions used to clarify the extent of the spread of the primary tumour or the amount of metastatic involvement at each stage.

While the TNM system provides a clearer system for staging colorectal tumours due to the increased detail given to describing the qualifying criteria for each TNM score, clarity in reporting this score is important as this system allows for the reporting of cancer staging based on clinical or pathological data. Some of these issues were raised by Compton in 2006 [61] which highlights that additional data, such as the level of lymphatic or vascular invasion into the primary tumour, is not included in the AJCC/UICC staging system but may be relevant for determining treatment options of the disease.

The prediction of prognosis for patients is also not as clear as is seen with the Dukes staging system, as the 2005 Surveillance, Epidemiology and End Results (SEER) data from the USA demonstrated that patients diagnosed with either stage I and stage IIIA colorectal cancer had similar 5-year survival rates [47]. However, recent analysis by Gao *et al* [62] and Hari *et al* [63] have shown that the 7th edition of the AJCC/UICC classification system is an improvement, in terms of predicting patient prognosis, over the 6th edition, although there is still room for improving the definitions for each stage to allow for better treatment decisions for those patients diagnosed with stage II or stage III colorectal cancer.

1.3 Cancer migration is a plastic process that leads to metastasis

As seen from the patient survival rates for colorectal cancer of different stages, the further a tumour has spread through the body, the worse the prognosis. This demonstrates that the cancer hallmark of ‘tissue invasion and metastasis’, as defined by Hanahan and Weinberg [6, 7], represents a key tipping point in patient outcomes and is, therefore, of great interest in the arena of cancer research. The localised spread of the tumour through the neighbouring tissue, either by expansion through growth or collective migration, eventually leads to the dissemination of the tumour through the body in the form of metastases.

Score	Definition
TX	Primary tumour cannot be assessed
T0	No evidence of primary tumour
Tis	Carcinoma in situ: intraepithelial or invasion of lamina propria
T1	Tumour invades submucosa
T2	Tumour invades muscularis propria
T3	Tumour invades through the muscularis propria into pericolorectal tissues
T4a	Tumour penetrates to the surface of the visceral peritoneum
T4b	Tumour directly invades or is adherent to other organs or structures
NX	Regional lymph nodes cannot be assessed
N0	No regional lymph node metastases
N1	Metastasis in 1-3 regional lymph nodes
N1a	Metastasis in one regional lymph node
N1b	Metastasis in 2-3 regional lymph nodes
N1c	Tumour deposit(s) in the subserosa, mesentery, or nonperitonealised pericolic or perirectal tissues without regional nodal metastasis
N2	Metastasis in four or more regional lymph nodes
N2a	Metastasis in 4-6 regional lymph nodes
N2b	Metastasis in seven or more regional lymph nodes
M0	No distant metastases
M1	Distant metastases
M1a	Metastasis confined to one organ or site (e.g. liver, lung, ovary, nonregional node)
M1b	Metastases in more than one organ/site or the peritoneum

A

Stage	T	N	M
0	Tis	N0	M0
I	T1	N0	M0
	T2	N0	M0
IIA	T3	N0	M0
IIB	T4a	N0	M0
IIC	T4b	N0	M0
IIIA	T1-T2	N1/N1c	M0
	T1	N2a	M0
IIIB	T3-T4a	N1/N1c	M0
	T2-T3	N2a	M0
	T1-T2	N2b	M0
IIIC	T4a	N2a	M0
	T3-T4a	N2b	M0
	T4b	N1-N2	M0
IVA	Any T	Any N	M1a
IVB	Any T	Any N	M1b

B

Figure 1.4: The AJCC/UICC staging criteria for colorectal cancer. The system uses A: the scoring of the spread of the primary tumour (T) through the localised tissue, the involvement of regional lymph nodes (N) and the presence of distant metastasis (M) to determine B: the prognostic groups to stage the disease based on its spread throughout the body.

1.3.1 Metastasis is a multistep process

The transition of cancer cells from those in an expanding primary tumour to those forming metastases at distant sites relies on the changing behaviour of cells as they disseminate, in addition to a permissive microenvironment at the site of metastasis. This was highlighted in Paget's 1889 paper [64] which discussed the incidence of secondary tumours in various cancer types and noted that there were certain sites in the body which are more likely to be the site of secondary tumours based on the location of the original tumour, such as the higher incidence of secondary liver tumours in breast cancer patients as opposed to spleen or kidneys. From this observation he hypothesised what has become known as the 'seed and soil' method of cancer metastases, where the process is reliant on the characteristics of the migrating cancer cell, the 'seed', and the microenvironment of the site of metastasis, the 'soil'.

The step-by-step process which is involved in the mechanics of metastasis formation has been outlined by many sources, including a 2003 review by Fidler [65]. Here the steps of metastatic dissemination are given as the formation of a primary tumour followed by proliferation and angiogenesis at this site. Single cells then detach and invade the surrounding tissues and blood vessels before being picked up by the circulatory system and transported to distant organs. Within the blood vessels of these organs, the cancer cells then attach to the wall of these vessels before extravasating into the local tissue, where a permissive microenvironment is established prior to the proliferation and vascularisation of the metastatic legion. From this sequence of events, it is clear that the cancer cells must adopt a variety of behaviours to navigate each step successfully and one of the earliest of these is the adoption of a migratory phenotype.

1.3.2 Cancer cells can adopt a variety of migratory mechanisms

The process of cell migration depends on the repeated action of three basic steps to move the cells, namely attachment of the leading edge, contraction of the cell body and detachment of the trailing edge [66]. The switching between migration modes is mediated by the variable expression and distribution of a large number of proteins, from integrins and cadherins regulating cell adhesion, matrix metalloproteases (MMP) and cathepsins degrading the surrounding extracellular matrix (ECM) and the dynamic behaviour of actin and actin binding proteins to change cell shape [67].

With this variability in the proteins which can be involved in cell migration, there are three main methods of cell migration that cells can employ [68]. Collective, or epithelial-sheet, migration (Figure 1.5A) is a commonly occurring process in development and regeneration, particularly in epidermal wound healing [69]. In this mode of migration, adherens junctions between the cells are retained and the active actin polymerisation and ECM remodelling occurs at the front of the leading cells of migration which creates a path for the following cells to move through [68].

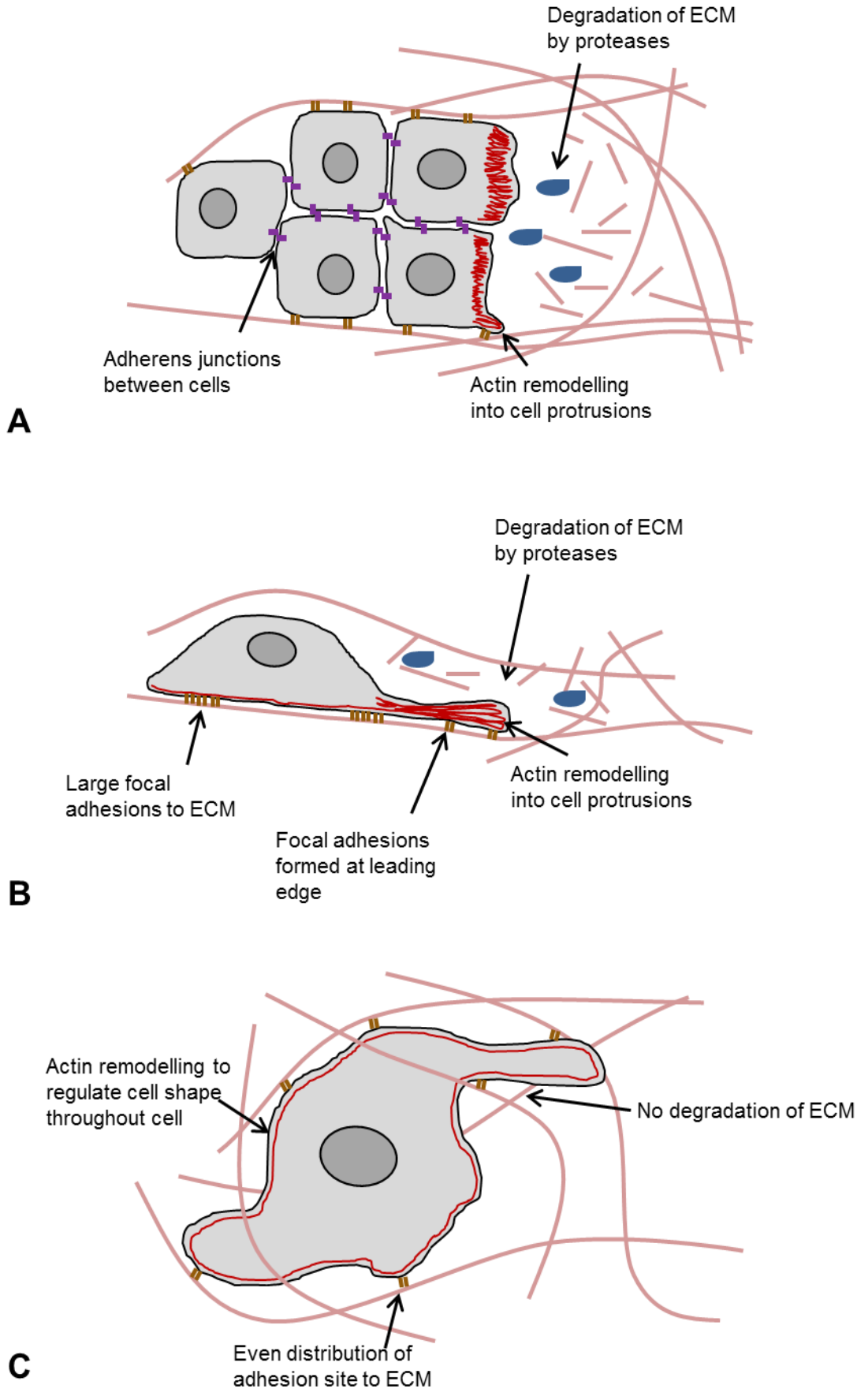

Figure 1.5: Migrating cells can adopt one of three modes of migration. A: cells moving via collective migration retain cell-cell adhesion sites, with ECM degradation occurring in front of the leading cells, B: cells moving via mesenchymal migration do not retain cell-cell adhesion sites but still degrade the ECM in front of the migrating cell and C: cells migrating via amoeboid migration do not degrade the local ECM and use a dynamic actin cytoskeleton to squeeze through gaps in the ECM, adapted from Sahai (2005) [68].

There are also two forms of single cell migration, mesenchymal and amoeboid [68]. Mesenchymal type migration (Figure 1.5B) is similar to the collective cell migration, with the degradation of ECM occurring in front of the migrating cell to generate a migration pathway. Cells undergoing this form of migration are characterised by a stereotypical elongated shape with the actin remodelling at the leading edge of the cell producing a variety of cell protrusions to allow the cells to form attachments to the ECM in the wake of the MMP activity. Cells migrating using the amoeboid method (Figure 1.5C) have a more rounded cell shape and weaker adhesion to the surrounding ECM. These cells do not rely on the secretion of MMPs, or similar, to produce a pathway through the ECM and instead rely on a dynamic cell shape to squeeze between ECM filaments.

With these different modes of migration available to cells, the mode of migration employed by the cells can be altered by the cells in response to environmental cues, with the physical characteristics of the ECM impacting the mode of migration utilised [70]. Cellular migration on 2D ECM gels is seen to favour collective migration, whereas the migration of cells through loose 3D ECM gels is mainly via amoeboid migration. The switching between the different types of migration in response to the environment is mediated by the altered expression of key protein groups, namely integrins, proteases and cadherins [71], which allows for the alteration of migration mode to suit the environment of the cells.

1.3.3 The tumour microenvironment can direct migratory behaviour

It is not just the ECM architecture that can direct the migratory behaviour of cancer cells, other factors in the microenvironment of the tumours can also affect cell migration. Larger solid tumours develop a hypoxic interior, necessitating the need for angiogenesis to sustain the tumour growth, one of the cancer hallmarks described by Hanahan and Weinberg [6, 7]. This oxygen deficient environment stimulates the activation of the transcription factor hypoxia-inducible factor (HIF) which mediates the cellular response [72]. Failure to adapt to the hypoxic environment via the growth of new blood vessels or alterations to cellular metabolism leads to the activation of migration associated genes in order to migrate out of the hypoxic environment. Another microenvironment trait which is linked to tumour hypoxia is the acidity of the tissue, as the lack of oxygen causes increased metabolism resulting in lactic acid and the lack of blood vessels leads to the poor removal of this lactic acid and CO_2 [73]. Together this reverses the balance of intracellular and extracellular pH seen in healthy tissues and can affect the behaviour of proteins including actin-binding proteins, leading to the activation of a migratory phenotype.

In addition to the non-cellular factors which can drive migration, additional cell types within the tumour can act to progress cancer cells towards a migratory phenotype [74], while the presence of immune cells and fibroblasts in tumours have been implicated in poor patient survival [58, 75]. In particular, the presence of fibroblasts in cancer models has been shown to increase the level of cancer cell migration over that seen in fibroblast free models [76]. Further work looking at the mechanism by which the fibroblasts aid migration demonstrated that squamous cell carcinoma cells were able to migrate in a collective manner along pathways generated by the fibroblasts in ECM gels and that the presence of live fibroblasts aided their migration into the gels [77].

1.3.4 The epithelial-mesenchymal transition is a key step in metastasis formation

The epithelial-mesenchymal transition (EMT) has been implicated in the shifting patterns of gene expression seen in cancer cells during the development of a migratory phenotype. This transition acts to convert an epithelial cell to a mesenchymal cell and is common in development in order to allow the migration of cells to form organ structures [78]. The most basic protein markers for EMT are the upregulation of vimentin, coupled with the downregulation of E-cadherin [79], although the expression of many other proteins are also altered during EMT inducing the downregulation of adhesion proteins such as desmoplakin and occludin and the upregulation of selected MMPs [80]. The downstream effects of these changes to gene expression impact the adhesion and migratory capabilities of the cells, including the loss of adhesion to neighbouring epithelial cells and increased actin remodelling due to the increased activity of Rho [81].

It has also been shown that an EMT signature is correlated with the progression of colorectal cancer, as the expression of mutated H-Ras in the colorectal cancer cell line CaCo-2 was sufficient to induce an alteration in gene expression which correlated with the expected EMT signature in terms of vimentin and E-cadherin expression [82]. This EMT signature was also correlated with the altered expression of other proteins, such as the transcription factor Slug, which has previously been shown to be correlated with the progression of colorectal cancer. Another research group also demonstrated that the division of colorectal cancers into those with and without an EMT signature was sufficient to be a predictor of prognosis in separate patient cohorts and was determined to be a dominant program in the progression of colorectal cancer [79].

1.3.4.1 The physical characteristics of the growth environment impacts cell behaviour

In addition to the changes seen when the dimensionality of the culture environment is altered, the physical characteristics of the 3D environment provided to the cells also affects cell behaviour. The stiffness of the 3D microenvironment can affect the adhesion of cells, with cells found to spread out more and produce larger colonies when cultured on stiffer gels, which is seen in conjunction with an increase in actin stress fibres [83]. As the elastic modulus of tissue culture plastic, as used for standard 2D culture, is far higher than that seen in healthy or tumorous tissue, this suggests one mechanism behind the difference in gene expression between 2D and 3D cultures which is not solely reliant on the spatial characteristics of the growth environment.

Another research group has also demonstrated that the culture of 3D spheroids in a high-stress environment, as induced by the variable inclusion of microbeads in the agarose gels, directed the growth of the spheroid to form an oblate shape in relation to the stress fracturing of the gel [84]. This increase in external stress also induced a significantly higher amount of caspase-3 mediated apoptosis in the centre of the spheroids compared to those grown with no or low compressive stress.

With the microenvironment playing a large role in directing the behaviour of cells it has been suggested that the application of engineering to tumours to revert the tumorous microenvironment back to a healthy microenvironment is one avenue for cancer research to pursue [85], as the reversion to a softer ECM environment may provide environment cues to the cancer cells to

modulate the expression and localisation of proteins, such as adhesion proteins, which may then have an impact on the migratory behaviour of the cells.

1.4 The Wnt signalling pathway is key in the development of colorectal cancer

Wnt signalling is vital for the development of the healthy colonic epithelium, but it has been shown to hold a key place in the development of colorectal cancers as it is consecutive mutations to genes in this pathway that forms the initial trigger point in Fearon and Vogelstein's adenoma-carcinoma progression of colorectal cancer [35].

1.4.1 The canonical Wnt pathway

In the canonical Wnt pathway [86], in the absence of a Wnt ligand, the scaffold protein Axin forms a complex with APC and glycogen synthase kinase 3β (GSK-3β) (Figure 1.6A). The β-catenin binding domains of APC bring the β-catenin protein into contact with GSK-3β, which in turn phosphorylates β-catenin and this phosphorylation of β-catenin then targets it for proteasomal degradation in the cytoplasm. However, once a Wnt ligand has bound to the Frizzled/lipoprotein receptor-related protein (LRP)5/6 co-receptor at the plasma membrane, the Axin/APC/GSK-3β complex is distupted as Axin is recruited up to the Frizzled/LRP5/6 co-receptor (Figure 1.6B). As β-catenin is no longer targeted for proteasomal degradation, it translocates to the nucleus where it finds its transcription binding partners which include TCF-4 and LEF-1 [87]. This results in the transcription of many genes, including those implicated in EMT and tumour progression [88].

1.4.2 Wnt signalling determines cell behaviour in the healthy colonic epithelium

The colonic epithelium is a tightly regulated system where the axis of proliferation vs. differentiation must be maintained to ensure a healthy, functional tissue. The cell types of the colonic epithelium each have distinct roles which collectively deliver the functionality of the colon. The absorptive enterocytes and mucous secreting goblet cells make up roughly 95% of the differentiated cells of the epithelium and are responsible for the functionality of the colon in terms of maintaining the homeostatic balance of water and electrolytes via the transport of ions including H^+, Cl^-, Na^+ and HCO_3^- across the apical membrane of the cells into and out of the colon lumen [89]. A further 1% of the remaining differentiated cells consist of the enteroendocrine cells which regulate the function of the gut via hormone secretion [90].

In addition to the different cell types found on the surface of the colonic epithelium, there is a population of cells, the Paneth cells, which reside at the base of the colonic crypts below the population of colonic stem cells [90]. The proteins secreted by these cells have a role in the innate immunity of the colon and may help to regulate the healthy gut flora which is found there. The differentiation pathways to each of these mature cell types is controlled by a balance of Wnt and Notch signalling, with Wnt signalling driving the proliferation vs. differentiation axis, while the Notch signalling controls the balance between the secretory and absorptive cell types [90].

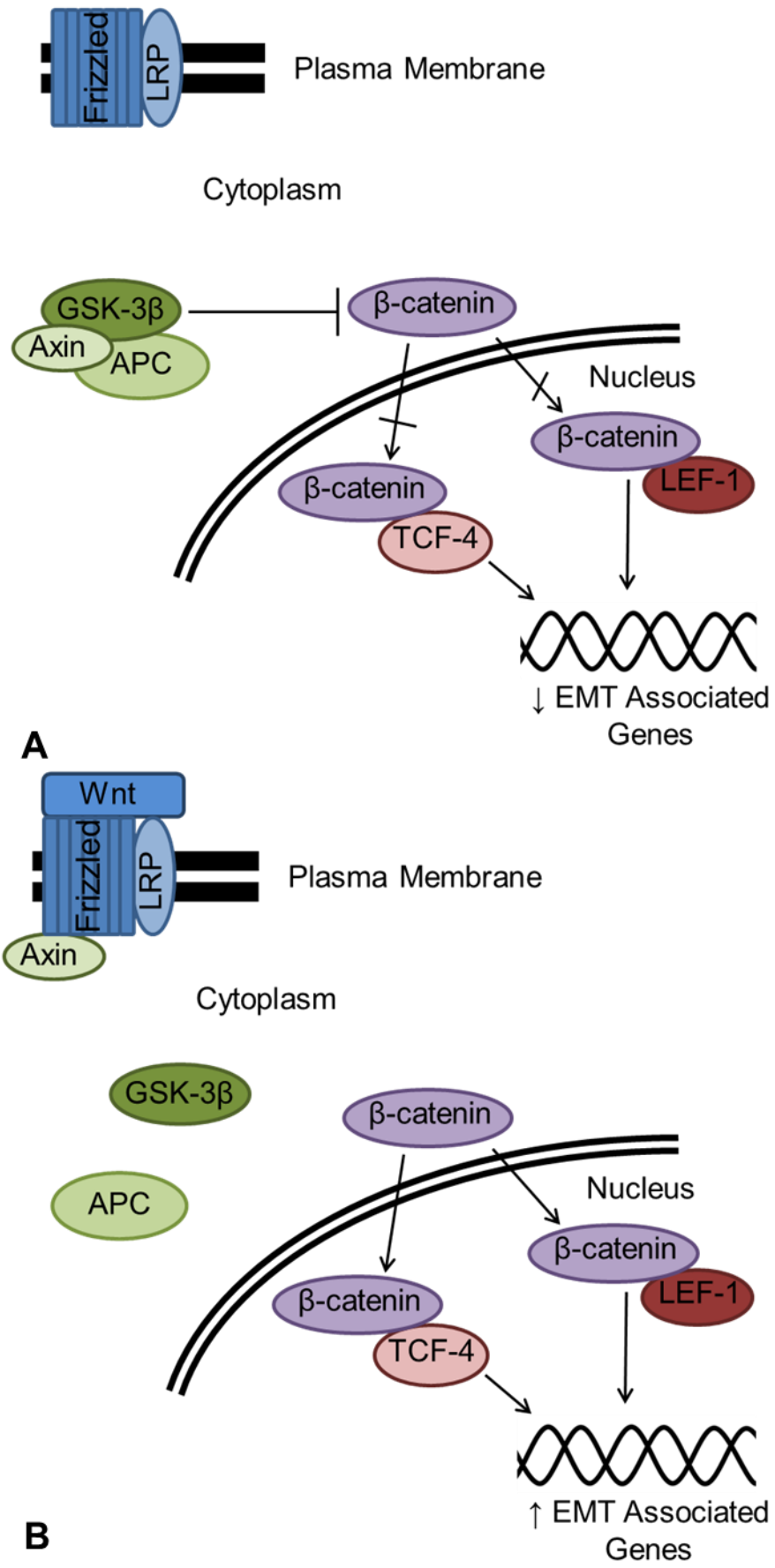

Figure 1.6: Schematic of the Wnt signalling pathway. A: In the absence of the Wnt ligand Axin, APC and GSK-3β form a complex which targets β-catenin for proteasomal degradation and prevents its translocation to the nucleus. B: In the presence of the Wnt ligand, the Axin/APC/ GSK-3β complex is disrupted by the recruitment of Axin to the plasma membrane, β-catenin is no longer targeted for proteasomal degradation and translocates to the nucleus to find its binding partners TCF-4 and LEF-1 to initiate transcription of β-catenin target genes, including those associated with EMT.

In mice, inhibition of the Wnt pathway by transgenic overexpression of its protein antagonist Dickkopf1 (Dkk1), which interacts with the membrane protein LRP6 [91], inhibits the proliferative activity of the cells, as seen by the lack of the proliferation marker Ki-67 or low uptake of the synthetic nucleoside Brd-U [92]. This overexpression was also found to disrupt the morphology of crypts seen on histological sections, in addition to disrupting the pattern of nuclear β-catenin localisation. This aberration of the natural patterning of Wnt leads to a loss to crypt phenotype, as visualised by the absence of the crypt marker Enc-1, and the depletion of the three secretory cell types of the epithelium, the goblet, enteroendocrine and Paneth cells, while preserving the distribution of absorptive enterocytes, as visualised by the alkaline phosphatase (AP), across the epithelium.

Studies on mice which are homozygous negative for the *Tcf7l2* gene, which encodes the β-catenin binding partner TCF-4, also demonstrate a disruption in intestinal epithelial morphology [93], although this study looked at the role in the development of the small intestine as opposed to the colon. The lack of TCF-4 disrupted the formation of intestinal crypts in the intervilli regions by producing cells which have characteristics of cells found in the villi, such as microvilli and the supranuclear arrangement of Golgi bodies. The lack of true crypts led to no detectable enteroendocrine cells in the *Tcf7l2*$^{-/-}$ mice and a lack of detectable cell division, again seen by analysing Ki-67 expression and Brd-U uptake, in the latest stages of embryonic development from E16.5 onwards. This disruption to cellular organisation was confined to the small intestine and led to *Tcf7l2*$^{-/-}$ pups dying within 24 hours of birth. Other work with TCF-4 null mice has also show that the removal of TCF-4 activity removes the expression of β-catenin/TCF-4 transcription targets, such as Enc-1, in the prospective crypts while promoting the expression of the differentiation markers p21 and FABP2 [94].

Downstream targets of Wnt signalling have also been found to drive cellular behaviour [95]. The proliferating compartment of the epithelium expresses the tyrosine kinase receptors EphB2 and EphB3, while the differentiating cells of the colonic epithelium express the ligands ephrin-B1 and ephrin-B2. Null mutations or kinase inactivity in the receptors negatively impacts the rate of cell proliferation but does not affect the level of apoptosis seen in the epithelial cells, while overexpression of ephrin-B2 causes an increase in observed cell proliferation. The lack of kinase activity also affects the distribution of the proliferative and Paneth cells within the crypt. It is thought that the inhibition of cell proliferation is caused by a reduction of cells entering the cell cycle as opposed to a reduction in size of the stem cell population and that the interaction between the ephrin ligands and the Wnt induced EphB receptor defines the domain of proliferation inside the colonic crypt.

1.4.3 Colorectal cancers have abnormal patterns of Wnt signalling

While Wnt signalling has a key physiological role in the maintenance of a healthy colonic epithelium, mutations to proteins within the pathway have been implicated in driving the development and progression of colorectal cancer [35]. Analysis by Albuquerque *et al* of the mutations present in the Wnt pathway genes *APC*, *CTNNB1* and *AXIN2* in HNPCC in addition to sporadic cases [96] was pooled with the data from 12 separate cohorts [21, 97-107] to demonstrate that ~90% of colorectal cancers possess a mutation in any of these three genes.

Many genes which are found to be upregulated in colorectal cancer are either genes which are directly involved in the Wnt signalling pathway, namely *APC*, *LGR6* and *TCF7L2*, or downstream transcription targets of the Wnt pathway, such as *MMP2*, *EPHB6*, *RET* and *K61RS3* [108]. Additionally, during EMT mediated progression of the disease, the expression Wnt signalling transcription mediator β-catenin and Wnt transcriptional target keratins are found to vary, which may be a result of Wnt signalling driving the EMT [109].

Mutations to APC are common in a variety of colorectal cancer cell lines [110] and tumour samples taken from patients with both hereditary and sporadic colorectal cancers [34]. This protein has long been one of interest to those studying the genetic causes of colorectal cancer as it was originally identified as the mutated gene which causes the autosomal dominant condition FAP. Due to the incidence of loss of heterozygosity (LOH) mutations during the progression of colorectal tumours [39], the inheritance or the sporadic acquisition of a mutated *APC* gene is seen as important step along the adenoma-carcinoma transition [37, 38].

The introduction of a full-length APC protein into the colorectal cancer cell line SW480, which possesses a truncated APC protein [110], causes a variety of changes to the cells [111]. The change of β-catenin localisation from nuclear in control SW480 cells to peripheral localisation in APC transfected cells leads to a change in the cell morphology in 2D cultures, with the APC transfected cells producing colonies where the cells had an increasingly epithelial morphology and the cells within the colonies were more tightly packed together. This alteration to cell morphology is accompanied by an upregulation of E-cadherin expression and its redistribution to the plasma membrane. This redistribution of both the β-catenin and E-cadherin does not appear to be mediated by the cortical distribution of actin filaments seen in the APC transfected cells, as disruption of the actin cytoskeleton via cytochalasin D does not affect the peripheral distribution of either. The introduction of APC also decreases the cell proliferation rate of the SW480 cells, resulting in smaller colonies formed on soft agar and significantly less tumour growth after injection into Balb/c mice. The migratory capacity of the cells is also reduced with fewer single cells moving into the wound of a 2D scratch wound assay after 24 hours, as the introduction of the APC protein appears to push the cells towards the epithelial sheet form of migration.

Inhibition of β-catenin/TCF-4 mediated gene transcription by transfection with a dominant negative variant of TCF-4 (dnTCF-4) led to a reduction in the proliferation rate of colorectal cell lines and induced the expression of the cell cycle regulator p21 [94]. It is thought that the diversion of the colorectal cancer cells from a proliferative phenotype to a differentiated phenotype is mediated via the downregulation of the Wnt target gene and transcriptional regulator *c-MYC* lifting the inhibition of p21 expression and leading to cell cycle arrest induced differentiation. This data suggests that the extended range of nuclear β-catenin localisation in colorectal cancers is a primary driver of the excessive proliferation seen in tumours and that targeting the β-catenin/TCF-4 transcriptional activity in these cells would cause the spontaneous differentiation of tumours and may be of value as a therapeutic strategy.

When taken with the increased β-catenin mRNA and protein expression at the leading edge of invasion in liver metastasis [112], it becomes clear that the transcription of Wnt target genes is involved in both driving colorectal cancer formation and its dissemination into distant tissues. This

pathway is therefore of interest when investigating colorectal cancer cell migration as disruption of Wnt signalling may disrupt the migratory behaviour of the cancer cells.

1.5 IGF-I signalling has been implicated in the cancerous transformation of cells

Another biological pathway which can feed into the Wnt signalling pathway and affect cell behaviour is the IGF-I pathway.

1.5.1 Biological function of Insulin-like Growth Factor-I

Insulin-like Growth Factor-I (IGF-I) is a 70 amino acid, 7.649kDa polypeptide with high homology to proinsulin [113]. The action of IGF-I is mainly mediated by the IGF-I receptor (IGF-IR), a transmembrane receptor tyrosine kinase which shares high homology with the insulin receptor, 85 and 65% for the cytoplasmic and extracellular domains respectively [114]. Due to the high homology between these two receptors, cross-reactivity between insulin and IGF-I and both of their receptors has been demonstrated [115]. Additionally, due to the high homology between IGF-I and IGF-II [116], there is also binding of IGF-II to the IGF-IR [117] and all of these binding partnerships were visualised by the displacement of ^{125}I labelled peptides from the receptors. While binding with different substrates has been demonstrated, the IGF-IR displays a higher binding affinity for IGF-I, with IGF-II and insulin displaying 2- and 100-fold less potency, respectively, at displacing ^{125}I labelled IGF-I from the IGF-IR binding site than unlabelled IGF-I [118].

IGF-I expression is induced by growth hormone (GH), with long and short term effects on mRNA and protein levels reported. A single dose of GH led to an increase in mRNA production in liver cells without a corresponding increase in the serum protein levels, whereas daily doses over 5 days significantly increased the serum levels of IGF-I detected via a radioimmunoassay [119]. This study also assessed the effect of administering GH on IGF-I related proteins such as IGF-II and the IGF binding proteins IGFBP-1, IGFBP-2, IGFBP-3 and ALS, demonstrating that changes in mRNA and serum protein levels are different for the different proteins and alter over time. Administration of GH to GH-deficient adults over a two week course has also been shown to increase serum levels of IGF-I, with the continual infusion of GH via a pump resulting in higher levels than induced by single daily injections of the same dose [120]. The changes induced by GH are also seen to have longer term effects with continual daily doses injected into patients, as after 3 or 6 months treatment the base level of IGF-I, either unbound or total, was increased relevant to the control [121]. This increase to the baseline levels did not dampen the immediate response to the administration of GH, the level of IGF-I still rose the same amount after the GH dose, however the starting value was higher in the samples at 6 months.

The production of IGF-I has been found to be localised to mesenchymal derived cells in a variety of human fetal tissues by histochemical hybridisation analysis [122], which demonstrates the capacity for tissue-specific paracrine signalling via IGF-I in addition to secretion into the circulating blood. A similar study on rat fetal and adult tissues also demonstrates the wide range of fetal tissues which express IGF-I mRNA, although they do not look at the specific tissue components that are responsible for this [123]. This paper demonstrates that the abundance of IGF-I mRNA is

decreased in the adult tissue comparative to the fetal samples, with the exception of the liver where there is a 10-fold increase in the amount of IGF-I mRNA in the adult tissue. The blood serum levels of IGF-I have been characterised in different populations [124-126] and shown to peak in childhood before declining with age, with slight variation between the levels seen in men and women, although it is noted that this may be a product of experimental variation between cohorts [124].

The IGF-IR is a homodimer tyrosine kinase receptor which comprises two extracellular α subunits and two transmembrane β subunits which possess intercellular kinase domains [114]. Binding of a ligand to the extracellular domain of IGF-IR leads to the autophosphorylation of the intercellular domains of the β subunits [127] and interaction with further target proteins, insulin response substrate-1 (IRS-1) [127, 128] and Shc [129] (Figure 1.7), both of which are signalling mediators also activated by the insulin receptor. When activated by the insulin receptor, IRS-1 is phosphorylated and has been shown to recruit phosphatidylinositol 3-kinase (PI3K), via the SH2 domains of the p85 regulatory subunit, in order to stimulate further signalling interactions [130], although it has been noted that the p85 subunit of PI3K is not phosphorylated at the tyrosine residues after stimulation by insulin and that this is not required for successful activation of PI3K [131]. Furthermore, the mitogenic activity stimulated by IGF-I in the human breast cancer cell line MCF-7 is mediated by PI3K, as the increase in DNA synthesis, as visualised by ^{3}H-thymine incorporation, and cyclin D1 mRNA and protein expression, as visualised by Northern and Western blots respectively, are all eliminated by the small molecule PI3K inhibitor LY294002 [132].

Binding of IGF-I to the IGF-IR causes the phosphorylation of tyrosine residues within the Shc protein, causing it to associate with the intercellular domain of IGF-IR [129]. This association between the proteins is not mediated by the SH2 domains of Shc [129] and are instead via interaction of the amino domain of Shc [133] with the Shc and IRS-1 NPXY binding (SAIN) domain of IGF-IR [134]. Although the binding domain on IGF-IR is not within the tyrosine kinase region of the protein, the autophosphorylation of IGF-IR is necessary for the binding of Shc, as mutations of the tyrosine residues to phenylalanine inhibits this binding [133]. Additionally, while IRS-1 and Shc share the same binding site on IGF-IR, there is no detectable interaction between these two proteins *in vitro* [135]. The signalling cascade mediated by the interactions of IGF-IR and Shc is continued via the association of Shc with SH2 domain of Grb2 and further signalling cascades via Ras [136]. This signalling cascade also affects the mitogenic behaviour of cells as microinjection of a Shc antibody or the dominant-negative N17 ras protein into rat fibroblasts inhibited IGF-I induced DNA synthesis, visualised via BrdU uptake [129, 137].

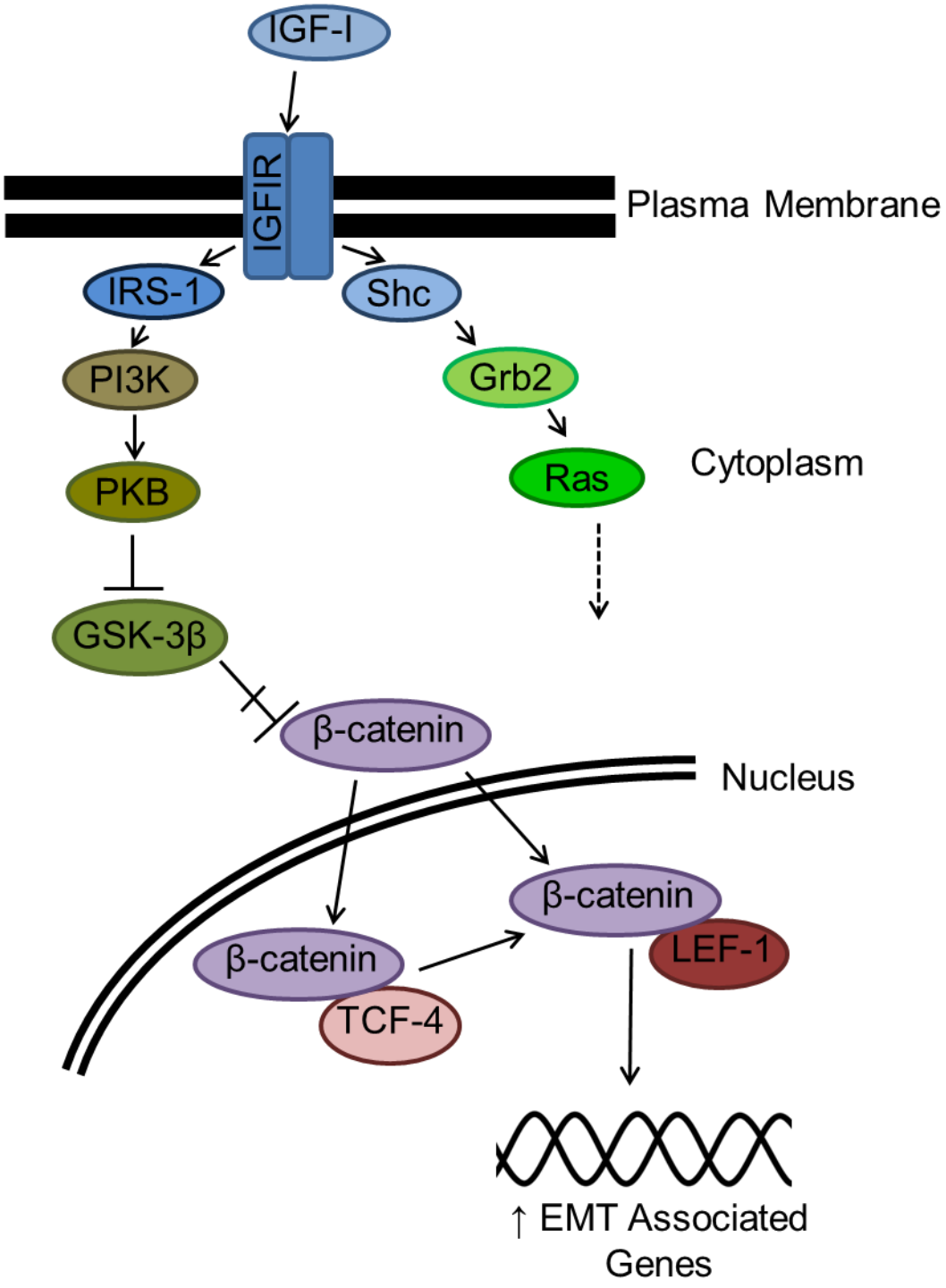

Figure 1.7: Schematic of the IGF-I signalling pathway demonstrating the interaction with the Wnt signalling pathway. IGF-I binds to the IGF-IR which results in signalling cascades via IRS-1 and Shc. The Shc mediated cascade feeds into the Ras/MEK/ERK pathway. The IRS-1 mediated cascade results in the PI3K/PKB mediated inhibition of GSK-3β. This results in the accumulation of β-catenin, which translocates to the nucleus and mediates transcription of EMT associated genes via interaction with various binding partners.

1.5.2 Interaction between the IGF-I and Wnt signalling pathways

Cross talk between the downstream signalling cascades of IGF-IR and the Wnt signalling pathway were first noted by Cross *et al* in 1994 [138] with a demonstration of the IGF-I inhibition of the activity of both GSK-3α and GSK-3β in L6 rat skeletal muscle cells, with GSK-3β being a key protein component of the Wnt signalling pathway. This IGF-I mediated GSK-3β inactivation was reversed by the pre-incubation of the L6 cells with the potent PI3K inhibitor wortmannin. As wortmannin was also shown to inhibit the IGF-I mediated activation of a variety of protein components of the MAPK cascade, it was initially suggested that the mechanism of the GSK-3β inhibition was via members of this pathway, such as MAPKAP kinase-1β. Further work from this group later demonstrated that it was protein kinase B (PKB), a protein found downstream of PI3K signalling, which was the signalling mediator of the IGF-I induced GSK-3β inactivity [139] (Figure 1.7). This was demonstrated via the relative activation half-times for PKB and MAPKAP kinase-1β, 1 and 5 minutes respectively, compared to the 2 minute half-time for GSK-3β inhibition, in addition to its sensitivity to wortmannin and not the MAPK signalling inhibitor PD 98059.

Further evidence of the role of PKB in the inactivation of GSK-3β was provided by the utilisation of a dominant negative PKB mutant which possesses a C-terminal CAAX motif which targets it to the plasma membrane [140]. This domain negative mutant was sufficient to reverse the insulin mediated inactivation of GSK-3β. This paper also demonstrated that the inhibition of GSK-3β activity was via a direct interaction between PKB and GSK-3β, as the two proteins were seen to co-immunoprecipitate from lysates of a variety of cell lines.

Following the work examining the inhibition of GSK-3β activity by IGF-I, the effect of IGF-I signalling on β-catenin and E-cadherin was examined in a variety of colorectal cancer cell lines [141]. This work demonstrated the highly variable expression of the IGF-IRβ subunit mRNA across the cell lines, but also demonstrated that the higher levels of expression were correlated with a lack of mutation to the APC, β-catenin and E-cadherin proteins. Working on the c10 cell line, which expresses wild-type APC, β-catenin and E-cadherin and a high level of IGF-IR, it was demonstrated that stimulation of these cells with IGF-I decreased the binding of β-catenin to E-cadherin. As the IGF-I altered the phosphorylation of E-cadherin bound proteins; the same effect of decreased β-catenin was mimicked with the use of the tyrosine phosphatase inhibitor pervanadate. This dissociation from E-cadherin led to the relocation of β-catenin from the plasma membrane to the cytoplasm of the cells following IGF-I stimulation. Together with the inhibitory effect of IGF-I on GSK-3β activity, stimulation of cells with IGF-I doubled the half-life of β-catenin within these cells, although this was not sufficient to cause an increase in β-catenin mediated gene transcription and required incubation with the GSK-3β inhibitor lithium chloride to induce a transcriptional response.

While IGF-I stimulation alone was not sufficient to induce β-catenin mediated gene transcription in the c10 cell line with wild-type β-catenin, it is sufficient to induce β-catenin mediated gene transcription in the HepG2 hepatoma cell line which expresses the wild-type isoform of β-catenin in addition to a truncated version which lacks the GSK-3β regulatory subunits [142]. This activation of gene transcription relied on PI3K/PKB signalling, as expression of the dominant negative versions of PI3K and PKB resulted in a ~90% reduction in the IGF-I induced gene transcription, while the expression of constitutively active versions of these proteins both resulted in an increase of transcriptional activity of β-catenin target genes in unstimulated cells. The alteration to β-catenin

mediated gene transcription in the HepG2 cell line was also reliant on the inactivation of GSK-3β, as previously seen in the c10 cells, as the expression of the uninhibitable A9GSK-3β mutant protein removed the IGF-I induced gene transcription. However, expression of the inactive R85GSK-3β mutant displayed an additive effect with IGF-I on the induction of β-catenin mediated gene transcription, which implies the role of a second downstream pathway of IGF-I signalling in the alteration of gene expression. This additional signalling was identified as the Ras/MEK/ERK pathway downstream of Ras activation, as expression of R85GSK-3β along with either activated Ha-Ras or constitutively active MEK1 induced a greater level of β-catenin mediated gene transcription than R85GSK-3β alone.

Together these papers demonstrate that signalling via components of the Wnt signalling pathway is one means of signal transduction from IGF-I stimulation of cells and from this it is hypothesised that the induction of IGF-I signalling would provide cellular responses in line with those seen when there is a high level of Wnt signalling. In the context of the experimental work here, it is hypothesised that IGF-I signalling would induce a migratory response in cells within a migration assay, while inhibition of IGF-I signalling would decrease the amount of cell migration.

1.5.3 Role of IGF-I in cancer

With its interaction with a range of downstream signalling mediators, IGF-I signalling has been implicated as a pathway with an involvement in cancer development and prognosis. The initial work on the role of the IGF-I pathway in the transformation of cells to an immortalised phenotype was carried out on mouse embryonic fibroblasts by Sell *et al* [143], where the group established a fibroblast cell line, R^- cells, from *Igf1r*$^{-/-}$ mice. These cells were found to have half the growth rate of the wild type (W) cells during adherent culture in standard DMEM supplemented with 10% FCS, while being unable to increase in number when the media supplement was a combination of platelet-derived growth factor (PDGF), epidermal growth factor (EGF) and IGF-I. Upon transfection with a plasmid for the temperature sensitive simian virus 40 large tumor antigen (SV40 TAg tsA58), a known transforming agent of mouse cells, W cells show a 2.7-fold increase in cell growth under hygromycin selection, whereas the R^- cells only display a 30% increase over the same culture period.

In addition to the negative impact on standard *in vitro* culturing, the homozygous null mutation in IGF-IR also retards the ability of the fibroblasts to form colonies on soft agar following transfection with SV40 TAg [143]. Only one example of colony formation in an experiment utilising the SV40 TAg tsA58 transfected R^- cells observed, while transfection with the wild-type SV40 TAg resulted in no colonies. In comparison, SV40 TAg transfected W cells were capable of forming colonies at all seeding densities tested, regardless of if the SV40 TAg plasmid contained the wild-type or temperature sensitive variant. Transfection of the R^- cells with human IGF-IR cDNA resulted in a partial rescue of the wild-type phenotype, with these cells capable of colony formation after SV40 TAg transfection, although with lower efficacy than demonstrated by W cells.

Further work by the same group demonstrated that an underlying reason for the alteration in cell proliferative behaviour between the W and R^- cells was an extension of the length of the cell cycle, with R^- cells spending longer in all stages of the cycle resulting in a 2.5-fold increase in total duration when compared to W cells [144]. Additionally, while the distribution of cells found in each

stage of the cell cycle was comparable between the W and R^- cells in the early stages of culture, R^- cells were less susceptible to re-entry into S phase following quiescence than their W cell counterparts, with only the inclusion of 10% FBS in the growth media capable of inducing DNA replication.

As this work demonstrated a clear alteration to cellular behaviour in cells lacking functional IGF-IR, the R^- cells were transfected with an activated variant of Ras, as it is a known downstream mediator of many tyrosine kinase growth factor receptors, such as IGF-IR, to investigate if this could rescue the observed phenotype. This transfection had no effect on the ability of R^- cells to form colonies in soft agar, even in conjunction with SV40 TAg transfection, thus suggesting that the presence of a functional IGF-IR occupies a critical role in the transformation of cells and has since been an object of investigation in the arena of cancer research.

Circulating IGF-I levels have been found to impact the establishment of colorectal cancer tumours in mouse models and liver-specific IGF-I deficient (LID) mice have been used to achieve this as they have lower levels of serum IGF-I than control mice [145, 146]. Intraperitoneal injection of the potent colorectal cancer inducer azoxymethane for a period of 2-4 weeks can be used to induce aberrant crypt foci and, subsequently, tumours, with the mice killed at 4 and 26-27 weeks for the examination of each respectively [145]. The occurrence of aberrant crypt foci was found to be significantly reduced in female LID mice, but not males, compared to the control mice, while the incidence of tumours was found to be reduced in LID mice regardless of the gender. At least 85% of the tumours produced had progressed from adenoma to adenocarcinoma in both female and male, control and LID mice although the tumours from control mice were consistently larger than those from LID mice.

Another study induced tumours by suturing Colon 38 mouse adenocarcinoma tissue to the cecum of control and LID mice before harvesting 6 weeks later [146]. Again, it was observed that more control mice produced tumours, 57% of control mice compared to 31% LID mice, which were larger than those produced in the LID mice and they had a shorter latency period before the growth was visible. In addition, the control tumours had a higher abundance of blood vessels, which were observed from counts made on histologically prepared samples. Intraperitoneal injection of IGF-I into the LID mice raised the serum levels of IGF-I to a level which is comparable to the control mice injected with saline. IGF-I injection increased the percentage of mice displaying tumour growth by 20% in the control mice and by 32% in the LID mice and it also increased the size of these tumours in both groups. The effects seen were thought to be due to the differing levels of serum IGF-I between the subject groups, as the level of IGF-IR expression within the tumour tissue obtained from all four groups was consistent.

With the growing body of evidence for the involvement of IGF-I signalling in colorectal cancer behaviour, there have been multiple studies investigating if plasma levels of IGF-I could be used as an indicator of risk for the development of colorectal cancer in patients. The results from these studies are variable, with some, a study looking at Cretan men and women and another at US men, demonstrating an increased risk for colorectal cancer with elevated plasma IGF-I levels [147, 148], while others, one looking at Chinese men and another at European men and women, demonstrate no association between plasma IGF-I levels and risk [149, 150]. Similarly, there has been study looking at Swedish men and women demonstrating that elevated plasma IGF-I has a role in colon

cancer development, but not rectal cancer [151]. Meta-analysis across multiple studies shows a small association between elevated plasma IGF-I levels and increased risk of colorectal cancers [150, 152], this meta-analysis is a benefit of pooling the data from multiple cohorts, as IGF-I levels are known to vary in healthy adults. Additionally, a study into colorectal cancer mortality rates in American men found that elevated plasma IGF-I levels are associated with a higher mortality rate from colorectal cancer, for age adjusted data as age is also a mortality risk [153].

1.6 3D culture models are more relevant to the in vivo biological situation

For many years there has been ongoing work on the development of 3D models in order to capture aspects of the *in vivo* environment, such as the diffusion of molecules through tissues or the effect of interstitial fluid flow on the concentration of secreted proteins [154]. The advantages of 3D culture methods were identified early in the development of techniques, when tissue explants and spheroids were the main methods in use [155], and many reviews have been produced outlining the progress of this field, particularly in the arena of 3D cancer models [156-164].

1.6.1 Standard 2D culture imparts changes to gene expression in cells

The emergence and increase of research into the development and characterisation of 3D models for cell culture has been carried out in line with increasing evidence supporting the problems with standard cell culture in 2D. Alterations to gene expression have been noted in a wide variety of cellular functions, such as proliferation and metabolism, with cell lines demonstrating an altered gene expression profile when compared back to the tissue of origin [165].

A study into the 3D morphology of breast cancer cell lines demonstrated that there was a significant alteration to the expression of proteins associated with signal transduction when 2D and 3D cultures were compared, in addition to differences between cultures with differing 3D morphologies [166]. In addition to this change in gene expression, when cultured in 3D, the cell line adopted one of four distinct morphologies, round, stellate, mass and grape-like, which did not correlate with the morphology of the cells under standard 2D culture on tissue culture plastic. The culture of hepatocellular carcinoma cells in a 3D gel also induced alterations to gene expression, including the upregulation of a range of MMPs and the focal adhesion proteins paxillin and focal adhesion kinase (FAK) [167]. With the protein composition of cell adhesion sites also altered between 2D and 3D culture [168], the body of evidence demonstrating a difference in protein expression and localisation between 2D and 3D is showing an increased need for 3D culture systems.

With the demonstration that the 3D culture of breast cancer cell lines can alter their response to chemotherapy and promote drug resistance [169], the use of 3D cultures to aid drug development in the pharmaceutical industry has been proposed as another application of 3D technology in addition to more investigative biological research [170]. However, as the authors of this paper note, there needs to be a standardisation of 3D culture methods which meet various criteria of the industry, such as the scalability of the models and the option for high-throughput screening, before the wide spread use of 3D technology as a tool in this industry.

1.6.2 3D models are becoming more biologically relevant

The induction of *in vivo* like characteristics can be achieved through a variety of methods which are now available to biological researchers, from the use of perfusion on cell monolayers to mimic interstitial fluid flow [171] to the use of 3D culturing techniques. As technology in other fields, such as engineering, has progressed, the methods of 3D culture have become more complex in the aim to model the microenvironment found in tissues [172].

1.6.2.1 Explant cultures

One of the earliest forms of 3D culture employed was the maintaining of tumour explants *in vitro*. Tumour samples were cut down to explants 1-2mm^3 in size before placing onto culture plates (Figure 1.8A), allowing them to remain viable for long time periods [173] whilst maintaining characteristics of the original tumour tissue such as structural characteristics and carcinoembryonic antigen production as seen in colorectal cancers [174]. The primary culture of these explants is also able to predict the chemosensitivity of tumours, as the response of explant tissue to the antimitotic drug SN-38 was comparable to the *in vivo* response observed in patients [175].

As explant cultures are a method of primary culture, these cultures retain many of the characteristics of the original tumours and have an application in determining the best course of treatment to take for individual patients. However, the tumour samples from which these explants are derived need to be prepared immediately after excision to retain the viability of the sample, which limits their usage as a laboratory model to those research laboratories with ties to surgical departments and with the appropriate licenses to work on primary human tissues. As the excised tumours contain a proportion of fibroblast cells, which will outgrow the other cell types in the explant, the explants need to be plated in an environment which limits this fibroblast outgrow, such as on poly-2-hydroxyethylmetacrylate (PolyHEMA) coated plates [175]. Additionally, these primary cultures are prone to infection [174] and require extensive treatment with antibiotics and antifungals in order to maintain uninfected cultures.

1.6.2.2 Spheroids

Spheroids are another form of 3D cancer cultures which have been around for many years. These multicellular aggregates (Figure 1.8B) do not contain many of the structural features prevalent in tumour samples, however, they do provide a model for the heterogenic distribution of oxygen, nutrients and waste products across a tumour [176]. With a declining supply of oxygen in the centre of these *in vitro* spheroids, the proliferating cells are found in the outer layers of the structure, surrounding a necrotic core, which is analogous to the regions of cell necrosis seen in regions between capillaries in tumours [177]. This system also permits co-culture, with studies into the infiltration of monocytes into spheroids [178] and the interaction between spheroids and collagen embedded fibroblasts [179] documented.

This simple model of cancer has applications for use on many cell lines where the formation of aggregates is possible and does permit co-culture with additional cell types to increase the complexity of the model. However, from the evidence presented in the literature, the size of the generated spheroids has the potential to vary which could give rise to variable results when subjected to cellular assays and must be controlled for.

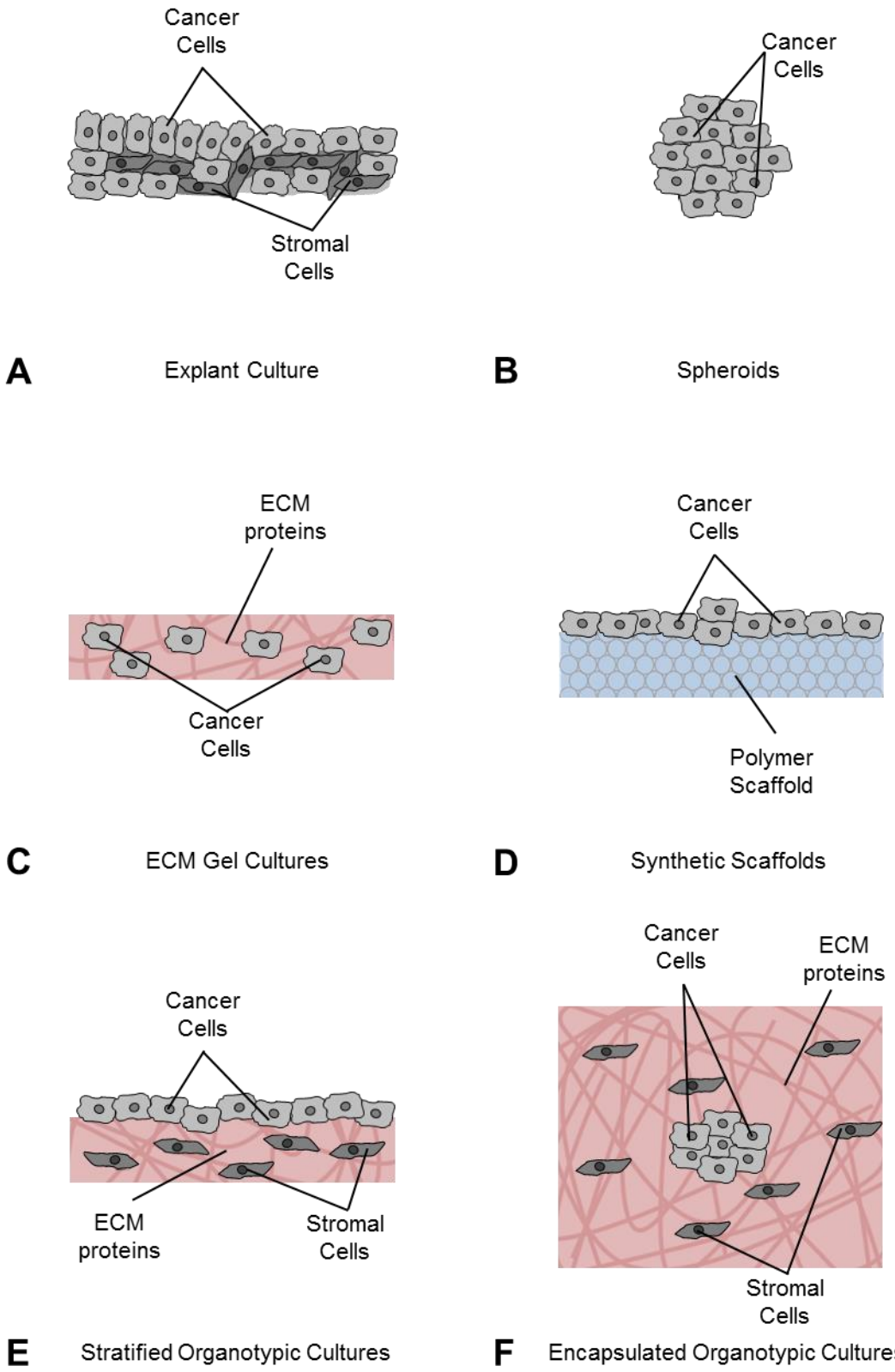

Figure 1.8: 3D models of cancer can model different aspects of the tumour microenvironment. A: explant cultures retain structural features of the original tumours, B: spheroid cultures model cell-cell interactions and the hypoxic interior of tumours, C: ECM gel cultures provide a 3D protein environment for cancer cells, D: scaffold cultures provide a 3D environment in the absence of biologically signalling, E: stratified organotypic cultures combine a 3D microenvironment with biological signalling from ECM proteins and secondary cell types and F: encapsulated organotypic cultures combine the aspects of the stratified organotypic cultures with the hypoxic gradients seen in spheroid cultures.

1.6.2.3 ECM gel cultures

The seeding of cancer cells in an ECM gel recreates some of the spatial and protein cues of the tumour microenvironment (Figure 1.8C). The protein composition of these gels can be varying to study the effect of different ECM components, from how mutations in colorectal or breast cancer cells disrupts the formation of crypts [180] or acini [181] in response to basement membrane proteins as provided by Matrigel, a commercially available soluble extract of Engelbreth-Holm-Swarm (EHS) mouse sarcoma tumours which gels at 37^{o}C [182]. The presentation of these ECM gels can be as large scale gels in well plates, or encapsulated in synthetic hydrogels to provide an array for high throughput screening [183]. In addition to gels made from extracted ECM proteins, decellularised gels derived from the culture of secondary cell lines, such as fibroblasts, can be employed [184]. A variation of collagen gel cultures is the collagen gel droplet embedded culture drug sensitivity test (CD-DST), where cells from tumour samples are suspended in collagen and plated as 30µl droplets into well plates [185]. This CD-DST method has been used to assess the chemosensitivity of human colorectal carcinomas in response to a range of chemotherapy drugs, in addition to assessing the effect of the expression of multidrug resistant proteins has on chemosensitivity [186].

When compared to thin gel coating on tissue culture plastic, these 3D gels have been shown to affect the proliferative response and response to chemotherapeutic drugs [184], demonstrating that the 3D environment they recreate is affecting cell behaviour. While they also provide a protein substrate, in gels which are composed of a single protein, the microenvironment provided is not as complex as the *in vivo* situation, whereas those made from multiple proteins, such as Matrigel [182], may lack the organisation of the different protein types seen *in vivo*, leading to conflicting microenvironment cues. These models also lack the interaction between the cancer cells and alternative cell types, limiting the intercellular signalling, which can direct cell behaviour.

1.6.2.4 Synthetic scaffolds

Another method of introducing a 3D environment to *in vitro* cultured cells is by the use of synthetic scaffolds (Figure 1.8D). These polymer based scaffolds can be made from a wide range of materials to highly specialised specifications to produce materials with differing culturing characteristics [172]. These materials can be biologically active or inert and can be used with [187] or without [188] an ECM coating to promote cellular adhesion.

When biologically inert scaffolds are employed, they provide the opportunity to observe the effects of dimensionality of the culturing environment in the absence of signalling cues which may arise in an ECM gel based system. These systems also allow for ECM coatings and co-culture, so they can be used to build a step-wise model of cancer to investigate the effect of different components of the microenvironment on the behaviour of the cancer cells. If these scaffold systems are commercially manufactured and distributed, then the quality control processes would provide a consistent product, eliminating variability between experiments and allowing the accumulation of a wide data set. However, due to the wide variety of materials and structures available [172], the process of optimising the growth of cancer cells on materials would need to occur to ensure consistent, viable cultures and the optimal methods for one material may not transfer across to others.

1.6.2.5 Organotypic cultures

The combination of cancer cells, ECM gels and secondary cell types combine to form organotypic models. These generally take the form of a collagen gel embedded with fibroblasts which have been allowed to establish a stromal equivalent before the addition of the cancer cell line on top (Figure 1.8E). Studies using this method have been carried out with colorectal cancer [189, 190] and squamous cell carcinoma (SCC) [191] cell lines, with the expression of proteins in the organotypic SCC cultures comparable to those seen in primary SCC tumour samples. There have also been examples of excised leiomyoma, a benign smooth muscle neoplasm, being used as the stromal equivalent for cancer cells, with this inducing a greater amount of cancer cell penetration than a collagen and fibroblast based organotypic culture [192]. A variation of these organotypic cultures sees an artificial cancer mass (ACM), consisting of cancer cell embedded in a collagen hydrogel and compressed to increase the collagen stiffness, encapsulated in a second collagen gel containing fibroblasts and/or endothelial cells (Figure 1.8F) [193].

These organotypic models allow for interactions between the cancer cells and both ECM component proteins and secondary cell types. These allow for the generation of a variety of collagen based stromal equivalents by altering the source of fibroblasts or culturing them in conjunction with other cell types, such as endothelial cells [193]. The pre-culture of these stromal equivalents also allows the secondary cell type to remodel these gels, which usually results in gel shrinkage [190], to produce a microenvironment which is closer to that seen *in vivo*. The encapsulation culture combines the hypoxia gradient seen in spheroid cultures with a more biologically relevant microenvironment to provide multiple signals to the cancer cells to drive their behaviour. However, due to the variable nature of ECM gels which are made in batches or between patient samples which are decellularised to provide the ECM environment, this technique may not provide a consistent 3D environment for large scale investigations into cellular behaviour.

1.7 2D and 3D in vitro migration and invasion models assess a range of cell behaviours

With the range of cancer models now available, there are a wide range of *in vitro* migration and invasion assays which can be employed to study cell behaviour and these have been extensively reviewed in the literature [194, 195]. These techniques can be used in conjunction with *in vivo* techniques to study migration and metastasis formation, such as the chick embryo chorioallantoic membrane (CAM) model [196] or xenografts [197], which provide a complete biological microenvironment to direct the behaviour of the cancer cells.

Each of the techniques discussed require varied techniques and have applications which can be more suited to the different modes of migration as described previously. While the increasingly complex models provide a more biologically relevant assay environment, the amount of analysis and the complexity of techniques required to obtain results is greatly increased over an assay which acts on monolayer cultures and there is a trade-off between biological relevance and ease of extracting results from the assays.

1.7.1 2D models of migration and invasion

Common 2D models of migration in use in research are based on cells migrating across a flat substrate, usually tissue culture plastic, and can be easily assayed by imaging the live cultures and performing image analysis to obtain the necessary results.

1.7.1.1 Outgrowth of explants

One of the basic forms of assaying cell migration is to view the migration of cells out of a tissue explant (Figure 1.9A) [198]. In this system it is possible to view both single migrating cells and cells migrating in a collective manner. However, due to the multicellular nature of explants, there is the potential for ambiguity regarding the identification of the migrating cells, which could be cleared up by the fixing and staining of cell outgrowth at the end of the assay. While the identification of the migrating cells would prove straightforward using light microscopy, the preparation and maintenance of these cultures would encounter similar problems to the explant cultures, as previously mentioned above.

1.7.1.1 Scratch wound assays

A commonly used migration assay is the scratch wound assay (Figure 1.9B), which is inexpensive and does not require specialist equipment to execute. The assay relies on the growth of a confluent 2D monolayer of cells which is then wounded using a pipette tip to scrape cells off the plastic. Images are taken immediately after wounding and at selected time periods afterwards and can be assessed for single cell migration, via the counting of cells which cross into the wound area or using cell tracking software, or collective migration, by assessing the closing distance between wound edges [199, 200]. While this assay is accessible and can be generated using standard laboratory equipment, there is the potential to damage cells when wounding the monolayer culture, resulting in unwanted cell signalling occurring during the course of the assay. Additionally, the cells are assayed for their migratory behaviour in a highly unnatural environment, with few biological cues which would be found in the *in vivo* situation.

1.7.1.2 Ring assays

Another assay which is similar to the scratch wound assay is the ring, or fence, assay (Figure 1.9C), where the cells are assayed for their migration across a 2D substrate, however the risk of cellular damage is removed. The set-up for this assay requires a confluent layer of cells to form within a circular ring, which is then removed to allow the cells to migrate out radially [201]. Again, this assay is easily analysed via image analysis on the resulting cultures to measure the increased area occupied by the migrating cells, although the cells are maintained in an unnatural microenvironment.

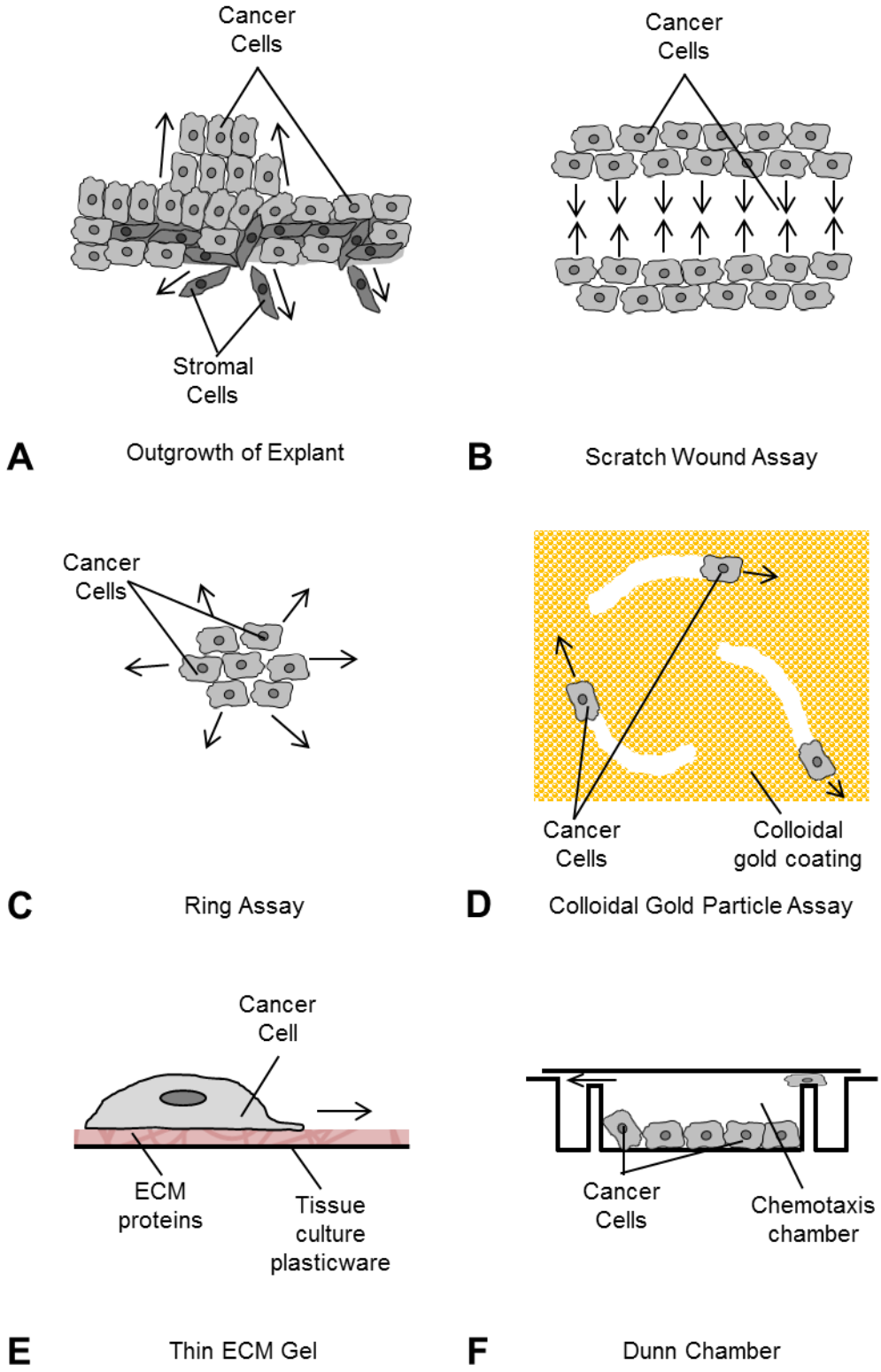

Figure 1.9: 2D migration models provide an easy method of obtaining data on cell migration. Different 2D migration assays include A: the migration cells out of explants across a coated 2D surface; B: scratch wound assays, where a monolayer culture is 'wounded' using a pipette tip and cells migrate to close the wound; C: ring assays, where cells are grown in a monolayer inside a ring which is removed and the cells migrate out radially; D: colloidal gold particle assays, where cells are seeded onto a 2D surface covered colloidal gold, which the cells remove as they travel over it; E: thin ECM gel assays, where single cells migrate across an ECM gel coating and digestion of this coating can be viewed via microscopy, and F: Dunn chamber for chemotaxis, where cells are seeded in the central chamber and migrate over the bridge towards a chemotatic agent in the outer ring.

1.7.1.3 Colloidal gold particle assays

A 2D migration assay which detects the migration of single cells is the colloidal gold particle assay, where a 2D substrate is thinly coated with colloidal gold particles which are removed by phagocytosis as the cells migrate across them (Figure 1.9D). The tracks produced by the migrating cells are clearly visible via microscopy, with cultures where the cells have migrated large distance displaying large areas of cleared particles, where the paths of cells have overlapped and the individual tracks are no longer visible [202]. This assay requires the use of more complex techniques to assay the cellular migration, but does allow for the monitoring of the routes taken by individual cells without the need for complex computerised tracking systems.

1.7.1.4 Thin ECM gels

The coating of a 2D surface with protein gels can increase the biological relevance of migration assays by providing an adhesion substrate which is closer to that seen *in vivo* (Figure 1.9E). The provision of the ECM proteins directs the migrating cells to degrade the coating at the point of cell extension, which is a behaviour that is seen in collective and mesenchymal migration. When a coating which incorporates a fluorescent tag is used, the points of ECM degradation can be viewed via fluorescence microscopy and distinctions between the types of actin protrusions employed during migration can be made [203]. Assays of this type begin to introduce more complexity into the study of cellular migration, however, the spatial aspect this assay does not match up with *in vivo* tumours as the signalling from ECM proteins is confined to one side of the cell.

1.7.1.5 Dunn chambers

A method of analysing 2D cell migration in the presence of a chemotactic gradient is the use of a Dunn chamber [204]. This assay uses a modified microscope slide with a central chamber and surrounding ring depressed into the slide surface with a raised bridge between them. The cells are seeded into the central chamber and the outer chamber is filled with media before the coverslip is placed over the chambers and secured such that a small gap over the edge of the outer chamber is left. Through this gap, the media in the outer well is drained and media containing the chemotactic agent under study is inserted, before sealing the gap over the outer chamber (Figure 1.9F). The migration of cells due to chemotaxis can then be observed via microscopic viewing of the bridge between chambers. While this method for assaying the migration of single cells adds an element of biological relevance by introducing molecules which may direct the migration of these cells, the cells remain in a 2D environment without the environmental cues from ECM proteins or other cell types. Additionally, the specialised equipment and nature of the set-up required for this assay mean it is unsuitable for high throughput studies.

1.7.2 3D models of migration and invasion

While 2D migration assays are relativity easy to execute, with little in the way of specialised equipment or techniques, they lack the ability to model the correct microenvironment for the cancer cells. With the introduction of another spatial dimension in 3D migration assays, the opportunity to model interactions between the cancer cells and surrounding ECM proteins or secondary cell types

is increased. However, this increasing complexity results in the need for more specialist techniques and equipment, with more processing required to obtain results.

1.7.2.1 Boyden chambers and Transwell® inserts

A highly adaptable 3D migration assay comes in the form of Boyden chambers [205] and Transwell® inserts, which are based on Boyden chambers [206]. The cell culture well is divided into two separate chambers by a highly porous filter with defined pore sizes, where the cells are seeded on top of the filter and allowed to pass through the pore to the underside of the filter (Figure 1.10A). This assay can be adapted to incorporate an element of cell invasion by coating the top side of the filter with an ECM gel prior to cell seeding. This assay is also highly adaptable, as chemotactic agents can be added to the bottom chamber to assess the cellular migratory response to these compounds, or a secondary cell type can be maintained on the bottom of the well plate to investigate the paracrine signalling between the two groups of cells. The adaption of the Boyden chamber technique to a disposable well insert allows the technology to be available to a wider research group and the analysis method of counting the number of cells which have migrated through the filter rapidly provides results.

1.7.2.2 Spheroid Confrontation Assays

The spheroid method of 3D culture can also be adapted to form a migration assay as a spheroid confrontation assay [207]. In this assay, two spheroids of differing cell types are placed in close proximity and allowed to migrate into each other to form a single large spheroid (Figure 1.10B). This assay can also be adapted to assay the invasion of cells from a single cell suspension into the spheroid body, which has applications to model the interactions between tumour cell and the immune system. This assay is does not require a large amount of specialist equipment, with the results viewable following the histological processing and staining of the samples. However, while this assay models cell-cell interactions, it does not model the interaction between cells and an extensive ECM network and the role that can play on the migratory behaviour of cells. Additionally, quantification of results can be difficult, as there is no distance of migration to measure or clearly defined area to count cells from where they have clearly undergone a migration from their starting position.

1.7.2.3 ECM gels

With the range of ECM proteins that can be purchased from biochemical suppliers, the use of ECM gels to generate invasion assays is widespread [208]. Assays of this type can take many forms, from cells seeded on the surface of an ECM gel and allowed to invade down into the gel (Figure 1.10C) [209, 210], to single cells encapsulated in ECM gels and their movement tracked using microscopy and cell tracking software (Figure 1.10D) [211, 212]. The encapsulation method has been adapted for use with robotics to produce a high-throughput assay, with a plate of 192 microchannels which are open at both ends [213]. The channel is filled with an ECM gel from one end and cells are added to the other and allowed to migrate along the channel, which can be monitored using microscopy. This style of assay provides the opportunity of signalling from ECM proteins, although it does lack the cell-cell interaction seen with other assays.

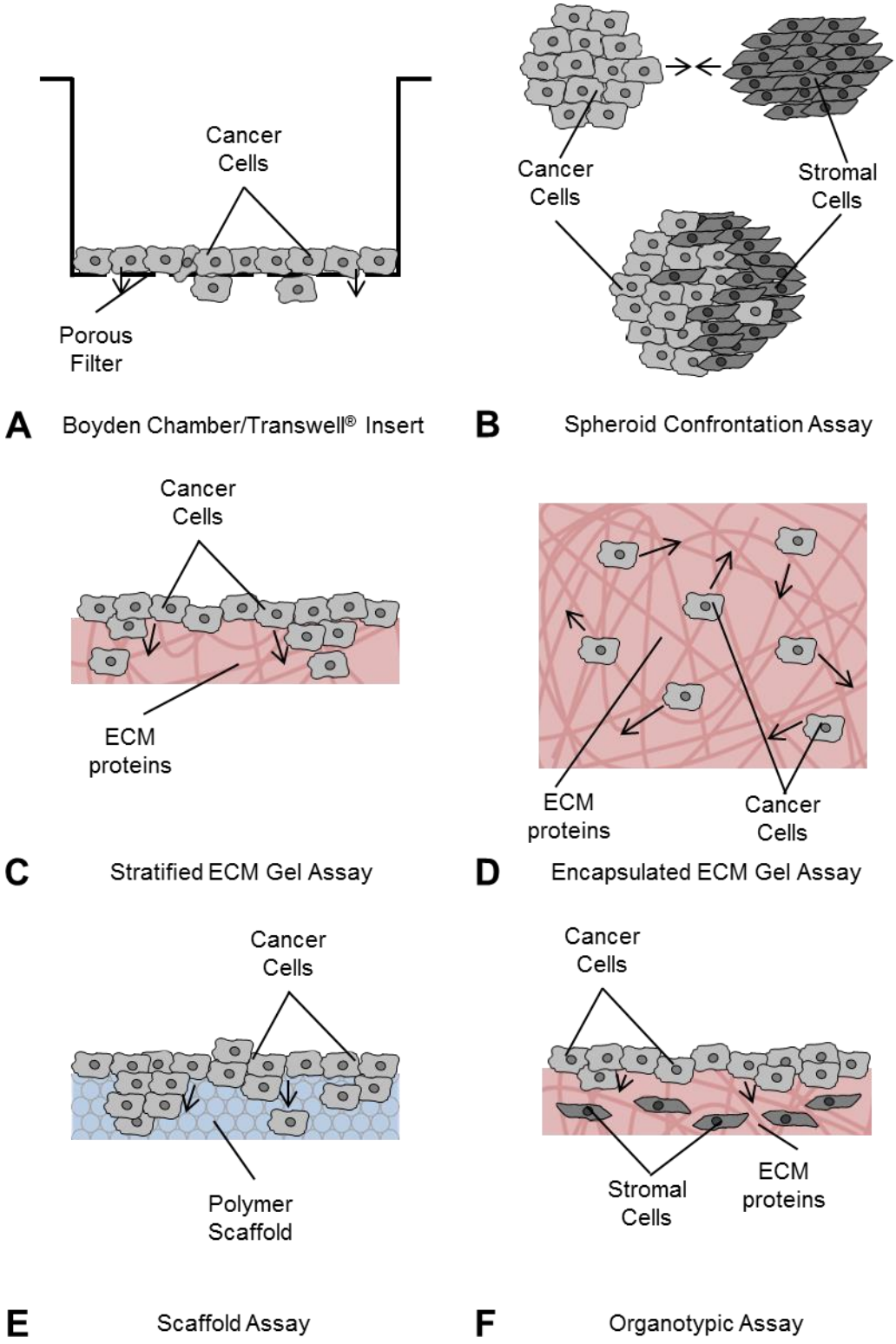

Figure 1.10: 3D migration models provide a microenvironment which is more biologically relevant. Different 3D migration assays include A: Boyden chambers/Transwell® inserts, where cells are seeded on top of a thin porous membrane (in the absence or presence of an ECM gel) and allowed to migrate to the other side of the membrane; B: spheroid confrontation assays, where two spheroids are placed in close proximity and form a single spheroid by invading each other; C: stratified ECM gel invasion assays, where the distance invaded vertically into ECM gels is measured; D: encapsulated ECM gel invasion assays, where the invasion of single cells through the ECM gel is tracked; E: scaffold assays, where the distance invaded vertically into the scaffold is measured, and F: organotypic assays, where the invasion of cancer cells into a stromal equivalent is measured.

While the larger gels can require specialist microscopy equipment or processing skills to obtain results, the technology required to set them up is accessible by many research groups. The adaption of this style of assay to a high-throughput method lends itself towards the style of assay that would be appealing to drug discovery and development.

1.7.2.4 Scaffolds

Despite the large number of scaffold technologies available, either as commercially available products or manufactured by individual research groups, there are few examples of the use of them in the application of migration assays. The methodology is similar to that used for Boyden chambers, with cells seeded on top of a synthetic material and allowed to penetration through it (Figure 1.10E) [214, 215]. However, unlike the Boyden chamber, the migrating cells are kept in a 3D environment for a greater period while migrating due to the greater depth of the scaffolds. While the basic form of this type of assay involves cells in a synthetic 3D environment, this technology has the potential to be adapted in similar ways to the Boyden chamber assays with the addition of ECM coatings or secondary cell types to increase the biological relevance of the model. Additionally, the amount of processing required to obtain results from this type of assay is likely to be similar to that required for ECM gel and organotypic assay, with histological processing required to quantify the level of cell penetration into the material.

1.7.2.5 Organotypic models

An invasion assay which recreates many aspects of the 3D microenvironment is the use of organotypic models (Figure 1.10F) [76, 216]. This style of assay contains the correct dimensionality of the *in vivo* situation, while incorporating signalling cues from ECM proteins and secondary cell types. However, while these systems are still reasonably simple to set up, provided the methodologies for the growth of a stromal equivalent are established, the analysis of this type of assay is more complex due to the multicellular nature of the culture. Here, tagging of different cell lines or staining for appropriate markers must be used to highlight the different cell populations and allow for an accurate assessment of the invasive behaviour of the cancer cells.

Together these demonstrate that there are many different options available for investigating the migratory and invasive behaviour of cancer cells. However, some of them do not model the microenvironment of tumours, which can lead to results which are not comparable to the *in vivo* situation, while others require specialist equipment or techniques which can prevent them from being readily available to researchers. Unfortunately, there appears to be a trend that the more biologically relevant a model is, the harder it is to extract results from the system, which hinders the development of highly biologically relevant systems into high-throughput systems for use in drug discovery.

1.8 Hypothesised Outcomes

From the literature reviewed here, the following experimental outcomes are hypothesised:

- A novel 3D model of colorectal cancer migration can be generated using a synthetic scaffold to provide the culturing environment;

- The migratory behaviour of colorectal cancer cells within the 3D model will differ from their 2D migratory behaviour due to the difference in the dimensionality of the culturing environment;
- Inhibition of the Wnt signalling pathway will result in inhibition of the migratory or proliferative behaviours of colorectal cancer cells;
- Modulation of IGF-I signalling will result in alterations to the migratory or proliferative behaviours of colorectal cancer cells;
- Adaption of the 3D model to include ECM proteins or a secondary cell line will also result in alterations to the migratory or proliferative behaviours of colorectal cancer cells.

1.9 Thesis Overview

This project aims to assess the feasibility of using a commercially available scaffold technology for the development of a 3D *in vitro* migration assay for colorectal cancer cells. This model will then be tested by investigating the role of signalling on the migratory behaviour colorectal cancer cells. The flexibility of the model will also be examined, with an aim of increasing the biological relevance of the model by the introduction of ECM protein coatings and co-culture into the assay. Throughout the process of development and testing, the aim is to use commercially available products to ensure that the methods employed during this project are available to a wide range of researchers and can be replicated and adapted by other research groups.

Chapter 3 will look at establishing and optimising the 3D culture of colorectal cancer cell lines on the 3D material by looking at varying cell seeding density and techniques. Once this has been established, the maintenance of viable 3D cell cultures on this material over longer time courses will be assessed to allow for the selection of an appropriate time frame for the migration assay. Finally, the amount of cell penetration into the different forms of the material will be assessed to allow for the selection of the appropriate material for the assay, before a clear protocol for this migration assay is defined, which will be followed throughout the rest of this thesis.

In Chapter 4 the effect of Wnt signalling on the migratory behaviour of colorectal cancer cells will be examined using small molecule inhibitions of this pathway. Side-by-side comparisons between 2D and 3D assays will be made to assess the efficacy of these compounds and to identify where the dimensionality of the assay is affecting the outcome.

Chapter 5 will follow a similar line of investigation to Chapter 4, but instead will focus on the IGF-I signalling pathway. Here recombinant IGF-I and a small molecule inhibitor of the pathway will be used in 2D and 3D assays to investigate the role this pathway has on cell migration. Interactions between the Wnt and IGF-I pathways will also be investigated here by the application of effective compounds identified in Chapter 4 to cultures in conjunction with IGF-I.

Finally, Chapter 6 will look at the feasibility of increasing the biological relevance of the assay. This would initially involve the addition of an ECM coating prior to cell seeding to recreate a protein environment for invasion. Secondly, the establishment of a stromal equivalent within the 3D material will be investigated, in addition to the ability to maintain a culture of colorectal cancer cells on top of this stromal equivalent to investigate the paracrine signalling between the different cell types.

2 Materials and Methods

2.1 Routine 2D Cell Culture

2.1.1 Cell Line: SW480

The human colorectal adenocarcinoma cell line SW480 (ATCC®, CCL-228™) was maintained in high glucose Dulbecco's Modified Eagle Medium (DMEM, Lonza) supplemented with 10% v/v heat-inactivated Foetal Bovine Serum (FBS, Sigma), 2 mM L-glutamine (Lonza) and 100 U/ml Penicillin/Streptomycin (Lonza) on Nunc plasticware (Fisher) at 37°C in a 5% CO_2 environment and enzymatically passaged, as outlined in 2.1.6, when cell growth reached 70%.

2.1.2 Cell Line: SW620

The human colorectal adenocarcinoma cell line SW620 (ATCC®, CCL-227™) was maintained in high glucose DMEM (Lonza) supplemented with 10% v/v heat-inactivated FBS (Sigma), 2 mM L-glutamine (Lonza) and 100 U/ml Penicillin/Streptomycin (Lonza) on Nunc plasticware (Fisher) at 37°C in a 5% CO_2 environment and enzymatically passaged, as outlined in 2.1.6, when cell growth reached 70%.

2.1.3 Cell Line: 3T3

The mouse embryonic fibroblast cell line NIH/3T3 (ATCC®, CRL-1658™) was maintained in high glucose DMEM (Lonza) supplemented with 10% v/v heat-inactivated FBS (Sigma), 2 mM L-glutamine (Lonza) and 100 U/ml Penicillin/Streptomycin (Lonza) on BD plasticware (Fisher) at 37°C in a 5% CO_2 environment and enzymatically passaged, as outlined in 2.1.6, when cell growth reached 70%.

2.1.4 Cell Line: 3T3/GFP

The mouse embryonic fibroblast cell line NIH3T3/GFP (Cell Bio Labs, AKR-214) was maintained in high glucose DMEM (Lonza) supplemented with 10% v/v heat-inactivated FBS (Sigma), 2 mM L-glutamine (Lonza), 100 U/ml Penicillin/Streptomycin (Lonza), 10µg/ml Blasticidin (Invitrogen) and 0.1mM MEM Non-essential Amino Acids (Sigma) on BD plasticware (Fisher) at 37°C in a 5% CO_2 environment and enzymatically passaged, as outlined in 2.1.6, when cell growth reached 70%.

2.1.5 Growth Curve of Cells Cultured on Conventional 2D Plastic

All cell lines were seeded into T25 flasks, manufacturer as appropriate to the cell line, at a density of 2.5 x 10^5 cells per flask and cultured for 7 days with media changes every other day. Timepoints were taken every other day by putting 3 flasks through the MTT Assay, as described in 2.9.1, and trypsinising the cells out of a further 3 flasks, as described in 2.1.6, for the determination of cell number, as described in 2.5.1.

2.1.6 Routine Passaging and Propagation of Cells

All cell lines were enzymatically passaged by removal of the growth media, washing of the cell monolayer with sterile Magnesium and Calcium free Phosphate Buffered Solution (PBS, Lonza) and incubation with Trypsin-Versene (Trypsin-EDTA) (Lonza) at 37^{o}C for 1 minute (NIH/3T3 and NIH3T3/GFP cell lines) or 5 minutes (SW480 and SW620 cell lines). Following neutralisation with complete culturing media, the cells were returned to fresh culture flasks as a single cell suspension.

2.1.7 Cryopreservation of Cells

All cell lines were cryopreserved at -140^{o}C in Nunc cryovials (Fisher) following suspension of cells in freezing media at a density of a T75 flask per 3ml. The freezing media for the SW480, SW620 and NIH/3T3 cell lines comprised 5% v/v Dimethyl Sulfoxide (DMSO, Sigma) in complete culturing media. The freezing media for the NIH3T3/GFP cell line comprised 20% v/v FBS (Sigma) and 10% v/v DMSO (Sigma) in DMEM (Lonza).

Cells were retrieved from cryopreservation by defrosting at 37^{o}C and diluting the freezing media with complete growth media. The resulting cell suspension was centrifuged at 200g for 3 minutes using an Eppendorf Centrifuge 5810 R, the supernatant removed and the remaining cell pellet resuspended in fresh complete growth media. The cells were transferred to cell culture plasticware and incubated to obtain a monolayer culture.

2.2 Scratch Wound Assays

2.2.1 Growth of 2D Cultures

For all experiments, the SW480 and SW620 cells used were taken from flasks within 10 passages of each other. The SW480 and SW620 cell lines were seeded into 48-well plates (SLS) and allowed to grow to 95% confluency over 5 days with media changes every other day.

2.2.2 Scratch Wound Assay Set-up

Scratch Wound Assays were initiated by introducing a scratch wound with a 10µl pipette tip (Sarstedt) into the cell monolayer. Cultures were then washed 3 times in sterile PBS and media containing media additives at appropriate concentrations added into the wells. The cultures were then returned to an incubator at 37^{o}C in a 5% CO_2 environment for 24 hours.

2.2.3 Scratch Wound Assay Analysis

Images of the wounds were taken at wounding and at 24 hours post wounding using a Leica DM13000 B light microscope with an attached Leica DFC310 FX camera at 10x magnification to obtain measurements for the movement of the leading edge, which were carried out using the Leica Application Suite software (Leica, Version 3.7). At 24 hours the cultures were fixed, as described in 2.10.1, stained for Phalloidin and DAPI, as described in 2.13.4, and imaged using a

Leica DM13000 B light microscope with an attached Leica DFC310 FX camera at 10x magnification to obtain data for single cell migration into the scratch wound.

2.3 3D Culture

2.3.1 Preparation of Scaffold Inserts

The commercially available windowed 6-well insert (Figure 2.1A) format of Alvetex® (Reinnervate, AVP004) required no preparation prior to material pre-treatment. The full-sided 6-well insert (Figure 2.1C) format of Alvetex® required the sterilisation of material and insert with 70% Ethanol prior to construction, with the 200µm thick section then clipped between the two halves of the insert.

For short-term culturing, the well inserts were placed into Greiner 6-well plates, with each well supplying 10ml of culture media to a single well insert. For long-term culturing, three well inserts were placed into a triplet well insert holder in a deep well Petri-dish (Reinnervate, AVP015); with each dish supplying 50ml of culture media to three inserts.

2.3.2 Media Changes

Media changes were made by aspirating off the culture media from the gap between the well insert and the edge of the well or petri-dish before replenishing the plate with fresh media into the same gap as to not disturb the cell growth on top of the material.

For short-term culturing (up to 7 days) in 6-well plates (Figure 2.2B), the culturing media was replaced every 2 days. For long-term culturing in (over 7 days) in deep well Petri-dishes (Figure 2.2F), the culturing media was replaced every 3-4 days. Additionally, the dishes were replaced to remove the build-up of cells growing on the bottom of the plastic at days 7 and 17 of culture, for the 21 day growth curve experiments, and at day 5 of culture, for the 10 day migration assay experiments. For migration assays, any media additives were initially introduced to the cultures at day 5 and replenished at the day 7 media change.

2.3.3 Construction of Co-cultures

The 3D fibroblast cultures were established for 7 days in a 6-well plate before transferring to a deep well Petri-dish. From there the colorectal cancer cell lines were seeded and cultured on top of the fibroblast growth as previously described in 2.3.2. Where co-cultures employed the NIH3T3/GFP cell line, the co-culture was maintained in the NIH3T3/GFP complete growth media.

2.4 Media Additives

2.4.1 Insulin-like Growth Factor-I

Human Insulin-like Growth Factor-I (IGF-I, Sigma, I3769) was reconstituted in Molecular Biology Water (Sigma) to a concentration of 1mg/ml and stored in aliquots at -20^{o}C.

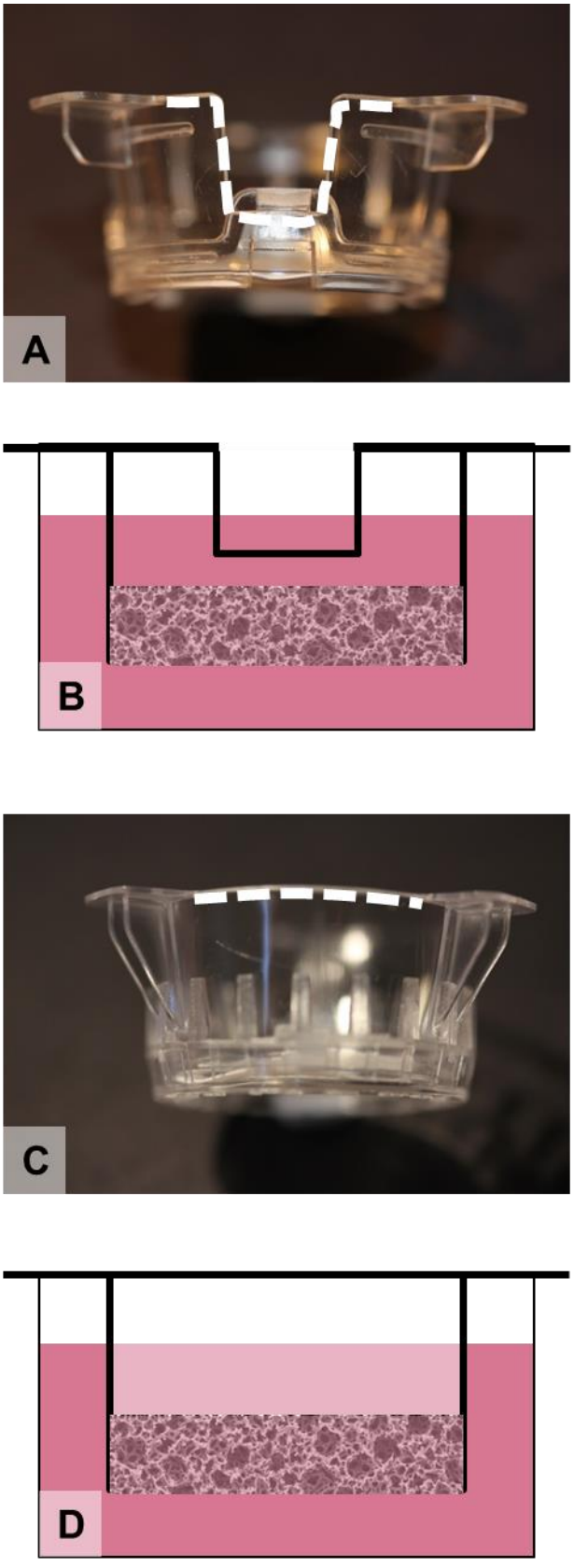

Figure 2.1: Schematics of the different types of well insert. A: The windowed inserts allow for the free exchange of culture media between the top and bottom surfaces of the material via three windows in the top half of the insert as highlighted in white. B: this keeps the media composition equal throughout the culture well. C: The full-sided inserts keep the culture media on top of the material separate from the media under the material by having a continuous top half, as highlighted in white. D: this results in an unequal media composition when the media on top of the insert is compared to the media surrounding the insert.

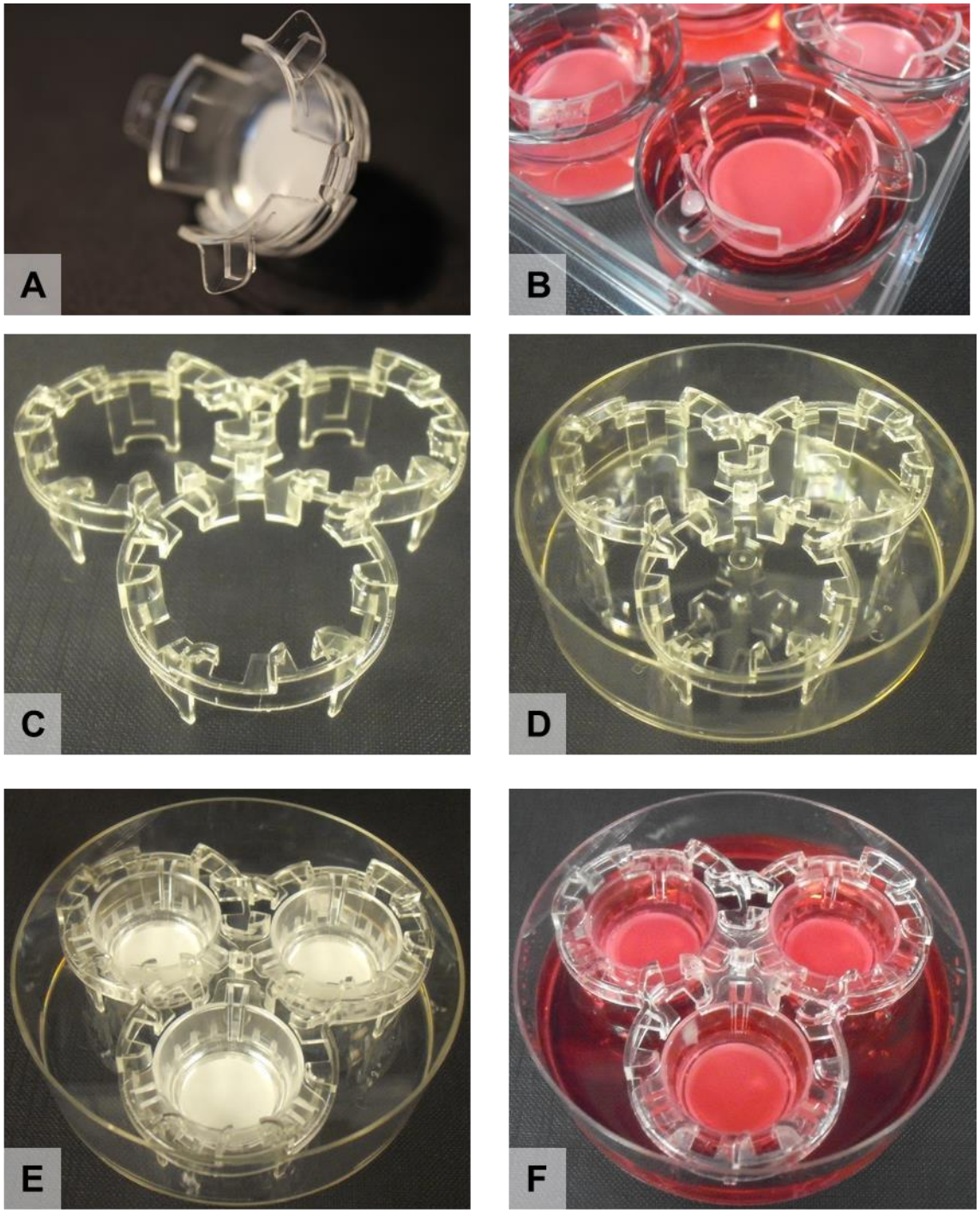

Figure 2.2: The culture plasticware used for 3D cell culture. For short-term culture, A: a 6-well insert is housed in B: the well of a 6-well plate, supplying 10ml of media per well. For long-term culture C: The cradle allows for three inserts to be cultured in the same dish and has three heights for positioning of inserts within the culture dish. D: The deep well petri dish that houses the cradle and allows for free media movement around the cradles. E: The height of the inserts can be selected to allow for different amounts of media on top of the scaffold. F: The inserts can be cultured in volumes of media up to 75ml which is shared between all three inserts.

2.4.2 Small Molecule Inhibitors

Small molecules were reconstituted in DMSO at the concentrations listed in Table 2.1 and sterile filtered prior to storage at -20^{o}C. All cultures maintained in media containing small molecule additives were compared to a DMSO control.

Small Molecule	Supplier	Catalogue Number	Working Stock Concentration
Cardamonin	Sigma	C8249	5mM
ICG 001	Tocris	4505	5mM
IWR-1	Sigma	I0161	10mM
NVP-AEW541	Cambridge Bioscience	CAY13641	1mM
XAV 939	Tocris	3748	10mM

Table 2.1: Small molecule additives with suppliers and concentration of stock solutions.

2.5 Cell Counting

2.5.1 Neubauer Improved Haemocytometer

For determination of cell number for calculating the 2D growth curves and seeding into 3D cultures, 2D cell cultures were trypsinised to a single cell suspension, as described in 2.1.6, and counted using a Neubauer Improved Haemocytometer. To ensure the accuracy and consistency of results, cell suspensions of the density 0.5-1.5 x 10^6 were used and suspensions outside of this range were resuspended to achieve the appropriate cell density.

2.5.2 Calculation of Generation Time

Determination of generation time for cell populations was carried out following the calculations laid out in Hayflick's work on culturing fibroblasts [217]. These equations contain the following variables: n, number of generations; N, final population size at time = t_2; X_0, initial population size at time = t_0; r, multiplication rate and g, generation time. These equations are:

$$n = 3.32(\log_{10} N - \log_{10} X_0),$$

$$r = n/(t_2 - t_0),$$

$$g = 1/r.$$

2.6 Seeding Method

2.6.1 Preparation of Cell Suspensions

For all experiments, the cancer and fibroblast cells used were taken from flasks within 10 passages of each other. 2D cell cultures were trypsinised and counted, as described in 2.5.1, before centrifugation 200g for 3 minutes using an Eppendorf Centrifuge 5810 R followed by resuspension of the cell pellet such that the resulting cell suspension had a cell density of 5 x 10^6 cells per ml, for

the NIH/3T3 and NIH3T3/GFP cell lines, or 10 x 10^6 cells per ml, for the SW480 and SW620 cell lines.

2.6.2 Seeding Cells by the Concentrated Method

To seed cells in the concentrated manner, 100µl of the seeding suspension was applied directly to the centre of each disc of prepared material (Figure 2.3A). Lids were then placed onto the culture dishes and they were placed into a cell culture incubator for 15 minutes to allow cell attachment before growth media was added (Figure 2.3B).

2.6.3 Seeding Cells by the Diffuse Method

To seed cells in the diffuse manner, the growth media was added to the culture dish prior to the application of 100µl of the seeding suspension to the media in the centre of the well insert and placement into a cell culture incubator (Figure 2.3C & D).

2.7 Scaffold Pretreatment

2.7.1 Ethanol Wetting

For the ethanol pre-treatment of Alvetex® discs, the discs housed within their well inserts were submerged in 70% v/v ethanol for 15 minutes, followed by 3 washes in sterile PBS (Figure 2.4A & B). Materials could be stored in sterile PBS until use to prevent them drying out and returning to their hydrophobic state.

2.7.2 Plasma Treatment

For the plasma pre-treatment of Alvetex® Scaffold, discs were subjected to an oxygen plasma for 5 minutes at 40W using an Emitech K1050X Plasma Asher (Figure 2.4C & D). For the plasma pre-treatment of Alvetex® Strata, discs were subjected to an oxygen plasma for 30 minutes at 10W using an Emitech K1050X Plasma Asher.

2.8 Scaffold Coating

2.8.1 Collagen I Coating

For the coating of Alvetex® Scaffold, Rat-tail Collagen I (SLS, 354236) was diluted down to a concentration of 0.8µg/ml in Molecular Biology Water. 100µl of the Collagen I solution was pipetted onto the centre of a plasma pre-treated disc and was allowed to set for 1 hour at room temperature before the addition of growth media.

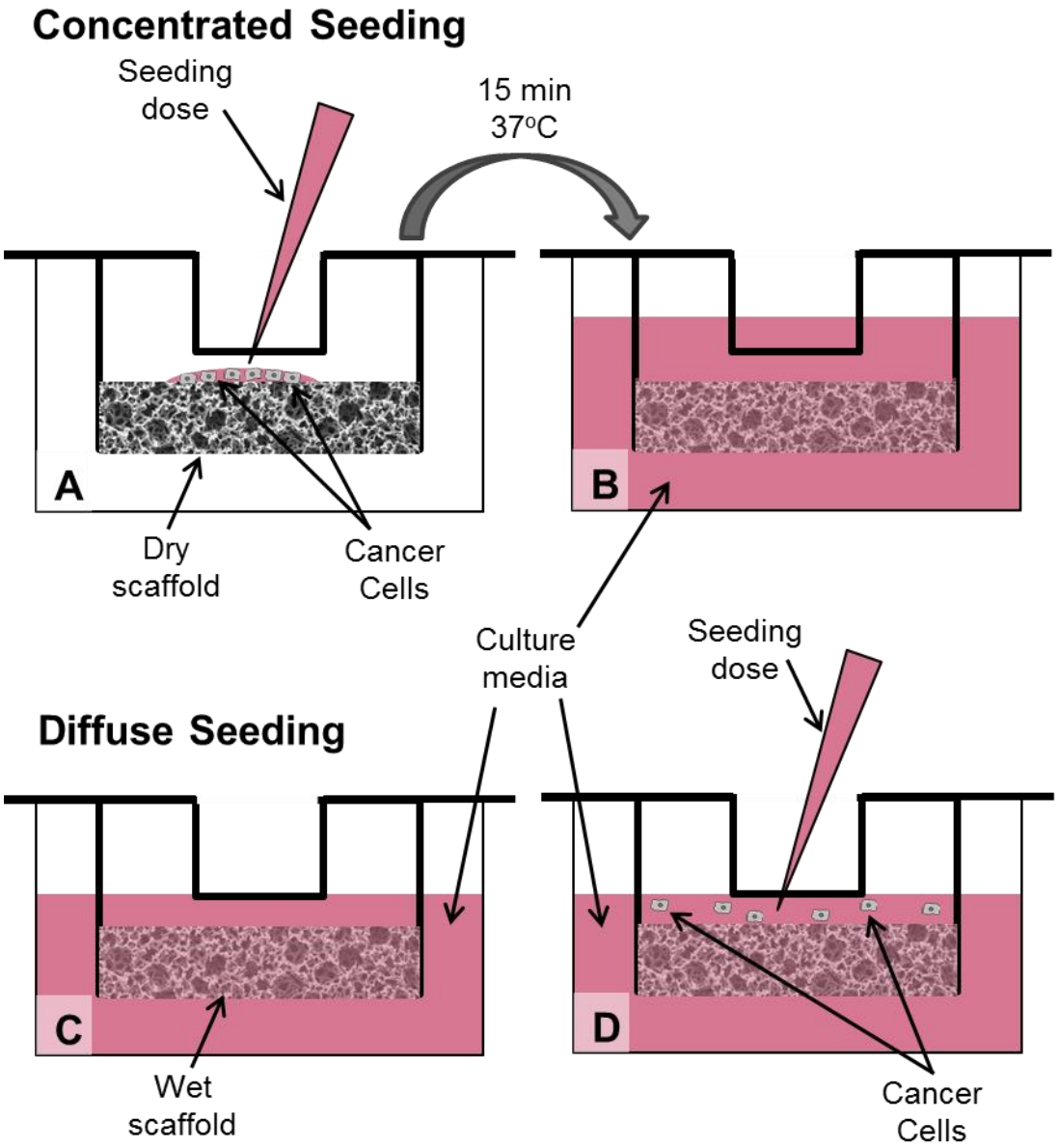

Figure 2.3: Schematics of the different methods for cell seeding onto the scaffold. For concentrated seeding, A: the 100µl seeding dose is applied to the scaffold in the absence of culture media. After a 15 minute attachment period, B: the well is filled with media. For diffuse seeding, C: the well is filled with enough media to cover the scaffold but without linking the two reservoirs of media. D: the 100µl seeding dose is applied to the scaffold through the media on top of the scaffold. After 24 hours the media level is topped up to link the two reservoirs of media.

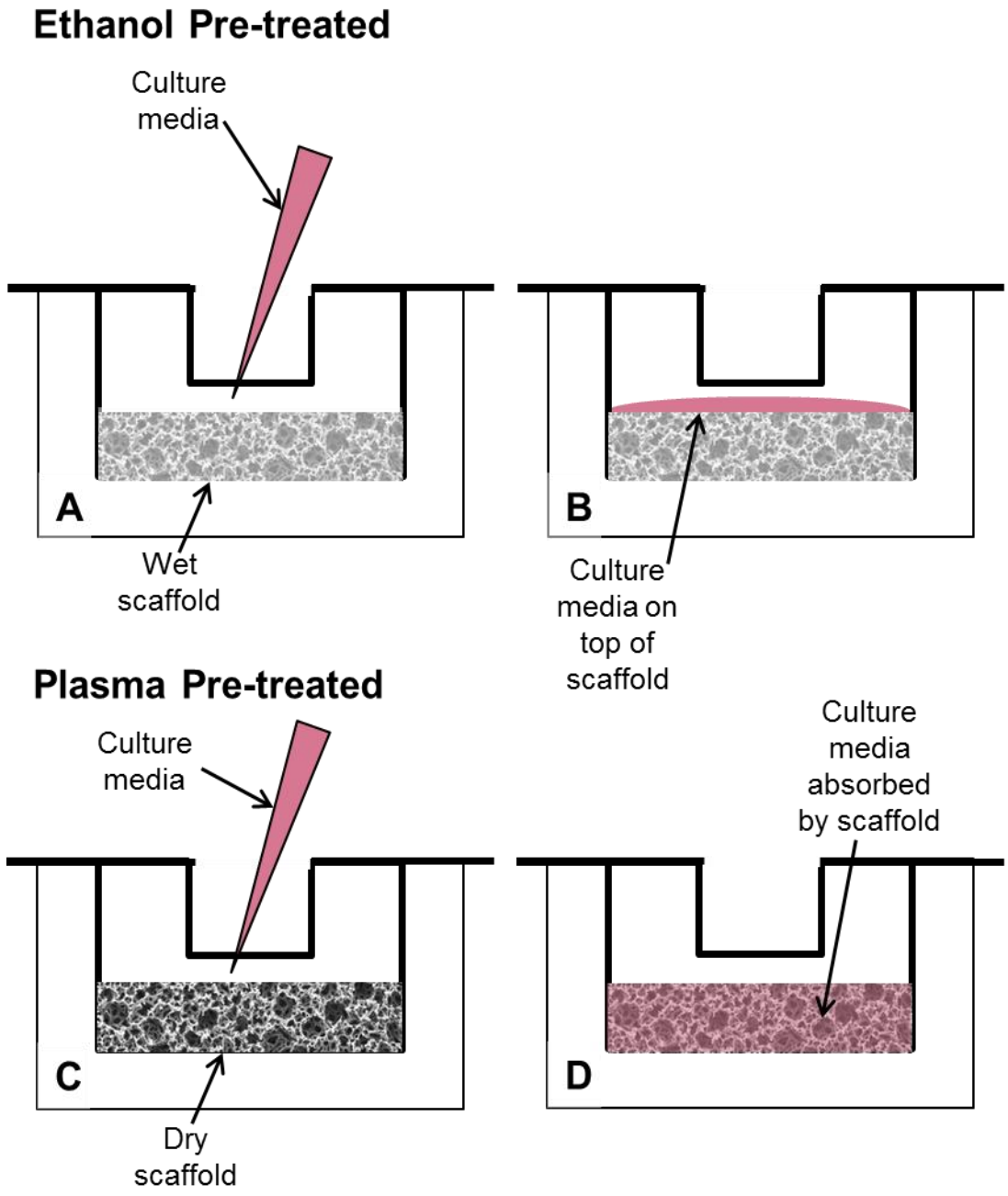

Figure 2.4: Schematics of the different scaffold pre-treatment methods. When scaffolds are ethanol pre-treated, A: the scaffold is full of the PBS when media is introduced to the scaffold, B: this results in the slow infiltration of the media into the material. When scaffolds are plasma pre-treated, C: the scaffold is dry when media is introduced to the scaffold, D: this results in the instant uptake of media into the material.

2.8.2 Fibronectin Coating

For the coating of Alvetex® Scaffold, Fibronectin from bovine plasma (Sigma, F1141) was diluted down to a concentration of 1µg/ml in sterile PBS. 100µl of the Fibronectin solution was pipetted onto the centre of a plasma pre-treated disc and was allowed to set for 1 hour at room temperature before the addition of growth media.

2.9 Assays

2.9.1 MTT Cell Viability Assay

Each sample to be subjected to the MTT Cell Viability Assay was removed from the well inert, washed in sterile PBS and placed into a 12-well plate (Greiner). Each sample was incubated with 1ml of the MTT solution, 1mg Thiazolyl Blue Tetrazolium Bromide (Sigma, M5655) dissolved per 1ml of phenol-red free DMEM (Sigma, D1145), for 1 hour in the dark at 37^{o}C. The samples were then lysed in Acidified Isopropanol, 1µl Hydrochloric Acid (Fisher) per 1ml Isopropanol (Fisher), for 10 minutes on a rotator plate at 100rpm.

To read the assay, 20µl of each sample was diluted in 180µl Isopropanol in a flat-bottom 96-well plate (Greiner) and read at 570nm on a BioTek ELx800 plate reader. The MTT Cell Viability Assay was performed in triplicate for each condition tested.

2.9.2 Bradford Assay

2.9.2.1 Protein Extraction

Each 3D sample for protein lysis was removed from the well insert, washed in sterile PBS 3 times and placed into a 1.5ml microcentrifuge tube (Starlabs). Each sample was incubated in 150µl Protein Lysis Buffer, 0.85% v/v Igepal CA-630 (Sigma), 42.55µM Tris-Base (Fisher) at pH8.0, 127.66µM Sodium Chloride (NaCL, Fisher), 0.85µM Magnesium Chloride ($MgCl_2$, Sigma) and 14.30% v/v 7x Complete Mini Protease Inhibitor Cocktail (Roche Diagnostics, 11 836 153 001), at room temperature for 30 minutes with the tubes vortexed half way through. Each sample was transferred to a fresh microcentrifuge tube and incubated in 150µl fresh Protein Lysis Buffer at room temperature for a further 30 minutes with the tubes vortexed half way through. The discs were then discarded and each set of protein lysate combined to give 300µl per sample. The samples were subsequently homogenised by passing through a 25G needle (Fisher) and centrifuged at 10,000rpm for 5 minutes. The resulting supernatant was transferred to a fresh microcentrifuge tube and denatured on a heat block at 95^{o}C for 3 minutes; the pellet resulting from the centrifugation was discarded. Each sample was stored at -80^{o}C until used for the Bradford Assay or Western Blot.

For protein lysis of 2D samples, the same procedure was followed with the lysis steps occurring in the well plates containing the cell growth.

2.9.2.2 Protein Quantification

For the Bradford Assay, 20µl of each sample was diluted 1 in 50 in dH_20 and placed into a 1.5ml microcentrifuge tube (Starlabs). A Bovine Albumin (BSA, Sigma) protein ladder was generated to obtain 10 standards ranging for 5mg/ml to 0mg/ml BSA in 0.1% v/v Triton X-100 (Fisher) and these were diluted in the same manner as the protein lysates. 250ml Bio-Rad Protein Assay Dye Reagent Concentrate (Bio-Rad Labs, 500-0006) was added to each microcentrifuge tube, the tubes inverted to mix the samples with the dye and incubated at room temperature for 40 minutes.

To read the assay, 200µl of each sample pipetted into a flat-bottom 96-well plate (Greiner) and read at 595nm on a BioTek ELx800 plate reader. The Bradford Assay was performed in triplicate for each condition tested.

2.9.3 Pico Green dsDNA Assay

2.9.3.1 Sample Lysis

Each 3D sample for lysis was removed from the well insert, washed in sterile PBS 2 times, cut into smaller pieces and placed into an RNase free 1.5ml microcentrifuge tube (Starlabs). Each sample was covered in 1ml RNase-free Pico Lysis Buffer, 10mM Tris-Base (Fisher) at pH8.0, 1mM EDTA (Sigma) and 0.2% v/v Triton X-100 (Fisher) in Molecular Biology Water, vortexed and frozen down to -80^{o}C overnight. Upon defrosting, each lysate was transferred to a fresh microcentrifuge tube and the discs discarded. The samples were subsequently homogenised by passing through a 21G needle (Fisher) and diluted 1 in 10 in Pico Lysis Buffer. Each sample was stored at -80^{o}C until used for the Pico Green Assay.

A ladder was created for each cell line used by trypsinising and counting 2D monolayer cultures, as described in 2.5.1, and spinning down cell pellets with 1.25 x 10^5 to 6.40 x 10^7 cells in centrifuge tubes at 1000rpm for 3 minutes. Each cell pellet was resuspended in 1ml RNase-free Pico Green Lysis Buffer, vortexed and frozen down to -80^{o}C overnight. From there the lysis procedure is the same as described above.

2.9.3.2 dsDNA Quantification

For the Pico Green Assay, the Quant-iT™ PicoGreen® dsDNA Assay Kit (Invitrogen, Fisher, VXP7589) was used with the appropriate protocol which is summarised below. 10µl of each sample and the appropriate ladder was diluted 1 in 10 in RNase-free Pico Green Lysis Buffer in black bottom 96-well plates (Fisher). 100µl of the Quant-iT™ PicoGreen® dsDNA Reagent, made up to a 0.5% v/v solution in 1x TE Buffer, was added to each well and the plate incubated for 5 minutes in the dark at room temperature. The plate was subsequently read with excitation 460/40nm and emission 540/35nm on a BioTek Synergy H4 Hybrid Multi-Mode Microplate Reader. The Pico Green Assay was performed in triplicate for each condition tested.

2.10 Fixation of Samples

2.10.1 2D Monolayer Cultures

The 2D cultures for fixing were washed 2 times in PBS and covered in a 4% w/v Paraformaldehyde (PFA, Sigma) solution pH 7.4 for 30 minutes at room temperature. Samples were washed 2 times in PBS prior to staining and could be stored in PBS at 4^{o}C until used.

2.10.2 3D Culture Samples

Each 3D sample for fixing was removed from the well insert, placed into a 6-well plate (Greiner) washed in sterile PBS 2 times and covered in a 4% w/v PFA (Sigma) solution pH 7.4 overnight at 4^{o}C. Samples were washed 2 times in PBS prior to further processing and could be stored in PBS at 4^{o}C until used.

2.11 Histological Processing

2.11.1 Dehydration and Embedding

The histological processing of cultures grown on Alvetex® discs followed the protocol published by Knight *et al* [218] for the dehydration and embedding of Alvetex® samples and is briefly summarised below. PFA fixed samples were washed 2 times in PBS and dehydrated through 15 minute steps in 30%, 50%, 70%, 80%, 90%, 95% and 100% v/v ethanol at room temperature. Each disc was subsequently cut in half along its diameter and placed into Histoclear (Fisher, 12358637) at 60^{o}C for 15 minutes before an equal volume of liquid paraffin wax (Fisher, 12624077) was added for a further 30 minute incubation. The Histoclear/wax mixture was fully replaced with fresh paraffin wax for a final hour of incubation before vertical embedding, with the cut surface pointing down, into disposable 33x25x13mm embedding moulds (Cellpath Ltd, GAD-5302-02A) topped with labelled embedding cassettes (SLS, HIS0029).

2.11.2 Sectioning

Wax blocks were sectioned on a Leica RM2125RT microtome using MB Dynasharp Microtome Blades (Fisher, 12056679) to a thickness of 10µm for H&E staining of SW480, SW620 and NIH/3T3 cultures and consecutive 7µm sections for H&E and DAPI staining of NIH3T3/GFP cultures and antibody staining of all cultures. Sections were floated on a 42^{o}C water bath, mounted onto Superfrost+ microscope slides (Fisher, 10149870) and allowed to dry overnight on slide dryers.

2.12 Pathological Samples

Pre-sectioned human pathological samples were obtained from the Liverpool Tissue Bank (LTB). Prior Ethical Approval and Consent was established by the LTB under its Board of Governance. A formal application and research proposal was submitted to access samples in line with the needs of this project. The LTB Board of Governance granted approval 4/3/2014, a Material Transfer

Agreement was signed, and the specimens were shipped and received. All samples were recorded and maintained securely in dedicated storage boxes. The samples were provided as 10 consecutive 5µm sections on glass slides. A total of 10 tumour samples, 5 from Dukes' Stage B tumours and 5 from Dukes' Stage C tumours, and 3 corresponding healthy colonic epithelium samples were provided for histological and immunohistochemical analysis.

2.13 Staining

2.13.1 Haematoxylin and Eosin (H&E) Staining

For the histological staining of samples, wax was cleared from slides using Histoclear (Fisher, 12358637) for 5 minutes prior to gradual rehydration through sequential ethanols, 2 minutes at 100% ethanol and 1 minute for 95% and 70% ethanol and dH_2O. The nuclei were stained by a 5 minute incubation in Mayer's Haematoxylin (Sigma, H1532) followed by a wash in distilled water and blueing of the nuclei in Alkaline Ethanol, 3% Ammonia in 70% Ethanol, for 30 seconds. The slides were then dehydrated for 30 seconds in 70% ethanol, followed by 30 seconds in 95% ethanol and the cytoplasm was stained in 0.5% Eosin (Sigma, E4009) in 95% ethanol for 1 minute. The slides were then further dehydrated in two 10 second washes in 95% ethanol and two washes in 100% ethanol, one of 15 seconds and one of 30 seconds. The slides were cleared by two 3 minute incubations in Histoclear prior to mounting with DPX mounting media (Fisher, 10050080) and covered with 50 x 22 mm coverslips (Fisher, 12383138). Once dry, these slides were imaged using a Leica DM500 light microscope with attached ICC50 HD camera at 10x and 20x magnification using the LAS EZ software (Leica).

2.13.2 Immunohistochemical Staining

Immunohistochemical staining, via a horseradish peroxidase (HRP) and 3,3' Diaminobenzidine (DAB) reaction, of 5 and 7µm thick consecutive sections was carried out using the IHC select HRP/DAB kit (Millipore, DAB150), which contains 20x Rinse Buffer, Blocking Buffer, Secondary Antibodies, Streptavidin HRP, DAB Chromogens A and B and Hematoxylin, with the protocol as follows. Wax was cleared from slides using Histoclear (Fisher, 12358637) for 5 minutes prior to gradual rehydration through sequential ethanols, 2 minutes at 100% ethanol and 1 minute for 95% and 70% ethanol and dH_2O.

Antigen retrieval was carried out by microwaving for three 2 minute periods at 800W in 10mM Citrate Buffer at pH6 (Fisher, BPE339-500) followed by a cooling period of 20 minutes in the heated Citrate Buffer. The samples were permeabilised and endogenous peroxidases quenched by incubation in 3% v/v Hydrogen Peroxide (Sigma, 216763) and then washed in 1x Rinse Buffer, containing 0.1% v/v Tween 20 (Sigma, P9416). The samples were blocked using the Blocking Buffer for 30 minutes and incubated with the primary antibody diluted in PBS at the concentrations given in Table 2.2 for 1 hour at room temperature in a humid environment.

Antibody	Clonality	Supplier	Catalogue Number	Working Concentration
E-cadherin (HECD-1)	Mono	Abcam	ab1416	1 in 50
Vimentin	Mono	Sigma	V6630	1 in 40
Slug	Mono	Cell Signalling Technology	C19G7	1 in 400
β-catenin	Mono	Millipore	05-665	1 in 300
Collagen I	Poly	Abcam	ab34710	1 in 500
Collagen IV	Poly	Abcam	ab6586	1 in 1000

Table 2.2: Antibodies for immunohistochemical staining with suppliers and concentrations.

Samples were washed in 1x Rinse Buffer, incubated with the Secondary Antibody, a combination of rabbit and mouse IgG raised in goat, for 1 hour at room temperature and washed again in 1x Rinse Buffer. The chromogen reaction was achieved by incubating the slides in Streptavidin for 20 minutes, followed by a wash in 1x Rinse Buffer followed by 20 minutes in the Chromogen Reagent, consisting of a 1:25 ratio of DAB Chromogens A and B, followed by a wash in 1x Rinse Buffer. The slides were counterstained for cell nuclei using Hematoxylin for 1 minute and washed for a final time in 1x Rinse Buffer. The slides were then dehydrated through distilled water and sequential ethanols, 1 minute each for the water, 70% and 95% ethanol and 2 minutes for 100% ethanol, before clearing in Histoclear for 5 minutes. The samples were mounted with DPX mounting media (Fisher, 10050080) and covered with 50 x 22 mm coverslips (Fisher, 12383138). Once dry, these slides were imaged using a Leica DM500 light microscope with attached ICC50 HD camera at 20x and 40x magnification using the LAS EZ software (Leica).

2.13.3 DAPI on Co-cultures

The counterstaining of nuclei in the sectioned NIH3T3/GFP co-cultures was achieved by clearing the wax from slides using Histoclear (Fisher, 12358637) for 5 minutes prior to gradual rehydration through sequential ethanols, 2 minutes at 100% ethanol and 1 minute for 95% and 70% ethanol and dH2O. The slides were then incubated with Hoescht 33342 (Molecular Probes, H3570), diluted 1 in 1000 in PBS, for 10 minutes. Slides were then washed for three 10 minutes in PBS on a rotating plate at 45rpm before mounting with Vectashield mounting media (Vector Laboratories, H-1000), covered with 50 x 22 mm coverslips (Fisher, 12383138) and sealed with nail varnish. Once dry, these slides were imaged using a Leica DM13000 B light microscope with attached DFC310 FX camera at 20x magnification using the Leica Application Suite software (Leica, Version 3.7).

2.13.4 Phalloidin/DAPI on Scratch Wounds

Scratch wounds were counterstained using Phalloidin to allow the counting of single migrating cells. Samples fixed with 4% PFA were washed twice in PBS prior to staining with 14µM Phalloidin (Universal Biologicals, PHDG1-A) in PBS, with a 1 in 1000 dilution of Hoescht 33342 (Molecular Probes, H3570) to highlight the cell nuclei, for 30 minutes in the dark at room temperature. Samples were then washed for three 10 minutes in PBS on a rotating plate at 45rpm and imaged in

PBS using a Leica DM13000 B light microscope with attached DFC310 FX camera at 10x magnification using the Leica Application Suite software (Leica, Version 3.7).

2.13.5 Antibody Staining of 2D Monolayer Cultures

Samples were permeabilised in 0.1% v/v Triton X-100 (Fisher) in PBS for 15 minutes, followed by blocking in 1% v/v newborn goat serum (Sigma, G6767), 0.1% v/v Tween 20 (Sigma, P9416) in PBS for 30 minutes on ice. Primary antibodies were diluted in the blocking buffer to the dilutions given in Table 2.2 and the samples incubated on ice for with them 1 hour. The samples were washed for three 5 minutes in blocking on a rotating plate at 45rpm before an hour incubation with a 1 in 600 dilution of the secondary antibody Alexa-fluor 488 goat anti-mouse IgG (Fisher, 1025630) and a 1 in 1000 dilution of Hoescht 33342 (Molecular Probes, H3570) in blocking buffer for 1 hour at room temperature. Samples were then washed for three 5 minutes in blocking on a rotating plate at 45rpm and imaged in PBS using a Leica DM13000 B light microscope with attached DFC310 FX camera at 10x magnification using the Leica Application Suite software (Leica, Version 3.7).

2.14 Measurement of Cell Penetration in 3D Culture Model

Two methods to analyse the amount of cell penetration were examined to ensure that the method selected would provide accurate results which were reflective of the histological data. The ‘linear’ method sampled the penetration at 3 separate points of the images and the ‘area’ method took data from the full image. Both methods of measuring cell penetration used the ImageJ software (NIH, Version 1.46a) to carry out image processing on the central 10 images acquired for each full length scaffold. Cell penetration measurements were performed in triplicate for each condition tested.

2.14.1 Linear Method

Determination of cell penetration via the linear method involved acquiring 3 linear measurements from each image, from the left, middle and right of the image, using the ‘Straight Line’ tool. Each measurement was made such that it was perpendicular to the top surface of the material and expressed as a distance and the 30 measurements were averaged to produce a result for each sample (Figure 2.5B).

2.14.2 Area Method

Determination of cell penetration via the area method involved determining the area covered by cell growth within the material and the total area covered by the piece of material on the image using the ‘Freehand Section’ tool. Each cell area measurement was expressed as a percentage of the total area measurement and the 10 measurements were averaged to produce a result for each sample (Figure 2.5C).

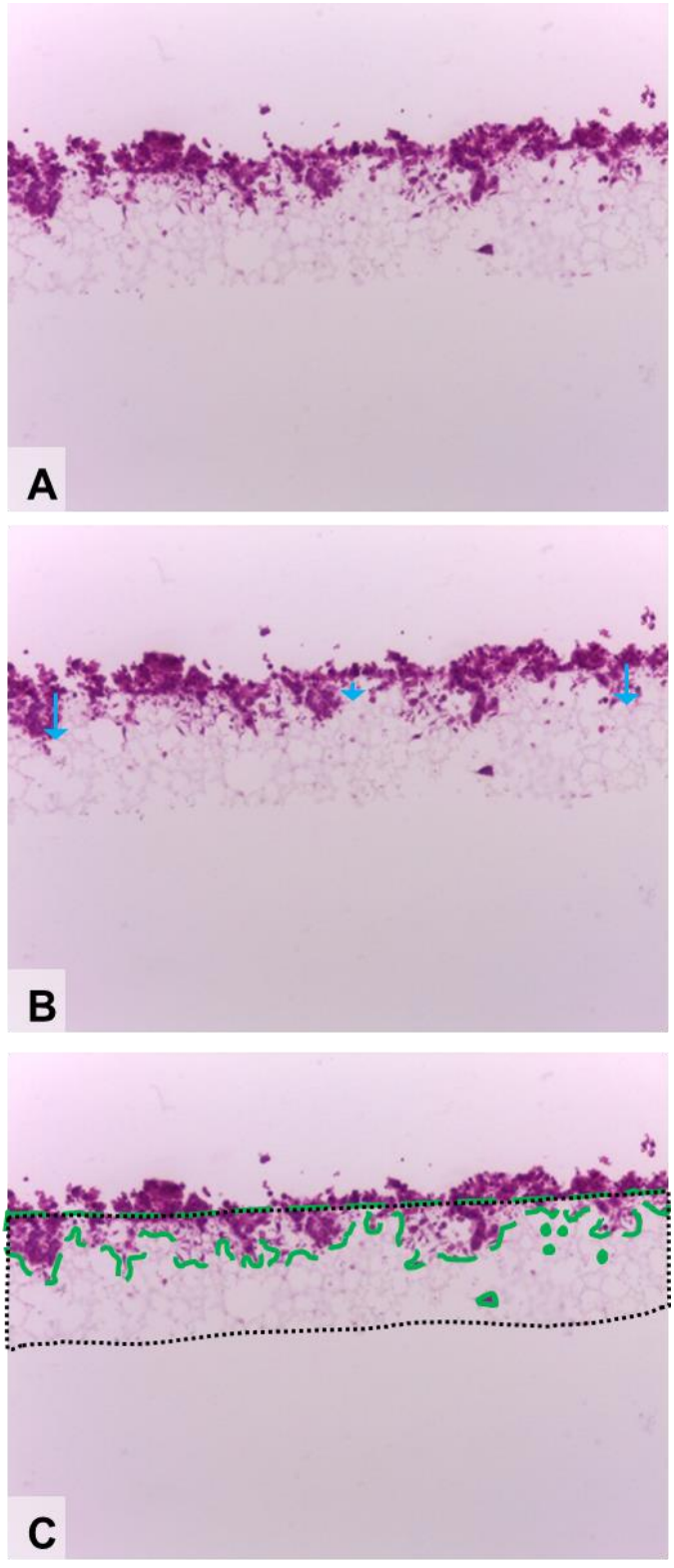

Figure 2.5: Methodological schematic for measuring cell penetration of the SW480 and SW620 cell lines on Alvetex®. A histological image (A) can be assessed for cell penetration by B: the 'linear' method, which involves taking 3 straight line measurements perpendicular to the top surface of the material down to the lowest level of cell penetration at that point (blue arrows), or C: the 'area' method, which involves determining both the total area of the image taken up by the material (black dotted line) and the total area of the image taken up by cells within the material (green dashed line) and subsequently showing the area filled with cells as a percentage of the total area of the material. For each replicate of each condition examined, this was done for 10 consecutive images and averaged. Both method utilised the ImageJ software, the 'linear' method utilised the measure length function after straight line selection while the 'area' method utilised the measure area function after free-hand area selection.

2.15 Western Blot Analysis

2.15.1 Preparing SDS-PAGE Gels

A 10% Sodium Dodecyl Sulphate (SDS) polyacrylamide gel was cast by mixing 9ml of the 10% gel solution, 375mM Tris HCl (Fisher) at pH8.8, 10% v/v Protogel Acrylamide (PAA, Fisher, 12381469) and 0.1% w/v SDS (Sigma, L3771), with 22µl 10% Ammonium Persulfate (APS, Sigma, A3678) and 10µl Tetramethylethylenediamine (TEMED, Sigma, T9281) to catalyse the polymerisation of the PAA. Once set, this gel was topped with a 4% loading gel, made by mixing 3ml of the 4% gel solution, 171.53mM Tris HCl at pH8.8, 4% v/v PAA and 1.72% w/v SDS, with 30µl 10% APS and 16µl TEMED, with a comb inserted to from the wells.

2.15.2 Running the Gels and Resolving Proteins

Once the gel had set, the samples and protein ladder (Fisher, 11872124) were loaded into the top of the gels and ran for 1-2 hours at 120V in an SDS Running Buffer, 3.03% w/v Tris (Fisher), 14.4% w/v Glycine (Sigma) and 1% w/v SDS (Sigma).

2.15.3 Blotting the Gels and Protein Transfer

The gel was then transferred to a Polyvinylidene Difluoride (PVDF, Millipore, IPVH00010) membrane in Blotting Buffer, 10% v/v Ethanol, 0.3% w/v Tris Base (Fisher), 1.4% w/v Glycine (Sigma) and 0.1% w/v SDS (Sigma), at 10V overnight. This was followed by 1.5 hours at 40V the following morning to complete the transfer.

2.15.4 Immunoblotting the Membrane to Examine Protein Expression

Following transfer from the gel, the PVDF membrane was washed in methanol and allowed to dry. The dried membrane was then blocked in 5% milk powder (Sigma, 70166) in PBS for 30-60 minutes and washed for three lots of 5 minutes in 0.1% Tween 20 (Sigma, P9416) in PBS. The primary antibodies were diluted in 5% milk powder in PBS to the concentrations given in Table 2.3 and the PVDF membrane was incubated in these overnight at 4^{o}C on a rotator plate at 45rpm.

Antibody	Supplier	Catalogue Number	Working Concentration
E-cadherin (HECD-1)	Abcam	ab1416	1 in 1000
Actin	Sigma	P1951	1 in 600

Table 2.3: Antibodies for Western Blotting with suppliers and concentrations.

The PVDF membrane was then washed for three lots of 5 minutes in 0.1% Tween 20 in PBS and incubated in the secondary antibody (Goat anti-mouse IgG, Abcam, ab150115) in 5% milk powder in PBS at room temperature for 1 hour. The membrane was washed for three lots of 5 minutes in 0.3% Tween 20 in PBS, followed by three lots of 5 minutes in 0.1% Tween 20 in PBS. The excess liquid was removed from the membrane and incubated with the ECL detection solution, 2.51mM Luminol (Sigma, 123072), 413.58µM pCoumaric Acid (Sigma, C9008), 103.65mM Tris HCl (Fisher) at pH8.5 and 0.01% v/v Hydrogen Peroxide (Sigma), for 1 minute. The membrane was then developed onto photographic film (Fisher, 10381544).

2.16 Statistical Analysis

All data presented in graphs within this thesis are averaged from three independent repeats, denoted by n = 3 in the figure legends. Statistical analysis of data was carried out using SPSS software (IBM, Version 20). Where two experimental groups were compared, the Student's t-test was used. For more than two experimental groups, Univariate Analysis of Variance (ANOVA) was used to determine general trends, with the post-hoc analysis of Dunnett's t-test, where experimental groups were compared back to the control only, or Tukey's test, where all experimental groups were compared to each other. The type of statistical analysis used is stated in the figure legends of the graphs where the significant statistical differences between groups are shown with * representing a statistical difference where $p < 0.05$, ** where $p < 0.01$ and *** where $p < 0.005$.

3 The Establishment and Characterisation of a Novel 3D Culture Model to Study Cell Migration in Colorectal Cancer

3.1 Introduction

3.1.1 Cell migration in cancer is an area of research interest

3.1.1.1 Cell migration negatively impacts patient survival

While the survival rates in England for both men and women diagnosed with colon cancer are increasing, with five-year survival rates of 53.4% and 52.3%, respectively, for those diagnosed in 2006 [10], the odds of survival are highly dependent on the stage of the cancer at diagnosis. This trend is seen in data from both England [59] and the USA [47], with patients diagnosed with the earliest stage of the disease, documented via Dukes staging for the English data and AJCC/UICC staging for the American data, seeing a 13-14 fold increase in the probably of surviving for five years after diagnosis compared to those patients diagnosed with the latest stage of the disease.

Under both methods of colorectal cancer staging, the disease is seen to progress via the spreading of the tumour from the original site through the neighbouring tissue of the colon and culminates in the formation of metastatic legions in lymph nodes and distant organs [46, 47]. Due to this, the change of cellular behaviour required for metastases to form is an area of research interest, as disrupting this process may have positive implications for patient survival.

3.1.1.2 Cell migration can be directed by the culture environment

One of the events in this multistep process is the invasion of cancer cells into the surrounding tissues [65], a complex process which relies on many environmental cues such as cell-cell interactions [219]. With such a large number of proteins implicated in the migratory behaviour of cancer cells, including the actin regulating Arp2/3 complex [220] and cell adhesion mediating integrins [221], and the expression patterns of these proteins directing the mode of migration adopted by cells [71], the recreation of an appropriate environment to study these processes in the lab is critical.

One such example which has been highlighted in the literature is the modulation of the expression known tumour suppressor *CDH1* gene for the cell adhesion protein E-cadherin. The loss of E-cadherin expression has been linked to increased cell migration and invasion in both 2D and 3D *in vitro* models for squamous cell carcinoma [222], demonstrating that this protein occupies a key position in the regulation of cell migratory behaviour. However, it has also been demonstrated that in the colorectal cancer cell lines SW480 and HCT116, the expression and localisation of E-cadherin can be modulated by the density of cell growth in 2D cultures [223]. When grown in sparse cultures, with reduced cell-cell contacts, the amount of E-cadherin detected via Western blot was reduced compared to dense cultures maintained over the same time period. In addition to this, the E-cadherin protein was found to be localised throughout the cytoplasm of the cells in sparse cultures, whereas in dense cultures it was predominantly found at the plasma membrane

and co-localised with β-catenin, which was itself seen to have a nuclear localisation in sparse culture conditions. This change in E-cadherin expression was seen to be negatively correlated with the expression of Slug, a transcription factor which is known to be correlated with EMT in colorectal cancer cells [82]. The authors of this paper then determined that β-catenin mediated induction of Slug expression was a mechanism responsible for the suppression of E-cadherin expression and the loss of cell-cell contacts between cells, leading to a more migratory phenotype. Together this demonstrates that the migratory behaviour of these cell lines may be modulated by changing the culturing environment and therefore it is important to culture them in a manner that accurately reflects the *in vivo* environment.

The critical nature of recreating a biologically relevant culturing environment is further highlighted by the role that the architecture of the surrounding environment, usually in reference to the ECM components of this environment, has on directing the mode of migration, with the dimensionality of this substrate a factor which can impact cell behaviour [70]. Hence, the use of 2D *in vitro* migration models, such as scratch wound assays [199, 200], provides cells with a culture environment which may direct the cells away from behaviours that they would otherwise exhibit *in vivo* and produce results which do not correlate with the observations made from patient data. Therefore, the development of a 3D *in vitro* migration assay which provides more appropriate environmental cues to cells would be well placed to bridge the gap between standard 2D *in vitro* studies and *in vivo* drugs testing to help reduce the high failure rate for anti-cancer treatments [224, 225].

3.1.2 The growing field of 3D cell culture

The expansion in 3D cell culture research in recent years has been reflected in the number of papers discussing the use of 3D cancer models, with a PubMed search finding over 500 published within the past five years [226, 227]. As this is still a growing area of research, there remains a large amount of investigation and optimisation to be carried out to find the methodologies best suited to the experimental aims of the field.

3.1.2.1 3D cell culture models mimic characteristics of tumour microenvironments

There are a variety of cancer models which are currently employed for research purposes [163] which aim to model certain aspects of the tumour environment in an *in vitro* setting. The main benefit each of these models has is the increase in appropriate signalling cues provided to the cultured cells, such as the provision of an attachment substrate beyond the planar surface provided by standard 2D tissue culture plastic. Each of these have their own advantages and disadvantages, with some suitable for adaption for use as an *in vitro* migration model.

3.1.2.1.1 Spheroid models provide an oxygen gradient to cancer cells

One of the 3D cancer models which has been in use the longest is the spheroid model [176]. This model relies on the aggregation of cells without the use of ECM protein gels or synthetic scaffolds to direct the distribution of cells. This process naturally produces an aggregate with an oxygen gradient where the cells the centre of the spheroid are maintained in a hypoxic environment which leads to necrosis of the cells found there [177]. Taken along with the diminishing availability of nutrients in the core of spheroids, this provides a simple model for poor growth environment found in the centre of small tumour legions or in the regions between blood vessels in larger vascularised

tumours. As hypoxia is a driver of cell behaviour modification in growing tumours, either directly via the action of HIF [72] or through secondary effects such as the lowering of pH [73], it is an environmental factor that can push cancer cells towards a migratory phenotype to allow them to escape the detrimental growth environment.

This model also allows for investigations into interactions between multiple cell types, via co-culture with either immune cells [178] or fibroblasts [179]. Both of these studies created spheroids from colorectal cancer cell lines before being covered in a cell suspension containing either the macrophages or fibroblasts. In the study involving the macrophages [178], the spheroids were plated on to anti-adherent agarose or adherent collagen I coated plates and cultured in the macrophage containing suspension, while in the study involving fibroblasts [179], the fibroblasts were introduced to the spheroid surface via centrifugation prior to embedding in a collagen I gel.

Spheroid cultures have also been used to assay the migratory behaviour of cells in the multicellular environment that they provide. This can take the form of observing the migration of cancer cells out of the spheroid into a surrounding ECM gel [179] or as a spheroid confrontation assay to observe the migration of cancer cells into a spheroid structure formed from a secondary cell type [207].

3.1.2.1.2 ECM gels provide relevant protein signalling and can support co-culture

Another common method for obtaining 3D cancer cultures is the use of ECM gels to either encapsulate cancer cells [180] or to act as a seeding surface [184]. The gels utilised in these cultures can be obtained from the polymerisation of commercially available ECM gels products, such as collagen I [185] or Matrigel [182], or the decellularisation of ECM gels generated via the culture of a secondary cell type, such as fibroblasts [184]. These cultures provide a 3D protein environment for cell culture which allows for signalling to the cells via cell surface receptor, such as integrins [168]. They also differ from the culture of cancer cells on 2D gel coatings, as thicker gels are more flexible than the thin coatings on tissue culture plastic they recreate the physical cues of ECM rigidity more accurately than 2D cultures [83]. This alteration to the rigidity of the microenvironment of the cells, in addition to the presentation of ECM protein to a greater proportion of the cell surface, has been shown to alter the protein composition of cell-ECM adhesion sites [168], which can have knock-on signalling effects as some of those proteins, such as vinculin, are known to interact with the actin cytoskeleton and have roles in the modulation the migratory behaviour of cells [228].

In addition to providing a biologically relevant *in vitro* protein environment to cells in culture, this technique can be adapted to incorporate a secondary cell line, such as fibroblasts, to produce an organotypic cancer culture [189]. This results in a more complex culture model with provides paracrine signalling from this secondary cell type in addition to the spatial cues from the 3D protein gel. The generation of these organotypic models can provide the opportunity for the user to construct a culture which reflects the morphology observed in pathology samples to allow for the study of cells in an environment which closely mimics the organisation seen in patient tumours to provide more accurate results.

These ECM gel based cultures have also been used to study the migratory behaviour of cancer cells. Methodologies include the tracking of single migrating cells encapsulated in a collagen I gel

[211] and the vertical invasion of tumour cells into collagen I gels [209] or an organotypic tissue construct [216].

3.1.2.1.3 Synthetic scaffolds provide a further opportunity for 3D cell culture

A further methodology for obtaining 3D cell cultures is the use of synthetic scaffolds. With an increasing number of materials and fabrication methods available [172], the opportunity to tailor scaffolds to a specific culturing application allows this technology to have applications in a wide range of research areas. Many scaffold models currently have applications in the modelling of functional tissue, such as the hyaluronic acid fibre reinforcement of skin equivalents [229], the differentiation of human embryonic stem cells (hESCs) on poly(DL-lactic-co-glycolic acid) (PLGA) scaffolds [230] or osteogenesis on mPEG-PCL-mPEG/hydroxyapatite composite scaffolds [231], with the physical traits of the materials tested for their ability to support the cell types under investigation in each situation.

This type of model can also have applications for cancer research, although these are less common than functional tissue models. Published examples of scaffold use for cancer research include the culturing of hemangioendothelioma and angiosarcoma vascular tumour cell lines on a polystyrene scaffold [232], a non-small-cell lung cancer cell line on a polyester based scaffold [188] and lung cancer cell line on electrospun copolymer scaffolds [233]. This type of model may be advantageous over ECM gel based models as the scaffold provides 3D environment for cell culture in the absence of biological signals from ECM proteins, which would allow for comparisons with standard 2D cultures on uncoated plasticware to assess the impact of the increased dimensionality of the culture environment. Additionally, these models can be coated with ECM proteins and support multiple cell types [229] which would allow the step-wise development of a more biologically realistic model with the ability to assess the impact that each step, increased dimensionality or increased biological signalling, has on the behaviour of cells.

While there are few examples of cancer culture models using synthetic scaffolds, there have been attempts to quantify the amount of cell migration attained by cells cultured in the manner by assessed the penetration of cancer cells into the material from the seeding surface [215]. A synthetic material which has been adapted for use as a migration or invasion assay is the Transwell® insert system, which utilises a 10µm polycarbonate filter with 8µm diameter pores to provide a barrier which migrating cells must cross [206]. The Transwell® system can be adapted for use with ECM protein coatings [234] or co-culture [235] to mimic the biological signals present in tumours and provide a simple 3D system for assaying cell migration.

3.1.2.2 3D migration assays assess cell behaviour in a more realistic microenvironment

The introduction of 3D culture systems allows for the maintenance of cells in environments which are closer replications of the *in vivo* system than standard 2D methodologies which have been in use for many years. In the context of assessing the migratory behaviour of cells, the incorporation of features such as increased dimensionality [215], the provision of biological signalling via ECM proteins or a secondary cell type [216] or the heterogeneous nature of these cultures [179] enhances the behavioural cues in the system, which may direct the cells to adopt a mode of migration which reflects the *in vivo* behaviour of cells more accurately than the mode adopted by

cells grown in a highly artificial 2D environment by altering the expression of key proteins involved in the migration of cells, such as integrins [168].

3.1.2.2.1 Disadvantages of 3D migration assays

While the biological relevance of models is increasing, the means of extracting data from models is becoming increasing complex and sophisticated. The wide range of 2D migration assays provide a simple means of measuring cell movement via microscopy, whereas 3D work requires more complex methods of cell tracking, as all cells may not be visible in the same plane of focus [194]. There is also a trade-off to be made when utilising 3D migration assays between using easy-to-use systems that have the potential to cause cellular damage, with systems which are less disruptive but more process intensive [195]. Additionally, while the most commonly form of 3D migration assay, the Transwell® assay [206], provides a relatively simple method of quantifying cell motility via counting the cells which have passed through the filter, when used without an ECM gel coating the 10µm thick membrane provides a limited 3D environment which may mean that results obtained from this assay may not truly reflect *in vivo* behaviour. These are all considerations to be made when selecting the tools and methodologies to develop a new assay.

3.1.3 Selection of appropriate tools for 3D cell culture is important

With the generation of any new system of methodology for scientific research, the tools selected play a vital role in ensuring that valuable data is obtained by the experimenter. In the case of developing a colorectal cancer migration assay, selection of both the cell lines involved and the means of 3D culture will help to shape the subsequent work carried out.

3.1.3.1 Cancer Cell Lines

As the aim of this project is to model the migratory behaviour of colorectal cancer in a 3D *in vitro* environment, the selection of cells which reflect the *in vivo* behaviour of the cancer is vital. While the use of cells extracted directly from a primary tumour may provide a closer model to the clinical situation there is a large amount of patient variability [79, 186] and tumour heterogeneity [236] which may lead to high variation in the results obtained from *in vitro* experimentation. This is particularly problematic during the optimisation of the model, as the lack of a consistent culturing profile would make the determination of the optimal conditions for the 3D model harder to visualise.

Cell lines have a more consistent growth profile in standard 2D *in vitro* culture, which is advantageous trait for the optimisation of a new protocol, so therefore colorectal cancer cell lines will be used to assess this model. There are a variety of commercially available cell lines derived from colorectal adenocarcinomas at various stages of the tumour progression. The focus of finding appropriate cell lines was concentrated on cell lines thought to be representative of the stages of colorectal cancer either side of the metastatic progression of the tumour, namely those at Duke's stages B and C [46].

A literature search highlighted four cell lines which were confirmed to be derived from Dukes' stage B cancers and initially cultured during the 1970s and 1980s, namely HCA-7 [237], LS123 [238], LS-174T [239] and SW480 [48]. Each cell line has distinct characteristics when cultured which allow for a selection to be made between them subject to the needs of the experimental work. The

optimisation process relies on using cells which are representative of the system in question, here colorectal cancer and the migratory behaviour it exhibits, and which provide consistent cultures, so that conclusions may be accurately drawn from many experiments, hence, these two criteria will be used to select the appropriate cell line.

3.1.3.1.1 HCA-7

The HCA-7 cell line was initially cultured by Kirkland and Bailey [237] and while this cell line was observed to retain some of the characteristics of the original tumour, such as microvilli, the morphological features of this cell line decreased with increased time in culture and the cells lost much of their adherent properties.

While this cell line has been used to assess cell migration, via scratch wound and Transwell® assays [240], or colony formation of sublines of this cell line [241], there is little data in the literature regarding the migratory behaviour of this cell line, with PubMed returning just 4 papers [242]. When this is taken with the loss of cell adhesion to tissue culture plastic over extended culture periods, the HCA-7 is unsuitable for use while optimising a 3D migration assay.

3.1.3.1.2 LS123

The LS123 cell line was initially isolated and cultured by Rutzky et al [238], however, this cell line failed to demonstrate tumorigenic potential when assayed via tumour formation in xenografts and colony formation in soft agar, although they did demonstrate the ability to invade in chick embryonic skin assay. The lack of tumorigenic potential has also been confirmed by work from another research group [243].

The lack of tumorigenic behaviour may contribute to the low number of papers found utilising this cell line, a PubMed search only returning 8 papers [244] with none of these in relation to migration [245]. This cell line has been used in the literature to assess the adhesion of colorectal cancer cells to laminin 5 [246] and derivatised agarose beads [247]. The lack of prior data regarding this cell line and its migratory behaviour means that it is an inappropriate choice for use in the optimisation of this migration assay and will not be discussed further.

3.1.3.1.3 LS-174T

The LS-174T cell line is a trypsinised variant of the LS-180 cell line original established by Tom *et al* [239]. This cell line initially produces monolayer cultures after plating into culture flasks; however, the cell morphology was seen to revert back to the tightly packed morphology of the LS-180 cell line, which exhibited a tendency to produce multicellular aggregates.

This cell line is more commonly used than either of the two previously discussed, with 872 entries found in the PubMed database [248], and has been documented as used in a variety of migration assays, including scratch wound assays [249] and Transwell® migration and invasion assays [250]. However, as the morphological properties of this cell line have been documented to alter over extended culture periods, this cell line is unlikely to provide a consistent tool for the optimisation of a novel model and will not be used here.

3.1.3.1.4 SW480

The final cell line under consideration for this model was the SW480 cell line, which was originally established by Leibovitz *et al* [48], and has been featured in over 1700 journal articles, as found in the PubMed database [251], of which nearly 10% were investigating migration [252]. The paper describing the initial culture of this cell line cultured them to high passage number and did not note any perturbation in cell behaviour, with the exception of a gradual decrease in the generation time of the cells [48], which is common as cells adapt to the standard culture conditions and has been noted during the isolation of the other Dukes' stage B colorectal cell lines discussed [237-239].

This cell line has been routinely used in standard scratch wound assays [253] and Transwell® migration [254] and invasion [255] assays, providing a large amount of published data regarding the migratory behaviour of this cell line for the results obtained from this model to be compared to. Taken with the stability of this cell line over long term *in vitro* culture, the SW480 cell line has been selected as the Dukes' stage B cell line which will be used to assess the suitability of this 3D migration assay.

A second advantage to the SW480 cell line is that there exists a counterpart Dukes' stage C cell line, the SW620 cell line, which was isolated from a lymph node of the same male patient one year after the original surgery [48]. At the time of isolation, subtle differences between the two cell lines were noted, such as variations in cell morphology and proliferation rate, with the SW620 cell line being comprised of smaller, faster dividing cells. A study in 2000 examined both of these cell lines and determined that they have each retained their characteristics over the subsequent years in culture and remain a suitable tool for the assessment of changes occurring in colorectal cancer during disease progression [256]. Together these cell lines represent states of the tumour either side of the metastatic progression of the disease and eliminate any differences seen by gross genetic variation between the cell lines.

Together, the SW480 and SW620 cell lines will reflect different aspects of colon cancer progression to allow for investigating how tumour progression alters the way in which cancers react to changes to their environment. Additionally, these two cell lines, with their behavioural differences, will provide the opportunity to optimise the use of the 3D culture system to provide a methodology which has the potential for application to other cell types without the need for extensive further optimisation.

3.1.3.2 Method of 3D culture

To avoid the variability and difficulty of processing that can be encountered with natural scaffolds and gels; a synthetic scaffold was selected for 3D culture. While most of the focus of synthetic scaffold use in cell culture is on biologically active materials [257, 258], the commercially available highly porous, biologically inactive polystyrene based material, Alvetex® [218], was selected to provide a reproducible platform for 3D culture to generate consistent results. The manufacturing method for the material is described by Carnachan *et al.* [259] and the dimensions of the characteristics can be altered depending on the additives present during the polymerisation.

This material is available in two formats, namely Alvetex® Scaffold and Alvetex® Strata, which are structurally similar, but have differing microscopic characteristics which lend them to varied applications. As these materials are manufactured from materials used to make standard tissue

culture plasticware, they are biologically inert and non-biodegradable. These material properties lead to a culturing system which is reproducible and will maintain its integrity over long culture periods. The biologically inert nature of this system also allows for a step-wise construction of a 3D migration model to allow the role of the dimensionality of the culture environment to be assessed, as opposed to the assessment made in the presence of ECM proteins as seen with ECM gel and organotypic models.

When working with a 3D system such as Alvetex®, it is important to understand the characteristics of the material. From the high magnification SEM images in Figure 3.1A & B it is clearly visible that gross morphology of the material is consistent between Alvetex® Scaffold and Alvetex® Strata, although the morphological features are present at different scales. Both materials are approximately 90% porous, with the polymer material surrounding air voids which are linked via smaller void interconnects [259, 260]. Alvetex® Scaffold is the larger void-sized variant of the two materials, with a modal diameter of 40µm (Figure 3.1C) and interconnect size of 13µm (grey line, Figure 3.1E). Alvetex® Strata, on the other hand, has a denser packing of the material, leading to modal void diameter of 15µm (Figure 3.1D) and interconnect size of 6µm (black line, Figure 3.1E). Each of these materials are presented in a variety of formats, the one selected for this project is the 22mm diameter, 200µm thick 6-well insert format (Figure 3.1F) as this is the largest size format available, which will allow for the maximal collection of data from the cultures, and is surrounded by culture media (Figure 3.1G) to aid the maintenance of rapidly proliferating cultures of cancer cell lines. From the structural presentation of these materials, it is hypothesised that the cells cultured on them will find it easier to move into the Alvetex® Scaffold, as the Alvetex® Strata may provide a physical barrier to the migration of the cells.

Use of this 3D system has also been documented with a wide variety of cell types, including adipose tissue-derived stem cells [261], neurons [262], hepatocytes [263], osteoblast-like cells [260] and cancer cell lines [232]. These papers also demonstrate the capability of 3D cultures grown with this system to be subjected to many forms of analysis to provide a rounded data set in order to allow for detailed conclusions to be drawn from experiments. This shows that it is a versatile system which has a high probability of producing successful 3D cultures with cell lines which have not been previously tested, subject to growth optimisation.

3.1.4 Aspects of Optimisation of 3D Cell Culture

The successful generation of 3D cultures relies on methods which have been optimised to obtain the best outcome for cell culture by looking at each aspect of the set up process. In the Alvetex® system, these areas are the pre-treatment and seeding of cells on the material, in addition to the parameters used throughout the culturing of cells on the material.

3.1.4.1 Surface Pre-treatment

As Alvetex® is a polystyrene based system, it retains the hydrophobic properties of polystyrene [264] and requires treatment prior to successful cell culture. The standard preparation of Alvetex® is to submerge it 70% v/v ethanol and then wash in sterile PBS prior to use [263]. This leaves the user with a pre-wetted scaffold to which a cell suspension can be applied.

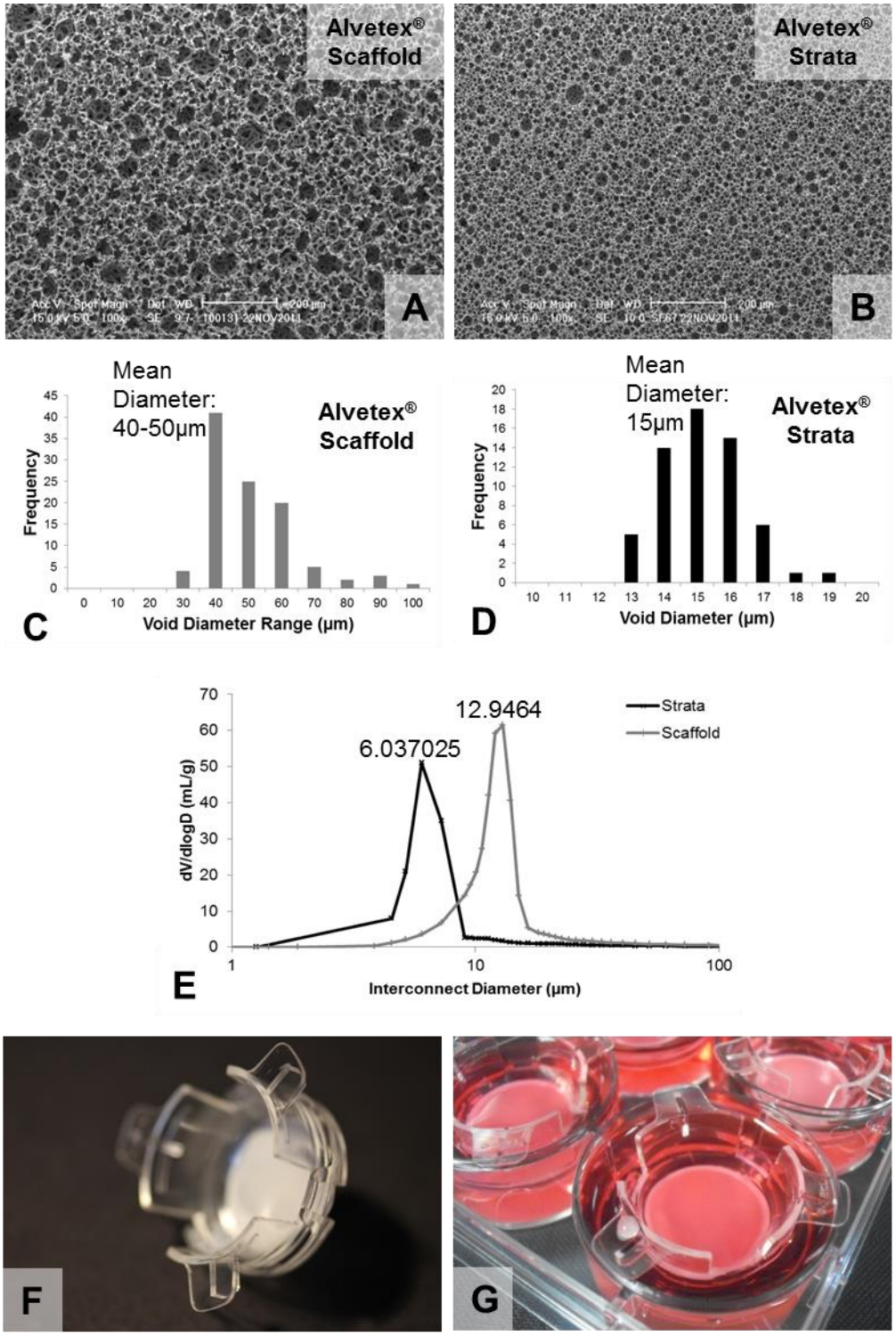

Figure 3.1: Both Alvetex® Scaffold and Alvetex® Strata possess a highly porous morphology, but on different scales. SEM images for A: Alvetex® Scaffold and B: Alvetex® Strata, void diameter distribution (as determined from measurements from SEM images) for C: Alvetex® Scaffold and D: Alvetex® Strata and E: interconnect size (as determined from mercury intrusion porosimetry) for both materials showing the difference in size of the microstructure. F: Both materials are presented as 200µm thick 22mm discs housed in a plastic insert, G: this insert fits standard 6-well plates and allows the cells to be cultured with media surrounding the insert with the media on top of and under the insert connected. Alvetex® Scaffold data supplied by Ross Carnachan and Alvetex® Strata data supplied by Adam Hayward.

The other option for surface pre-treatment is to expose the material to an oxygen plasma, as used in the preparation of commercial plasticware for cell culture [265]. This procedure changes the surface chemistry of the material by adding oxygen into surface functional groups [266], providing more sites for cells to attach to. Indeed the amount of oxygen found on the material surface is inversely related to the contact angle of the material, as a measure of surface wettability, as removal of this oxygen from tissue culture polystyrene by an n-hexane plasma results in an increased contact angle [264].

The wettability of a surface has a direct impact on the ability of proteins and cells to adhere to the surface, as a highly wettable surface will permit stronger adhesion of proteins to the surface than a poorly wettable one [267], this in turn leads to an increased cell density on the highly wettable surfaces [264]. However, there appears to be a limit on the range of contact angles which result in optimal cell adhesion, with the maximal number of cells attached to the surface observed around 70^{o} and dropping off either side of that [267]. Pre-treatment of Alvetex® with an oxygen plasma results in a lowering of the contact angle from 122^{o} to 76^{o} [268], putting it in the optimal range for cell adhesion.

3.1.4.2 Cell Seeding Methodology

The method by which cells are applied to the pre-treated Alvetex® is another aspect of the set up protocol which has the potential to have a large effect on the characteristics of the resulting 3D culture. There are a variety of methods which may be used to introduce the cells to the material and these can be divided into two groups, static and dynamic techniques.

Thevenot *et al* [214] carried out an evaluation of the efficacy of four techniques for cell seeding onto 3mm thick PLGA copolymer scaffolds, two static methods, namely surface and injection seeding, and two dynamic methods, centrifuge and orbital seeding. These methods produced similar levels of cells present in the material after 7 days of culture, although the centrifuge method resulted in a greater percentage of dead cells found 3 hours post seeding. The main difference between the techniques was seen in the profile of cell distribution throughout the scaffolds, with surface seeding resulting in the greatest number of cells found at the extremities of the scaffold, while injection seeding results in a higher density of cells toward the bottom of the scaffold. The two dynamic methods, centrifuge and orbital seeding, both resulted in the greatest density of cells residing in the centre of the scaffolds.

As the endpoint of the research question addressed here is to investigate the migratory capacity of colorectal cancer cells in a 3D environment, the employment of a seeding method which causes cells to become evenly distributed throughout the depth of material would hinder the analysis of cultures to determine if the migratory behaviour alters when the cultures are exposed to different conditions. Due to this two static, surface seeding methods will be investigated, the concentrated and diffuse seeding methods. Both apply cells to the uppermost surface of the material; however the concentrated method applies the cells directly to the surface via a small seeding dose, while the diffuse method allows the cells within the seeding dose to settle out onto the surface of the material through the culture media in the dish. A comparison of these should highlight if they have an effect on the lateral distribution of cells across the material and if that has an effect on the cultures they produce.

3.1.4.3 Period of Growth

It is expected that the culturing of cells in a 3D environment will affect their protein expression and, in turn, their behaviour. One such example of this is FAK and phosphorylated FAK, which is known to be altered when cells form different types of adhesion sites and specifically decreased at 3D adhesion sites [168], the expression of which has been shown to affect the growth rates of colorectal cancer cell lines *in vitro*, with higher FAK expression correlated with higher rates of proliferation [269]. As it has also been demonstrated that the increase in the dimensionality of collagen I gels reduces the proliferation of human breast epithelial cells [270], it is expected that the proliferation of cells in the 3D cultures would be reduced compared to 2D cultures.

With the a reduction in cell proliferation expected, the model must be examined to ascertain how long Alvetex® can support viable cultures as this time period is likely to be longer than that seen in 2D and the culture of cells for an extended period may provide the opportunity to make a more accurate assessment of the migratory behaviour of the cells.

3.1.4.4 Protein Coating of Materials

It has been demonstrated that the ECM environment of cells can direct the migratory behaviour of cells [271] and is also correlated to the progression of tumours [272]. The inclusion of ECM coatings in the model under development here represents a more advanced model by the increasing of the biological relevance of the model and will be discussed fully in Chapter 6.

3.1.4.5 Utilisation of a Co-culture Model

The involvement of stromal cells in tumour development has implications for cancer cell migration [273] and overall patient survival [58, 274]. Again, as with the inclusion of ECM coatings, the inclusion of a secondary cell line to form a stromal equivalent represents a more advanced model by the increasing of the biological relevance of the model and will be discussed fully in Chapter 6.

3.1.4.6 Medium Type

An end goal of this project is to produce a co-culture of these cell lines with fibroblasts, therefore, the selection of a suitable growth medium for both cell types is critical. The paper which documented the original culturing of the SW480 and SW620 cell lines used supplemented L-15 media [48], however, the original isolation of the NIH/3T3 cell line which will be used for co-culture, see Chapter 6, shows that this was carried out in Dulbecco's modification of Eagle's medium (DMEM) [275]. A search of the literature has demonstrated that since their initial isolation both the SW480 and SW620 cell lines have been successfully maintained in DMEM and subjected to a variety of experimental procedures [276, 277]. Due to this, DMEM has been selected as the growth media for these experiments to allow the model to be assessed for the ability to support a co-culture model without the need for extensive re-optimisation.

3.2 Chapter Aims

This Chapter aims to assess the suitability of a novel polystyrene scaffold for use in a 3D migration assay for colorectal cancer and to develop a standard protocol for this assay. To achieve this, the lateral distribution of cells across the material should be maximised to increase the opportunities for data collection. Additionally, the optimisation process should result in cultures which have little variation in the distribution of the cells across the depth of the material.

3.2.1 Objectives

- To assess the 2D growth characteristics of the two colorectal cancer cell lines;
- To assess the impact of seeding methodology, scaffold preparation and scaffold presentation on 3D cultures of two colorectal cancer cell lines;
- To assess the long term viability of 3D cultures on different sized variants of the material;
- To assess the amount of cell movement into the materials and develop an appropriate method to quantify cell migration in a 3D system.

3.3 Results

3.3.1 The SW480 and SW620 cell lines display different characteristics when grown in standard 2D culture

Although both the SW480 and SW620 cell lines were isolated from the same patient at different stages of the disease progression, characteristics of the cells in standard 2D culture differ. The two cell lines possess distinct morphology which allows for easy distinction between the two lines.

3.3.1.1 Both the SW480 and SW620 cell lines possessed a mixed morphology in 2D culture

Both cell lines culture as mixed morphologies, as noted in the original paper at their isolation [48], with both of them containing populations with an elongated bipolar phenotype (arrows, Figure 3.2B & D), although the size of these individual cells is larger in the SW480 cell line, roughly 36µm by 13µm, than the SW620 cell line, roughly 26µm by 10µm. The SW480 cell line also had a population of larger cells, roughly 36µm by 23µm, which grew with a triangular shape and possess a more epithelial phenotype (solid arrowheads, Figure 3.2B). Whereas the SW620 cell line contained a cell population with a smaller rounded morphology, roughly 11µm in diameter (outline arrowheads, Figure 3.2D). Within both cell lines, the different cell morphologies were found with equal distribution throughout the cultures and together, along with the differences in cell size, these allow for the easy identification of the cell lines in standard 2D *in vitro* culture.

3.3.1.2 Both the SW480 and SW620 cell lines retained a rapidly proliferating phenotype

At the original derivation of these two cell lines, they were noted as having population doubling times which characterised them as two of the faster growing cell lines discussed in the paper. Their generation times were listed as 50 and 30 hours for SW480 and SW620 respectively for the higher passage numbers documented [48]. It was also noted that many of the cell lines generated in this collection underwent a shortening of generation time as their passage number increased, as they adapted to *in vitro* culturing conditions.

When these cell lines were seeded at a density of 0.5 million cells per T25 culture flask, they maintained the rapidly dividing phenotype noted in the original article (Figure 3.3). When trypsinised cells were manually counted at the end of the seven day culture period, the SW480 cell line reached a final population of 16.90×10^6 while the SW620 appeared to retain the faster dividing phenotype and had increased to a final population of 20.75×10^6 cells per flask. However, the subsequent years of cell culture maintenance appear to have led to the two cell lines developing a shorter generation time and displaying a comparable generation time of 28 and 26 hours for SW480 and SW620 respectively, the calculations for these made using the experimental data and Hayflick's formula as stated in his 1973 paper on subculturing fibroblasts [217] and subsequently used by Leibovitz *et al.* to calculate the original values for the generation time [48].

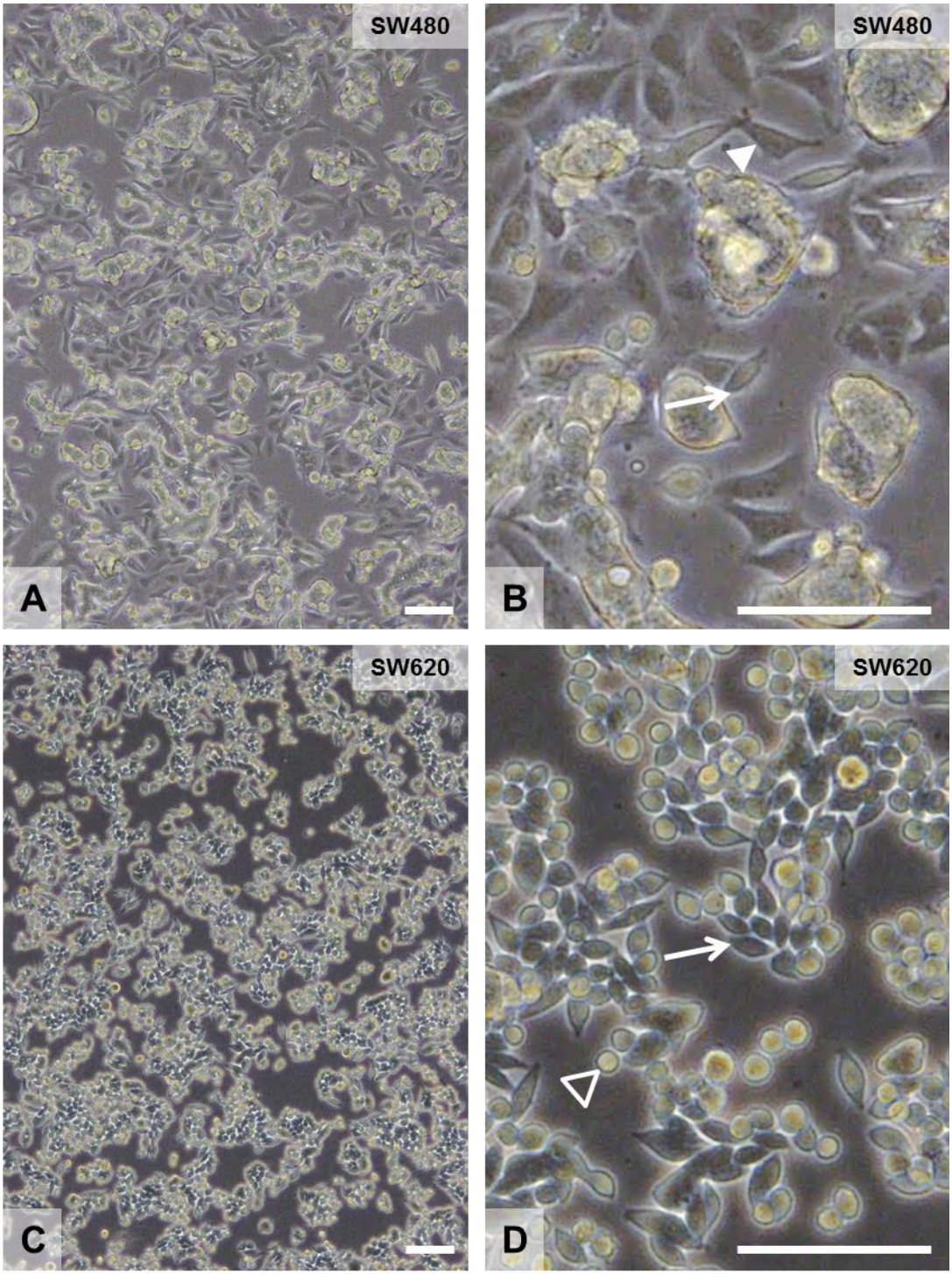

Figure 3.2: Both the SW480 and SW620 cell lines display distinct mixed morphologies of cells in standard 2D culture, with the SW480 cell lines having larger cells than the SW620 cell line. Phase contrast images of the A and B: SW480 and C and D: SW620 cell lines at low and high magnification respectively, with both cell lines having a bipolar type cell (arrow) The SW480 cell line also has an epithelial type cell (solid arrowhead) while the SW620 cell line has a spherical type cell (empty arrowhead). Scale bars = 100µm for all images.

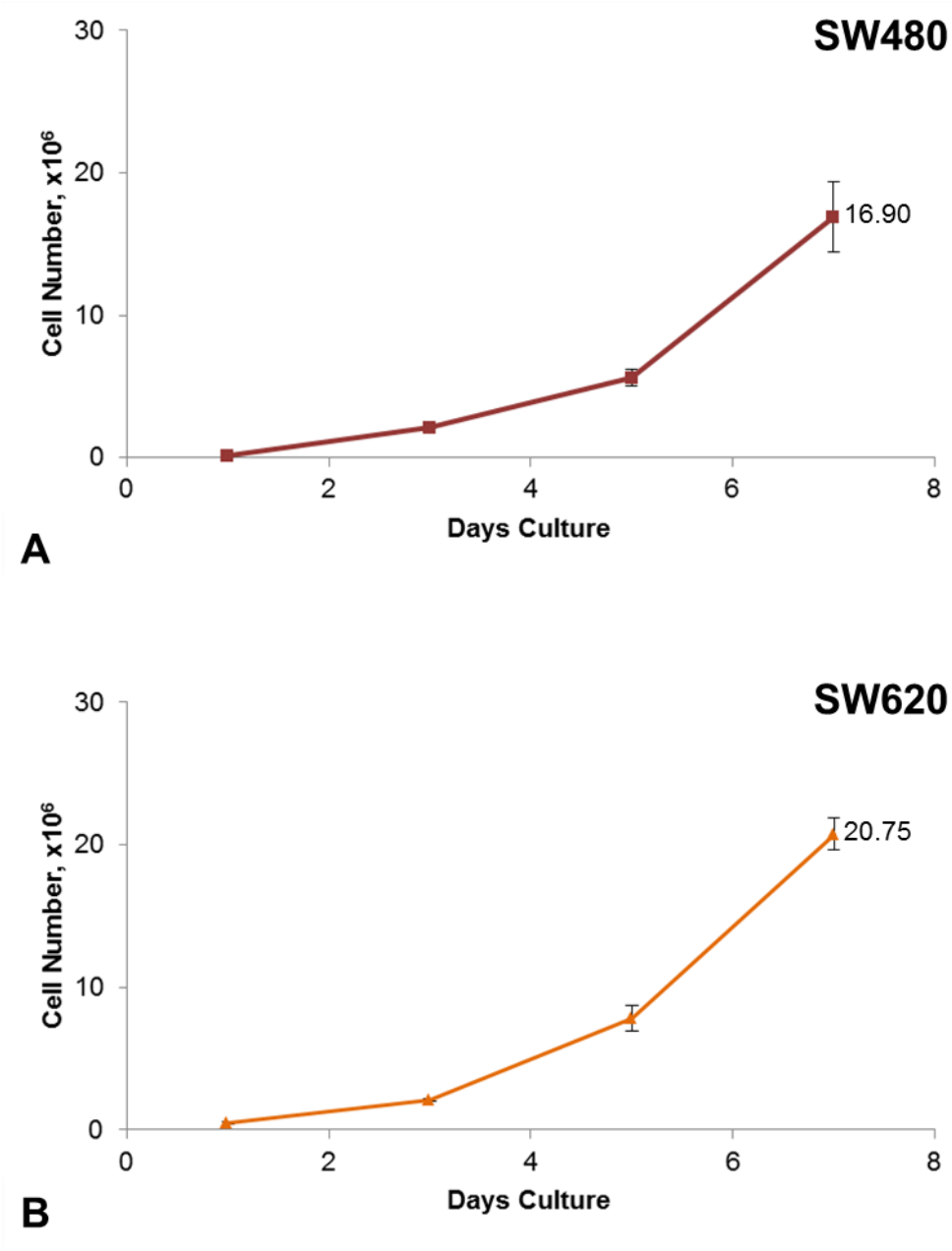

Figure 3.3: Both the SW480 and SW620 cell lines expand rapidly in 2D culture over 7 days, with the SW620 cell line maintaining a faster rate of division than the SW480 cell line as seen by the final cell counts. Cell counts from trypsinised monolayer cultures in T25 culture flasks with 0.5 x10^6 cells at initial seeding for A: SW480 and B: SW620 cells. Data represent mean, n = 3, ±SEM for both graphs.

Furthermore, the cultures of both the SW480 and SW620 cell lines were found to retain cell viability (Figure 3.4) throughout the complete seven day culture period. This suggests that the speed of population doubling across the culture period was not constrained by limited nutrient supply from the media or limited space to accommodate the newly generated biomass.

Together these data display that the two cell lines both retain a rapidly dividing phenotype, which will need to be accounted for when optimising the protocols for their growth in the 3D culture system. However, as it has been previously noted that the culturing of cells in a 3D environment reduces their rate of cell division [270], it is expected that the proliferation rate of the SW480 and SW620 cell line will be reduced compared to the rate observed in 2D. Additionally, the distinct morphologies of each cell line when maintained in standard 2D culture have the potential to result in a distinct 3D growth pattern on the material.

3.3.2 Pilot assay to determine whether the SW480 and SW620 cell lines can be maintained in a 3D culture system

The SW480 and SW620 cell lines were cultured on Alvetex® Scaffolds provided in a standard 6-well insert format. Each 22mm diameter, 200µm thick disc of material was housed in an insert which is suspended in a well of a 6-well culture plate. The material was ethanol pre-treated to prepare the Scaffold for culture, as per the manufacturer instructions and standard protocol used in previously published research papers [263], and each cell line was subsequently seeded in a concentrated manner at a density of 1 million cells per scaffold. Scaffolds were incubated for 15 minutes to allow for cell adhesion before the remaining media was added to each of the wells.

3.3.2.1 The SW480 and SW620 cell lines demonstrated different cell distributions when culture on Alvetex® Scaffold

From the histological data presented in Figure 3.5, Alvetex® Scaffold can support the culture of both the SW480 and SW620 cell lines for up to 7 days. The composite images in Figure 3.5A, for SW480, and Figure 3.5B, for SW620, demonstrate that the growth of the cell lines was found across the entire 22mm diameter of the material after 7 days in culture. When higher magnification images of the cultured material are viewed, it is clear that both cell lines had moved into the material over the culture period.

At 4 days culture, the SW480 cell line (Figure 3.5C) was found distributed at low density within the polymer material, with few cells growing on top. However, by 7 days culture (Figure 3.5D), the cell growth had increased in density. The majority of this increase was seen by the thickening of the cell layer found at the surface of the material, with a modest increase in the density of the cells distributed within the material.

In contrast, the SW620 cell line did not have a cell layer on the top of the material after 4 days culture (Figure 3.5E) and only presented a layer that is one or two cells thick by 7 days culture (Figure 3.5F). Instead, this cell line appeared to enter the material and to continue to proliferate within it, producing a higher density of internal cell growth by the end of the culture period when compared back to the SW480 cell line.

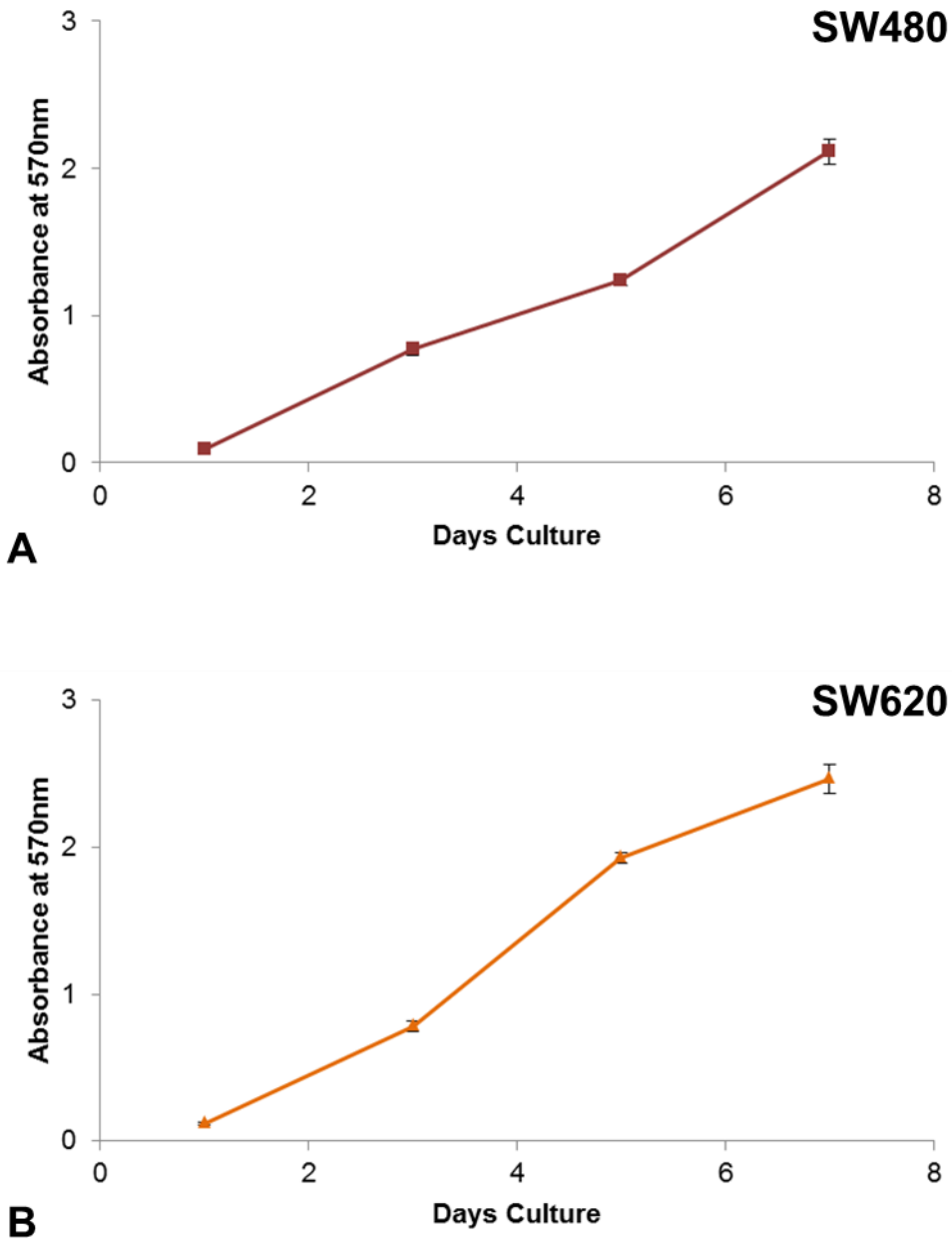

Figure 3.4: The SW480 and SW620 cells maintain similar increasing levels of cell viability when maintained in 2D culture over 7 days. Absorbance at 570nm of monolayer cultures in T25 culture flasks with 0.5 x10^6 cells at initial seeding for A: SW480 and B: SW620 cells as determined by the MTT Cell Viability Assay. Data represent mean, n = 3, ±SEM for both graphs.

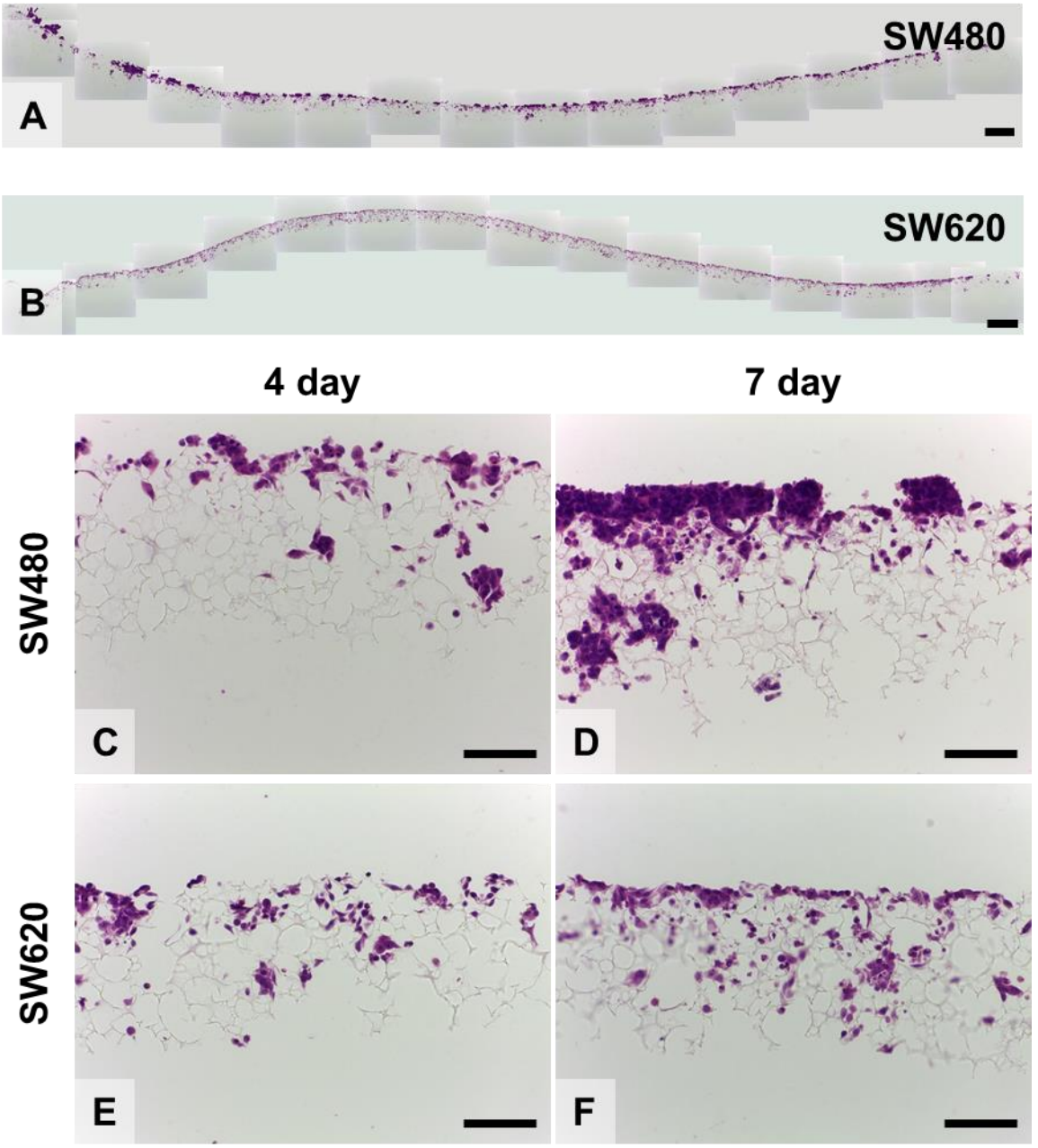

Figure 3.5: The SW480 and SW620 cell lines have different growth characteristics when cultured for 4 or 7 days on Alvetex® Scaffold. Both cell lines also display an increase in cell growth when left to grow for 7 days when compared to 4 days culture. H&E stained full scaffold images of 7 day cultures with A: SW480 and B: SW620 cells and high magnification images of scaffolds cultured with C: SW480 for 4 days, D: SW480 for 7 days, E: SW620 for 4 days and F: SW620 for 7 days. Scale bars = 500µm for images A and B, 100µm for images C-F.

Furthermore, the manner in which the cells grow in the 3D culture varies between the two cell lines. The SW480 cell line was more likely to be found as groups of cells both on top of and within the material, whereas the SW620 cells filled the material as a culture of loosely associated individual cells, without packing together in tightly associated groups.

3.3.2.2 SW480 and SW620 cultures on Alvetex® Scaffold remained viable for up to 7 days

From the cell viability data (Figure 3.6), it was seen that the extension of the culturing period from 4 days to 7 days results in a significant increase in the viability of the SW480 3D cultures (Figure 3.6A). As the assay used is based on the metabolic activity of the cells within a given culture, this increase may be correlated with the increased cell population seen in the material at 7 days. However, such a viability increase was not seen in the SW620 cultures (Figure 3.6B), even with the visible increase in the amount of cell growth within the cultures between the two time points (Figure 3.6E & F).

This data demonstrated that both the SW480 and SW620 cell lines could be maintained on Alvetex® Scaffold for up to 7 days without a loss of cell viability. Therefore, a 7 day culture period was selected to assess further aspects of the optimisation of the 3D cultures, as this extended culture period would allow any differences in the cultures resulting from the different setup protocols tested to be more apparent than a 4 day culture.

3.3.3 Seeding method affects the viability of 3D SW620 cultures

One possible variable in the setup of 3D cultures is the method by which cells are applied to the culture material [214]. To investigate the effect of seeding method on the growth characteristics of 3D SW480 and SW620 cultures, two different methodologies were selected for comparison, here termed the concentrated and diffuse seeding methods. For consistency across other variables, the cells were applied to an ethanol pre-treated material in a seeding dose of 100µl, which contained 1 million cells in a single cell suspension.

The concentrated seeding method applies the cells directly to the material before the addition of culture media. A seeding dose was pipetted into the centre of pre-treated discs (Figure 2.3A), after which the 6-well plates were placed in a cell culture incubator at 37^{o}C, 5% CO_2 for 15 minutes to allow the cells to attach to the material. Following the attachment period, media was added to each culture well such that the reservoir of media on top of the material, which is within the top part of the well insert, links with the reservoir of media found surrounding the well insert via the cut-away sides of the well insert (Figure 2.3B).

When the diffuse seeding method is employed, the cells are introduced to the material after the addition of the culture media. The well was filled with media such that the material is covered by media, but the two reservoirs of media, one directly over the material and the other between the insert and the well wall, are not linked via the cut-away sides of the well insert (Figure 2.3C) to prevent cells from settling onto the bottom of the well plate The seeding dose was added into the media sitting above the material (Figure 2.3D) and the 6-well plates placed into a cell culture incubator to allow the cells to settle onto the material over time, in a manner similar to standard 2D culture. The wells were topped up with media after the initial 24 hours to allow cell attachment.

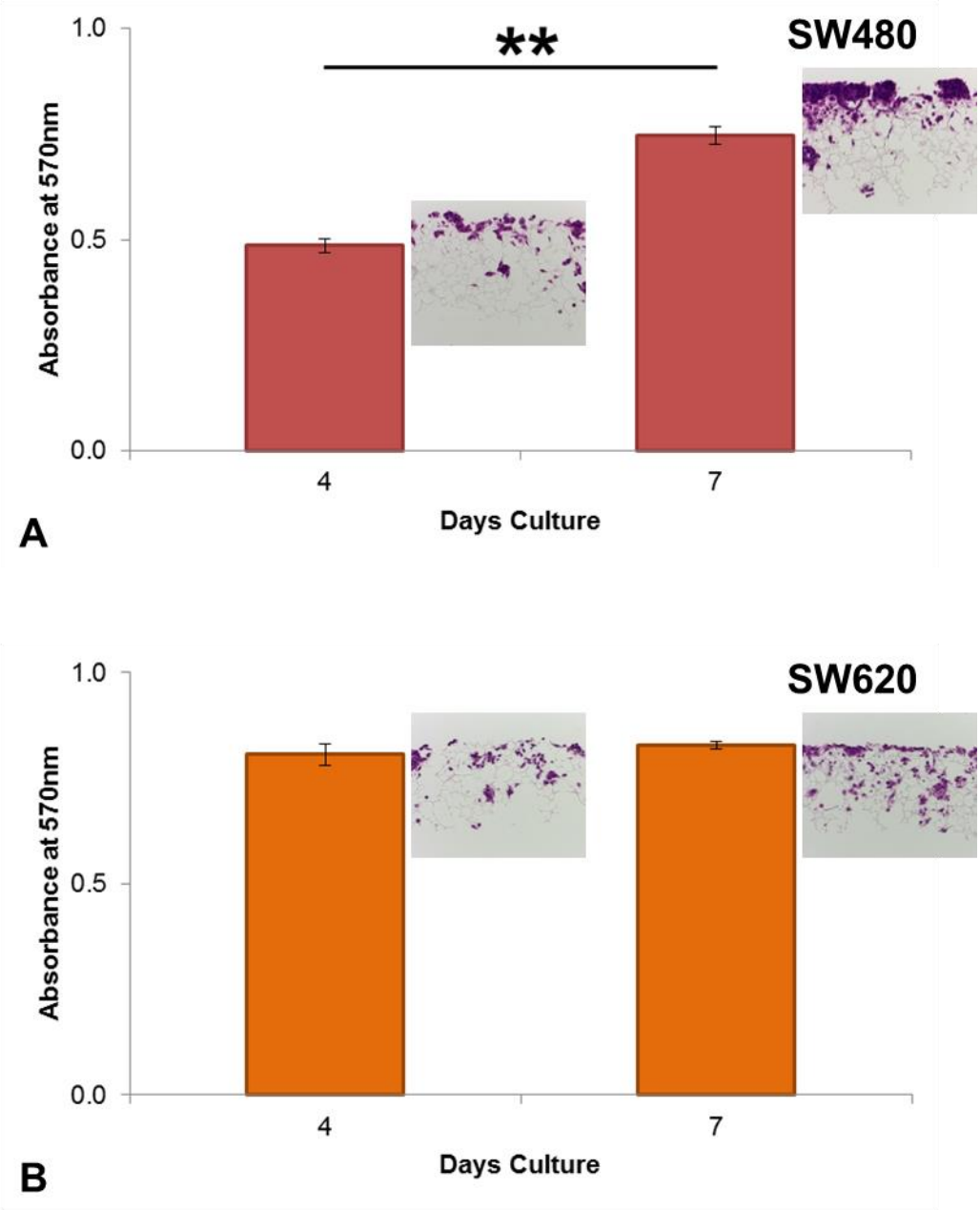

Figure 3.6: The viability of the SW480 cell line increases according to time cultured on Alvetex® Scaffold, while the viability of the SW620 cell line was unaffected, when 1 million cells were seeded in a concentrated manner and cultured for 4 or 7 days. Absorbance at 570nm of A: SW480 and B: SW620 cells as determined by the MTT Cell Viability Assay, with corresponding histological images for each condition. Data represent mean, n = 3, ±SEM for both graphs, ** $p < 0.01$ by a Students t-test.

3.3.3.1 Diffuse seeding provided a more even cell distribution

When 3D cultures of the SW480 cells seeded by the two methods are compared, it was seen that the diffuse seeding protocol produces a culture which is evenly distributed across the entire width of the material, as seen in the composite image in Figure 3.7A, which was comparable to the results from applying the concentrated seeding protocol (Figure 3.5A). However, the 7 day culture after concentrated seeding resulted in a build-up of cells on the top surface of the material (Figure 3.7C), diffuse seeding did not lead to a build-up of cells, while still maintaining a cell population within the material (Figure 3.7D).

The alteration of seeding method also affects the behaviour of the SW620 cell line during 3D culture. Again, cell distribution after 7 days of culture was even across the width of the material with both the concentrated (Figure 3.5B) and diffuse (Figure 3.7B) seeding protocols. When viewed at a higher magnification, differences were visible between the two cultures. While cultures seeded by the concentrated protocol had a low build-up of cells at the top surface of the material, with most cells found distributed within the material (Figure 3.7E), in the cultures produced by seeding the cells by the diffuse protocol the cells were distributed towards the top surface of the material, with a thicker layer of cells at the top surface (Figure 3.7E).

3.3.3.2 Diffuse seeding increased the viability of SW620 cultures

Additionally, the viability of SW480 cultures was unaltered by the seeding method employed (Figure 3.8A), suggesting that there is no distinct advantage or disadvantage to applying either method to this cell line. The same was not seen in the SW620 cultures, where the diffuse seeding protocol resulted in increased viability over the concentrated seeding protocol (Figure 3.8B), suggesting that an advantage could be gained from seeding these cells using the diffuse method.

Whilst this data shows that there minimal differences in cell distributions in 3D culture, when viewed via histological images, when the method of seeding cells is varied, the viability data displayed a significant difference for the SW620 cell line. The increase in viability seen in diffusely seeded SW620 cultures, which did not appear to be correlated with an observable increase in the number of cells distributed throughout the material, suggesting that this culture method is preferable for the 3D culture of SW620 cells. As the use of the diffuse seeding method did not have a negative impact on the viability of SW480 cultures, both cell lines will continue to be seeded via the diffuse method for further optimisation of this 3D system.

3.3.4 The method of scaffold pre-treatment affects cell distribution in 3D cultures

As previously mentioned, the material used to provide the 3D culturing environment for this research is a polystyrene based scaffold. Whilst having a porosity of 90% due to the large number of voids found within the material [260], and therefore having the capacity to take up comparatively large volumes of liquid when compared to a similar material with a lower porosity, the material itself is hydrophobic and requires a pre-treatment before it will absorb aqueous solutions, such as cell culture media.

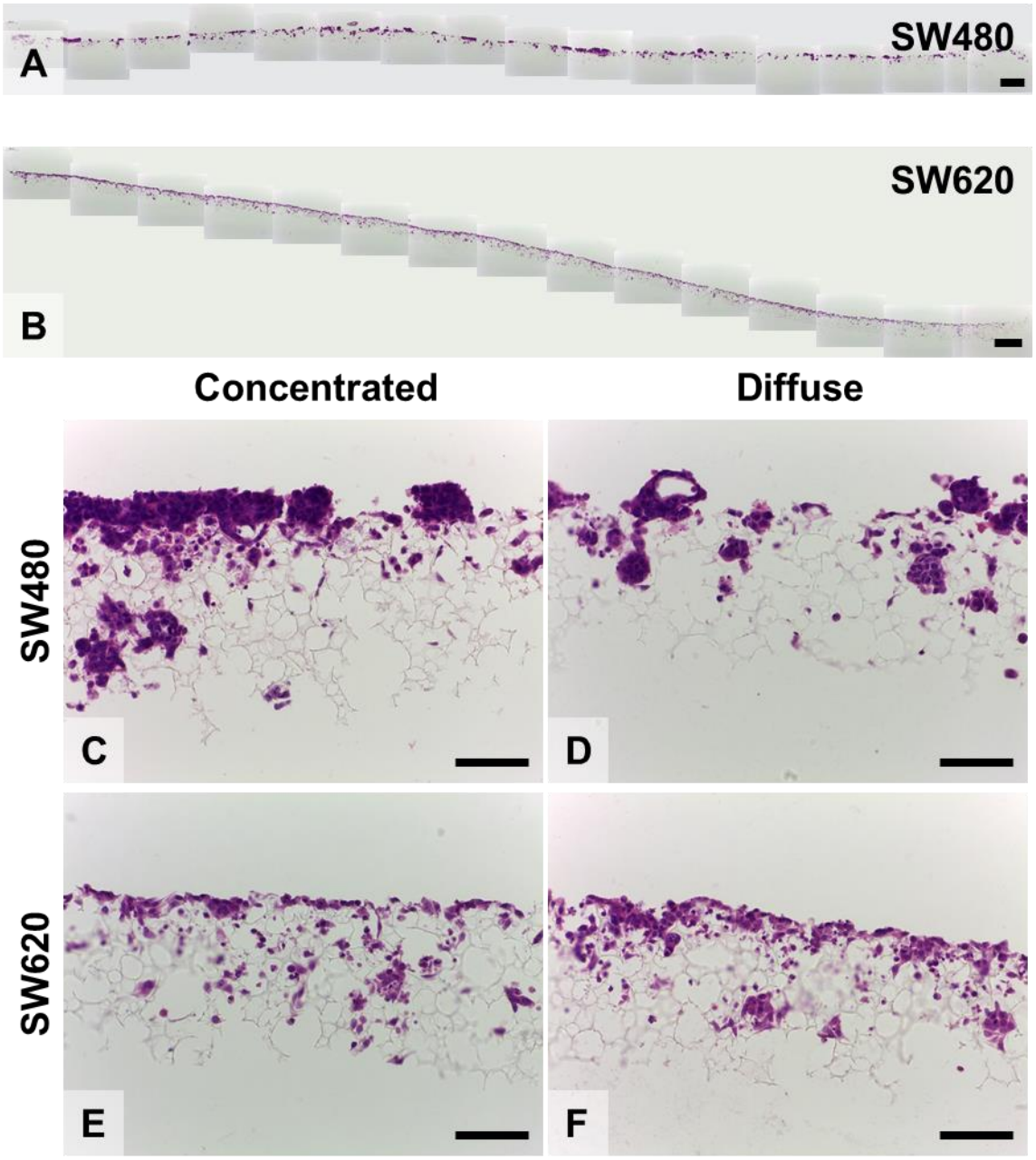

Figure 3.7: Diffuse seeding of 3D cultures onto Alvetex® Scaffold affects the distribution of the SW480 and SW620 cell lines. The SW480 cell line displays a smaller amount of growth on top of the material, whereas SW620 cell line displays a more consistent layer of growth across the whole scaffold when diffusely seeded. H&E stained full scaffold images of diffusely seeded cultures with A: SW480 and B: SW620 cells and high magnification images of scaffolds seeded with C: SW480 in a concentrated manner, D: SW480 in a diffuse manner, E: SW620 in a concentrated manner and F: SW620 in a diffuse manner. Scale bars = 500µm for images A and B, 100µm for images C-F.

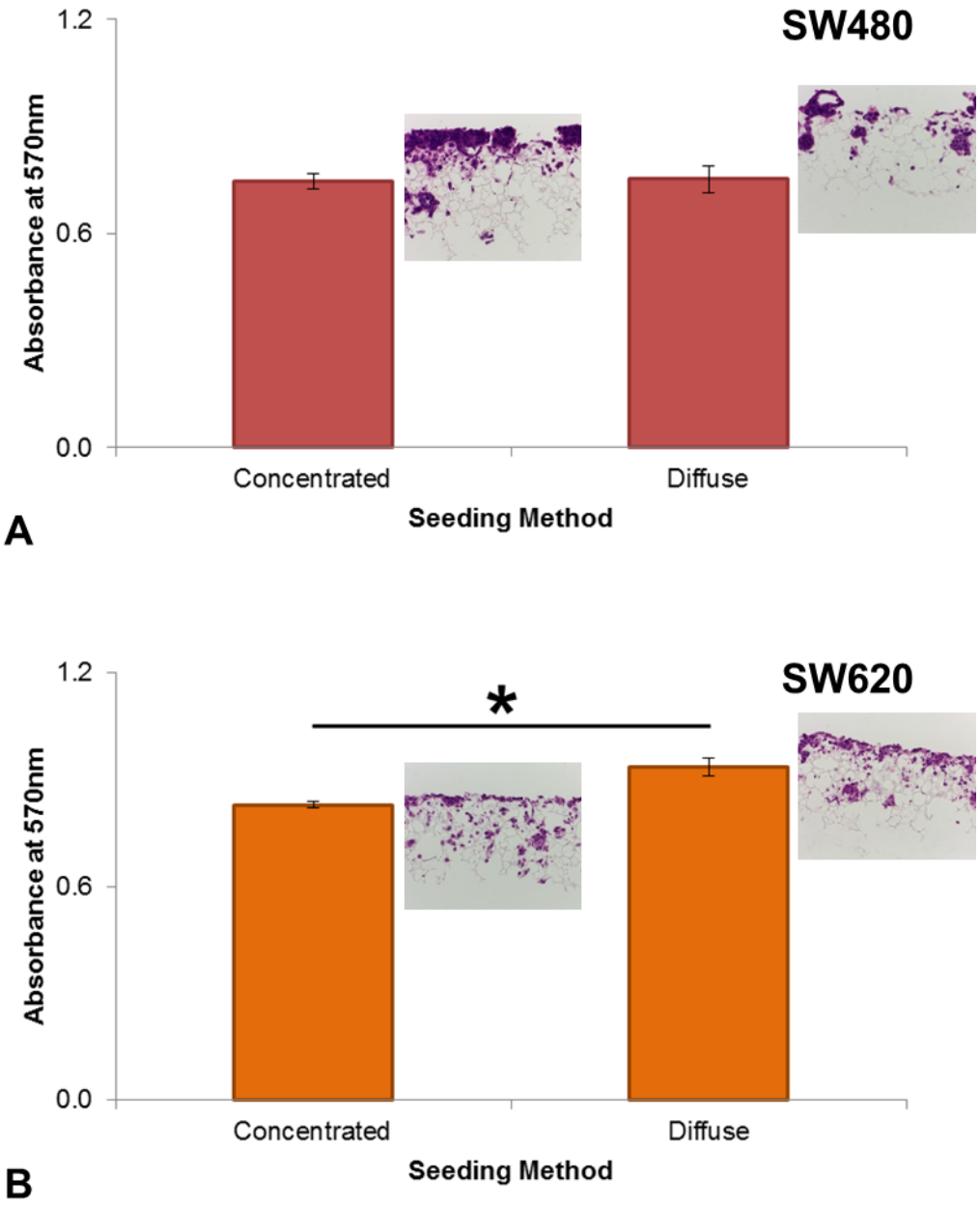

Figure 3.8: The viability of the SW620 cell line is increased when diffusely seeded onto Alvetex® Scaffold, while the viability of the SW480 cell line was unaffected, as compared to cells seeded in a concentrated manner when 1 million cells were cultured for 7 days. Absorbance at 570nm of A: SW480 and B: SW620 cells as determined by the MTT Cell Viability Assay. Data represent mean, n = 3, ±SEM for both graphs, * $p < 0.05$ by a Students t-test.

Alvetex® Scaffold can be pre-treated in one of two different ways to prepare it for cell culture, either by an ethanol wash or an oxygen plasma. For the ethanol wash procedure, discs were submerged in a 70% ethanol solution and subsequently washed in PBS to remove the ethanol from the voids, after which they remain hydrophilic until they dry out. This means that when an aqueous liquid is applied to the top surface of the material, it spreads across the surface of the material before it is absorbed (Figure 2.4A & B), as the voids of the material are filled with PBS, preventing the rapid uptake of the liquid.

Oxygen plasma pre-treatment instead results in a hydrophilic material which is still dry. Application of liquid to the top surface of the material leads to a rapid uptake of the liquid (Figure 2.4C & D), as the voids do not contain a different liquid which needs to be displaced. For ethanol pre-treated discs, the media is slower to flow through the material to the internal part of the well insert, which may result is it floating in the culture media until sufficient media has come through the material, or the cut-away sides of the well insert, to equilibrate the media levels inside and outside the well insert. In contrast, the media flows straight through a plasma pre-treated disc and the insert is not dislodged from its position in the well temporarily.

3.3.4.1 SW480 and SW620 cells grew in a less clustered manner on plasma pre-treated scaffold

The method of pre-treatment of the Alvetex® Scaffold prior to seeding with either SW480 or SW620 cells had an impact on the distribution of cells within the material after a 7 day growth period. Both cell lines demonstrated an increased cell penetration across the entire length of the material (Figure 3.9A & B) when cultured on scaffolds which had a plasma pre-treatment when compared to scaffolds that were ethanol pre-treated (Figure 3.7A & B).

When cultured on plasma pre-treated scaffolds, the SW480 cells grew in a spread out distribution within the material (Figure 3.9D), whereas on ethanol pre-treated scaffolds the cell growth within the material tended to be found in clusters of densely packed cells (Figure 3.9C). Additionally the plasma pre-treatment produced a larger build-up of cells on the top surface of the material, which was a feature seen across the full length of the material.

Culturing the SW620 cells on plasma pre-treated scaffolds also lead to a difference in cell distribution after 7 days of growth. On ethanol pre-treated scaffolds, the cells were mostly confined to the upper half of the material and usually found as loosely associated collections of cells (Figure 3.9E). Plasma pre-treatment of scaffolds resulted in the SW620 cells adopting a distribution throughout the depth of the material, with more cells found as isolated cells within the material (Figure 3.9F).

3.3.4.2 Plasma pre-treatment increased the viability of SW480 cultures

The method of pre-treatment of the scaffolds also affected the viability of the resulting SW480 cultures, with cells grown on plasma pre-treated scaffolds displaying increased cell viability when compared to cells grown on ethanol pre-treated scaffolds (Figure 3.10A). In contrast there was no significant advantage to either scaffold pre-treatment method in the viability of SW620 cultures over the same time scale (Figure 3.10B).

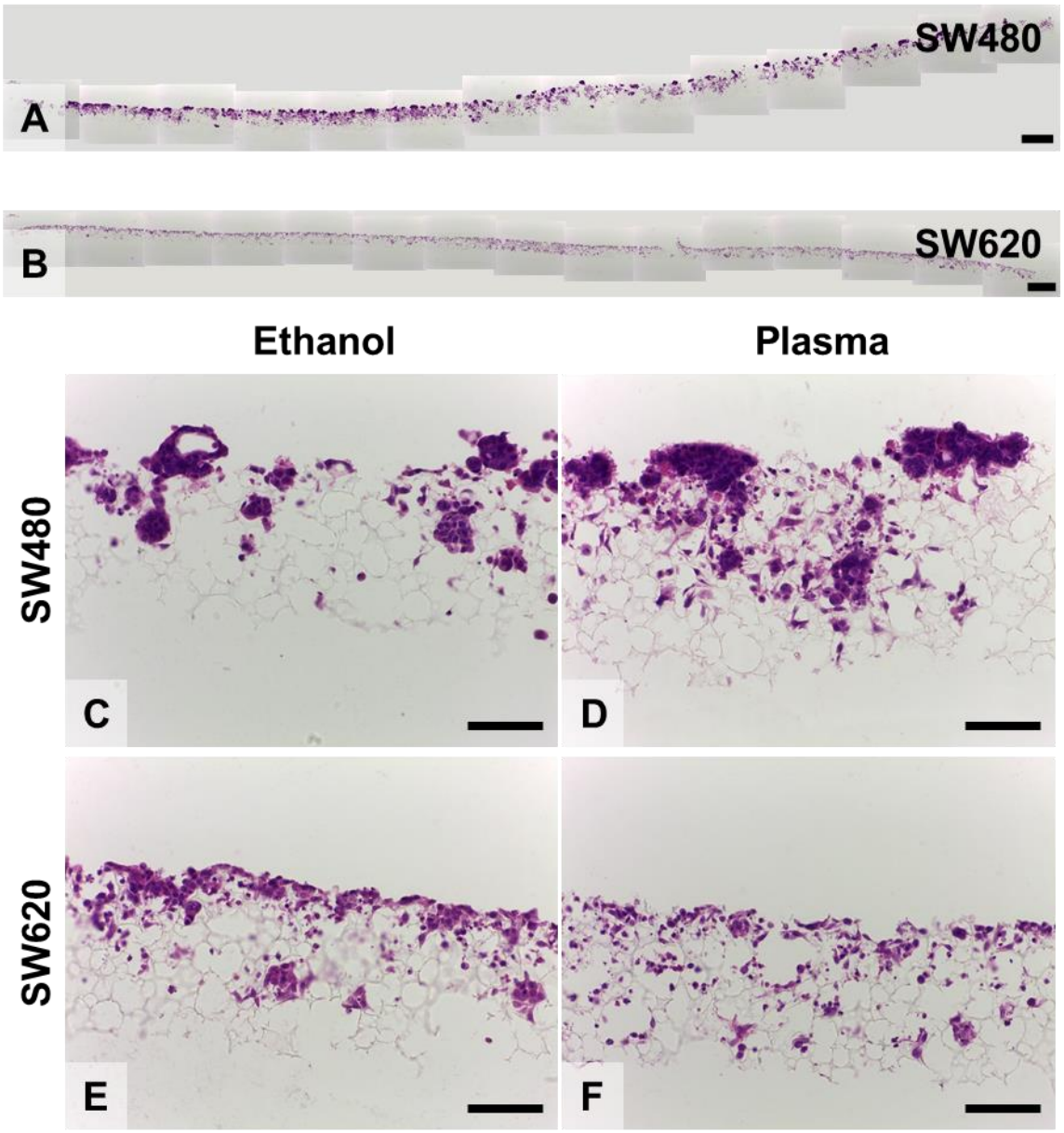

Figure 3.9: Both the SW480 and SW620 cell lines display deeper cell penetration when seeded on plasma pre-treated Alvetex® Scaffolds. H&E stained full scaffold images of plasma pre-treated scaffolds with A: SW480 and B: SW620 cells and high magnification images of scaffolds with C: SW480 on an ethanol pre-treated scaffold, D: SW480 on a plasma pre-treated scaffold, E: SW620 on an ethanol pre-treated scaffold and F: SW620 on a plasma pre-treated scaffold. Scale bars = 500µm for images A and B, 100µm for images C-F.

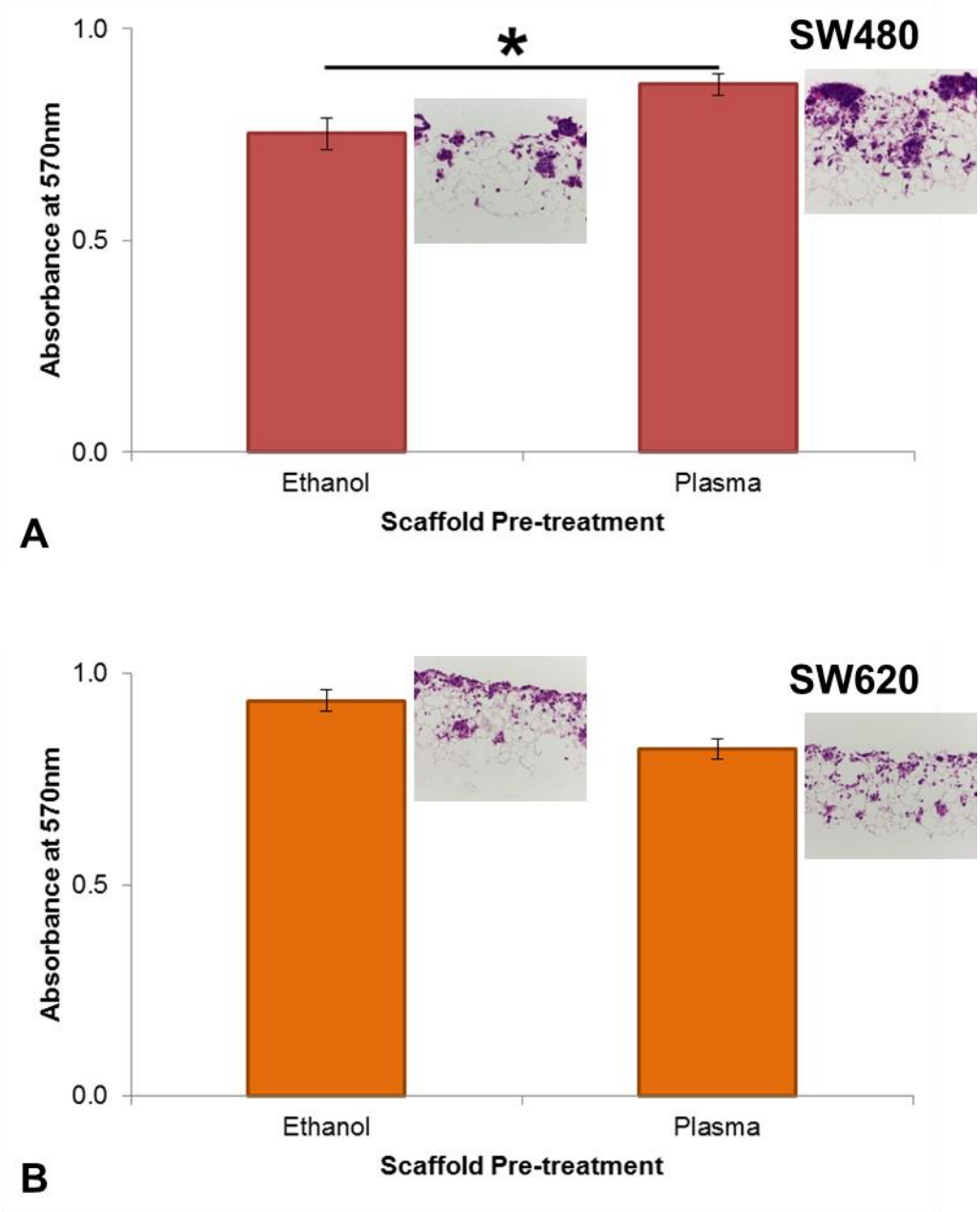

Figure 3.10: Plasma pre-treatment of Alvetex® Scaffold increases the viability of the SW480 cell line, but not the SW620 cell line, as compared to ethanol pre-treatment when 1 million cells were diffusely seeded scaffolds and cultured for 7 days. Absorbance at 570nm of A: SW480 and B: SW620 cells as determined by the MTT Cell Viability Assay. Data represent mean, n = 3, ±SEM for both graphs, * $p < 0.05$ by a Students t-test.

Collectively, these data show that the method of scaffold pre-treatment had a significant effect on the resulting 3D cultures of colorectal cancer cell lines. Plasma pre-treatment of scaffolds resulted in cultures which had cells distributed throughout a larger proportion of the material than those grown on ethanol pre-treated scaffolds. The cells were also more likely to be found as individual cells within the material when it has been plasma pre-treated, as compared to the clusters seen in ethanol pre-treated scaffolds. Taking into account this and the data showing that plasma pre-treatment of scaffolds had a slight increase in the cell viability of SW480 cultures without negatively impacting SW620 cultures, plasma pre-treatment of scaffolds will be employed for further 3D culturing experiments.

3.3.5 The presentation of the 3D culture does not significantly affect the cell growth

The presentation of the material within the well is another variable which has the potential to affect the behaviour of the 3D cultures. The format of Alvetex® Scaffold well insert employed so far during this investigation was the windowed insert where a 22mm diameter disc is held between the top and bottom halves of the well insert which subsequently sat inside the well of 6-well plates (Figure 2.1A). This design allows for the free exchange of media from on top of the material with media from underneath by passing through the three windows cut into the sides of the insert. This results in a more homogeneous media composition throughout the well [278] (Figure 2.1B).

A second style of insert for the 22mm disc format of Alvetex® Scaffold is the full-sided insert. This insert does not have the windows cut into the top half of the walls, resulting in a solid ring which surrounds the media on top of the material (Figure 2.1C). This full-sided insert segregates this reservoir of media from the media underneath/surrounding the material, meaning that any exchange of media occurs via movement through the Scaffold and any cells found in culture there, resulting in two reservoirs of media with varying media composition within the well [278] (Figure 2.1D).

It has been shown that while the amount of glucose and lactic acid in the media is consistent both above and below the windowed insert, the full-sided insert provides a barrier to media mixing between these compartments that results in an unequal distribution of lactic acid, with higher lactic acid concentrations seen in the media compartment above the scaffold [278]. This increased concentration of lactic acid when using the full-sided insert may prove beneficial to the culturing of cancer cells, as this may mimic the hypoxic interior of unvascularised tumours and induce a migratory response in the cancer cells in response to this environmental cue [72].

3.3.5.1 The use of the full-sided insert produced a more even distribution of SW480 cells

Alteration of the insert style when culturing the SW480 cell line produced a difference in the distribution of cells at the end of the culturing period, as the SW480 cells grew in a more even distribution across the width of the material when cultured used a full-sided insert (Figure 3.11A). In contrast, the overall distribution of the SW620 cell line across the width of the material did not alter when the style of well insert is changed (Figure 3.11B).

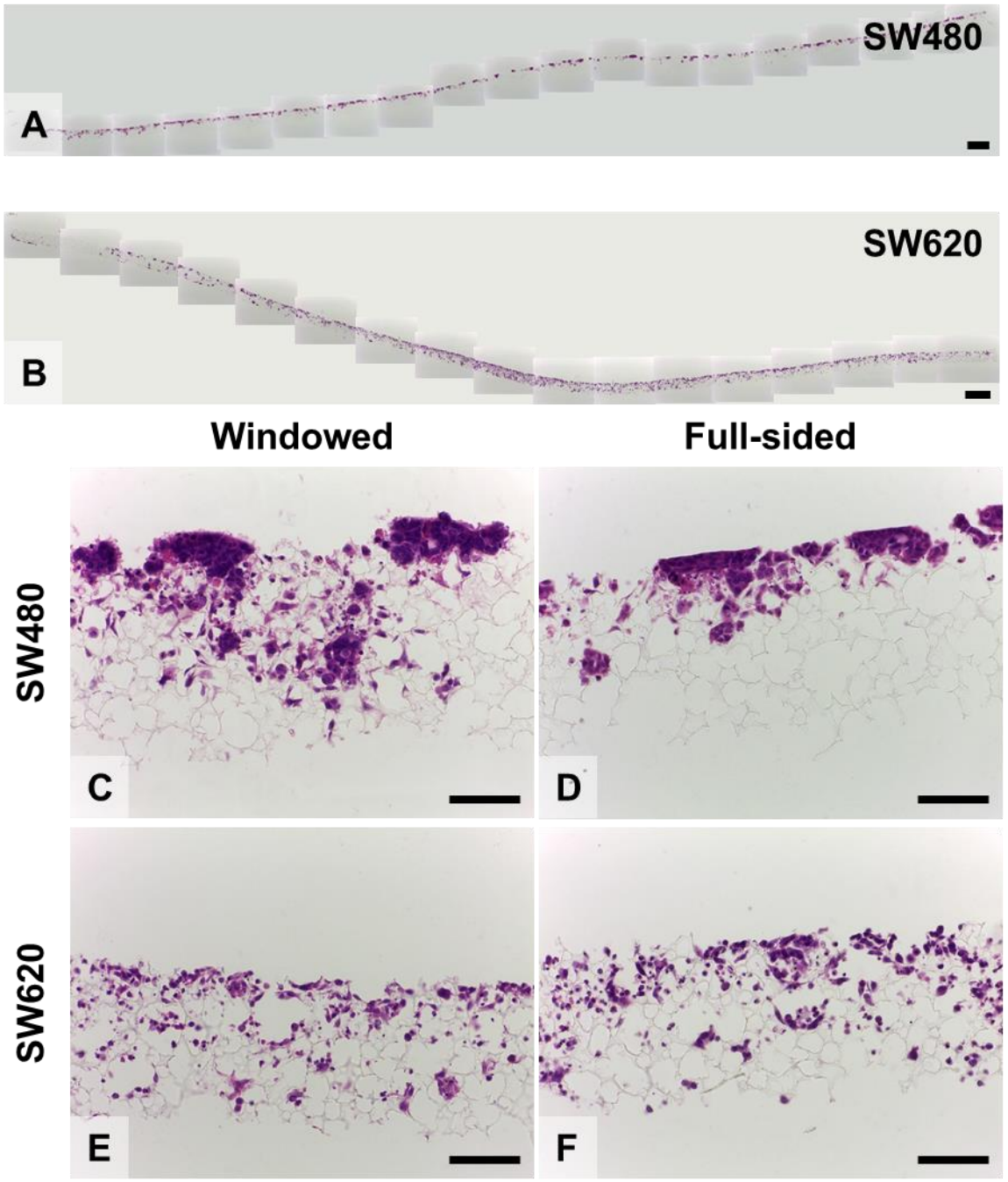

Figure 3.11: Both the SW480 and SW620 cell lines display similar distribution profiles when cultured on Alvetex® Scaffolds placed in full-sided inserts, when compared to culturing in the standard windowed insert. H&E stained full scaffolds cultured in a full-sided insert cultured with A: SW480 and B: SW620 cells and high magnification images of scaffolds with C: SW480 in a windowed insert, D: SW480 in a full-sided insert, E: SW620 in a windowed insert and F: SW620 in a full-sided insert. Scale bars = 500µm for images A and B, 100µm for images C-F.

When viewed at higher magnification, SW480 cells grown in a full-sided insert did not penetrate as far into the material as seen with the windowed insert, with the cell growth confined to the upper half of the material (Figure 3.11C & D). Additionally, the growth on top of the material was found to be more consistent across the culture, with fewer gaps between areas of cell growth and the cells growing at a similar thickness across the width of the material.

Such changes in cell behaviour are not seen with the SW620 cell line when the style of insert was altered. When cultured with either insert type, the SW620 cells were found to be distributed throughout the depth of the material, with a mixture of individual cells and cells growing in clusters with others (Figure 3.11E & F).

3.3.5.2 Cell viability was not affected by the well insert style

The alteration of the style of well insert did not have a significant effect on the viability of the 7 day 3D cultures of either the SW480 or SW620 cell lines (Figure 3.12). Whilst this was not unexpected with the SW620 due to the consistency of growth patterns when either insert type was used, the viability data suggested that the change in insert type only altered the growth pattern of the SW480 cells without diminishing their capacity to produce viable cultures.

These data show that the style of insert did not have a significant effect on the behaviour of SW620 cultures, but changed the distribution of the SW480 found both within and on top of the material. As the aim of this optimisation process is to produce cultures with a minimum of internal variation within the sample to allow for accurate data retrieval, the full-sided insert is selected over the windowed insert. The use of the full-sided inserts results in more consistent SW480 cultures, without a detrimental effect on the consistency of cell distribution in SW620 cultures.

3.3.6 Alvetex® Scaffold allows for more viable long term cultures than Alvetex® Strata

This optimisation process has resulted in a set of conditions for the experimental set up of 3D colorectal cancer cultures using Alvetex® Scaffold which result in consistent, viable cultures after 7 days of growth. The diffuse seeding of 1 million cells per plasma pre-treated scaffold housed in a full-sided insert provided conditions which are suited to short term culture of the SW480 and SW620 cell lines. This protocol will now been assessed for its suitability for the maintenance of long term cultures of both SW480 and SW620 cells on both Alvetex® Scaffold and Alvetex® Strata.

To facilitate this, the cultures will be maintained in deep-well petri dishes (Figure 2.2) instead of the 6-well plates previously used. This system allows for the culture of three well inserts in the same dish with 50ml of culture media shared between them. This provides better long term viability of cultures by allowing the cells access to a larger reservoir of nutrients, leading to less fluctuation in media composition over the culture period [218].

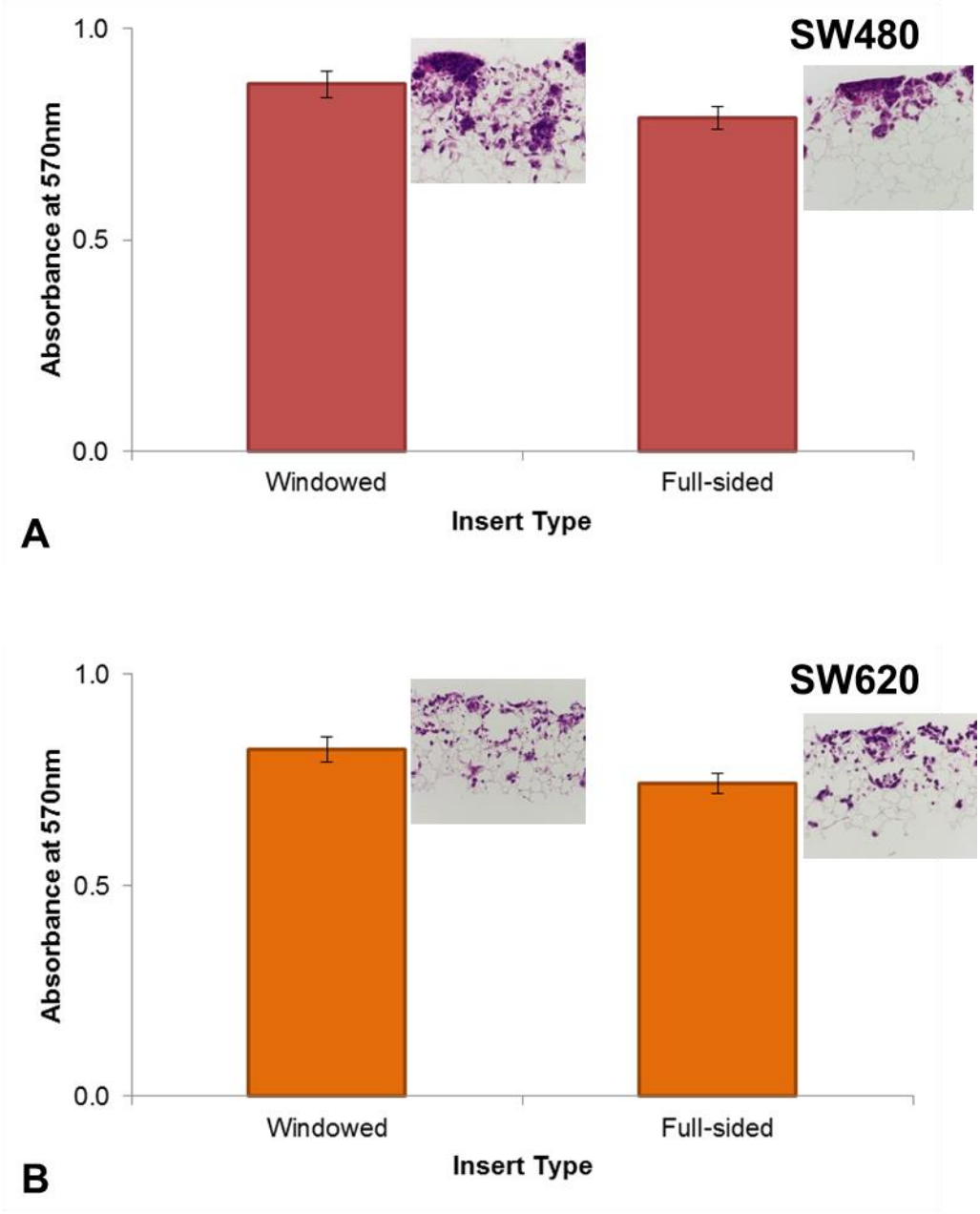

Figure 3.12: The viability of the SW480 and SW620 cell lines is not altered by the insert type for the presentation of Alvetex® Scaffold when 1 million cells were diffusely seeded onto plasma treated scaffolds and cultured for 7 days. Absorbance at 570nm of A: SW480 and B: SW620 cells as determined by the MTT Cell Viability Assay. Data represent mean, n = 3, ±SEM for both graphs, no significance by a Student's t-test.

3.3.6.1 The SW620 cell line penetrated Alvetex® Scaffold quicker than the SW480 cell line over 21 days

When the SW480 cell line is seeded onto Alvetex® Scaffold, it can be maintained in culture for up to 21 days (Figure 3.13). Over this time course, the cell growth began as sparsely distributed cells confined to the top half of the material for the first 7 days of culture (Figure 3.13B). Once this culture was established, the cells built up a thicker layer of growth on top of the material over the next 11 days, while maintaining their distribution within the top half of the material only (Figure 3.13E). It was only in the final days of this culture period that the cells then penetrated down into the material and were found to be distributed throughout the entire depth of the material (Figure 3.13F).

In contrast the SW620 cells line could not be maintained on Alvetex® Scaffold for the full 21 day culture period (Figure 3.14). As with the SW480 cells, the SW620 cells had a 7 day establishment period with cells found to be sparsely distributed throughout the depth of the material with no cell growth found at the surface (Figure 3.14B). However, after this establishment period, the cell growth expanded rapidly to fill the majority of the available space within the material by 11 days of culture (Figure 3.14C). This pattern of cell growth was then maintained for a further week (Figure 3.14E) before cell death, as seen by changes in cell morphology and a decreased cell density within the material, by day 21 (Figure 3.14F).

3.3.6.2 The viability of SW480 and SW620 cultures decreased after the first 11 days of culture on Alvetex® Scaffold

The differing behaviour of each cell line in terms of cell distribution within Alvetex® Scaffold is also reflected in the viability of each cell line over the culture period. The viability data for the SW480 cell line showed that there is a steady level of viability for the first 11 days of the culture period, followed by a small increase between 11 and 18 days before a crash in viability at 21 days (Figure 3.15A). In contrast, the SW620 cell line displayed a steady increase in the viability of the culture for the first 11 days, followed by a progressive decline after that until the end of the culture period (Figure 3.15B).

3.3.6.3 Long term cultures of SW480 and SW620 demonstrated increasing protein content

This viability data was not reflected in the amount of protein for long term cultures of either cell line on Alvetex® Scaffold. Both the SW480 and SW620 cells displayed a general trend of increasing protein content over the course of the culture period. The protein content of the SW480 cultures appeared to increase in staggered jumps, such as between 11 and 14 days, with a period where the level remains steady between jumps, such as between 7 and 11 days (Figure 3.16A). Whereas the increase in protein content in the SW620 cultures was more gradual over the full 21 day culture period (Figure 3.16B). Together this data would suggest that SW480 cells can be maintained in long term cultures on Alvetex® Scaffold for longer than the SW620 cell line without compromising the viability of the culture.

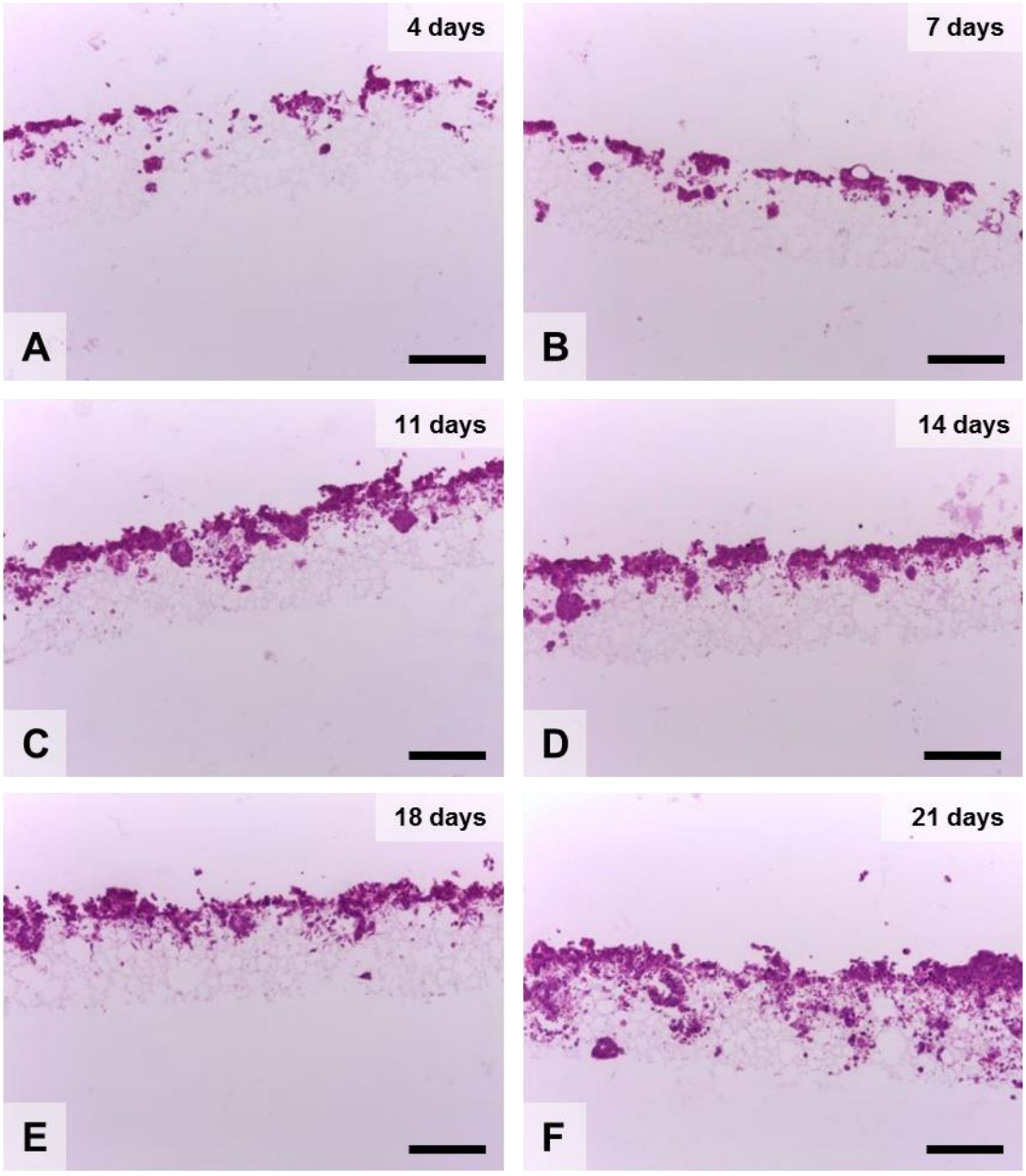

Figure 3.13: The SW480 cell line can be maintained in 3D culture on Alvetex® Scaffold for up to 21 days. The cell growth starts as a layer at the top surface of the material and penetrates the material as the cell growth builds up over the full 21 day culture period. H&E stained images of scaffolds which had been cultured for A: 4 days, B: 7 days, C: 11 days, D: 14 days, E: 18 days and F: 21 days. Scale bars = 200µm for all images.

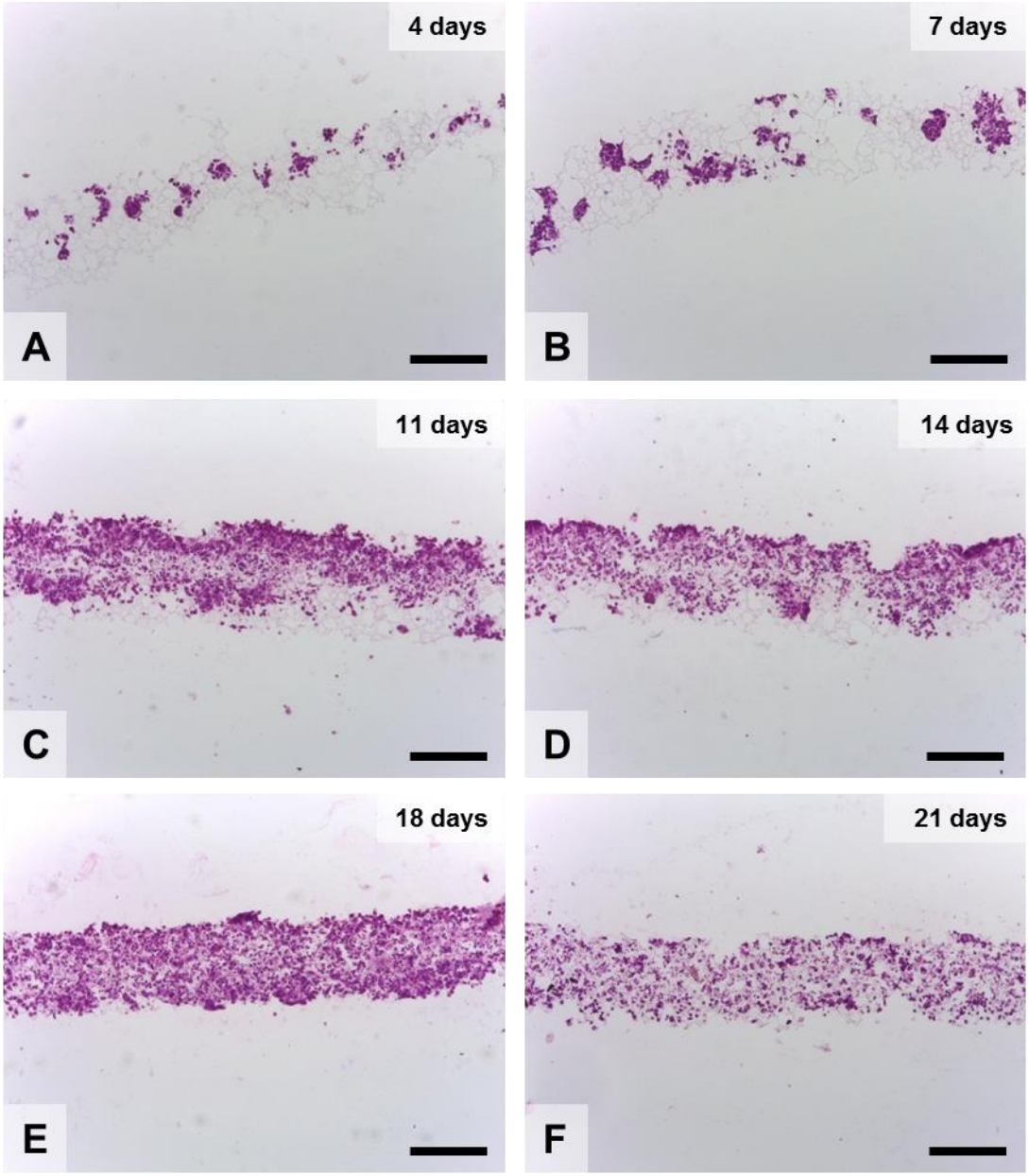

Figure 3.14: The SW620 cell line does overgrow when maintained in 3D culture on Alvetex® Scaffold for up to 21 days. Cells quickly penetrate into the material and the build-up of cells expands from these initial penetrating cells until 18 days culture, at which point the culture over grows the material as seen by the apparent cell death at 21 days culture. H&E stained images of scaffolds which had been cultured for A: 4 days, B: 7 days, C: 11 days, D: 14 days, E: 18 days and F: 21 days. Scale bars = 200µm for all images.

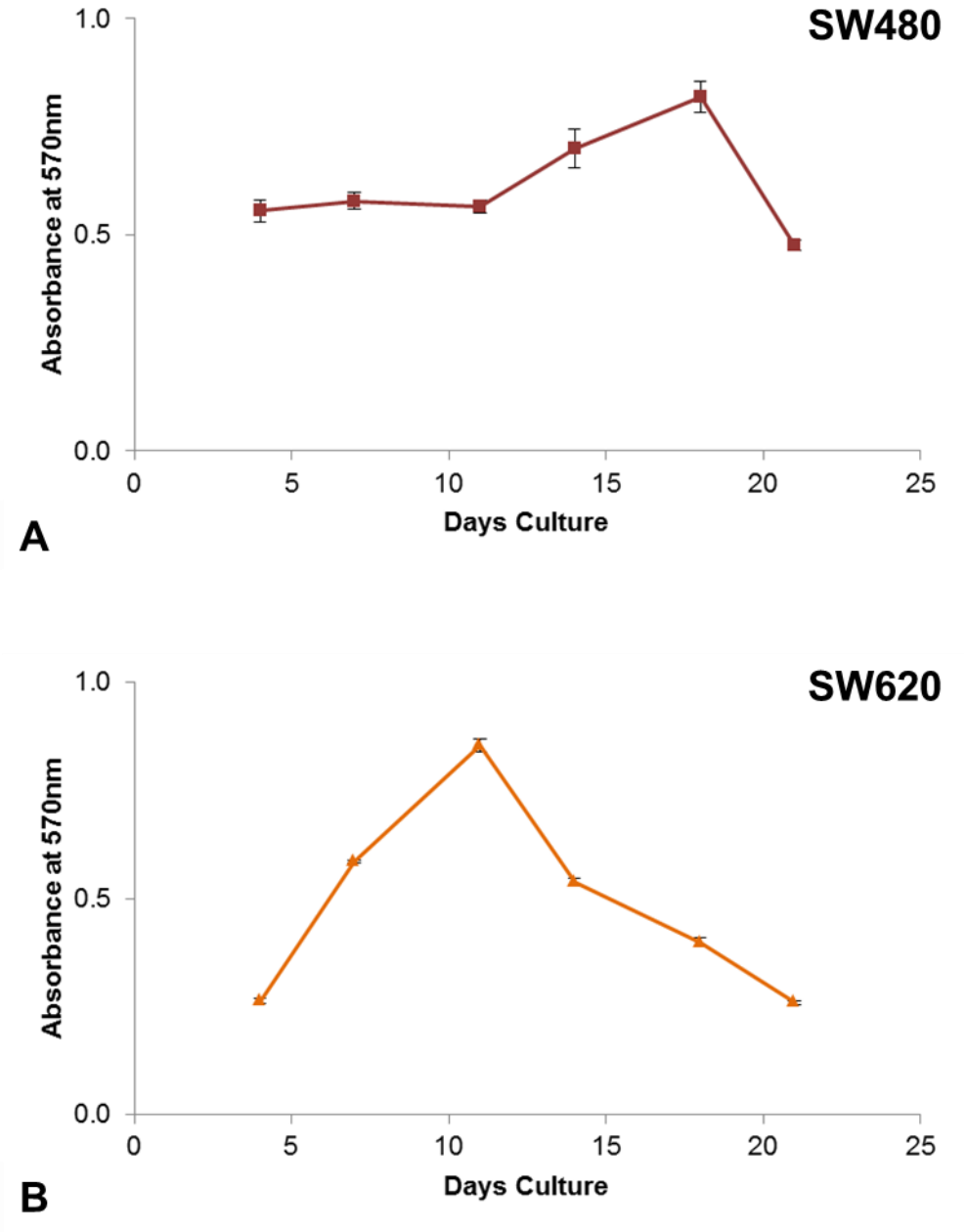

Figure 3.15: The SW480 and SW620 cell lines remain viable cultures for different culture periods when maintained on Alvetex® Scaffold for up to 21 days, with the SW480 cells remaining viable for up to 18 days, while the SW620 cells remain viable up to 11 days. Absorbance at 570nm of A: SW480 and B: SW620 cells as determined by the MTT Cell Viability Assay. Data represent mean, n = 3, ±SEM for both graphs.

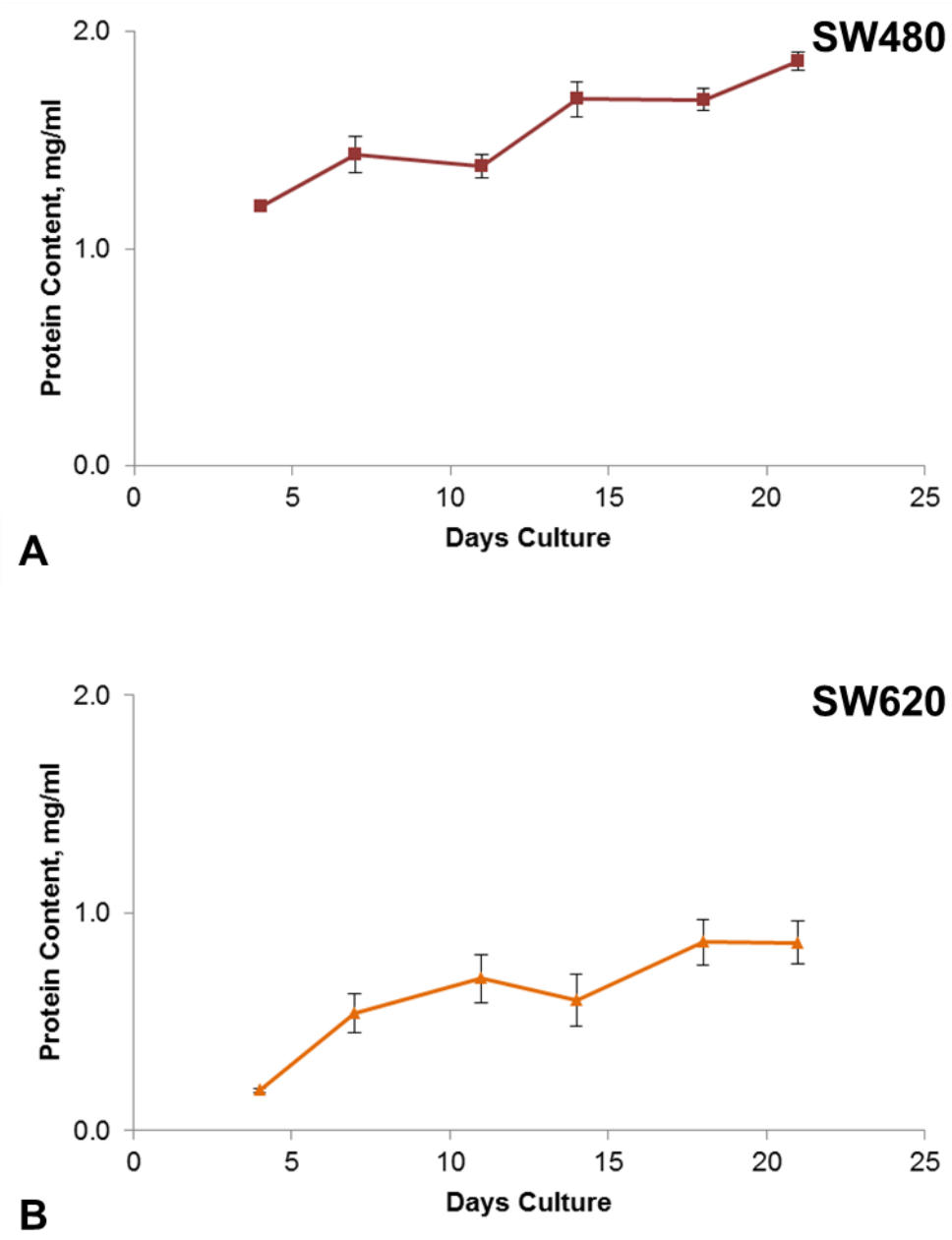

Figure 3.16: The SW480 and SW620 cell lines produce different amounts of proteins when maintained on Alvetex® Scaffold for up to 21 days, with both displaying a slight increase over the total culture period. Protein content in mg/ml of A: SW480 and B: SW620 cells as determined by the Bradford Assay. Data represent mean, n = 3, ±SEM for both graphs.

3.3.6.4 The distribution of SW480 and SW620 cells on Alvetex® Strata is limited compared to Alvetex® Scaffold

Long term culture on Alvetex® Strata was also investigated for only 14 days due to the observations in Alvetex® Scaffold suggesting a longer culture period would be detrimental to cell viability. The growth of SW480 cells on Alvetex® Strata resulted in a culture in which cells adopted a distribution that is distinct from cultures grown on Alvetex® Scaffold, as the cells did not penetrate into the material to the same extent (Figure 3.17). The density of cells found on the top surface of the material was established within the 4 days of culture (Figure 3.17A), with this level of cell growth maintained through to 7 days of culture (Figure 3.17B). It was only after the initial culturing period that SW480 cells began to move into the material, with the small amount of cell growth found within the material by day 14 confined to the upper quarter (Figure 3.17D). Throughout the culturing period, the cell growth on the top surface did not increase beyond the level seen by day 4, unlike the long term cultures on Alvetex® Scaffold (Figure 3.13).

Similarly, the SW620 cell line displayed an impaired ability to grow on Alvetex® Strata (Figure 3.18). Unlike cultures on Alvetex® Scaffold, SW620 cultures on Alvetex® Strata did not initially penetrate into the material and form a small layer of growth at the top surface (Figure 3.18A). Cells were seen to penetrate into the material by later time-points (Figure 3.18C); however, once again they were confined to the top quarter of the material. It also appeared that the cells found in the material by day 11 are cells which had migrated into the material as the build-up of cells inside the material was correlated with a loss of cell from the top surface of the material at day 7 (Figure 3.18B). By day 14 most of the cell growth both within and on top of the material had been lost (Figure 3.18D), suggesting an inability of Alvetex® Strata to maintain long term culture of the SW620 cell line.

3.3.6.5 Cultures on Alvetex® Strata demonstrated poor viability

Histological analysis reflected the data for both the viability and protein content of the cultures grown on Alvetex® Strata. Both the SW480 and SW620 cultures displayed a steady level of viability over the first 11 days of culture, with a drop by the end of the 14 day culturing period (Figure 3.19). This viability data was also more variable that the viability data from cultures grown on Alvetex® Scaffold, as viewed by comparing the error bars with Figure 3.15, suggesting that culture on Alvetex® Strata did not produce consistent samples at any time-point in culture.

3.3.6.6 Cultures on Alvetex® Strata had a lower protein content than those on Alvetex® Scaffold

Similarly, the protein content data for Alvetex® Strata cultures differed from the data for Alvetex® Scaffold cultures. The protein content of the SW480 cultures on Alvetex® Strata was seen to decline over the 14 day culture period (Figure 3.20A), while the protein content of the SW620 cultures on Alvetex® Strata was found not to vary across all time-points (Figure 3.20B). For both cell lines, the amount of protein found in the Alvetex® Strata cultures was at a much lower level than found in the Alvetex® Scaffold cultures.

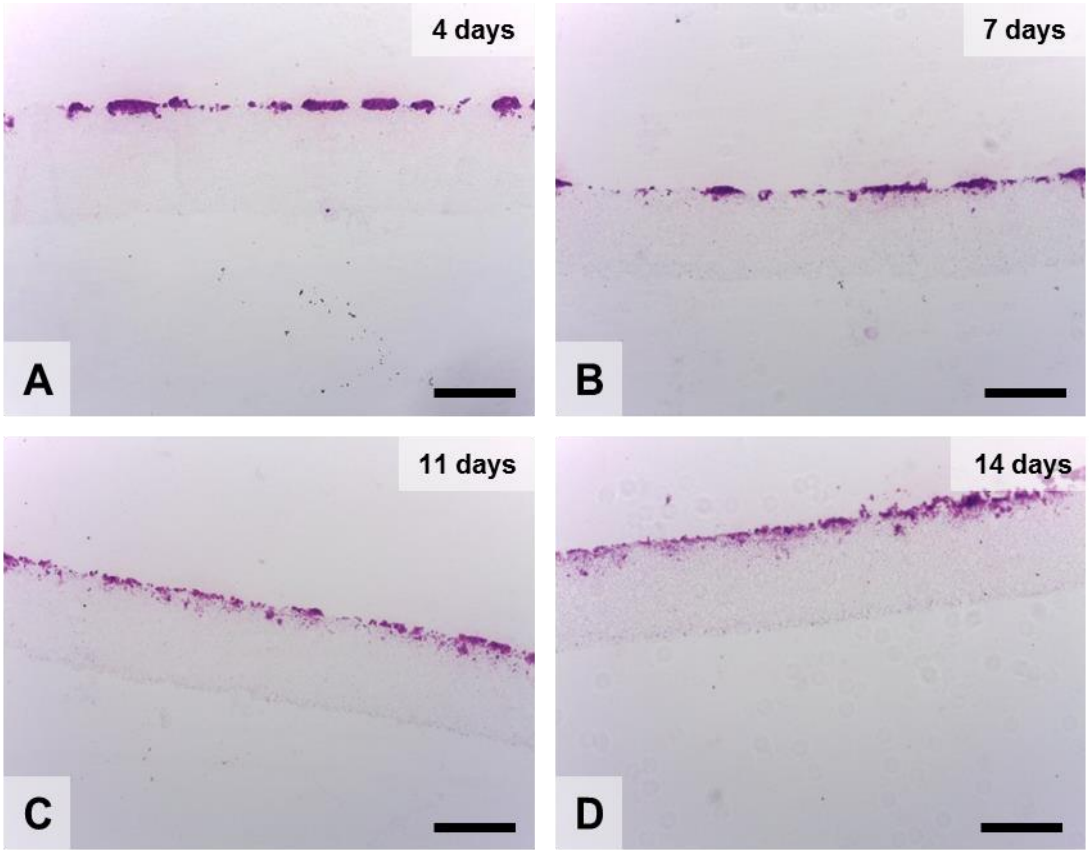

Figure 3.17: The SW480 cell line can be maintained in 3D culture on the top layer of Alvetex® Strata for up to 14 days with fewer cells visible than seen when cultured on Alvetex® Scaffold. Cells maintain a layer of growth on top of the material with little penetration into the material over the culture period. H&E stained images of scaffolds which had been cultured for A: 4 days, B: 7 days, C: 11 days and D: 14 days. Scale bars = 200µm for all images.

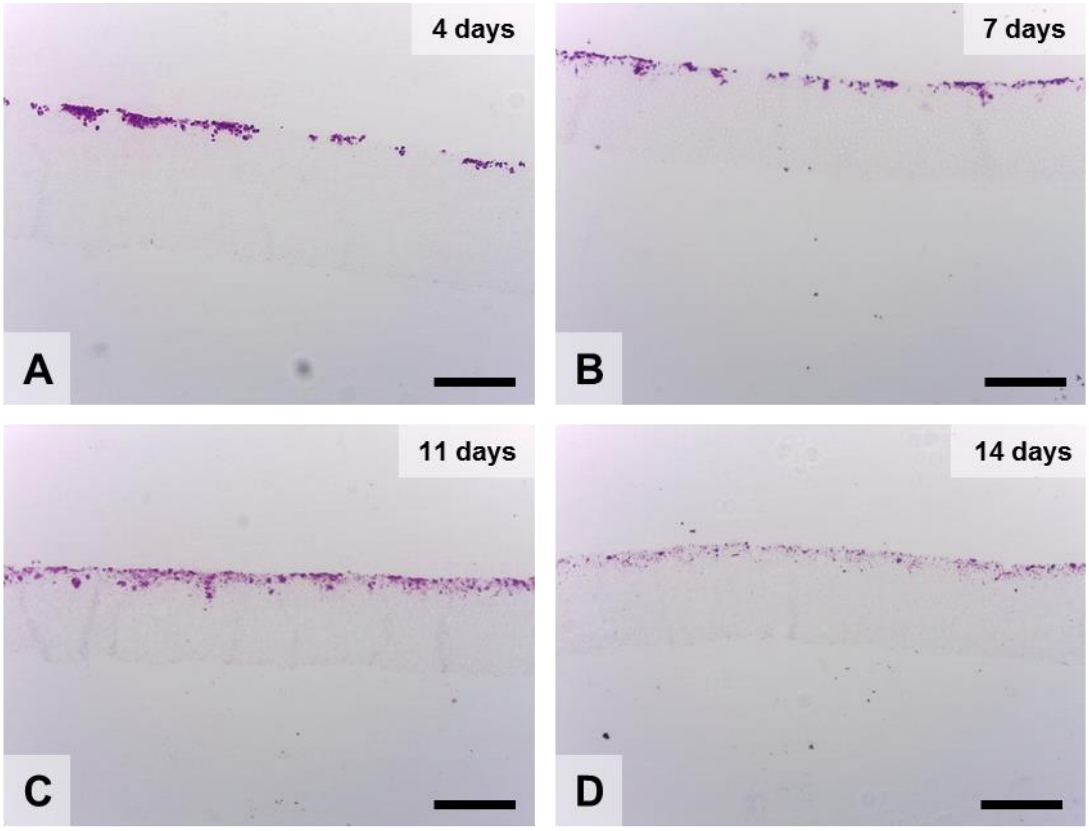

Figure 3.18: The SW620 cell line shows a poor ability to be maintained in 3D culture on the top layer of Alvetex® Strata for up to 14 days. The initial cell attachment to the top surface of the material is lost over the culture period, with few cells penetrating the material. H&E stained images of scaffolds which had been cultured for A: 4 days, B: 7 days, C: 11 days and D: 14 days. Scale bars = 200µm for all images.

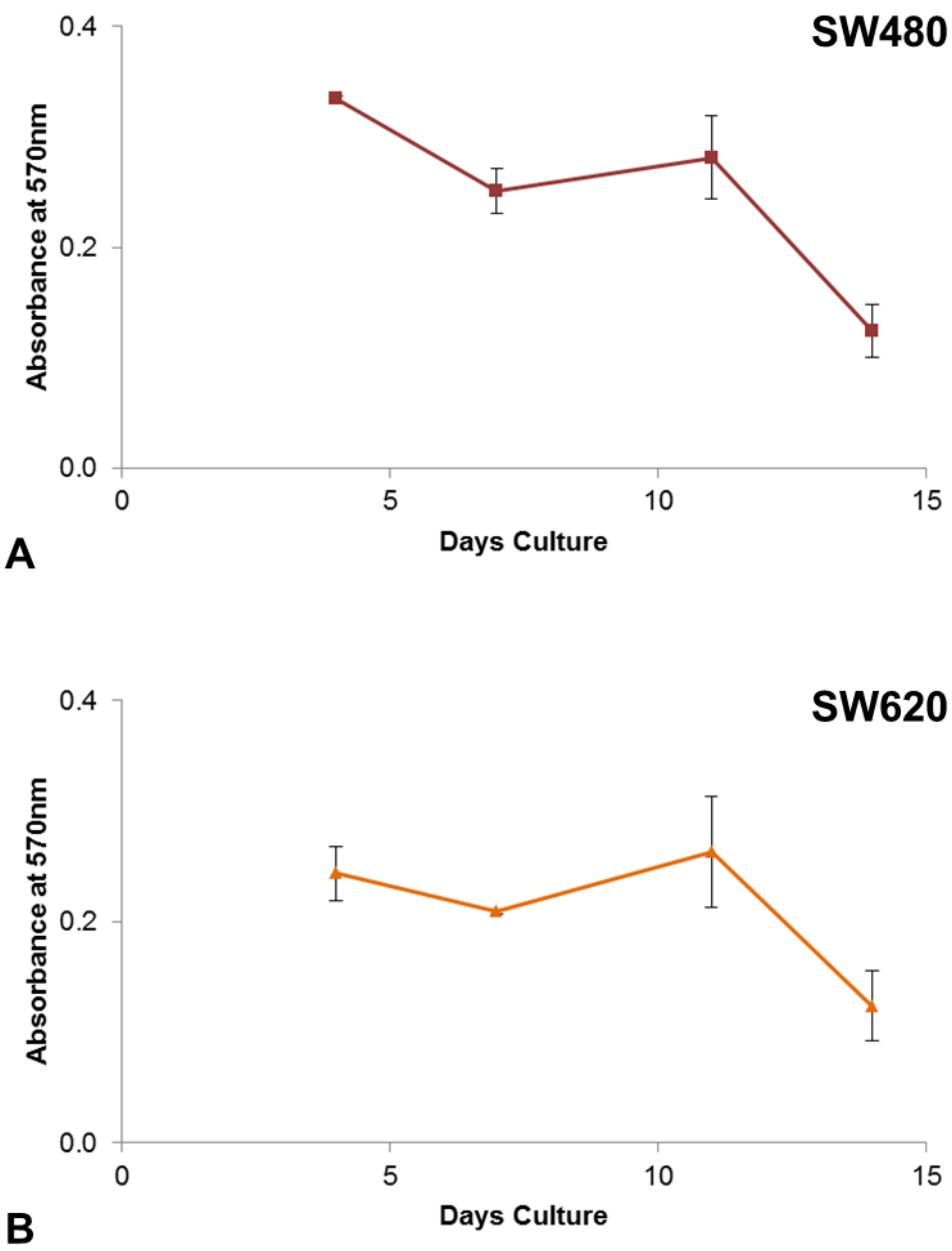

Figure 3.19: Low levels of cell viability of cells cultured on Alvetex® Strata for up to 14 days reflects the low low amount of cell growth build up for both the SW480 and SW620 cell lines. Absorbance at 570nm of A: SW480 and B: SW620 cells as determined by the MTT Cell Viability Assay. Data represent mean, n = 3, ±SEM for both graphs.

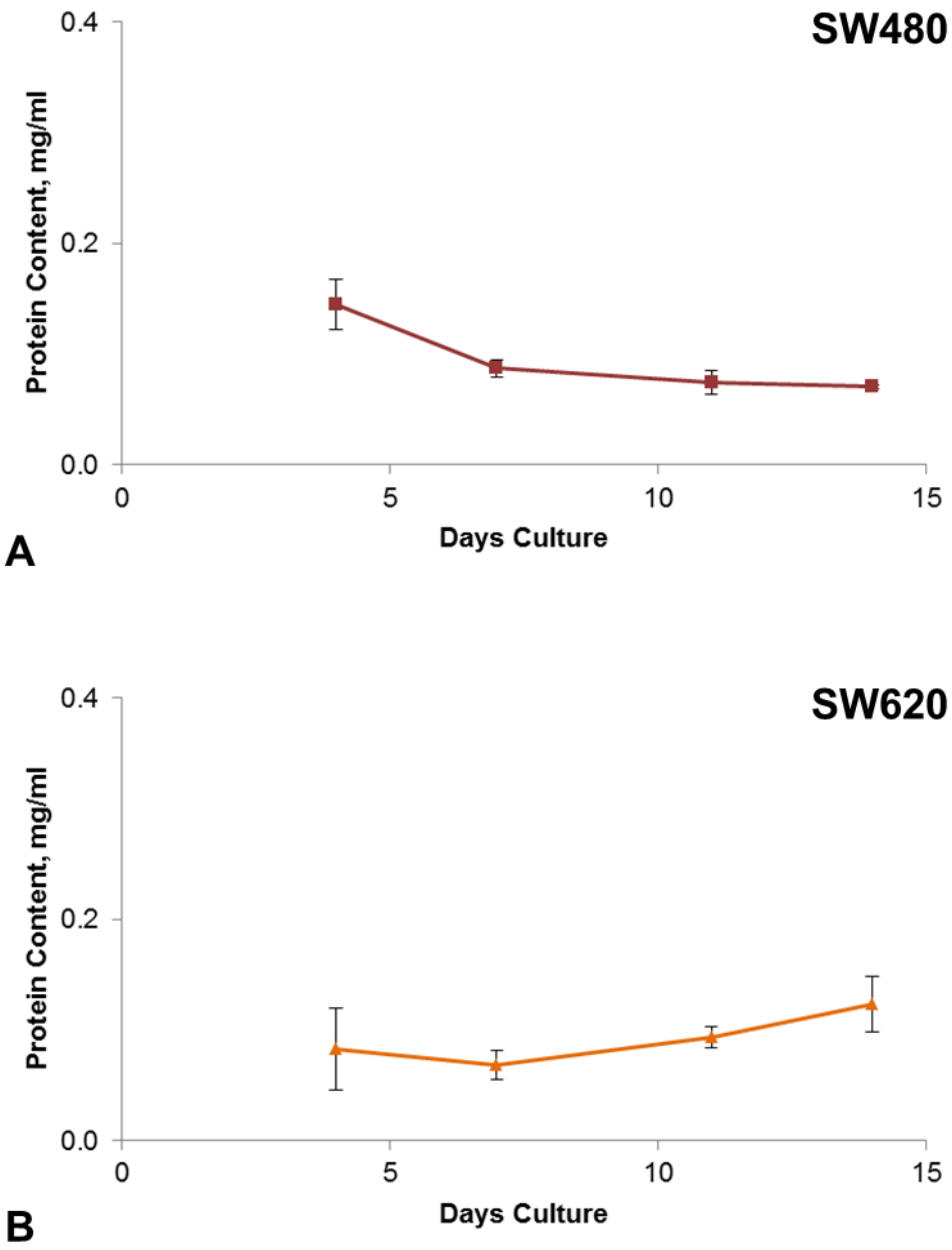

Figure 3.20: Low levels of protein extracted from cells on Alvetex® Strata for up to 14 days reflects the low amount of cell growth build up for both the SW480 and SW620 cell lines. Protein content in mg/ml of A: SW480 and B: SW620 cells as determined by the Bradford Assay. Data represent mean, n = 3, ±SEM for both graphs.

Collectively, this data suggests that Alvetex® Scaffold is a better choice of material for long term culture of both the SW480 and SW620 colorectal cancer cell lines as it could support the growth of cells at a high density before there was a decrease in their viability. This is not without limitations, as each cell line reaches a point of declining cell viability at different timepoints throughout the growth period. In comparison, Alvetex® Strata did not appear to provide either cell line with a growth environment which encourages the maintenance or expansion of cultures, even at the shortest timepoint investigated.

3.3.7 Culturing colorectal cancer cells in 3D changes the expression of E-cadherin

The data presented so far has demonstrated that there were differences in the cell distribution profile of each cell line in 3D cultures on Alvetex® Scaffold; furthermore this distribution altered over extended culture periods. Protein lysates from 2D and 3D cultures of both cell lines were compared to investigate if this difference in cell distribution and cell density had an effect on the protein expression profile of these cells. To assess this, the expression of E-cadherin and vimentin were examined as the expression of these key proteins can be used to identify which cells have undergone EMT [79] and have developed a more migratory phenotype via the alteration of a wide range of proteins [80].

Immunostaining of 2D and 3D SW480 and SW620 cultures for E-cadherin showed clear differences between the two cell lines, in addition to variation due to the cell density (Figure 3.21A). E-cadherin expression in the SW480 cell line appeared to be dependent of the culture conditions, with staining seen in both 2D cultures and in the more densely packed 3D culture (Figure 3.21A). This was reflected in the Western blot analysis, where a band was found at 110kDa in both of the samples taken from moderately and densely packed 2D monolayer cultures (Figure 3.21B, lanes 1 & 2). In the 3D cultures, the band was found to be absent in 7 day cultures (Figure 3.21B, lane 3) where the cells were sparsely packed into the scaffold (Figure 3.13B) with the band present in the sample taken from 11 day cultures (Figure 3.21B, lane 4) where the cells were more densely packed at the top surface of the scaffold (Figure 3.13C).

In contrast, the SW620 cell line did not appear to express E-cadherin at any of the cell densities investigated in either 2D or 3D cultures when analysed by both immunostaining (Figure 3.21A) and Western blots (Figure 3.21B, lanes 5, 6, 7 & 8). This corresponds to cells which have undergone EMT during metastatic tumour progression and have lost any E-cadherin expression that the original tumour had.

Additional immunostaining analysis was carried out to determine the expression of vimentin in the 2D and 3D cultures of these cell lines. Both the SW480 and SW620 cell lines were seen to express vimentin regardless of the density or dimensionality of the *in vitro* culture conditions (Figure 3.21A). Together this shows that the expressional behaviour of certain proteins in certain cell lines, such as E-cadherin in the SW480 cell line, may be altered by the dimensionality of the culture environment.

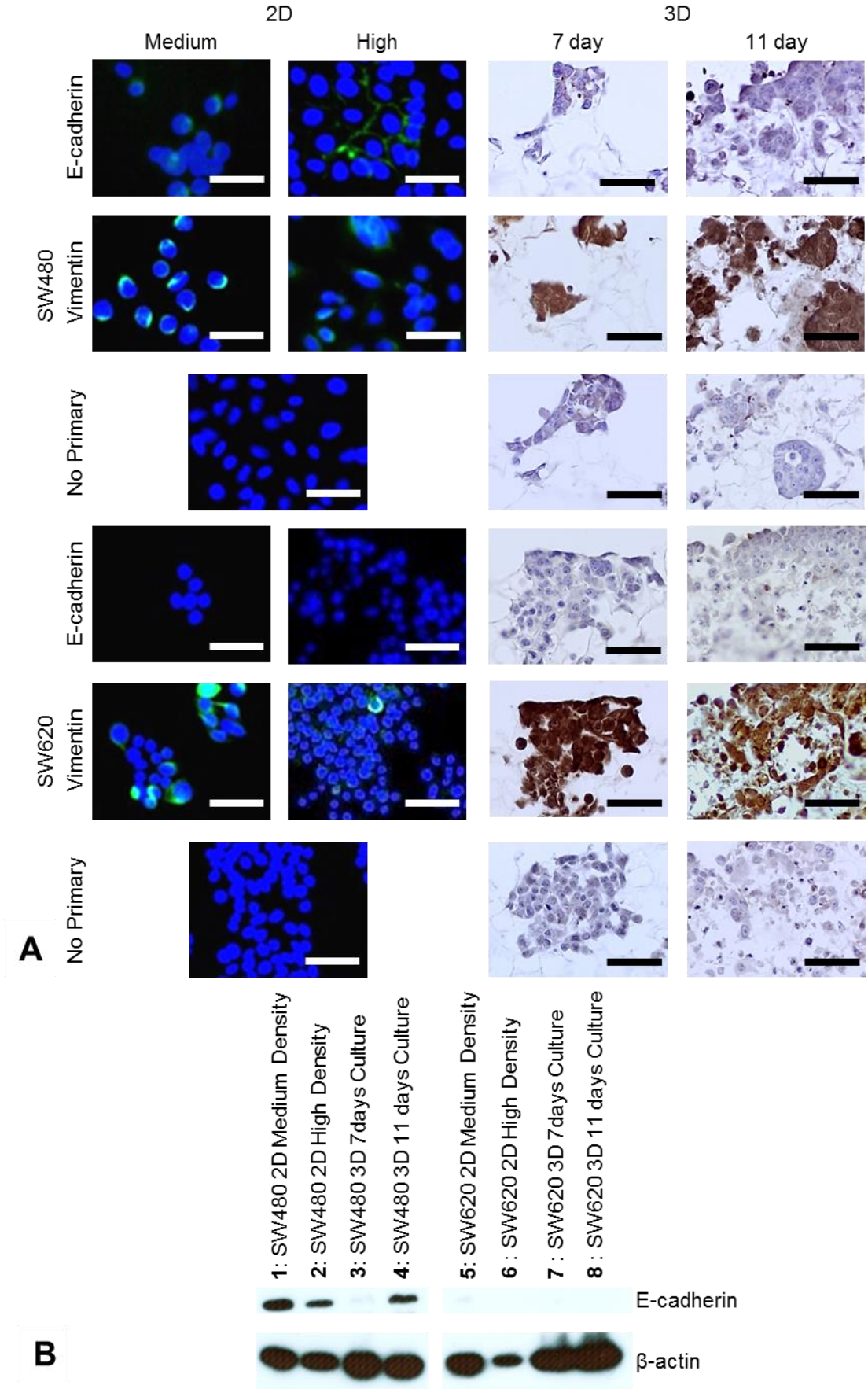

Figure 3.21: The conditions of cell culture alter the expression levels of E-cadherin but not vimentin in SW480 and SW620 cells. A: Immunocytochemical and immunohistochemical staining for E-cadherin and vimentin in 2D and 3D cultures of SW480 and SW620 cells, demonstrating the absence of E-cadherin expression in the SW620 cell line and in the lower density 3D SW480 cultures. B: Western blot analysis of E-cadherin expression in SW480 cells grown in 2D at lane 1: medium and lane 2: high density and in 3D for lane 3: 7 days and lane 4: 11 days and SW620 cells grown in 2D at lane 5: medium and lane 6: high density and in 3D for G: lane 7 days and lane 8: 11 days. Scale bar = 50μm for all images.

3.3.8 Long term culture on Alvetex ® Scaffold provides the basis for a 3D cell migration assay

As the aim of this Chapter is to generate and optimise a 3D migration assay for the assessment of the impact of signalling events and culture microenvironment on the behaviour of colorectal cancer cells, the migratory behaviour of both the SW480 and SW620 cell lines on both Alvetex® Scaffold and Alvetex® Strata were assessed to establish the most appropriate time point to use for the assessment of this behaviour.

Two methods of analysing the level of cell penetration into the material will be compared to determine which provides the most accurate results for use in a migration assay. Each method utilises the histological images taken from processed samples from each time-point of the culturing period (Figure 2.5A). The images used for analysis were the 10 consecutive images encompassing the central portion of the material; this ensures that the analysis was not skewed by the areas of lower cell density found towards the edge of the material.

The first method of analysis, the 'linear' method, samples the depth of penetration at 3 points on each image by taking straight line measurements from the top surface of the material perpendicularly downwards to the greatest depth of penetration at that point (blue arrows, Figure 2.5B). An alternative method was also assessed and is referred to as the 'area' method. This method takes the area of the material filled with cell growth (green dashed line, Figure 2.5C) as a percentage of the total area of the material (black dotted line, Figure 2.5C). When the cell penetration of the Alvetex® Scaffold and Alvetex® Strata cultures with both cell lines were assessed using the two methods, both methods produced results with similar trends, which reflected the histological images seen in Figure 3.13, Figure 3.14, Figure 3.17 and Figure 3.18.

3.3.8.1 The SW620 cell line penetrated further into Alvetex® Scaffold than the SW480 cell line over 14 days

When the SW480 cultures on Alvetex® Scaffold are assessed by the linear method, the cell penetration was seen to peak at 88µm by 11 days into the culturing period (Figure 3.22A), however assessment by the area method showed a maximal penetration of 22%, equivalent to 44µm, by the same time-point (Figure 3.22B). This reflected the distribution of cells as seen at the relevant time-point images in Figure 3.13, as the amount of cells visible within the material increased between 7 and 11 days, without filling the whole of the material.

Similar trends in data generated by each method are seen when the SW620 cells were cultured on Alvetex® Scaffold. The area method detected a lower level of cell penetration than the linear method for the same data set. Assessment via the linear method of these cultures showed a continual increase in the level of cell penetration which peaks at 185µm by 14 days (Figure 3.22C), whereas the area method put the maximal penetration at 70%, equivalent to 140µm, with a smaller increase in penetration seen between days 11 and 14 (Figure 3.22D). Again, this was a good reflection of the histological images presented in Figure 3.14, with the amount of cell growth found within the material shown to increase over the culturing period to 14 days.

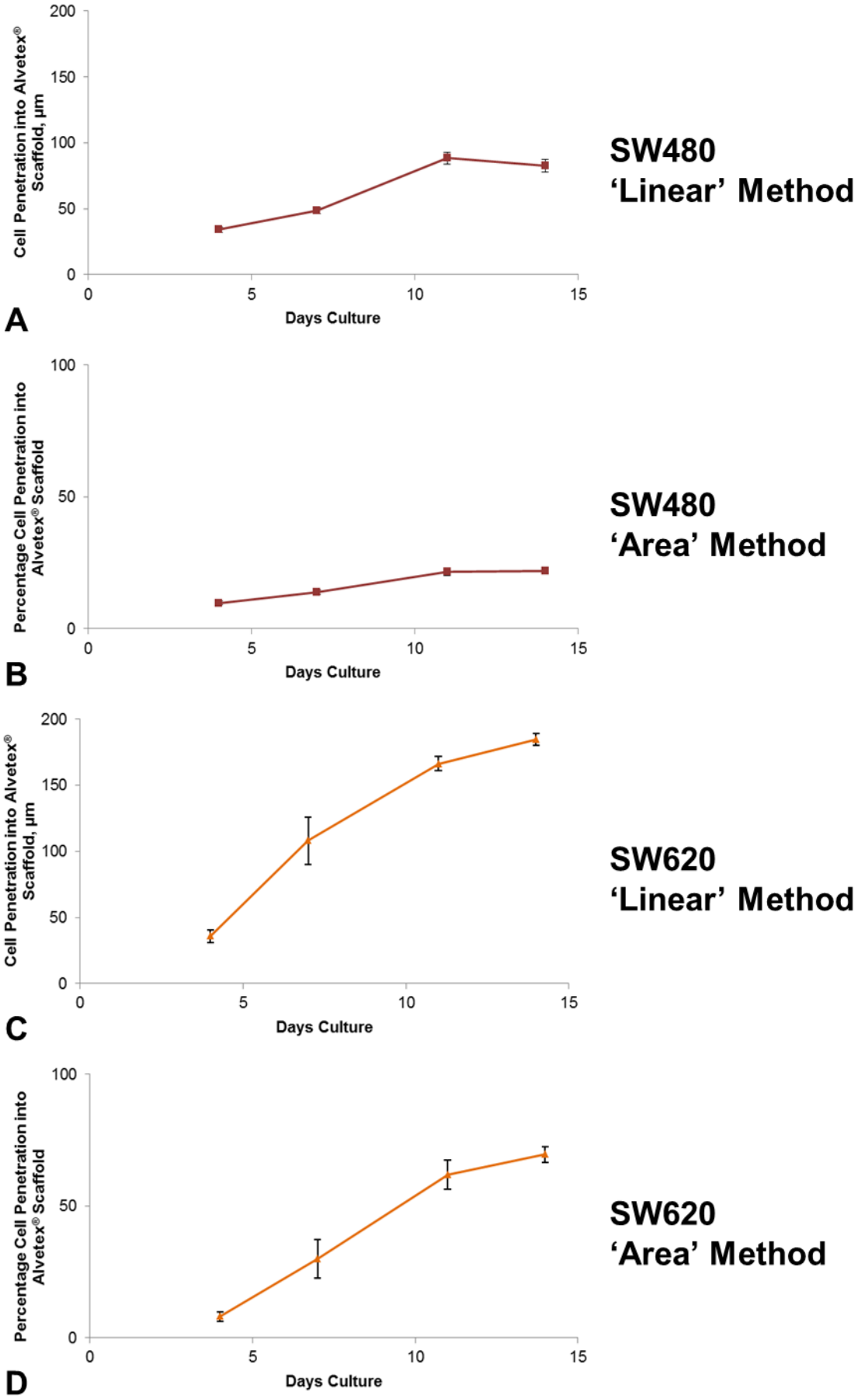

Figure 3.22: 3D culture of cells on Alvetex® Scaffold for up to 14 days demonstrates a difference in cell penetration ability between the SW480 and SW620 cell lines, with the SW620 cells achieving a greater penetration over the culture period. Cell penetration of A and B: SW480 and C and D: SW620 cells as determined by the linear method, expressed in µm, and by the area method, expressed as percentage, respectively. Data represent mean, n = 3, ±SEM for all graphs.

3.3.8.2 Both the SW480 and SW620 cell lines demonstrated impaired penetration into Alvetex® Strata

The results from the Alvetex® Strata cultures show that the two cell lines exhibited different migratory behaviours on this material. Linear assessment of the SW480 cultures showed a gradual increase in cell penetration over the full 14 days of the culturing period with it peaking at 51µm (Figure 3.23A). Use of the area method did not show an increase in penetration over the 14 day culturing, with it remaining at 6%, equivalent to 12µm, throughout (Figure 3.23B). With these assessments, it was the cell penetration detected by the linear method that best reflects the histological data as presented in Figure 3.17, as these images showed a gradual movement of cells into the upmost part of the material.

The penetration of the SW620 cell line into Alvetex® Strata was also found to be at a much lower level than the penetration seen into Alvetex® Scaffold. A gradual increase in penetration was detected by both the linear and area methods, although again the area method detected a lower level. The linear method detected a maximum penetration of 55µm at 14 days (Figure 3.23C), while the area method only placed the maximum penetration at 18%, equivalent to 36µm (Figure 3.23D). These numbers again reflected the histological data seen in Figure 3.18, with only a small amount of cell penetration seen by the end of the culture period.

From these assessments of cell penetration, the linear method produced results which appear to be a more accurate reflection of the cell distribution seen in the corresponding histological images. This main reason for this seems to be that the area method tended to under estimate the level of cell penetration within a sample as it works on the assumption that the cells migrate down through the material as a solid block, whereas it was clearly seen in the histological data presented throughout this Chapter that it is not the case with the two cell lines assessed here.

Additionally, due to the increased amount of user input required to obtain results using the area method over using the linear method, the potential for introducing errors into the data obtained was greatly increased when using the area method and may lead to incorrect conclusion being drawn from the data. Therefore, for the assessment of cell penetration in the migration assay, the linear method will be used as it is more sensitive to small alterations in cell penetration that the area method does not detect.

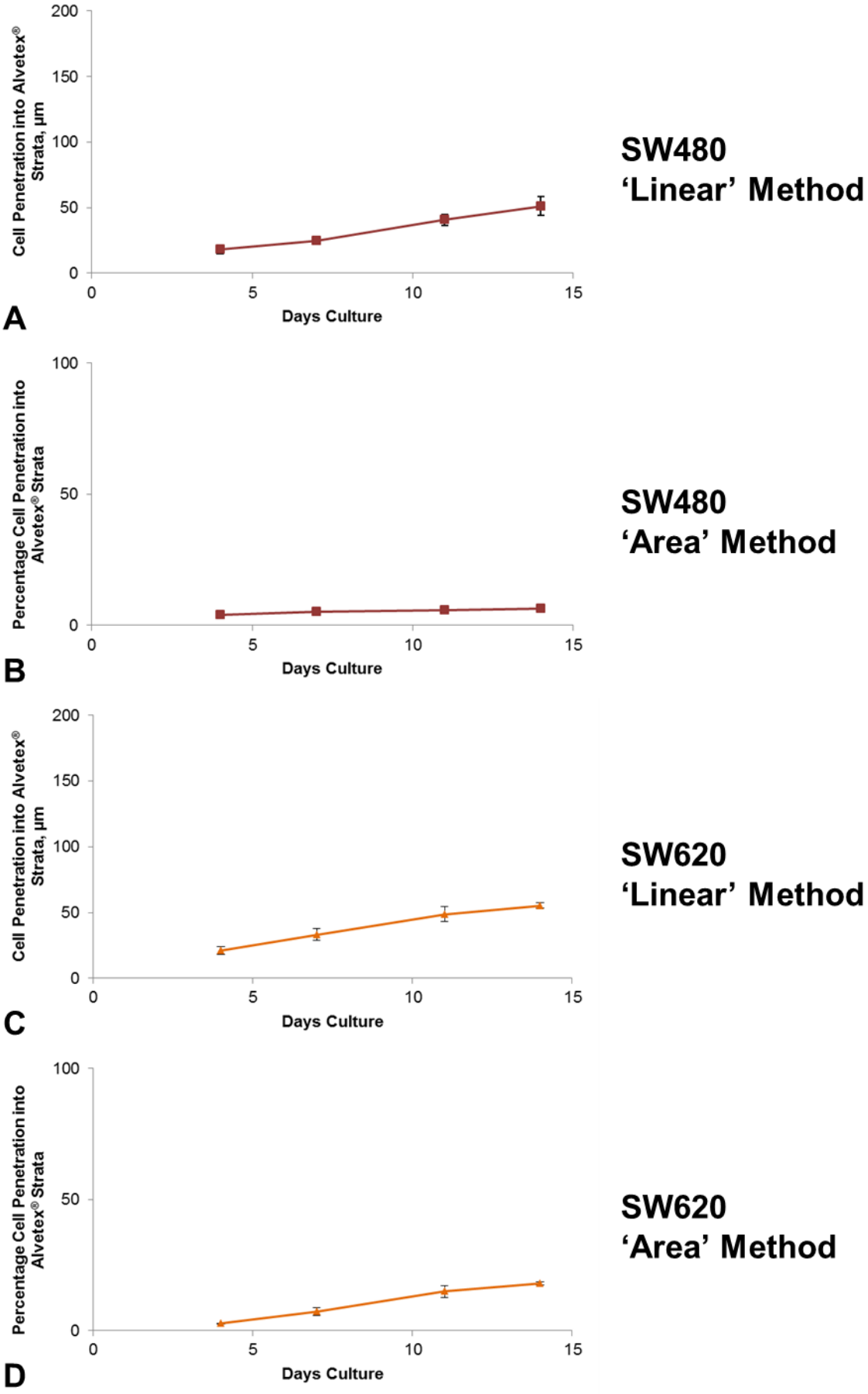

Figure 3.23: 3D culture of cells on Alvetex® Strata for up to 14 days limits the amount of cell penetration for both the SW480 and SW620 cell lines. Cell penetration of A and B: SW480 and C and D: SW620 cells as determined by the linear method, expressed in µm, and by the area method, expressed as percentage, respectively. Data represent mean, n = 3, ±SEM for all graphs.

3.4 Discussion

This Chapter has sought to assess the suitability of a 3D cell culture system, Alvetex®, for use in a 3D cell migration assay for colorectal cancer. This system was selected as there is currently a lack of synthetic scaffold based 3D migration assays and it has already been shown to support a wide variety of cell lines [232, 260-263]. The optimisation process examined the outcome of altering different aspects of the preparation of the cultures on the cell distribution, as assessed from histologically processed samples, and cell viability, as assessed using the MTT Cell Viability Assay. The outcomes of the four areas examined, namely seeding method, scaffold pre-treatment, well insert format and Alvetex® format, are summarised in Table 3.1.

Area of Optimisation	Selected Outcome	Effect on 3D Cultures
Seeding Method	Diffuse Seeding	− Cell distribution more even when diffuse seeding was used, for both SW480 and SW620 cell line − Increased viability of SW620 cultures when diffuse seeding was used
Scaffold Pre-treatment	Plasma Pre-treatment	− Cell distribution was less clustered on plasma pre-treated scaffolds, for both SW480 and SW620 cell lines − Increased viability of SW480 cultures when plasma pre-treatment was used
Well Insert Format	Full-sided Insert	− Cell distribution of SW480 cells was more even when the full-sided insert was used − No effect on cell viability of either the SW480 or SW620 cell lines when the full-sided insert was used − Media quality is unequal between media on top of and media below the insert, which may mimic the poor nutrient conditions seen in tumours
Alvetex® Format	Alvetex® Scaffold	− Better cell adhesion to Alvetex® Scaffold than Alvetex® Strata, for both SW480 and SW620 cell lines − Increased cell viability and protein production on Alvetex® Scaffold than Alvetex® Strata, for both SW480 and SW620 cell lines

Table 3.1: Summary of the outcomes of protocol optimisation for growing SW480 and SW620 cells on Alvetex®.

Work carried out here has demonstrated that the standard method of pre-treatment, ethanol wetting, is sufficient to allow cultures of the SW480 and SW620 cell lines to grow in 3D, as has previously been demonstrated for a variety of other cell lines [232, 260-263]. However the data from plasma pre-treated samples demonstrates that this is also sufficient for cultures to be maintained on Alvetex®. Using side-by-side comparisons of cultures grown on ethanol and plasma pre-treated material (Figure 3.9 and Figure 3.10); it is shown that the plasma pre-treated membranes provided the opportunity for a more consistent growth profile in the resulting cultures. As more consistent cultures would remove internal variation in the cell distribution within the material and would provide the homogeneous environment throughout the culture, this would lead to less variation in the protein expression [223], in turn the migratory behaviour of the cells will be more consistent, leading to more reliable penetration data.

The two methods of cell seeding, concentrated and diffuse, were equally effective at introducing the cell lines to the material and both led to successful cultures. The choice of static seeding methods minimises damage to both cells and the substrate that can be seen in dynamically seeded cultures by introducing excessive forces to the system [214]. The other advantage of investigating these methods is that they do not require specialist equipment to carry out the protocol and are relatively quick to complete. The alteration in seeding method had a large effect on the SW480 cell line by eliminating the thick layer of cell growth seen on top of the material (Figure 3.7C & D) without having a negative effect on the overall viability of the culture. While the SW620 cultures did not appear to have an altered cell distribution with a change in cell seeding method, the change from concentrated to diffused seeded cultures increased the viability of the cultures (Figure 3.8B). As with the selection of material pre-treatment, the selection of the diffuse seeding method achieved cultures which have a more consistent growth profile to provide reliable results.

Changing the culturing environment by altering the well insert did not have an effect on the viability of the cultures of either cell line (Figure 3.12), while only effecting the distribution of the SW480 cells (Figure 3.11). However, it has previously been demonstrated that the use of the full-sided insert leads to increased lactic acid build up in the reservoir of media above the scaffold compared to the media below it [278]. While this is not desirable for most cultures, this may prove advantageous for use in a migration assay as it may provide a simple way of mimic the hypoxic interior of tumours and produce biological cues which drive cell migration in a manner to that seen *in vivo* [72]. Additionally, with the culture media divided into two separate compartments within the well, there is the potential for introducing media additives to either compartment to produce a concentration gradient to alter the migration of the cells during 3D culture and this is a method that is often used in other migration protocols during standard 2D culture [204, 279].

From the Western blot presented in Figure 3.21, it was clear that the 3D culture environment has an effect on the protein expression profile of cells. The data for the expression of E-cadherin is in agreement with previously published studies. The SW480 cell line has been found to have variable levels of expression depending on the confluency of the 2D cultures from which the protein was extracted [223]. This carries over to culturing the SW480 cell line in a 3D system, as the lower density culture of these cells expressed E-cadherin at a lower level than the higher density culture. The lack of bands for E-cadherin from the SW620 cell lysates has also been previous noted in the literature, with multiple sources finding no detectable expression via Western blots and only limited expression when probed via immunohistochemistry [280, 281]. This variation seen in protein expression profile could have a knock-on effect when it comes to comparing the migration of the cell lines in 2D and 3D cultures, particularly as the loss of E-cadherin is one of the defining factors in determining whether cells have undergone EMT and have an increase metastatic potential [79].

The comparison between Alvetex® Scaffold and Alvetex® Strata has demonstrated that their morphological characteristics have a large impact on the behaviour of the SW480 and SW620 cell lines during 3D culture. The smaller void and interconnect size of Alvetex® Strata appeared to limit the number of cells which can attach to the material in the first instance, as seen when MTT data was compared to that from Alvetex® Scaffold cultures (Figure 3.15 and Figure 3.19), and provides an environment where it was more difficult for the cells to remain attached to maintain the viability of the cultures (Figure 3.19). This led to a smaller volume of cells moving into the material over the

14 day culture period when compared to the counterpart Alvetex® Scaffold cultures. This agrees with the original hypothesis that Alvetex® Strata may provide a physical barrier to cell migration into the material and, therefore, is not an appropriate material for a 3D migration assay with these cell lines and so all further studies will work solely with Alvetex® Scaffold.

From the viability and penetration data for long term cultures of the SW480 and SW620 cells on Alvetex® Scaffold, an overall methodology for a 3D migration assay has been established (Figure 3.24). The timescales for this protocol were determined by the behaviour of both cell lines over the 21 day culture period tested. The endpoint of 10 days was selected due to the behaviour of the SW620 cell line, as these cells had penetrated 185µm into the 200µm thick scaffold by 14 days (Figure 3.22C). This would make visualising differences in cell penetration more difficult in cases where media additives increase the level of migration, whereas the penetration depth of 166µm by 11 days would allow for more opportunity to visualise these differences. Additionally, viability of the long term cultures of SW620 dropped off after 11 days in 3D culture, so using a culturing period which is shorter than this ensures that the migration assay is being carried out on healthy cells and the results obtained would not be affected by cell death. A 10 day culture of the SW480 and SW620 cell lines still demonstrated a similar level of distinction between the amount of cell penetration demonstrated by each cell line as previously seen at 11 days (Figure 3.25).

Furthermore, the selection of an even number of days for the total assay period allows for an even split between the establishment and assessment periods of the assay. Histology data for both cell lines demonstrated that both of them have established cultures by 4 days (Figure 3.13A and Figure 3.14A), so the introduction of media additives at day 5 would lead to them acting on cells which have already adapted to the scaffold environment and would not alter the outcome of the assay by affecting cell attachment.

As with all assays, a control needs to be included in order to validate the results obtained and to allow for the best possible conclusion to be drawn from the data available. As the role of the Wnt signalling pathway in colorectal cancer is the biological focus of this project, the control aspect is particularly important in this assay, as the Wnt pathway plays a crucial role in the proliferative behaviour and differentiation of cells in the colonic epithelium [94] and disruption of the pattern of Wnt signalling causes major disruption to the final organisation of the epithelial cells in the colon [92]. The control selected for this migration assay is the Quant-iT™ PicoGreen® dsDNA Assay, which is a fluorescence assay which quantifies the amount of double-stranded DNA [282], which in turn provides the user with either the concentration of dsDNA or the cell number within a sample. This will allow the assessment of the effect of any media additives to ensure that the any alteration seen in the penetration of cells into the scaffold is due to changes in cell migratory behaviour and not proliferative behaviour.

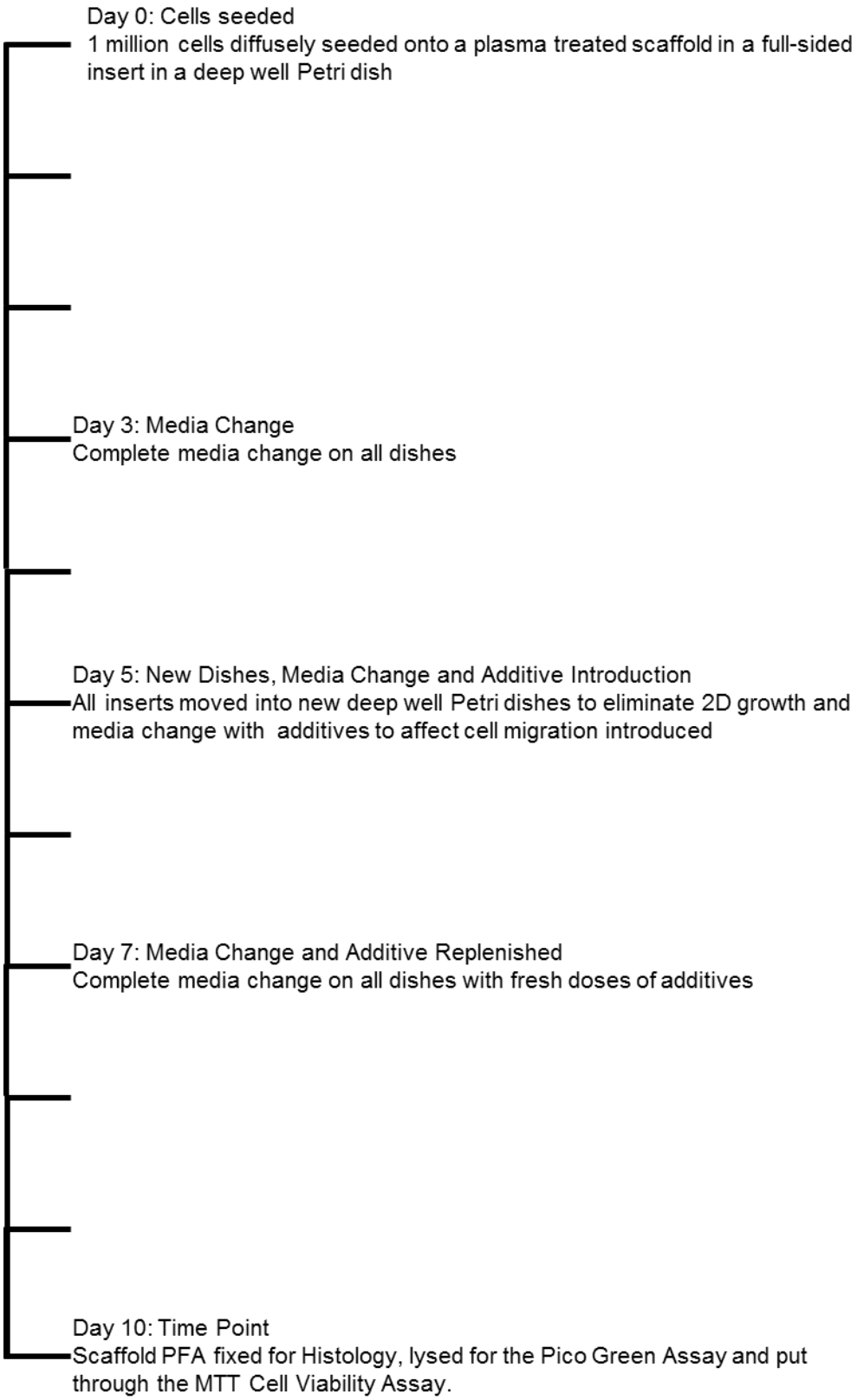

Figure 3.24: Schematic for the 3D cell migration assay using Alvetex® Scaffold, a novel polystyrene scaffold. This experimental outline allows for an establishment period for cell growth before the introduction of media additives to influence cell penetration during the second phase of the culture period.

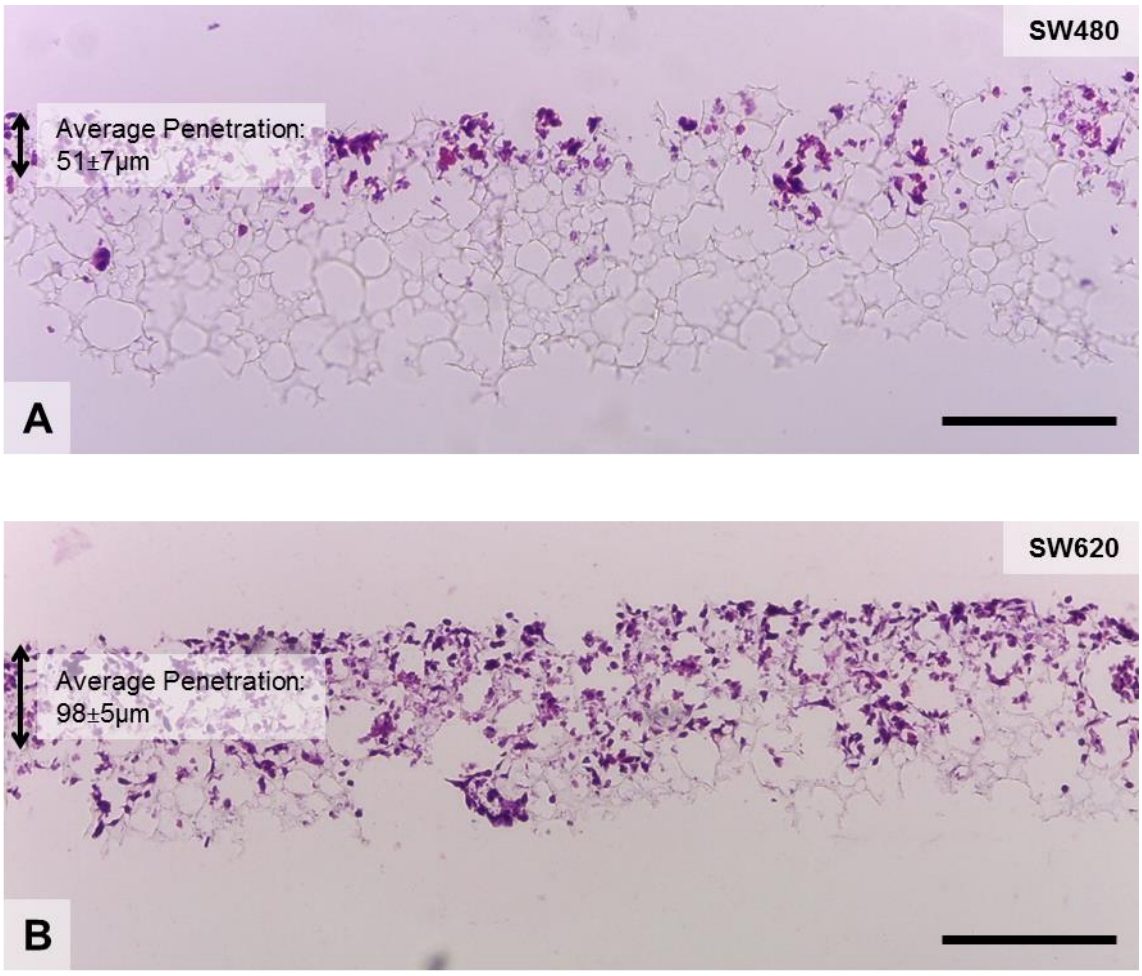

Figure 3.25: The SW620 cell line shows a greater capacity than the SW480 cell line to penetrate into Alvetex® Scaffold over the time course of the migration assay. H&E stained images of scaffolds which had been cultured for 10 days with A: SW480 and B: SW620 cells showing an average penetration (n=3) of 51±7µm and 98±5µm respectively. Scale bars = 200µm for both images.

Together, this work will aim to investigate cancer cell migration in a setting that has not been examined in great detail in the literature, which is using a synthetic scaffold to provide a 3D cell culture environment. Using this variety of system has advantages over other methods of obtaining 3D cancer cultures, such as spheroids or ECM gel based cultures. Spheroids have been used for many years as a method of obtaining 3D multi-cellular cultures [176] and naturally provide an oxygen and nutrient gradient which mimics the intravascular regions of tumours. However, it has been demonstrated that the size of these spheroids needs to be tightly regulated, the behaviour of cells is affected by spheroid size and this can affect experimental outcomes [155]. The system under development here provides a platform for producing consistent 3D cultures, removing some of the variability in cell behaviour and experimental outcomes seen with spheroids. Additionally, with the employment of the full-sided well insert, the 3D culture can be subjected to a lactic acid concentration gradient [278], providing a simple way of modelling the gradient seen in tumours.

ECM gels are another commonly used method for obtaining 3D cancer cultures, with the cancer cells cultured on top of [209] or encapsulated by the gel [211] and with the option of co-culturing with a secondary cell type to form an organotypic model [216]. While these systems provide a 3D microenvironment which is highly biologically relevant, the determination of biological responses which are due to biological signalling from the protein environment or the increased dimensionality of the culture environment may be complex. As the Alvetex® system is polystyrene based [259], the same material used for tissue culture plasticware [265], it provides an opportunity to study the role that the increased dimensionality has in the alteration of cell behaviour in the absence of the increased biological cues from the ECM gel. Additionally, as the culture of cells on ECM coated Alvetex® Scaffolds has been demonstrated [283], it provides the opportunity for the stepwise building of a biologically relevant 3D model to examine the effect of each component individually.

The closest model to the Alvetex® system which is routinely used to assay cell migration and invasion is the Transwell® model [206], which is used with or without an ECM coating to investigate cell invasion or migration respectively. The Transwell® system also works on the concept of utilising well inserts to allow the rapid set up of experiments which require little in the way of specialist equipment, which may account for their widespread usage in the literature. However, Transwell® insert membranes are only 10μm thick, which, when used to assay cell migration, provides a limited 3D environment for the cells to migrate through, while the 200μm thickness of Alvetex® Scaffold provides a 3D environment to the migrating cells for a longer period of their migration, which more accurately reflects the *in vivo* tissue morphology. Additionally, the relatively short time periods that Transwell® assays are run for, in the region of hours as opposed to days [284], may fail to identify compounds of interest if their effects work over a longer time period. It is proposed that the Alvetex® system is a more advanced migratory system than the Transwell® system by providing a more biologically relevant 3D microenvironment than the Transwell® system.

This migration assay will now be utilised for investigating the role of Wnt signalling in modulating the migratory behaviour of colorectal cancer cells and if the nature of the 3D culture environment has an effect by looking at ECM protein coatings and co-culture with fibroblasts to mimic the stromal compartment of tumours.

4 Inhibition of Wnt Signalling in Colorectal Cancer Cells Alters Cell Migratory Behaviour

4.1 Introduction

This Chapter will seek to investigate the role of Wnt signalling in mediating cell migration within colorectal cancer models. From roles in controlling the proliferation vs. differentiation axis of colonic epithelial cells [92, 93] to the positioning of cells to form crypts [92] or the functional intercrypt epithelium [95], the Wnt signalling pathway has been shown to be fundamental to the maintenance of the healthy colonic epithelium. With ~90% of colorectal tumours possessing a mutation to key proteins within this pathway [96], Wnt signalling also plays a key role in the initiation of colorectal cancers, leading to it holding a position of interest within the field over many of the other signalling pathways which have been implicated in cancer development [6].

As the protein interactions within the Wnt signalling pathway were fully identified in the 1990s [285-287], there has been the opportunity to develop a range of molecular tools to manipulate the activity of this pathway. As the Wnt pathway is found to be inappropriately activated in colorectal cancers, as demonstrated by the high levels of nuclear β-catenin [288], it is the search for antagonists of this pathway that have the potential to provide the basis for the treatment of this disease. While there is Dkk1, a protein antagonist of the Wnt pathway [91], there are also a range of small molecules which act as antagonists to the Wnt signalling pathway by targeting different protein interactions (Figure 4.1).

4.1.1 Small molecule inhibition of the Wnt signalling pathway

A screen of the literature has highlighted four commercially available Wnt antagonists, cardamonin, ICG 011, IWR-1 and XAV 939, for testing in the migration assay optimised in Chapter 3 to evaluate their effect on the migration of colorectal cancer cell in *in vitro* migration assays.

4.1.1.1 Cardamonin

Cardamonin (Figure 4.1A) belongs to the chalcone family of compounds and has been isolated from a variety of plant species, including *Boesenbergia pandurata* [289] and *Alpinia henryi* [290]. It is one of a group of plant derived compounds termed ‘nutraceuticals’ which have been implicated for roles in cancer prevention and treatment due to their interaction with a variety of signalling pathways which are crucial to cancer initiation and development [291, 292].

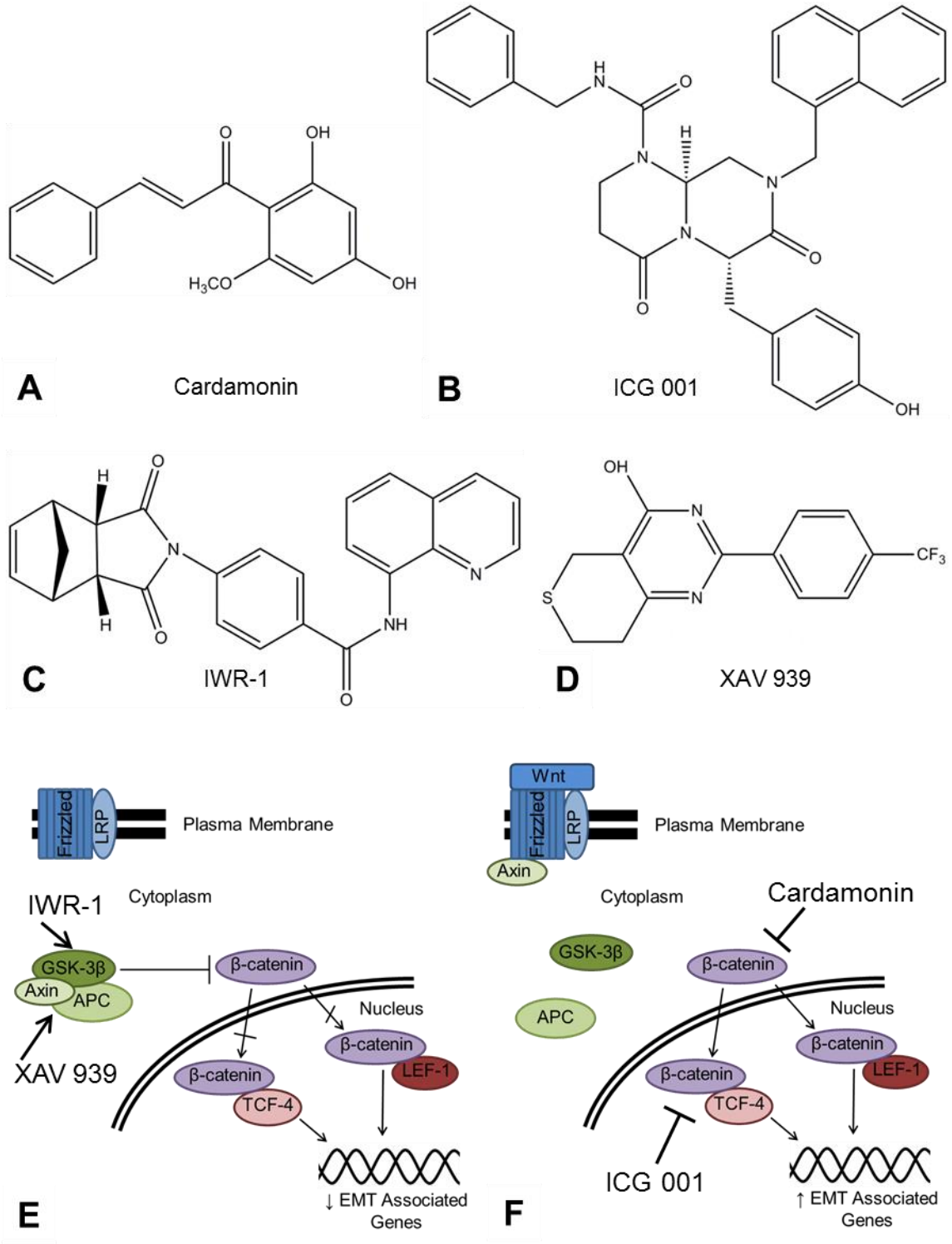

Figure 4.1: Chemical structure of small molecule Wnt inhibitors and schematic of their interaction with the Wnt signalling pathway. Chemical structure of A: cardamonin, B: ICG 001, C: IWR-1 and D: XAV 939. E: both XAV 939 and IWR-1 stabilise the Axin/APC/GSK-3β complex, leading to β-catenin phosphorylation even when the Wnt ligand is present. F: cardamonin decreases the levels of free β-catenin in a GSK-3β independent manner, while ICG 001 inhibits β-catenin/TCF-4 mediated transcription by interaction with transcriptional coactivators. The inhibition of Wnt signalling leads to a decrease in the transcription of EMT associated genes.

4.1.1.1.1 Cardamonin inhibits NF-κB target gene activation

Work carried out on RAW 264.7 macrophages has shown that cardamonin inhibits bacterial lipopolysaccharide stimulated NF-κB target gene activation, including inflammatory associated proteins such as COX-2, iNOS [293] and TNF-α [294]. The reduction seen in Cox-2 and iNOS protein levels leads to a decrease in the production of prostaglandin E2 and NO_2^- respectively [295]. The proposed mechanism for this action is the inhibition of IKK, the protein complex responsible for the phosphorylation of I-κBα. The inhibition of this phosphorylation process leads to the cytosolic accumulation of the unphosphorylated form of I-κBα, masking the nuclear localisation signal of NF-κB, preventing nuclear translocation and transcriptional activation of target genes [295].

Cardamonin has also been shown to have an inhibitory effect on the migration of a variety of cancer cell lines, including breast cancer, neuroblastoma and fibrosarcoma cell lines [296]. This work was carried out looking at both migration and invasion assays, using multi-well chambers and Matrigel coated Transwell® units respectively with FBS as a chemoattractant. Cardamonin dose dependently inhibited migration and invasion via the NF-κB mediated suppression of transglutaminase-2 expression, in addition to suppression of the activity of the matrix metalloproteinases MMP-2 and MMP-9, both in the presence and absence of the invasion inducer TPA.

4.1.1.1.2 Cardamnonin decreases β-catenin protein levels independently of the Wnt signalling pathway

In addition to its role as an anti-inflammatory compound, cardamonin has also been shown to inhibit Wnt signalling. In human melanocytes, cardamonin has been shown to decrease the levels of β-catenin protein in a dose dependent manner without altering the level of β-catenin mRNA [297]. Further to this, the decrease of β-catenin protein levels was found to be independent of the Wnt pathway, as it was unaffected by the presence of the Wnt3a ligand or BIO, a Wnt signalling agonist. The action of cardamonin was blocked by addition of the proteasome inhibitor MG-132, indicating that the mechanism by which the compound acts on β-catenin is via proteasome-mediated degradation (Figure 4.1F). In the melanocytes, decreased levels of β-catenin led to decreased melanin production in response to the Wnt3a ligand by lowering the levels of tyrosinase and microphthalmia-associated transcription factor, both of which are required to catalyse tyrosine into melanin.

Cardamonin has also been used to investigate the role that Wnt signalling has to play in control cardiac function [298]. Using the murine derived atrial-like cells HL-1, cardamonin was used to determine the mode of action by which MSC conditioned tyrodes affected the conduction velocity of the cells. Application of cardamonin in addition to the conditioned tyrodes lead to a decrease in Cx43 protein expression and, due to its role in synchronised contraction of cardiac tissue, a decrease of the conduction velocity of the cells. As this complemented data using the GSK3-β inhibitor lithium chloride, this lead to the conclusion that the signalling pathway activated to control the conduction velocity was the canonical Wnt signalling pathway.

4.1.1.1.3 The cardamonin mediated decrease in β-catenin suppresses the proliferation of colorectal cancer cells

More recently, cardamonin has been shown to suppress the proliferation of a variety of colorectal cancer cell lines, including the SW480 cell line, in standard 2D monolayer cultures [299]. Again, this action was found to be via the proteasome mediated degradation of the β-catenin protein without affecting the mRNA levels, as seen in melanocytes [297]. This decrease in β-catenin protein level led to the decreased expression of cyclin D1 and c-myc [299], both of which are β-catenin target genes, with a knock-on effect to the viability of cell lines upon exposure to the compound. Together the data for the interactions between cardamonin and the Wnt signalling pathway suggests that it has potential as a therapeutic agent for targeting cancer, along with other compounds which modulate the transcriptional activity of β-catenin [300].

4.1.1.1.4 Cardamonin sensitises cancer cells to TRAIL mediated apoptosis

In addition to the interactions with NF-κB and the Wnt pathway, cardamonin has been shown to sensitise a variety of cancer cells to TRAIL mediated apoptosis by down regulating various anti-apoptotic proteins such as Bcl-2 and survivin [301]. While the authors of the paper eliminated p53 involvement in this process, they did not confirm the signalling pathway which the cardamonin was interacting with to mediate this result.

While the action of cardamonin is not limited to interactions with the Wnt pathway, the evidence linking it to roles in mediating cell migration and invasion shows that it has potential in a novel migration assay, although the migration data obtained should be viewed in light of cell number data to determine whether that the compound is primarily affecting the migratory or proliferative behaviour of the cells.

4.1.1.2 ICG 001

4.1.1.2.1 ICG 001 inhibits tumour growth

ICG 001 (Figure 4.1B) is an organic compound which interacts with CBP, a transcriptional coactivator of β-catenin, in a dose dependent manner (Figure 4.1F). First utilised by Emami *et al* [302], it has shown to be effective in both *in vitro* and *in vivo* colorectal cancer studies by directly inhibiting the binding between β-catenin and CBP without inhibiting the binding of β-catenin to the CBP homolog p300. As the IC_{50} of ICG 001 is raised from the initial 3μM seen in SW480 cells by transfection of CBP into the cell line, this demonstrates that ICG 001 actively competes with β-catenin as a binding partner for CBP and, by blocking the β-catenin/CBP interaction, switches the balance of β-catenin binding towards transcriptional complexes with p300. ICG 001 downregulates the expression of survivin and cyclin D1, both β-catenin/TCF transcriptional targets, which in turn results in an inhibition of growth of the colorectal cancer cell lines SW480 and HCT116 without effect the growth of the normal colonic epithelial cell line CCD-841Co *in vitro*. *In vivo* studies using SW620 xenografts into Balb/c nude mice and the Min mouse model of human FAP reflect the *in vitro* data regarding survivin expression and inhibition of tumour cell growth, suggesting that ICG 001 may have clinical applications.

4.1.1.2.2 ICG 001 suppresses gene expression, including EMT associated genes

Application of ICG 001 to *in vitro* cultures alters the expression of a range of genes, including the downregulation of survivin expression in various colorectal cancer cell lines mediated by the lack of CBP binding to the gene promoter [303] and was also seen in a variety of hepatic [304], breast and prostate [303] cancer cell lines tested. This downregulation was seen found without alteration to the levels of either β-catenin or TCF proteins found at the promoter [303]. In addition to the blocking of CBP from the survivin promoter, ICG 001 mediated the recruitment of the transcriptional repressors HDAC6 and SUMO-1 to the promoter, further enhancing the inhibition of expression [303]. When utilised with the MCF-7 breast cancer cell line, ICG 001 was found to repress leptin mediated EMT by supressing the levels of Snail, Zeb2 and Slug expression when compared to treatment with leptin alone, resulting in monolayer cultures with cellular phenotypes resembling the untreated controls [305].

4.1.1.2.3 ICG 001 inhibits Wnt signalling in response to dietary fibre breakdown

ICG 001 has been used to investigate the signalling events that mediate the effect of butyrate, a histone deactylase inhibitor (HDACi) breakdown product of dietary fibre, on the behaviour of colorectal cancer cells. ICG 001 inhibited butyrate induced Wnt signalling in both the HCT-116 and SW620 cell lines, which in turn had a variable effect on the induction of apoptosis in these cell lines with ICG 001 increasing the apoptotic response, as visualised by caspase activity, in the HCT-116 cells while inhibiting the level of apoptosis seen in the SW620 cells [306]. In addition to affecting apoptosis induction, ICG 001 and butyrate have a negative impact on the proliferation rate of the two cell lines tested, when used individually and in combination, with the expression levels of both p21 and survivin supressed by ICG 001 treatment. Further work from the same group has shown that ICG 001 mediates similar effects on the level of Wnt activity of the p300 deficient colorectal cell lines HCT-R and HCT-15 in response to butyrate [307]. The authors of these papers suggest that with further investigations into the action of β-catenin/p300 on cell proliferative and apoptotic behaviours, joint therapies of ICG 001 and HDACis may have a role in the treatment of p300 deficient patients where treatment with butyrate alone does not elicit the desired cellular response. A further role for ICG 001 in joint therapies has been suggested for the treatment of multidrug resistant hepatoblastoma, as is has been shown that combinatorial therapy with either the MET kinase inhibitor SU11274 or common hepatoblastoma chemotherapy agent cisplatin had a greater decrease on the cell viability of 2D monolayer cultures than any compound used in isolation [308].

4.1.1.2.4 ICG 001 has application in the modulation of Wnt signalling in different cell types

The documented use of ICG 001 in the literature is not limited to studies looking at the behaviours of cancer, as it has been used to look at the effect of inhibiting β-catenin/CBP mediated gene transcription in rat epicardial cells following induced myocardial infarction [309]. ICG 001 was found to upregulate the *Gdf15*, *Ctgf* and *Nppa* genes which are associated with healthy cardiac function and this causes an increase in contractile function of the left ventricle. Additionally, inhibition of the Wnt pathway via ICG 001 is able to upregulate the expression of the cartilage specific collagen *COL2A1* gene after injury to the growth plate of hind legs of rats and this effect can accentuate the increase caused by the chondrogenesis enhancer TGF-β1 [310]. By 10 days post injury, the application of ICG 001 increased the proportion of cartilaginous tissue and decreased the

proportion of bony trabecular whilst leaving the proportions of mesenchymal tissue and bone marrow unaffected in the sampled population.

With ICG 001 displaying a wide variety of uses both in vitro and in vivo models, from those discussed here to models of neuron outgrowth [311] and pulmonary fibrosis [312], it has demonstrated its capacity to modulate the regulation of Wnt target genes and it has potential for use with the novel 3D migration model under testing here.

4.1.1.3 IWR-1

4.1.1.3.1 IWR-1 modulates Wnt signalling by stabilising the β-catenin degradation complex

IWR-1 (Figure 4.1C) is one of a group of organic small molecules termed 'inhibitors of Wnt response' capable of inhibiting Wnt signalling via promoting the stability of the β-catenin degradation complex comprising of Axin, APC and GSK-3β (Figure 4.1E) [313], in addition to being a potent inhibitor of tankyrase (TNKS) 2 [314]. Application of IWR-1 to the colorectal cell line DLD-1 results in the upregulation of the Axin2 protein relative to DMSO treated controls and this is not mirrored by changes to the protein levels of other components of the Wnt pathway such as APC, GSK-3β, β-catenin and Dvl. The upregulation of Axin2 is not mediated by upregulation of *AXIN2* gene, as IWR-1 downregulates the expression of the *AXIN2* gene, or inhibit the action of the proteasome; neither does it alter the localisation of Axin2 within the cells or its affinity for β-catenin. This paper also demonstrates the ability of IWR-1 to modulate the activity of the Wnt pathway in cell lines with a mutated APC protein, as is found in many colorectal cancers.

4.1.1.3.2 IWR-1 has been used to downregulate Wnt signalling in development models

IWR-1 has been utilised to investigate the role of Wnt signalling in various developmental processes in zebrafish and *Xenopus*. It is found to retard the regrowth of amputated caudal fin and inhibit the regeneration of the lining of the gastrointestinal tract of six-month old zebrafish, as visualised by the lack BrdU uptake in the base of intestinal folds [313]. In addition to those effects of Wnt signalling inhibition in zebrafish, the use of IWR-1 retards swimbladder development in the developing embryo [315, 316]. The smaller swimbladder is also associated with a lack of smooth muscle, visualised by the lack of *acta2* expression, in addition to disrupted tissue layers, as visualised by disrupted *hb9*, *has2* and *elov1a* expression. In *Xenopus* embryos, application of IWR-1 reduced the expression of *AXIN2*, as well as the markers for blood development *hba1* and *lmo2* [317].

4.1.1.3.3 IWR-1 had been shown to be effective in non-cancer models

There has also been work carried out utilising IWR-1 as a modulator of Wnt signalling in mammalian culture experiments. When used in conjunction with BMP2 on mouse dental papilla cells, IWR-1 is capable of reversing the BMP2 induced increase in DMP1, Dspp and β-catenin expression and reduces the level of AP activity induced after a 48 hour exposure to BMP2 [318]. Inhibition of the Wnt signalling pathway in human iPSCs can switch the differentiation pathway from alveolar epithelial type II (AETII) to alveolar epithelial type I (AETI) cells by increasing the gene expression levels of *caveolin-1*, *AQ5* and *T1α*, all of which are markers of the AETI phenotype [319]. During hESC differentiation into cardiomyocytes via exposure to BMP-4 and activin A, inclusion of IWR-1 in the induction media increased the percentage of cardiomyocytes produced

over a DMSO control [320], with IWR-1 producing a greater proportion of atrial cells over ventricular cells, as visualised by the relative gene expression of the *MYL7* and *MYL2* respectively.

IWR-1 has had limited usage so far in the area of cancer research, however it has been used on a variety of murine and human lung cancer cell lines [321]. Across all cell lines tested, IWR-1 dose dependently decreased the viability of the 2D monolayer cultures, an effect which could be reversed by the overexpression of β-catenin in the cells. As this paper also demonstrated the inhibition of Wnt signalling by IWR-1, this molecule has the potential to affect the migratory outcome of Wnt signalling in a colorectal cancer model.

4.1.1.4 XAV 939

4.1.1.4.1 XAV 939 also stabilises the β-catenin degradation complex

XAV 939 (Figure 4.1D) is another small molecule which has the capability to stabilise the Axin/APC/GSK-3β destruction complex by stabilising axin2 (Figure 4.1E), which results in an increase in the protein levels of phosphorylated β-catenin and a decrease the level of Wnt dependent gene transcription [322]. The action of XAV 939 is mediated by the inhibition of TNKS1 and TNKS2 and it is the inhibition of these which in turn stabilise the axin2 protein levels, as treatment of SW480 with TNKS1/2 siRNA also increased the levels of axin2. TNKS1 and TNKS2 add several ADP-ribose units to their targets, a process called poly-ADP-ribosylation (PARsylation). PARsylation of axin2 targets it for ubiquitin mediated proteasomal degradation, as demonstrated by the exposure of XAV 939 treated SW480 cells to the proteasome inhibitor MG132, which leads to a build-up of PARsylated and ubiquitinated axin2 relative to untreated controls. When the DLD-1 colorectal cancer cell line was exposed to XAV 939, it caused a decrease in colony formation relative to untreated controls. As IWR-1 is also a TNKS2 inhibitor [314], it is possible that its action to stabilise axin2 is also mediated by TNKS2.

4.1.1.4.2 XAV 939 inhibits Wnt signalling in development models

Like IWR-1, XAV 939 has also been used to look at developmental processes in *Xenopus* embryos, where it reduced the expression of *AXIN2*, as well as the markers for blood development *hba1* and *lmo2* [317]. XAV 939 has also been used to investigate the role of Wnt signalling in cardiomyogenesis of mouse ES cells [323], with the application of XAV 939 to embryoid bodies (EBs) during days 3 through 5 of differentiation producing a greater proportion of spontaneously beating EBs by day 10. The increase in XAV 939 induced spontaneously beating EBs is comparable to the increase induced by the Wnt antagonist Dkk1. The increase in spontaneously beating EBs was accompanied by gene upregulation of the cardiac markers *Myh6* and *Nkx2.5* as well as upregulation of α-actinin protein levels at the expense of gene expression of *Gata1*, *Myh11*, and *KDR*, which are hematopoietic, smooth muscle and endothelial markers respectively.

4.1.1.4.3 XAV 939 sensitises cancer cells to apoptosis and decreases viability

XAV 939 has been used to investigate the role of Wnt signalling in a variety of cancer types. As with IWR-1, XAV 939 also dose dependently decreased the viability of 2D monolayer cultures of a variety of murine and human lung cancers cell lines, an effect which could be reversed by the overexpression of β-catenin in the cells [321]. When the human neuroblastoma cell line SK-N-SH is exposed to XAV 939 in conjunction with the chemotherapy agent Doxorubicin (DOX), the

percentage of live cells is lower than when the cells are exposed to DOX alone for 24 hours [324]. Additionally, the use of XAV 939 equalises the effect of DOX on the $CD133^+$ and $CD133^-$ populations within the cell line, as DOX causes a larger drop in live cells in the $CD133^-$ population than the $CD133^+$ population, the putative stem cell compartment of the tumour cell populations.

In colorectal cancers, XAV 939 has been shown to increase apoptosis mediated by the PI3K inhibitors LY-294002 and BKM120 or the PKB inhibitor API-2 in spheroid cultures of cells from patient samples with high levels of nuclear β-catenin [325]. However, the same effect was not seen in dual treatment with the chemotherapy agents 5-FU or oxaliplatin. As the Wnt signalling pathway is disrupted in many colorectal cancers, there have been many review articles suggesting that XAV 939 has the potential to be effective in the treatment of colorectal cancers by switching the balance of β-catenin behaviour within the cells [326-328], hence its selection as a Wnt signalling antagonist to be assessed for its potential to reduce colorectal cancer cell migration in a 3D model.

Based on the available literature when this study was initiated, XAV 939 was selected as the first small molecule to be screened for effectiveness in the 3D migration model developed here. This selection was based on characteristics of all four of the small molecules. Cardamonin was discounted as it has been shown to interact with multiple signalling pathways and so its mechanism of activity is not confined to the Wnt pathway. Hence, any results obtained using this molecule would need to be assessed to determine which pathways were responsible for any changes in behaviour observed.

As ICG 001 acts to inhibit the binding of β-catenin and CBP, not p300, it does not uniformly block Wnt signalling and appears to favour inhibiting the proliferative activity of cells. As the aim of this study is to investigate the migratory behaviour of the cancer cells, this molecule was also discounted as there is evidence to suggest that it would target a wider range of cellular behaviour beyond migration.

The two remaining small molecules, IWR-1 and XAV 939, both work to stabilise the Axin/APC/GSK-3β degradation complex to decease the available amount of β-catenin, which decreases the expression of Wnt target genes. Of these, IWR-1 has had limited applications in cancer research and, therefore, was not selected for initial study.

While XAV 939 has been used with a variety of cancer types, it was the effect on cell viability, not migration, which was investigated. As its effect on β-catenin mediated gene transcription is well documented, it is hypothesised that it would decrease Wnt mediated cell migration. However, any data obtained would need to be assessed in conjunction with cell number data to ensure that the molecule is not affecting cell viability as previously noted.

4.2 Chapter Aims

This Chapter aims to assess the role of the Wnt signalling pathway in modulating the behaviour of colorectal cancer cells by utilising small molecule inhibitors of the Wnt pathway in both 2D and 3D cell migration assays. Screens of these molecules will highlight whether they have an inhibitory effect on the cell migration whilst also considering their influence on the proliferative behaviour of the cells.

4.2.1 Objectives

Overall, the aims of the small molecule assessment in this Chapter will be met by:

- Screening a selection of small molecule Wnt signalling inhibitors to assess their impact on the migration and proliferation of colorectal cancer cells in the 3D model;
- Performing counterpart assessments on the efficacy of the small molecule Wnt signalling inhibitors for inhibiting colorectal cancer cell migration in standard 2D scratch wound assays;
- Obtaining the optimum concentration for usage of any small molecule Wnt signalling inhibitors which demonstrate their ability to inhibit colorectal cancer cell migration in the 3D model.

4.3 Results

4.3.1 XAV 939 is a Wnt signalling inhibitor which is ineffective in this 3D cell migration model

Due to previous examples of the effectiveness of XAV 939 in colorectal cancer cell lines [322, 324, 325], in particular the SW480 cell line which is in use during this study [322], it was selected as the first small molecule to be screened for its ability to inhibit Wnt mediated cell migration. The IC_{50} value of XAV 939 is 11nM and 4nM for TNKS1 and TNKS2 respectively [322] and it has previously been used at concentrations for 5nM [324] through to 20μM [322]. Therefore, a selection of concentrations within this range were used for the initial screen, clustered around the commonly used lower concentrations found in the literature, namely 1, 3 and 5μM [322, 323, 325, 329].

4.3.1.1 Low concentrations of XAV 939 do not effect cell migratory behaviour

The addition of the low concentrations of XAV 939 to the 3D migration assay after culture establishment did not cause any clearly visible alterations to the cell distribution of either of the SW480 or SW620 cell lines throughout Alvetex® Scaffold after the 10 day total culture period (Figure 4.2). The SW480 cultures produced after exposure to either XAV 939 or the DMSO (0μM XAV 939) control had the majority of the cell growth in the uppermost section of the scaffold, with the cells found to be growing in clusters (Figure 4.2A, C, E & G). The SW620 cells were also found to be distributed in the same manner as seen in previous experiments, with the cells found individually throughout a greater depth of the scaffold (Figure 4.2B, D, F & H).

When the cell penetration within each condition was analysed using the 'linear' method of measurement, neither cell line displayed a significant difference in cell penetration in the presence or absence of XAV 939 at concentrations of 5μM and below (Figure 4.3), with the SW620 cell line penetrating the scaffold roughly twice as much as the SW480 cell line, ANOVA, $F(1,19)=116.440$, $p<0.001$.

4.3.1.2 Low concentrations of XAV 939 affect the viability and proliferation of SW480 cells but not SW620 cells

While it does not affect the cell penetration at these concentrations, XAV 939 did have an overall effect on cell viability, ANOVA, $F(3,19)=3.259$, $p=0.044$, and significantly so on the viability of the 3D SW480 cultures (Figure 4.4A), with all concentrations of XAV 939 tested increasing the apparent cell viability of the whole culture when compared to the DMSO control using the MTT Cell Viability Assay. The greatest and most significant increase in viability was seen when XAV 939 was used at 1μM, with the increases seen at 3 and 5μM also being significant over the control. This change to cell viability was not seen with the SW620 cell line at any of the concentrations of XAV 939 tested (Figure 4.4B).

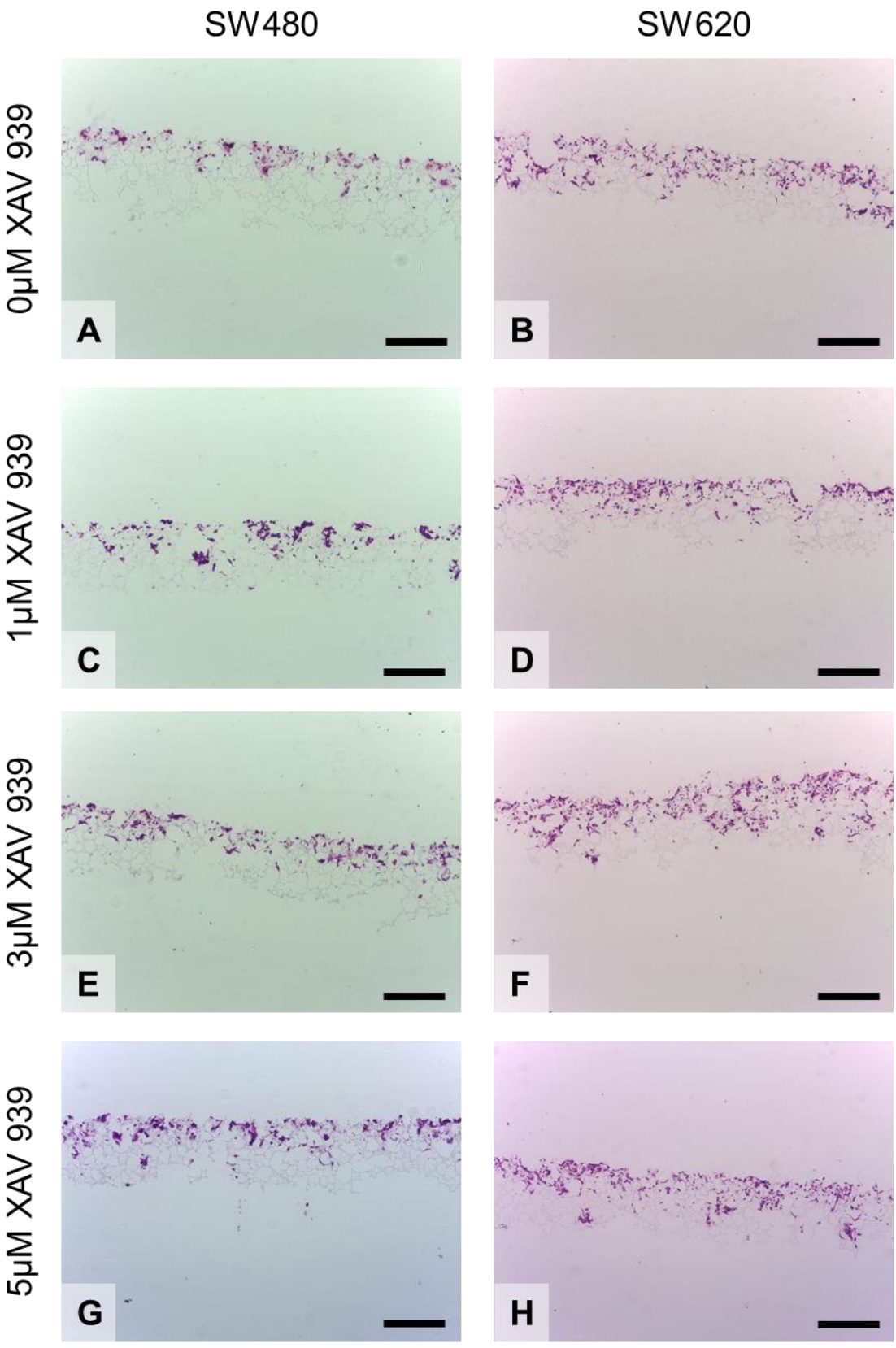

Figure 4.2: Neither cell line displayed an alteration in the build-up of cells when the Wnt inhibitor XAV 939 was present at concentrations of 5µM and below. H&E images of 10 day cultures with A and B: 0µM XAV 939 (DMSO control), C and D: 1µM XAV 939, E and F: 3µM XAV 939 and G and H: 5µM XAV 939 for both cell lines. Scale bars = 200µm for all images.

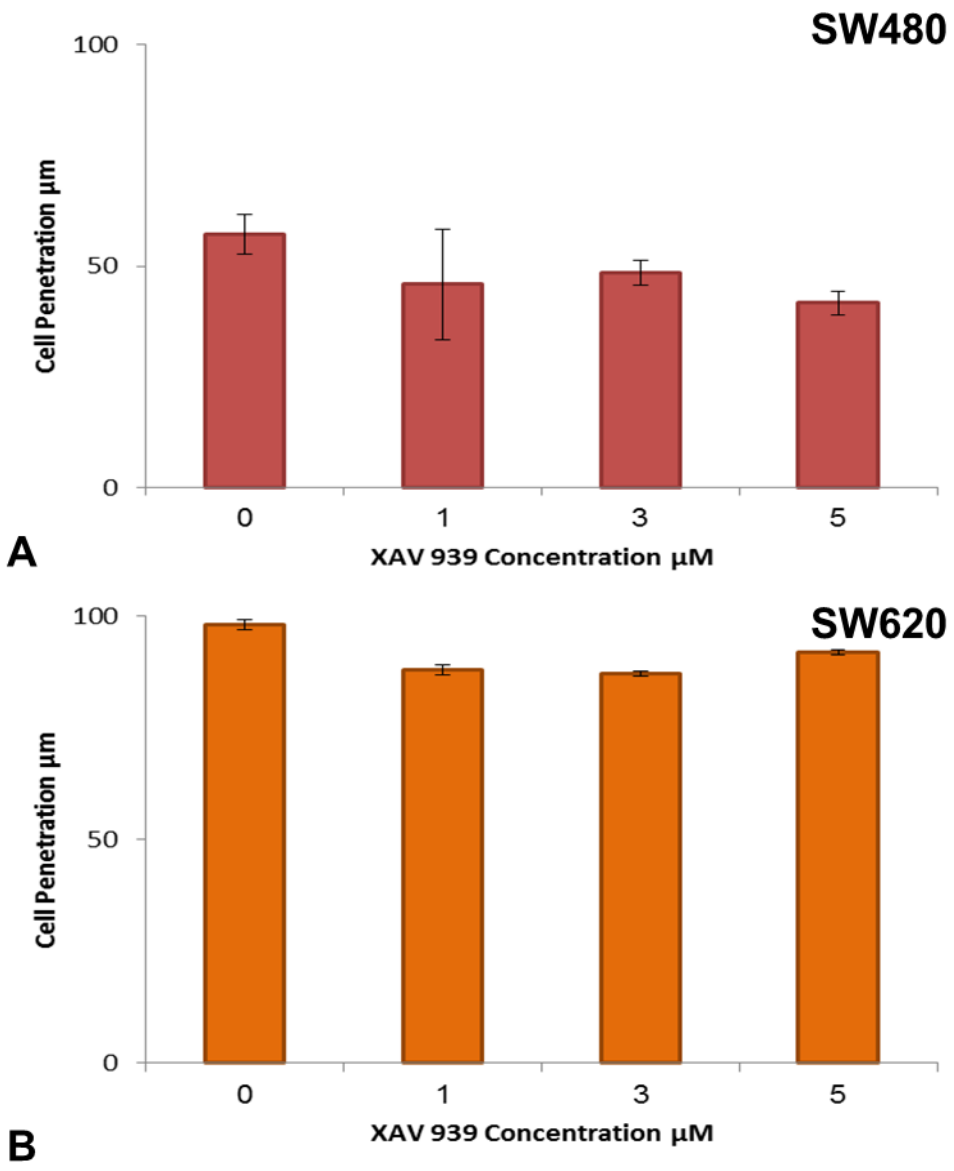

Figure 4.3: The 3D cell penetration of the both the SW480 and SW620 cell lines remained unaffected by the presence of XAV 393 at 5µm and below. Cell penetration in µm of A: SW480 and B: SW620 cells as determined by the linear measurement method. Data represent mean, n = 3, ±SEM for both graphs, no significance by a Dunnett's t-test.

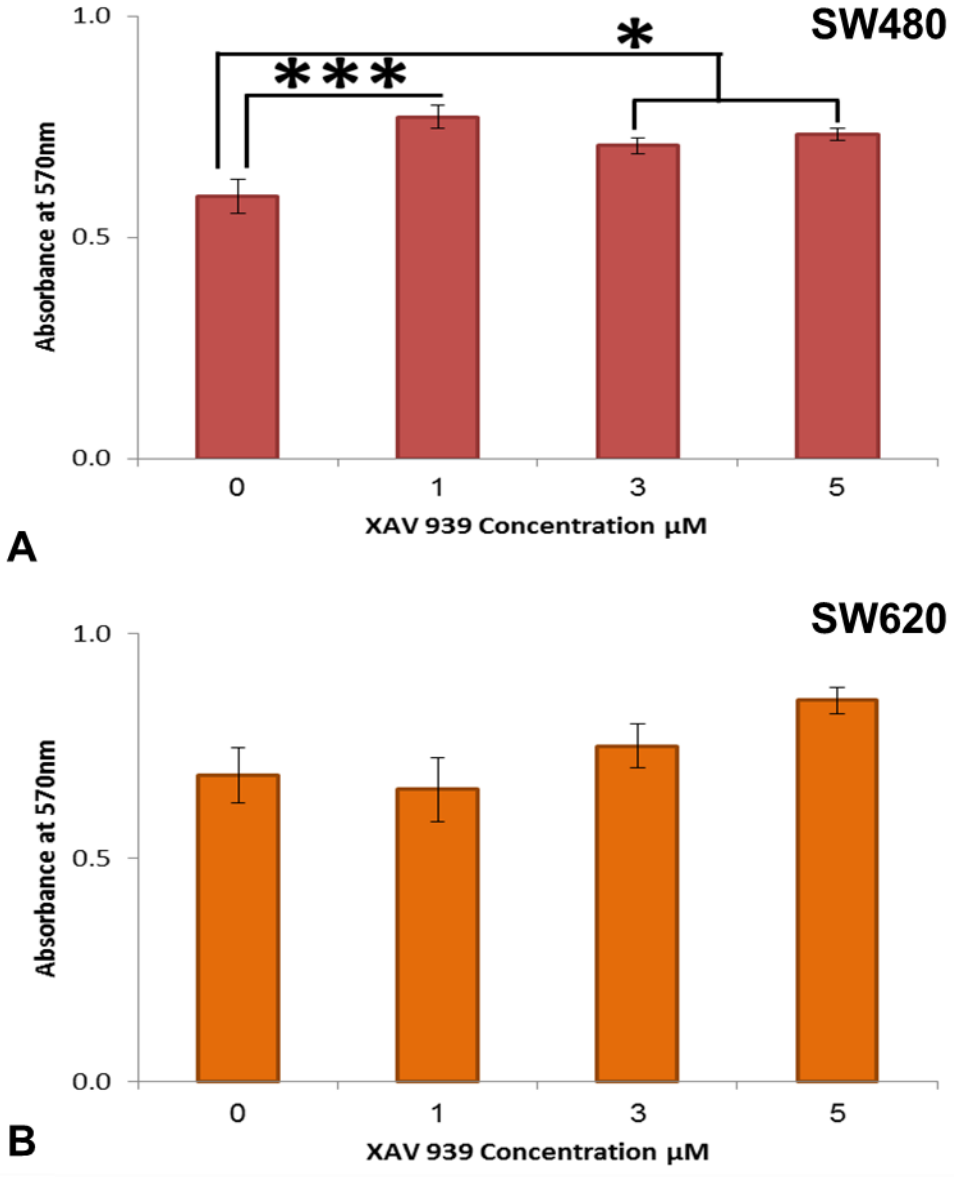

Figure 4.4: The 3D cell viability of the SW480 cell line increased when XAV 939 was present, while the viability of the SW620 cell line was unaffected. Absorbance at 570nm of A: SW480 and B: SW620 cells as determined by the MTT Cell Viability Assay. Data represent mean, n = 3, ±SEM for both graphs, * $p < 0.05$, 0.05, *** $p < 0.005$ by a Dunnett's t-test.

The increase in cell viability seen in the SW480 cell line was only correlated with an increase in cell number, as obtained by use of the Quant-iT™ PicoGreen® dsDNA Assay, at 5μM XAV 939, with all other concentrations failing to cause a change in cell number after the 10 day culture period (Figure 4.5A). There was also no significant alteration to cell number in the SW620 cell line after exposure to XAV 939 at concentrations up to 5μM (Figure 4.5B), although the SW620 cultures were found to have a significantly higher cell number than the SW480 cultures, ANOVA, $F(1,19)=196.740$, $p<0.001$.

4.3.1.3 The 2D migratory behaviour of the SW480 and SW620 cell lines was unaffected by low XAV 939 concentrations

As a comparison, these concentrations of XAV 939 were also utilised in a standard 2D scratch wound assay on uncoated tissue culture plastic. The scratch wounds were monitored over a 24 hour period, with the data obtained from images taken at 24 hours post wounding presented here within this thesis. At 24 hours post wounding both cell lines had moved into the wound from the wound edges at either side (Figure 4.6), although the SW620 also appeared to have a greater number of single cells within the wound which are not attached to either wound edge (Figure 4.6B, D, F & H). The scratch wound assay was quantified by two methods in order to assess the different forms of cell migration that cells can undertake. Measuring the distance between the two wound edges measured epithelial-sheet migration, where cells maintain E-cadherin cell-cell adhesion, whereas counting the number of single cells within the wound measured the mesenchymal-type migration, where each cell moves individually.

When the wound closure in terms of distance moved by the wound edges was quantified, the application of XAV 939 did not affect the amount of migration obtained by either cell line (Figure 4.7). Additionally, when quantified in this manner, the two cell lines appeared to migrate at similar rates in this 2D migration assay which was not seen in the 3D migration assay. For the single cell counting, the scratch wounds were fixed and stained with DAPI, to show individual nuclei, and fluorescently tagged Phalloidin, an actin binding molecule, to ease in determining if cells were attached to either wound edge. This staining confirmed that the SW620 cell line has more single cells present within the wound at 24 hours than the SW480 (Figure 4.8), which was further confirmed by the quantification of these cells (Figure 4.9), as the SW620 cell line had ~10 times the number of single cells in the wound after 24 hours than seen with the SW480 cell line, ANOVA, $F(1,16)=158.583$, $p<0.001$. These data also show that the application of XAV 939 at concentrations of up to 5μM did not inhibit single cell migration in this 2D model (Figure 4.9).

4.3.1.4 Cell migration was unaffected by high XAV 939 concentrations in 3D

As XAV 939 has been shown to be ineffective at curtailing the migratory behaviour of either the SW480 or SW620 cell lines in 2D and 3D migration assays at concentrations of 5μM and below, it was then screened for effectiveness at higher concentrations as it has been used at concentrations of up to 20μM in other models [321, 322, 329]. A range of higher XAV 939 concentrations, namely 10, 20 and 50μM, were selected to encompass the higher end of concentrations previously used in the literature.

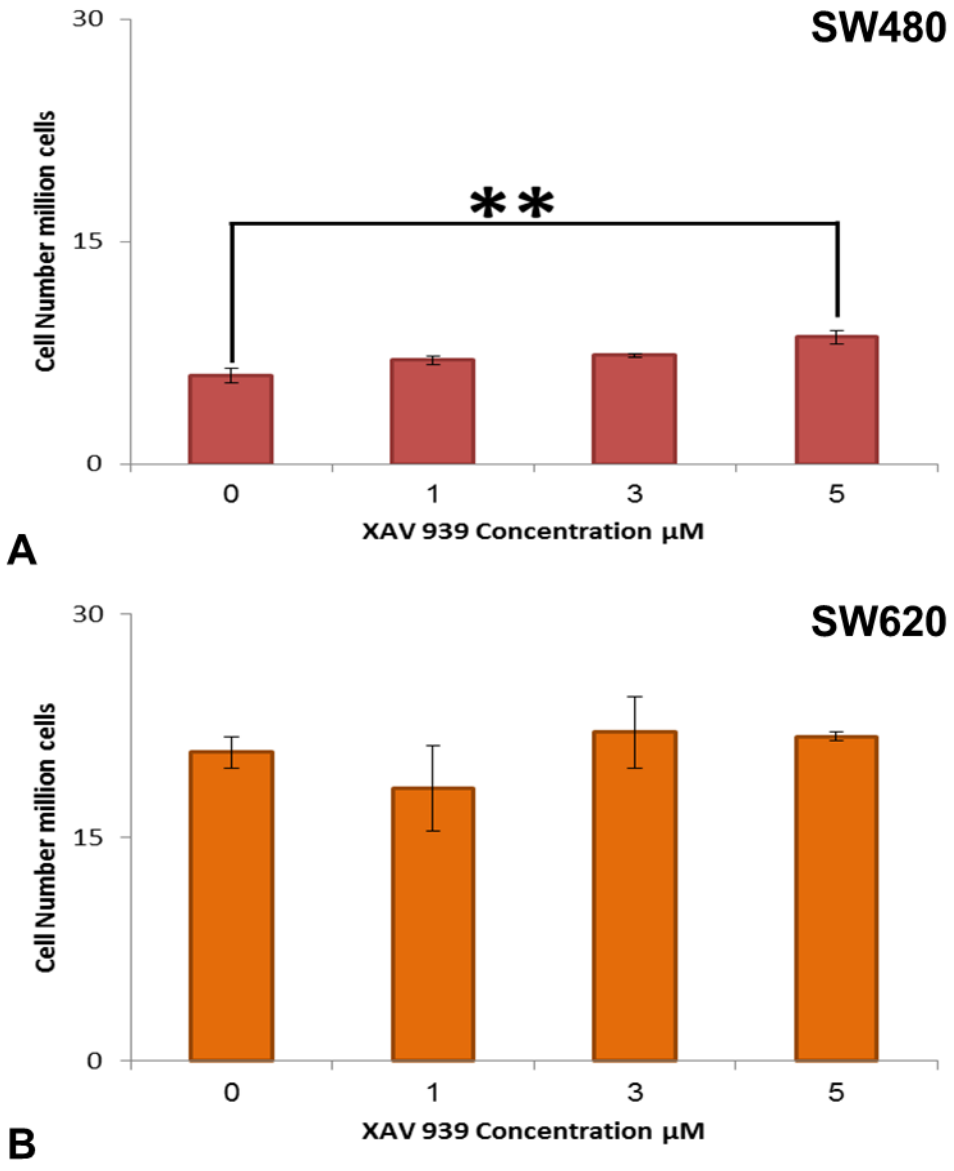

Figure 4.5: The number of SW480 cells in the 3D material increased when XAV 939 was present at a concentration of 5µM, while the number of SW620 cells was unaffected. Cell number in millions of cells of A: SW480 and B: SW620 cells as determined by the Pico Green dsDNA Assay. Data represent mean, n = 3, ±SEM for both graphs, ** $p < 0.01$ by a Dunnett's t-test.

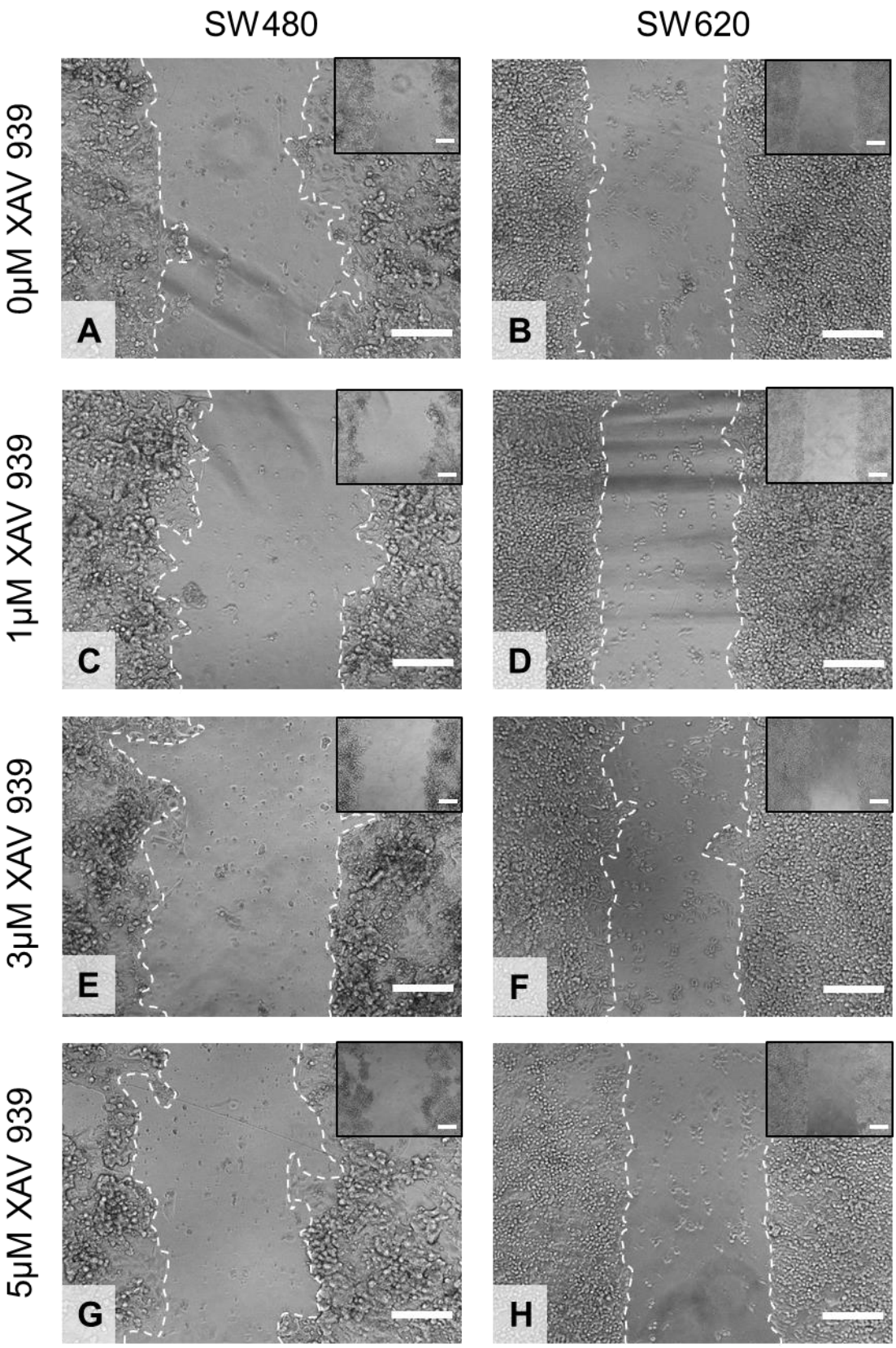

Figure 4.6: Both the SW480 and SW620 cell lines exhibited wound closing during a scratch wound assay with concentrations of the Wnt inhibitor XAV 939 of 5µM and below. Phase images of 24 hours post wounding, with 0 hours post wounding shown inset, with A and B: 0µM XAV 939 (DMSO control), C and D: 1µM XAV 939, E and F: 3µM XAV 939 and G and H: 5µM XAV 939 for both cells lines. Scale bars = 200µm for all images.

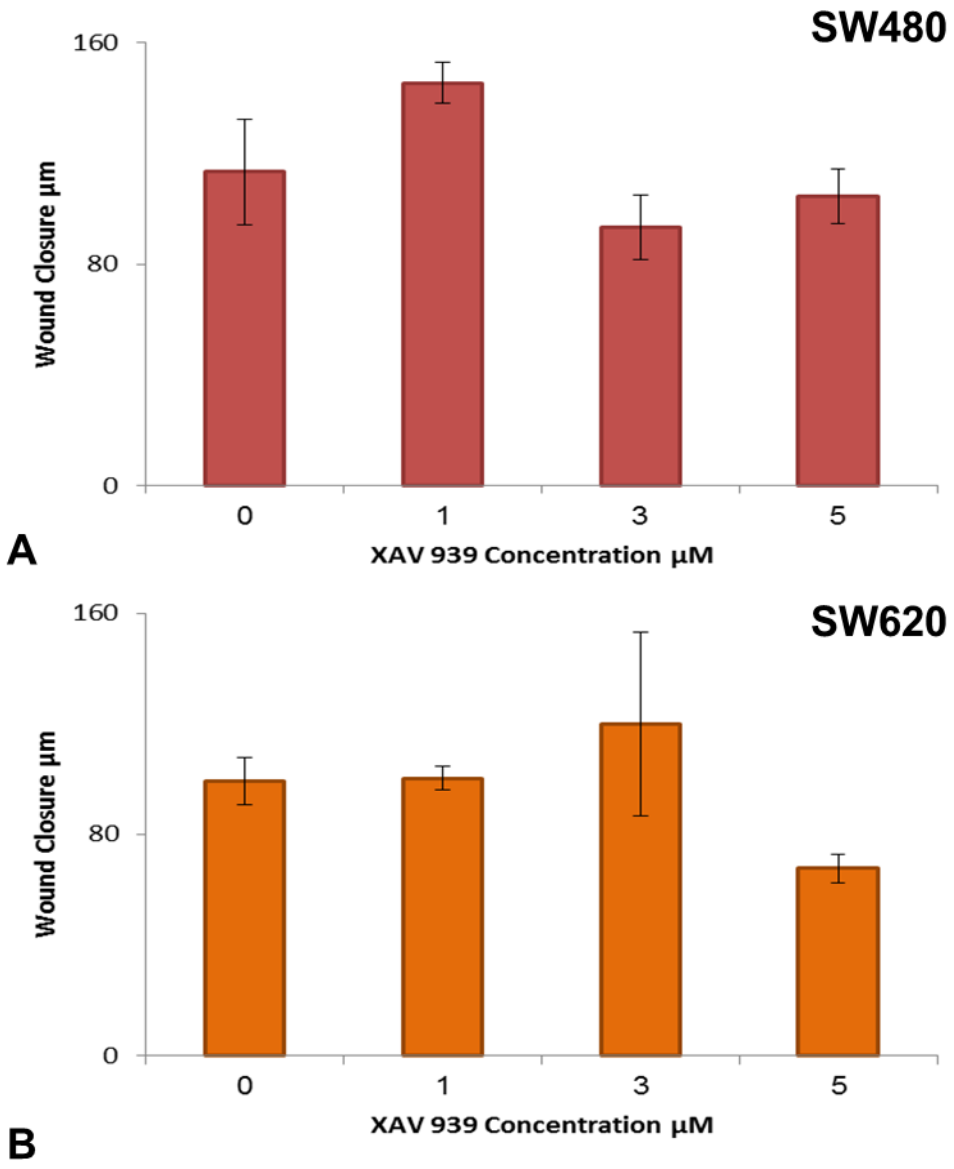

Figure 4.7: Neither the SW480 and SW620 cell lines showed a significant alteration in the distance moved by the edges of the 2D scratch wound in the presence of XAV 939 at concentrations of 5µM and below. Wound closure in µm of A: SW480 and B: SW620 cells as determined by measuring the width of the wound. Data represent mean, n = 3, ±SEM for both graphs, no significance by a Dunnett's t-test.

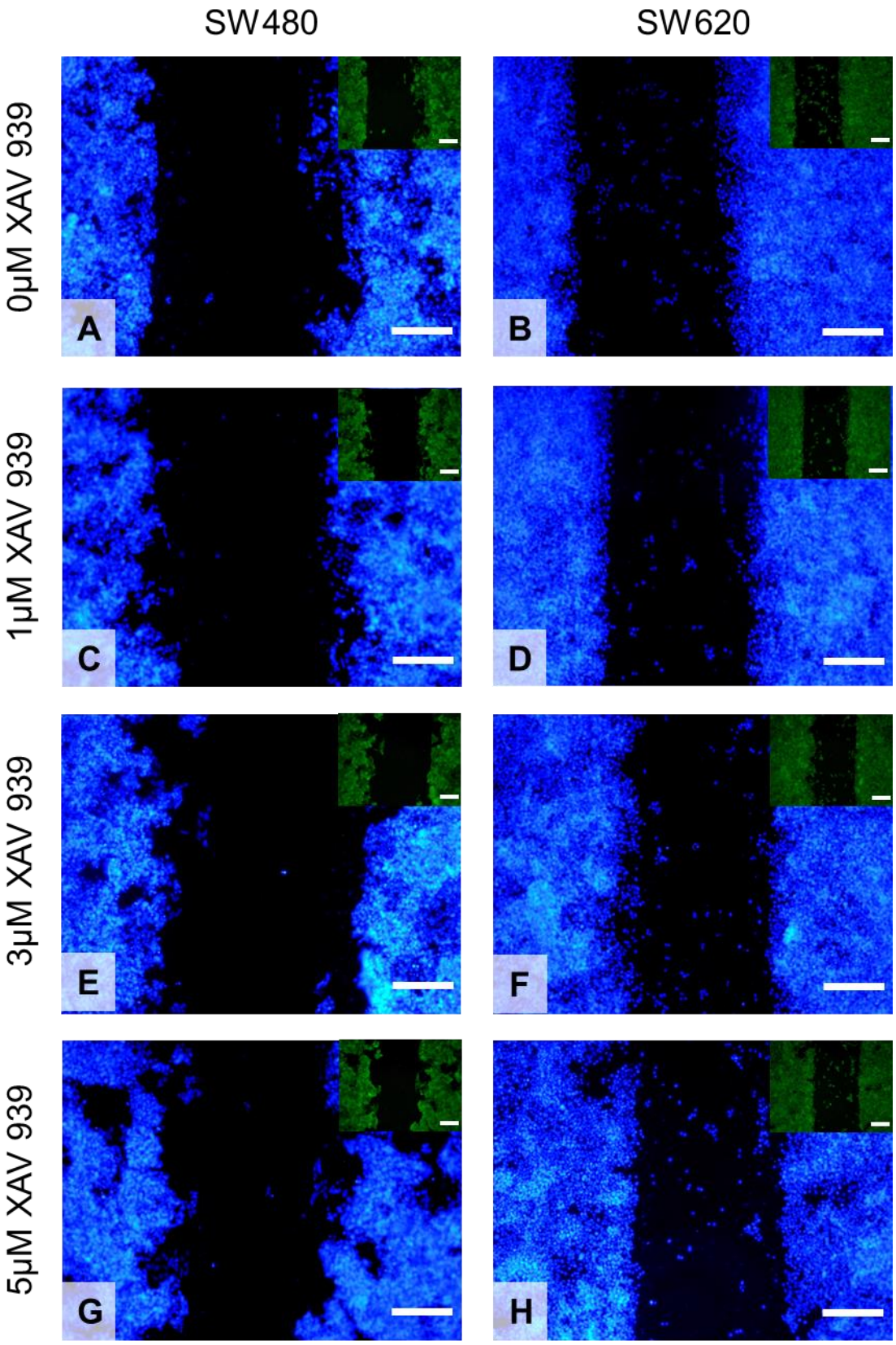

Figure 4.8: The SW620 cell line had more single migrating cells than the SW480 cell line during a scratch wound assay with concentrations of the Wnt inhibitor XAV 939 of 5µM and below. DAPI and Phalloidin (inset) images of 24 hours post wounding with A and B: 0µM XAV 939 (DMSO control), C and D: 1µM XAV 939, E and F: 3µM XAV 939 and G and H: 5µM XAV 939 for both cells lines. Scale bars = 200µm for all images.

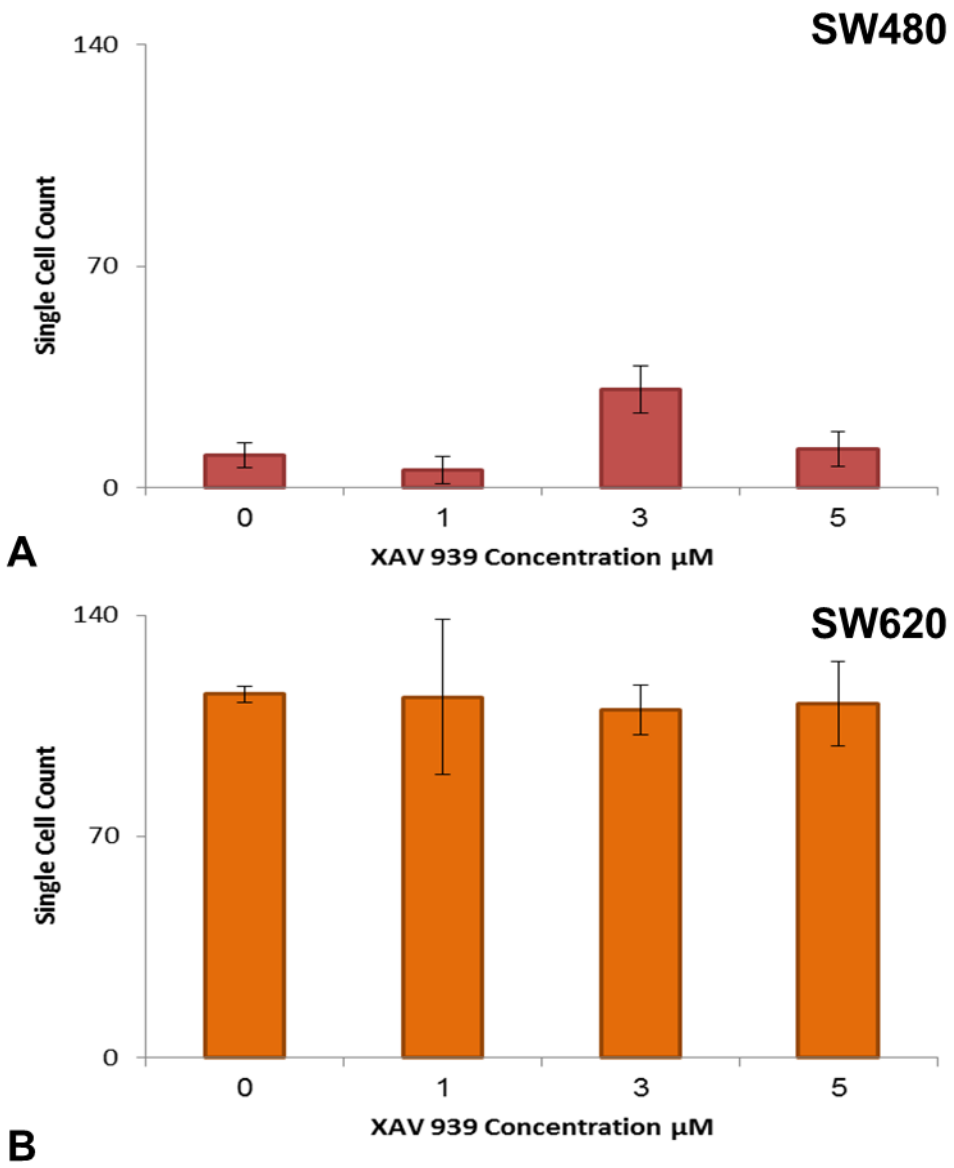

Figure 4.9: Neither the SW480 and SW620 cell lines showed a significant alteration in the number of single migrating cells within the 2D scratch wound in the presence of XAV 939 at concentrations of 5µM and below. Number of single migrating cells in A: SW480 and B: SW620 scratch wounds as determined from cell counts. Data represent mean, n = 3, ±SEM for both graphs, no significance by a Dunnett's t-test.

When used in the 3D migration assay, there was no alteration to the distribution of the cell growth for either the SW480 or SW620 cell lines upon exposure to the higher concentrations of XAV 939 (Figure 4.10). As expected, the SW480 cell line maintained a distribution of cells towards the seeding surface of the scaffold, with the cells found to be clustered together (Figure 4.10A, C, E & G), while the SW620 cells maintained their distribution pattern as individual cells throughout a greater depth of the scaffold (Figure 4.10B, D, F & H). These cell distribution patterns in the histological data were confirmed by the measurement of cell penetration into the scaffold, with the addition of XAV 939 at any of the concentrations tested resulting in no alteration to the level of cell penetration displayed by either the SW480 or SW620 cell lines (Figure 4.11), although, as previously seen, the SW620 cell line achieved a greater level of cell penetration, ANOVA, $F(1,19)=25.59$, $p<0.001$.

4.3.1.5 The viability and proliferation of the SW480 cell line only was affected by high concentrations of XAV 939

As with the lower concentrations of XAV 939, there was an overall effect of XAV 939 addition on cell viability, ANOVA, $F(3,19)=6.868$, $p=0.003$. There was also a specific impact of the cell viability of SW480 with the addition of XAV 939 when compared to the DMSO control (Figure 4.12A). However, unlike the response to low concentrations of XAV 939, the cell viability of the 3D cultures was decreased when XAV 939 was present at concentrations of 20 and 50μM, while the presence of XAV 939 at 10μM did not affect the cell viability. The SW620 cell line did not display any response to the addition of XAV 939 at concentrations of 10μM and above (Figure 4.12B), which reflects what was seen with the addition of XAV 939 at lower concentrations (Figure 4.4B). The decrease in apparent cell viability when XAV 939 was present at concentrations of 20 and 50μM is accompanied by a decrease in the number of SW480 cells within the 3D cultures after 10 days (Figure 4.13A), whereas XAV 939 did not induce a change in the cell number of the SW620 cell line at any concentration tested (Figure 4.13B), with the SW620 cultures producing a greater number of cells over the growth period, ANOVA, $F(1,19)=195.303$, $p<0.001$.

4.3.1.6 Higher concentrations of XAV 939 also failed to affect 2D migration

When these higher concentrations were used in a 2D scratch wound assay, XAV 939 failed to inhibit the migration of cells over a 24 hour period (Figure 4.14). The distribution of each cell line relative to the initial wound was comparable to the previous scratch wound assays with XAV 939 at a lower concentrations, with the movement of SW480 cells mostly confined to the wound edge (Figure 4.14A, C, E & G), whereas the SW620 cultures had more single cells within the wound after 24 hours (Figure 4.14B, D, F & H). The black particles seen at 24 hours in the wells which contained XAV 939 at 50μM (Figure 4.14G & H) were most likely to be the XAV 939 precipitating out into the culture media as opposed to an infection of the cultures as these were viewed in all cultures, both 2D and 3D, which contained 50μM XAV 939 across multiple independent experiments. When the wound closure was looked at in terms of the movement of the wound edges over 24 hours, XAV 939 did not have an impact on the amount of epithelial sheet migration achieved by either the SW480 or SW620 cell line (Figure 4.15).

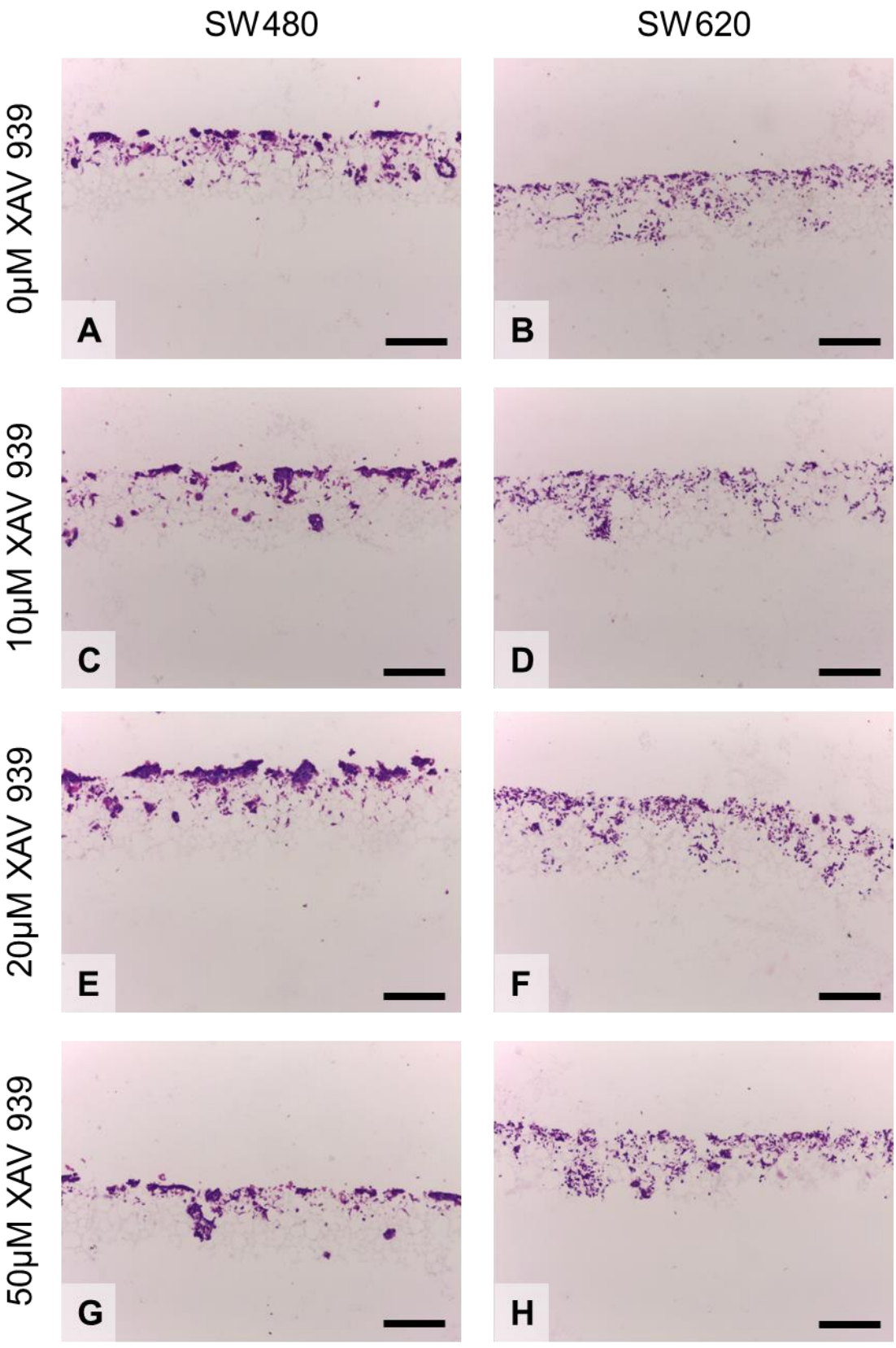

Figure 4.10: Neither cell line displayed an alteration in the build-up of cells when the Wnt inhibitor XAV 939 was present at concentrations of 10µM and above. H&E images of 10 day cultures with A and B: 0µM XAV 939 (DMSO control), C and D: 10µM XAV 939, E and F: 20µM XAV 939 and G and H: 50µM XAV 939 for both cells lines. Scale bars = 200µm for all images.

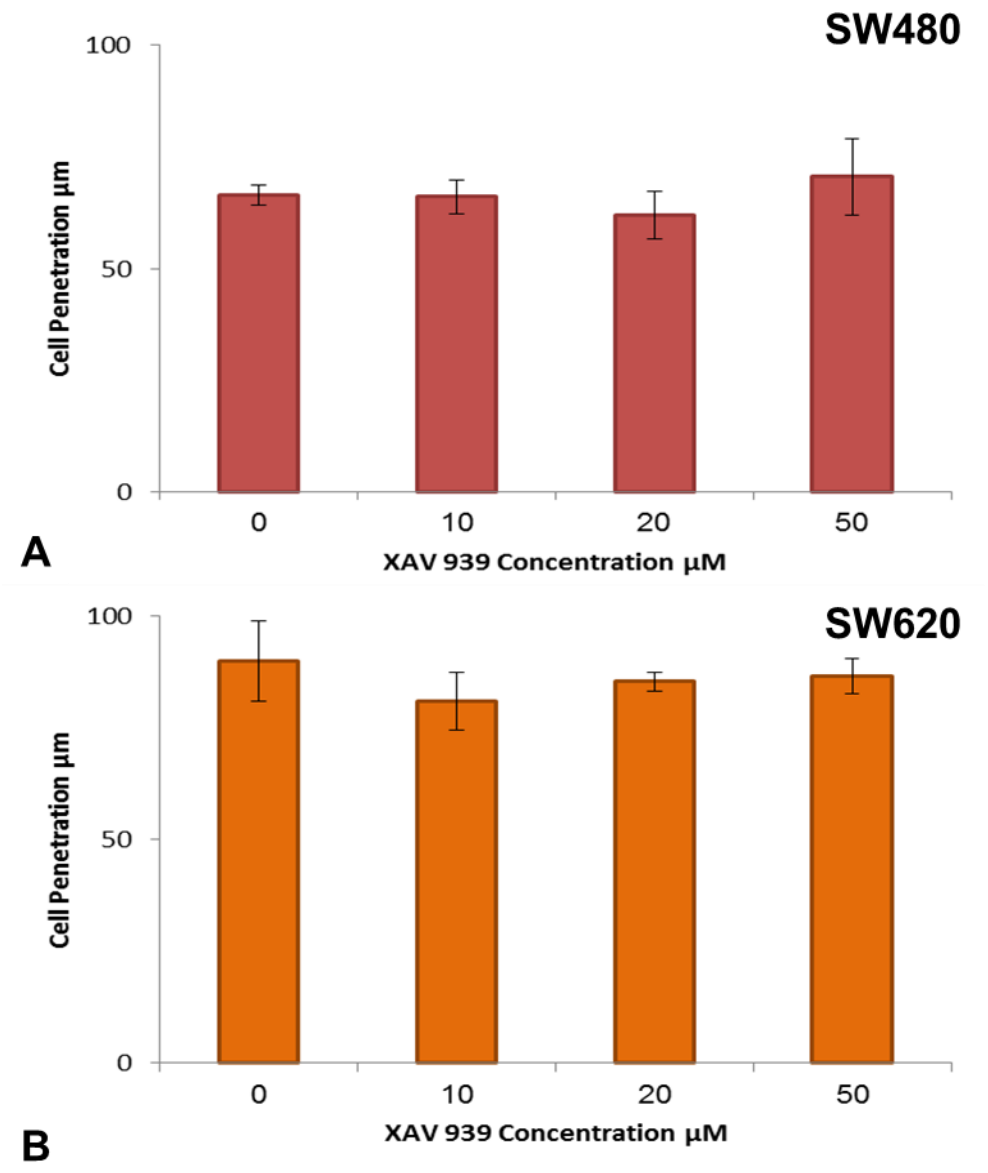

Figure 4.11: The 3D cell penetration of both the SW480 and SW620 cell lines remained unaffected by XAV 939 present at concentrations of 10µM and above. Cell penetration in µm of A: SW480 and B: SW620 SW620 cells as determined by the linear measurement method. Data represent mean, n = 3, ±SEM for both graphs, no significance by a Dunnett's t-test.

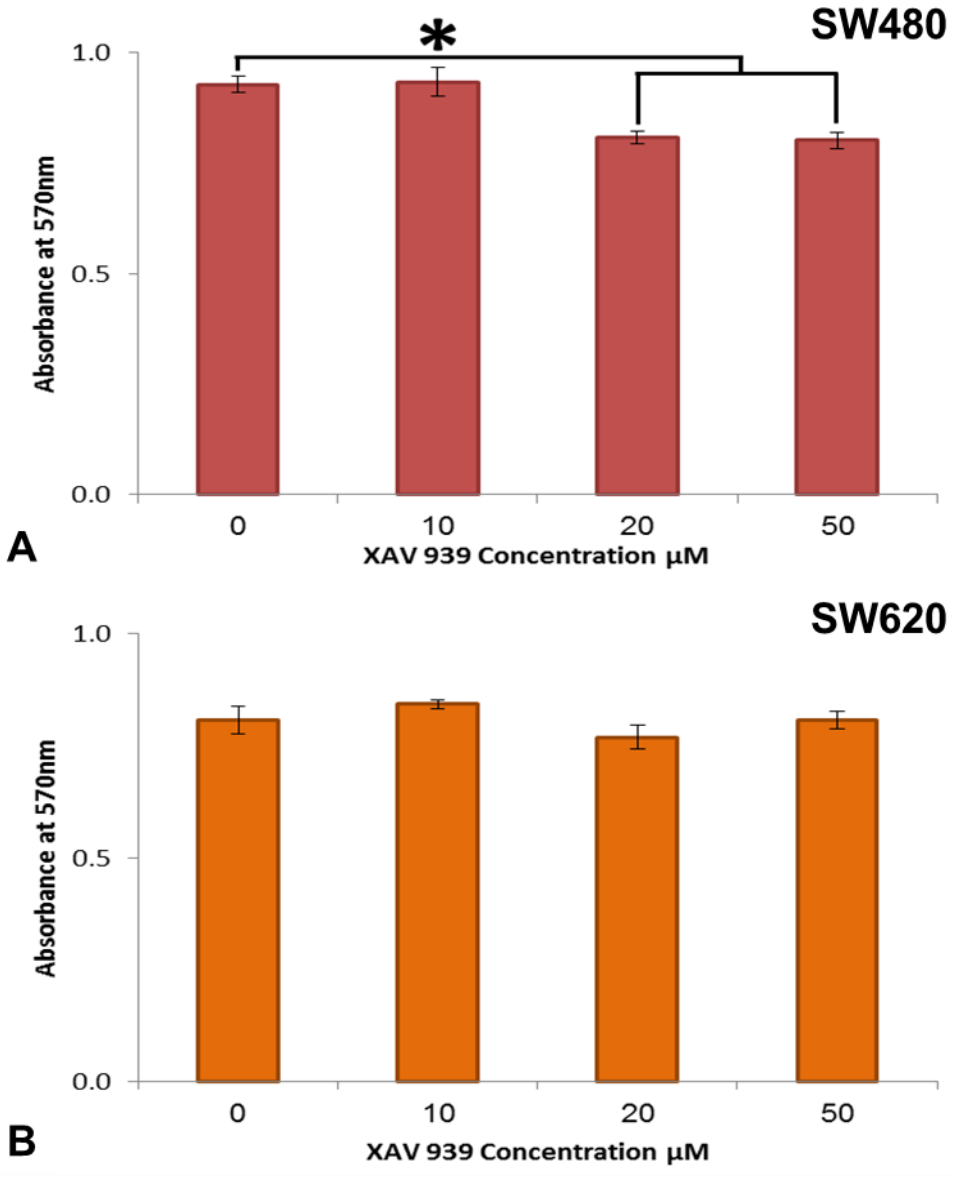

Figure 4.12: The 3D cell viability of the SW480 cell lines decreased when XAV 939 was present at concentrations of 20µM and above, while the viability of the SW620 cell line was unaffected. Absorbance at 570nm of A: SW480 and B: SW620 cells as determined by the MTT Cell Viability Assay. Data represent mean, n = 3, ±SEM for both graphs, * $p < 0.05$ by a Dunnett's t-test.

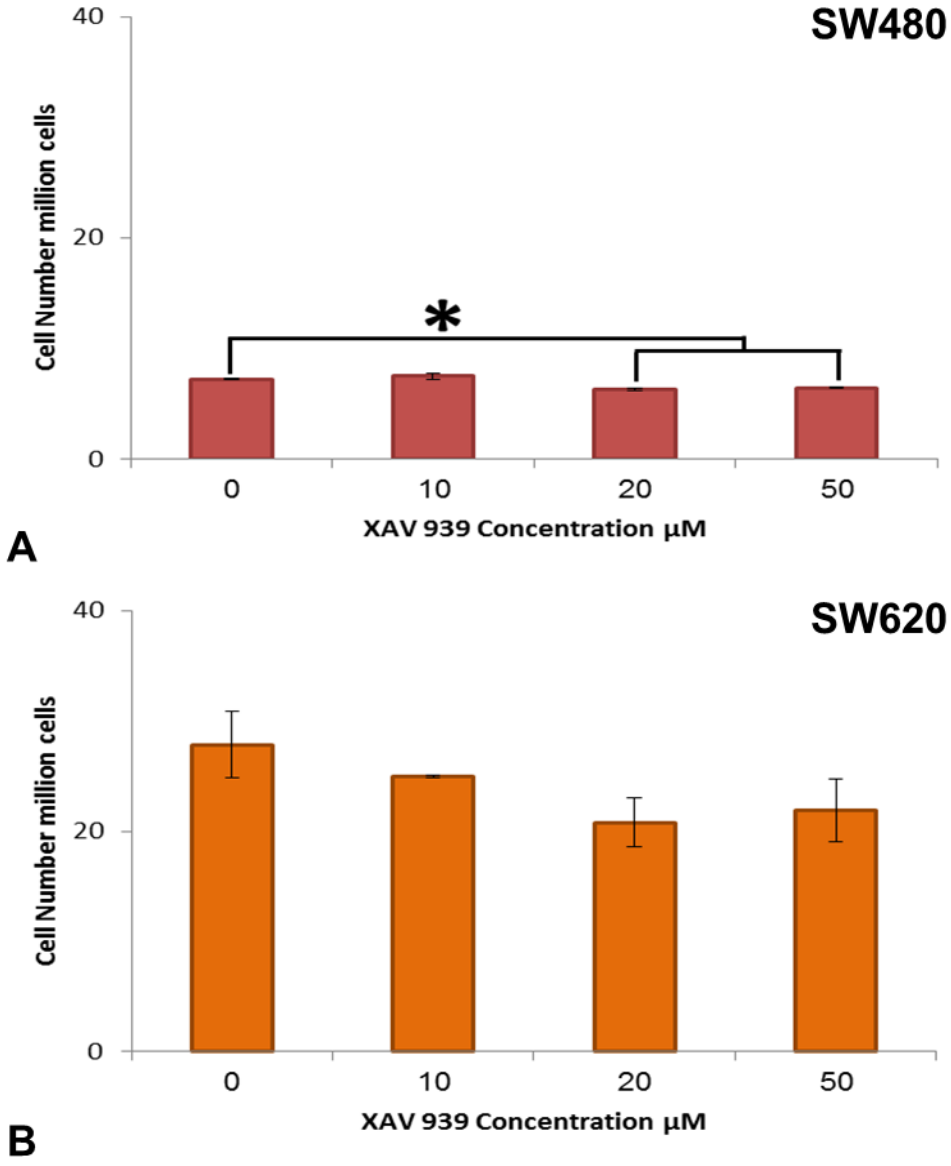

Figure 4.13: The number of SW480 cells in the 3D material decreased when XAV 939 was present at concentrations of 20µM and above, while the number of SW620 cells was unaffected. Cell number in millions of cells of A: SW480 and B: SW620 cells as determined by the Pico Green dsDNA Assay. Data represent mean, n = 3, ±SEM for both graphs, * $p < 0.05$ by a Dunnett's t-test.

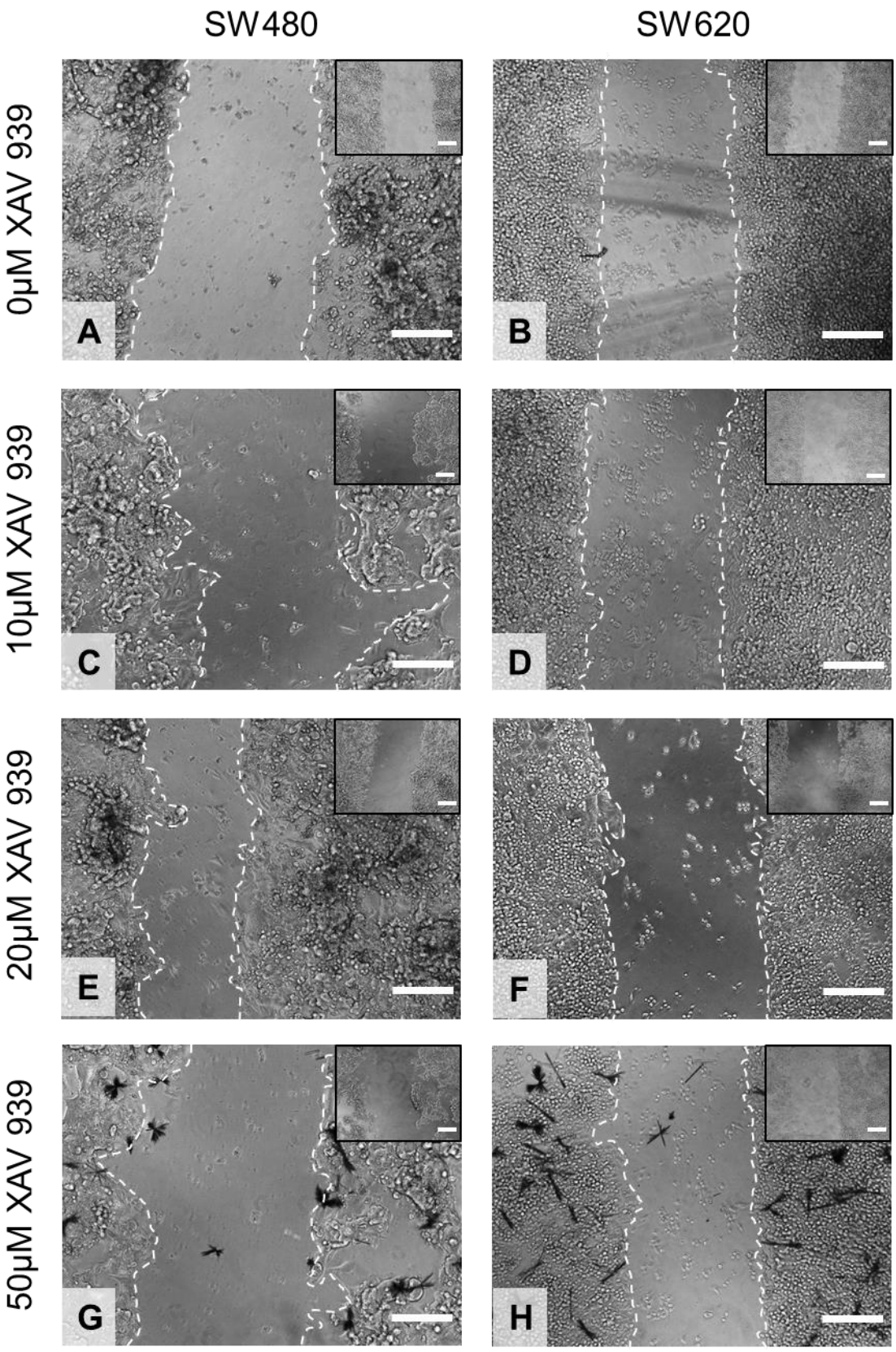

Figure 4.14: Both the SW480 and SW620 cell lines exhibited wound closing during a scratch wound assay with concentrations of the Wnt inhibitor XAV 939 of 10μM and above. Phase images of 24 hours post wounding, with 0 hours post wounding shown inset, with A and B: 0μM XAV 939 (DMSO control), C and D: 10μM XAV 939, E and F: 20μM XAV 939 and G and H: 50μM XAV 939 for both cells lines. The black particles seen in the cultures with 50μM XAV 939 present were assumed to be the XAV 939 precipitating out of solution as they were observed with all 50μM XAV 939 cultures, both in 2D and 3D. Scale bars = 200μm for all images.

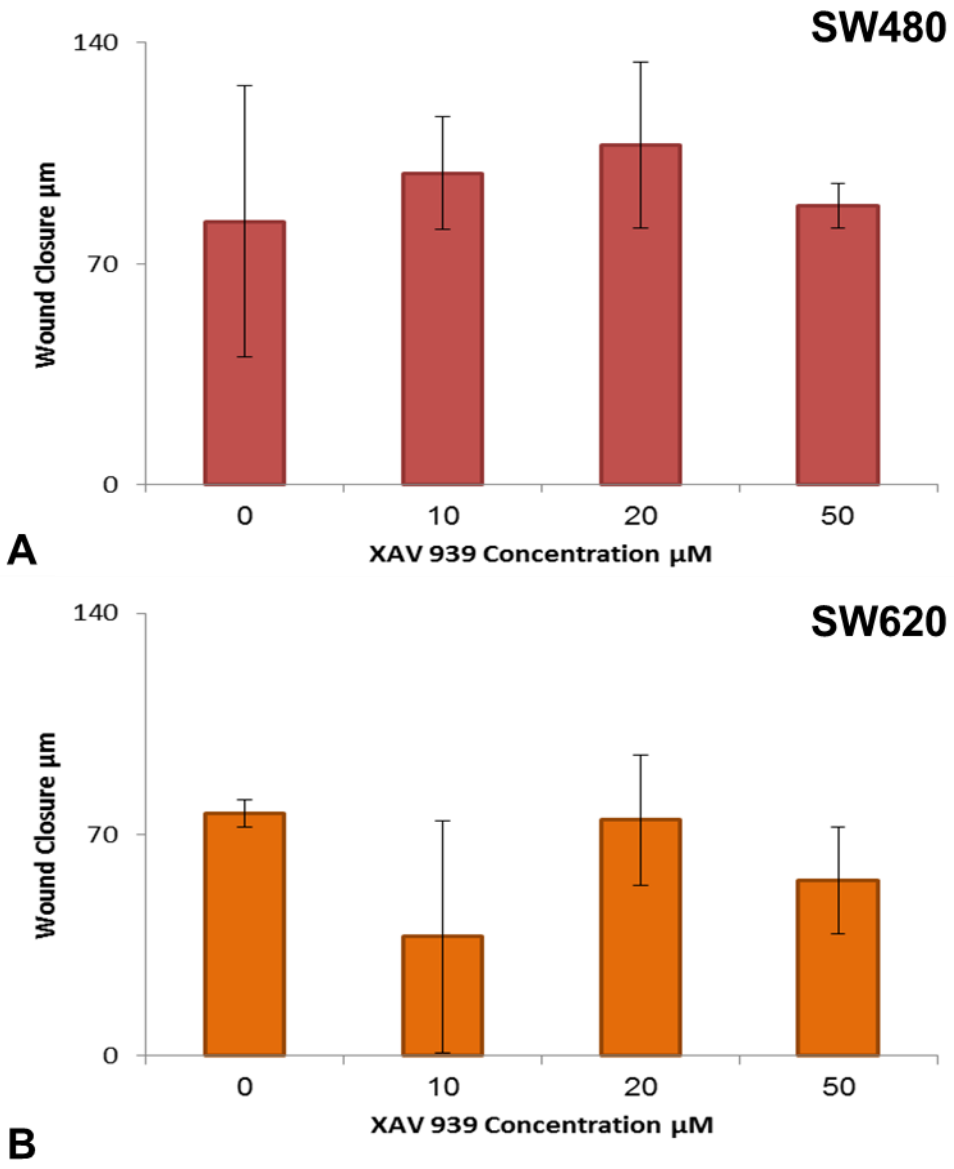

Figure 4.15: Neither the SW480 and SW620 cell lines showed a significant alteration in the distance moved by the edges of the 2D scratch wound in the presence of XAV 939 at concentrations of 10µM and above. Wound closure in µm of A: SW480 and B: SW620 cells as determined by measuring the width of the wound. Data represent mean, n = 3, ±SEM for both graphs, no significance by a Dunnett's t-test.

The images of the DAPI and Phalloidin stained cultures confirmed that scratch wounds to the SW620 cultures resulted in a greater number of single cells within the wound than was seen in the SW480 cultures (Figure 4.16), ANOVA, $F(1,16)=33.304$, $p<0.001$. Counts of these individual cells demonstrated that the application of XAV 939 to the 24 hour scratch wounds did not affect the number of these cells seen in either cell line (Figure 4.17).

Together these experiments demonstrate the XAV 939 is a Wnt signalling inhibitor which is ineffective in mediating the migratory behaviour of colorectal cancer cells in both 2D and 3D migration models and it is therefore an unsuitable candidate for further investigation.

4.3.2 Further 3D small molecule screens highlight an effective Wnt signalling inhibitor

With XAV 939 ruled out for use in investigating the role of the Wnt pathway in the migratory behaviour of colorectal cancer cells in *in vitro* models, the remaining three candidate small molecule inhibitors were screened. A single concentration was selected for each small molecule based on previous usage in the literature. The IC_{50} value of IWR-1 against Wnt signalling activity has been found to be 0.18μM when used in L-Wnt-STF cells [313], with the standard concentration of usage being 10μM [313, 315-317, 320, 321], hence the concentration of 10μM was selected for the screening process.

There has not been an IC_{50} value established for the action of cardamonin on β-catenin degradation, with the closest approximation coming from Cho *et al* demonstrating that β-catenin mediated Wnt signalling is inhibited in the presence of cardamonin at concentrations of 5μM and above [297] and other papers using concentrations of 10μM [298] or 20 to 80μM [299]. For the screening of compounds, the concentration of 10μM was selected for cardamonin as it sits in the midrange of concentrations used in a variety of models.

The small molecule ICG 001 has an IC_{50} value of 3μM for binding to the transcription co-activator CBP [302] and has been used at a variety of concentrations from 1μM [330] through to 100μM [302, 303, 307, 308], although it has been shown to have a negative impact on cell viability at higher concentrations [308]. For these reasons, ICG 001 was tested in the small molecule screen at a concentration of 5μM.

4.3.2.1 The distribution of colorectal cancer cells was affected by the inclusion of small molecule Wnt inhibitors

When these three small molecules were screened in a 3D migration assay, the distribution of the SW480 and SW620 cell lines was still found to display the same broad characteristics as before, with the SW480 cells growing in clusters towards the top of the material and the SW620 cells distributed as single cells (Figure 4.18). However, in this screen there were differences seen in the depth distribution of the two cell lines with some of the candidate molecules. When exposed to 5μM ICG 001, the SW480 cell line had a tighter distribution of cells, with more appearing to grow as clusters and fewer single cells found between the clusters (Figure 4.18G). Additionally, the distribution of the SW620 cells did not extend as far down into the scaffold as in the DMSO control in cultures treated with either 10μM IWR-1 (Figure 4.18D) or 5μM ICG 001 (Figure 4.18H).

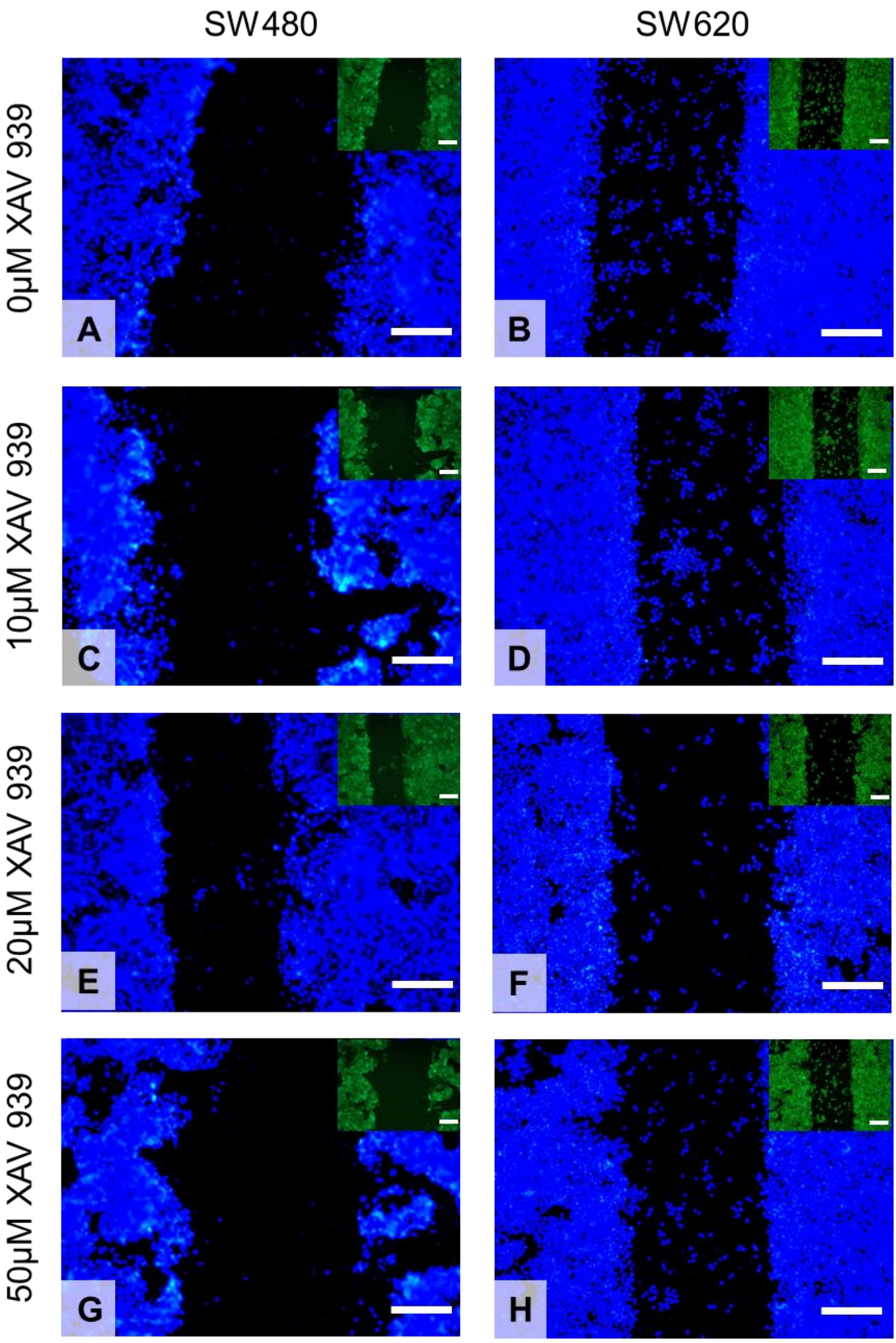

Figure 4.16: The SW620 cell line had more single migrating cells than the SW480 cell line during a scratch wound assay with concentrations of the Wnt inhibitor XAV 939 of 10µM and above. DAPI and Phalloidin (inset) images of 24 hours post wounding with A and B: 0µM XAV 939 (DMSO control), C and D: 10µM XAV 939, E and F: 20µM XAV 939 and G and H: 50µM XAV 939 for both cells lines. Scale bars = 200µm for all images.

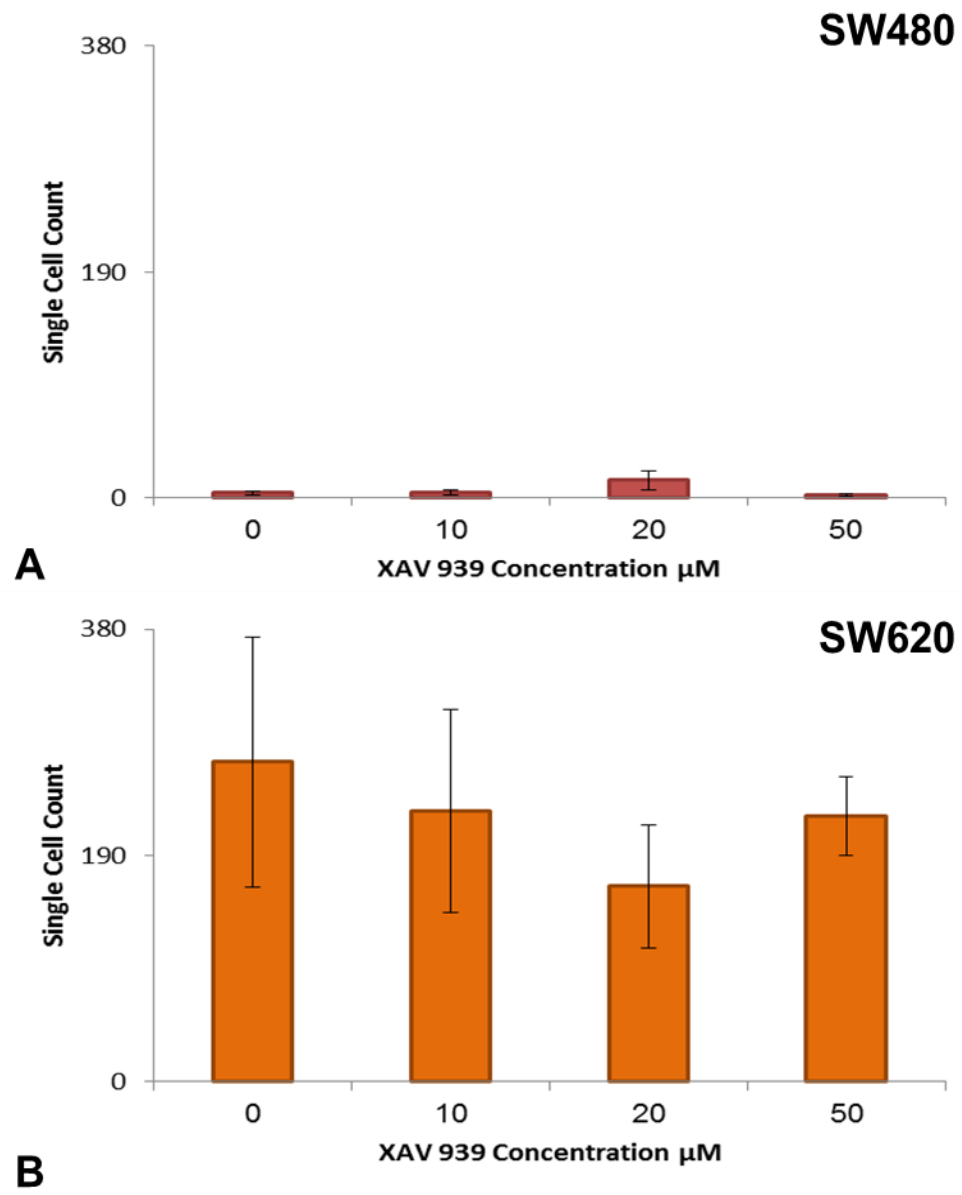

Figure 4.17: Neither the SW480 and SW620 cell lines showed a significant alteration in the number of single migrating cells within the 2D scratch wound in the presence of XAV 939 at concentrations of 10µM and above. Number of single migrating cells in A: SW480 and B: SW620 scratch wounds as determined from cell counts. Data represent mean, n = 3, ±SEM for both graphs, no significance by a Dunnett's t-test.

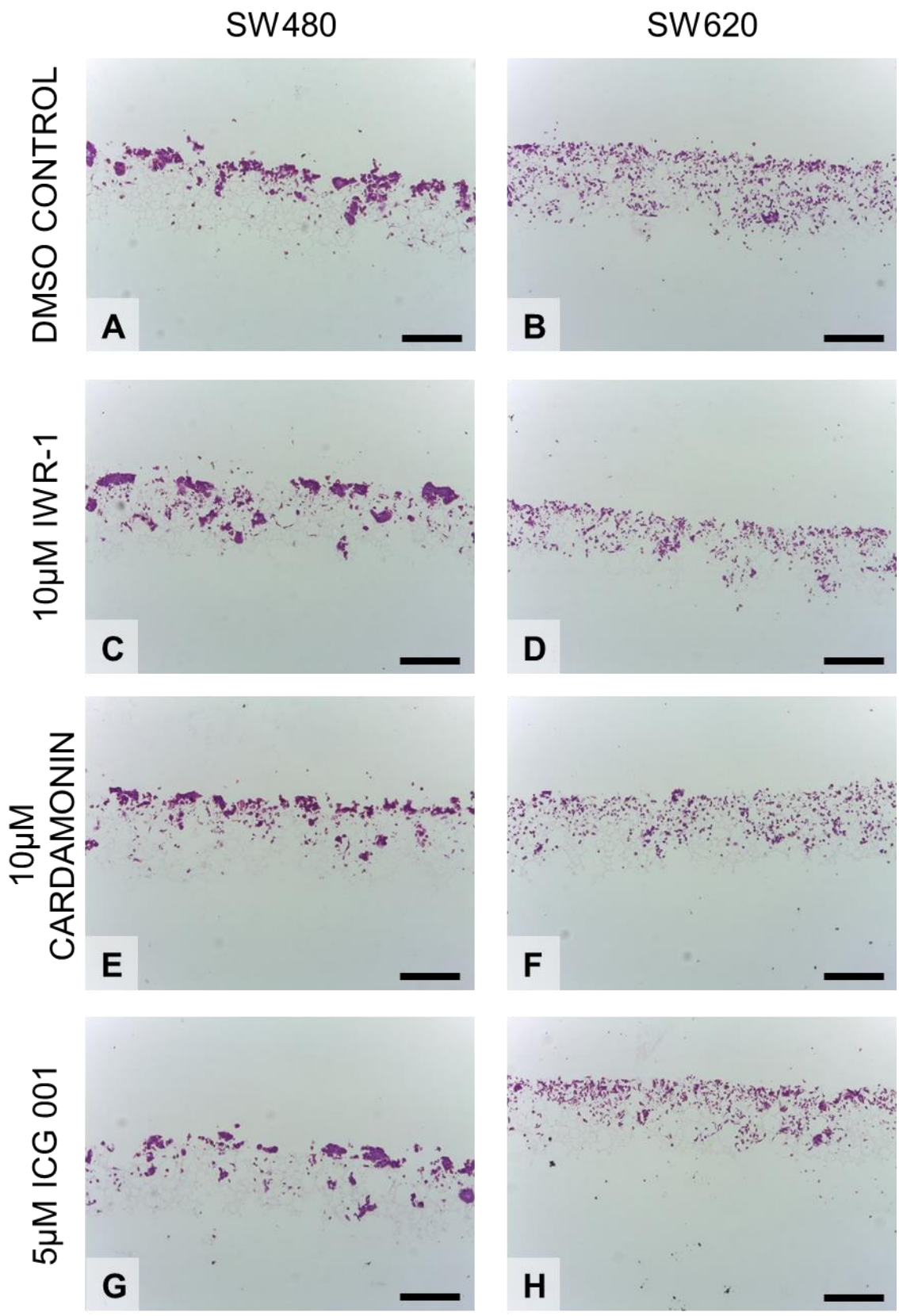

Figure 4.18: The application of Wnt inhibitors alters the distribution of SW480 and SW620 cells in 3D. The SW480 cell line displayed a decrease in the build-up of cells when 5µM ICG 001 was present, while the SW620 cell line displayed a decrease in the build-up of cells when either 10µM IWR-1 or 5µM ICG 001 were present. H&E images of 10 day cultures with A and B: DMSO control, C and D: 10µM IWR-1, E and F: 10µM cardamonin and G and H: 5µM ICG 001 for both cells lines. Scale bars = 200µm for all images.

The alteration in the distribution of the SW480 cells in the presence of 5μM ICG 001 was not reflected in the cell penetration observed under this condition (Figure 4.19A). This data confirms that none of the three small molecules tested were effective in altering the penetration behaviour of the SW480 cell line in this 3D model. In contrast, the cell penetration data for the SW620 cell line did show that molecules screened impact the behaviour of the cells in this model. Application of either 10μM IWR-1 or 5μM ICG 001 had a negative impact on the cell penetration achieved by the SW620 cell line after the 10 day culture period, while cardamonin failed to induce a significant change in cell behaviour (Figure 4.19B). Additionally, the SW620 cell line continued to demonstrate a greater ability to penetrate the scaffold than the SW480 cell line, ANOVA, $F(1,19)=15.94$, $p=0.001$.

4.3.2.2 Small molecule inhibition of Wnt signalling inhibited cell viability and proliferation

The viability data from this experiment also showed that the small molecules have a variable effect on both cell lines, ANOVA, $F(3,19)=7.573$, $p=0.002$. The application of either 10μM IWR-1 to the SW480 cell line or 10μM cardamonin to the SW620 cell line led to a decrease in cell viability, while culturing the SW620 cell line in the presence of 5μM ICG 001 resulted in an increase in the viability (Figure 4.20). While the addition of small molecules had an overall effect on the number of cells observed in the 3D cultures, ANOVA, $F(1,19)=106.315$, $p<0.001$, the decreased cell viability of SW480 cultures in response to 10μM IWR-1 was not mirrored by a decrease in cell number (Figure 4.21A), unlike the correlation seen between cell viability and cell number in the SW480 cell line in response to XAV 939 (Figure 4.4, Figure 4.5, Figure 4.12 & Figure 4.13). However, there was a decrease in the number of SW480 cells found in the 3D cultures after 10 days when the cultures have been exposed to 5μM ICG 001. The only alteration to cell number seen with the SW620 cell line was in cultures which have been exposed to 10μM cardamonin, with the other small molecules leaving cell number unaffected (Figure 4.21B). Despite the reduction in cell number mediated by 10μM cardamonin, the SW620 culture were found to contain more cells than the SW480 cultures, ANOVA small molecule, $F(3,19)=4.656$, $p=0.013$.

4.3.2.3 The single cell migration of SW620 cells was altered by small molecule inclusion

The counterpart 2D scratch wound screen of IWR-1, cardamonin or ICG 001 demonstrated that none of these small molecules fully inhibited the migration attained by 24 hours in this model (Figure 4.22). This is reflected in the wound closure data, where the distance moved by the wound edges was not significantly altered by the addition of any of the small molecules tested (Figure 4.23).

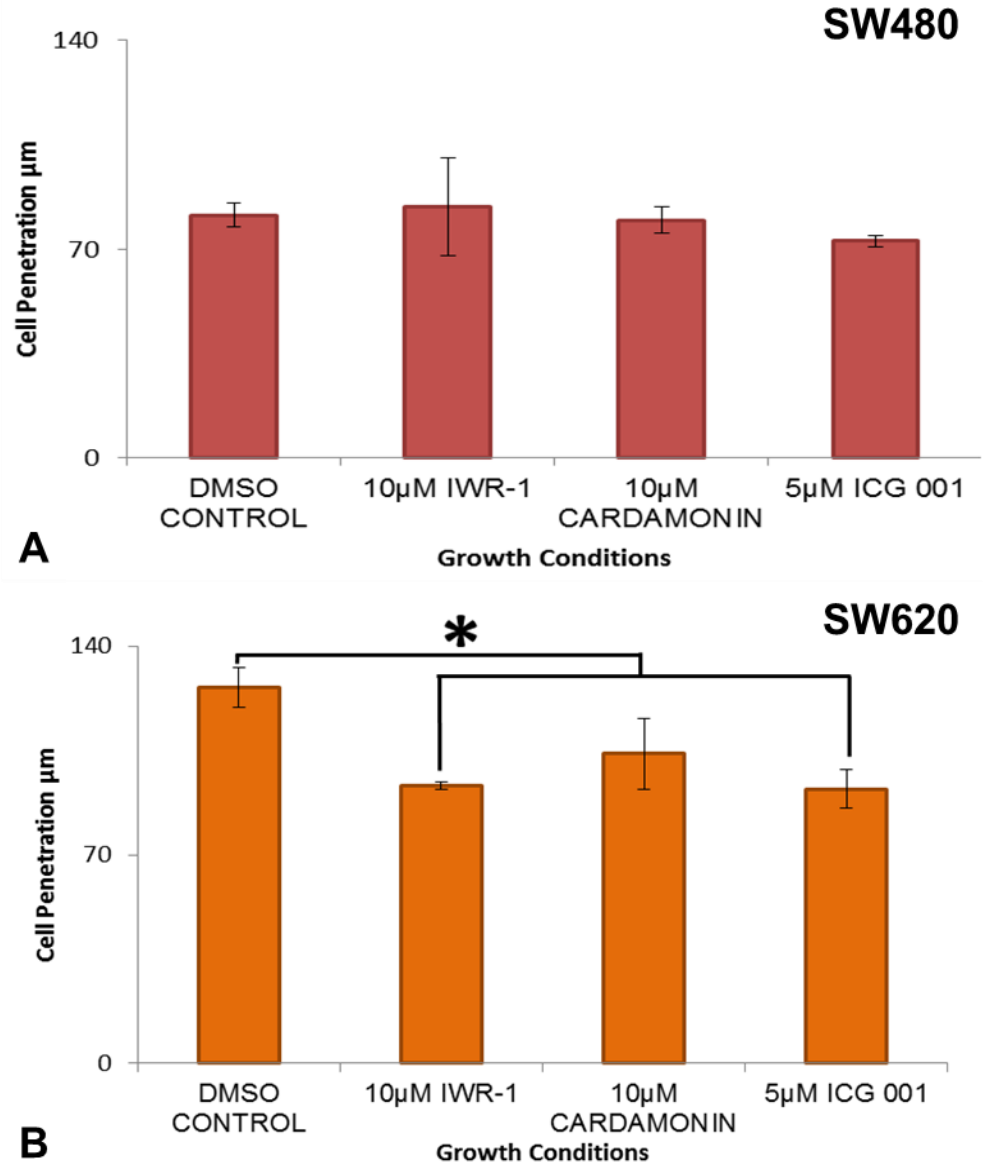

Figure 4.19: The 3D cell penetration of the SW620 cell line decreased in the presence of 10µM IWR-1 or 5µM ICG 001, but remained unaffected by 10µM cardamonin, while the penetration of the SW480 cell line remained unaffected by all small molecules. Cell penetration in µm of A: SW480 and B: SW620 cells as determined by the linear measurement method. Data represent mean, n = 3, ±SEM for both graphs, * $p<0.05$ by a Dunnett's t-test.

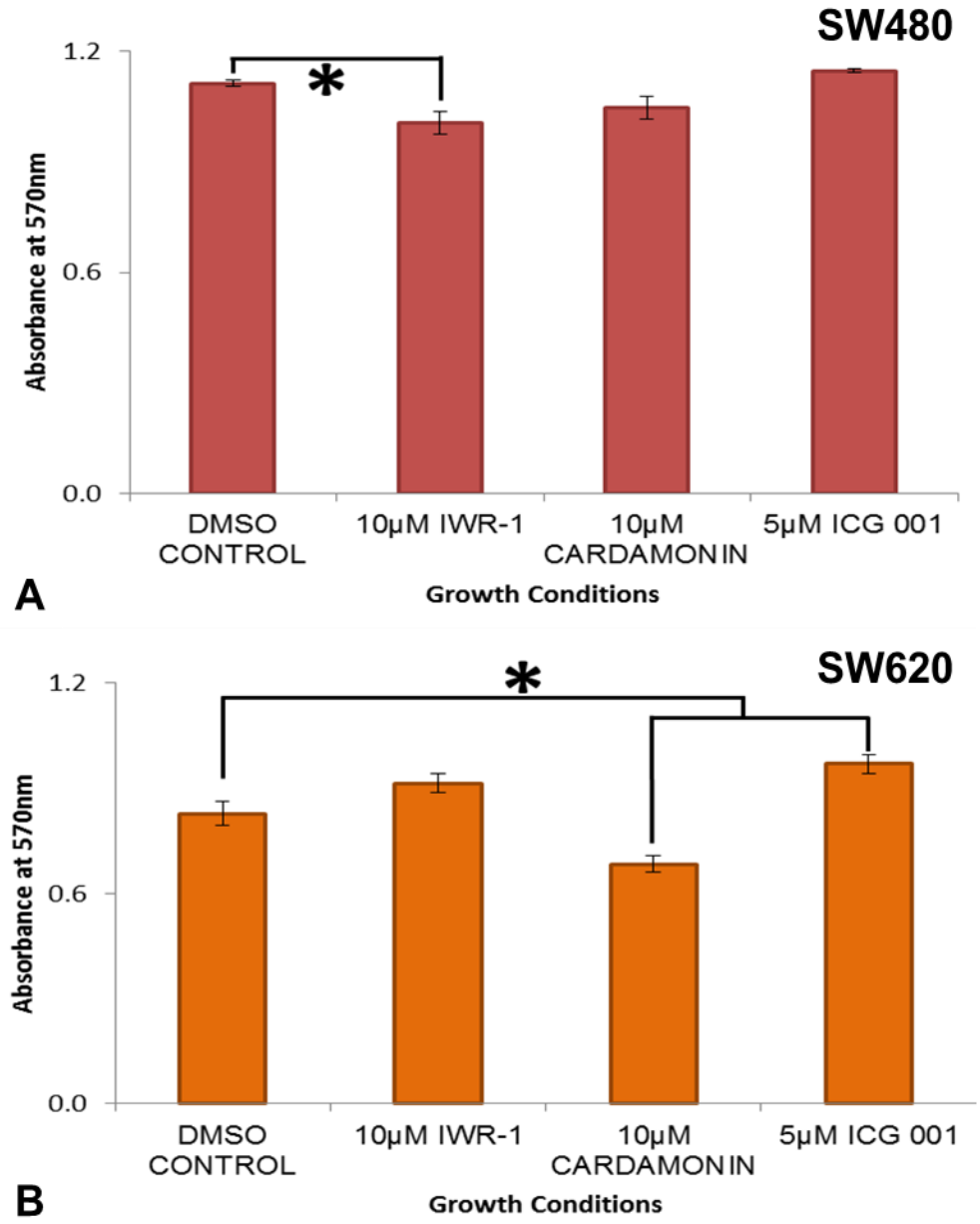

Figure 4.20: The 3D cell viability of the SW620 cell line increased in the presence of 5µM ICG 001, but decreased in the presence of 10µM cardamonin, while the viability of the SW480 cell line decreased in the presence of 10µM IWR-1. Absorbance at 570nm of A: SW480 and B: SW620 cells as determined by the MTT Cell Viability Assay. Data represent mean, n = 3, ±SEM for both graphs, * $p < 0.05$ by a Dunnett's t-test.

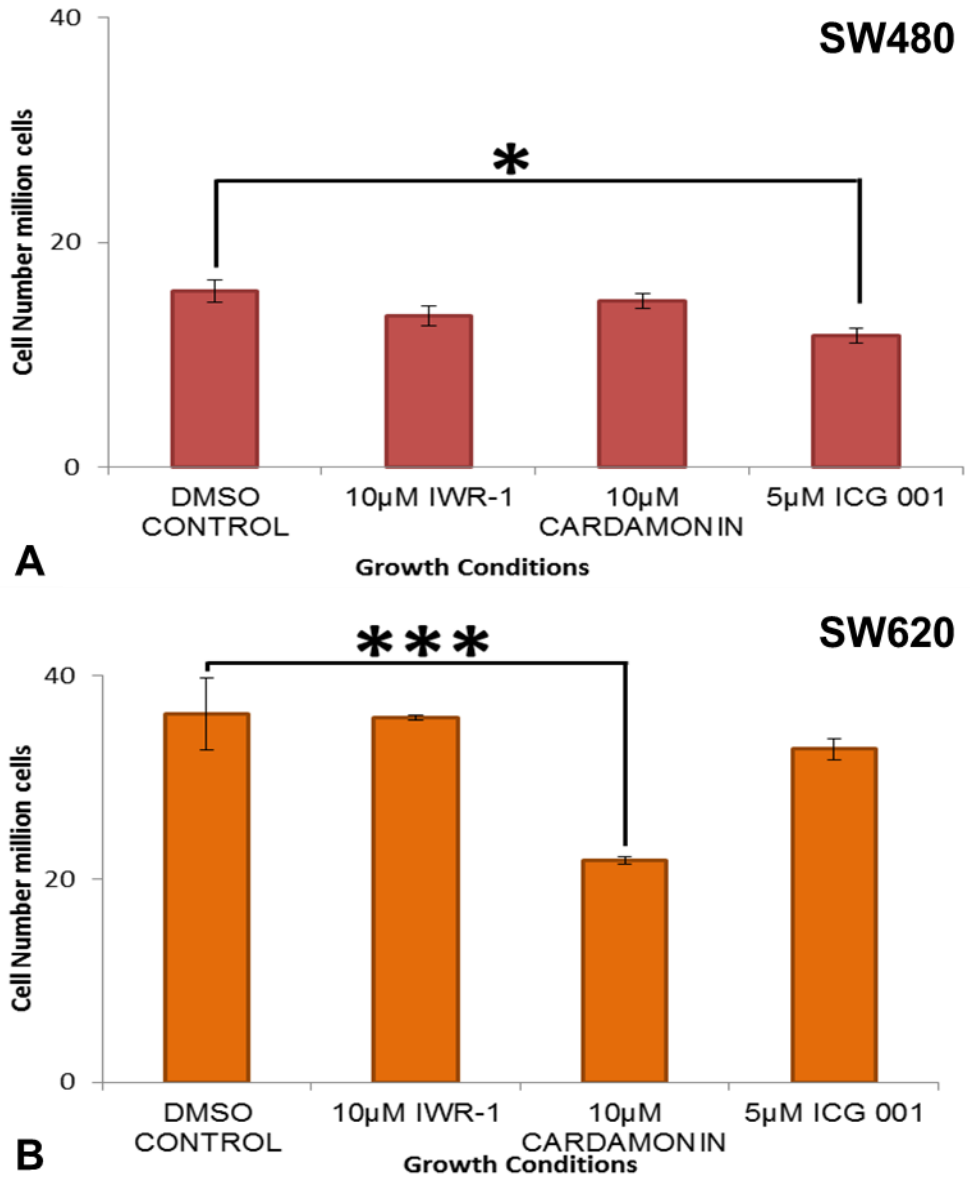

Figure 4.21: The number of SW480 cells in the 3D material decreased when 5μM ICG 001 was present, while the number of SW620 cells decreased when 10μM cardamonin was present. Cell number in millions of cells of A: SW480 and B: SW620 cells as determined by the Pico Green dsDNA Assay. Data represent mean, n = 3, ±SEM for both graphs, * $p < 0.05$, *** $p<0.005$ by a Dunnett's t-test.

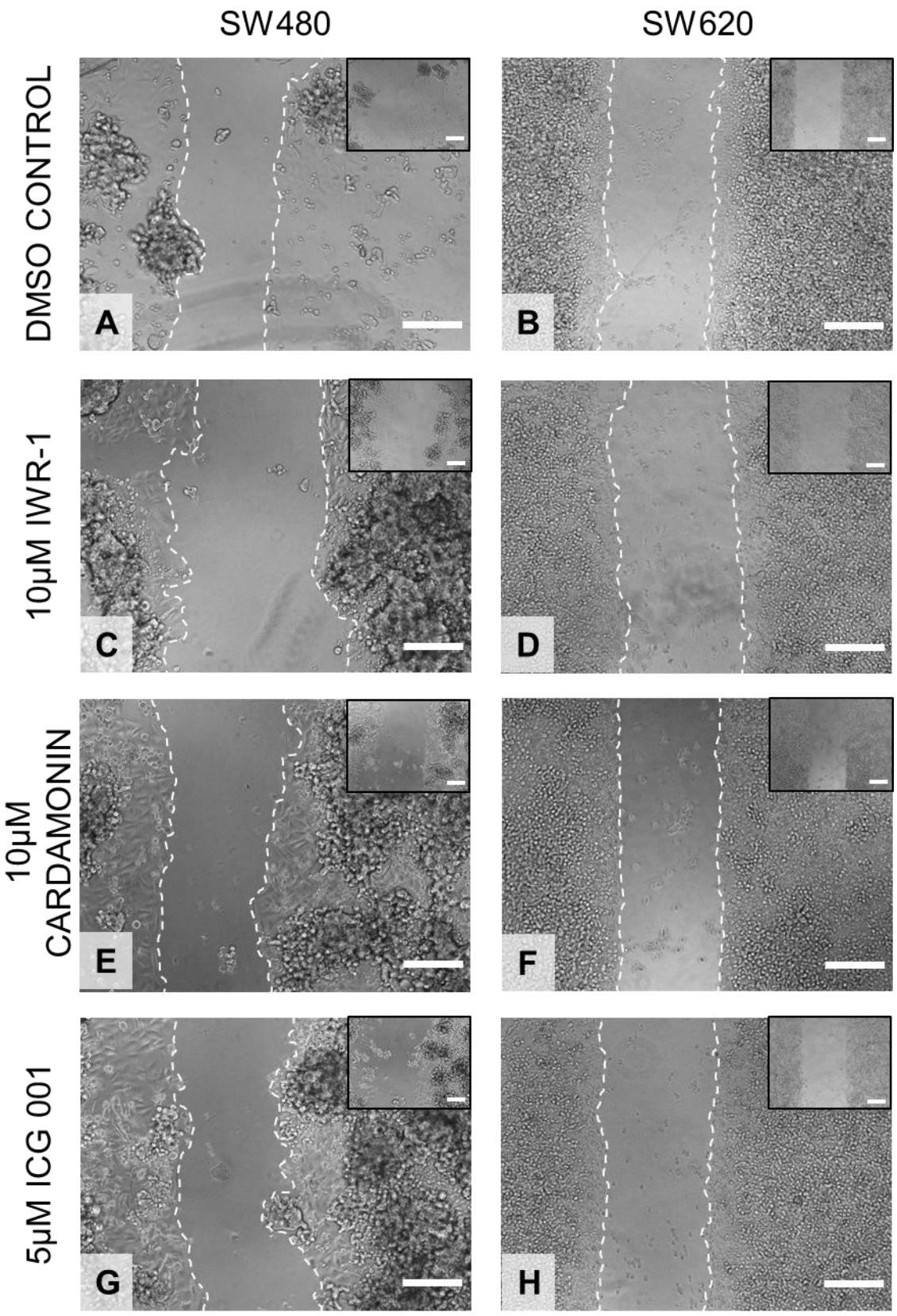

Figure 4.22: Both the SW480 and SW620 cell lines exhibied wound closing during a scratch wound assay with small molecule Wnt inhibitors. Phase images of 24 hours post wounding, with 0 hours post wounding shown inset, with A and B: DMSO control, C and D: 10µM IWR-1, E and F: 10µM cardamonin and G and H: 5µM ICG 001 for both cells lines. Scale bars = 200µm for all images.

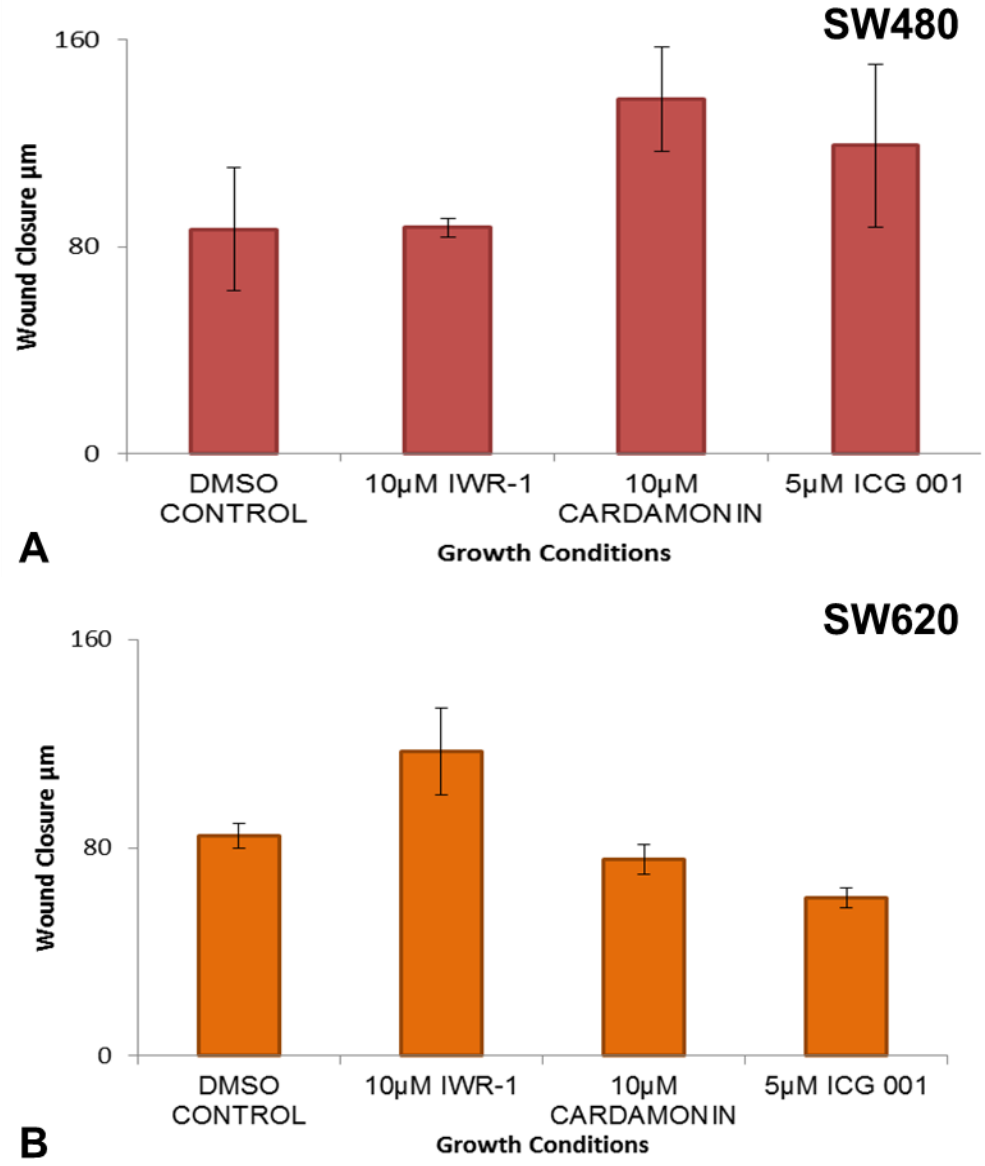

Figure 4.23: Neither the SW480 and SW620 cell lines showed a significant alteration in the distance moved by the edges of the 2D scratch wound in the presence of various small molecule inhibitors of the Wnt signalling pathway. Wound closure in µm of A: SW480 and B: SW620 cells as determined by measuring the width of the wound. Data represent mean, n = 3, ±SEM for both graphs, no significance by a Dunnett's t-test.

The DAPI and Phalloidin staining demonstrated that while the SW620 cell line produced more single cells in the wound after 24 hours than the SW480 cell line, the number of these appeared reduced in the cultures which have been exposed to either 10μM cardamonin or 5μM ICG 001 (Figure 4.24F & H). The quantification data for the number of single cells within the wound reflected this observation, as the numbers seen for the SW480 cell line were lower than those seen for the SW620 cell line, ANOVA cell line, $F(1,16)=667.283$, $p<0.001$, and were not altered by any of the small molecules. Whereas the SW620 scratch wounds maintained in the presence of either 10μM cardamonin or 5μM ICG 001 produced significantly fewer single cells in the wound after 24 hours (Figure 4.25) and the addition of small molecules was found to have an overall effect on single cell migration, ANOVA small molecule, $F(3,16)= 61.270$, $p<0.001$.

When viewed together, this small molecule screen highlights a clear candidate, IWR-1, for further use as it caused a decrease in the penetration of the SW620 cell line without adversely affecting the number of cells seen in the 3D cultures. As the aim of this project is to investigate the role of the Wnt pathway in modulating migratory behaviour of colorectal cancer cells and not the proliferative or apoptotic behaviour, neither cardamonin nor ICG 001 are suitable candidates for further use in this model, as they have a negative impact on the number of cells found in 3D SW620 and SW480 cultures respectively.

4.3.3 IWR-1 is only effective at inhibiting SW620 migration in 3D

As it has been demonstrated that IWR-1 is effective at limiting the amount of cell penetration achieved by the SW620 in the 3D migration assay at a concentration of 10μM, it was subsequently screened to observe its effectiveness at lower concentrations. The concentrations of 0.1 and 1μM were selected, as 0.1μM falls below the IC_{50} value for IWR-1 it was expected that this concentration would fail to induce a response in the assay.

4.3.3.1 SW620 cell distribution was disrupted by higher concentrations of IWR-1

When utilised in the 3D migration assay, the distribution of the SW480 cell line was unaltered within the scaffold in the presence of IWR-1 at any concentration (Figure 4.26A, C, E & G). In contrast, the distribution of the SW620 cell line was limited to the upper half of the scaffold when IWR-1 was present at concentrations of 1 or 10μM (Figure 4.26F & H), whereas there was not a clear difference in the cell distribution of cultures with 0.1μM IWR-1 and a DMSO (0μM IWR-1) control (Figure 4.26B & D). The alteration in the depth distribution of cells in response to the higher concentrations of IWR-1 was not correlated with a change to the clustering behaviour of the cells, as they were still found as individuals within the scaffold.

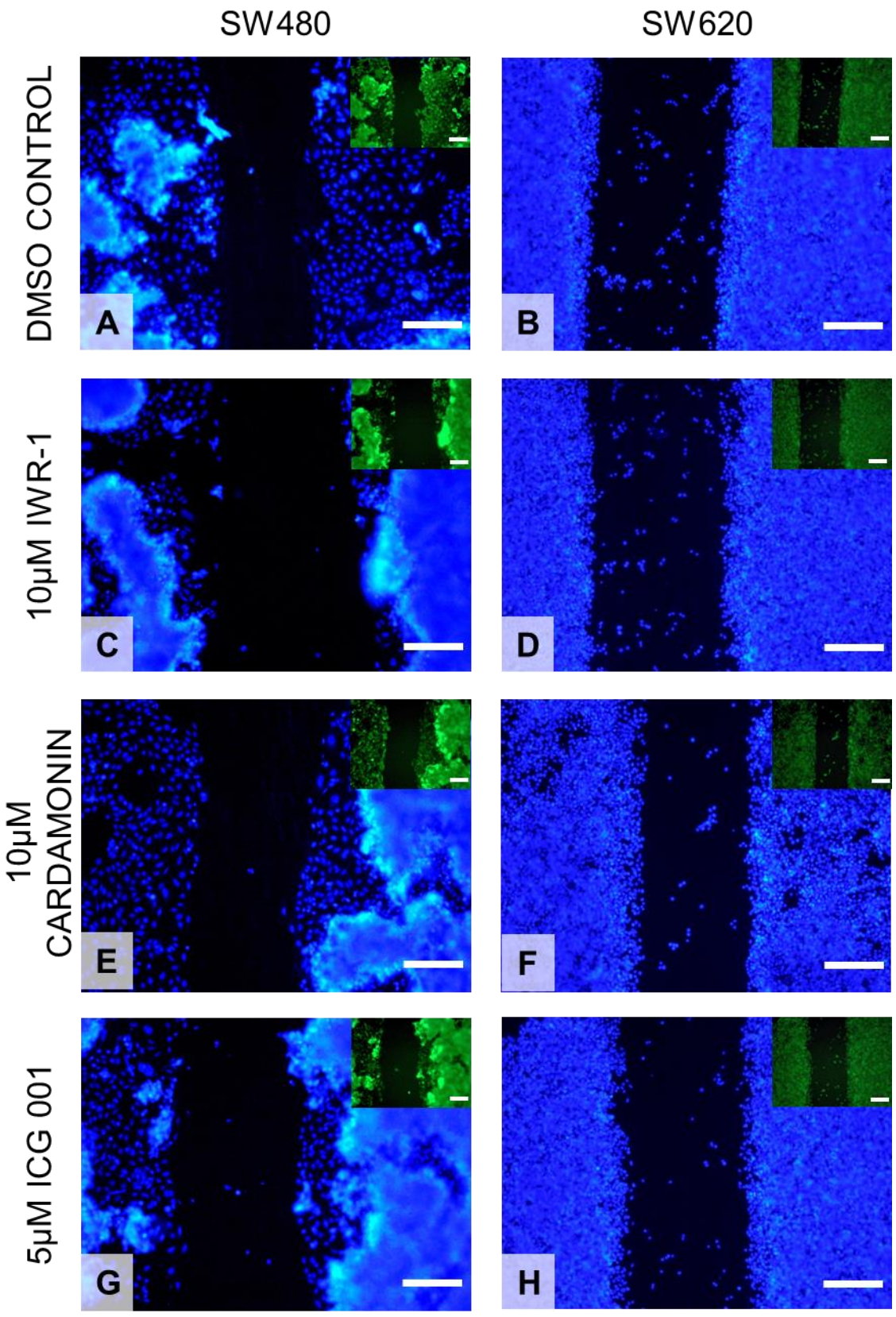

Figure 4.24: The SW620 cell line had more single migrating cells than the SW480 cell line during a scratch wound assay, with the numbers affected by small molecule Wnt inhibitors. DAPI and Phalloidin (inset) images of 24 hours post wounding with A and B: DMSO control, C and D: 10µM IWR-1, E and F: 10µM cardamonin and G and H: 5µM ICG 001 for both cells lines. Scale bars = 200µm for all images.

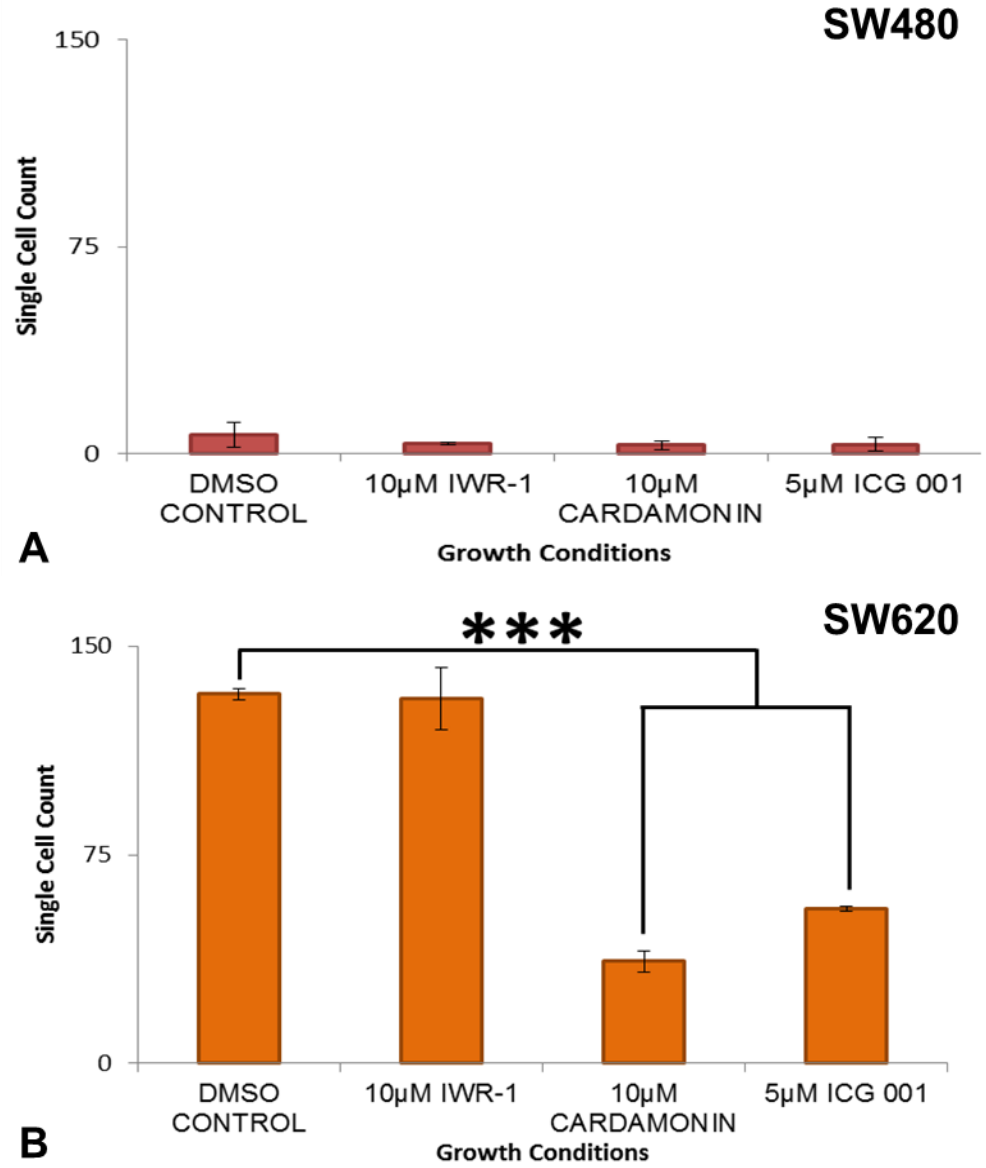

Figure 4.25: The SW620 cell line showed a significant alteration in the number of single migrating cells within the 2D scratch wound in the presence of 10µM cardamonin and 5µM ICG 001, whereas the SW480 cell line was not affected. Number of single migrating cells in A: SW480 and B: SW620 scratch wounds as determined from cell counts. Data represent mean, n = 3, ±SEM for both graphs, *** $p < 0.005$, by a Dunnett's t-test.

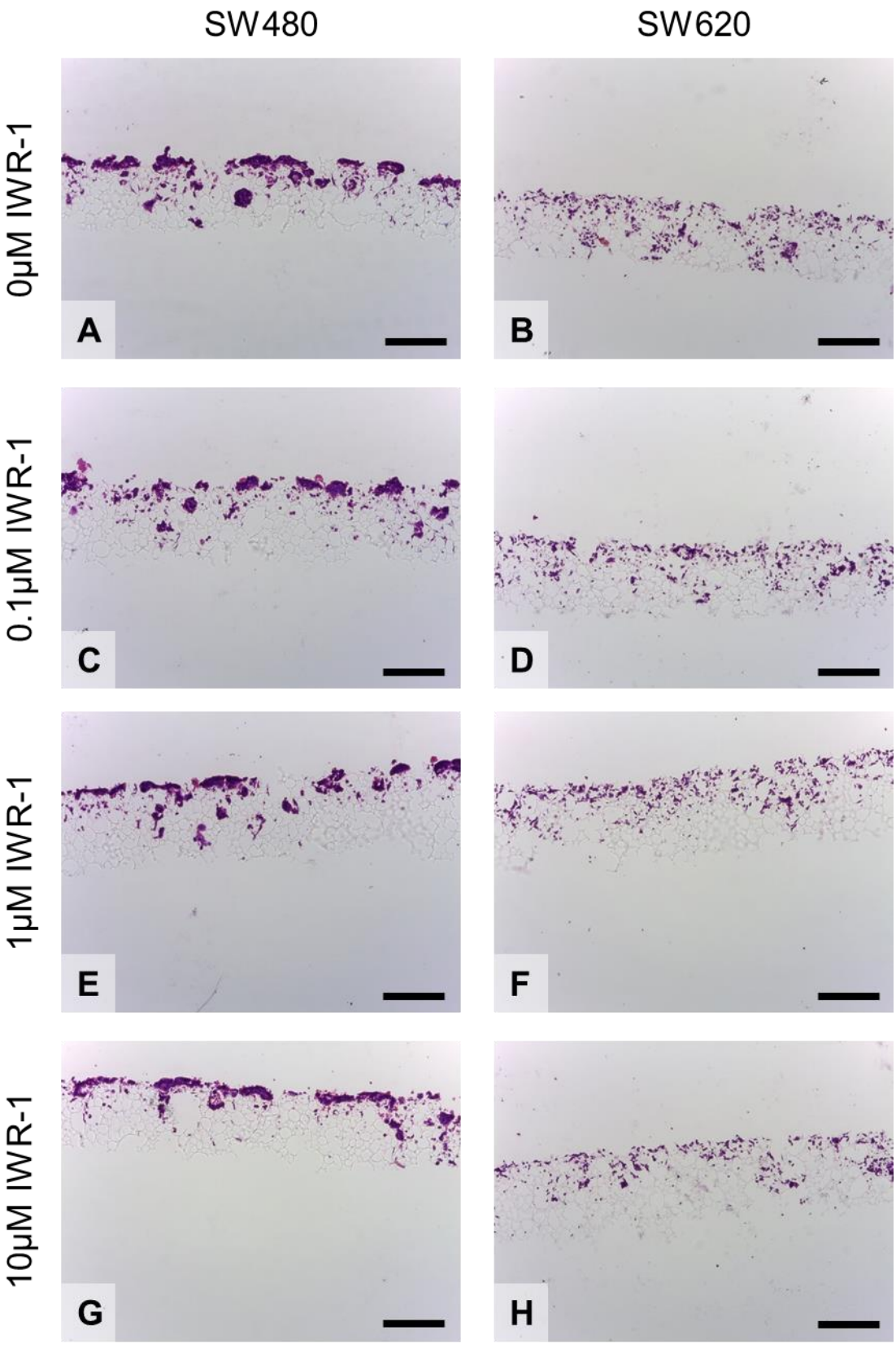

Figure 4.26: The SW620 cell line displayed a decreased build-up of cells when the Wnt inhibitor IWR-1 is present at a concentration of 1μM and above, while the SW480 cell line remained unaffected. H&E images of 10 day cultures with A and B: 0μM IWR-1 (DMSO control), C and D: 0.1μM IWR-1, E and F: 1μM IWR-1 and G and H: 10μM IWR-1 for both cells lines. Scale bars = 200μm for all images.

4.3.3.2 IWR-1 affected cell penetration without affecting viability or proliferation

In line with the histological data, the SW620 cell line was found to attain a greater depth of cell penetration than the SW480 cell line, ANOVA, $F(1, 19)=20.376$, $p<0.001$. The cell penetration of SW480 cell line into the scaffold was not altered by the addition of IWR-1 at any concentration (Figure 4.27A). Use of IWR-1 at a concentration of 0.1μM was also insufficient to induce a change in cell penetration in the SW620 cell line, whereas 1 and 10μM were both sufficient to significantly reduce the level of cell penetration seen in the SW620 cell line (Figure 4.27B). Application of IWR-1 did not alter the viability of either the SW480 or SW620 cell line for any of the concentrations tested (Figure 4.28). Additionally, there was no difference in cell number for either of the two cell lines after exposure to IWR-1 at any concentration (Figure 4.29), with a greater cell number measured for the SW620 cultures, ANOVA, $F(1,19)=126.167$, $p<0.001$.

4.3.3.3 2D migration was unaffected by IWR-1 at any concentration

As expected from the initial small molecule screen, addition of IWR-1 into the culture media for 2D scratch wounds did not have an effect on the appearance of the cellular distribution after 24 hours for either of the cell lines (Figure 4.30). This resulted in no significant alteration to the distance moved by either of the wound edges for either cell line upon exposure to IWR-1 (Figure 4.31). The DAPI and Phalloidin staining also confirmed that there was also a consistent pattern of single cell distribution within the wound after 24 hours for either cell line in the presence and absence of IWR-1 (Figure 4.32) and the quantification of these cells showed that the amount of them did not alter in the presence and absence of IWR-1 (Figure 4.33), although there were more SW620 cells observed in the wound, ANOVA, $F(1,16)=101.217$, $p<0.001$.

Together, these data show that IWR-1 is a small molecule inhibitor of Wnt which is an effective inhibitor of migration in a 3D model of colorectal cancer, without affecting the number of cells found in the material by the end of the culture period, but which is not effective in a standard 2D scratch wound model at the same concentrations.

4.3.4 IWR-1 suppresses β-catenin expression in the SW620 cell line

With this identification of IWR-1, which is capable of causing a 17% decrease in cell penetration in a 3D migration model, the effect of this molecule on the expression of key EMT and signalling proteins was examined. The proteins selected for investigation via immunohistochemistry were E-cadherin and vimentin, both key identifiers of cancer cells which have gone through EMT [79], β-catenin, the transcriptional mediator of Wnt signalling [86], and Slug, a transcriptional suppressor which mediates the effect of β-catenin on E-cadherin expression [223]. Together these proteins should provide information about the migratory capacity of the cells and the role of Wnt signalling in directing the migratory behaviour of the cells.

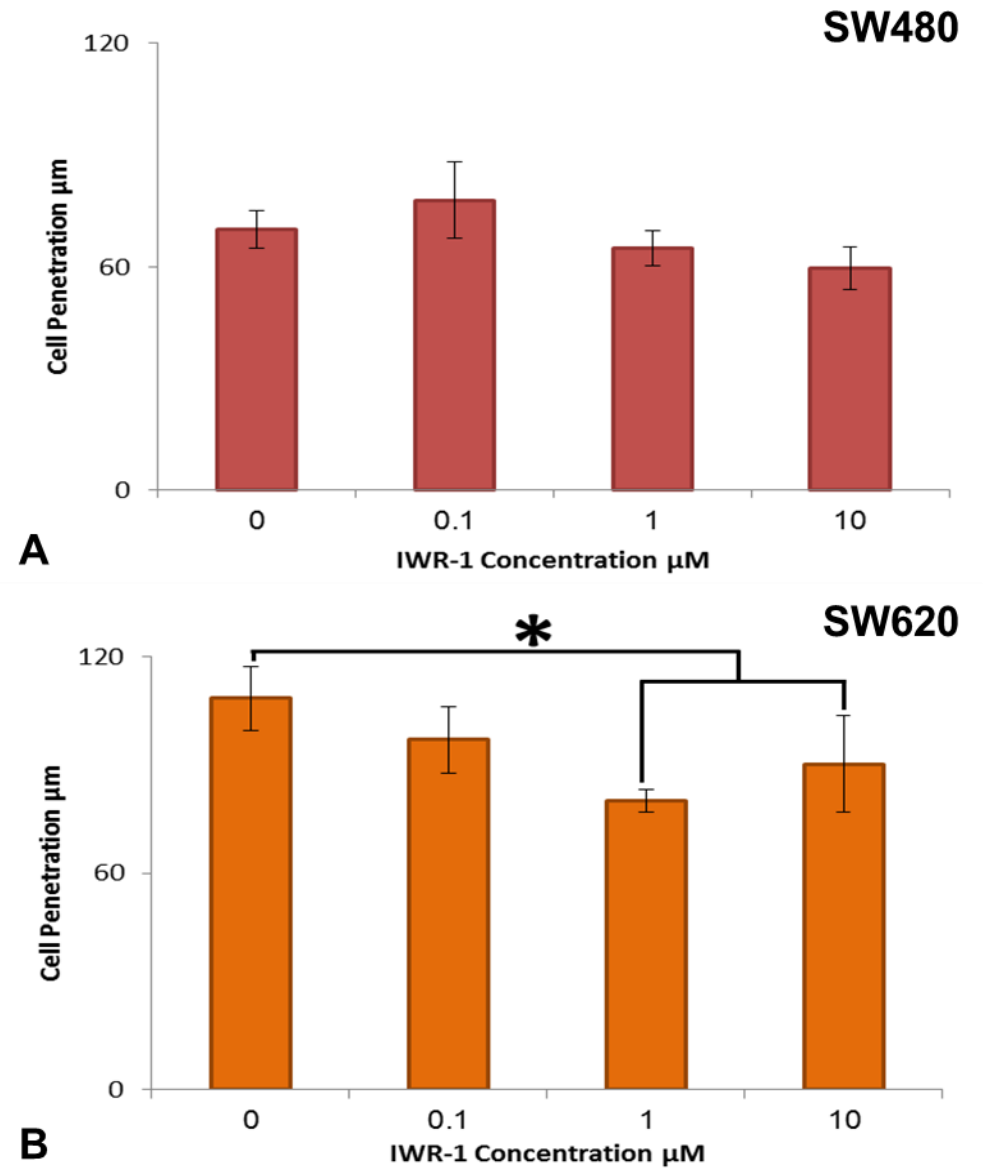

Figure 4.27: The 3D cell penetration of the SW620 cell line was decreased when IWR-1 was present at concentrations of 1µM and above, while penetration of the SW480 cell line remained unaffected. Cell penetration in µm of A: SW480 and B: SW620 cells as determined by the linear measurement method. Data represent mean, n = 3, ±SEM for both graphs, * $p < 0.05$ by a Dunnett's t-test.

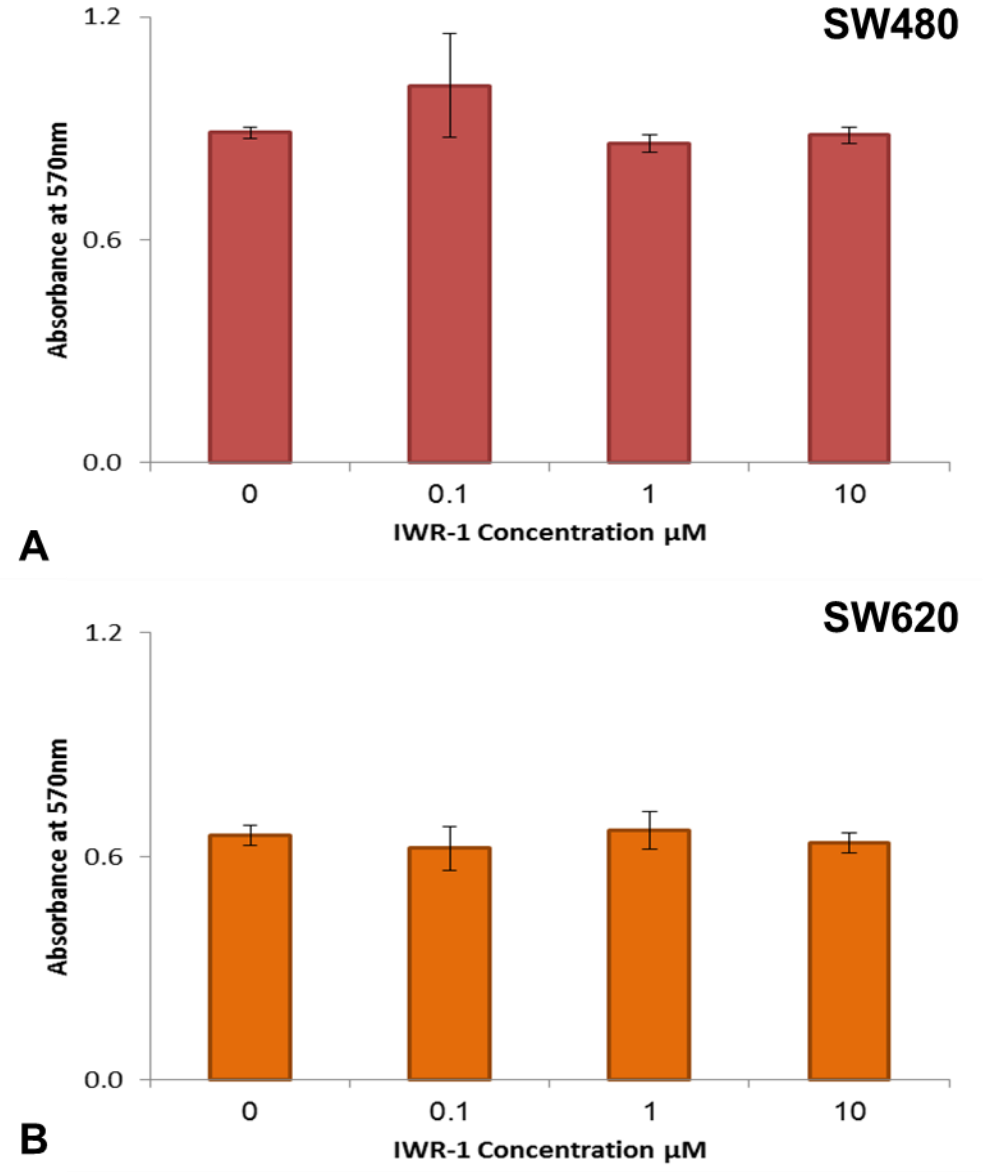

Figure 4.28: The 3D cell viability of both cell lines remained unaffected by IWR-1 present at concentrations of 10µM and below. Absorbance at 570nm of A: SW480 and B: SW620 cells as determined by the MTT Cell Viability Assay. Data represent mean, n = 3, ±SEM for both graphs, no significance by a Dunnett's t-test.

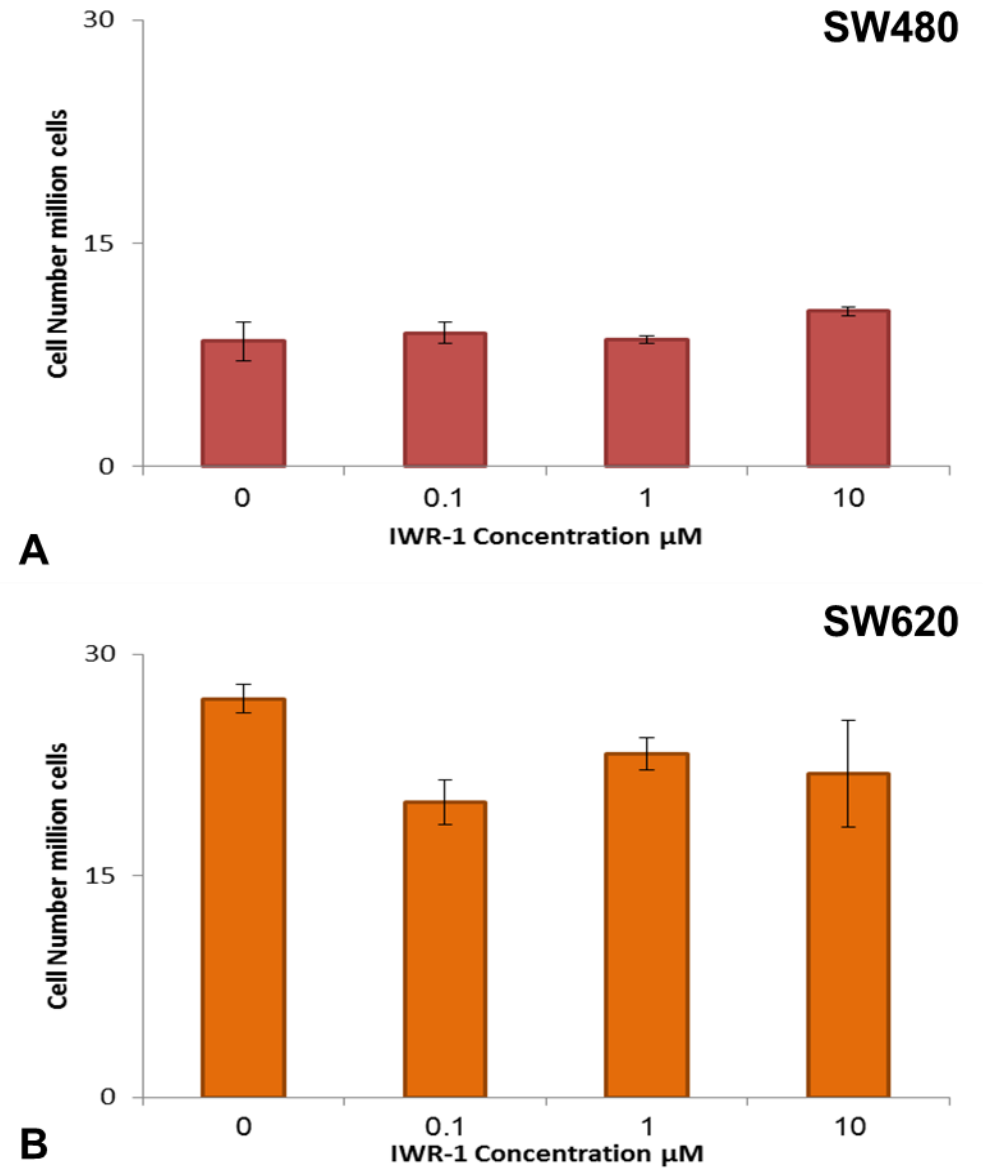

Figure 4.29: The number of cells present in the 3D material remained unaffected by IWR-1 present at concentrations of 10µM and below for both the SW480 and SW620 cell lines. Cell number in millions of cells of A: SW480 and B: SW620 cells as determined by the Pico Green dsDNA Assay. Data represent mean, n = 3, ±SEM for both graphs, no significance by a Dunnett's t-test.

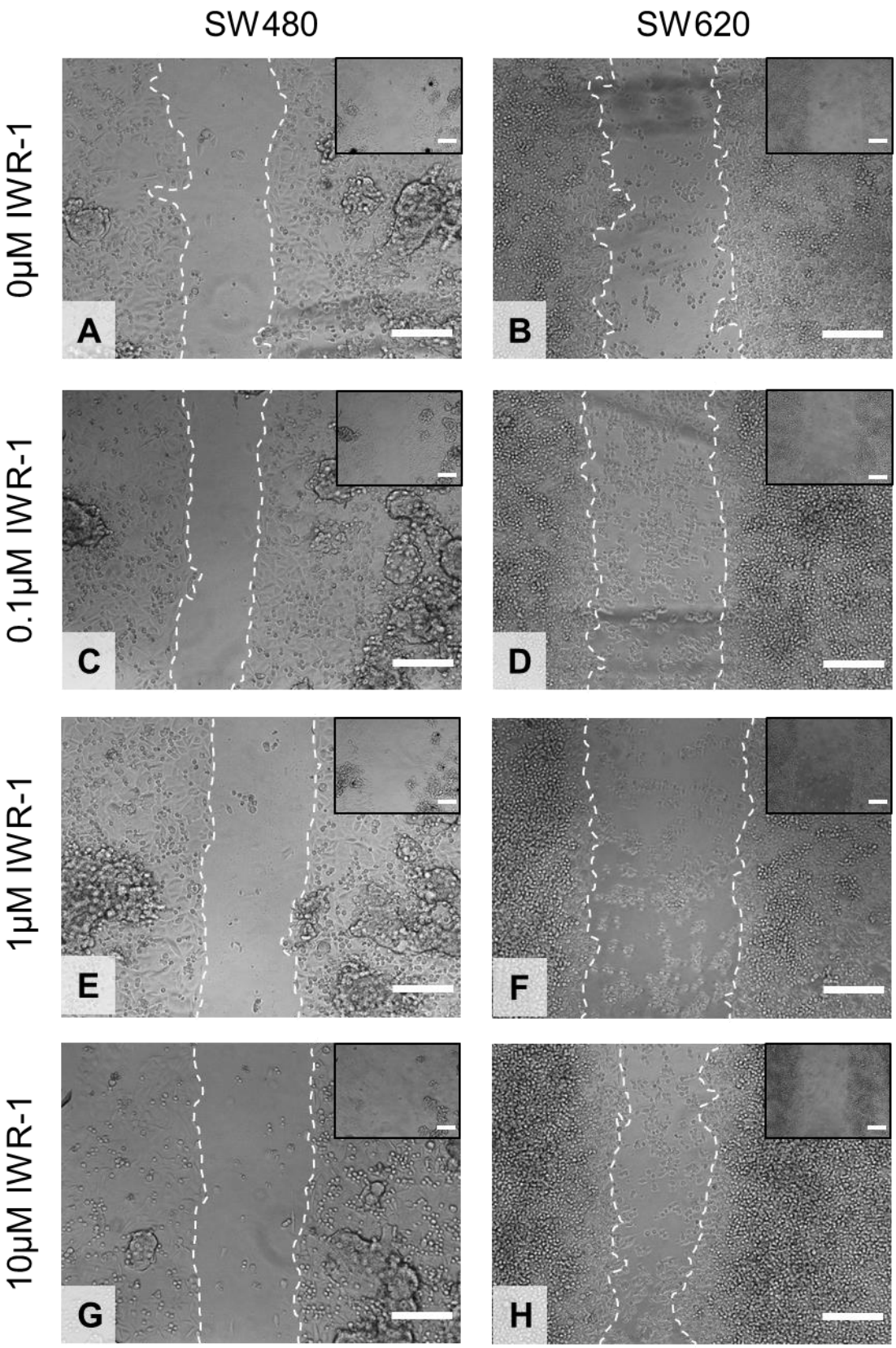

Figure 4.30: Both the SW480 and SW620 cell lines exhibited wound closing during a scratch wound assay with concentrations of the Wnt inhibitor IWR-1 of 10μM and below. Phase images of 24 hours post wounding, with 0 hours post wounding shown inset, with A and B: 0μM IWR-1 (DMSO control), C and D: 0.1μM IWR-1, E and F: 1μM IWR-1 and G and H: 10μM IWR-1 for both cells lines. Scale bars = 200μm for for all images.

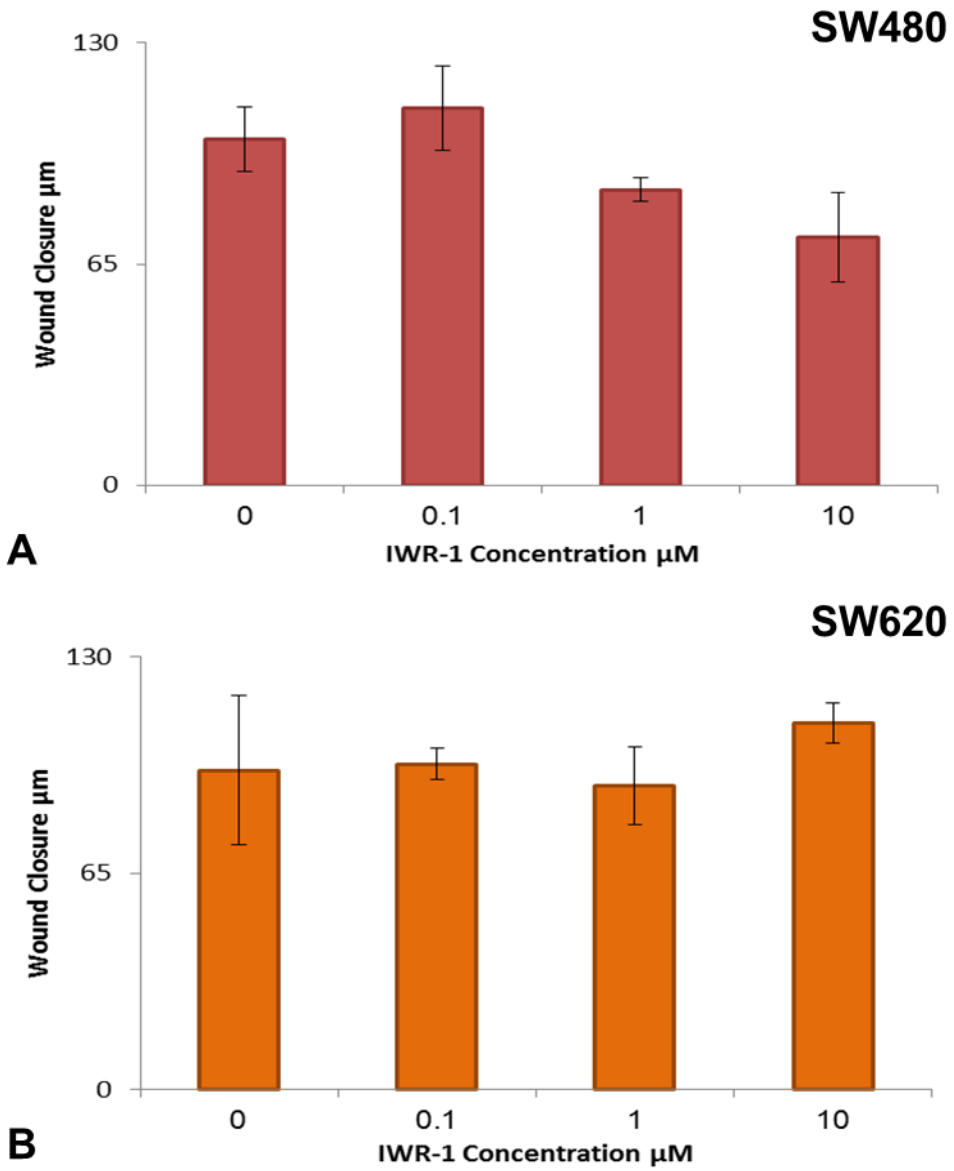

Figure 4.31: Neither the SW480 and SW620 cell lines showed a significant alteration in the distance moved by the edges of the 2D scratch wound in the presence of IWR-1 at concentrations of 10µM and below. Wound closure in µm of A: SW480 and B: SW620 cells as determined by measuring the width of the wound. Data represent mean, n = 3, ±SEM for both graphs, no significance by a Dunnett's t-test.

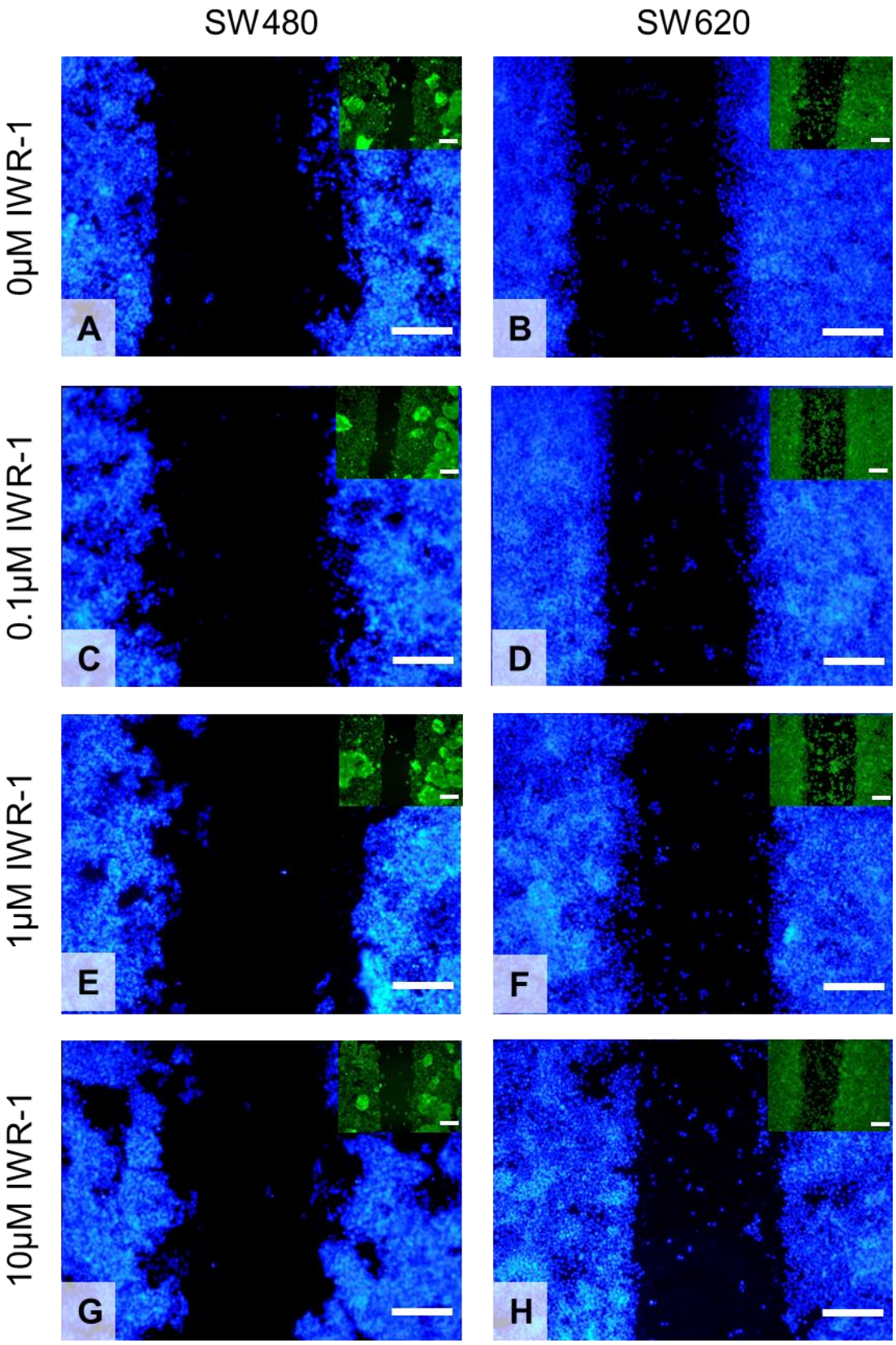

Figure 4.32: The SW620 cell line had more single migrating cells than the SW480 cell line during a scratch wound assay with concentrations of the Wnt inhibitor IWR-1 of 10µM and below. DAPI and Phalloidin (inset) images of 24 hours post wounding with A and B: 0µM IWR-1 (DMSO control), C and D: 0.1µM IWR-1, E and F: 1µM IWR-1 and G and H: 10µM IWR-1 for both cells lines. Scale bars = 200µm for for all images.

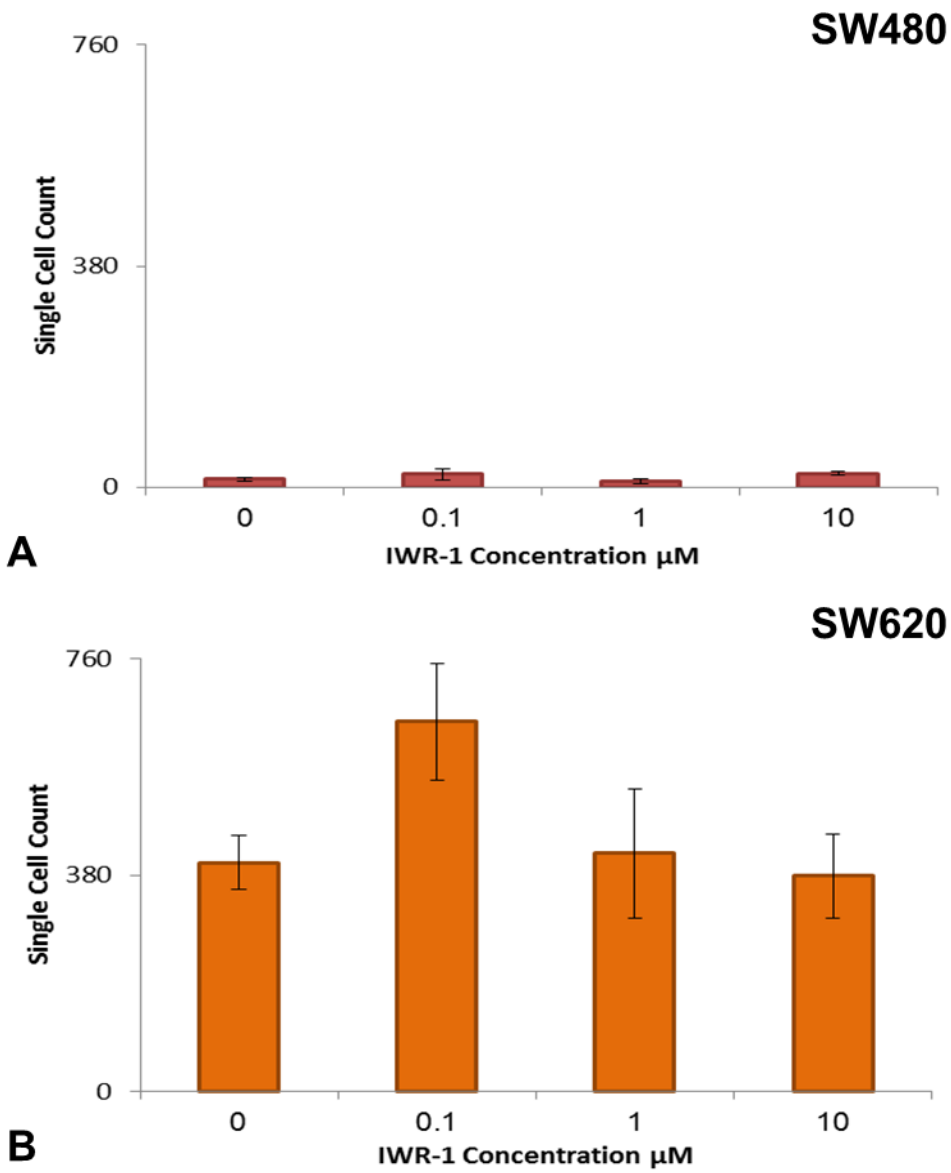

Figure 4.33: Neither the SW480 and SW620 cell lines showed a significant alteration in the number of single migrating cells within the 2D scratch wound in the presence of IWR-1 at concentrations of 10µM and below. Number of single migrating cells in A: SW480 and B: SW620 scratch wounds as determined from cell counts. Data represent mean, n = 3, ±SEM for both graphs, no significance by a Dunnett's t-test.

The immunohistochemical staining of 10 day 3D SW620 cultures in the absence and presence of 10μM IWR-1 demonstrated that the inclusion of this small molecule did affect the protein expression profile of these cells. When cultured in the absence of IWR-1, the SW620 cell line did not express E-cadherin (Figure 4.34A) or Slug (Figure 4.34G) and did express vimentin (Figure 4.34C) and β-catenin (Figure 4.34E), with the staining for vimentin appearing to be stronger than the staining for β-catenin, with more cells demonstrating more intense positive staining. When IWR-1 was included in the culture media, the expression of E-cadherin (Figure 4.34B), vimentin (Figure 4.34D) and Slug (Figure 4.34H) in the SW620 cell line did not appear to alter. However, the expression of β-catenin was seen to decrease, with fewer cells demonstrating positive staining and that positive staining being less intense(Figure 4.34F), compared to the majority of cells seen to express β-catenin in the control cultures (Figure 4.34E).

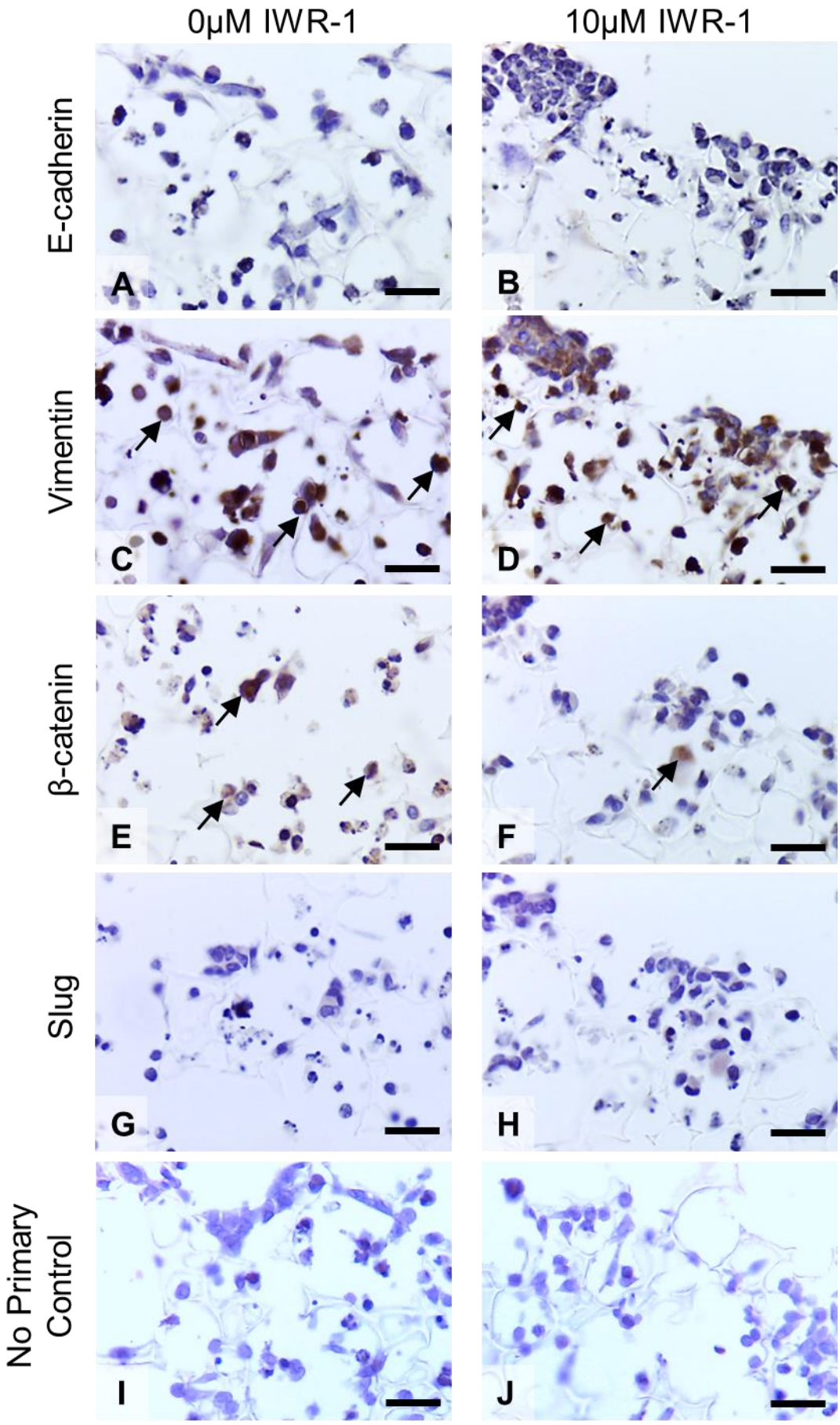

Figure 4.34: The inclusion of the Wnt inhibitior IWR-1 in culture media suppresses β-catenin expression in the SW620 cell line in 3D cultures. Immunohistochemical images of antibody staining for A and B: E-cadherin, C and D: Vimentin, E and F: β-catenin, G and H: Slug and I and J: no primary control on 10 day 3D cultures of SW620 cells in the absence and presence of 10μM IWR-1, where the brown precipitate (arrows) indicates positive staining. Scale bars = 25μm for all images.

4.4 Discussion

The primary effects on the small molecule Wnt inhibitors screened in this Chapter on both the SW480 and SW620 cell lines in the 3D migration model is summarised in Table 4.1. This demonstrates the range of effects that these molecules can have upon cells as the Wnt pathway is known to have roles in cell proliferation, differentiation and migration [90, 95].

Additive	Concentration	SW480	SW620
XAV 939	Up to 50µM	No effect on cell penetration, but variable changes to cell number	No effect on cell penetration
IWR-1	10µM	No effect	Up to 26% decrease in cell penetration with concentrations of 1µM and greater
Cardamonin	10µM	No effect	No effect on cell penetration, but 40% decrease in cell number
ICG 001	5µM	No effect on cell penetration, but 25% decrease in cell number	26% decrease in cell penetration

Table 4.1: Summary of the primary effect of small molecule Wnt inhibitors on cell culture in the 3D migration assay.

Of the small molecules tested, the TNKS inhibitor XAV 939 was found to have a variable effect on cell number, increasing the number of SW480 cells found after 10 days 3D culture at 5µM (Figure 4.5A) and decreasing those found when applied at 20 and 50µM (Figure 4.13A). The different responses of the 3D SW480 cultures to high and low concentrations of XAV 939 may be due to paradoxical activation of signalling mediators of the Wnt signalling pathway. This phenomenon was initially documented in Raf signalling, where the application of a Raf inhibitor resulted in an increase in c-Raf activation compared to control cells [331]. This effect was found to be due to the self-reactivation of Raf following inhibition. So far there have been no reports in the literature of instances of paradoxical activation of the Wnt signalling pathway by Wnt inhibitors, however, this does not rule out the possibility of it occurring in the 3D system under investigation here.

This XAV 939 data partially correlates with the effect on colorectal cancer cell behaviour previously reported, with inhibited colony formation by the DLD-1 cell line in the presence of XAV 939 [322]. Additionally, this molecule did not have any effect on the cell migration of either cell line tested in either of the 3D or 2D migration models used here (Figure 4.3, Figure 4.7, Figure 4.9, Figure 4.11, Figure 4.15 & Figure 4.17). When this is taken with the lack of published data regarding the effect of XAV 939 on cell migration, it would suggest that the downstream effects of this molecule result in alterations to cell viability and that it may be better placed to reduce the growth of tumours via limiting cell proliferation and increasing apoptosis than by inhibiting cell migration.

Cardamonin was also found to be an unsuitable candidate for a small molecule inhibitor of colorectal cancer migration as it failed to elicit a change in the migratory behaviour of either the SW480 or SW620 cell lines in the 3D model (Figure 4.19), despite significantly decreasing the amount of single cell migration observed in the 2D SW620 scratch wounds (Figure 4.25). With its negative impact on the number of SW620 cells found in the 3D cultures (Figure 4.21B), cardamonin demonstrates that cellular responses that it elicits are not limited to cell migration. This correlates with the published data for this molecule, as cardamonin has been shown to inhibit cell migration, via NF-κB signalling [296], and cell proliferation, via β-catenin suppression [299]. The data presented here failed to demonstrate a reduction in the cell number in the SW480 cell line (Figure 4.21A), which had been previously observed [299]. However, a reduction in the number of SW620 cells upon exposure to cardamonin was demonstrated (Figure 4.21B). This difference in the observed behaviour of the SW480 cell line may be due to the dimensionality of the cultures, as Park *et al*. assessed cells in 2D monolayer cultures and here the cell number was obtained for 3D cultures only.

The small molecule ICG 001 showed promise as an anti-migratory compound, as was able to inhibit the migration of the SW620 cell line in both 3D (Figure 4.19B) and 2D models (Figure 4.25B). However, it also had a negative impact on the number of SW480 cells found after 3D culture (Figure 4.21A). The inhibition of migration in the SW620 cell line may be due to a repression of EMT via suppression of Snail, Zeb2 and Slug expression, as previously seen in MCF-7 cells [305]. The negative impact of ICG 001 on the number of cells in 3D SW480 cultures also correlates with previously published data, where ICG 001 downregulated survivin and cyclin D1 in the SW480 cell line, resulting in an inhibition of 2D growth [302].

While IWR-1 is also a TNKS inhibitor like XAV 939 [314], it caused a different cellular response in the migration models tested here, as it affected the 3D migration of the SW620 cell line (Figure 4.19B) without affecting the cell number of either cell line (Figure 4.21). The initial screen demonstrated its effectiveness at a concentration of 10μM (Figure 4.19B), which is the most commonly used concentration in a variety of studies utilising this molecule [313, 321], and further experiments also demonstrated its effectiveness at the lower concentration of 1μM (Figure 4.27B). An exhaustive search of the published literature demonstrated that the application of this small molecule to 2D cultures of lung cancer cells decreased cell viability [321]. However, no mentions of a role for this small molecule as an anti-migratory compound were found, suggesting that the data presented here for the effect of IWR-1 on the 3D migration of SW620 cells represents a novel experimental result.

The immunohistochemical staining of 3D SW620 cultures grown in the absence and presence of IWR-1 also highlighted its mechanism of action, as the inclusion of IWR-1 decreased the amount of β-catenin staining compared to the control (Figure 4.34E&F), which correlates with other papers demonstrating the mechanism of IWR-1 on 2D cultures [313]. When taken with the cell penetration data, this would suggest that the action of IWR-1 is mediated by a decrease in β-catenin availability, which would in turn affect the downstream transcriptional targets of the Wnt signalling pathway. This mechanism appears to be independent of pathways involving the Slug mediated downregulation of E-cadherin, as the expression of both of these proteins was unaffected by the inclusion of IWR-1 in the culture media.

Together these data demonstrate that IWR-1 is a small molecule which can inhibit the 3D migration of the SW620 cell line while leaving the viability of cells unaffected in multiple cell lines. This small molecule may be of use in limiting the spread of later stage cancers, while avoiding the negative impact on cell proliferation in a wide range of cell types, as seen with conventional chemotherapy agents. However, the results presented here are drawn from observations of the behaviour of the cell cultures. A more direct assessment of Wnt signalling, via a TOPFLASH assay to assess TCF mediated gene transcription [329], would provide clearer information regarding the inhibition of Wnt signalling by the small molecules tested in this Chapter.

These data demonstrate the need to screen large numbers of compounds in order to identify those which have the potential to be of clinical significance in the treatment of cancers. From the previously published literature, it would be a reasonable hypothesis that IWR-1 and XAV 939 would elicit the same response in a 3D cancer migration model as they are both TNKS inhibitors [314] and produce similar phenotypes when utilised in *Xenopus* development models [317]. However, when used in 2D and 3D models of colorectal cancer cell migration these two compounds produce different responses; with IWR-1 affecting the 3D migration while XAV 939 did not and instead affected the cell number. This difference in cell response could arise from a variety of causes, from the difference in binding interactions with target proteins to differences in IC_{50} and molecular stability when reconstituted in culture media, and highlights the difficulties in accurately predicting experimental outcomes in different models.

However, many high-throughput screening methods rely on 2D culture models, as more complex 3D models are unsuitable for use in a high-throughput format, although there are examples of the adaption of these 3D models for use in compound screening [183, 225]. This reliance on 2D culture methods to carry out initial compound screens with further validation in 3D models has the potential to identify compounds which do not prove to be effective in further testing, or to fail to identify compounds of interest that have an effect in a more complex model, as demonstrated here by the lack of IWR-1 activity in 2D scratch wounds (Figure 4.31 and Figure 4.33) while causing a significant reduction in 3D cell migration (Figure 4.27).

Additionally, this data highlights the problems with using 2D models which have already been discussed. With a high rate of failure during drug discovery, the discussion in the literature is turning towards the accuracy of 2D *in vitro* models in identifying targets and drug development [332], with 3D models offered as a more biologically relevant alternative [157, 159]. Of the three compounds tested here which elicited a response in terms of the migratory behaviour of the cells, only one, ICG 001, was effective in both the 2D and 3D models. Cardamonin was only effective at inhibiting single cell migration in the 2D scratch wound and only affected cell number in 3D, whereas the effectiveness of IWR-1 in the 3D model was not mirrored in the 2D model at any of the concentrations tested. This correlates with previously published data demonstrating that the JIMT1 breast cancer cell line displayed differing responses to antineoplastic agents when assayed in 2D and 3D culture conditions [333]. This highlights the need for more biologically relevant models to guide the development of treatments for diseases, as 2D *in vitro* data alone can falsely identify targets of interest.

5 Use of Insulin-like Growth Factor-I Increases the Biological Relevance of a 3D Migration Assay

5.1 Introduction

This Chapter will aim to assess the role that the growth factor IGF-I plays in the migratory behaviour of colorectal cancer cells. The secretion of IGF-I by mesenchymal cells, predominantly from the liver [123], allows for both paracrine and endocrine signalling. The blood serum levels of the protein follows a characteristic pattern over the human lifespan, with a peak during puberty and tailing off in later life [124], while an elevation of these levels is correlated with an increased risk of developing colorectal cancer [150]. As the downstream signalling processes of IGF-IR are mediated by the signalling intermediaries PI3K [130], which subsequently feeds into the Wnt signalling pathway [141], and Ras [136] (Figure 5.1B), IGF-I signalling appears well placed as a target subject for cancer research. This is confirmed from published literature in the area of cancer cell migration, as *in vitro* exposure of colorectal cancer cells to IGF-I results in an increase in cell migration and invasion [334], while the induction of xenograft colorectal tumours in LID mice results in a lower rate of metastasis formation [146].

5.1.1 Role of IGF-I in cancer

5.1.1.1 IGF-I signalling provides a small protective effect against apoptosis in colorectal cancer cells

IGF-I has been shown to modulate cellular response in the human colon carcinoma cell line DiFi by reducing the level of apoptosis which is induced upon exposure to mAb 225, a ligand blocking antibody to EGF receptor, by reducing the activity of caspase-3, caspase-8 and caspase-9 [335]. However this reduction of apoptosis was only effective in the short term, as longer exposure to mAb 225, here up to 72 hours, in the presence of IGF-I still resulted in a decrease in cell number relative to the control cells which were exposed to neither, although it did provide a small protective effect at this time point relative to cells exposed to mAb 225 in the absence of IGF-I. IGF-I was also ineffective in inhibiting the mAb 225 induced G1 cell cycle arrest, as the reversal of the mAb 225 induced PI3K/PKB inhibition was limited to the initial hours after exposure and the level of IGF-I activation of the MAPK pathway was not sufficient to overcome the apoptosis.

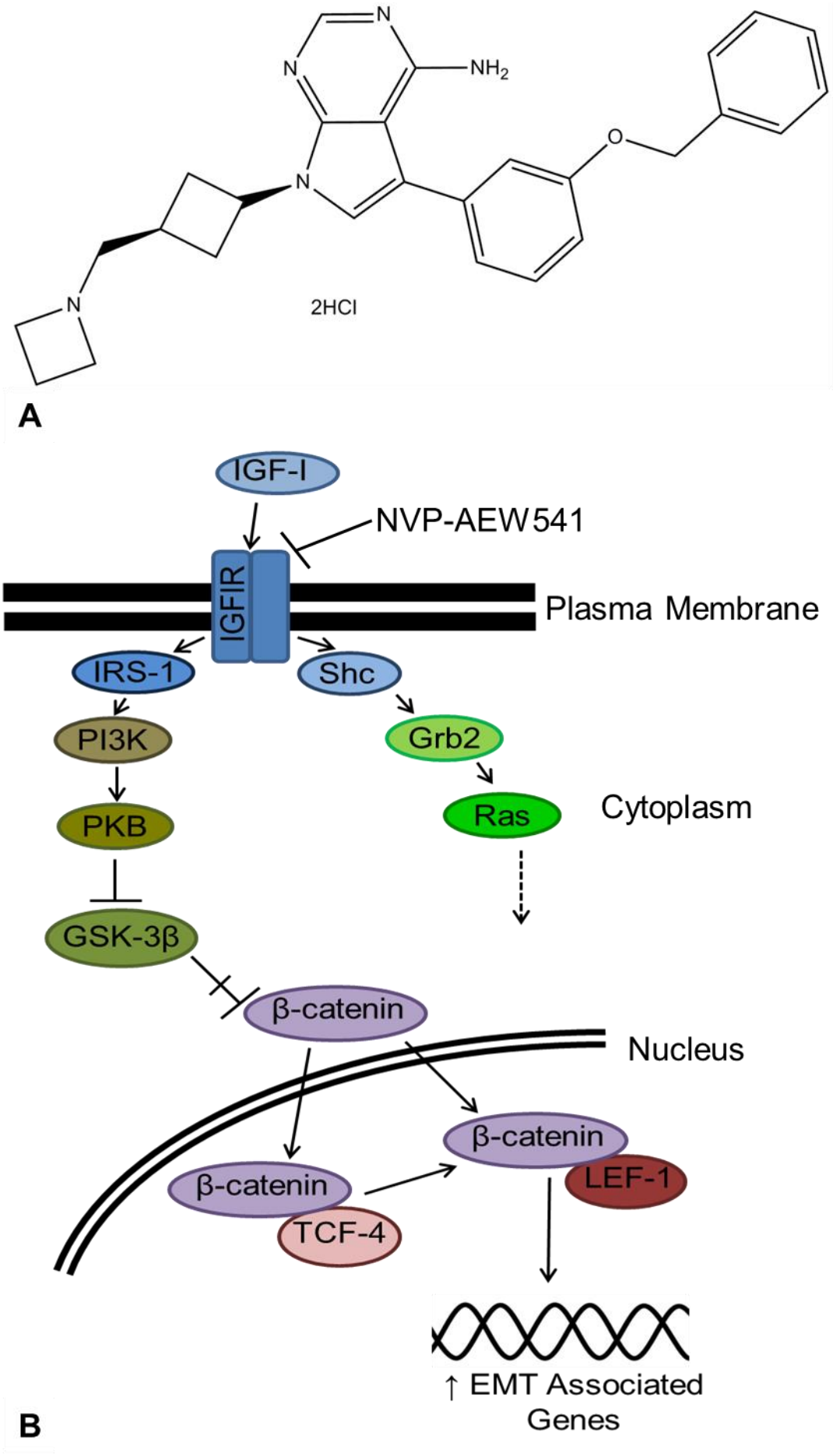

Figure 5.1: Chemical structure of the small molecule inhibitor of the IGF-IR, NVP-AEW541, and schematic of its interaction of the IGF-I signalling pathway. A: chemical structure of NVP-AEW541. B: NVP-AEW541 competitively binds the receptor, blocking IGF-I interaction and inhibiting IGF-I signalling, leading to a decrease in the transcription of EMT associated genes.

5.1.1.2 Inhibition of IGF-I signalling limits colorectal cancer cell proliferation

With the increased expression of IGF-IR in colorectal cancer [336], IGF-I has also been found to influence the proliferative behaviour of colorectal cancer cell lines in a variety of *in vitro* and *in vivo* experiments. Transfection of a dominant negative variant of IGF-IR (dnIGF-IR) in the HT29 colorectal cancer cell line results in lower levels of vascular endothelial growth factor (VEGF) being induced in the cells after stimulation with IGF-I in addition to a decrease in the levels of phosphorylated IRS-1 and ERK1/2 when compared to control cells [337]. This group again observed a decrease in cell proliferation in standard 2D culture conditions and severe inhibition of colony formation on soft agar as has been seen with mouse fibroblasts [143]. When the dnIGF-IR cells were used in xenograft experiments in nude mice subcutaneous tumours were observed after 25 days, although these tumours were significantly smaller and lighter than control tumours generated from untransfected or mock transfected HT29 cells. The dnIGF-IR cells also showed a compromised ability to form tumours when directly injected into the livers of nude mice, with 30% of mice producing significantly smaller tumours than those produced in 88% of the control mice after 30 days. Histological analysis of the subcutaneous dnIGF-IR tumours showed decreased staining for proliferating cell nuclear antigen (PCNA), VEGF and CD31, an endothelial cell marker, while displaying an increased number of TUNEL positive cells, an apoptosis indicator. Manual counts of the CD31 stained blood vessels in these tumours showed that the dnIGF-IR tumours had a reduced number of vessels compared to controls which demonstrates that impaired IGF-I signalling affects angiogenesis within tumours in addition to the proliferative behaviour of the tumour cells.

Inhibition of IGF-I signalling can also be obtained via transfection with siRNA and produces similar results in terms of cell proliferation of the SW480 cell line, with a ~35% reduction in cell number observed over a 72 hour period [338]. This method of inhibiting IGF-IR function was also used to investigate the effect it has on the sensitivity of the SW480 cell line to doses of radiation ranging from 1 to 20Gy over a 72 hour period [339]. Transfection with the IGF-IR siRNA increased the cellular sensitivity to all radiation doses over the time course when compared to mock transfected cells, with the maximal radiation dose of 20Gy inhibiting cell growth by 35%, 70% and 95% at 24, 48 and 72 hours, respectively, in IGF-IR siRNA transfected cells while only achieving 13%, 23% and 63% inhibition in the mock transfected cells. From the data it was calculated that the ID_{50} at 72 hours required for the control cells was 8.3Gy, compared to the 4.3Gy for the IGF-IR siRNA transfected cells, demonstrating the level of increased sensitivity that IGF-IR inhibition causes.

5.1.1.3 IGF-I signalling modulates migration and metastasis formation

In addition to affecting the establishment and growth of colorectal cancers, IGF-I signalling also affects the migratory behaviour of colorectal cancer cells, as exposure of the colorectal cancer cell line KM12L4 to IGF-I over 48 hours results in a 17.5-fold increase in migration in a standard Transwell® assay and a 1.8-fold increase in invasion in a Matrigel coated Transwell® assay [334]. This increase in migratory behaviour appeared to be mediated by the urokinase plasminogen activator (uPA)/uPA receptor (uPAR) system, as treatment with antibodies to either uPA or uPAR inhibited both migration, by 85% and 92% respectively, and invasion, by 75% and 85% respectively. Use of the uPA inhibitor amiloride, in conjunction with IGF-I also reduced the migration and invasion observed by 92% and 75% respectively.

The effect of IGF-I is not limited to localised migration, as it also has been shown to have an impact on the development of metastasis in *in vivo* models. In addition to the investigation into adenocarcinoma establishment carried out in LID mice as described preivously [146], this paper also looked at the effect of circulating IGF-I on liver metastasis. It was found that the control mice had a higher incidence of metastasis, 44% compared to 31% of LID mice, and the number of metastatic nodes per liver was increased. Additionally, the intraperitoneal injection of IGF-I increased the metastasis rate in both groups, as well as the frequency of metastatic nodes found in the control mice.

Direct blockade of the IGF-IR also inhibits the metastatic growth colorectal cancer [340]. Application of the cytotoxic chemotherapy agent oxaplatin or the IGF-IR targeting monoclonal antibody AVE1642 to 2D cultures of the colorectal cancer cell lines HT29 and KM12L4 significantly inhibits the growth of both cell lines, with the greatest effect observed when both oxaplatin and AVE1642 are used together. These agents also have an impact on cell growth when HT29 cells are directly injected into the livers of nude mice. Intraperitoneal injection of oxaplatin with a control antibody did not significantly decrease the tumour volume observed after 54 days, however it did increase the level of cell apoptosis observed and decrease the level of BrdU uptake in the last 16 hours prior to tumour harvest. Intraperitoneal injection of AVE1642 was found to be effective, both with and without administration of oxaplatin; the tumours from these mice were smaller, with a higher level of apoptotic cells and lower BrdU uptake. As with the *in vitro* work, the application of oxaplatin and AVE1642 had a synergistic effect on the growth of xenograft tumours.

5.1.2 Small molecule inhibition of IGF-I signalling

With the body of evidence for the role of IGF-I signalling in the development of cancers, targeting this pathway has been viewed as a viable method for controlling the behaviour of cancer cells and providing chemotherapy treatments for a wide range of cancers. There are different methodologies for this targeting which are currently undergoing experimentation, these consist of antibody targeting of IGF-I or IGF-IR, or small molecule tyrosine kinase inhibition of the receptor. In the pursuit of this line of investigation, a wide range of compounds that been isolated and are undergoing further testing in various stages of preclinical and clinical trials, the status of some of these are reviewed by Ewing and Goff [341] and Gao *et al* [342].

One of the small molecules identified for its role in modulating IGF-I signalling via the IGF-IR is NVP-AEW541 [343] (Figure 5.1A). This molecule is highly selective for both the IGF-IR and the insulin receptor over a range of other tyrosine kinase receptors, with IC_{50} values of 0.15μM and 0.14μM respectively when used on purified GST-fusion recombinant proteins. However, when tested on cell lines expressing the receptors, the selectivity for the IGF-IR far outweighed the selectivity for the insulin receptor, with the compound obtaining an IC_{50} value of 0.086μM against IGF-IR expressed on NWT-21 cells and 2.3μM against insulin receptors on A14 cells, a 27-fold selectivity for the IGF-IR.

With the confirmation of the selectivity of NVP-AEW541 for the IGF-IR, it has subsequently been used on a variety of cancer cell lines to examine its effect on cellular behaviour. These include cancers originating from epithelial cells, such as hepatocellular carcinomas [344, 345], colorectal cancer [345-347] and pancreatic cancer [345, 348, 349], in addition to musculoskeletal tumours

[350, 351], neural-tissue derived tumours [352-355], acute myeloid leukaemia (AML) [356, 357] and multiple myeloma cells [358]. The effects of NVP-AEW541 have been shown to be consistent across many of this cell lines, demonstrating the specificity of its targeting.

Application of NVP-AEW541 has been shown to inhibit the phosphorylation of various protein signalling mediators of IGF-IR signalling, without affecting the overall level of protein expression. These include IGF-IR itself [345, 348, 352-354, 356, 358], in addition to the downstream signalling mediators IRS-1 [348, 353], PKB [343, 345, 347-353, 356, 358-361], ERK [345, 348, 350, 351, 353, 358, 361], MEK [348], MAPK [343] and GSK-3β [353, 356]. There was also an inhibition of phosphorylation of signal transducer and activator of transcription 3, STAT3, [348, 354] and the associated downregulation of protein levels of HIF1α [354], suggesting that inhibition of IGF-IR signalling via NVP-AEW541 affects the response of glioblastoma cells to hypoxic conditions.

5.1.2.1 NVP-AEW541 inhibits cell proliferation

NVP-AEW541 affects the behaviour of the cells tested by limiting the cell growth in standard 2D cultures [343-345, 347, 348, 350-352, 357], although this effect appears to be dependent on the endogenous expression of the IGF-IR exhibited by the cells [346]. One of the mechanisms for the lower cell survival appears to be the arrest of the cell cycle at the transition between G1 and S phase [343, 344, 352, 353, 358, 359]. The observed decrease in phosphorylated GSK-3β in AML cells is associated with an increased level of phosphorylated cyclin D1 [356]. This provides a potential mechanism for the G1 arrest seen after exposure of cells to NVP-AEW541 as cyclin D is targeted for degradation upon phosphorylation and cannot initiate the transition into S phase and results in a lower proliferation rate. This limitation to the proliferation rate can be seen as either lower ^{3}H-thymidine incorporation [361] or reduced uptake and metabolic conversion of MTT reagent [358].

In a reflection of the work carried out on R^- cells from *Igf1r*$^{-/-}$ mice [143], the use of NVP-AEW541 has also been used to retard the growth of cells on semisolid agar. This effect has been seen across cancer cell lines deriving from a variety of source tissues, including the mouse medulloblastoma cell line BsB8 and the two human medulloblastoma cell lines D364 and Daoy [353] and a variety of gastrointestinal tract cancer cell lines, including the colorectal cancer cell line HT29, esophageal squamous cell carcinoma cell line TE1, pancreatic adenocarcinoma cell line BxPC3 and hepatocellular carcinoma cell line PLC/PRF/5 [345]. In the study of AML, NVP-AEW541 is also effective in preventing the $CD34^+$ bone marrow cells, the stem cell population of the bone marrow, from forming colonies on soft agar [357].

5.1.2.2 NVP-AEW541 can inhibit cell growth by the induction of apoptosis

Another mechanism of NVP-AEW541 in limiting the rate of cell growth is the induction of apoptosis [355], as seen by a lower number of Trypan Blue excluding cells upon cell counting [353] or a higher number of Annexin V positive cells, a marker of apoptotic DNA changes [358]. This induction in apoptosis is linked with the NVP-AEW541 induction of caspase-3, caspase-7 and caspase-8 activity [344, 345, 357], in addition to downregulating the expression the anti-apoptotic proteins Bcl-2, Bax and survivin [344], leading to the stereotypical changes to cell shape associated with apoptotic induction.

5.1.2.3 The apoptosis of cells after exposure to chemotherapeutic agents can be enhanced by NVP-AEW541

When used in conjunction with standard chemotherapeutic agents, NVP-AEW541 has been shown to enhance the cytotoxic effect of some of them. NVP-AEW541 is effective at augmenting the effects of vincristine, actinomycin D and ifosfamide on the Ewing's sarcoma cell line TC-71 *in vitro*, but not doxorubicin and cisplatin and was also seen to augment the effect of vincristine on decreasing the size of TC-71 xenografts [350]. Similarly, NVP-AEW541 displayed a synergistic effect on the cell survival of biliary tract cancer cells when used in combination with gemcitabine, but only an additive effect when used with 5-fluorouracil (5-FU) and the PI3K inhibitor BI 2536 [359]. The downregulation of cell growth of multiple myeloma MM1S cells by the drugs lenalidomide, dexamethasone, bortezomib and melphalan was enhanced with the addition of NVP-AEW541, when each drug was used alone or in conjunction with dexamethasone, and a similar enhancement of apoptotic induction was seen with the use of NVP-AEW541 and dexamethasone or bortezomib [358]. The synergistic effect that NVP-AEW541 has on the cell death of HL60AR AML cells with etoposide is reflected when NVP-AEW541 is used in conjunction with etoposide on cells from chemoresistant patients, where the use of NVP-AEW541 sensitises the cells to the actions of the chemotherapy agent [356].

5.1.2.4 The migratory behaviour of cancer cells can be inhibited by NVP-AEW541

Application of NVP-AEW541 to cultures can also inhibit the migratory behaviour of the cells, with the compound able to inhibit the *in vitro* migration of the Ewing's sarcoma cell lines TC-71 and SK-N-MC [351], the pancreatic cancer cell line HPAF-II [348] and the colorectal cancer cell line HT29 [345]. This inhibition is seen even in the presence of IGF-I, suggesting that this compound may have use in a migration model for looking at cell migratory behaviour in response to IGF-I. In addition to the inhibited migration behaviour of the HT29 cells, NVP-AEW541 is also capable of inhibiting the invasion of these cells in Matrigel-coated Boyden Chambers and is associated with a downregulation of the matrix metalloproteinase-7 (MMP-7) protein, but not MMP-2 or MMP-9 [349].

5.1.2.5 NVP-AEW541 inhibits xenograft tumour formation in mice

The described *in vitro* behaviours of cells in response to exposure to NVP-AEW541 are reflected in the xenograft experiments which have been carried out with this compound. NVP-AEW541 has been shown to limit the size of xenograft tumours when administered to mice, without affecting the overall weight of the subject [343, 345], and this has also been used to augment the effects of chemotherapy agents on the size of tumours [345, 350]. The smaller xenograft tumours display protein phosphorylation profiles which are similar to those seen *in vitro*, with the NVP-AEW541 tumours demonstrating lower positive staining for phosphorylated IGF-IR [348], PKB [345, 349] and ERK [345, 348].

The smaller size of the xenograft tumours could be due to a variety of factors. The cells within the tumours have a higher number of pyknotic nuclei, where the DNA condenses prior to apoptosis [352], suggesting that apoptosis may be one of them. The level of vascularisation within the tumours is decreased [351, 352], with fewer CD31 positive cells detected [348]. This lack of vascularisation is seen in conjunction with lower levels of VEGF mRNA [348, 352] and protein [348, 351, 354] and limited metastatic spread of the xenograft tumours from their original site [351, 352].

While the work with NVP-AEW541 has shown the capability of this compound to modulate IGF-IR signalling, the overall experimental work targeting IGF-IR signalling to obtain a viable clinical treatment has not produced the results that were initially hoped for when IGF-I signalling was first identified as a pathway of interest for cancer research. In their 2013 review, Baserga discusses some of the underlying reasons for this lack of success and suggests that the targeting of signalling via the IGF-IR is not a successful strategy for single target cancer therapy, it still has the potential for use in supplementing current chemotherapy agents as the compounds can produce a synergistic effect on cell viable when used together [362].

The evidence that both IGF-I and NVP-AEW541 can modulate the migratory behaviour of a variety of cancer cell lines, with IGF-I increasing migration [334] and NVP-AEW541 decreasing migration [345], demonstrates that manipulation of IGF-I signalling is the 3D model in use here is likely to produce a change in migratory behaviour. However, as there is also extensive evidence that decreased IGF-I signalling decreases cell proliferation [143] while application of NVP-AEW541 inhibits cell proliferation [347], an assessment must be made to ensure that any changes in the amount of cell penetration seen with either cell line are not due to changes in cell number.

5.2 Chapter Aims

This Chapter aims to assess the role of IGF-I signalling via the IGF-IR in modulating the behaviour of colorectal cancer cells by utilising recombinant IGF-I and a small molecule inhibitor of IGF-IR in both 2D and 3D migration assays.

5.2.1 Objectives

Overall, the aims of the small molecule assessment in this Chapter will be met by:

- Assessing the impact of IGF-I addition on the migration and proliferation of colorectal cancer cells in the 3D model;
- Performing counterpart assessments of IGF-I addition on colorectal cancer cell migration in standard 2D scratch wound assays;
- Assessing the effectiveness of a small molecule IGF-IR inhibitor in affecting the IGF-I induced changes in migration and proliferation of colorectal cancer cells in the 2D and 3D models;
- Assessing the effect that the Wnt signalling inhibitor IWR-1 has on the IGF-I induced changes in migration and proliferation of colorectal cancer cells in the 2D and 3D models.

5.3 Results

5.3.1 IGF-I interacts with the Wnt pathway to induce a migratory response in this 3D model

As the levels of circulating IGF-I can vary within healthy populations, it is important to select a biologically appropriate range of IGF-I concentrations for testing in this 3D migration model. Many studies which have determined the circulating concentration of IGF-I, which is in the region of 100 – 200ng/ml [119, 124, 126], examine the total IGF-I which includes IGF-I which is bound to IGFBPs or ALS and is therefore inactive. It is the concentration of the unbound, or free, IGF-I which is of importance as it is this subset of the total IGF-I which has the capacity to bind to the IGF-IR and induce a cellular response. In a selection of healthy volunteers used as a control for a study into the levels of serum IGF-I and IGF-II in hormone disorders, the blood serum concentration of free IGF-I was found to range from 0.22 – 1.20ng/ml [363]. In another study into the effect of GH administration on the blood serum levels of IGF-I and other associated proteins, the baseline level of free IGF-I was found to be 0.26ng/ml, with it rising to 1.02ng/ml within the 24 hours after GH administration [121]. After 6 months of daily doses of GH, the base level of free IGF-I is 2.96ng/ml, which is still a small proportion of the total IGF-I, and rises up to 5.33ng/ml after GH administration. Together these data sets provide a biologically relevant range of IGF-I concentrations for testing in the 3D model used here, with the concentrations of 0.1, 1.0 and 10.0ng/ml selected here.

5.3.1.1 IGF-I enhanced the penetration of the SW480 cell line but not the SW620 cell line

Use of IGF-I at these concentrations in this 3D migration model affected the two colorectal cancer cell lines SW480 and SW620 differently. When added to the SW480 cultures, IGF-I altered the distribution of the cells within the scaffold (Figure 5.2). In the absence of IGF-I, the SW480 cells were found to be in the top quarter of the scaffold (Figure 5.3A), which was also seen when IGF-I added at a concentration of 0.1ng/ml (Figure 5.2C). However, when IGF-I was present at concentrations of 1 and 10ng/ml, the distribution of the cells was altered, with the cells found at a greater depth into the scaffold (Figure 5.2E & G). When the cell distribution was altered by the IGF-I, it is not only the depth at which the cells are found which was altered, as the cells were found in tighter association with other cells in the material when the IGF-I is present at 1ng/ml (Figure 5.3B) than when it was absent (Figure 5.3A). In contrast, the addition of IGF-I did not produce a clearly visible alteration to the cellular distribution of the SW620 within the scaffold (Figure 5.2B, D, F & H).

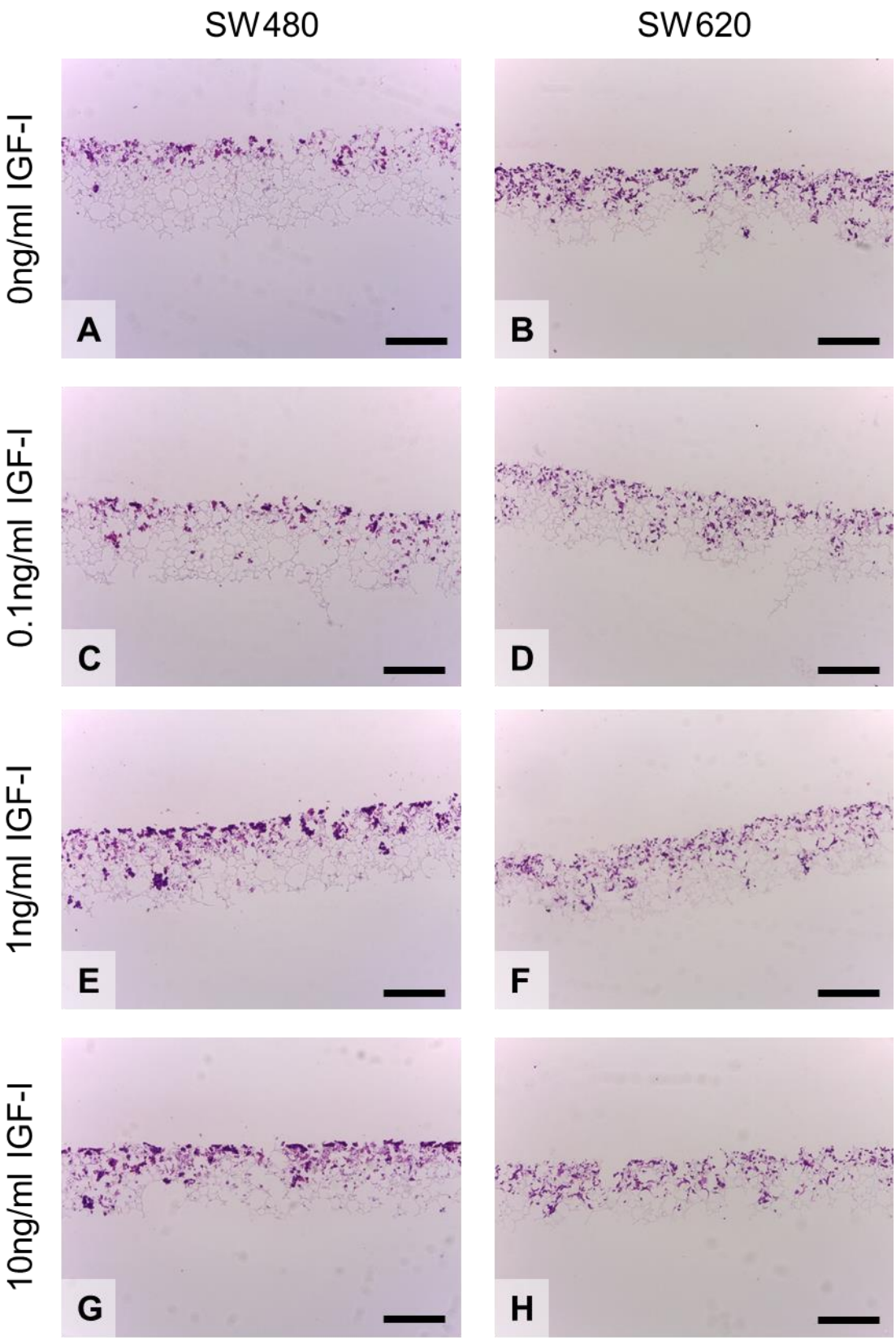

Figure 5.2: The SW480 cell line displayed an increased build-up of cells when IGF-I was present at concentrations of 1ng/ml and above, while the SW620 cell line remained unaffected. H&E images of 10 day cultures with A and B: 0ng/ml IGF-I, C and D: 0.1ng/ml IGF-I, E and F: 1ng/ml IGF-I and G and H: 10ng/ml IGF-I for both cells lines. Larger images of this data are presented in Figure 5.3. Scale bars = 200µm for all images.

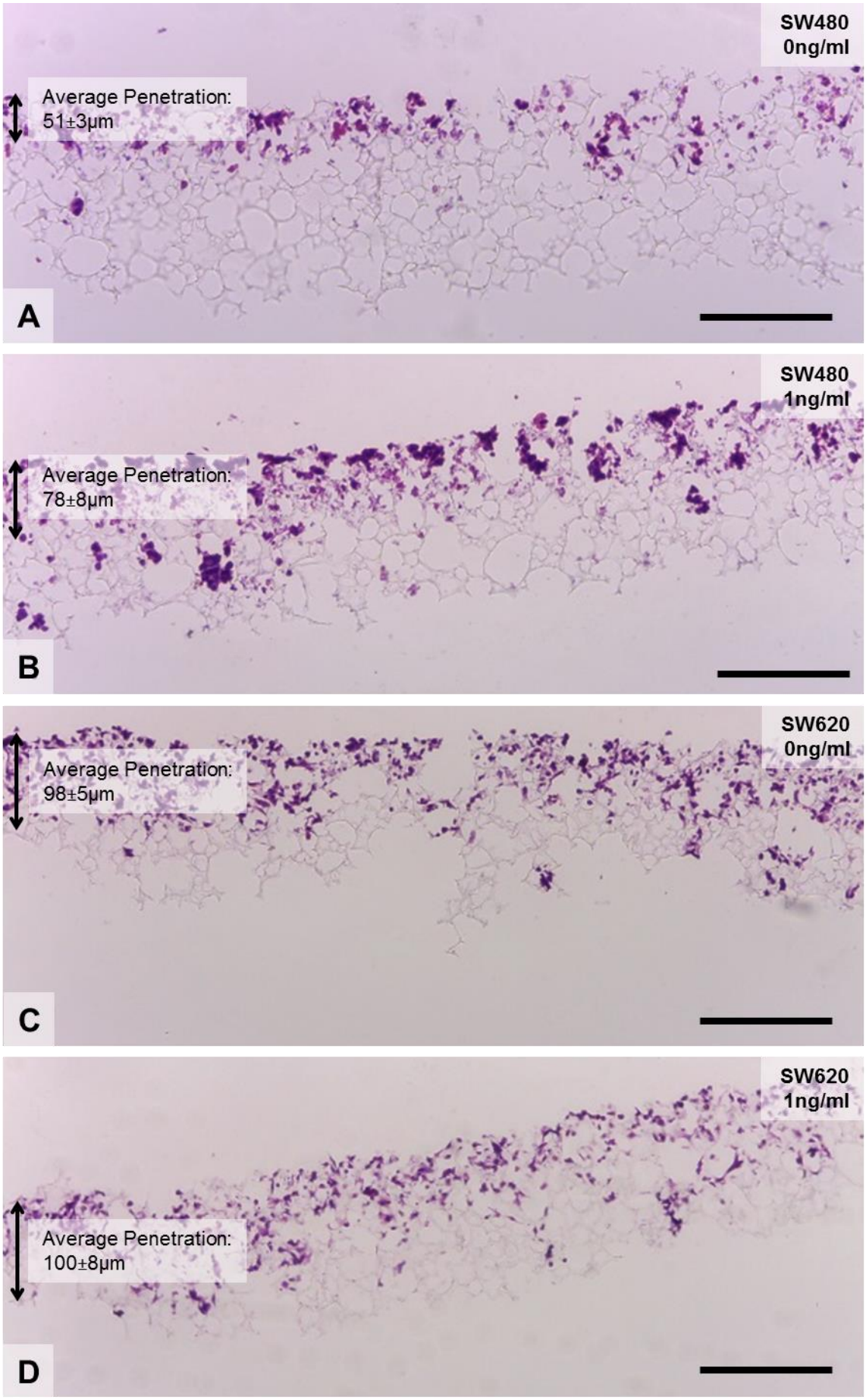

Figure 5.3: The use of IGF-I at 1ng/ml on the SW480 cell line produced a clear change in the observed cell distribution. H&E stained images of 10 days cultures of SW480 cells with A: 0ng/ml and B: 1ng/ml IGF-I showing an average penetration (n=3) of 51±3µm and 78±8µm respectively and SW620 cells with C: 0ng/ml and D: 1ng/ml IGF-I showing an average penetration (n=3) of 98±5µm and 100±8µm respectively. Scale bars = 200µm for all images.

When the cell depth was measured using the 'linear' method of cell penetration quantification, it was confirmed that the addition of IGF-I did affect the penetration of the SW480 cells in the scaffold but did not affect the penetration of the SW620 cells (Figure 5.4). The addition of IGF-I at a concentration of 0.1ng/ml did not cause a significant increase in the amount of cell penetration observed, however, when added at concentrations of 1ng/ml and above IGF-I did cause a significant increase in the level of cell penetration (Figure 5.4A). When added at a concentration of 1ng/ml, IGF-I induced a 54% increase in the level of cell penetration attained by the SW480 cell line, while the addition of IGF-I at a concentration of 10ng/ml induced a 50% increase in penetration. While the level of penetration attained by the SW620 cell line was unaffected by IGF-I at all concentrations tested (Figure 5.4B), although, as previously observed, it was found to be significantly higher than the penetration attained by the SW480 cell line, even in the presence of IGF-I, ANOVA, $F(1,19)=43.413$, $P<0.001$.

5.3.1.2 IGF-I did not affect the viability or proliferation of the SW480 cell line

As IGF-I is known to have an effect on the proliferative behaviour of cancer cells [337], it is important to check if the observed increase in cell penetration demonstrated by the SW480 cell line was due to an alteration in the migratory behaviour of the cells and not due to an alteration in the proliferative behaviour resulting in an increased number of cells within the material. When the viability of the 3D cultures was measured using the MTT Cell Viability Assay, the addition of IGF-I did not induce an alteration in the cell viability of either cell line at any of the concentrations screened (Figure 5.5). Additionally, when the number of cells within the material after 10 days of culture was quantified using the Quant-iT™ PicoGreen® dsDNA Assay, it was found to be unaltered by the presence of IGF-I in the culture media (Figure 5.6), although the number of SW620 cells was significantly higher than the number of SW480 cells, as previously observed ANOVA, $F(1,19)=113.399$, $p<0.001$. Together these suggest that the alteration in cell penetration seen in the SW480 cells cultured in the presence of IGF-I at concentrations of 1ng/ml and above was due to an alteration of the distribution of the cells as caused by a change in the migratory behaviour of the cells as opposed to the distribution of an increased number of cells within the material.

5.3.1.3 The 2D migratory behaviour was unaffected by IGF-I

With this data, the 2D migratory behaviour of colorectal cancer cells in the presence and absence of IGF-I at a concentration of 1ng/ml was examined. The phase contrast images of the scratch wounds at 24 hours post wounding showed that both cell lines display migratory behaviour, as seen with the alteration of the wound shape relative to initially after the wound was made (Figure 5.7). There was no clear visual difference between the cells cultured with or without the IGF-I, as the SW480 cells demonstrated partial closing of the wound (Figure 5.7A & C) and the SW620 cells demonstrated partial wound closing and the clear migration of single cells into the wound (Figure 5.7B & D). When the wound closure was quantified, it was found that IGF-I had no effect of the distance that the leading edges of migration move for either cell line (Figure 5.8).

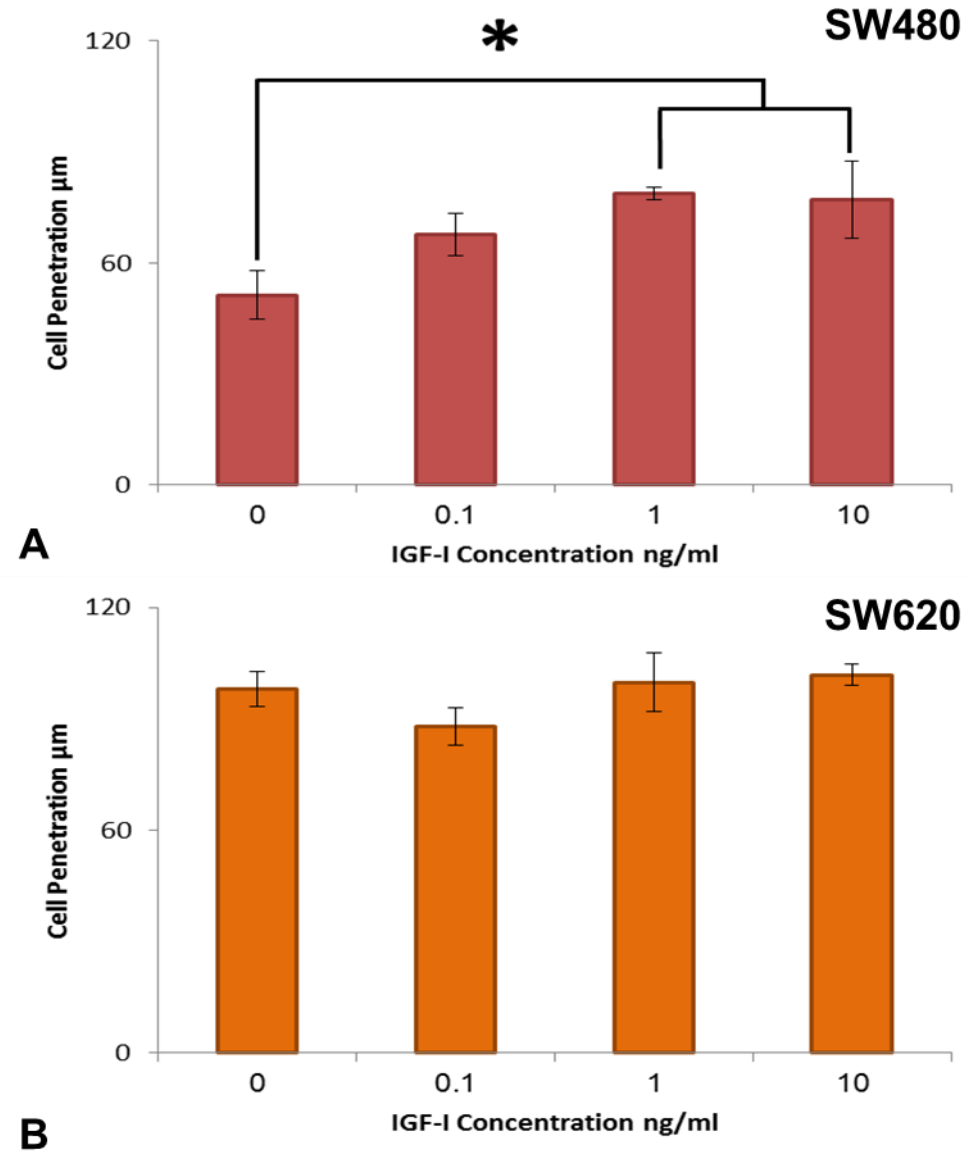

Figure 5.4: The 3D cell penetration of the SW480 cell line was increased when IGF-I was present at concentrations of 1ng/ml and above, while penetration of the SW620 cell line remained unaffected. Cell penetration in µm of A: SW480 and B: SW620 cells as determined by the linear measurement method. Data represent mean, n = 3, ±SEM for both graphs, * $p < 0.05$ by a Dunnett's t-test.

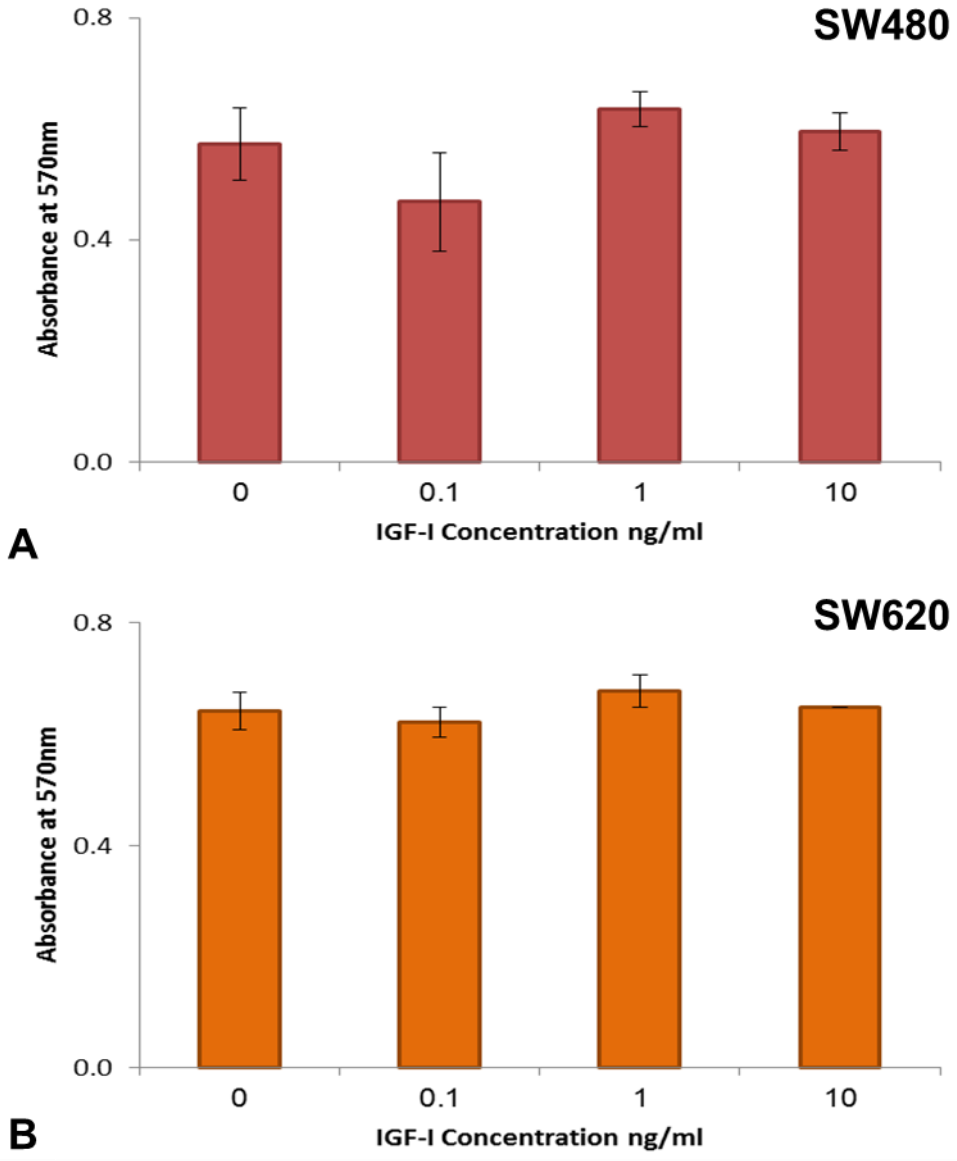

Figure 5.5: The 3D cell viability of both the SW480 and SW620 cell lines was unaffected by the presence of IGF-I. Absorbance at 570nm of A: SW480 and B: SW620 cells as determined by the MTT Cell Viability Assay. Data represent mean, n = 3, ±SEM for both graphs, no significance by a Dunnett's t-test.

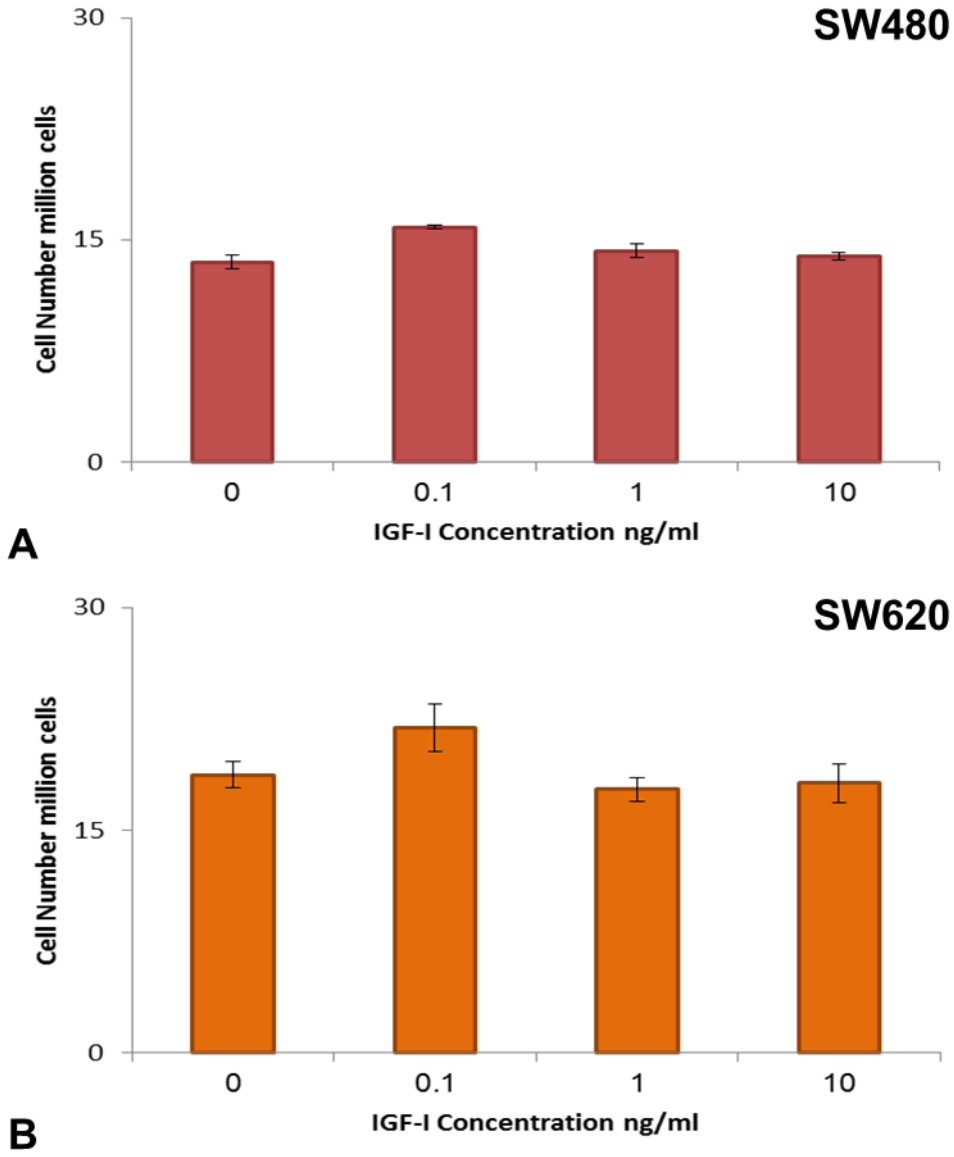

Figure 5.6: The number of SW480 and SW620 cells in the 3D material was unaffected when IGF-I was present at a concentrations up to 10ng/ml. Cell number in millions of cells of A: SW480 and B: SW620 cells as determined by the Pico Green dsDNA Assay. Data represent mean, n = 3, ±SEM for both graphs, no significance by a Dunnett's t-test.

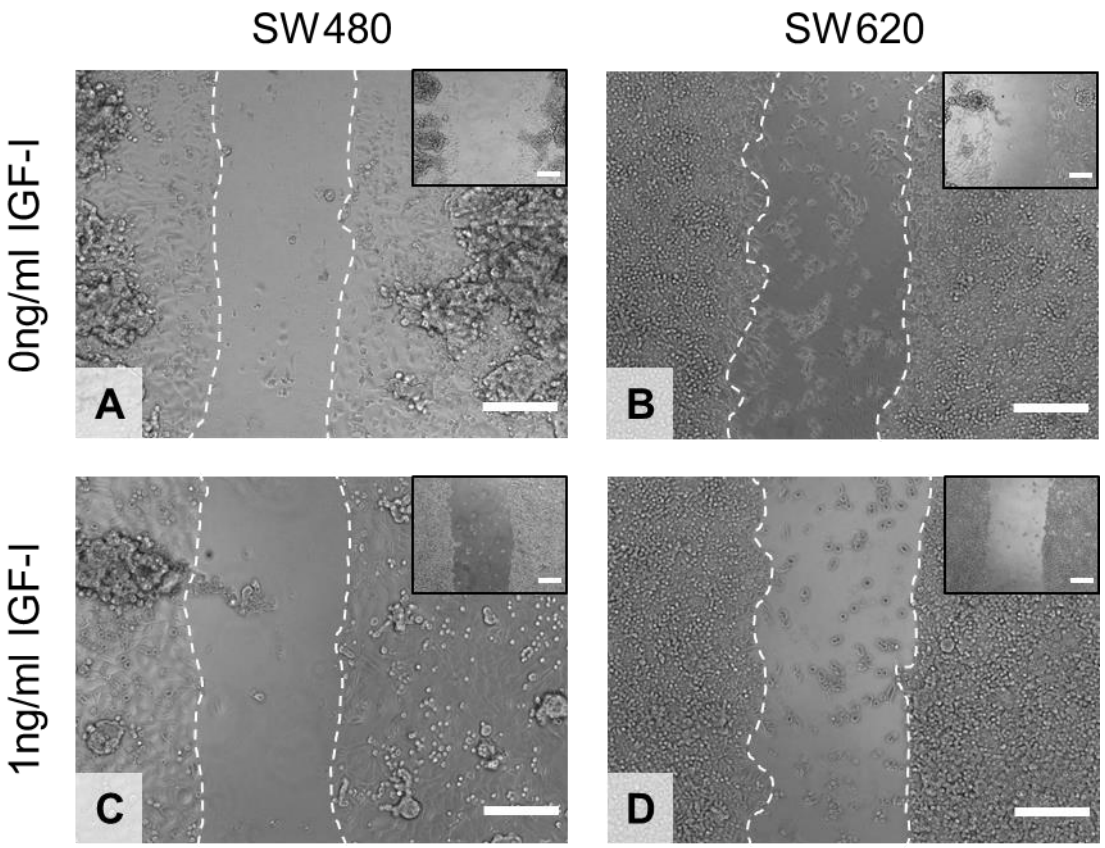

Figure 5.7: Both the SW480 and SW620 cell lines exhibited wound closing during a scratch wound assay with in the presence and absence of 1ng/ml IGF-I. Phase images of 24 hours post wounding with A and B: 0ng/ml IGF-I and C and D: 1ng/ml IGF-I for both cells lines. Scale bars = 200µm for all images.

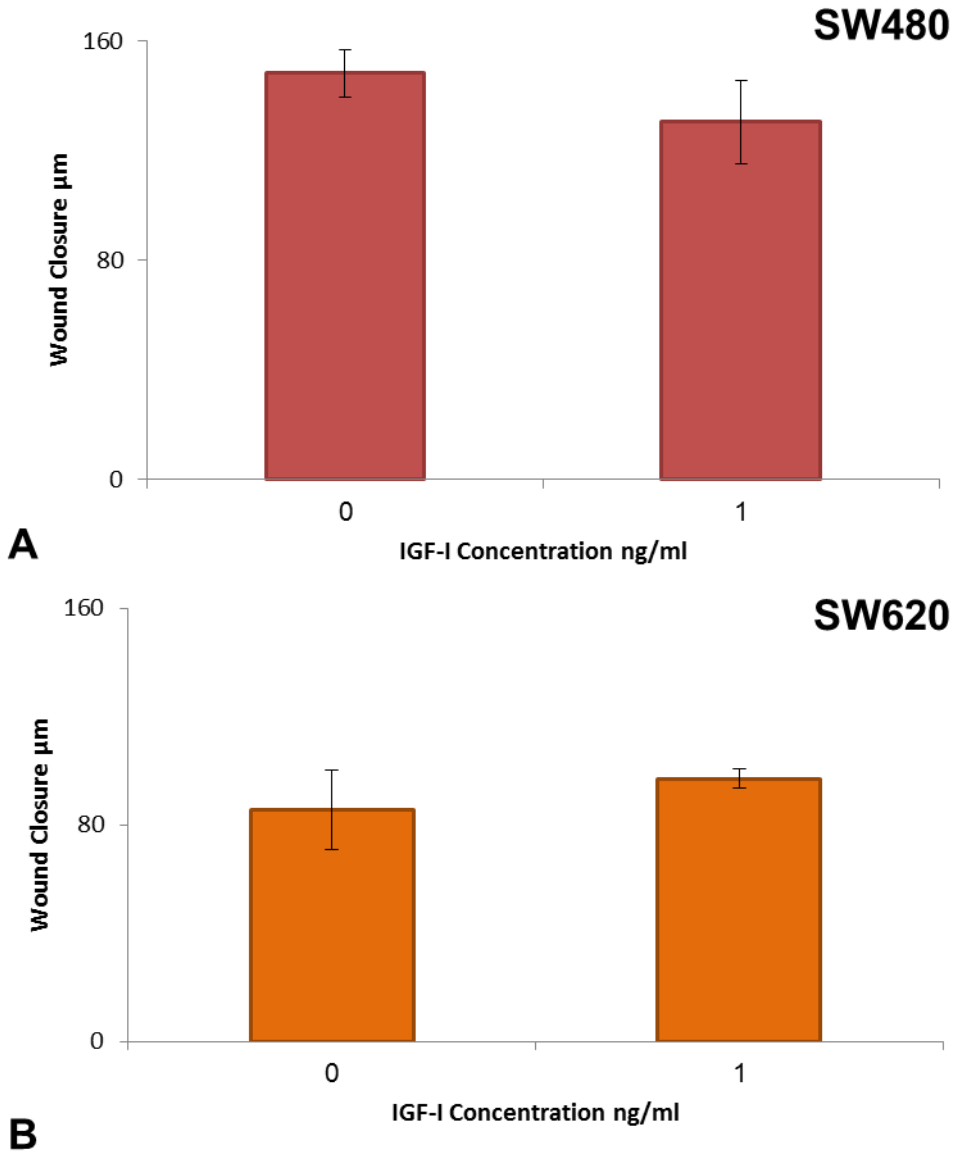

Figure 5.8: Neither the SW480 and SW620 cell lines showed a significant alteration in the distance moved by the edges of the 2D scratch wound in the presence of IGF-I at concentrations of 1ng/ml. Wound closure in µm of A: SW480 and B: SW620 cells as determined by measuring the width of the wound. Data represent mean, n = 3, ±SEM for both graphs, no significance by a Student's t-test.

When the number of single migrating cells was highlighted using DAPI and Phalloidin staining, there were fewer cells visible in the SW480 wounds (Figure 5.9A & C) than observed in the SW620 wounds (Figure 5.9B & D), which was consistent with previous observations, although there was no obvious difference between the cultures grown with or without 1ng/ml IGF-I. Quantification of these cells confirmed that the SW620 cell line has more single cells within the scratch wound after 24 hours than the SW480 cells line and that these numbers were not altered by the addition of IGF-I for either cell line (Figure 5.10).

Together these data show that IGF-I is capable of altering the migratory behaviour of the colorectal cancer cell line SW480 in a 3D migration model but not a 2D migration model, whilst having no effect on the migratory behaviour on the counterpart cell line SW620. It also demonstrates the an IGF-I concentration of 1ng/ml is sufficient to produce the observed migratory response in the 3D model.

5.3.2 NVP-AEW541 inhibits the IGF-I induced migratory response only and is ineffective when IGF-I is absent

As it has been demonstrated that IGF-I increases the migration of the SW480 cell line in a 3D migration model, the effect of the IGF-IR inhibitor NVP-AEW541 was then examined. The original paper describing the activity of NVP-AEW541 gives the cellular IC_{50} value of the molecule against the IGF-IR as 0.086μM, with it inducing cellular effects in a variety of cell lines at concentrations of 0.105 – 1.640μM [343]. When used in in vitro migration and invasion assays, NVP-AEW541 has been shown to inhibit the invasion of neuroblastoma cells through Matrigel at concentrations as low as 0.5μM [352]. With gastrointestinal tract tumour cells, including the colorectal cancer cell line HT29, use of NVP-AEW541 at 1μM is sufficient to decrease the migration by at least 50% [345, 348]. From these data the concentrations of 0.01, 0.10 and 1.00μM were selected as those which would be subjected to screening with the 3D migration model, as this was predicted to provide a concentration that is below effective concentrations noted in the literature and a concentration that has previously been shown to be effective, in addition to an intermediary one.

5.3.2.1 The migratory behaviour of both SW480 and SW620 cells lines was inhibited by NVP-AEW541

When the histological data of the 3D cultures in the screen for the effectiveness of NVP-AEW541 on inhibiting the action of IGF-I on the migratory behaviour of the colorectal cancer cells was examined, there was no clear difference in the distribution of either cell line (Figure 5.11). The SW480 cells were found to be distributed in the uppermost proportion of the material, with many of the cells found in distinct clusters and few cells found as individual cells (Figure 5.11A, C, E, G & I). The SW620 cells were once again found to be distributed as single cells throughout a greater proportion of the depth of the material (Figure 5.11B, D, F, H & J).

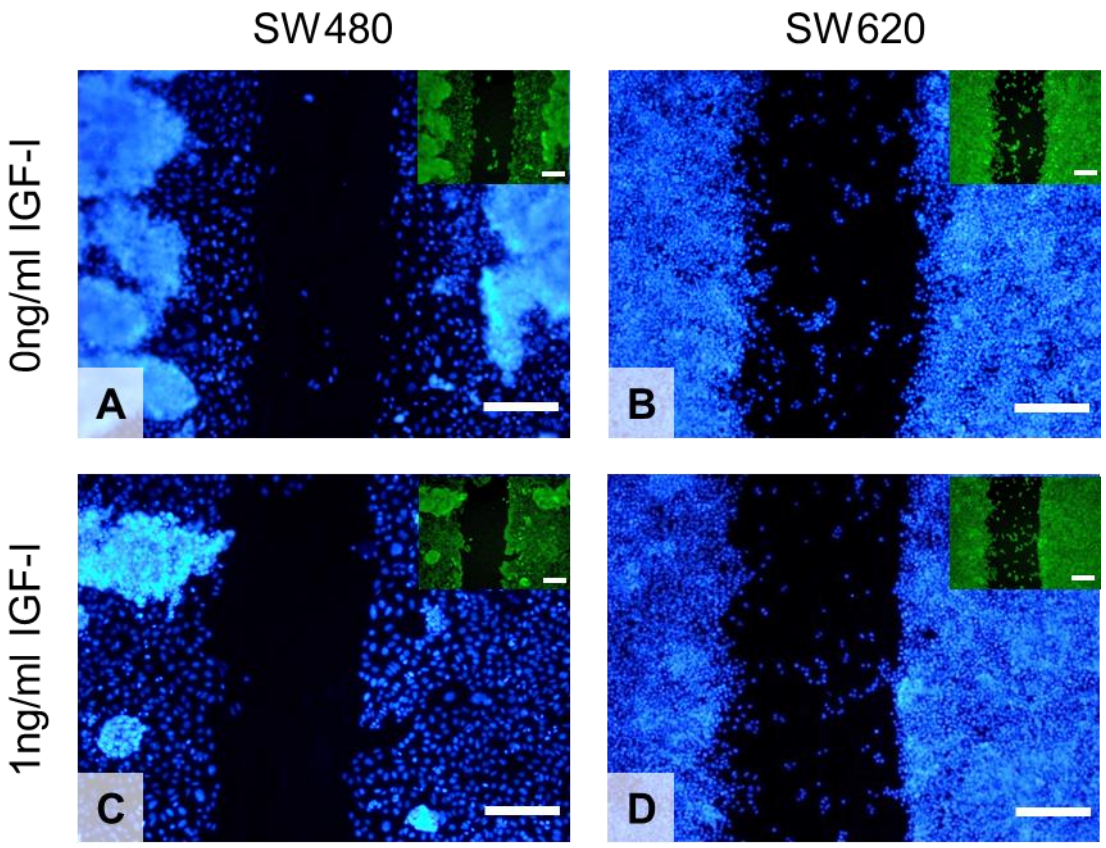

Figure 5.9: The SW620 cell line had more single migrating cells than the SW480 cell line during a scratch wound assay in the presence and absence of 1ng/ml IGF-I. DAPI and Phalloidin (inset) images of 24 hours post wounding with A and B: 0ng/ml IGF-I and C and D: 1ng/ml IGF-I for both cells lines. Scale bars = 200µm for all images.

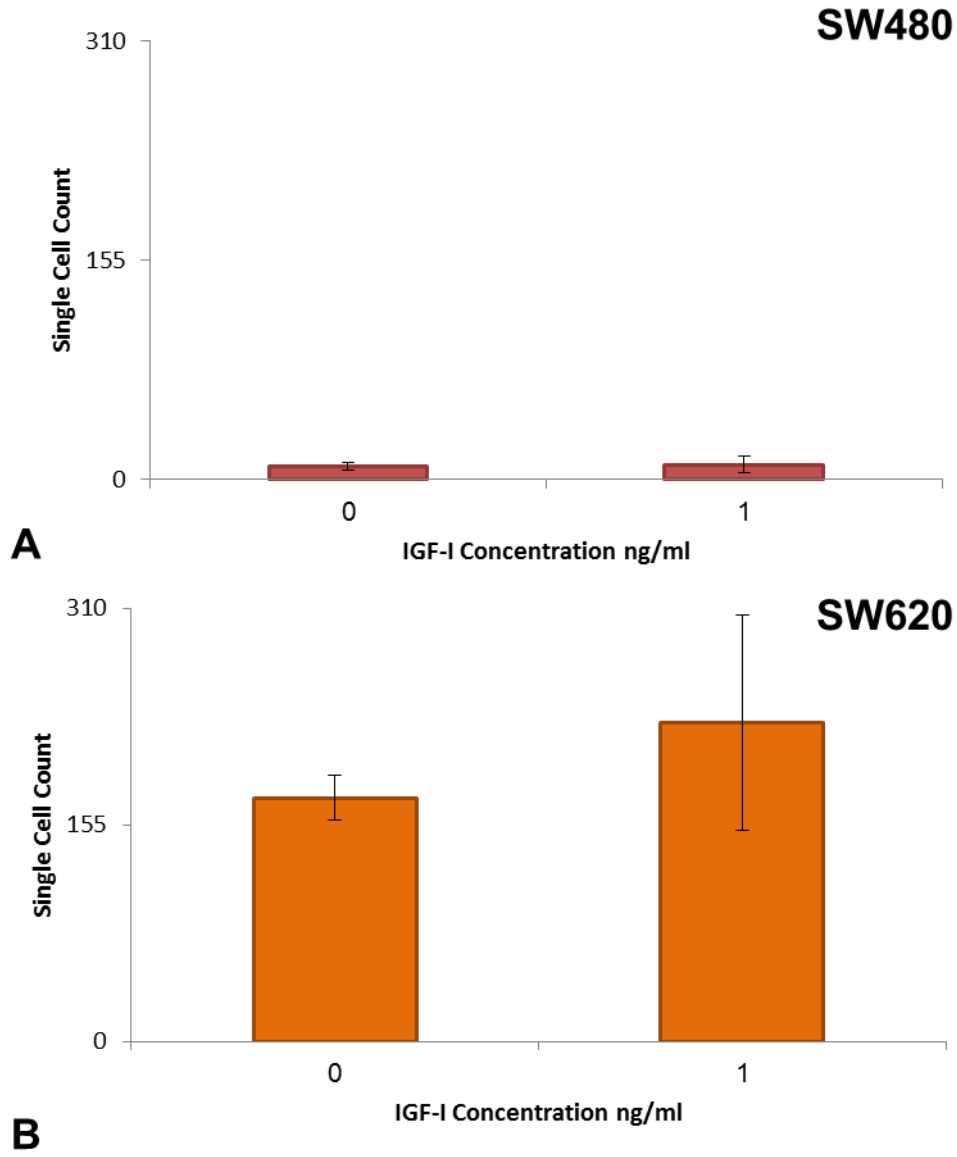

Figure 5.10: Neither the SW480 and SW620 cell lines showed a significant alteration in the number of single migrating cells within the 2D scratch wound in the presence or absence of IGF-I. Number of single migrating cells in A: SW480 and B: SW620 scratch wounds as determined from cell counts. Data represent mean, n = 3, ±SEM for both graphs, no significance by a Student t-test.

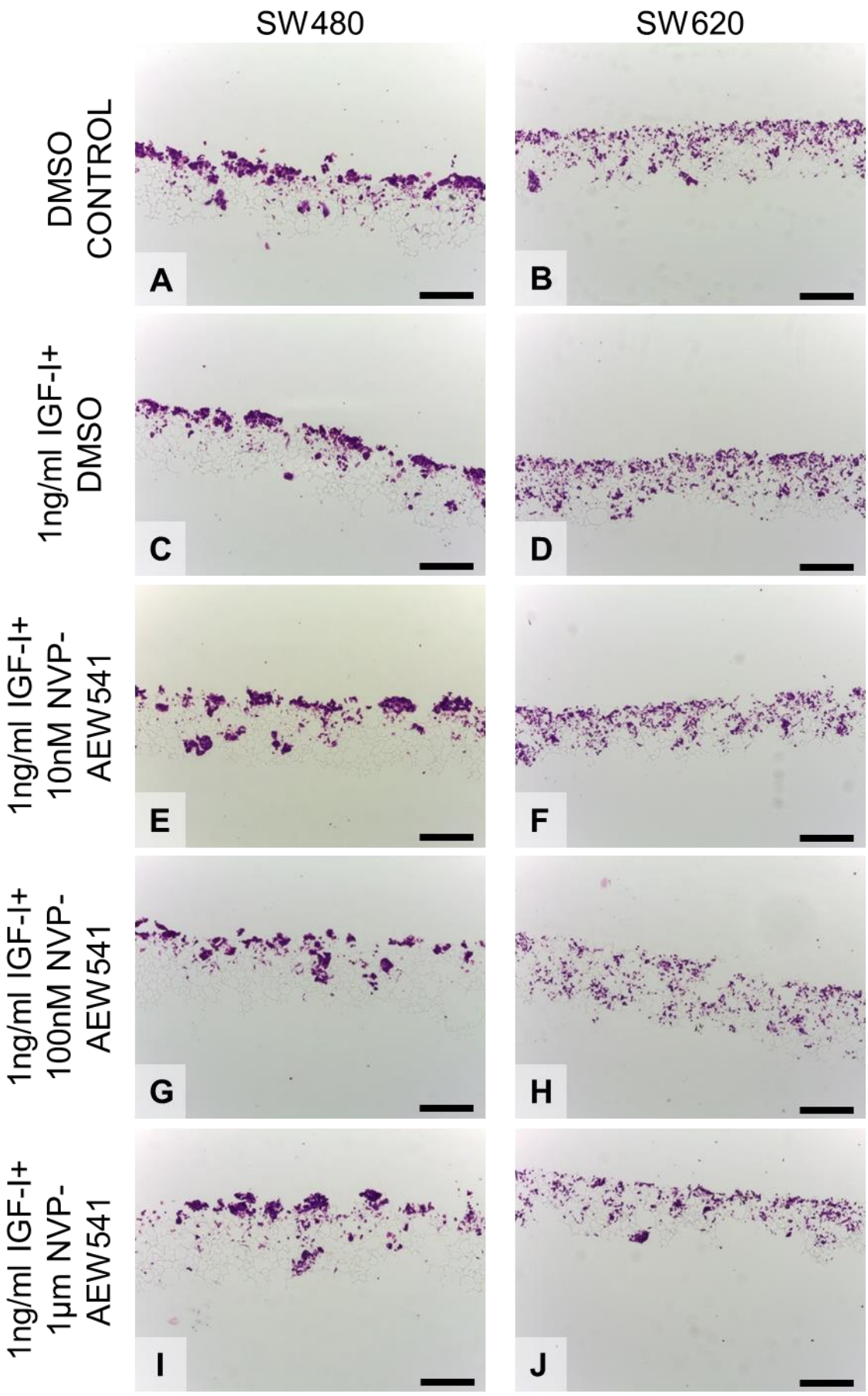

Figure 5.11: Both cell lines displayed a decreased build-up of cells when the IGF-I inhibitor NVP-AEW541 was present at a concentration of 1µM. H&E images of 10 day cultures with A and B: DMSO control, C and D: 1ng/ml IGF-I and DMSO control, E and F: 1ng/ml IGF-I and 10nM NVP-AEW541, G and H: 1ng/ml IGF-I and 100nM NVP-AEW541 and I and J: 1ng/ml IGF-I and 1µM NVP-AEW541 for both cells lines. Scale bars = 200µm for all images.

The quantification of the cell penetration again confirmed that more SW620 cells were present in the scaffold at 10 days than SW480 cells, ANOVA, $F(1, 24)=91.04$, $p<0.001$. This quantification also demonstrated that the inclusion of NVP-AEW541 significantly altered the penetration of cells into the scaffold, ANOVA, $F(4,24)=3.949$, $p=0.013$. NVP-AEW541 caused a significant decrease in the penetration for both cell lines when used at a concentration of 1µM in the presence of 1ng/ml IGF-I (Figure 5.12). Used on the SW480 cell line, the significant decrease seen with 1µM NVP-AEW541 was seen relative to the DMSO control (Figure 5.12A), whereas with the SW620 cell line, this decrease was seen relative to the 1ng/ml IGF-I control (Figure 5.12B). However, the increase in cell penetration induced by IGF-I in the SW480 cell line seen previously (Figure 5.4A) was not replicated here (Figure 5.12A), although this may be due to the use of different batches of IGF-I and the result presented in Figure 5.4 was replicated by other experiments presented later in this thesis.

5.3.2.2 NVP-AEW541 also affected cell viability and proliferation

The use of IGF-I with or without NVP-AEW541 was found to have no effect on the cell viability of the 3D SW480 cultures (Figure 5.13A); whereas the addition of 1ng/ml IGF-I without the presence of NVP-AEW541 at any concentration was found to increase the cell viability of the SW620 cultures (Figure 5.13B). However, as with the SW480 cell line, the addition of NVP-AEW541 did not alter the cell viability relative to the DMSO control (Figure 5.13B). In agreement with previous observations, when the number of cells within the material was quantified, there are more SW620 cells found per scaffold than SW480 cells (Figure 5.14), ANOVA, $F(1,24)=350.186$, $p<0.001$. Here it was observed that there was a small but significant increase in the observed cell number in SW480 cultures when 1ng/ml IGF-I was present in the absence of NVP-AEW541, compared to the DMSO control, (Figure 5.14A) and there was a significant increase in the number of SW620 cells when 1ng/ml IGF-I was present with 0.01µM NVP-AEW541 over the DMSO control (Figure 5.14B). Together these data show that at the concentration where NVP-AEW541 was effective in inhibiting the cell penetration into the material, this compound is not affecting the proliferative behaviour of the cultures, suggesting that the changes seen are due to NVP-AEW541 affecting the cellular migratory behaviour of the cells.

5.3.2.3 The combination of IGF-I and NVP-AEW541 did not affect the 2D migration of cells

When utilised in a 2D scratch wound assay, use of NVP-AEW541 did not completely inhibit the migration of the cells, as seen by the changes to the wound edges in the first 24 hours post wound (Figure 5.15). Quantification of the distance moved by the leading edges of migration demonstrated that none of the combinations of media additives tested were effective in significantly altering the amount migration attained by either cell line (Figure 5.16), although there was a difference observed between the two cell lines, ANOVA, $F(1,20)=8.703$, $p=0.008$. Fluorescent staining of the scratch wounds at 24 hours post wounding highlighted the number of single cells which have migrated into the wounds over 24 hours under each condition, as the SW620 cell line demonstrated a greater number of observed single cells than the SW480 cell line (Figure 5.17). The quantification of these cells confirmed that the SW620 cell line produces more of them over the 24 hour period than the SW480 cell line, ANOVA, $F(1, 20)=40.786$, $p<0.001$, with the media additives causing no alteration to the numbers observed within each cell line (Figure 5.18).

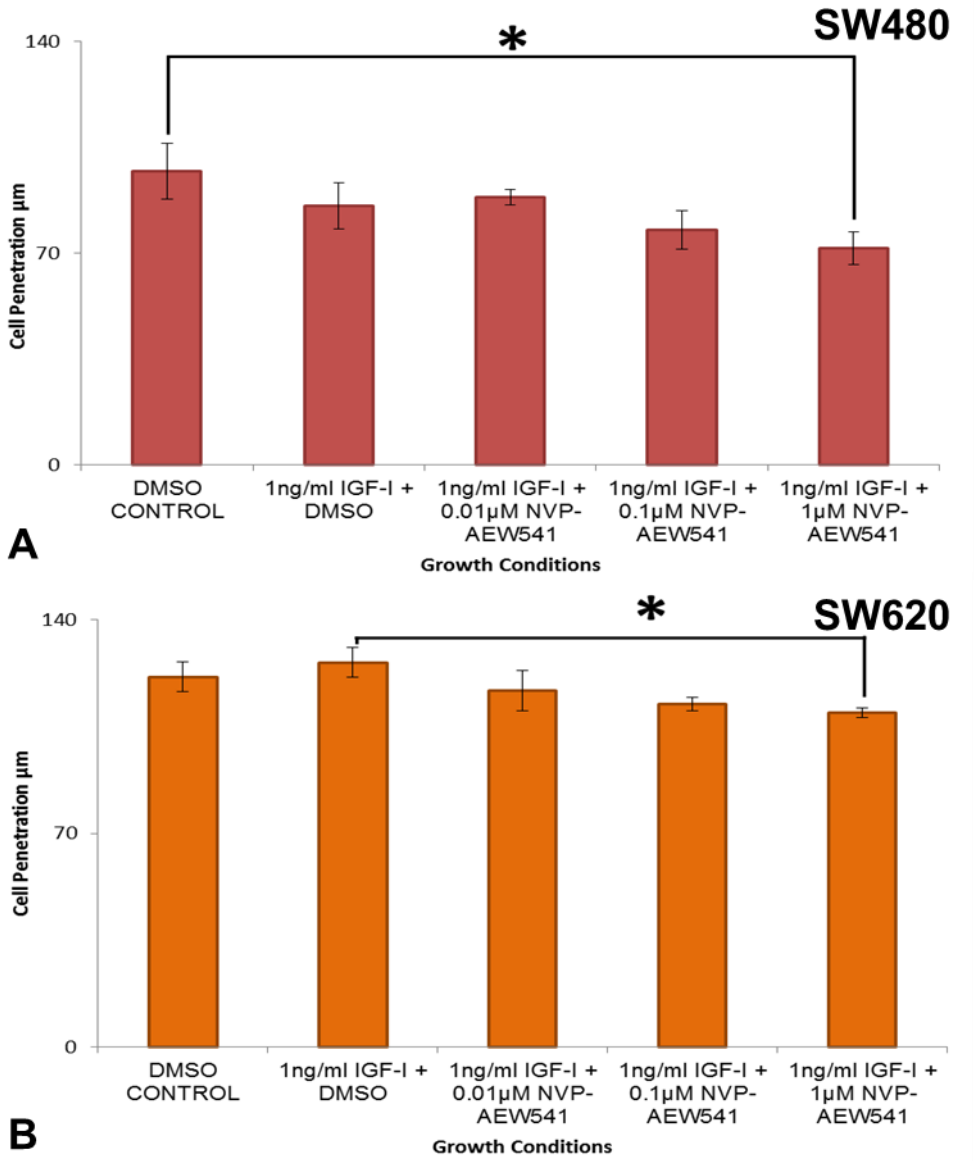

Figure 5.12: The 3D cell penetration of both the cell lines decreased when 1ng/ml IGF-I and 1µM NVP-AEW541 were present, relative to a DMSO control for the SW480 cells and a 1ng/ml IGF-I control for the SW620 cells. Cell penetration in µm of A: SW480 and B: SW620 cells as determined by the linear measurement method. Data represent mean, n = 3, ±SEM for both graphs, * $p < 0.05$ by a Tukey's test.

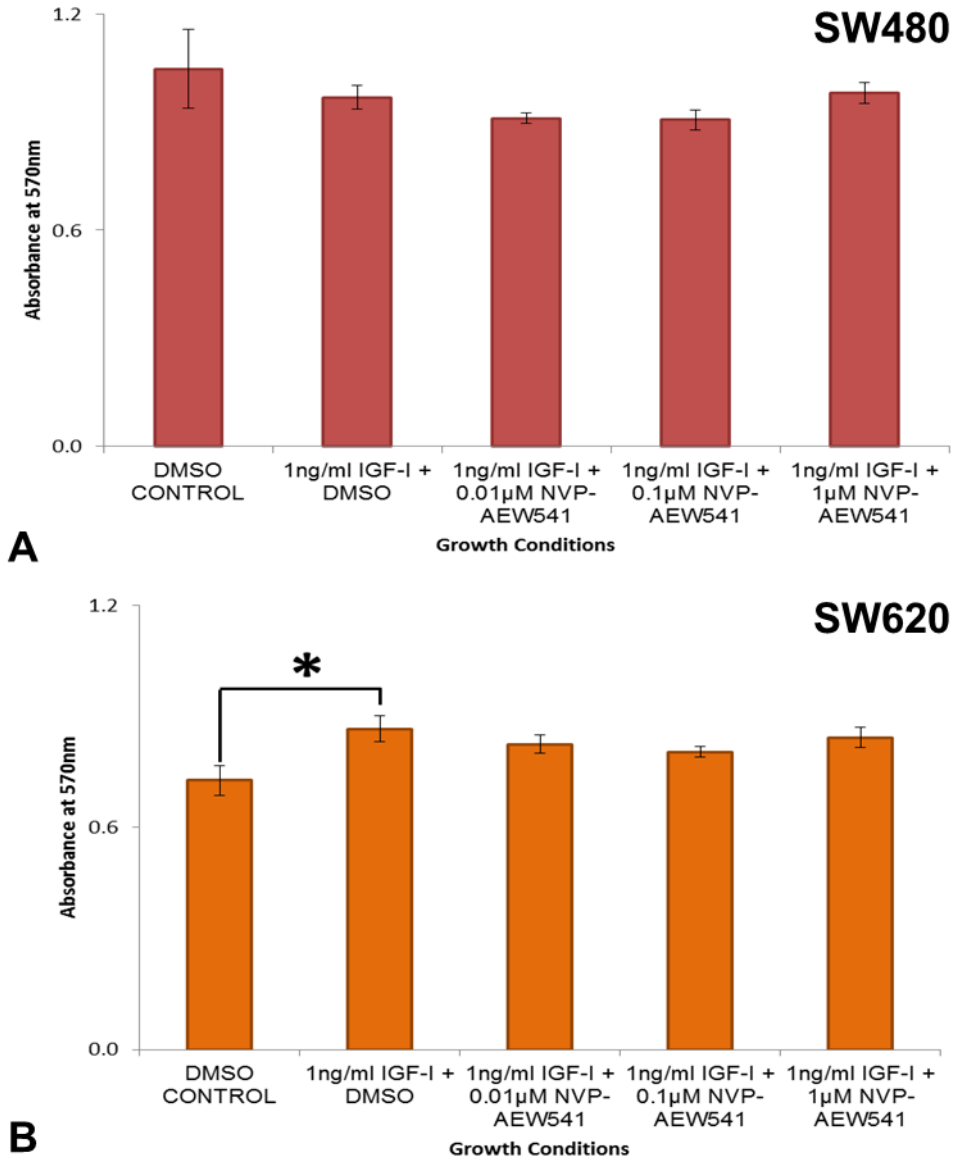

Figure 5.13: The 3D cell viability of the SW620 cell line increased when 1ng/ml IGF-I was present in the absence of NVP-AEW541, while the viability of the SW480 cell line was unaffected. Absorbance at 570nm of A: SW480 and B: SW620 cells as determined by the MTT Cell Viability Assay. Data represent mean, n = 3, ±SEM for both graphs, * $p < 0.05$ by a Tukey's test.

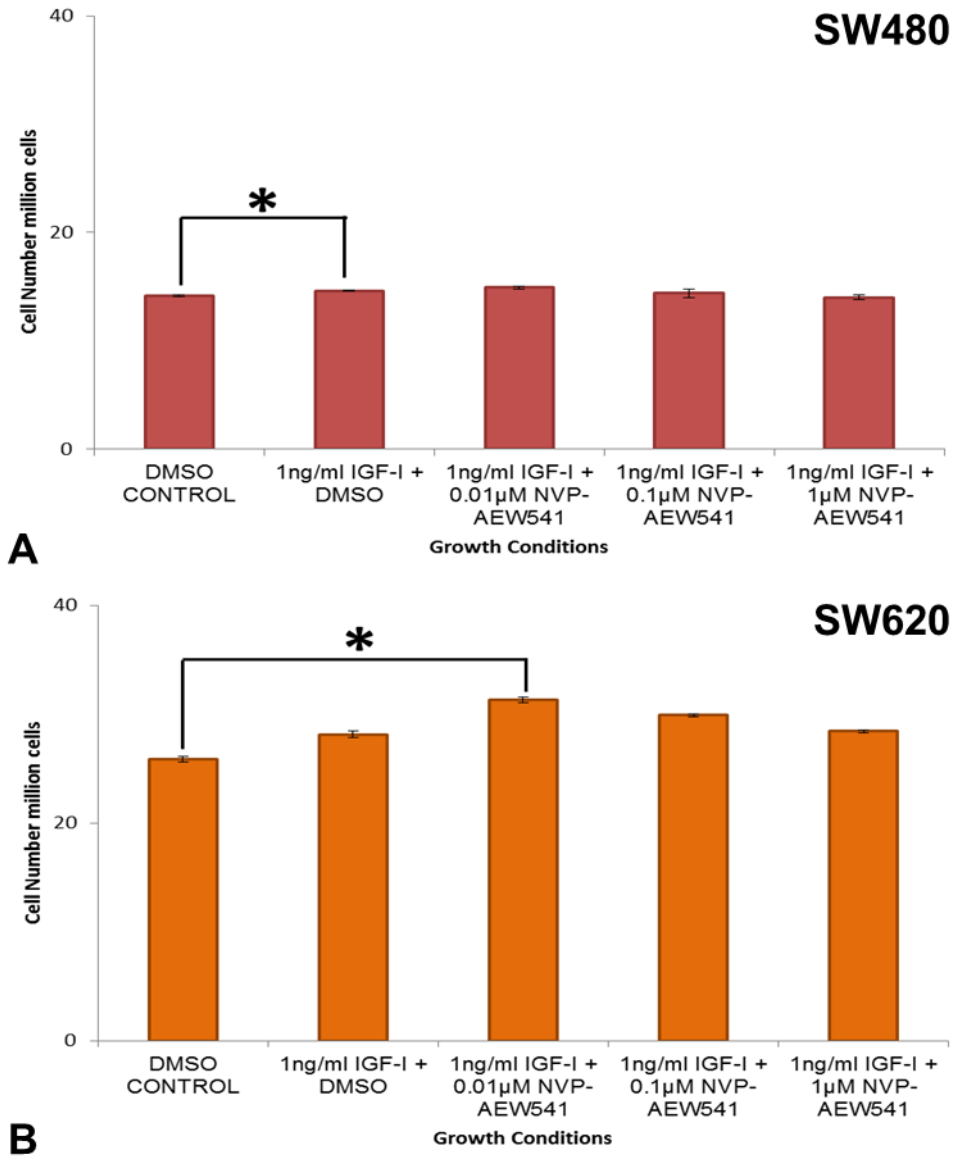

Figure 5.14: The number of SW480 cells in the 3D material increased when IGF-I only was present at a concentration of 1ng/ml and was unaffected by the presence of NVP-AEW541 at all concentrations, while the number of SW620 cells increased in the presence of 1ng/ml IGF-I and 0.01µM NVP-AEW541 and was unaffected by all other NVP-AEW541 concentrations. Cell number in millions of cells of A: SW480 and B: SW620 cells as determined by the Pico Green dsDNA Assay. Data represent mean, n = 3, ±SEM for both graphs, * $p < 0.05$ by a Tukey's test.

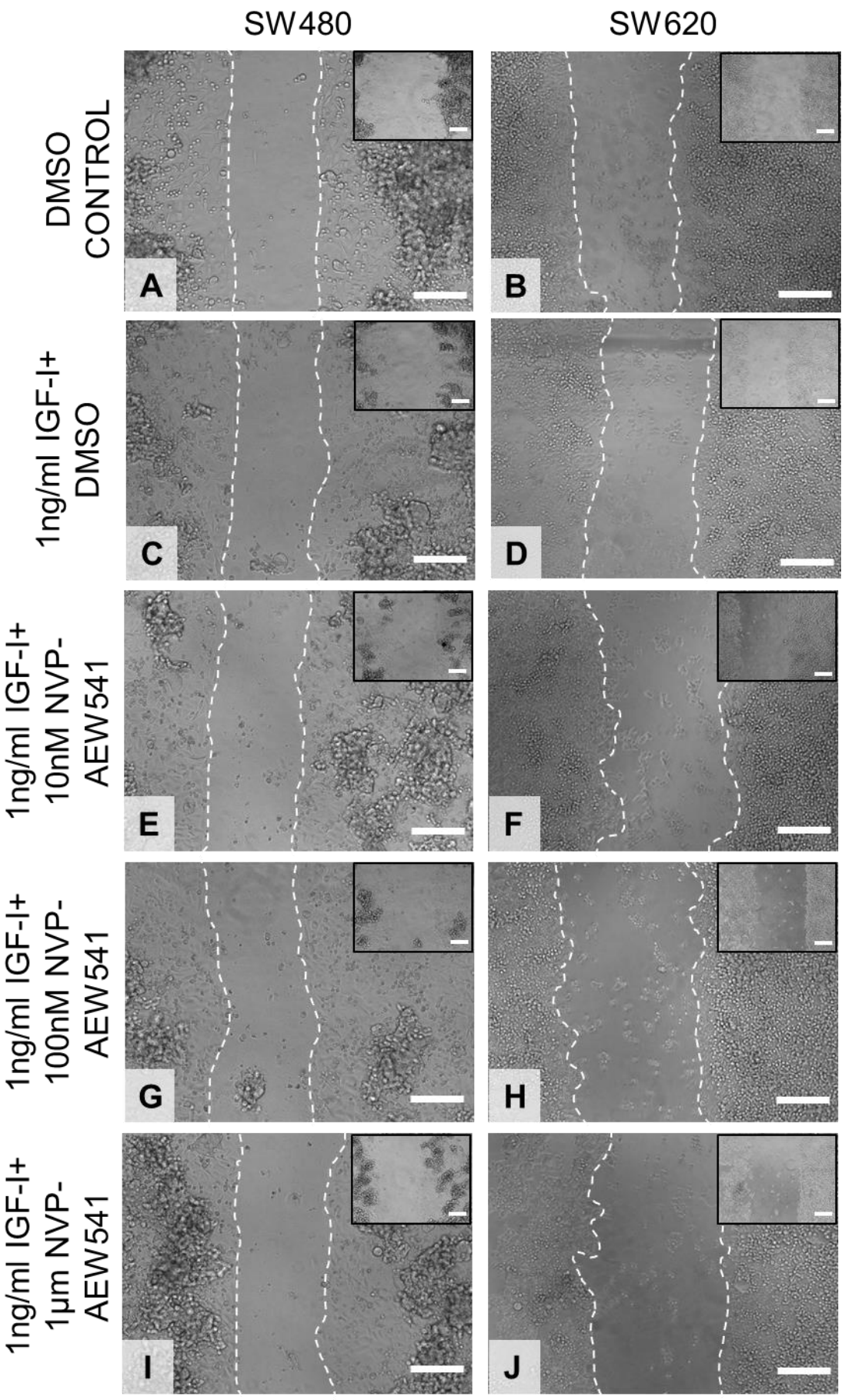

Figure 5.15: Both the SW480 and SW620 cell lines exhibited wound closing during a scratch wound assay in the presence of 1ng/ml IGF-I with and without the IGF-I inhibitor NVP-AEW541. Phase images of 24 hours post wounding with A and B: DMSO control, C and D: 1ng/ml IGF-I and DMSO control, E and F: 1ng/ml IGF-I and 10nM NVP-AEW541, G and H: 1ng/ml IGF-I and 100nM NVP-AEW541 and I and J: 1ng/ml IGF-I and 1µM NVP-AEW541 for both cells lines. Scale bars = 200µm for all images.

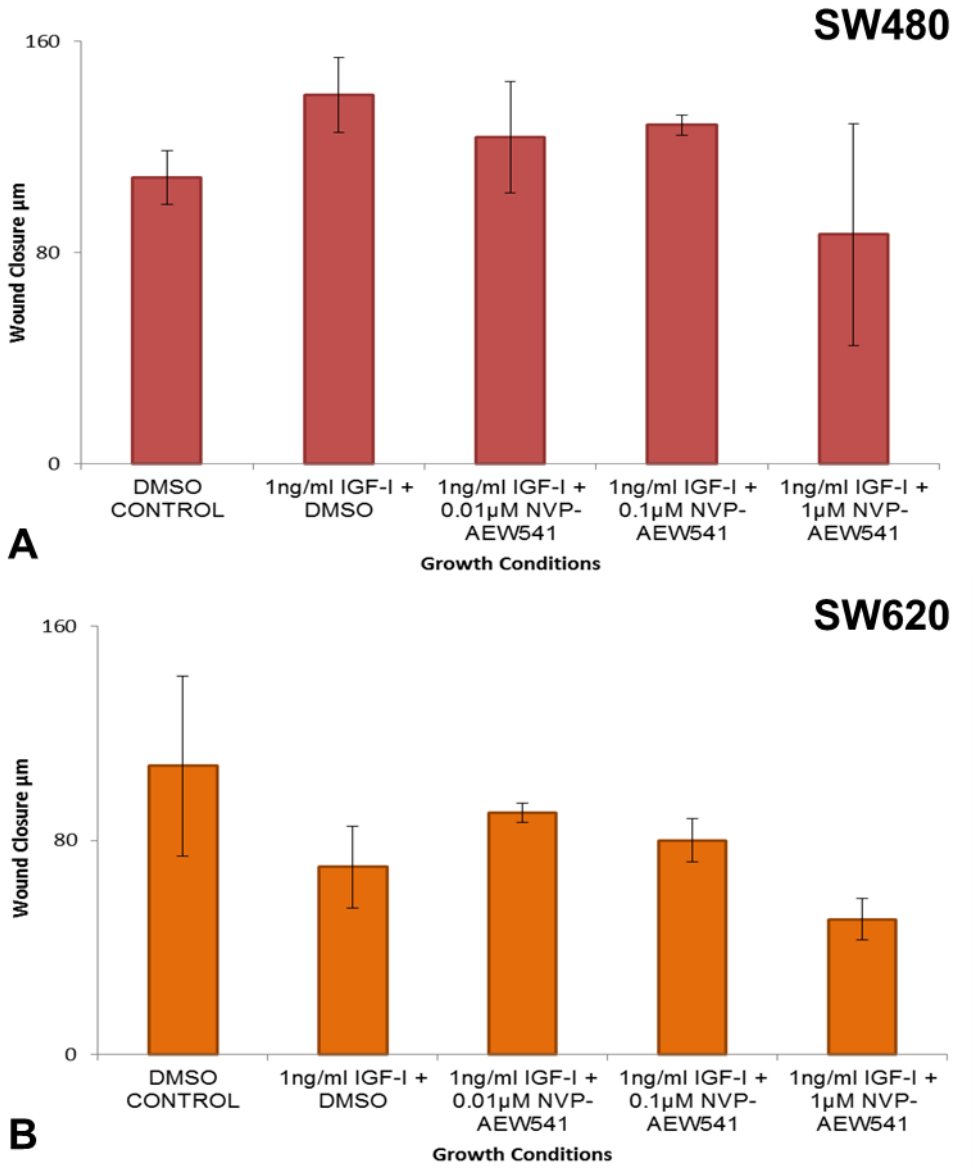

Figure 5.16: Neither the SW480 and SW620 cell lines showed a significant alteration in the distance moved by the edges of the 2D scratch wound in the presence of IGF-I with and without NVP-AEW541. Wound closure in µm of A: SW480 and B: SW620 cells as determined by measuring the width of the wound. Data represent mean, n = 3, ±SEM for both graphs, no significance by a Tukey's test.

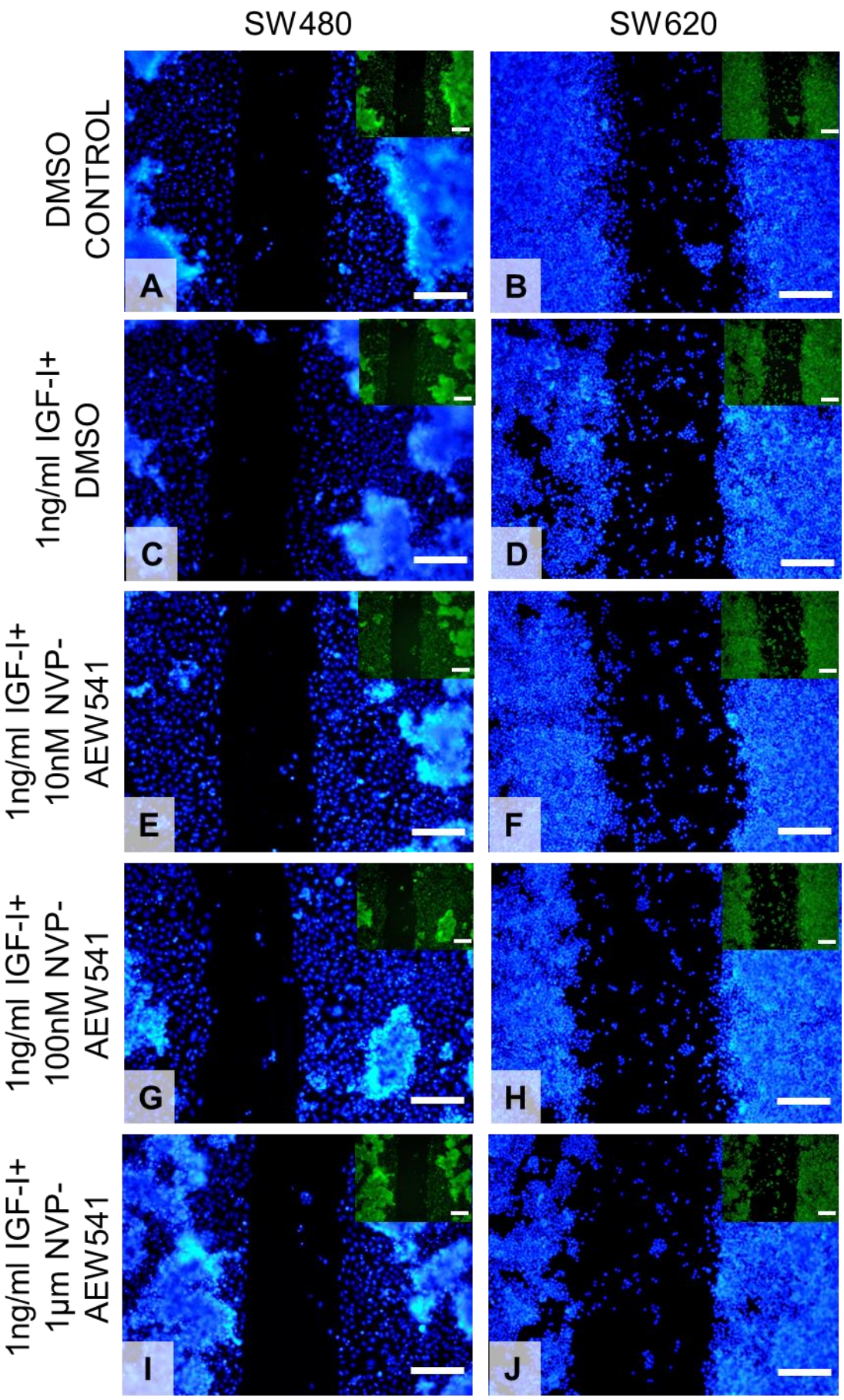

Figure 5.17: The SW620 cell line had more single migrating cells than the SW480 cell line during a scratch wound assay in the presence of 1ng/ml IGF-I with and without the IGF-I inhibitor NVP-AEW541. Phase images of 24 hours post wounding with A and B: DMSO control, C and D: 1ng/ml IGF-I and DMSO control, E and F: 1ng/ml IGF-I and 10nM NVP-AEW541, G and H: 1ng/ml IGF-I and 100nM NVP-AEW541 and I and J: 1ng/ml IGF-I and 1µM NVP-AEW541 for both cells lines. Scale bars = 200µm for all images.

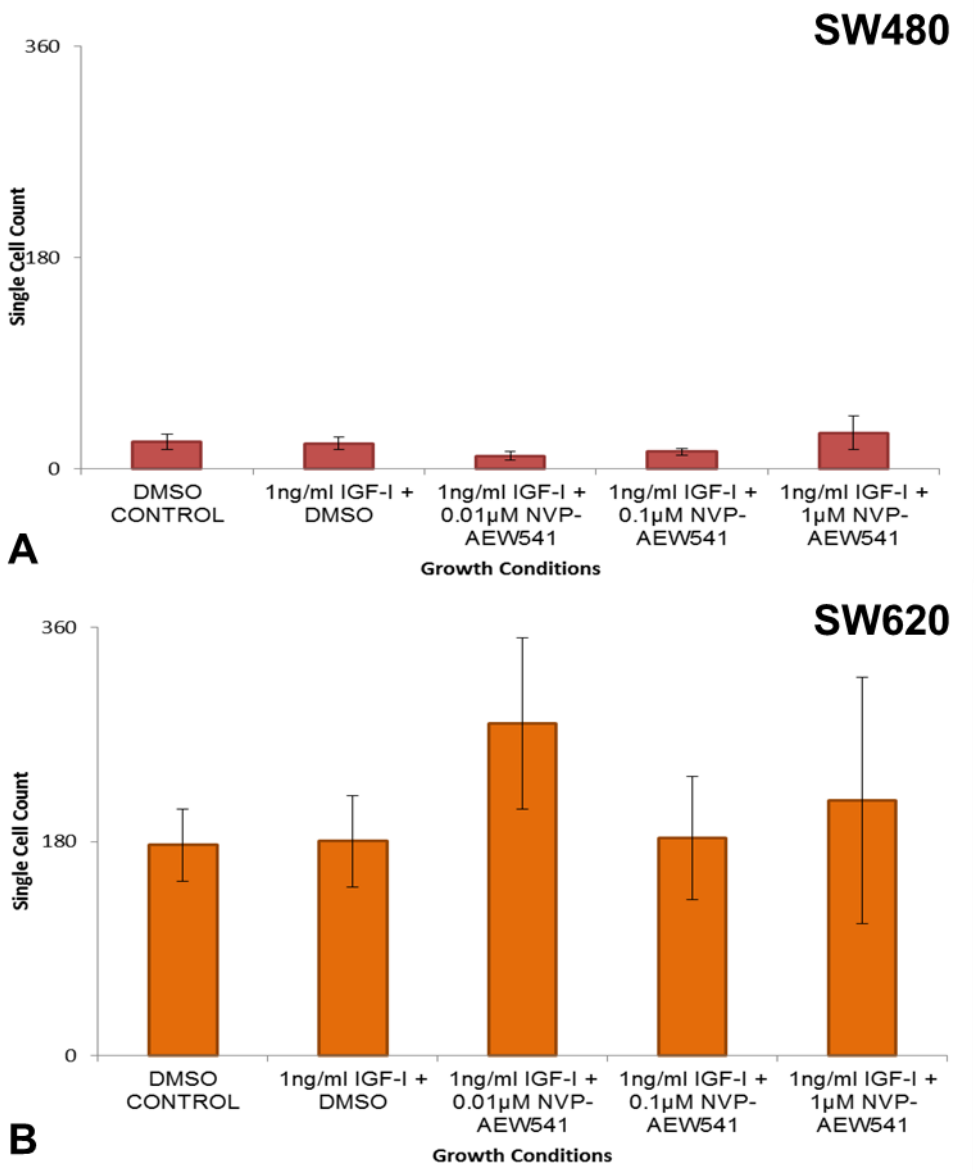

Figure 5.18: Neither the SW480 and SW620 cell lines showed a significant alteration in the number of single migrating cells within the 2D scratch wound in the presence of IGF-I with and without NVP-AEW541. Number of single migrating cells in A: SW480 and B: SW620 scratch wounds as determined from cell counts. Data represent mean, n = 3, ±SEM for both graphs, no significance by a Tukey's test.

5.3.2.4 The presence of NVP-AEW541 alone had no effect on cell penetration

As it has been demonstrated that 1µM NVP-AEW541 is capable of inhibiting 3D migration of colorectal cancer cells in the presence of IGF-I, the effectiveness of NVP-AEW541 in inhibiting migration in the absence of IGF-I was then examined. Upon histological examination of the 3D cultures grown with and without IGF-I and NVP-AEW541, the SW480 cell line displayed the build of cells previously observed when IGF-I alone is present (Figure 5.19C) when compared to the DMSO control (Figure 5.19A). The presence of NVP-AEW541, either with (Figure 5.19G) or without (Figure 5.19E) the presence of IGF-I, produced cultures where the cellular distribution is comparable to the DMSO control. The distribution of SW620 cells within the scaffold did not appear to be altered by the presence of either IGF-I or NVP-AEW541 (Figure 5.19B, D, F & H).

The quantification of cell penetration demonstrated that the SW620 cell line attained a greater depth of penetration than the SW480 cell line, ANOVA, $F(1,19)=14.317$, $P=0.001$, in addition to demonstrating that the inclusion of NVP-AEW541 also significantly affected the cell penetration, ANOVA, $F(3,19)=5.02$, $p=0.01$.The average penetration of SW480 cells into the scaffold was increased in the presence of 1ng/ml IGF-I and returned to a level comparable to the DMSO control when 1µM NVP-AEW541 was also present, as the presence of 1µM NVP-AEW541 alone failed to produce a significant alteration in cellular penetration when compared to the DMSO control (Figure 5.20A). In conjunction with the observation made from the initial assessment of the histological images, the cell penetration demonstrated by the SW620 cell line remained unaltered in the presence of the media additives examined here (Figure 5.20B).

5.3.2.5 The viability and proliferation of colorectal cancer cell lines was not affected by NVP-AEW541

Assessment of the cell viability of the 3D cultures showed that the addition of 1ng/ml IGF-I or 1µM NVP-AEW541 to the culture media did not have an effect on the viability of either cell line (Figure 5.21). The number of cells present in the cultures with either cell line was also unaltered by the addition of 1ng/ml IGF-I or 1µM NVP-AEW541 to the culture media, with the SW620 cultures yielding a higher cell number than the SW480 as previously observed (Figure 5.22), ANOVA, $F(1,19)=495.973$, $p<0.001$. These data showed that in the 3D migration model, NVP-AEW541 was effective in inhibiting the IGF-I induced cell migration and not the base-line cell migration observed, while leaving the proliferative behaviour of the cells unaffected.

5.3.2.6 The combination of IGF-I and NVP-AEW541 only effects 3D migration and did not affect 2D migration

The phase contrast images for the counterpart 2D scratch wound assays showed that the cell distribution after 24 hours was broadly similar to that previously observed in other experiments and shows no clear difference between each of the conditions tested (Figure 5.23). The quantification of the wound closure attained by these cultures confirmed the lack of significant variation in wound closure in the presence of 1ng/ml IGF-I or 1µM NVP-AEW541 for either the SW480 or SW620 cell line (Figure 5.24).

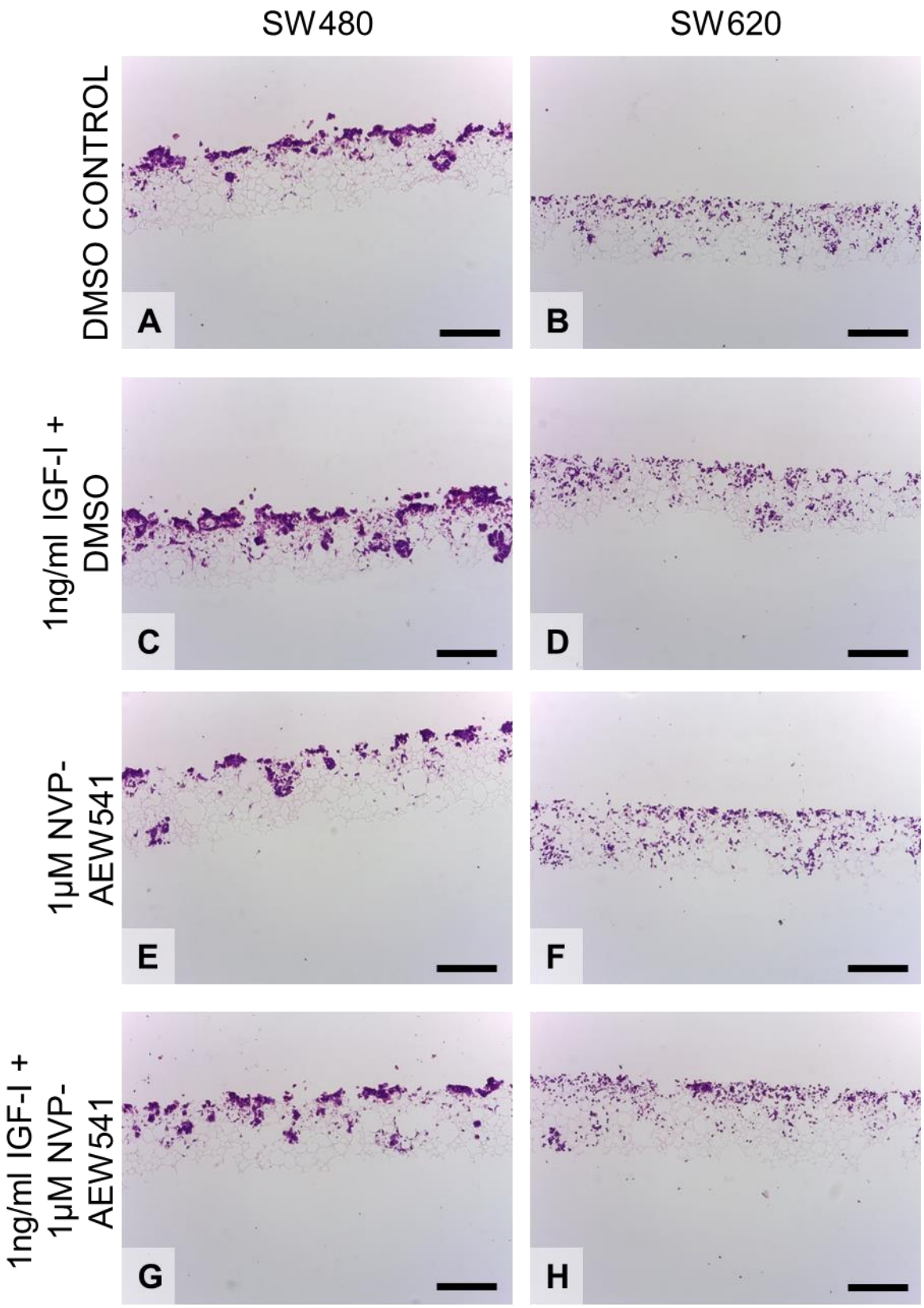

Figure 5.19: Neither cell line displayed an alteration in the build-up of cells when the IGF-I inhibitor NVP-AEW541 was present in the absence of IGF-I. H&E images of 10 day cultures with A and B: DMSO control, C and D: 1ng/ml IGF-I and DMSO, E and F: 1µM NVP-AEW541 and G and H: 1ng/ml IGF-I and 1µM NVP-AEW541 for both cells lines. Scale bars = 200µm for all images.

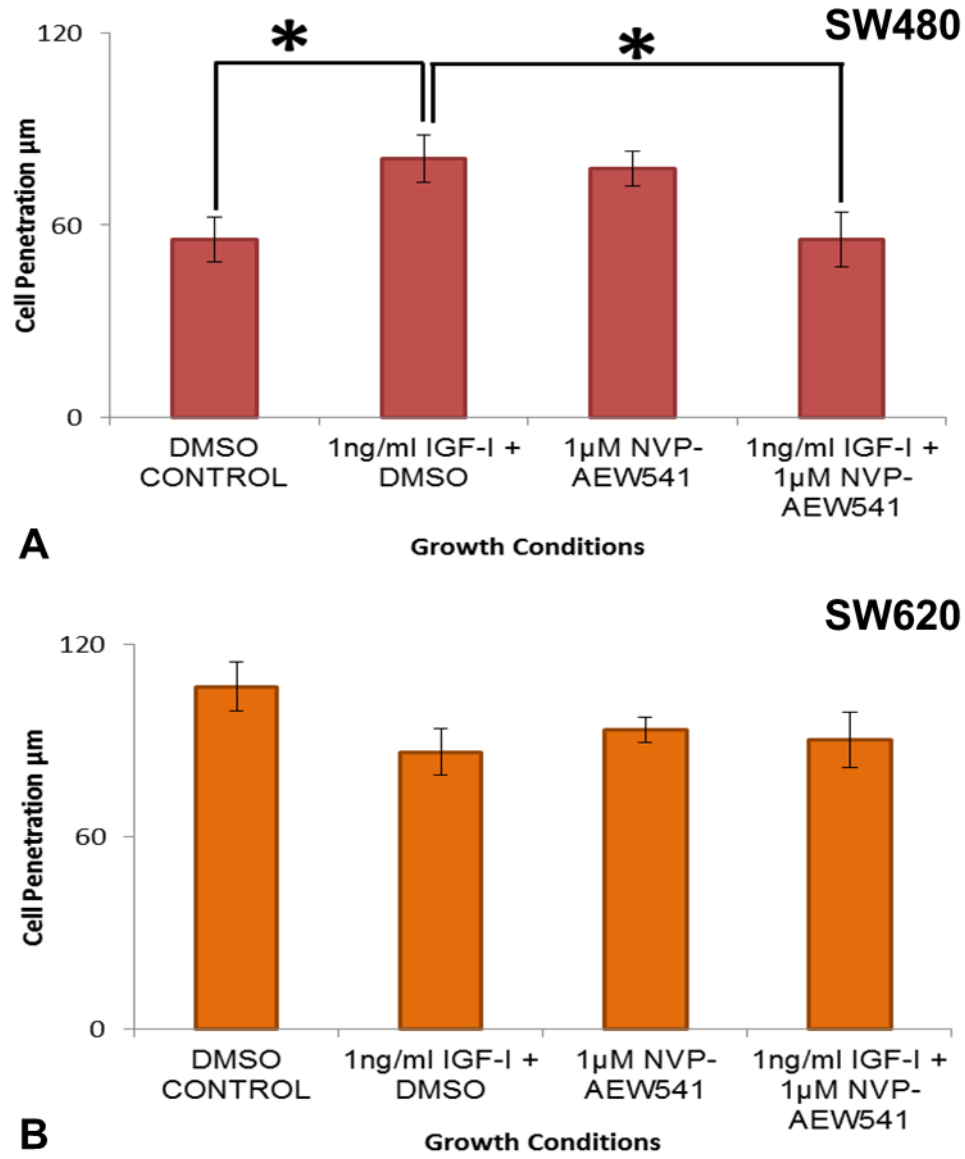

Figure 5.20: The 3D cell penetration of the SW480 cell line increased when IGF-I alone was present and decreased relative to this when 1µM NVP-AEW541 was present in the presence of 1ng/ml IGF-1, the penetration of both cell lines was unaffected when 1µM NVP-AEW541 alone was present. Cell penetration in µm of A: SW480 and B: SW620 cells as determined by the linear measurement method. Data represent mean, n = 3, ±SEM for both graphs, * $p < 0.05$ by a Tukey's test.

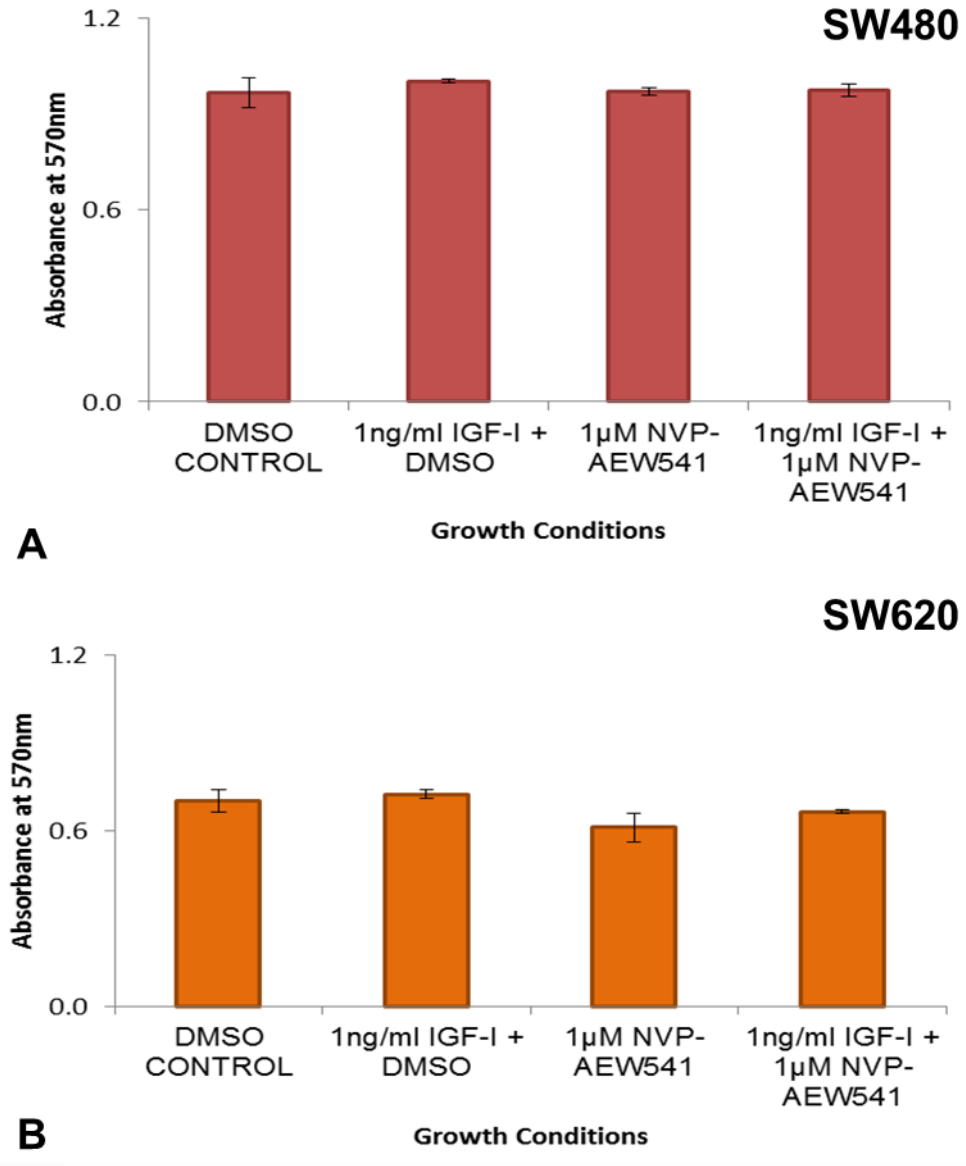

Figure 5.21: The 3D cell viability of both the SW480 and SW620 cell lines was unaffected by the presence of IGF-I or NVP-AEW541. Absorbance at 570nm of A: SW480 and B: SW620 cells as determined by the MTT Cell Viability Assay. Data represent mean, n = 3, ±SEM for both graphs, no significance by a Tukey's test.

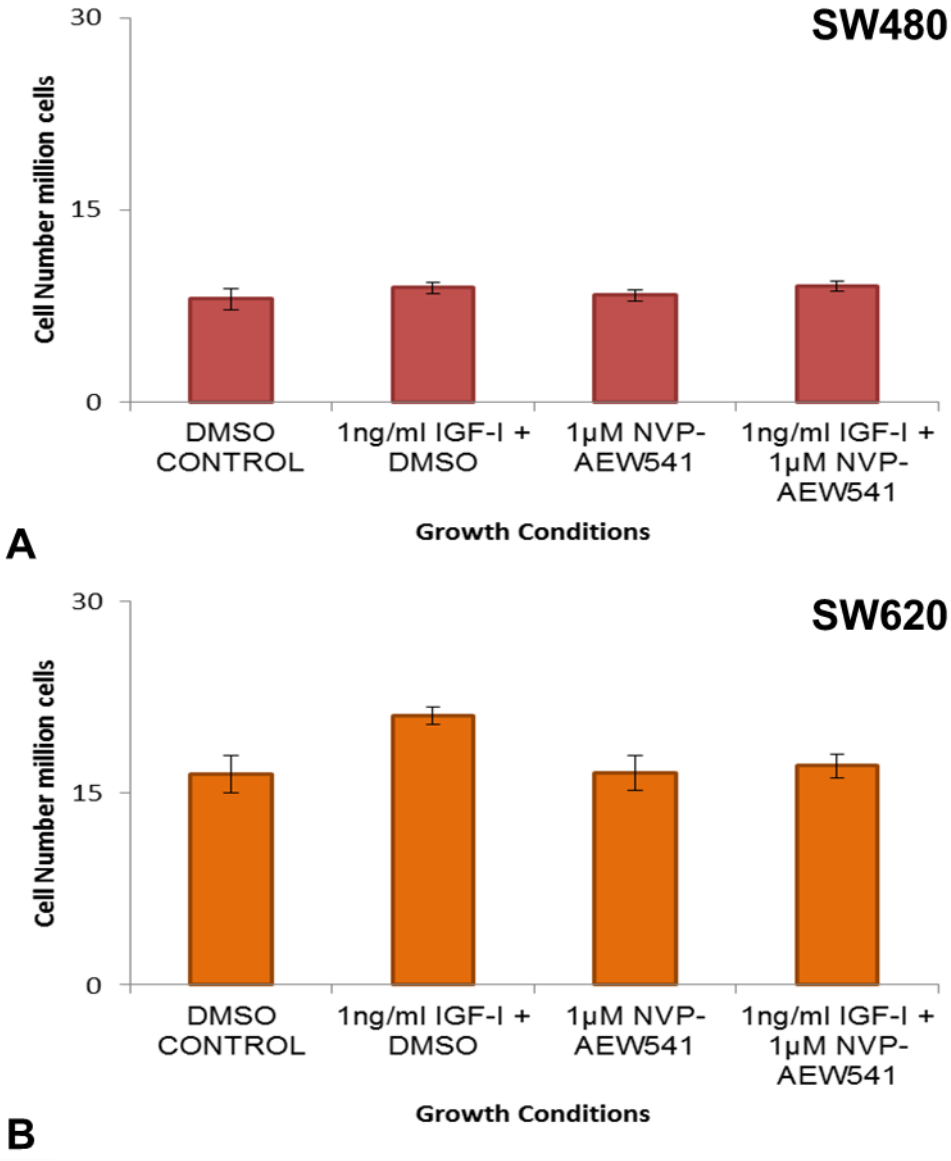

Figure 5.22: The number of cells present in the 3D material was unaffected by the presence of IGF-I or NVP-AEW541 for both the SW480 and SW620 cell lines. Cell number in millions of cells of A: SW480 and B: SW620 cells as determined by the Pico Green dsDNA Assay. Data represent mean, n = 3, ±SEM for both graphs, no significance by a Tukey's test.

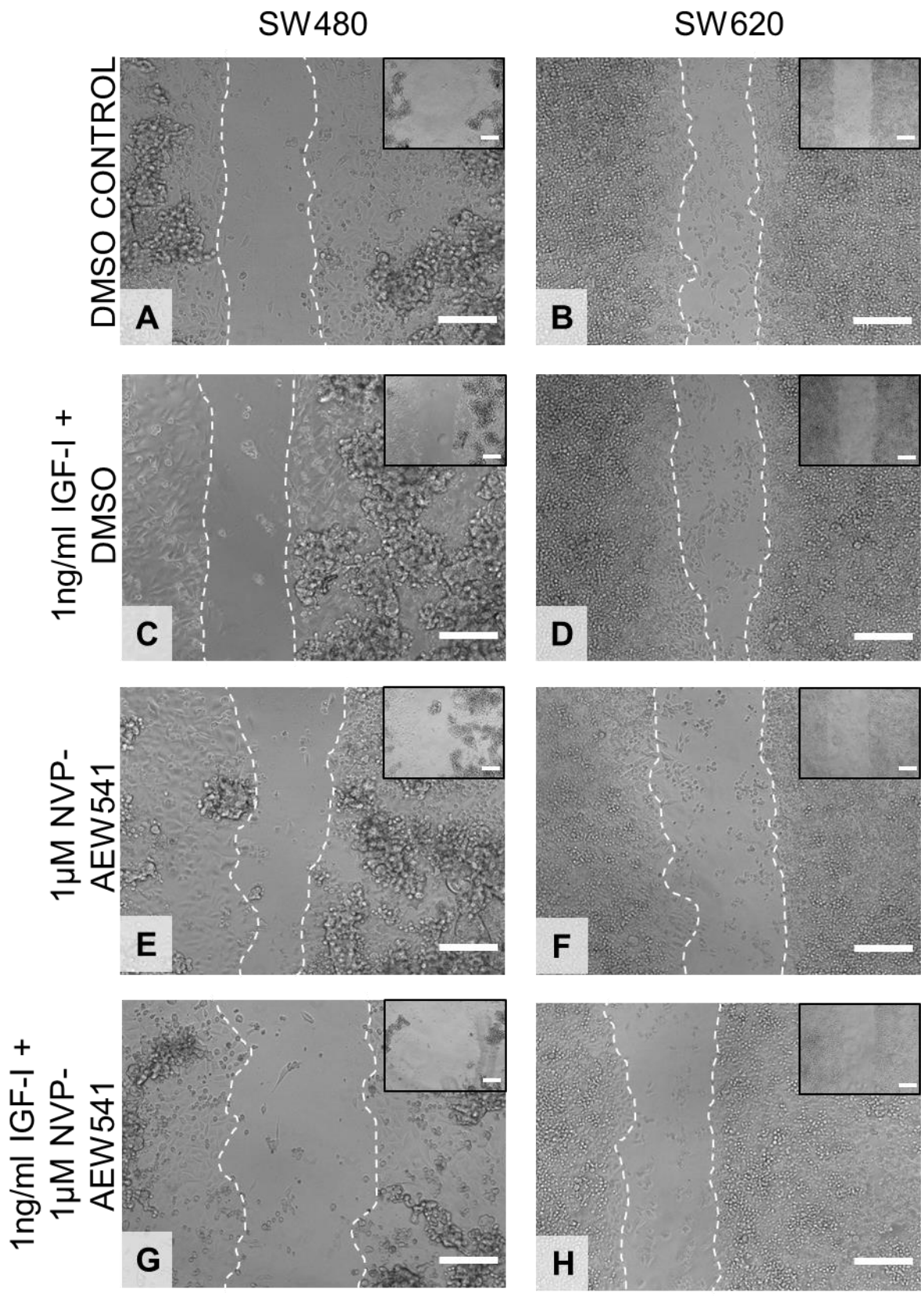

Figure 5.23: Both the SW480 and SW620 cell lines exhibited wound closing during a scratch wound assay in the presence of IGF-I or the IGF-I inhibitor NVP-AEW541. Phase images of 24 hours post wounding with A and B: DMSO control, C and D: 1ng/ml IGF-I and DMSO, E and F: 1µM NVP-AEW541 G and H: 1ng/ml IGF-I and 1µM NVP-AEW541 for both cells lines. Scale bars = 200µm for all images.

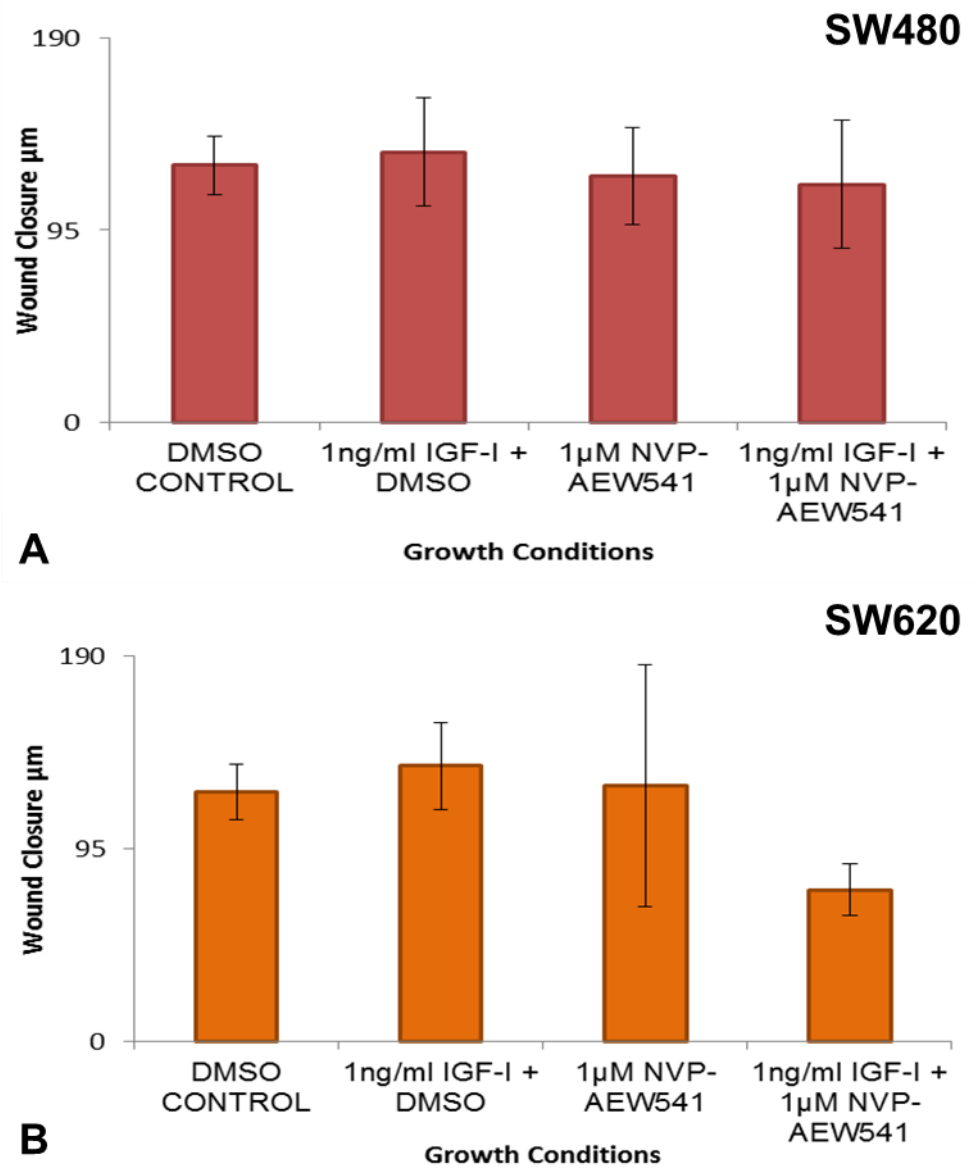

Figure 5.24: Neither the SW480 and SW620 cell lines showed a significant alteration in the distance moved by the edges of the 2D scratch wound in the presence of IGF-I or NVP-AEW541. Wound closure in µm of A: SW480 and B: SW620 cells as determined by measuring the width of the wound. Data represent mean, n = 3, ±SEM for both graphs, no significance by a Tukey's test.

The DAPI and Phalloidin staining of the scratch wounds did not reveal any clear alteration to the number of single cells within the scratch wound at 24 hours post wounding within the cultures for each cell line (Figure 5.25). A count of these cells confirmed that there is no significant alteration in the presence of 1ng/ml IGF-I or 1μM NVP-AEW541, with the SW620 cultures consistently resulting in a higher number of single cells within the wound after 24 hours than the SW480 cultures (Figure 5.26), ANOVA, $F(1,16)=122.785$, $p<0.001$. These data confirmed that the effect of IGF-I and NVP-AEW541 in altering the migratory behaviour of colorectal cancer cells was only effective in the 3D model and not the 2D scratch wound model used here.

5.3.3 Inhibition of the Wnt signalling pathway with IWR-1 can block the IGF-I induced migratory response of cells in the 3D model

As it has now been demonstrated that independent manipulation of both the IGF-I and Wnt signalling pathways can be used to alter the cell migratory behaviour of colorectal cancer cells in a 3D migration model, the interaction between these pathways was then examined. For this, IGF-I and IWR-1 were used in conjunction at the effective concentrations determined previously in this Chapter, 1ng/ml for IGF-I, and in Chapter 4, 10μM for IWR-1.

5.3.3.1 IWR-1 counteracts the effect of IGF-I on the penetration of SW480 cells

Histological processing of the 3D cultures grown in the presence of 1ng/ml IGF-I or 10μM IWR-1 shows a difference in the response of each cell line to the media additives. Culturing the SW480 cell line in the presence of IGF-I led to the cells being present in a greater proportion of the depth of the scaffold (Figure 5.27C) than when cultured in the presence of DMSO alone (Figure 5.27A), while there were no clear differences between the distribution of cells in the control cultures and those when IWR-1 was present (Figure 5.27E & G). The H&E images of the SW620 cultures did not display an alteration of cellular distribution within the scaffold in the presence of either of the media additives (Figure 5.27B, D, F & H). In confirmation of the histological data, the addition of media additives was found to alter the cell penetration achieved by the SW480 cell line, but not the SW620 cell line (Figure 5.28), although the SW620 cell line was found to penetrate a greater depth than the SW480 cell line, ANOVA, $F(1,19)=19.327$, $p<0.001$. The amount of cell penetration found in the SW480 cultures grown in the presence of IGF-I was found to be significantly greater than those cultures grown under any of the other conditions (Figure 5.28A).

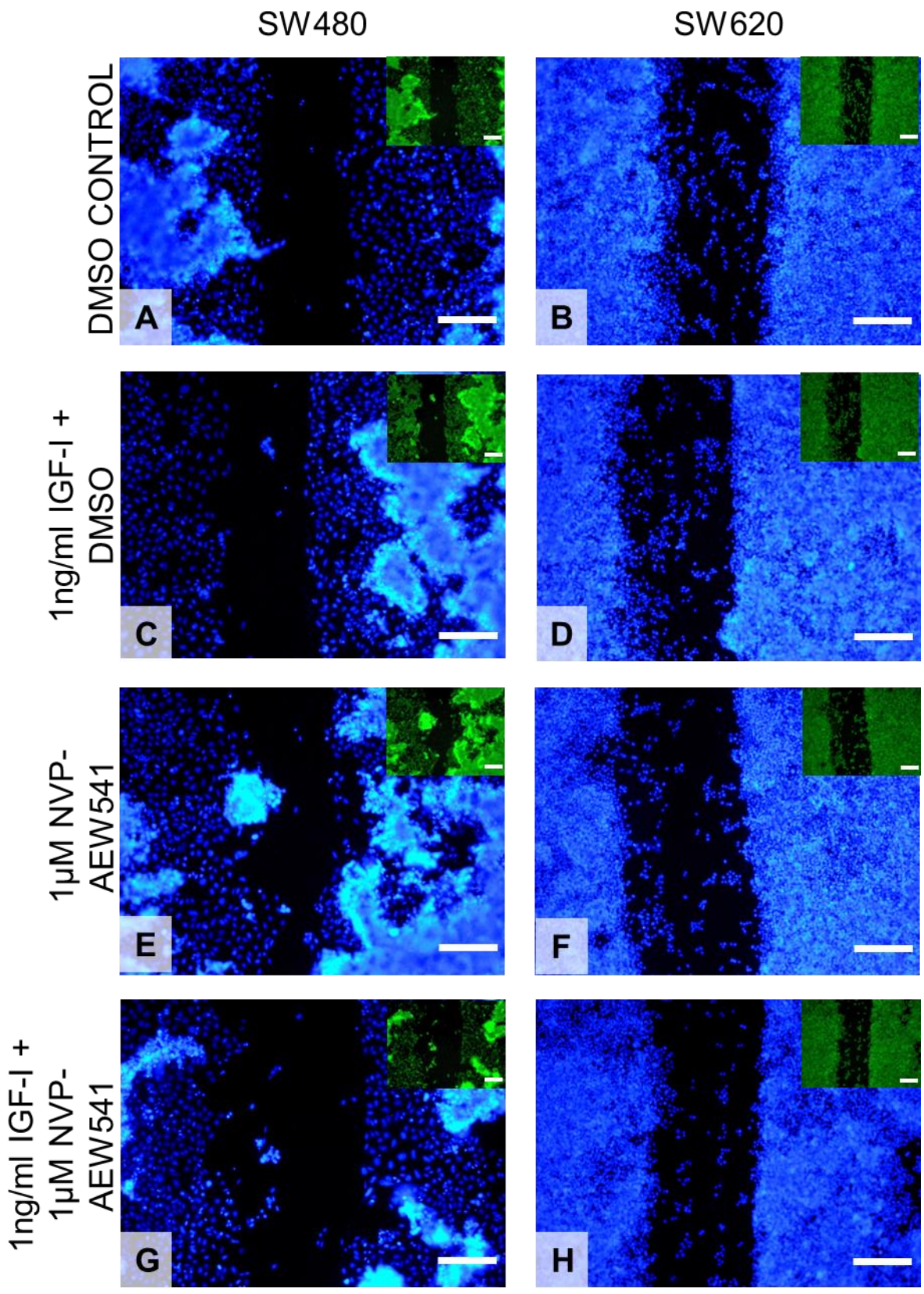

Figure 5.25: The SW620 cell line had more single migrating cells than the SW480 cell line during a scratch wound assay in the presence of IGF-I or the IGF-I inhibitor NVP-AEW541. DAPI and Phalloidin (inset) images of 24 hours post wounding with A and B: DMSO control, C and D: 1ng/ml IGF-I and DMSO, E and F: 1µM NVP-AEW541 G and H: 1ng/ml IGF-I and 1µM NVP-AEW541 for both cells lines. Scale bars = 200µm for all images.

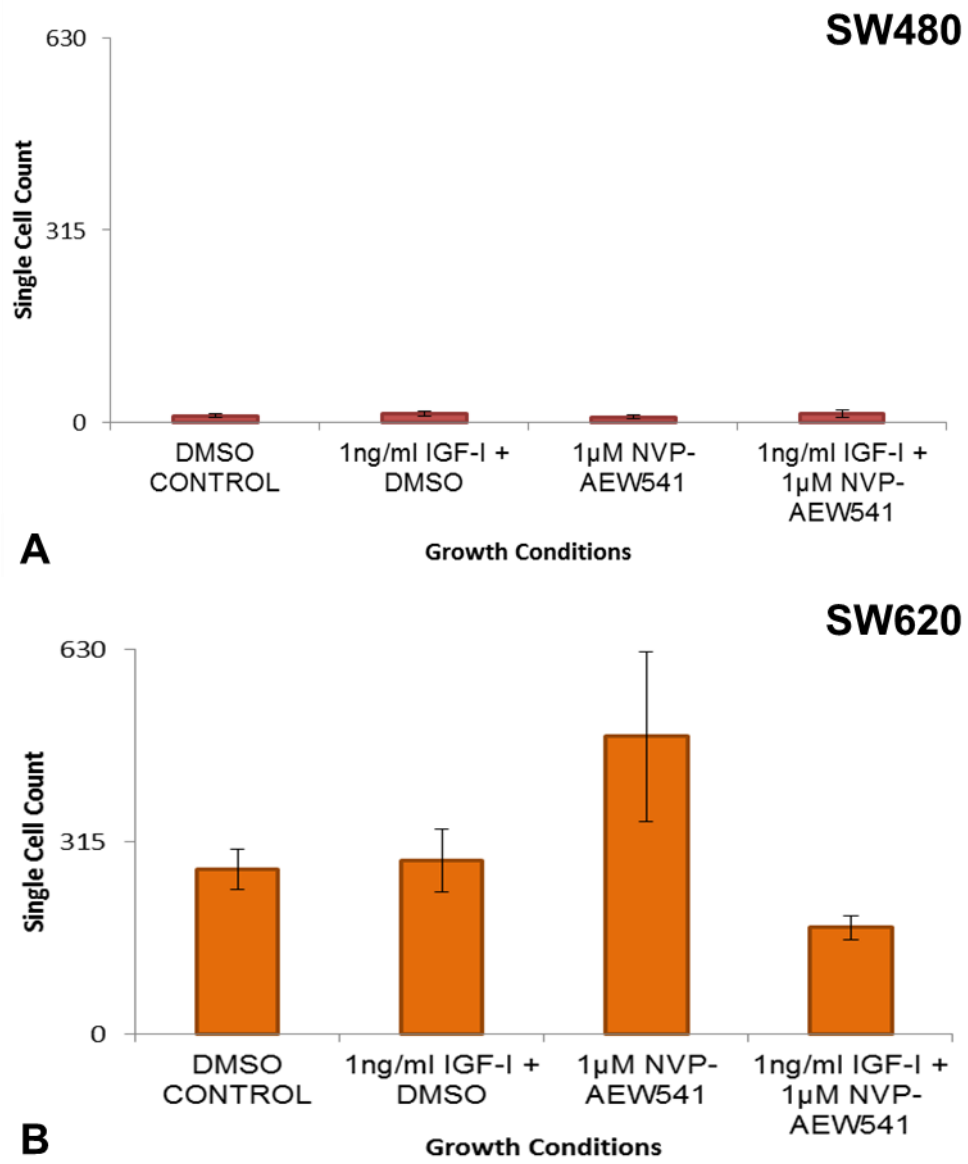

Figure 5.26: Neither the SW480 and SW620 cell lines showed a significant alteration in the number of single migrating cells within the 2D scratch wound in the presence of IGF-I or NVP-AEW541. Number of single migrating cells in A: SW480 and B: SW620 scratch wounds as determined from cell counts. Data represent mean, n = 3, ±SEM for both graphs, no significance by a Tukey's test.

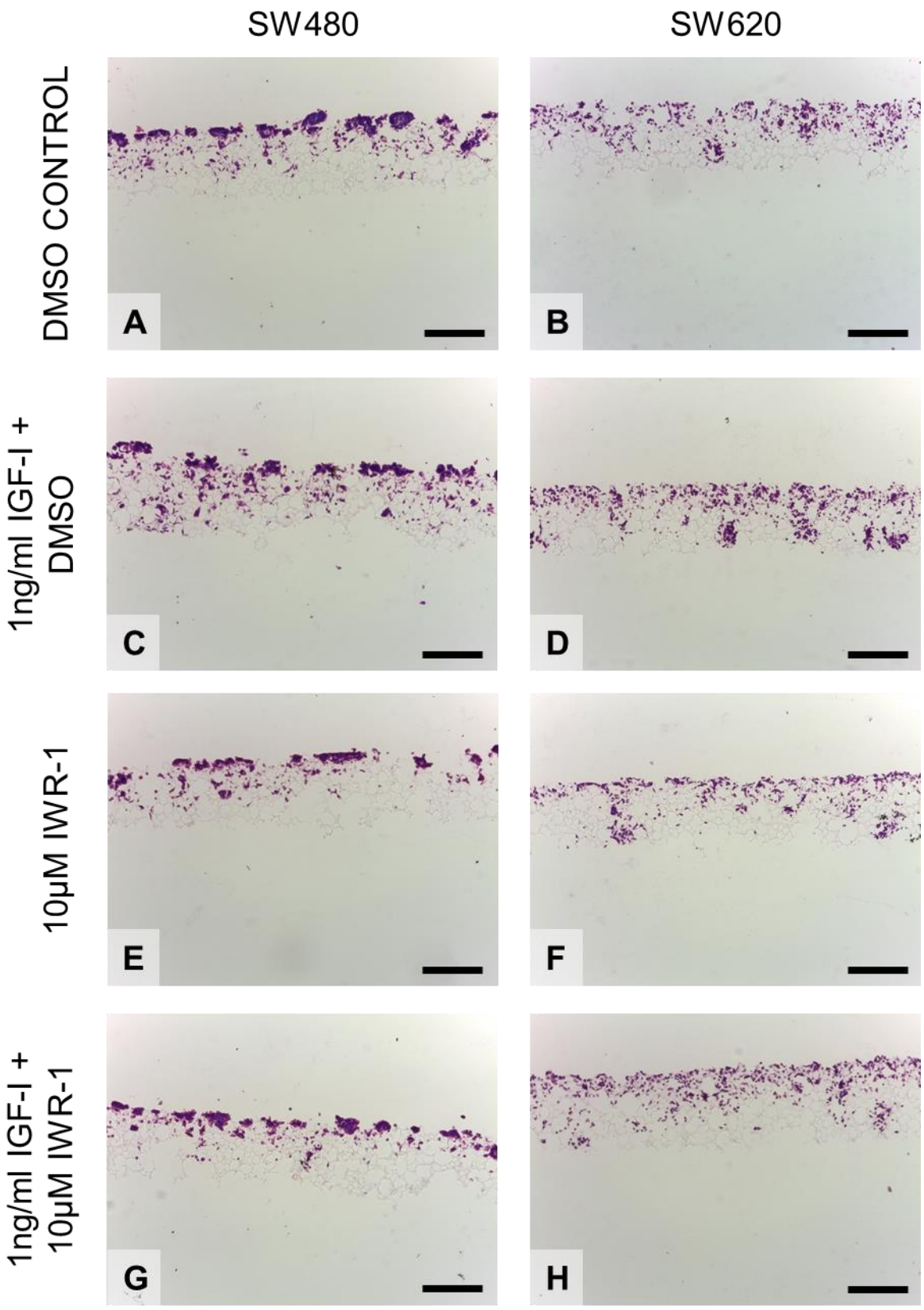

Figure 5.27: The SW480 cell line displayed a decrease in the build-up of cells when both IGF-I and the Wnt inhibitor IWR-1 were present, relative to those seen when IGF-I alone was present, while the SW620 cell line did not display a decrease under these conditions. H&E images of 10 day cultures with A and B: DMSO control, C and D: 1ng/ml IGF-I and DMSO, E and F: 10µM IWR-1 and G and H: 1ng/ml IGF-I and 10µM IWR-1 for both cells lines. Scale bars = 200µm for all images.

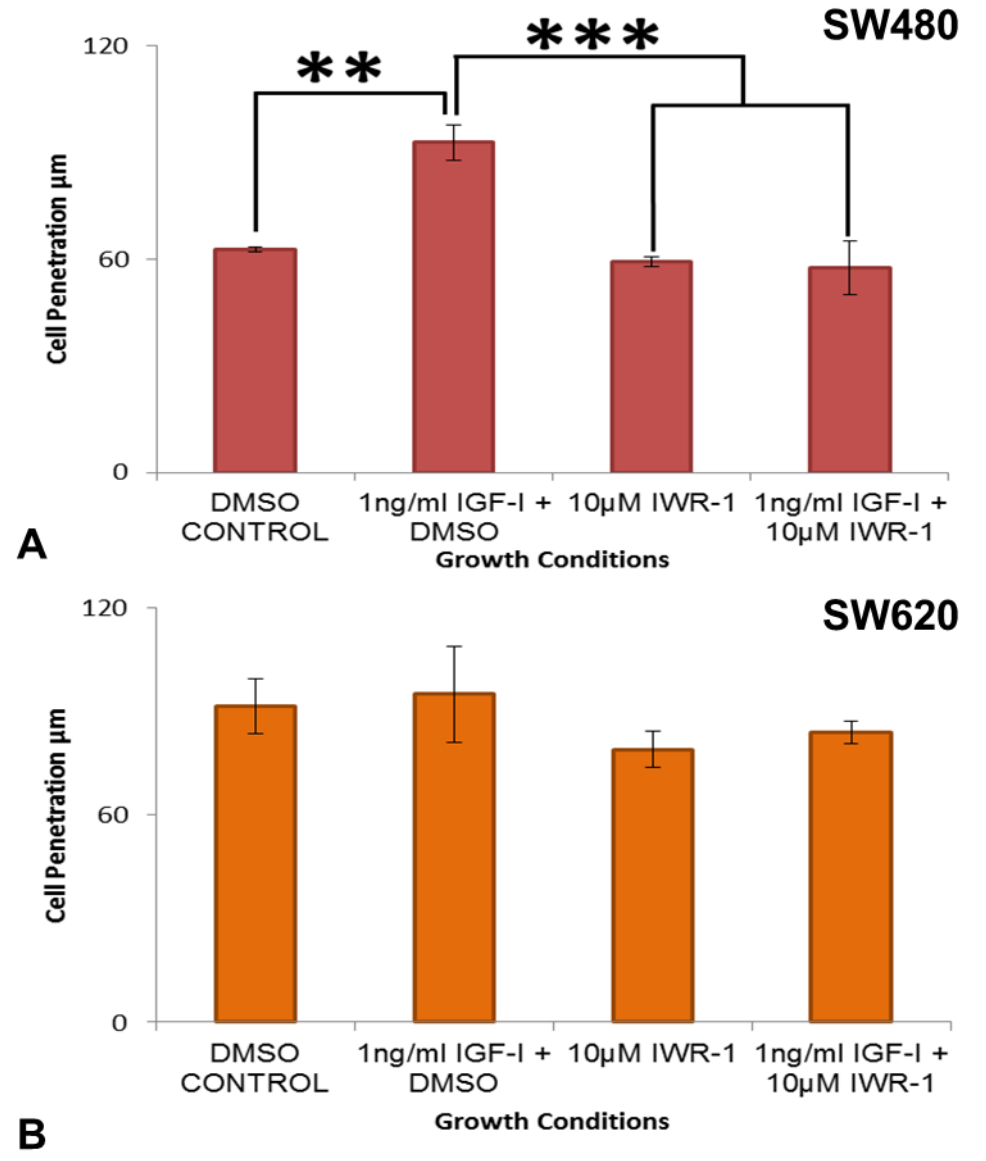

Figure 5.28: The 3D cell penetration of the SW480 cell line was increased when 1ng/ml IGF-I alone was present relative to all other conditions, while the penetration of the SW620 cell line remained unaffected. Cell penetration in µm of A: SW480 and B: SW620 cells as determined by the linear measurement method. Data represent mean, n = 3, ±SEM for both graphs, ** $p < 0.01$, *** $p < 0.005$ by a Tukey's test.

5.3.3.2 The viability of 3D cultures was unaffected while the final cell population was affected

The use of IGF-I or IWR-1, either on their own or in conjunction with each other, did not cause a significant variation in the viability of cultures grown with either cell line (Figure 5.29). When the cell numbers within the cultures was assessed, the SW620 cell line was found to have more cells in the scaffold than the SW480 cell line, ANOVA, $F(1,19)=213.238$, $p<0.001$. There was a small but significant increase in the number of SW480 cells present in the scaffolds cultured with IGF-I when compared to the DMSO (Figure 5.30A), while inclusion of media additives did not affect the final cell numbers found in the SW620 cultures (Figure 5.30B). Although in this case the inclusion of IGF-I in the culture media caused a 23% increase in the number of SW480 cells after 10 days of 3D culture, this increase was unlikely to wholly account for the 48% increase in cell penetration seen in these cultures. Additionally, as there was no significant difference between the cell number in the IGF-I and the IGF-I with IWR-1 cultures, but there was a significant difference in the depth of cell penetration attained by the cells found in each culture, it is thought that the addition of IWR-1 in the culture media inhibits the IGF-I induced cell migration in the SW480 cell line.

5.3.3.3 The inclusion of both IWR-1 and IGF-I did not affect 2D migration

When IGF-I and IWR-1 are included in the culture media of 2D scratch wounds, the appearance of the cultures containing both did not grossly differ from those cultures grown with either or neither of them (Figure 5.31). In conjunction with previously observed results, the inclusion of either IGF-I or IWR-1 on their own did not have an effect on the distance moved by the leading edges of the wound and the addition of both of them did not cause a significant alteration either (Figure 5.32).

The quantity and distribution of single cells within the scratch wound in the presence of IGF-I or IWR-1 appeared similar to those previously seen in the fluorescently stained samples, with little deviation from the DMSO control (Figure 5.33). Quantification of these cells confirmed that IGF-I and IWR-1 had no effect on the migratory behaviour of the SW480 cells in a 2D scratch assay (Figure 5.34A), with fewer cells observed than for the SW620 cell line, ANOVA, $F(1, 16)=57.400$, $p<0.001$. The number of single cells observed in the SW620 cultures grown with 1ng/ml IGF-I and 10μM IWR-1 was significantly lower than the DMSO control (Figure 5.34B), but as all cell counts were lower than the control and there was no significant difference between the IGF-I only and IGF-I with IWR-1 cell counts, it was likely that the control count was unusually high and therefore IWR-1 was unable to alter any effect that the addition of IGF-I is having on the 2D scratch wounds. Together these data shows that the manipulation of the migratory behaviour of the colorectal cancer cell line SW480 and SW620 using IGF-I and IWR-1 is only effective in the 3D model used here and not in the counterpart 2D scratch wounds.

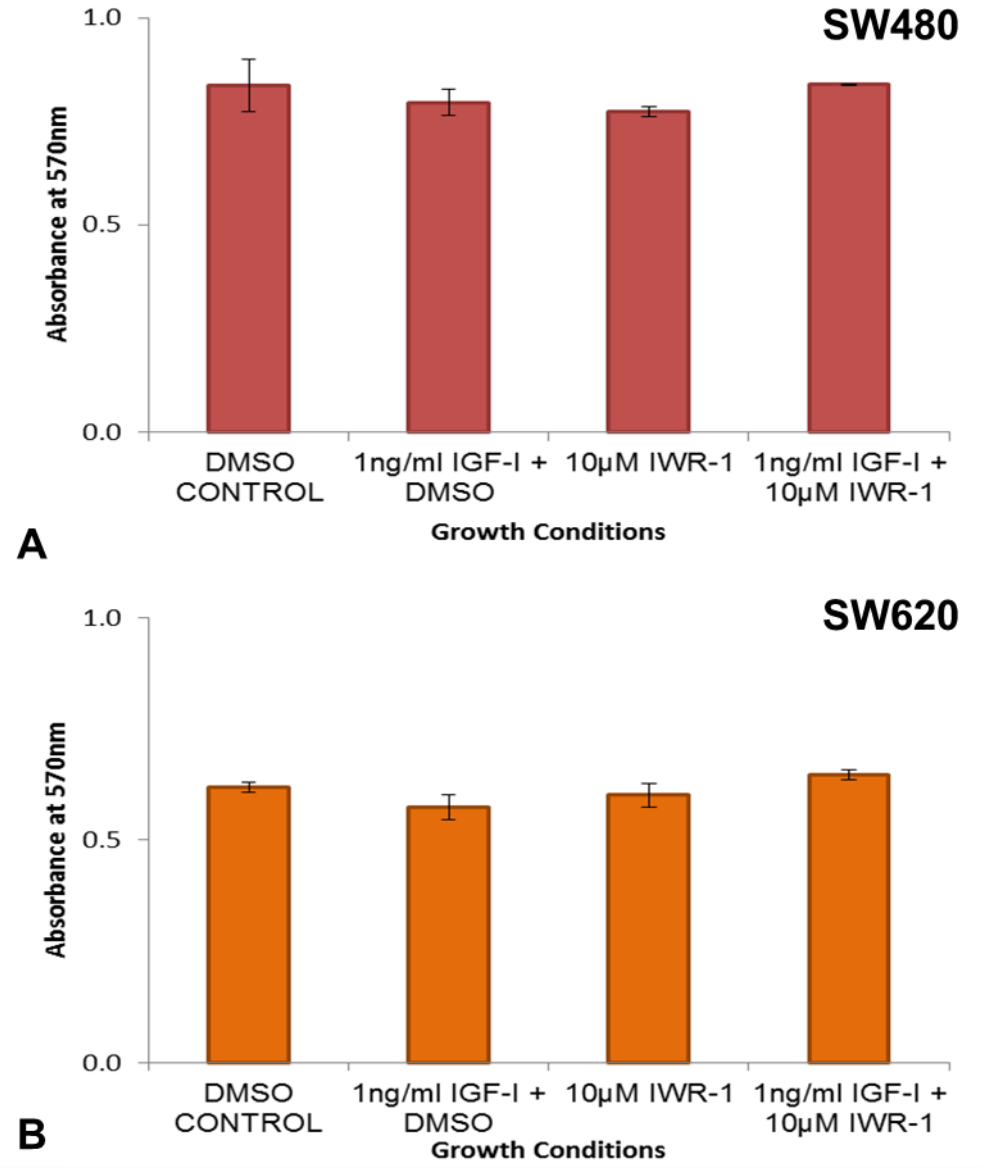

Figure 5.29: The 3D cell viability of both cell lines was unaffected by the presence of IGF-I or IWR-1. Absorbance at 570nm of A: SW480 and B: SW620 cells as determined by the MTT Cell Viability Assay. Data represent mean, n = 3, ±SEM for both graphs, no significance by a Tukey's test.

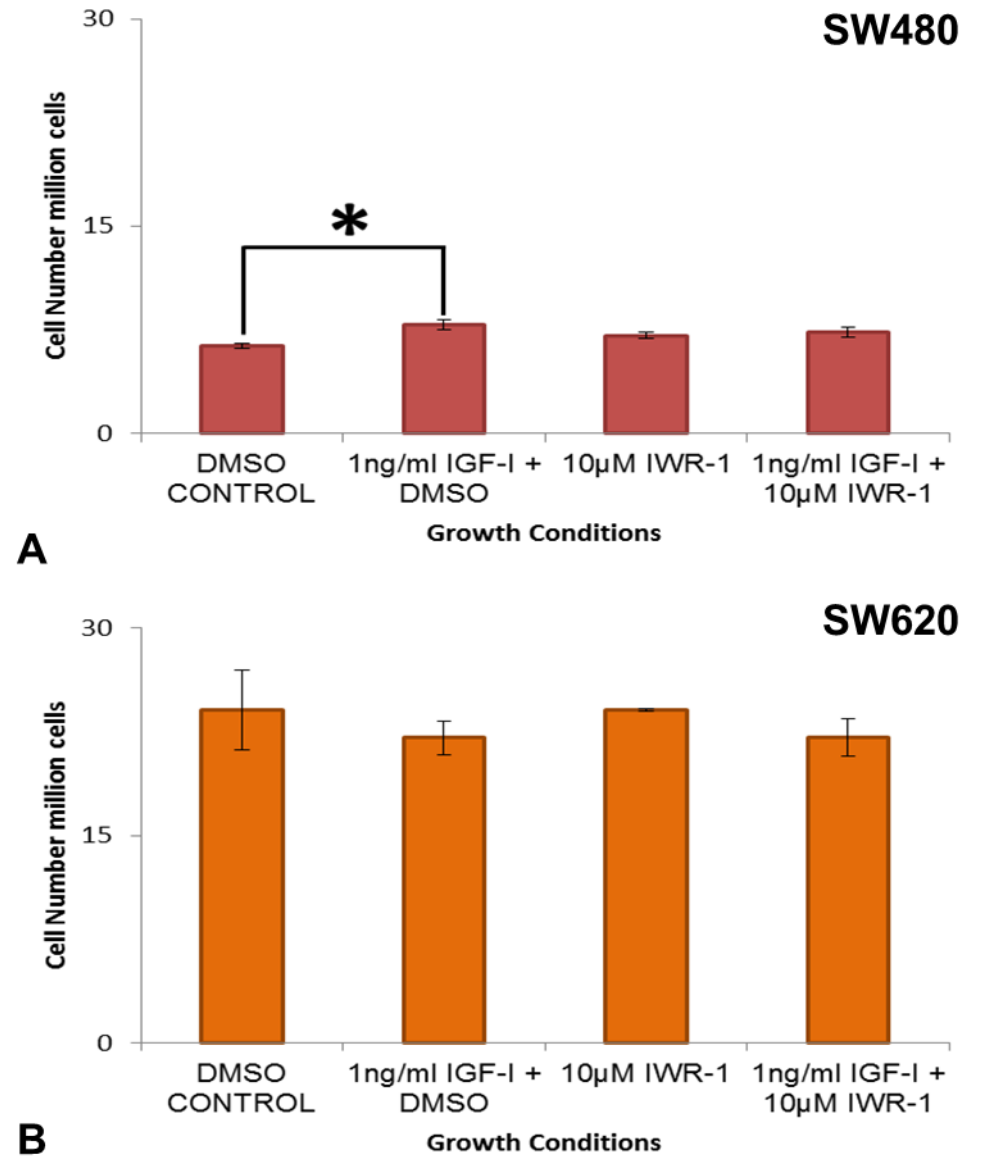

Figure 5.30: The number of SW480 cells in the 3D material increased when IGF-I alone was present, while the SW620 cell line was unaffected by all conditions. Cell number in millions of cells of A: SW480 and B: SW620 cells as determined by the Pico Green dsDNA Assay. Data represent mean, n = 3, ±SEM for both graphs, * $p < 0.05$ by a Tukey's test.

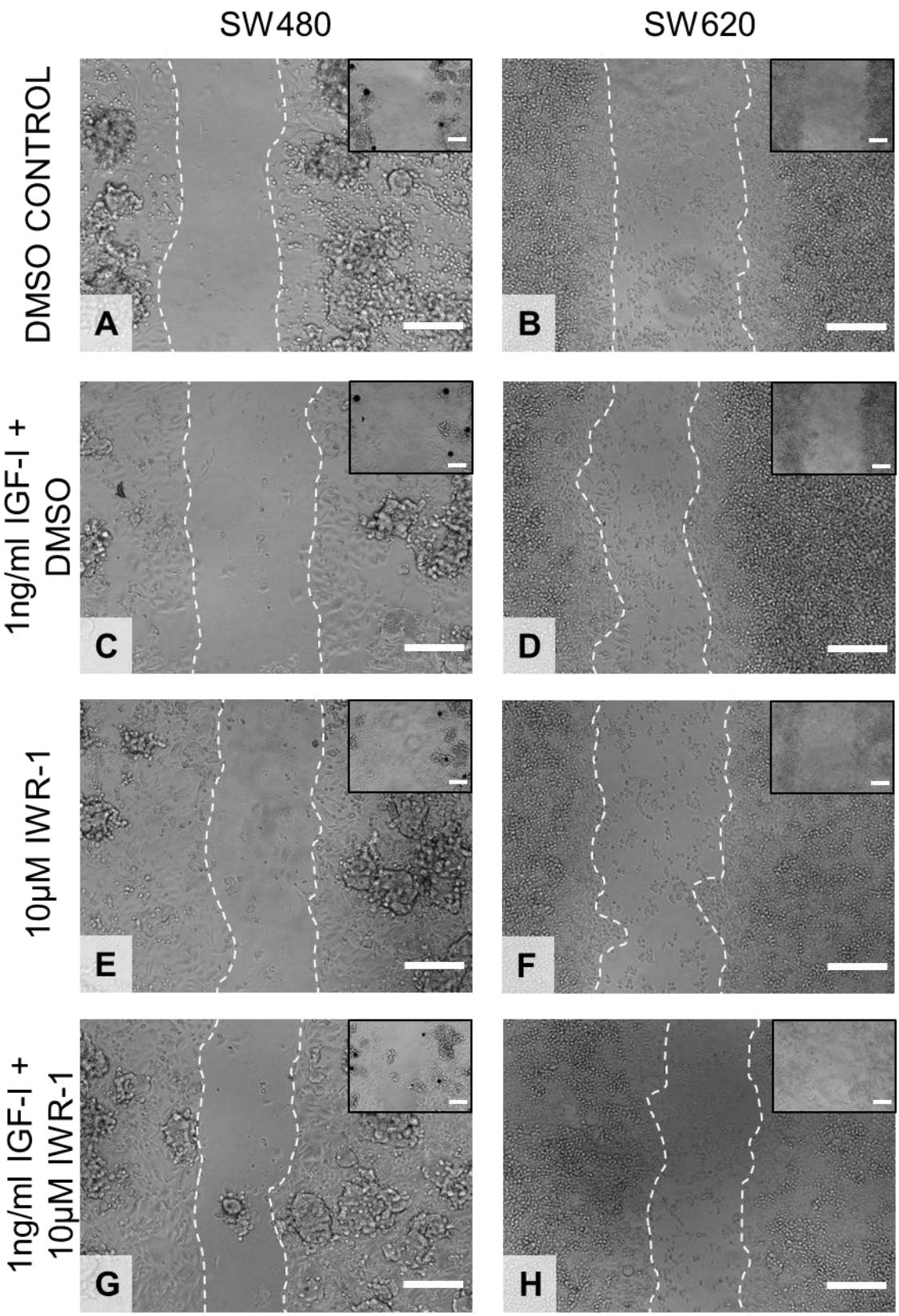

Figure 5.31: Both the SW480 and SW620 cell lines exhibited wound closing during a scratch wound assay in the presence IGF-I or the Wnt inhibitor IWR-1. Phase images of 24 hours post wounding with A and B: DMSO control, C and D: 1ng/ml IGF-I and DMSO, E and F: 10µM IWR-1 and G and H: 1ng/ml IGF-I and 10µM IWR-1 for both cells lines. Scale bars = 200µm for all images.

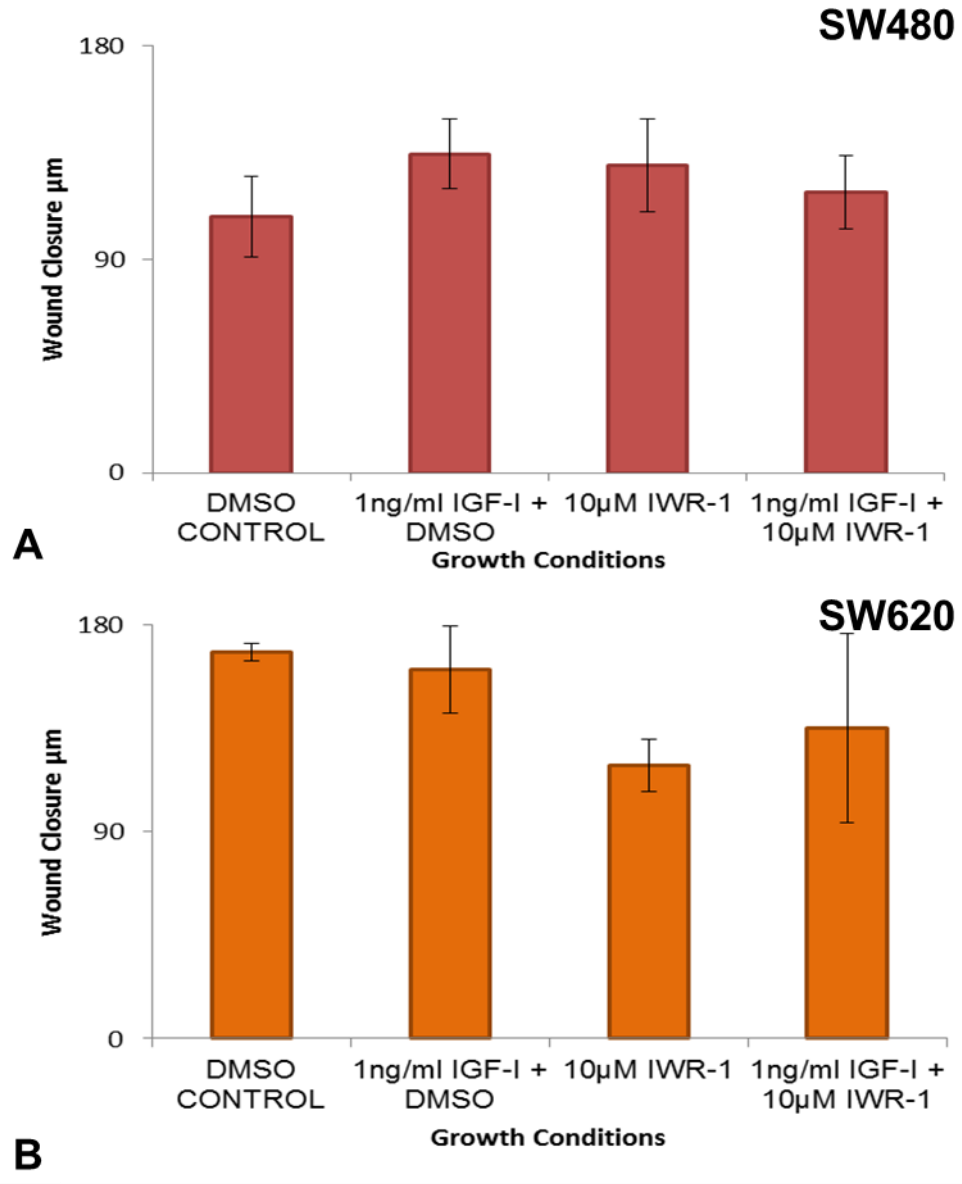

Figure 5.32: Neither the SW480 and SW620 cell lines showed a significant alteration in the distance moved by the edges of the 2D scratch wound in the presence of IGF-I or IWR-1. Wound closure in µm of A: SW480 and B: SW620 cells as determined by measuring the width of the wound. Data represent mean, n = 3, ±SEM for both graphs, no significance by a Tukey's test.

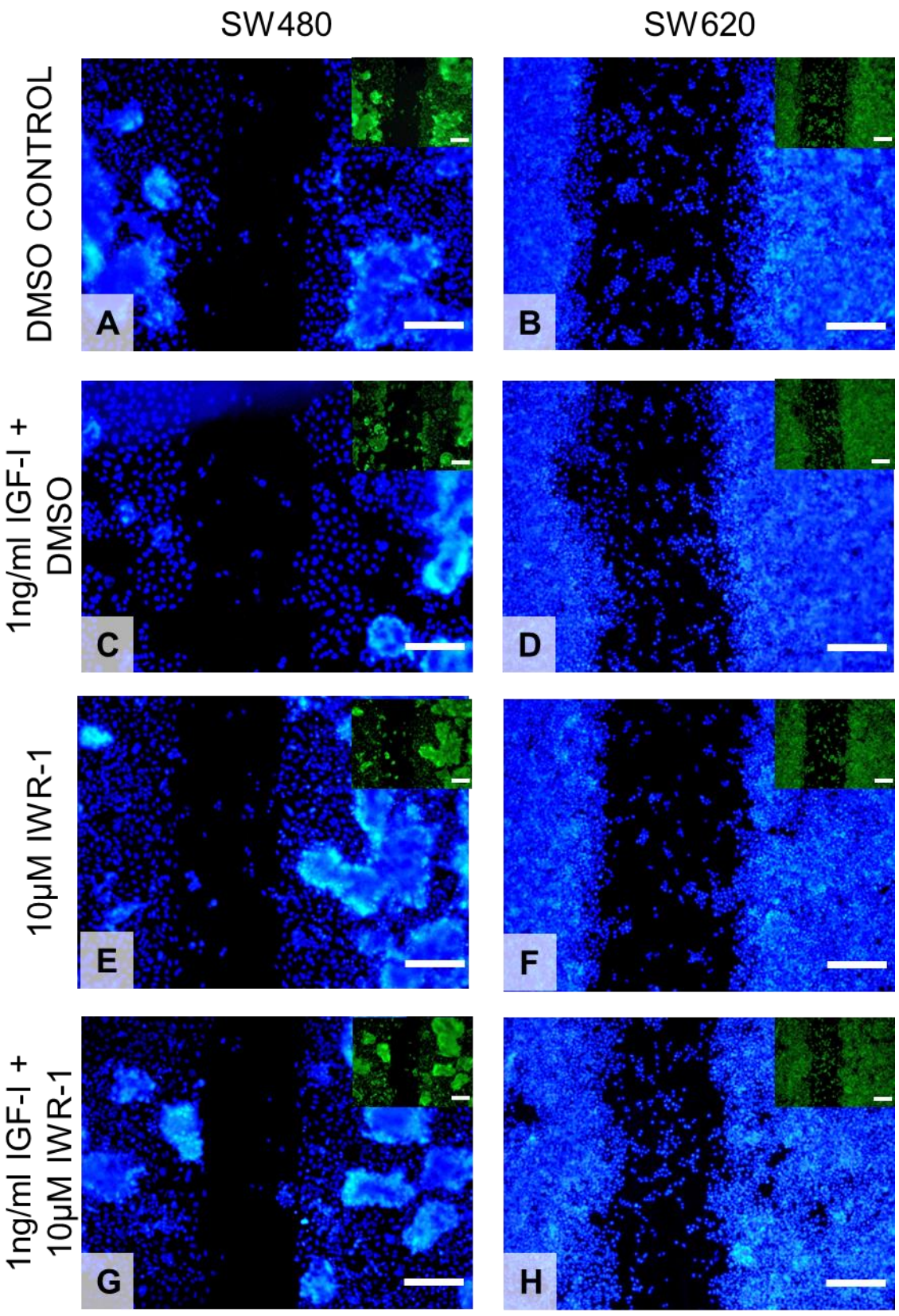

Figure 5.33: The SW620 cell line had more single migrating cells than the SW480 cell line during a scratch wound assay in the presence IGF-I or the Wnt inhibitor IWR-1. DAPI and Phalloidin (inset) images of 24 hours post wounding with A and B: DMSO control, C and D: 1ng/ml IGF-I and DMSO, E and F: 10µM IWR-1 and G and H: 1ng/ml IGF-I and 10µM IWR-1 for both cells lines. Scale bars = 200µm for all images.

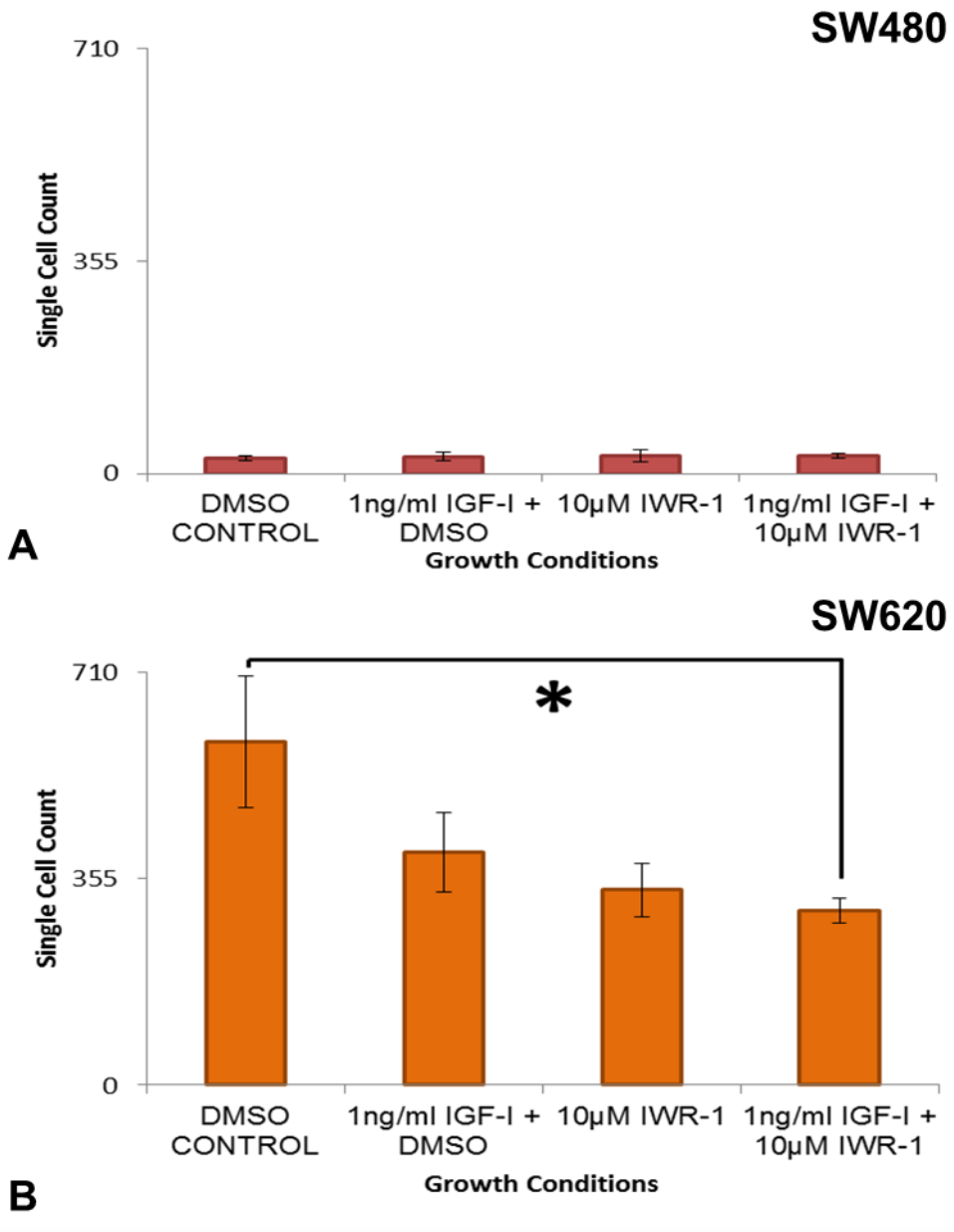

Figure 5.34: The SW620 cell line showed a significant decrease in the number of single migrating cells within the 2D scratch wound in the presence of IGF-I and IWR-1, while the SW480 cell line remained unaffected. Number of single migrating cells in A: SW480 and B: SW620 scratch wounds as determined from cell counts. Data represent mean, n = 3, ±SEM for both graphs, * $p < 0.05$ by a Tukey's test.

5.3.4 Manipulation of IGF-I signalling affected protein expression in both the SW480 and SW620 cell lines

In this Chapter, media additives which manipulate the IGF-I signalling pathway and effect the migratory behaviour of colorectal cancer cell lines in a 3D migration model have been identified, namely IGF-I and NVP-AEW541. The effect of these media additives on the key proteins identified in Chapter 4, E-cadherin, vimetin, β-catenin and Slug, was assessed to determine the underlying pathways involving in the altered migratory behaviour of the colorectal cancer cells.

5.3.4.1 IGF-I increases β-catenin expression in the SW480 cell line

The immunohistochemical staining of 10 day 3D SW480 cultures in the absence and presence of 1ng/ml IGF-I demonstrated that the inclusion of this growth factor did affect the protein expression profile of these cells. When cultured in the absence of IGF-I, the SW480 cell line did not express E-cadherin (Figure 5.35A) or Slug (Figure 5.35G) and did express vimentin (Figure 5.35C) and β-catenin (Figure 5.35E), with the staining for vimentin appearing to be stronger than the staining for β-catenin. When IGF-I was included in the culture media, the expression of E-cadherin (Figure 5.35B), vimentin (Figure 5.35D) and Slug (Figure 5.35H) in the SW480 cell line did not appear to alter. However, the expression of β-catenin was seen to increase, with stronger staining seen in the cells (Figure 5.35F) when compared to the control cultures (Figure 5.35E).

5.3.4.2 NVP-AEW541 affects the expression of different proteins in different cell lines

The analysis of 3D cultures of both colorectal cancer cell lines cultured with IGF-I and NVP-AEW541 via immunohistochemistry also demonstrated that the inclusion of NVP-AEW541 in the culture media affected protein expression. When cultured in the presence of IGF-I with DMSO, the SW480 cell line retained the same expression profile as previous seen, with no E-cadherin (Figure 5.36A) or Slug (Figure 5.36G) expression and vimentin (Figure 5.36C) and β-catenin (Figure 5.36E) expression. When 1μM NVP-AEW541 was included in addition to the IGF-I, the expression of E-cadherin (Figure 5.36B) and Slug (Figure 5.36H) in the SW480 cell line did not appear to alter. However, the expression of vimentin was entirely suppressed (Figure 5.36D) and the expression of β-catenin was seen to decrease, with less intense staining observed in the cells (Figure 5.36F).

The pattern of protein expression in the SW620 cell line in response to the addition of NVP-AEW541 was observed to differ from that seen in the SW480 cell line. When cultured in the presence of IGF-I with DMSO, the SW620 cell line retained the same expression profile as previous seen, with no E-cadherin (Figure 5.37A) or Slug (Figure 5.37G) expression and vimentin (Figure 5.37C) and β-catenin (Figure 5.37E) expression. When 1μM NVP-AEW541 was included in addition to the IGF-I, the expression of vimetin (Figure 5.37D), β-catenin (Figure 5.37F) and Slug (Figure 5.37H) in the SW620 cell line did not appear to alter. However, the expression of E-cadherin was seen to increase (Figure 5.37B) relative to the IGF-I control.

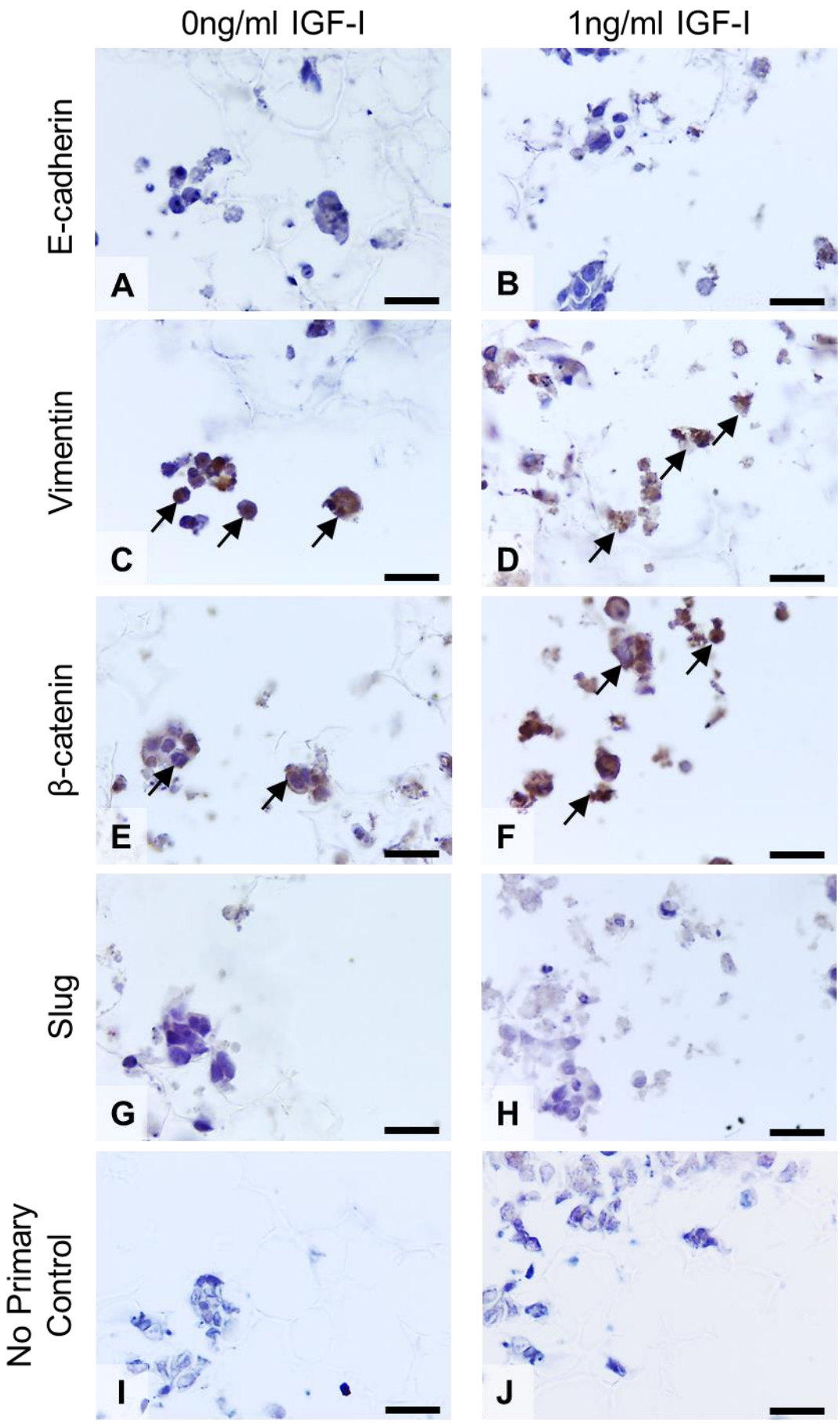

Figure 5.35: The inclusion of IGF-I in culture media enhances β-catenin expression in the SW480 cell line. Immunohistochemical images of antibody staining for A and B: E-cadherin, C and D: vimentin, E and F: β-catenin, G and H: Slug and I and J: no primary control on 10 day 3D cultures of SW480 cells in the absence and presence of 1ng/ml IGF-I, where the brown precipitate (arrows) indicates positive staining. Scale bars = 25µm for all images.

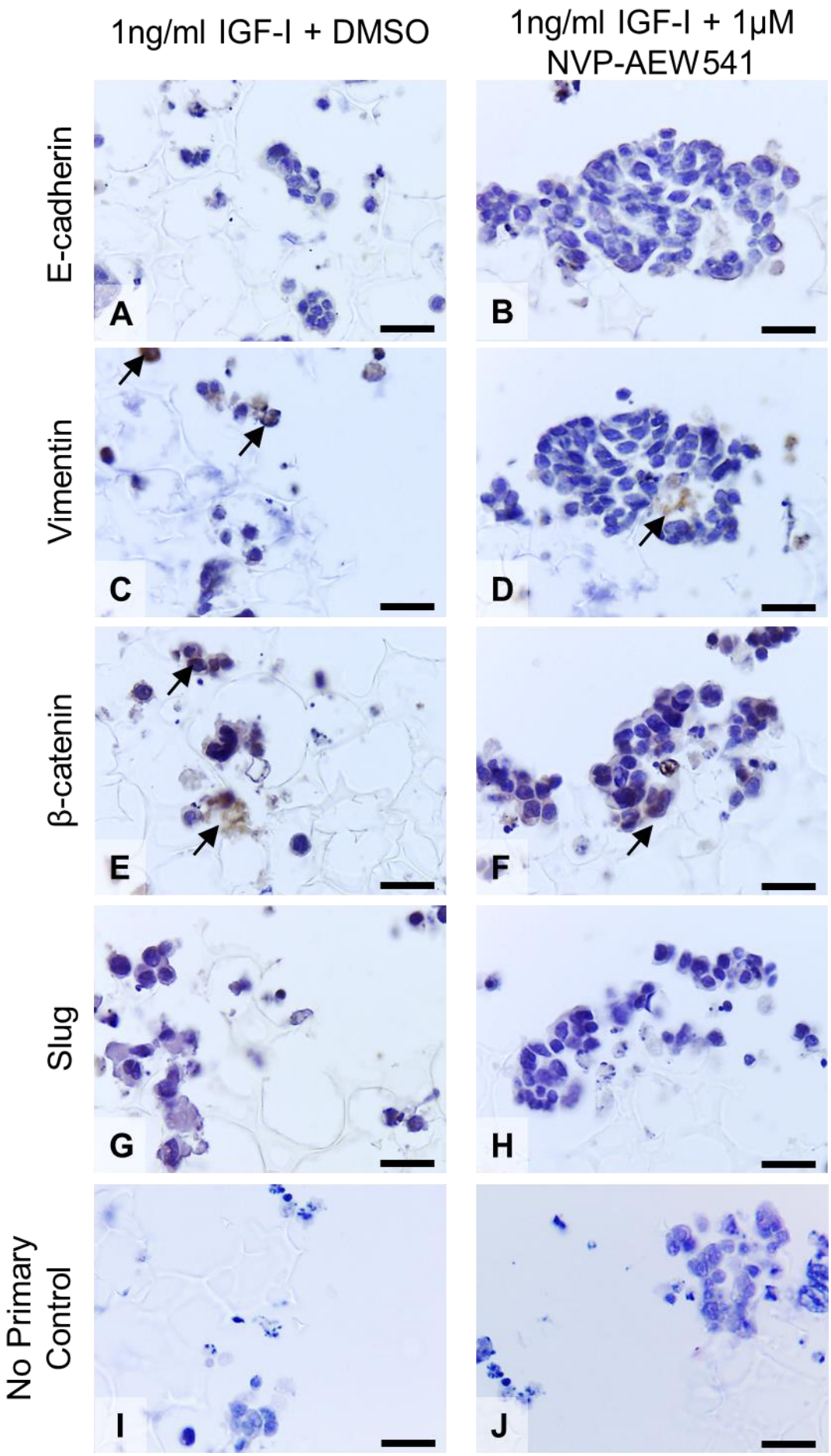

Figure 5.36: The inclusion of NVP-AEW541 with IGF-I in culture media suppresses vimentin and β-catenin expression in the SW480 cell line. Immunohistochemical images of antibody staining for A and B: E-cadherin, C and D: vimentin, E and F: β-catenin, G and H: Slug and I and J: no primary control on 10 day 3D cultures of SW480 cells in the absence and presence of 1μM NVP-AEW541 with 1ng/ml IGF-I, where the brown precipitate (arrows) indicates positive staining. Scale bars = 25μm for all images.

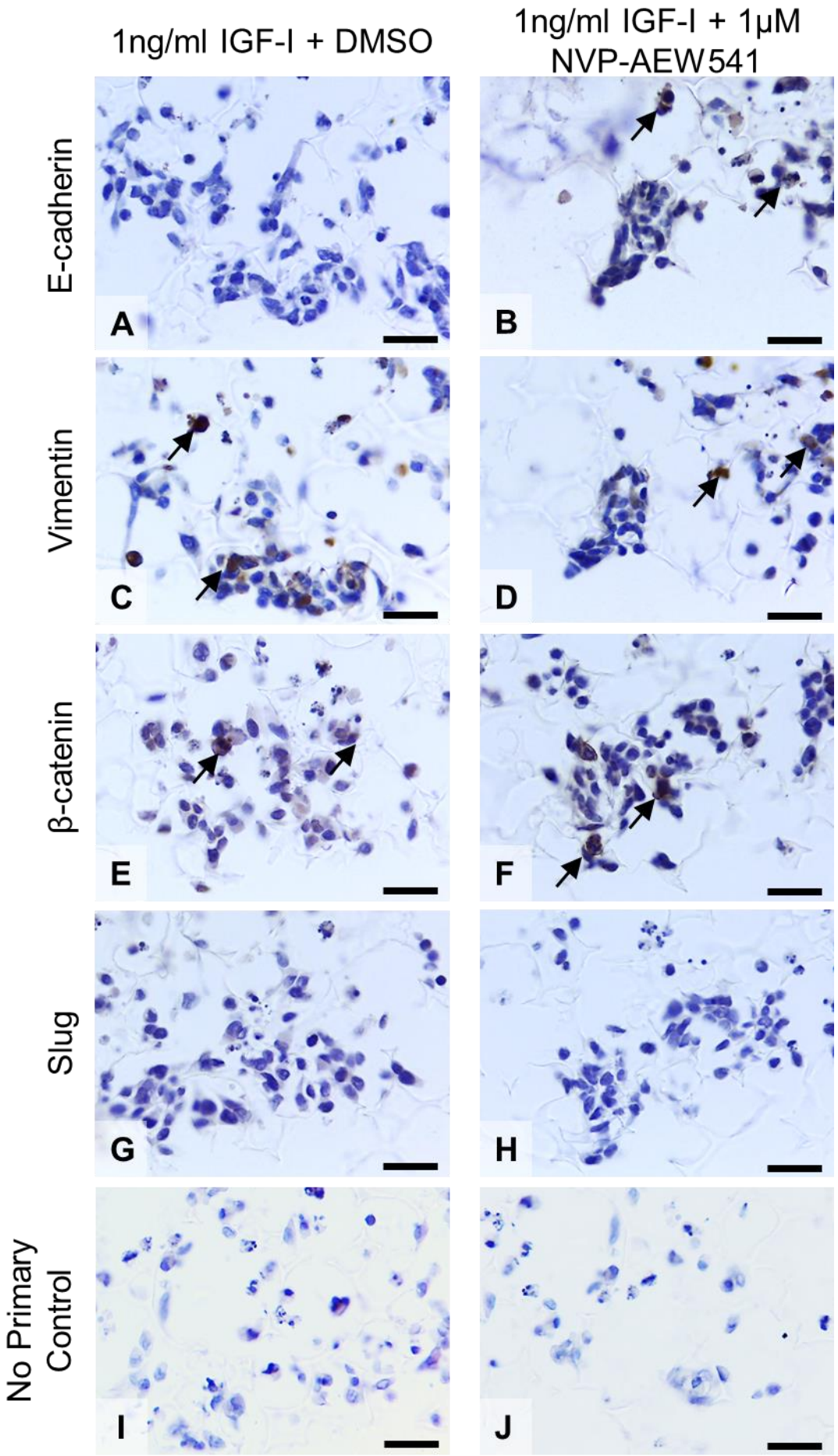

Figure 5.37: The inclusion of NVP-AEW541 with IGF-I in culture media enhances E-cadherin expression in the SW620 cell line. Immunohistochemical images of antibody staining for A and B: E-cadherin, C and D: vimentin, E and F: β-catenin, G and H: Slug and I and J: no primary control on 10 day 3D cultures of SW620 cells in the absence and presence of 1μM NVP-AEW541 in the presence of 1ng/ml IGF-I, where the brown precipitate (arrows) indicates positive staining. Scale bars = 25μm for all images.

5.3.4.3 IWR-1 reverses the effect of IGF-I on β-catenin expression

As the inclusion of IWR-1 along with IGF-I in 3D SW480 cultures has been shown to inhibit the IGF-I mediated increase in cell migration, the effect of the combination of these additives on protein expression profile of the SW480 cell line was investigated. The immunohistochemical staining of 10 day 3D SW480 cultures with combinations of IGF-I and IWR-1 added to the culture media demonstrated that the inclusion of IWR-1 did affect the IGF-I induced protein expression profile of these cells. The control and IGF-I SW480 cultures displayed the same protein expression profile as seen in (Figure 5.35), with E-cadherin (Figure 5.38A & B) and Slug (Figure 5.38J & K) not expressed and vimentin (Figure 5.38D & E) and β-catenin (Figure 5.38G & H) expressed. When IWR-1 was included in the culture media along with IGF-I, the expression of E-cadherin (Figure 5.38C), vimentin (Figure 5.38F) and Slug (Figure 5.38L) in the SW480 cell line did not appear to alter. However, the expression of β-catenin was seen to decrease, with few, if any, cells demonstrating positive staining (Figure 5.38I), compared to the majority of cells seen to express β-catenin in the control and IGF-I cultures (Figure 5.38G & H).

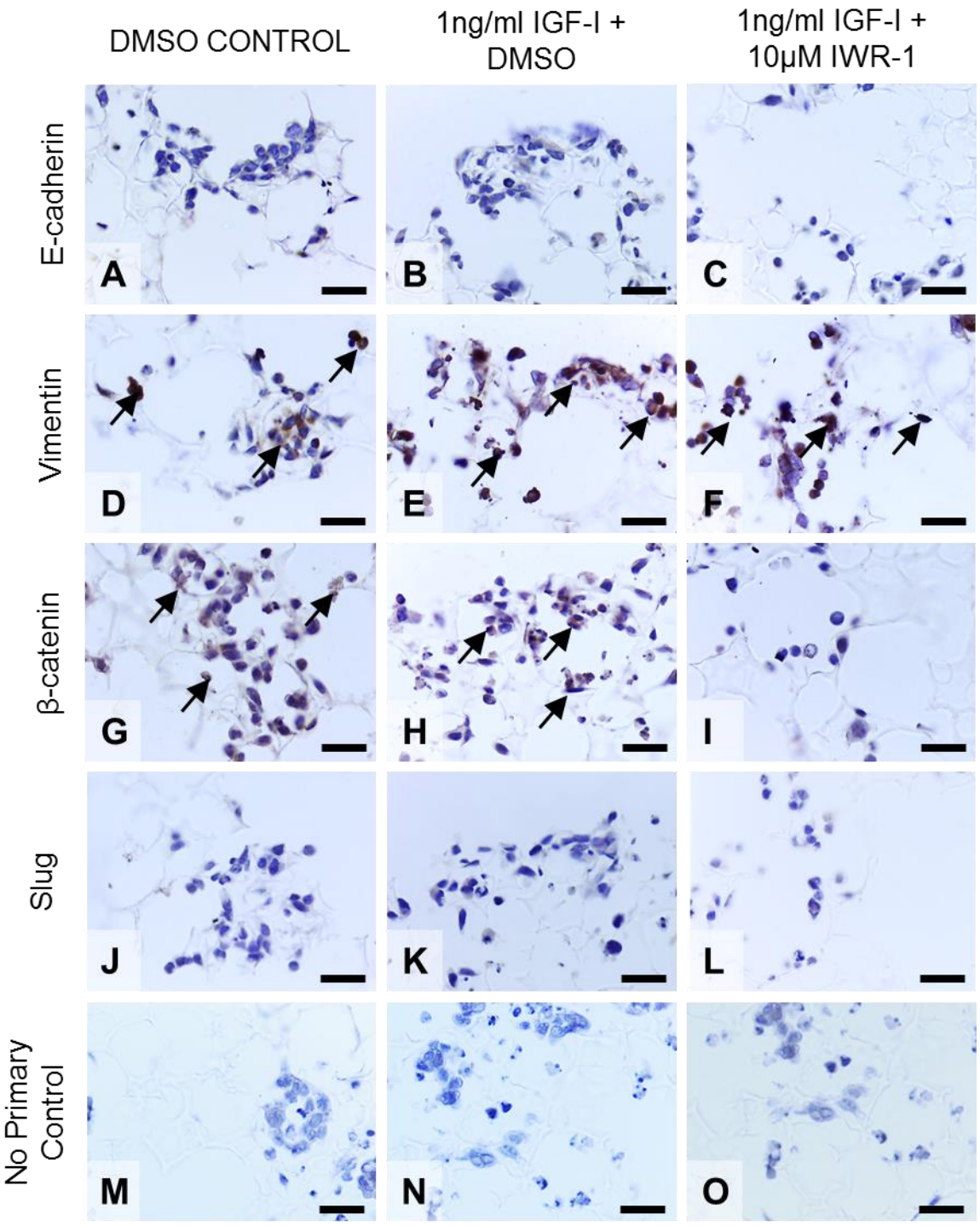

Figure 5.38: The inclusion of IWR-1 with IGF-I in culture media suppresses β-catenin expression in the SW480 cell line. Immunohistochemical images of antibody staining for A, B and C: E-cadherin, D, E and F: vimentin, G, H and I: β-catenin, J, K and L: Slug and M, N and O: no primary control on 10 day cultures of SW480 in the absence and presence of 1ng/ml IGF-I without and with 10μM IWR-1, where the brown precipitate (arrows) indicates positive staining. Scale bars = 25μm for all images.

5.4 Discussion

Following the application of the model developed here to investigate the role of Wnt signalling in directing the migratory behaviour of colorectal cancer cells, this 3D model was then used to analyse the role of IGF-I. The commercial availability of human recombinant IGF-I and the small molecule NVP-AEW541 has provided a useful set of tools for investigating the role of the IGF-I signalling pathway via the IGF-IR in the 3D migration model under development in this project. In both cases, the addition of these compounds to the culture media yielded results in the 3D migration assay but not the counterpart 2D studies and these are summarised in Table 5.1. This highlights that although IGF-I signalling is known to have an effect on the proliferative behaviour of cancer cells [338], in the model used here the action of IGF-I signalling has only affected the migratory behaviour of the cells.

Additive	Concentration	SW480	SW620
IGF-I	1ng/ml	54% increase in cell penetration	No effect
NVP-AEW541	1µM	16% decrease in cell penetration, only when 1ng/ml IGF-I is also present	13% decrease in cell penetration, only when 1ng/ml IGF-I is also present
IWR-1	10µM	Reduces the 54% increase in cell penetration induced by 1ng/ml IGF-I down to control levels	Up to 26% decrease in cell penetration

Table 5.1: Summary of the primary effect of growth factors and small molecules on cell culture in the 3D migration assay.

IGF-I was found to induce a 50% increase in the observed cell migration of the SW480 cell line when used at concentrations of 1ng/ml and above in the 3D model (Figure 5.3A), which resulted in changes in cellular distribution clearly visible in the histological images of the cultures (Figure 5.2A, E & G), but was unable to produce a response in the 2D model when either epithelial sheet (Figure 5.7A) or single cell (Figure 5.9A) migration was measured. The effect on the SW480 cell line was not mirrored by its counterpart cell line, SW620, as IGF-I failed to induce a migratory response when used on this cell line in 2D (Figure 5.7B & Figure 5.9B) or 3D (Figure 5.3B) models. This data correlates with previously published data, as the exposure of the colorectal cancer cell line KM12L4 to exogenous IGF-I resulted in increased migration and invasion in uncoated and Matrigel coated Transwell® assays [334]. This role of IGF-I in enhancing colorectal cancer cell migration is not limited to *in vitro* studies, as the intraperitoneal injection of IGF-I into both control and LID mice resulted in an increase in metastasis formation [146].

In contrast, the data regarding cell number obtained here does not correlate with previously published data, as manipulation of IGF-I signalling did not affect the overall cell number of cancer cells in the 3D model tested, this may be due to differences in experimental protocols, as cell proliferation in 2D cultures [143] and xenografts [340] have been assessed in the literature,

whereas a 3D model was assessed here. Additionally, the published studies looked at the effect of the manipulation of IGF-I signalling via inhibition of IGF-IR activity via transfection of a dominant negative variant of IGF-IR [337] or IGF-IR siRNA [338] as opposed to the addition of IGF-I into culture media. As the cell lines used here are derived from cancers, it is likely that their rate of proliferation is already elevated due to genetic mutations and signalling alterations within the cells, resulting in the cells having an impaired capacity to respond to elevated IGF-I signalling.

The alteration of protein expression mediated by the addition of IGF-I into the culture media also correlates with previously published data. An increase in β-catenin expression in response to IGF-I has previously been noted by Desbois-Mouthon *et al*. [142], which correlates with the increased staining presented here (Figure 5.35E & F). It has also been noted that exposure to IGF-I also changes the location of both E-cadherin and β-catenin in the colonic adenocarcinoma cell line HT29-D4, from a distribution based predominantly at the plasma membrane in the absence of IGF-I to a distribution through the cytoplasm in the presence of IGF-I [364].

The introduction of the small molecule inhibitor NVP-AEW541 at a concentration of 1μM was successful in inhibiting 3D cell migration in the presence of IGF-I (Figure 5.11), while failing to elicit a response when IGF-I was absent (Figure 5.19). Again, this manipulation of IGF-I signalling did not alter the migratory behaviour of either the SW480 or SW620 cell line in 2D (Figure 5.15, Figure 5.17, Figure 5.23 & Figure 5.25). Again, this data is not fully in correlation with the published data for this small molecule, as NVP-AEW541 has been shown to limit cell growth in the 2D cultures of a variety of cell types [345, 357]. However, the data presented here does correlate with the published data regarding the effect of NVP-AEW541 on cell migration, with NVP-AEW541 inhibiting the migration of both SW480 and SW620 cells in the presence of IGF-I, although in the literature this inhibition was also seen in the absence of IGF-I [351], which was not observed here. In terms of the effect of NVP-AEW541 on protein expression, no published data was found regarding the effects of NVP-AEW541 on any of the protein targets assessed here. However, the downregualtion of vimetin and β-catenin in SW480 cells (Figure 5.36C, D, E & F) and the upregulation of E-cadherin in SW620 cells (Figure 5.37A & B) would correlate with the decreased motility observed in the 3D model if the main mechanism of action of IGF-I is via the Wnt signalling pathway in this system.

As there is a known interaction between IGF-I signalling and the Wnt signalling pathway [141], the mechanism of the action of IGF-I in the induction of migration in the 3D cultures of the SW480 cell line was examined using the small molecule Wnt signalling inhibitor IWR-1. It has previously been demonstrated that use of IWR-1 at a concentration of 10μM is capable of causing a 26% reduction in the observed cell migration of the SW620 cell line (Figure 4.27B), while leaving the SW480 unaffected (Figure 4.27A). When used in conjunction, the addition of IWR-1 to the cultures with IGF-I resulted in the complete inhibition of the IGF-I induced 3D cell migration of the SW480 cell line (Figure 5.28A). As there is no evidence in the literature of IGF-I and IWR-1 being used in conjunction on cell cultures, there is no previous data to compare these results to. However, the increase in SW480 cell migration in response to IGF-I has been consistent across all experiments and correlates with published data [334], in addition to the effect of IWR-1 correlating with previously noted migratory inhibition which has not been recorded in any published data. This provides evidence that the main signalling cascade responsible for mediating the migratory

response of the SW480 cell upon exposure to IGF-I is acting via the Axin/APC/GSK-3β destruction complex, as this is the point in the Wnt signalling pathway at which IWR-1 interacts by stabilising axin2 [313]. Additionally, the observed reduction in IGF-I induced β-catenin expression seen in SW480 cells cultured in the presence of IWR-1 (Figure 5.38E & F) correlated with the previously seen decrease in β-catenin expression in SW620 cells (Figure 4.34E & F), although there is no evidence in the literature regarding the effect of IWR-1 on the expression of the proteins assessed in this study.

When taken with the cell penetration data, this immunohistochemical data would suggest that the downstream signalling action of IGF-I interacts with the Wnt signalling pathway. This interaction is likely to be via the PKB mediated inhibition of GSK-3β [139], as inclusion of exogenous IGF-I increased β-catenin expression, which would in turn affect the downstream transcriptional targets of the Wnt signalling pathway. In addition to this, inhibition of IGF-I signalling via the small molecule NVP-AEW541 appears to mediate changes to the cell migratory behaviour by affecting the expression of the key EMT indicators E-cadherin and vimentin. Along with the inhibition of the IGF-I mediated increase in migration in the SW480 cell line by the small molecule Wnt inhibitor IWR-1, this demonstrates that the IGF-I pathway can interact with the Wnt signalling pathway, a critical pathway for the development of colorectal cancer [96], to induce a migratory response in the model under investigation here.

6 Increasing the biological relevance of cell invasion models *in vitro* by utilising ECM coatings and co-culture

6.1 Introduction

The provision of a 3D environment for *in vitro* cultures is an important step towards mimicking the *in vivo* environment of cells in order to produce more accurate biological models. The microenvironment of extracellular matrix (ECM) proteins and secondary cell types have also been identified as important in the development and behaviour of cancers [365, 366]. Modification of the 3D migration assay in use herein to include ECM and co-culture components will be addressed in this Chapter and open opportunities for novel cell invasion models which reflect the tumour microenvironment more accurately (Figure 6.1).

6.1.1 The ECM has a role in modulating cellular behaviour

6.1.1.1 ECM proteins alter cellular behaviour both *in vivo* and *in vitro*

The *in vivo* ECM provides a wide variety of biochemical and mechanical information to cells and alterations to this environment can have a significant impact on the behaviour of cells and tumours. This also applies to cells cultured *in vitro* with the provision of an ECM substrate altering the biochemical and physical properties of the culturing environment.

6.1.1.1.1 The mechanical stiffness of the ECM alters during cancer and affects cell behaviour

Changes to the mechanical stiffness of the growth substrate of cells *in vitro* have been shown to alter the morphology and migration of cells [367]. The seeding of the rat kidney cell line NRK-52E or Swiss mouse 3T3 fibroblasts onto polyacrylamide (PA) gels with increasing bis-acrylamide content altered their morphology, as the higher the bis-acrylamide content gels were stiffer and allowed for the better spreading of cells. The softer substrates resulted in greater fluctuation of the lamellipodia of the NRK-52E cells and a faster rate of motility of the 3T3 cells, demonstrating that these cell lines appear to be more motile on the softer gels.

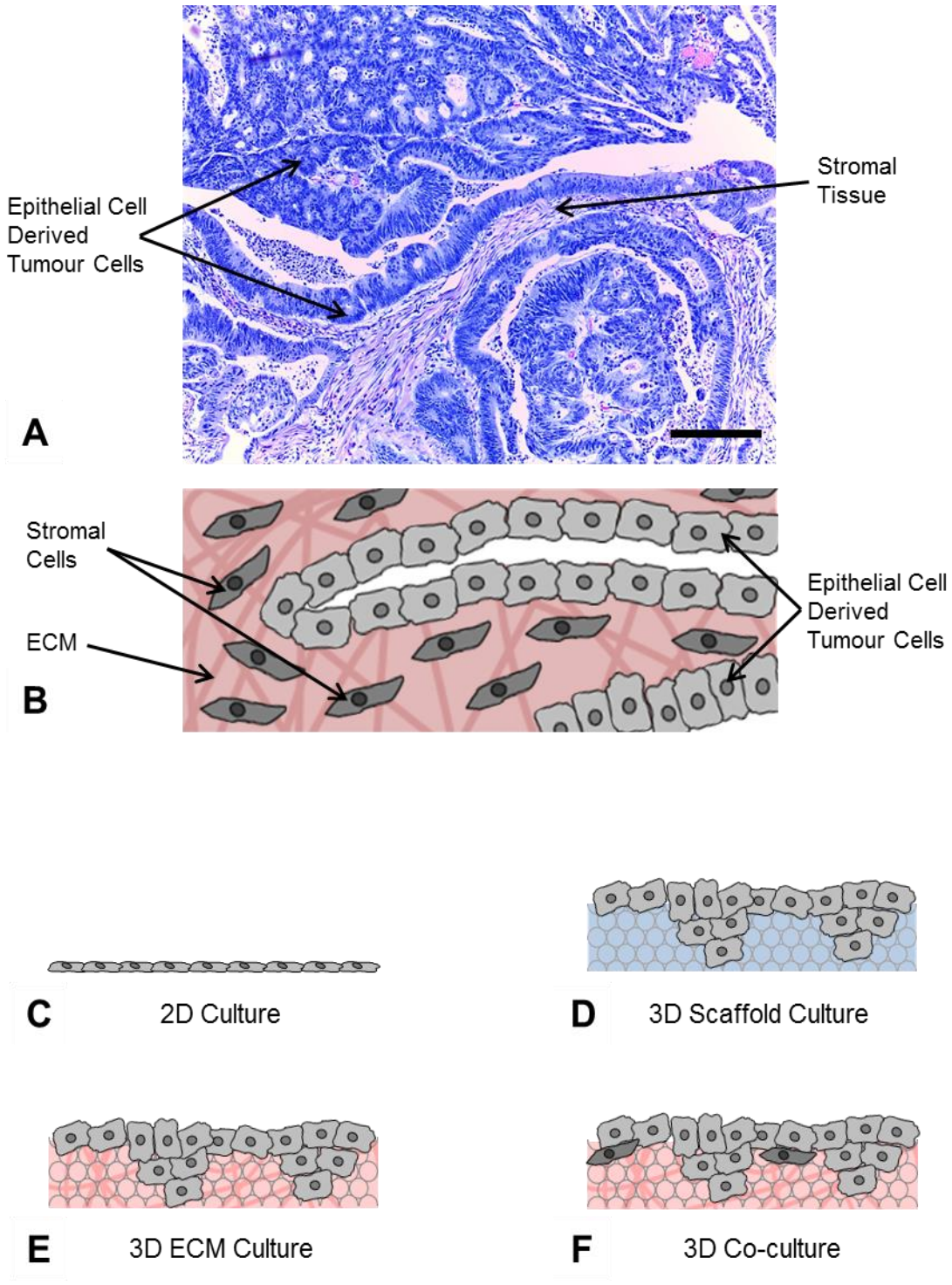

Figure 6.1: The tumour microenvironment is a complex multicellular environment which requires accurate in vitro modelling. A: H&E image of a Stage C colorectal cancer with B: a schematic representation of the components of the microenvironment. This microenvironment can be modelled via C: 2D culture, providing a limited microenvironment to model cancer behaviour, with limited cell-cell contacts, D: 3D culture on synthetic scaffolds, increasing the level of cell-cell interactions in the absence of ECM protein or cancer-stroma interactions, E: 3D culture with ECM, providing cell-protein interactions to direct cell behaviour, and F: 3D co-culture, providing a range of multicellular and protein interactions. Scale bar = 200µm.

The stiffness of protein matrices has been shown to have an effect on breast cancer cells, in both *in vivo* and *in vitro* studies. A study using the MMTV-Neu mouse model of breast cancer demonstrated that the stiffness of the mammary gland tissue increases with increasing tumour progression and that this stiffness also spreads to the stromal tissue adjacent to the invading tumour [368]. This increased stiffness is thought to be due to a combination of increased collagen expression and increased linearisation and cross-linking of these fibres. The increased detection of the collagen cross-links was also seen in correlation with an increase of lysyl oxidase (LOX), an amine oxidase which acts as a collagen cross-link initiator. The cross-linking of *in vitro* collagen gels with L-ribose also resulted in an increase in gel stiffness which was sufficient to disrupt the tissue organisation of non-malignant MCF10A acini and to increase the size of the observed colonies within the 3D gel. However, without the malignant activity of ErbB2, the stiffening of the collagen gels was not sufficient to induce the invasion of the mammary epithelial cells (MECs).

The authors of this study then went on to investigate the role of the LOX modulation of tissue stiffness in the initiation and progression of breast tumours [368]. The replacement of the native cells of the mammary fat pads of NOD/SCID mice with fibroblasts which express normal or elevated levels of LOX allowed the experimenters to prime the mice prior to the injection of MCF10AT MECs to induce premalignant legions. The elevated LOX expression resulted in stiffer glands with a higher linearised collagen content which promoted the growth and invasion of the injected MECs without directly affecting the behaviour of the MECs themselves, as the application of the LOX inhibitor β–aminopropionitrile (BAPN) did not affect the tumour growth. A complementary study treating five month old MMTV-Neu mice either BAPN or a LOX inhibiting antibody for a period of one month followed by a month recovery was sufficient to reduce the LOX activity levels and decrease amount of fibrillar collagen, crosslinks and the linearisation of fibres. This resulted in fewer, smaller tumours produced in the LOX inhibited mice and they took longer to appear. These tumours were found to express lower levels of proliferating cell nuclear antigen (PCNA) and were generally a lower grade of tumour when compared to the untreated MMTV-Neu mice.

LOX has also shown to have a role in the progression of colorectal tumours, as the injection of SW480 cells stably overexpressing LOX into nude mice resulted in an increased tumour volume and increased stiffness of the tumours produced when compared to either control mice or those expressing catalytically inactive LOX [369]. However, this model did not observe the increase in collagen as was observed in the mouse model described above as the collagen content was comparable across all conditions. The expression of active LOX in the SW480 cells was sufficient to promote the phosphorylation of focal adhesion kinase (FAK), while the culturing of unmodified SW480 cells on collagen I gels treated with either LOX or ribose to promote cross-linking and increase stiffness was also sufficient to promote FAK phosphorylation. Histological staining of the subcutaneous SW480 tumours also highlighted that expression of LOX increases the amount of phosphorylated Src, suggesting that the mechanism of signal transduction from the stiffened matrix via a FAK/Src signalling cascade. Application of either FAK or Src inhibitors to LOX expressing SW480 cells grown in collagen gels was sufficient to reduce the proliferation and invasion of these cells back to levels comparative to those seen with controls, with the FAK inhibitor reducing the proliferation of both the control and LOX mutant cells.

While both of these papers utilised cell lines which demonstrated increased growth and motility on stiffer matrix substrates, cancer cells have varied growth profiles on substrates of differing rigidity [370]. A variety of cell lines were assessed for their ability to grow on collagen coated PA gels with elastic moduli ranging from 150 to 9600 Pa, which covers the stiffness of normal lung or mammary tissue, breast tumours and striated muscle. Those which were found to grow better on the stiffer gels were termed rigidity-dependent and those which had a consistent growth profile across all gel were termed rigidity-independent, with no correlation between the growth patterns and the tumour origin or stage observed. Rigidity-dependent cell lines were found to have a cell-cycle blockade preventing entry into S phase or increased apoptosis, or a combination of the two, when cultured on softer gels which accounts for the decreased cell number overall as the attachment of cells to the range of gels remained comparable. The alteration of gel stiffness also affected the ability of the rigidity-dependent cells to spread on the substrate and to migrate through the gels. Altogether, these traits meant that the rigidity-dependent cell lines were less effective at generating xenograft tumours in soft lung tissue than rigidity-independent cell lines under the same conditions and highlight that the mechanical properties of ECM can play a large part in directing the initial growth and spread of tumours.

SW480 cells seeded onto soft collagen I gels, as opposed to collagen I coated glass or a hard collagen I gels, exhibited an inhibited ability to spread, which appeared to be under the control of receptor-type tyrosine-protein phosphatase alpha (RPTPα) [371]. While RPTPα expression reversed this inhibition in the soft gels and knock-down of RPTPα expression in cells grown on the harder substrates mimicked the inhibition seen on the soft gels. This process of spreading is Src dependent, as the transfection of C-terminal Src kinase (CSK), which acts to activate Src where RPTPα inactivates Src, is sufficient to decrease the amount of spreading on the hard gels when expressed alone and counteracts the effect of RPTPα when both proteins are expressed together. The authors demonstrated that cellular spread is also mediated via myosin light chain kinase (MLCK) but not via Rho-kinase (ROCK), as application of the MLCK inhibitor ML-7 was sufficient to inhibit the effect of RPTPα expression completely but the application of the ROCK inhibitor Y-27632 only resulted in a partial inhibition of the response to RPTPα. The expression of RPTPα also controls the invasion of SW480 across the chorioallantoic membrane (CAM) of eggs, as knock-down of RPTPα expression reduced the number of eggs exhibiting invasion of the membrane by the SW480 from ~75% seen in controls to ~20%, while overexpression of RPTPα resulted in a small increase in instances of invasion.

Together these data demonstrate that the mechanical properties of the microenvironment, in terms of its rigidity, can drive cell behaviour and the interaction of cells with ECM with differing rigidity can direct cancer progression and spread. The inclusion of an ECM substrate in the 3D model under development here may alter the rigidity of the 3D *in vitro* microenvironment, providing the cells with a culture environment which is closer to the *in vivo* situation.

6.1.1.1.2 ECM proteins can direct cell migratory behaviour

Modulation of the migratory behaviour of cells by ECM protein components has also been observed, with both collagen I and fibronectin facilitating the migration of cells in *in vitro* and *in vivo* assays. The remodelling interaction between cells and the ECM can also direct the mode of migration utilised in the 3D environment [271], as the inhibition of the protease degradation of ECM

forces cells to adopt a more amoeboid mode of migration to maintain migration speed. Using a Fluorescein Isothiocyanate (FITC) release assay, the migration of membrane type-1 matrix metalloproteinase (MT1-MMP, also known as MMP-14) overexpressing HT-1080 fibrosarcoma cells (HT-1080/MT1 cells) on FITC-labelled collagen matrices was examined in the presence of protease inhibitors. The addition of the broad spectrum matrix metalloproteinase (MMP) inhibitor BB-2516 was sufficient to cause an 80% reduction in the amount of FITC released from the matrix by collagen degradation over a 40 hour period, while the application of a protease cocktail which induced cathepsin and serine protease inhibitors in with BB-2516 increased this inhibition to 95%. This significant reduction in matrix degradation was not accompanied by a decrease in the migratory speed of the cells, with both the control and cocktail treated HT-1080/MT1 cells maintaining a median speed of ~0.5μm per minute across the 15 hours they were tracked. The lack of speed loss in the presence of the protease cocktail appears to be due to a shift in the migratory mode utilised by these cells, observed as a significant change from elongated mesenchymal type cells to spherical amoeboid type cells in the presence of the cocktail. This change was also seen in the breast cancer cell line MDA-MB-231, although the shift in the ratio of mesenchymal and amoeboid in the presence and absence of the protease cocktail was not significant, in addition to a lower inhibition of FITC release in the MDA-MB-231 cultures in the presence of the protease cocktail. This *in vitro* data was mirrored by the injection of HT-1080/MT1 cells into mouse dermis as those cells which were pre-treated with the protease cocktail exhibited a greater ability to disseminate throughout the dermal tissue, with the cells also maintaining a more spherical amoeboid shape.

The interactions of cancer cells with ECM components leads to alterations to their organisation as visible through histological analysis and has led to the identification of a series of tumour-associated collagen signatures (TACS) which are correlated with the disease progression [272]. The first of these signatures, TACS-1, is seen as a build-up of dense collagen deposits in the stromal tissue surrounding the initial site of tumour growth and can be used to local small tumours within a tissue sample. TACS-2 is associated with larger tumours and characterised by stretched, elongated collagen fibres found around the tumour boundary, with the angle between the tumour boundary and the fibres being 0^{o}. The authors of this study hypothesise that this alteration in collagen organisation is due to the expansion of the tumour exerting an outward force on the dense collagen deposits of TACS-1, causing the stretching of the individual fibres. The final signature, TACS-3, is associated with invasive tumours, as the smooth collagen organisation seen in TACS-2 is disrupted by the local invasive fronts of the tumour to a formation which is irregular and most commonly perpendicular to the tumour boundary. As these signatures were observed in fixed mammary tumours from MMTV-Wnt-1 mice, a common mouse breast tumour model, the study then looked at the remodelling of *in vitro* collagen gels by tumour explants from another common mouse breast tumour model, the MMTV-polyoma middle-T (PyVT) model where cells express the oncogenic middle antigen of the polyoma virus. Imaging of these gels after polymerisation but before the addition of the tumour explants highlights the randomly orientated collagen fibres, while imaging of gels after 8 hours of culturing with the explants shows a radically altered collagen organisation close to the explants. Collagen morphology analogous to TACS-2 was observed around the tumour boundary, while morphology analogous to TACS-3 was seen in areas where the

explant had begun to invade into the collagen gel, demonstrating that tumours are able to remodel the organisation of collagen fibres to promote the localised invasion of the tumours.

The deposition of collagen seen in the earlier stages of the mammary tumours may also have a role in the migration of tumours as it has been shown that glioblastoma spheroids attain a greater distance of invasion over a 12 hour period on gels with a higher content of collagen I [372]. Deposition of fibronectin may also increase the cell migration of both normal and transformed cells, as seen via the colloidal gold migration assay where cells remove the gold coating from coverslips as they migrate across the surface [202]. The addition of 50µg/ml of fibronectin at the time of cell plating enhanced the migration of both normal and transformed NIL8 hamster and 3T3 mouse fibroblasts in the initial two days after cell seeding. The migration of the NIL8 cells transformed by the hamster sarcoma virus (NIL8-HSV cells) was observed over the initial 24 hours after plating and the extent of this migration was dependant on the concentration of fibronectin present, as lower concentrations of fibronectin resulted in smaller areas cleared of their gold particle coating. The change in behaviour seen in response to fibronectin could also be directly observed from the cell morphology, as the NIL8-HSV cells adopted a spindle like morphology and were more spread out in the presence of 50µg/ml fibronectin, whereas they grew in tight colonies in the absence of fibronectin.

The presence of fibronectin can also increase the ability of cells to migrate across a collagen I substrate, as demonstrated *in vitro* with Chinese hamster ovary (CHO) cells [373]. The seeding of CHO cells on to 3D collagen I gels in the absence of fibronectin resulted in delayed attachment to the substrate as cells retained a spherical morphology over the initial two hours post seeding, whereas those seeded in the presence of fibronectin had adopted the characteristic spread out morphology of the cell line. This difference in cell attachment was lost by 24 hours post seeding, with the 3D cultures with or without fibronectin producing cells with comparable morphologies. This alteration in attachment behaviour did not lead to a significant alteration in the proliferative behaviour of the CHO cells over the first 3 days of culture post seeding, with the initial 2.5×10^4 cells expanding to 5.5×10^5 and 5.0×10^5 cells, with and without fibronectin in the serum respectively. However the migratory capacity of the CHO cells cultured on the 3D collagen I gels varied depending on the presence of fibronectin. After the initial 3 days of culturing, 12.4% of the CHO cells where found within the collagen gels when fibronectin was present in the serum, whereas the use of fibronectin depleted serum resulted in only 6.1% of the cells migrating into the gels.

While the presence of fibronectin has implications for the migration of cancer cells *in vitro*, the expression of fibronectin has been shown to not fully correlate to the metastatic behaviour of breast cancer cells [374]. Using mammary tumour clones generated from 7,12-dimethylbenz(α)anthracene (DMBA) induced tumours in rats, the group identified three clones taken from legions within the mammary tissue which exhibited a varied capacity to produce lung metastasis when xenografted into the mammary fat pads of further rats. Two lung metastases were also cloned and shown to have different capacities for metastasis formation in a xenograft model, with the more metastatic of these two also able to produce lymph node metastases which were not viewed with any of the other clones examined. Analysis of *in vitro* cultures on glass coverslips showed that both of the metastatic clones did not demonstrate any cell surface expression of fibronectin, regardless of the

confluency of cell growth, whereas the three clones from primary tumours did have surface fibronectin expression which was shown to increase with increased cell confluency. The same trend was observed with fibronectin secreted into the growth medium, with both the metastatic clones secreting ~2.5µg per 1 x 10^6 cells when in confluent cultures compared to the 26.7 - 77.0µg per 1 x 10^6 cells secreted by the confluent cultures of the primary clones. This pattern of expression of fibronectin was maintained *in vivo*, with xenograft tumours produced from the metastatic clones producing a much lower amount of fibronectin than those produced from the primary clones and this trend remained when either the primary mammary xenograft tumour or metastases were examined. As the authors of this paper found no clear correlation between the expression of fibronectin and the metastatic potential of the mammary tumour clones it is thought that any role that fibronectin may play in the metastatic progression of tumours is not as simple as changing expression levels of the protein.

6.1.1.1.3 The ECM can direct other aspects of cancer behaviour

While the ECM can modulate the migratory behaviour of cancer cells, other aspects of cancer behaviour and progression can also be affected by these proteins. The collagen content of subcutaneous xenograft tumours affects the elasticity of the tumours, with those containing a higher amount of collagen taking longer to relax after compression [375]. This difference in elasticity was seen in tumours generated from cancer cell lines originating from a variety of tissues and was not correlated to the glycosaminoglycan (GAG) content of the xenografts, as this was comparable across the four cell lines examined. The higher collagen content also affects the diffusion of macromolecules, as examined with a non-binding antibody, with those tumours with a lower collagen content attaining a diffusion rate of ~1.930 x 10^{-7} cm^2 per second as opposed to the ~0.915 x 10^{-7} cm^2 per second obtained in the tumours with a higher collagen content, demonstrating that the collagen content of tumours may be preventing the diffusion of chemotherapy agents into the centre of the tumour mass and limiting the effectiveness of these treatments. The treatment of these high collagen tumours with collagenase was able to increase the rate of diffusion by up to 100% and provides a potential solution to the problem of drug delivery if the collagenase can be appropriately targeted to the tumour mass and not disrupt the organisation of other tissues.

The regulation of collagen I can also affect angiogenesis in response to basic fibroblast growth factor (bFGF) and vascular endothelial growth factor (VEGF) [376]. Using a modified CAM assay where a collagen I gel is implanted into the membrane and the angiogenesis of the chick embryo into the collagen is observed, the addition of bFGF, either with or without VEGF, was sufficient to increase the amount of vascularisation of the collagen I gel, while the application of VEGF alone did not result in a significant increase in vascularisation. This increase in vascularisation was shown to be dependent on the action of MMPs degrading the collagen I gel as the inclusion of either the synthetic MMP inhibitor BB-3103 or the natural MMP inhibitor tissue inhibitor of metalloproteinase (TIMP)-1, here used in its C-terminally truncated form, were sufficient to reduce at least 60% of the angiogenesis activity. Immunofluorescence and polymerase chain reaction (PCR) analysis of the collagen gels demonstrated that the degradation of the gel was facilitated by a combination of MMP proteins, namely MMP-2, MMP-9, MMP-13 and MMP-16. This highlights

that the ECM can have roles in tumour progression which are not limited to modulating the migratory behaviour of the cells.

6.1.1.2 The distribution of ECM proteins in colonic tissue is altered during cancer progression

6.1.1.2.1 Collagen I and fibronectin are found in healthy colonic tissue

The composition of the colonic ECM in terms of major protein components has been documented in the literature for many years. As with most other tissues, one of the major components of the ECM is type I collagen, the most abundant of the fibrillar collagens, which comprises of 68% of the fibrillar collagens present in healthy intestinal samples [377] and is localised at the basement membrane found below the epithelial cells and within the stromal tissue of the colon [378]. Additionally the basement membrane marker, collagen IV, is also present in healthy colon and is mainly found at the basement membrane around the colonic epithelium [379] in addition to surrounding blood vessels within the stromal layer [378]. Another common ECM component, fibronectin, is distributed throughout the stromal layer of the colon [379]. As both collagen I and fibronectin are abundant ECM proteins and have documented effects on cancer cell behaviour they will be the two ECM components which will be focused on during this chapter.

Like many other aspects of normal cell behaviour, the expression and distribution of ECM components is found to be disrupted during cancer progression. However, as each cancer case is different, there is variation in the data presented in the literature, although some trends remain once all of the data is taken into account.

6.1.1.2.2 Collagen I expression is increased in the stromal compartment of tumours

Assessments of the variable expression of proteins in cancer have been made using the serial analysis of gene expression (SAGE) technique, which is capable of analysing large number of gene transcripts simultaneously, and has been applied to pancreatic [380-382], colorectal [381, 382], ovarian [382] and breast [382-384] cancers. Use of this technique has identified the variable expression of collagen I between normal and cancerous colonic tissue, Ryu *et al*. found that the expression of both the α1 and α2 collagen I chains is increased in tissue obtained from primary colorectal tumours compared to normal mucosa, but this increased expression is not maintained in the colorectal cancer derived cell lines CaCo-2 or SW837 [382]. This is comparable to results seen for breast cancer, with the collagen I α1 transcript found to be elevated during the later stages of disease progression when compared to normal mammary tissue [383], while the breast cancer cell line libraries LacZ, MCF70 h, and MDA453 did not show this elevated expression [384]. This result has been mirrored using microarray analysis of gene expression between primary and metastatic solid tumours which found an elevation of collagen I α1 and α2 expression [385].

Proteomic analysis of colorectal cancer tissue via mass spectrometry has also identified a variation in both collagen I α1 and α2 expression across all stages of the disease progression [386]. The mRNA and protein expression levels for both collagen I chains were found to be elevated at all stages compared to normal mucosa, with the elevation seen in stages I and II significantly greater than that in stages III and IV and stage II tumours consistently demonstrating the highest levels for all. Enzyme-linked immunosorbent assay (ELISA) analysis of the serum levels of the

carboxyterminal propeptide of type I collagen (PICP) and the C-terminal telopeptide of type I collagen (CTx) provide further information regarding the dynamics of collagen I processing across the progression of colorectal cancer. PICP is a marker of collagen I synthesis and found to be elevated in the serum of patients exhibiting all stages of the disease when compared to healthy patients. CTx is a marker of collagen I degradation and also found to be elevated in the serum of cancer patients, although this elevation increased with increasing progression of the disease. Kaplan-Meier analysis of the survival rates demonstrated that there is a correlation between elevated serum CTx levels and poor patient progression, as visualised by examining the 3-year disease free survival rates.

Immunohistochemical analysis of primary colorectal tumours highlights increased stromal distribution of collagen I in tumours when compared back to normal tissue from the same patient [378] and this change in collagen I distribution was seen regardless of tumour site within the colon or grade of tumour. When pre- and post-metastatic colorectal cancers are compared in this manner, there is a higher collagen I expression in the reactive stroma of the metastatic disease than the non-metastatic disease, with the expression of collagen I in tumour cells remaining comparable [387]. Additionally, when two different forms of metastatic growth patterns were compared, the level of collagen I expression was found to vary at the tumour border but not in the interior of the tumour. Metastasis displaying a desmoplastic growth pattern, that is metastasis formation separated from the liver parenchyma by a layer of stromal tissue [388], expressed a higher level of collagen I than metastasis displaying a pushing growth pattern [387], where the metastasis and liver tissue are found next to each other without the formation of a stromal layer [388].

Together this data shows that collagen I is an ECM component which is abundant in the stromal compartment of tumours, with the expression of both primary protein chains, collagen I α1 and α2, elevated relative to normal tissue. The proteomic analysis also demonstrated an increase in collagen I turnover in the later metastatic stages of colorectal cancer, which accounts for the highest expression seen in stage II of the disease, and this degradation is linked to decreased patient survival.

6.1.1.2.3 Fibronectin expression is increased in colorectal cancer

Fibronectin is commonly produced by fibroblasts and secreted to a pericellular localisation around many cell types [389]. This localisation of fibronectin is commonly lost during transformation of cells to a malignant cell type and has been demonstrated in gliomas [390], rhabdomyosarcoma and transformed fibroblasts [391], however it was noted that this loss is not due to an inhibition of fibronectin production.

Indeed, an increase in fibronectin expression has been noted in different types of cancer, with a 6.53-fold increase noted in a study which compared microarray analysis of pancreatic cancer cell lines and primary tumours to the SAGE data for healthy pancreatic tissue [392]. There have also been studies made on colorectal cancer which have detected increases in the expression of fibronectin. SAGE analysis of two primary colorectal tumours highlights an 11-fold increase in fibronectin expression over normal colonic tissue, while comparisons between normal tissue and the colorectal cancer cell lines SW837 and CaCo-2 shows a 28-fold increase in fibronectin expression in the cell lines over the normal tissue [381].

The analysis of protein expression carried out via mass spectrometry that detected an increase in the expression of both collagen I α1 and α2 also detected a smaller, but still significant, increase in fibronectin expression across stages I, II and III of the disease [386]. Microarray analysis of colon cancers which were sorted into epithelial-type and mesenchymal-type cells using the citeria of high E-cadherin/low vimentin expression to denote an epithelial-like gene expression pattern and low E-cadherin/high vimentin expression to denote a mesenchymal-like gene expression pattern also identified a change in fibronectin expression [79]. This identification criteria was sufficient to identify genes which are associated with the epithelial-mesenchymal transition (EMT) in colorectal cancer and fibronectin was found to be upregulated in cells displaying the mesenchymal phenotype over the epithelial phenotype and therefore a gene which is correlated with EMT.

This result from Loboda *et al*. appears to be a contradiction of data previous obtained by Smith *et al*. which found that the amount of fibronectin found within and secreted by cells was reduced in cell lines derived from metastatic tumours when compared to cell lines derived from primary tumours [393]. However, together these data may mean that the cells which make up the metastatic tumours from which the six cell lines tested were derived have gone through the reverse process of EMT, namely mesenchymal-epithelial transition (MET), whereby cells regain a more epithelial phenotype and this may account from the drop in fibronectin expression in the metastatic tumours.

In addition to the variation in the expression level of fibronectin between normal and cancerous colonic tissue, there is also a variation in the specific isoforms of fibronectin that are present too. One of the means of generating isoform differences in the fibronectin protein is by alternate splicing at a 270 nucleotide long splice site, the ED splice site [394], which results in the ED-A^+ and ED-B^+ isoforms [395]. It is the ED-A^+, not the ED-B^+, isoform which is present in healthy human colonic tissue, whereas the ED-B^+ isoform is only found in colorectal cancer tissue. The amount of the ED-A^+ isoform appears to be increased in cancer, as the immunohistological staining for this isoform was stronger in the cancer samples than in the healthy tissue. The source of these isoforms of fibronectin is from both the colorectal cancer cells and tumour-associated myofibroblasts, as demonstrated by both Northern and Western blot analysis of the colorectal cancer cell line CaCo-2 and primary rat tumour-associated myofibroblasts.

Together these data show that there is generally an increase in the production of fibronectin at the primary site of tumour growth which is correlated with an altered extracellular distribution of the protein. This increase in expression is also correlated with other EMT associated genetic changes and may be part of the metastatic process of colorectal cancer cells.

6.1.2 Solid tumours are comprised of multiple cell types

While the protein environment in terms of the localised ECM is clearly important in the development and progression of colorectal cancers, the stromal compartment of tumours also plays a role in the disease and the addition of stromal components into *in vitro* assays can increase the biological relevance of the models.

6.1.2.1 Tumours are multicellular environments

6.1.2.1.1 The stromal compartment of tumours can comprise of a variety of cell types

Over the years many different types of stromal cell have been identified in cancers, including vascular endothelial cells [396, 397], fibroblasts [398] and immune cells such as T-cells [75] and macrophages [399]. As each of these cell types can have differing protein expression profiles and each may originate from different populations of healthy cells [400], together these add a great deal of complexity to understanding the precise mechanisms involved at any point during cancer progression.

6.1.2.1.2 The stromal content of tumours is a marker of prognosis

While the involvement of stromal tissue in cancerous tumours has been under investigation for many years, a study into the role of stromal content of colorectal cancers in terms of predicting patient prognosis was published in 2007 by Mesker *et al*. [58], with a follow up study published in 2009 [274]. The amount of stromal tissue within the tumour was scored from histological samples from human colorectal cancers graded from I to III under the AJCC classification system and designated as either the carcinoma percentage (CP) or stroma ratio, with a low CP equivalent to a high stromal ratio and vice versa. The initial study found that a CP of 50%, that is a tumour which is comprised of cancerous tissue and stromal tissue in equal parts, was a sufficient cut off point to provide a significant variation in the patient prognosis, visualised by both the disease-free and overall survival [58]. The initial study set used in this paper demonstrate that patients with CP-low tumours had a worse prognosis for both disease-free and overall survival, 1.36 and 1.40 years respectively vs 4.82 and 5.40 years for CP-high tumours, with the validation series providing a similar trend. This difference in survival prospects is as significant as when the T-stage, N-stage or overall tumour grade is used as a factor of prognosis and remains valid when the microsatellite instability (MSI) status or stage of the tumours is considered. The follow up study from this group, which drew data from a larger study group, confirmed the finding of the initial study that the CP is a marker of patient prognosis [274]. Here they demonstrated that in addition to there being a statistically significant difference in the disease-free and overall survival between CP-low and CP-high group, there is also a significant difference in the metastasis-free survival, again with the CP-high patients faring better than the CP-low patients. In addition, this study also showed that the expression of the transcription factor SMAD4 could be used as a further marker of prognosis in CP-low tumours. The expression of SMAD4 had no effect in CP-high tumours, but in CP-low tumours the expression of SMAD4 correlated to an increase in the disease-free and overall survival rates.

This work was backed up by the use of a different patient cohort, again demonstrating that colorectal cancer patients with CP-low grade II or III tumours had a poorer prognosis in terms of both disease-free and overall survival [401]. The relationship between CP and the T- and N-stages of tumours was also examined, with the percentage of CP-high tumours decreasing from 100.0% of T1 tumours down to 55.0% of T4 tumours. Similarly, a drop in CP-high tumours is seen when lymph nodes are metastasised, with 76.1% of N0, lymph node negative, tumours falling into the CP-high classification compared to ~64.7% of N1-2, lymph node metastasised, tumours. This scoring via analysis of histologically stained samples demonstrates the value of the stromal compartment of tumours as a diagnostic tool and the authors of these papers suggest that this

could be used to identify high-risk patients that could benefit from further treatment after surgical resection of the initial tumour mass.

6.1.2.1.3 The production of proteins by cancer associated stroma can affect patient prognosis

While the volume of stromal tissue within tumours has been shown to have implications for patient survival, the production and secretion of proteins by this stromal compartment can also have a value as a marker of patient prognosis. A variety of research groups have published data demonstrating that high protein expression of vimentin [402] and toll-like receptor 4 (TLR-4) [403] in the stroma is linked to poor patient prognosis in terms of disease-free survival, and overall survival in the case of vimentin. Conversely, stromal expression of the MMP-related disintegrin and metalloproteinase with thrombospondin motifs (ADAMTS)-12 protein, a known inhibitor of tumour growth which acts via modulation of the ERK signalling pathway, correlates with improved patient prognosis for both disease-free and overall survival and this improvement is seen with the increasing percentage of positively staining stromal cells [404]. The mRNA expression of fibroblast activation protein-α (FAP-α) and stromal cell-derived factor-1 (SDF-1) are both associated with cancer-associated fibroblasts (CAFs) and are poor prognostic markers for distant recurrence of the cancer and survival, while the blood serum levels for these two proteins do have a prognostic significance [405].

It is not just the expression of proteins in the stromal compartment of the primary tumour which can affect patient outcome. The expression of a range of MMPs, growth factors and other pro-angiogenic proteins varies between the tumour and stromal compartments of primary colorectal cancers, liver and lung metastases [406]. Some proteins such as angiopoietin-2 were found at a higher concentration in the stromal compartment of all locations analysed, while others such as MMP-9 were elevated in the tumour compartment of liver metastases with no variation at the other sites. While this information can provide clues to the role of these proteins in the vascularisation of tumours at the primary and metastatic sites, the variation in expression can also be used as prognosis markers. In the primary tumours and lung metastases, high stromal expression of MMP-2 and MMP-3 correlated with a better overall survival rate while not being significantly correlated with survival in liver metastases.

6.1.2.2 Fibroblasts involvement in tumours affects cancer behaviour

A major component of the stromal portion of tumours is the CAFs and these have been shown to produce proteins which can direct the progression of the disease.

6.1.2.2.1 Recruitment of CAFs alters their protein expression

Interactions between the tumour cells and the recruited CAFs result in alteration of the protein expression profile of the CAFs. Culturing of fibroblasts derived from human skin, colon and lung in the presence of tumour cell-derived collagenase-stimulatory factor (TCSF), derived from the cell membranes of the LX-1 human lung carcinoma cell line, induced an increase in mRNA expression and protein secretion of MMP-1, MMP-2 and MMP-3 [407]. These MMPs target a variety of ECM proteins and have been implicated in the progression of colorectal cancer [408]. The overexpression of MMPs by CAFs has also been assessed via *in situ* hybridisation of colon cancer

samples [409]. While the overexpression of MMP-14 was seen in both the populations of tumour cells and CAFs, the overexpression of MMP-2 and type-1 procollagen was confined to the fibroblast compartment of the tumour mass.

It is not only the expression of secreted ECM proteins and MMPs in fibroblasts which is altered during cancer progression, the expression of cytoskeletal proteins is also altered [410]. When the expression of cytoskeletal proteins is examined via immunohistochemistry, there is an increase of staining in the nonpericryptal stroma of the diseased tissue when compared to the normal mucosa. While the expression of vimentin does not alter across the tissues examined, there is focal expression of the muscle specific intermediate filament, desmin, in the diseased colonic tissue which is absent from the healthy nonpericryptal stroma. Additionally, the expression of α-SMA and the associated actin motor protein smooth muscle myosin (SMM) is also increased in the diseased tissues, with the adenomatous polyps displaying a greater intensity of staining than the non-tumorous hyperplastic polyps examined.

It is not just the recruited CAFs at the site of the primary tumours which have an altered protein expression profile relative to the healthy colonic fibroblasts, the recruited CAFs at the site of metastatic legions in the liver also have an altered expression profile [411]. Microarray analysis of mRNA extracted from subcultured fibroblasts isolated from metastatic colorectal cancer legions in the liver and counterpart healthy liver fibroblasts from the same patients reveals that there is a wide variety of genes which are either up- or downregulated in the CAFs. While some of the genes were unidentified, the majority of genes which were found to be downregulated in the CAFs were transcription factors or transcription regulators. The upregulated genes were found to come from a variety of cellular processes including cell signalling pathways, migration and cell proliferation.

The matter of altered protein expression profile in CAFs is further complicated by the variable expression of proteins depending on the origin of the colorectal cancer [412]. This study examined the expression of the focal adhesion protein four and a half LIM domain protein-2 (FHL2) in sporadic and HNPCC cases of colorectal cancer with or without lymph node involvement. This protein is absent from the stromal tissue of tumour samples which have been immunohistochemically stained and present in the peritumoural fibroblasts found within the centre of the tumour mass. The expression of FHL2 was also seen to be variable in the fibroblasts in the invasive margin of the tumours. When the amount of FHL2 expression was quantified in each of the four types of cancer, either sporadic or HNPCC, with or without lymphatic involvement, it is seen that positive FHL2 expression is significantly correlated with lymphatic involvement in sporadic tumours and significantly inversely correlated in HNPCC cases.

One of the pathways which has been implicated in the mechanism of expression alteration in CAFs is the TGFβ signalling pathway [413]. Culturing of the colorectal cancer cell lines HT29 and HCT116 produces conditioned media which is high in TGFβ, with the HCT116 cultures producing a higher amount of TGFβ than the HT29 cultures. When this conditioned media is subsequently used to culture CAFs isolated from colorectal cancer patients, it was able to induce a similar pattern of expression induction to that seen when cultured with human recombinant TGFβ. Some of the proteins which were analysed include MMP-2, MMP-3 and MMP-14, which were seen to increase the most with the conditioned media from the HCT116 cell line, which is in line with the amount of TGFβ these cultures secreted into the culture media.

With the alteration of protein expression in the recruited CAFs of colorectal tumours, there is a greater potential for the behaviour of cancers to also be altered via paracrine signalling.

6.1.2.2.2 CAFs alter cancer behaviour

The recruitment of CAFs to colorectal cancer tumours, both primary and metastatic, has been shown to affect different aspects of the tumour progression, including tumour growth and dissemination. The activation of fibroblasts in the tumour microenvironment can be visualised by the expression of FAP-α on the cell surface and inhibition of this protein has been shown to limit tumour growth in a murine lung carcinoma model [398]. The cross breeding of BALB/c LSL–K-ras^{G12D} mice, a model which produces lung adenoma when infected with an adenovirus expressing Cre recombinase, with FAP-deficient mice produced a collection of animals which either had two functional copies of the *FAP* gene, two non-functional copies or one of each. The induction of tumours in these animals highlighted the role the stromal compartment has on the establishment of the tumours, with tumours occurring more readily in the mice which had at least one functional copy of the *FAP* gene than those without a functional copy of the gene. This difference was also visualised by the decreased area of tumour growth observed on histologically stained slides and the decreased expression of Ki67 in the homozygous null mice. This result was also mirrored in a xenograft model where the colorectal carcinoma cell line CT26 was subcutaneously injected into *FAP*$^{+/+}$ and *FAP*-null mice, where the tumour size and number of proliferative cells were significantly lower in the *FAP*-null mice.

With this demonstration that FAP-α plays a role in tumour establishment, the potential of this protein as a diagnostic marker has been examined [414]. A study of human colorectal cancer samples obtained from tumour resections examined the expression of FAP-α in both the tumour centre and invasive front, with a negative correlation seen between the level of FAP-α staining and the TNM grading of the tumour. However, when the survival data was examined for these patients it was seen that FAP-α expression at the tumour front did not have a correlation with the cancer-specific survival rates. However, it was observed that higher levels of FAP-α expression in the tumour centre were correlated with a significant decrease in the cancer-specific survival rates of patients diagnosed with colon cancer, but not rectal cancer.

The expression of *FAP* mRNA has also been shown to be correlated with the expression of *SNAI1* mRNA in colorectal CAFs, as CAFs were show to express higher levels of *SNAI1* than normal fibroblasts and detection of *SNAI1* expression in tumour samples was positively correlated with *FAP* expression [254]. The expression of *SNAI1* also has an effect on tumour growth in a xenograft model where the colorectal cancer cell line HT29-M6 was subcutaneously injected into mice with fibroblasts which were either the wild-type cells or knock-outs for *SNAI1* expression. Tumours obtained from mice injected with both the cancer and knock-out fibroblasts were smaller and had fewer proliferative cells than tumour obtained from mice injected with either HT29-M6 cells alone or with wild-type fibroblasts.

The source of fibroblast cells can have a significant effect on proliferative activity of cancer cells, as has been demonstrated by the culture of gastric cancer cell lines with varying states of differentiation with conditioned media from the growth of fibroblast cell lines derived from a variety of human tissues [415]. It was observed that the poorly differentiated cell lines exhibited enhanced proliferation in the presence of conditioned media from stomach fibroblast cell lines when

compared to serum free media and that the use of conditioned media from fibroblasts with a different tissue of origin did not enhance the proliferation over the levels seen in the control cultures. Meanwhile the proliferation of the well differentiated cancer cell lines did not alter with the addition of conditioned media, regardless of the source of the fibroblasts. The tissue source of fibroblast also affects the migratory behaviour of cancer cells, as demonstrated by the co-culture of the colorectal cancer cell line KMl2SM on monolayers of primary mouse fibroblasts [416]. While the monolayer co-culture did not affect the proliferation of the KMl2SM cells, the cancer cells were seen to migrate through colon derived fibroblasts grown on 0.8μm pore filters at a greater rate than cultures of skin or lung derived fibroblasts or filters without fibroblasts.

The origin of CAFs from different stages of tumours also affects the behaviour of cancer cells *in vitro* [417]. The culturing of the DLD1 colorectal cancer cell line in the presence of conditioned media obtained from either normal fibroblasts or CAFs obtained from primary tumours (CAF-PT) or liver metastases (CAF-LM) increased the colony formation observed compared to cultures grown with normal media. Additionally, the rate of colony formation was increased in the cultures grown with conditioned media from either of the CAF populations compared to normal fibroblasts, although there was no significant difference between them. However, prolonged culturing with the CAF-LM conditioned media resulted in a decreased number of cells from a variety of colorectal cancer cell lines when compared to culturing with standard media, while culturing with the CAF-PT conditioned media resulted in cultures which had cell counts which were similar to or greater than the controls. However, this decrease in cell number was not due to increased apoptotic activity, as the level of caspase-3 activity was reduced in cultures grown with either type of CAF conditioned media, and the authors hypothesised that this decrease in cell number was due to an induction of cell necrosis. In addition to the effect that the conditioned media had on cell proliferation and survival, it also had an effect on the migration and invasion of colorectal cancer cell lines. The DLD1 cell line was found to exhibit a significant increase in migration in both scratch wound and Transwell® assays in response to culturing with the CAF-LM media, whereas the SW480 cell line showed enhanced invasion through basal membrane extract coated Transwell® inserts in response to the CAF-LM media, regardless of the concentration of the coating.

One of the means by which CAFs can direct the migratory behaviour of colorectal cancer cells is by the secretion of the glycoprotein stanniocalcin-1 (STC1) [418]. Platelet-derived growth factor (PDGF) stimulation of the BJhTERT immortalised fibroblasts elevated STC1 mRNA expression and increased the migration and invasion of the LIM1215 colorectal cancer cell line in co-culture models using Transwell® inserts without or with a Matrigel coating. Similarly a decrease in cell invasion was observed for a variety of colorectal cancer cell lines co-cultured with STC1-deficient fibroblasts. Xenograft experiments, where mice were injected with HCT116 colorectal cancer cells with fibroblasts which were either wild-type or STC1-deficient, demonstrate that STC1 expression affects tumour volume and metastatic potential, as the tumours formed in the mice injected with the STC1-deficient fibroblasts were both significantly smaller and spread to fewer sites throughout the body.

Another protein which is upregulated in CAFs and has an effect on cell migration is the actin binding protein transgelin (TGALN) [273]. Co-cultures of the gastric cancer cell line MKN-45 with CAFs showed a greater ability to migrate and invade in modified Boyden chambers than cultures

with fibroblasts derived from tissue adjacent to tumours or fibroblasts from healthy tissue. As the CAFs expressed a significantly higher level of TAGLN than either of the non-CAF fibroblast types, the role of TAGLN in the migratory behaviour was examined using siRNA. The knockdown of TAGLN expression by the siRNA was sufficient to reduce the observed level of TAGLN expression in the three types of fibroblasts and to also significantly reduce the migration and invasion of the MKN-45 cells in the co-cultures, compared to control siRNA.

6.1.2.2.3 Xenograft tumour formation is altered when the behaviour of CAFs is altered

With CAFs affecting many areas of cell behaviour, it is not surprising that altering the fibroblast compartment of tumours in *in vivo* xenograft models can have a large impact on the outcomes of these experiments. A study published in 1993 by Noël *et al*. demonstrated that the subcutaneous injection of human skin fibroblasts with human breast carcinoma cell lines increased both the instance of tumour growth and the size of the resulting tumours [419]. With the MCF7 breast cancer cell line, injections which had neither fibroblasts nor Matrigel failed to produce tumours at either the low or high cell number injected, whereas the inclusion of fibroblasts produced tumours in 60% of cases with a latency period of 65-70 days. When Matrigel was included in the injections, those without fibroblasts produced tumours in 67% and 80% of cases, for low and high cell numbers respectively, with respective latency periods of 36 and 22 days. The inclusion of both Matrigel and fibroblasts increased the tumorigenicity of the injections to 100% tumour formation with a latency period of 20 days. A similar decrease in latency time and increase in tumour size at any given time point was also observed when the MDA-MB-231 cell line was injected with Matrigel and fibroblasts, as compared to with Matrigel alone. It was hypothesised that the mechanism by which the fibroblasts were affecting the tumour growth was due to soluble factors secreted from the fibroblasts, as the repeated, weekly injection of conditioned media from 2D culture of fibroblasts into the inoculation site produced a similar increase in tumorigenicity that the repeated injection of fibroblasts into the inoculation site produced.

Another study demonstrated that the characteristics of the fibroblasts included in the inoculation injection also affect the tumorigenic potential of the cells used in the xenograft models [420]. Injection of either the human epidermal keratinocyte cell line HaCAT or its tumorigenic derivative Ha(Pk) into the dorsal flap of nude mice did not produce any tumours over the initial 40 days post injection when injected without fibroblasts. When presenescent WI-38 lung fibroblasts were included in the injections, both cell lines were able to produce tumours in a small number of mice. However the greatest change was seen when the WI-38 fibroblasts were used when they were senescent, with over half the mice used producing tumours which were larger than the tumours produced in mice injected with presenescent fibroblasts. A similar trend was mirrored when the mammary epithelial cell line SCp2 was injected into the nipple region of nude mice, with the injection of these cells on their own or with presenescent fibroblasts failing to produce tumours within 120 days. Again, when this cell line was injected with the senescent fibroblasts, large tumours were produced within the observation period in more than 50% of the mice.

Blocking the action of CAFs has been investigated in a xenograft model to assess the impact this has on tumour development and response to treatment [421]. The oral pre-immunisation of BALB/c mice with a DNA vaccine for FAP-α prior to subcutaneous injection of the colorectal carcinoma cell line CT26 or injection of the breast carcinoma cell line D2F2 into the mammary fat pads

significantly reduced the size of the tumours formed in this xenograft model. It was further noted that this reduction was not enhanced by the complementary vaccination against the chemokine CCL21 or IL-2, an inducer of T-cell proliferation. The oral immunisation against FAP-α was also sufficient to reduce the occurrence of lung metastases after the intravenous injection of CT26 cells, where the vaccination was carried out after the introduction of the cancer cells. When this immunisation was carried out in conjunction with doxorubicin (Dox) treatment, a synergistic effect was seen, with the size of tumours drastically reduced when the mice were pre-immunised against FAP-α and treated with Dox after the injection of the D2F2 cells compared to either of the two treatments given separately. In a therapeutic model where the FAP-α immunisation was delivered after the intravenous introduction of the D2F2 cells, again the combined therapy of immunisation and Dox treatment resulted in a significant increase in survival when compared to the single treatment mice, although these single treatment groups themselves had a better outcome than the control group. While there was a marked effect on tumour growth, the treatment of mice with the FAP-α vaccine did not affect the speed of wound closure in the back skin of these mice, suggesting that it is targeting the fibroblasts within the tumours and not the healthy fibroblasts populations elsewhere in the body.

These studies provide evidence to suggest that the inclusion of fibroblasts to provide a stromal equivalent in *in vitro* cancer models would increase the biological relevance of these models and lead them to produce results which are more easily translated into cancer treatments.

6.1.2.3 The immune system can also affect cancer behaviour

6.1.2.3.1 The infiltration of regulatory T-cells into tumours is a marker of patient prognosis

T-cells are one of the many immune cell types that have been implicated in tumour progression and this group of cells is composed of various subsets which can be identified by their cell surface markers. The influence of these different subsets of colorectal cancer patient survival was examined using the CD3, CD8 and CD45RO cell surface markers and the transcription factor FOXP3 to identify all T-cells, cytotoxic T-cells (T_c cells), memory T-cells and regulatory T-cells (Tregs) respectively [75]. This study found that the amount of tumour infiltrating $CD3^+$ cells did not affect either the disease-specific and overall survival, while higher levels of $CD8^+$, $CD45RO^+$ and $FOXP3^+$ cells were correlated with better patient survival. Furthermore, it was also found that that there was a correlation between the infiltration of $CD45RO^+$ cells and the other three cell types examined.

Another study looking specifically at the correlation between Tregs and patient prognosis also found associations between the number of Tregs observed within the tumours and the T-stage of the primary tumour, the involvement of the lymphatic system and the overall disease grading [422]. The tumours with a lower grading or lacking lymphatic involvement were found to have a significantly higher number of Tregs within the tumour. The expression of FOXP3 in the nuclei of the cancer cells was also negatively correlated with lymphatic invasion and tumour grading, with higher levels of expression seen in patients with less developed examples of the disease. In addition to these correlations with tumour grading, this study also demonstrated a correlation with overall patient survival. A higher number of tumour-infiltrating Tregs, a lower number of Tregs in the

tumour epithelium and normal mucosa and a lower level of FOXP3 expression in the cancer cells were all correlated with increased patient survival when evaluated via Kaplan-Meier analysis.

6.1.2.3.2 Macrophages can play a role in metastasis development

Another type of immune cell which has been implicated in cancer is macrophages. Depletion of colony-stimulating factor-1 (CSF-1), a hematopoietic growth factor which directs macrophage differentiation, via anti-sense oligonucleotides is sufficient to limit the growth of embryonal carcinoma xenograft tumours in the testicles of SCID mice [423]. Of the three oligonucleotides tested, each of them demonstrated a different capacity to limit CSF-1 production and this inhibition was directly correlated with the inhibition of tumour growth of seen by either testicular weight or the area of tumour tissue visible on processed slides. The lower levels of CSF-1 expression were also correlated with lower levels of vascularisation of the xenograft and lower expression of the angiogenesis associated proteins VEGF, VEGF receptor 2 (VEGFR-2) and angiopoietin 1 (Ang-1). When these oligonucleotides were tested in a colorectal carcinoma xenograft model, the same pattern of decreased CSF-1 expression and tumour size was also observed. Survival analysis demonstrated that oligonucleotide treatment increased the survival rate, as all control animals has died by 65 days and over 50% of the treated mice survived past 6 months.

Depletion of the liver specific Kupffer cells, a specialised type of macrophages found lining the sinusoids of the liver, also affects the development of liver metastases in a rat xenograft model [424]. This depletion was mediated by intravenous injection of clodronate encapsulated in liposomes and was sufficient to completely eliminate the Kupffer cells in the liver. The rat colon carcinoma cell line CC531 was subsequently injected into the hepatic portal vein to induce the liver metastases and the animals were sacrificed at day 14. The tumours produced in the Kupffer cell depleted rats were larger and occurred at a higher frequency than in the control rats, while the tumours produced in the control rats had a higher amount of immune cell infiltration and desmoplastic reaction from the surrounding tissue.

Like T-cells, the number of macrophages observed within clinical samples of colorectal cancer has been found to be inversely correlated with various markers of tumour progression [425]. The presence of macrophages in the tumour stroma and borders was assessed via expression of the macrophage marker CD68. Higher numbers of $CD68^+$ macrophages in the tumour stroma were observed in tumours with a lower histological grading, those which had no distant metastases and those with a higher level of inflammatory response at the invasive front. These correlations were also seen when the number of macrophages at the tumour border was assessed and there were further correlations between high number of macrophages in this location and those tumours with low TNM grading, no vascular or lymphatic invasion or localised lymph node metastases. The correlation between high macrophage density in the tumour border and the characteristics listed here translate into a correlation with patient survival, with 50% of patients surviving for ~28 months after surgery when a low macrophage number is observed and over 50% of patients surviving over the ~40 month follow up period when a high macrophage number is observed.

The secretion of proteins from tumour infiltrating macrophages is also correlated with colorectal cancer progression. The secretion of the anti-angiogenic MMP-12 is correlated with better patient prognosis, with a 3-year survival rate of 75.86% for those patients with a higher level of MMP-12 compared to 36.00% of those patients with lower MMP-12 expression [426]. This survival analysis

was accompanied by an analysis of the correlation between MMP-12 mRNA levels and clinicopathologic characteristics of the tumours examined. Minimal invasion from the initial tumour site and low levels of lymphatic and vascular invasion were all significantly correlated with higher MMP-12 levels and while fewer microvessels were observed in the low MMP-12 tumours, this decrease was not significant.

6.1.2.3.3 Immune cell involvement has the potential for use in cancer classification

It has recently been proposed that the involvement of the immune system in cancers could be used as a method of classification of the disease, in a similar way that information about the differentiation of cells within the tumour or the mutation status of key genes is used to supplement the AJCC/UICC classification, and a proposal has been made following research on the prognostic importance of T-cells infiltration into tumours [427]. Some of the research drawn on by this article includes studies which have confirmed that high Treg infiltration is positively correlated with patient survival [75, 428, 429] and that low T_c cell involvement is correlated with patient relapse [430]. Taken together with the general correlation between high numbers of T-cells and patient survival, as assayed by CD3 staining [429, 431], Galon *et al*. propose that an 'immunoscore' devised from the staining of histopathological samples for a combination of CD3, CD8 and CD45RO to determine the density of T-cells and specifically T_c and Treg cells within different areas of the tumour has the potential to be a simple diagnostic tool to be used in conjunction with the standard TNM grading system to provide a clearer picture of patient prognosis.

6.1.2.4 *In vitro* co-cultures highlight the biological relevance of stromal cells to cancer models

With the emergence of data highlighting the influence that secondary cell types have on tumours, there have been developments in *in vitro* research to develop models which incorporate these additional cells in order to increase the biological relevance of the models.

6.1.2.4.1 In vitro *models can utilise conditioned media to examine the role of soluble factors in the directing of cancer cell behaviour*

One of the easiest ways of modelling the interactions between two cell populations is to investigate the role that secreted factors have on the behaviour of the cell type of interest. There are many examples of conditioned media being used to determine the effect that additional cell types can have on tumour cells in *in vitro* culture. One such example is the use of conditioned media from human pancreatic stellate cells (HPSCs) to culture human pancreatic cancer cell lines and examine for any resulting change in cell behaviour [432]. It was observed that the addition of the HPSC conditioned media resulted in dose dependent increase in the proliferation, invasion through Matrigel and colony formation on soft agar of the cells, over the serum free media controls. In some cases, the increase seen with the addition of the highest concentration of conditioned media was comparable with the increase induced by the addition of 10% FCS to the culturing medium. However, in other examples, such as the invasion of the Panc1 cell line, there was a significant difference between the conditioned media and the FCS media, with the conditioned media inducing a higher invasive response than the FCS. The apoptotic response of the BxPC3 cell line in response to chemotherapy treatment gemcitabine or radiation treatment was also measured when

the cells were cultured in serum free or conditioned media, with the conditioned media providing protection against apoptosis in both cases.

Another method of analysing the soluble factors involved in cell-cell interactions is to grow the two cell lines as segregated co-cultures, with the cell lines usually separated by a Transwell® insert or similar. This method has been used to access the impact of MSC co-culture on the characteristics of colorectal cancer cell lines [235]. The cancer cells grown in the co-cultures have a different morphology compared to the cancer cells which had been cultured in media alone, with the HCT116 and HT29 cell lines adopting an elongated shape in response to the MSCs, while the LS180 cells formed spheroid-like structures in the co-cultures. Regardless of the morphological response, the expression levels of proteins which are associated with EMT were found to be significantly altered by the introduction of the MSCs, with E-cadherin expression downregulated and the upregulation of the EMT associated transcription factors Twist, Snail1 and Slug in all three cancer cell lines. As a result, the colorectal cancer cells which had been maintained as co-cultures were found to be more invasive in a Matrigel-coated Transwell® model. It was further noted that these alterations in cell behaviour were due to an increase in surface bound TGF-β on the cancer cell lines after co-culture, as alterations to gene expression induced by the co-culture were reversed by the use of TGF-β inhibitors latency-associated peptide or SB431542.

Opposite trends in terms of cell migratory behaviour were observed with the segregated co-culture of the hepatocellular carcinoma cell line Bel-7402 with either the endothelial cell line RF/6A or the normal liver cell line HL-7702 [433]. After co-culturing with either of these two cell lines, the Bel-7402 cells were removed from the 0.4μm pore inserts and subjected to migration and invasion assays on 8μm Transwell® insert in the absence and presence of a Matrigel coating. In all cases, the migratory capacity of the Bel-7402 was significantly inhibited after co-culture and this inhibition was seen after the co-cultures had been maintained for a variety of time periods. Protein analysis via Western blots and immunofluorescence staining demonstrated that the co-cultured Bel-7402 cells expressed a greater amount of E-cadherin and a decreased amount of F-actin, which the authors of this paper considered was sufficient to account for the impaired motility of these cells. In contrast, the culture of the Bel-7402 cell line with conditioned media from the lung fibroblast cell line MRC-5 induced a distinct change in Bel-7402 cell morphology, with the cells adopting a more rounded phenotype. These cells demonstrated a significant increase in motility when subjected to Transwell® assays and immunofluorescence analysis highlighted that the actin cytoskeleton in these cells had adopted a morphology more commonly seen in highly motile cells with many protrusions from the main cell body. The authors of this paper hypothesise that the MRC-5 cells were able to induce EMT in the Bel-7402 cells due to their production of HGF, which was not seen with either the RF/6a or HL-7702 cell lines.

The segregated co-culture of the colonic fibroblast cell line CCD-18Co with the two colorectal cancer cell lines SW480 and SW620 showed that the presence of the cancer cell lines could also affect the behaviour of the fibroblast cell line [434]. In standard monolayer culture, the CCD-18Co cells had a mixed morphology of spindle-like and rounded cells, with the amount of spindle-like cells decreasing over the 72 hour culture period which was coupled with a significant reduction in cell viability when compared to the viability at 24 hours of culture. In contrast, when maintained in co-culture, a higher percentage of the CCD-18Co cells had the spindle-like morphology and

retained this throughout the culture period. The co-culture was also beneficial to the viability of the fibroblasts, as this did not significantly alter over the 72 hour culturing period. The improved maintenance of the fibroblast cultures was due to a decrease in cells undergoing apoptosis when maintained in co-culture and an increase in the percentage of cells found in the G1 phase of the cell cycle. In addition to the changes in the proliferative behaviour of the CCD-18Co cells, the co-culture also induced changes in the expression of VEGF mRNA in these cells. While the CCD-18Co cells expressed a higher level of VEGF mRNA in monolayer cultures than either the SW480 or SW620 cell line, this expression was significantly increased in the co-cultures, with the SW620 cell inducing a greater increase than the SW480 cell lines. In contrast, only the SW620 cells demonstrated a more modest increase in VEGF mRNA expression in co-cultures when compared to the monolayer cultures.

These experiments using conditioned media or segregated co-cultures demonstrate that soluble factors secreted from both cancer and secondary cell types can influence many aspects of cell behaviour. However, cancers occur in a microenvironment where they grow along side and in contact with secondary cell types and so modelling the physical interactions between these cells would provide a more relevant model.

6.1.2.4.2 In vitro *models utilising gels in addition to co-culture can develop structures which mimic the* in vivo *situation*

While experiments which utilise the soluble factors produced by additional cell types to influence cancer cell behaviour model a more complex cellular environment, these experiments are generally carried out in standard 2D culture conditions, which mean that cells are still subjected to the unnatural culture conditions that this imposes. Another approach is to adapt 3D models of cancer to incorporate a co-culture element. One example of this is the adaption of the tumour spheroid model to allow two spheroids, one consisting of breast tumour cells, the other of fibroblasts, to invade into each other [435]. However, as observed from the phase-contrast and immunohistochemical images presented in this paper, the result of this appears to be the engulfing of one spheroid by the other so that when the cells are stained for fibronectin to highlight the fibroblasts or cytokeratin 18 to highlight the breast cancer cells, the two stains are not found to overlay each other and there is a distinct boundary between the expressing and non-expressing cells. However, this paper does highlight that different breast cell lines exhibited varying behaviour in terms of the infiltration of the fibroblast spheroids.

Another model which mimics a 3D environment to study the migratory ability of cancer cells is one which supplements collagen I gels with Swiss 3T3 fibroblasts and plates the cancer cells either directly on top of the gel/fibroblast base or on top of an intervening collagen I layer [436]. This model was used to demonstrate that the oral epithelial cancer cell lines YD-10B and YD-38 would only infiltrate the collagen I gel when fibroblasts were present within it. This behaviour was seen in conjunction with an increase in expression of both MMP-2 and MMP-9 mRNA when the oral cancer cell lines were co-cultured adjacent to fibroblast containing collagen I, as opposed to cell-free collagen I gels or those where there was an intervening layer of collagen I. This change in MMP expression levels in 3D co-cultures was mimicked in the mixed and segregated 2D co-cultures of these cell lines, with the mRNA expression of both MMP-2 and MMP-9 found to be higher in the co-cultured YD-10B and YD-38 cells than in the monolayer cultured YD-10B or YD-38 cells. This data

supports the hypothesis that the fibroblast compartment of tumours plays a vital role in the migration of cancer cells by inducing changes in the expression of genes within the cancer cells.

An extension of this method using collagen I gels is the study by Nyga *et al*. which documents the creation of an artificial cell mass (ACM) and the subsequent culture of this in a collagen I hydrogel containing fibroblasts and/or endothelial cells [193]. The ACM was generated by suspending HT29 colorectal carcinoma cells in a collagen I hydrogel and then compressing this gel to increase the stiffness of the collagen so that it more closely mimicked the denser collagen I fibres seen in tumours. The ACMs were then cut to a standard size of 5.5 x 10 x 10 mm and embedded into collagen I gels with or without a secondary cell type. When subjected to this type of 3D culture, the centre of the ACM reached hypoxic conditions faster than the outer edges of the ACM and the growth of the HT29 cells was decreased compared to standard 2D monolayer cultures. Over the course of 21 days culture in an acellular collagen I gel, the HT29 initially migrated towards the edge of the ACM before breaking into the surrounding collagen I gel as tumour spheroids. The inclusion of fibroblasts in the surrounding collagen I gel resulted in a contraction of this gel, even in the presence of endothelial cells, although in this case it was to a lesser extent, which resulted in smaller spheroids migrating out of the ACM at 21 days. As the hypoxic environment in the ACM was thought to be a large driving factor in the migration of the HT29 cells, the expression of VEGF in these cultures was examined and positive staining was observed via immunofluorescence at day 14 and 21 of culture.

These studies demonstrate that there is a move toward developing in *vitro* models which incorporate additional aspects of the tumour microenvironment, be it ECM proteins or supplementary cell types, which are better representative of the situation *in vivo*. Therefore the 3D *in vitro* model under development here will be assessed for it potential to allow the incorporation of ECM and co-culture components to better model the cancer microenvironment.

6.2 Chapter Aims

This Chapter aims to assess the potential of including ECM and co-culture components in the 3D *in vitro* migration assay under development in this project by looking at protein coatings and co-culture with a stromal equivalent. These basic assays will help to determine whether this system can be developed into a model of greater biological significance taking into account ECM and alternative cell types. This is an important step toward recreating a cancer tissue-like microenvironment *in vitro*.

6.2.1 Objectives

Overall, the aims of the assessment of assay adaptability in this Chapter will be investigated by:

- Assessing the feasibility of the utilisation of ECM coatings of collagen I and fibronectin for the culture of colorectal cancer cells in the 3D model;
- Assessing the impact that these coatings, if successful, have on the behaviour of the colorectal cancer cells in the 3D model;
- Assessing the feasibility of the adaption of the 3D migration assay to include a stromal equivalent for co-culture;
- Comparing the *in vitro* 3D cultures obtained with ECM coating and co-cultures to patient samples to investigate if the increased biological relevance of the 3D model produces cultures with protein expression patterns which are closer to those seen in tumour samples.

6.3 Results

6.3.1 ECM coatings effect cell behaviour in a 3D model

Collagen I and fibronectin have both been identified as the ECM proteins which have altered expression level and distribution in colorectal cancer progression [79, 378, 381, 382]. They have therefore been selected as ECM components to assess the impact of incorporating a protein coating into the 3D migration model herein.

6.3.1.1 ECM coatings affected cellular distribution in 3D culture

When cultured on 3D scaffolds which had been pre-coated which either 0.8µg/ml rat-tail collagen I or 1.0µg/ml bovine plasma fibronectin both the SW480 and SW620 cell lines demonstrated altered distribution on Alvetex® Scaffold after 10 days of culture. As previously observed on uncoated scaffolds, the SW480 cell line was found to be distributed across the entire width of the scaffold, however the growth of these cells did not form a continuous layer across the material (Figure 6.2A). When cultured on either collagen I or fibronectin (Figure 6.2C & E), the SW480 cells maintained a distribution across the entire length of the material as seen with the cultures on uncoated scaffolds. In contrast, cell cultures on coated scaffolds produced a cellular distribution which was found to be more consistent over the width of the material. Interestingly, the depth of growth did not appear to differ from that observed in the cultures on uncoated scaffolds.

The culture of the SW620 cell line on coated scaffolds demonstrated that this cell line was more sensitive to the presence of protein coatings than the SW480 cell line. As expected, on uncoated scaffolds the SW620 cell line mainly grew as single cells scattered throughout the width and depth of the material (Figure 6.2B). However, when a coating of collagen I was present, the behaviour of these cells was altered, with two distinct behaviours observed within each sample. On the collagen I coated scaffolds, the SW620 cells were observed as growing in tight clusters on top of the collagen I coating at the top of the material or they had grown through the collagen I and were seen to penetrate into the scaffold as previously observed (Figure 6.2D). In contrast, the pre-coating of Alvetex® Scaffold with fibronectin did not lead to the SW620 cells growing in clusters at the top of the material and the cells were observed to be spaced more evenly within the material when compared to the uncoated scaffolds (Figure 6.2F).

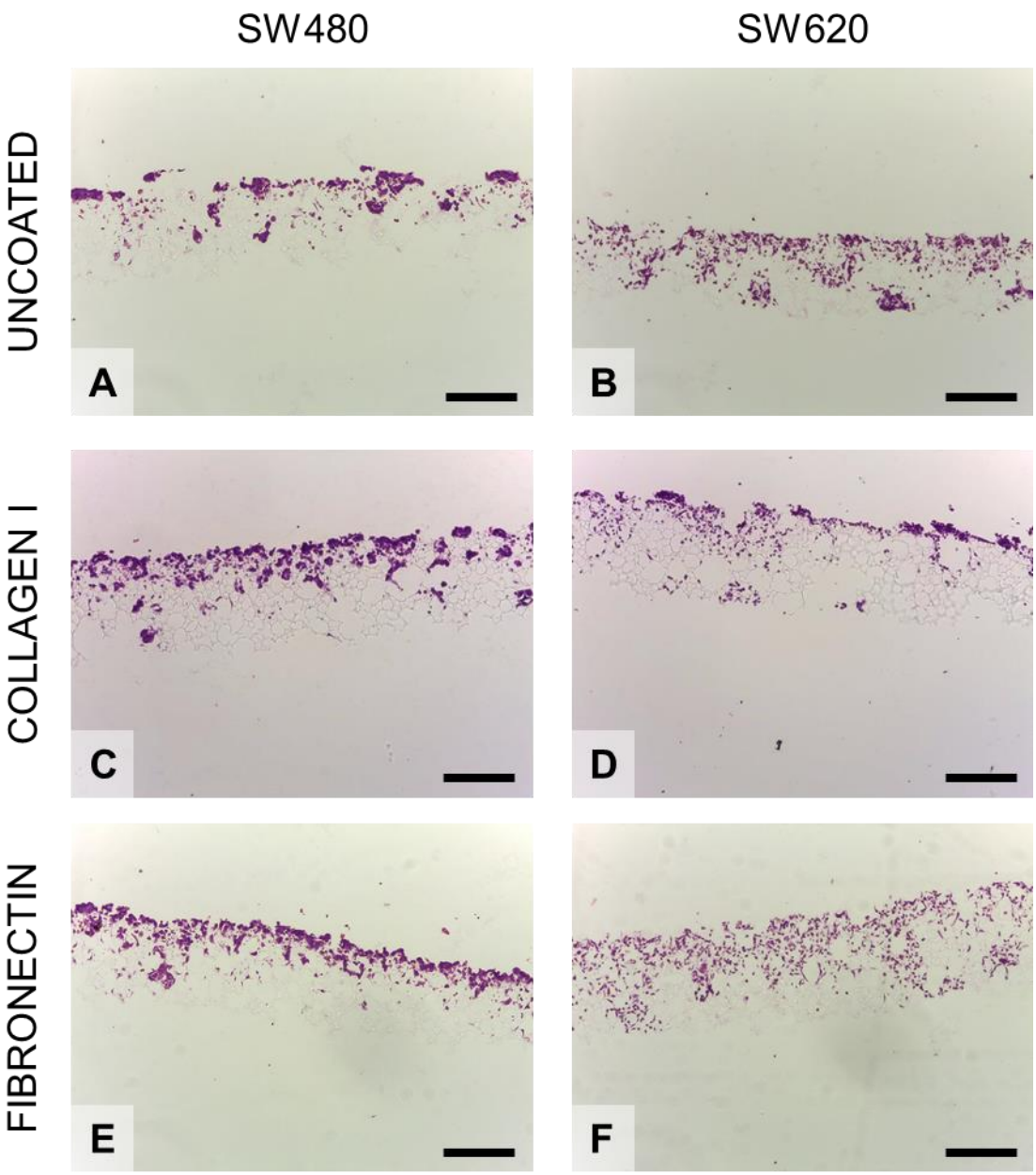

Figure 6.2: Both the SW480 and SW620 cell lines displayed an altered cell distribution when cultured on collagen I or fibronectin coated scaffolds. H&E images of 10 day cultures on A and B: uncoated, C and D: collagen I coated and E and F: fibronectin coated scaffolds for both cells lines. Scale bars = 200μm for all images.

The observed differences in cellular distribution of the SW480 and SW620 cell lines when cultured on uncoated and coated scaffolds were reflected in the observed cell penetration achieved by each cell line over the 10 day culture period, with a significant difference seen between the two cell lines, ANOVA, $F(1,12)=13.025$, $p=0.004$. When the cell penetration achieved by the SW480 cell line was quantified, there was a small, but not significant, 20% decrease in cell penetration on the collagen I coated scaffolds, whereas the SW480 cells cultured on fibronectin coated scaffolds achieved a significant 27% increase in cell penetration (Figure 6.3A). In comparison, the depth of cell penetration attained by the SW620 cell line was not significantly affected by the protein pre-coating of the scaffold, with the cell penetration decreased by 14% on collagen I and increased by 13% on fibronectin coated scaffolds, compared to uncoated scaffolds (Figure 6.3B). The main variation to note between the three coating tested is that the cell penetration of the SW620 cell line measured on the collagen I coated scaffolds was found to be more variable than that measured on the uncoated or fibronectin coated scaffolds, as seen here by the increased size of the error bars for this data set compared to the other conditions. This variability is likely to be due to the two behaviours observed, with the collagen I restricting penetration into the scaffold in some areas and allowing penetration in others.

6.3.1.2 ECM coatings affected the proliferation of colorectal cancer cells in a 3D model

When the apparent cell viability of the 3D cultures was examined using the MTT Cell Viability Assay, the addition of an ECM pre-coating was seen to have a significant effect on viability overall, ANOVA, $F(2,12)=33.866$, $p<0.001$. It was also observed that a coating of collagen I negatively affected the viability of 3D cultures of both the SW480 and SW620 cell lines (Figure 6.4). With both cell lines, the cell viability was significantly decreased for cultures grown on scaffolds which had been pre-coated with collagen I, when compared to uncoated controls, whereas a pre-coating of fibronectin did not affect the viability of the 3D cultures of either cell line.

The assessment of the number of cells present in the material after 10 days of culture also highlighted that the pre-coating of Alvetex® Scaffold had a significant effect on cell number, ANOVA, $F(2,12)=12.548$, $p=0.001$. The number of SW480 cells found in the material was significantly reduced when the cultures had been maintained on ECM pre-coated scaffolds compared to uncoated control scaffolds, with a collagen I coating resulting in a greater decrease than a fibronectin coating (Figure 6.5A). However, there was no significant variation in cell number for the SW620 cell line cultured on uncoated and coated scaffolds, although a small, non-significant dip in cell number was observed with the collagen I coated scaffolds (Figure 6.5B), with the SW620 cell line maintaining a higher cell number overall, ANOVA, $F(1,12)=142.522$, $p<0.001$.

6.3.1.3 ECM coatings significantly affected cell attachment

Coating of scaffolds with ECM components has been shown to affect the resulting viability and cell number of SW480 and SW620 cells cultured for 10 days. The attachment of cells was then investigated as a potential cause for this difference. The cells were seeded onto uncoated and coated scaffolds as before and assessed after 24 hours of culture to determine if the ECM coatings had an effect on the attachment of either the SW480 or SW620 cell lines to the material.

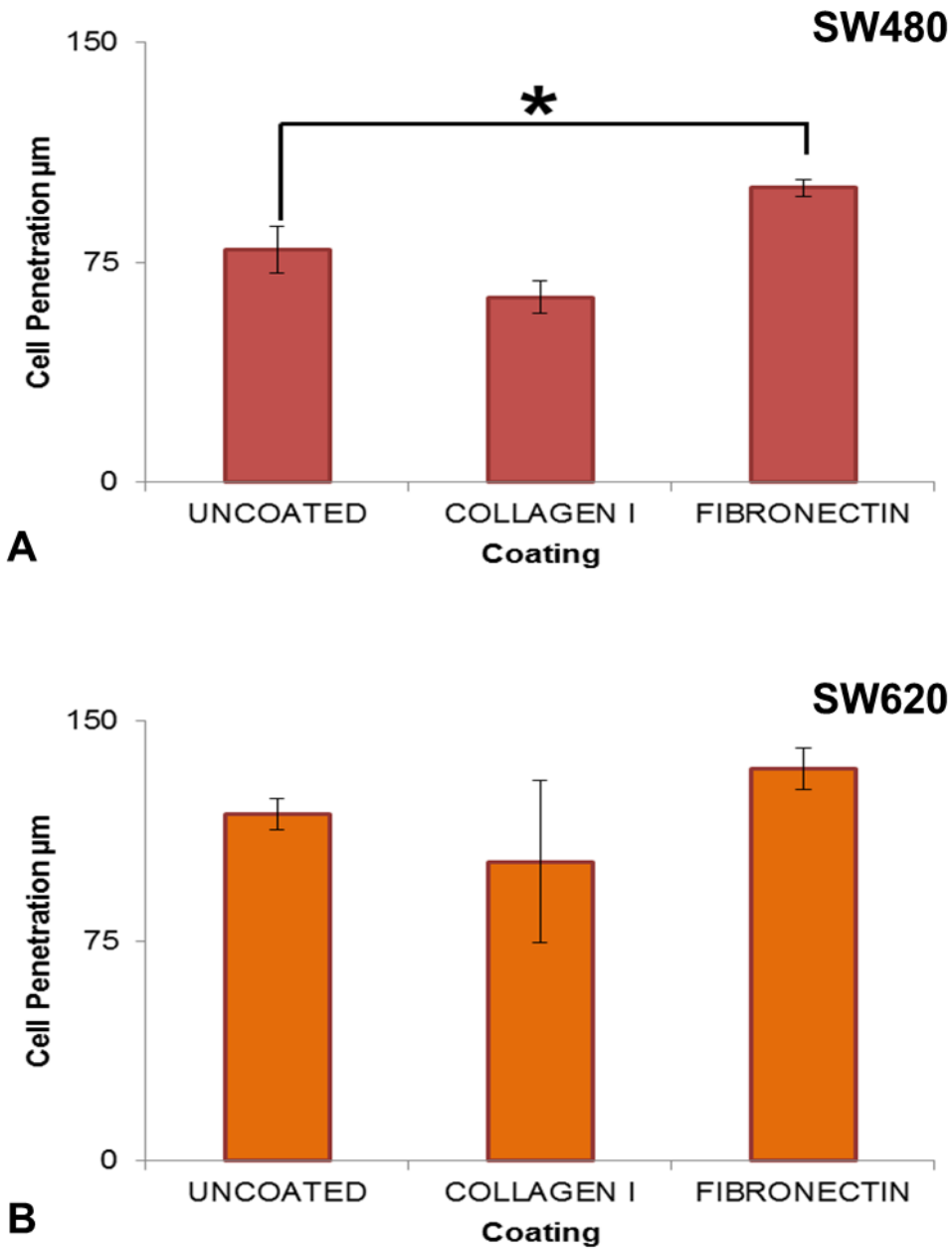

Figure 6.3: The 3D cell penetration of the SW480 cell line was increased when the scaffolds were fibronectin coated, while penetration of the SW620 cell line remained unaffected. Cell penetration in µm of A: SW480 and B: SW620 cells after 10 days of 3D culture, as determined by the linear measurement method. Data represent mean, n = 3, ±SEM for both graphs, * $p < 0.05$ by a Dunnett's t-test.

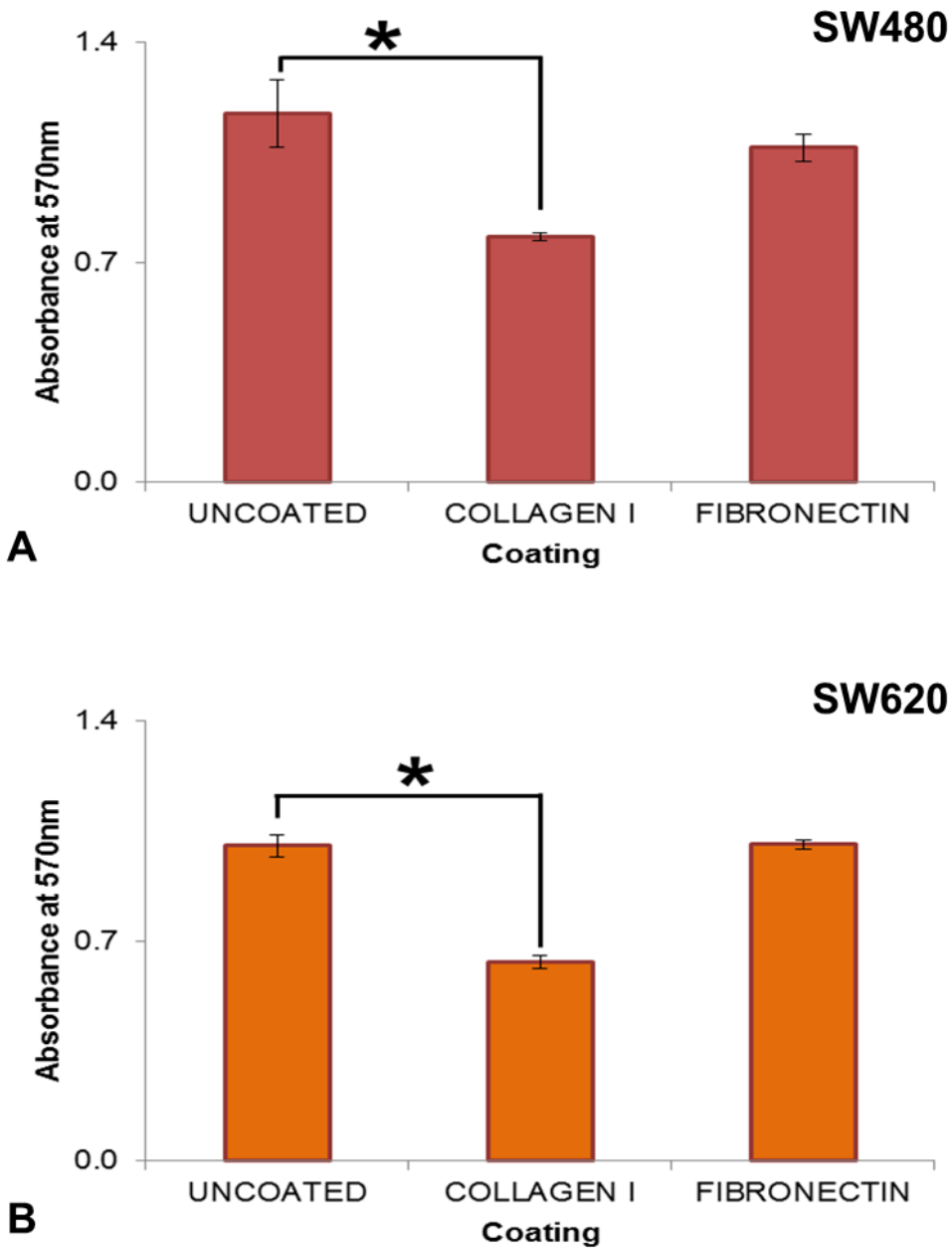

Figure 6.4: The 3D cell viability of both the SW480 and SW620 cell lines was decreased following culturing on collagen I coated scaffolds. Absorbance at 570nm of A: SW480 and B: SW620 cells after 10 days of 3D culture, as determined by the MTT Cell Viability Assay. Data represent mean, n = 3, ±SEM for both graphs, * $p < 0.05$ by a Dunnett's t-test.

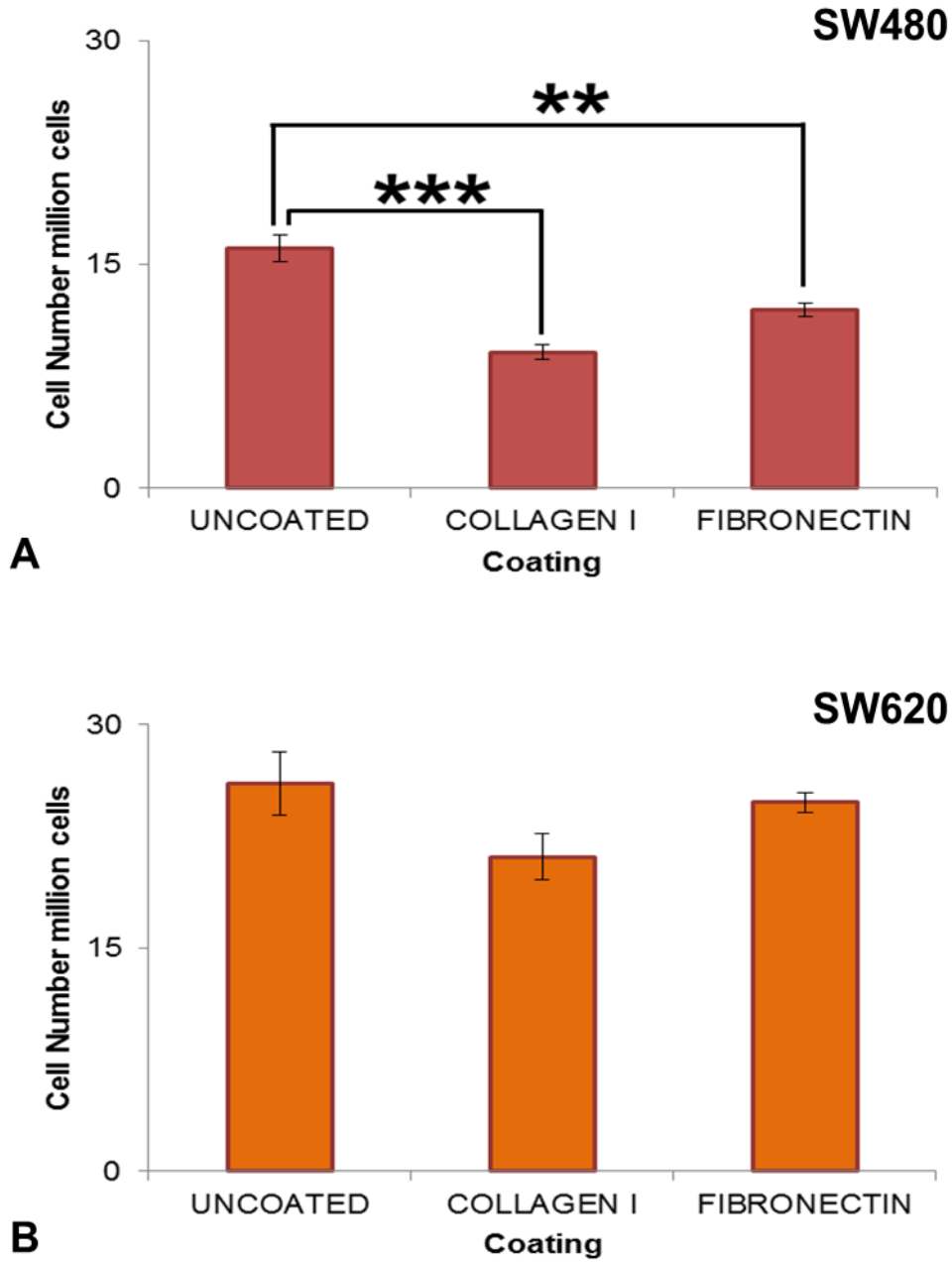

Figure 6.5: The number of SW480 cells in the 3D material was decreased both the presence of both collagen I and fibronectin, while the SW620 cell line remained unaffected. Cell number in millions of cells of A: SW480 and B: SW620 cells after 10 days of 3D culture, as determined by the Pico Green dsDNA Assay. Data represent mean, n = 3, ±SEM for both graphs, ** $p < 0.01$, *** $p < 0.005$ by a Dunnett's t-test.

When samples which had been fixed and prepared for histological examination were imaged, a small number of cells were observed to be attached to the material for all conditions (Figure 6.6). The distribution of the SW480 cells appeared to be unaffected by the presence of ECM coating, with a small number of cells visible in the top quarter of the material regardless of the type of coating present (Figure 6.6A, C & E). The distribution of the SW620 appeared to be affected by a pre-coating of collagen I, but not by fibronectin, as the cells were observed on the top seeding surface of collagen I coated scaffolds (Figure 6.6D), but were seen distributed throughout a greater proportion of the depth of the material on either the uncoated or fibronectin coated scaffolds (Figure 6.6B & F). Additionally, there appears to be a variation in the attachment of the two cell lines, with more SW480 cells visible on the material at 24 hours than SW620 cells.

The observed variation in cell attachment between the SW480 and SW620 cell lines was also reflected in the cell viability data, as the SW480 cells produced a higher reading than the SW620 cells after 24 hours (Figure 6.7), ANOVA, $F(1,12)=11.106$, $p=0.006$. As expected from the consistent cellular distribution seen in the SW480 cultures, the level of cell viability did not vary between cultures with the various protein coatings (Figure 6.7A). In contrast, the observed difference in the depth distribution of the SW620 cells on collagen I coated scaffolds was not reflected in the MTT data, with no significant variation seen between all cultures (Figure 6.7B).

The assessment of the number of attached cells after 24 hours highlighted a significant difference between the cultures grown on different coatings, ANOVA, $F(2,12)=8.396$, $p=0.005$; in addition to a significant difference between the number of SW480 or SW620 cells attached to the scaffolds, ANOVA, $F(1,12)=5.670$, $p=0.035$ (Figure 6.8). For both cell lines, there was a non-significant drop in the number of cells attached to collagen I coated scaffolds when compared to either uncoated or fibronectin coated scaffolds, with a comparable number of cells attached to either of these scaffolds.

Together these data show that the pre-coating of Alvetex® Scaffold significantly affected the attachment of the SW480 or SW620 cell lines over a 24 hour period. Differences in the number of SW480 cells after 10 days of 3D culture may also be due to changes in the proliferative behaviour of the attached cells. This is further confirmed when the cell number data after 24 hours and 10 days is used to calculate the population doubling times using the equations given by Hayflick in 1973 [217]. On uncoated scaffolds, the SW480 cell line achieved a generation time of 55 hours. This was extended on collagen I and fibronectin coated scaffolds to 58 and 68 hours respectively, demonstrating that the SW480 cells proliferate at a slower rate on protein coated scaffolds. The SW620 cell line demonstrated a faster rate of proliferation than the SW480 cell line, with a generation time of 43 hours on uncoated scaffolds. Again, the rate of proliferation was altered when the cells were cultured on pre-coated scaffolds, with the cells cultured on collagen I coated scaffolds achieving a generation time of 40 hours, while those cultured on fibronectin scaffolds achieve a generation time of 45 hours. This data correlates with the 2D generation times for these cell lines, 28 and 26 hours for SW480 and SW620 respectively as shown in Chapter 3, with the SW620 cell line maintaining a quicker rate of cell proliferation than the SW480 cell line for all conditions, however it also highlights that subjecting these cells to 3D culture decreases the rate of proliferation, a phenomena which has been noted in many different systems [165].

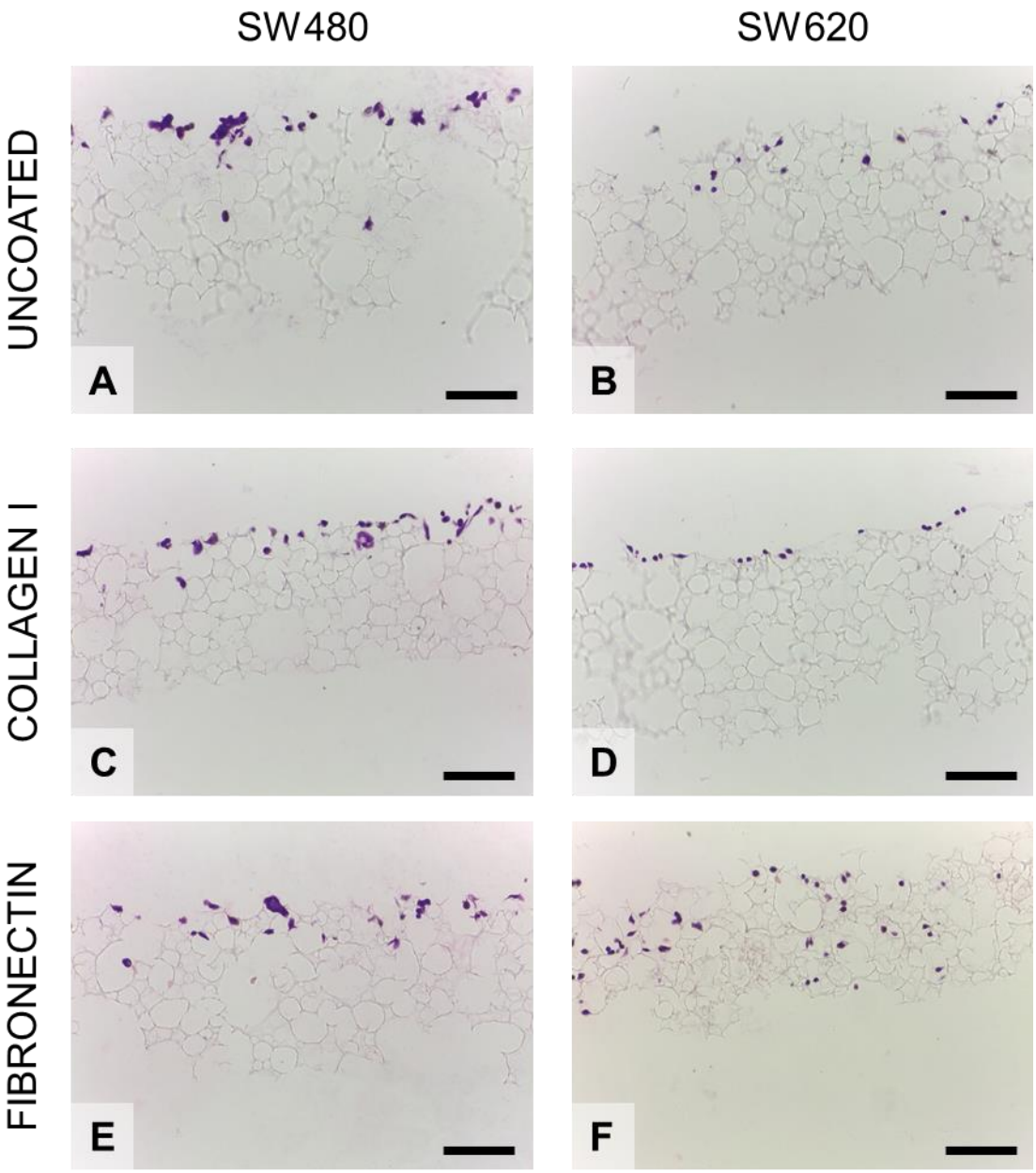

Figure 6.6: Both the SW480 and SW620 cell lines displayed attachment to the scaffolds after 24 hours on uncoated and collagen I or fibronectin coated scaffolds. H&E images of 24 hours cultures on A and B: uncoated, C and D: collagen I coated and E and F: fibronectin coated scaffolds for both cells lines. Scale bars = 100µm for all images.

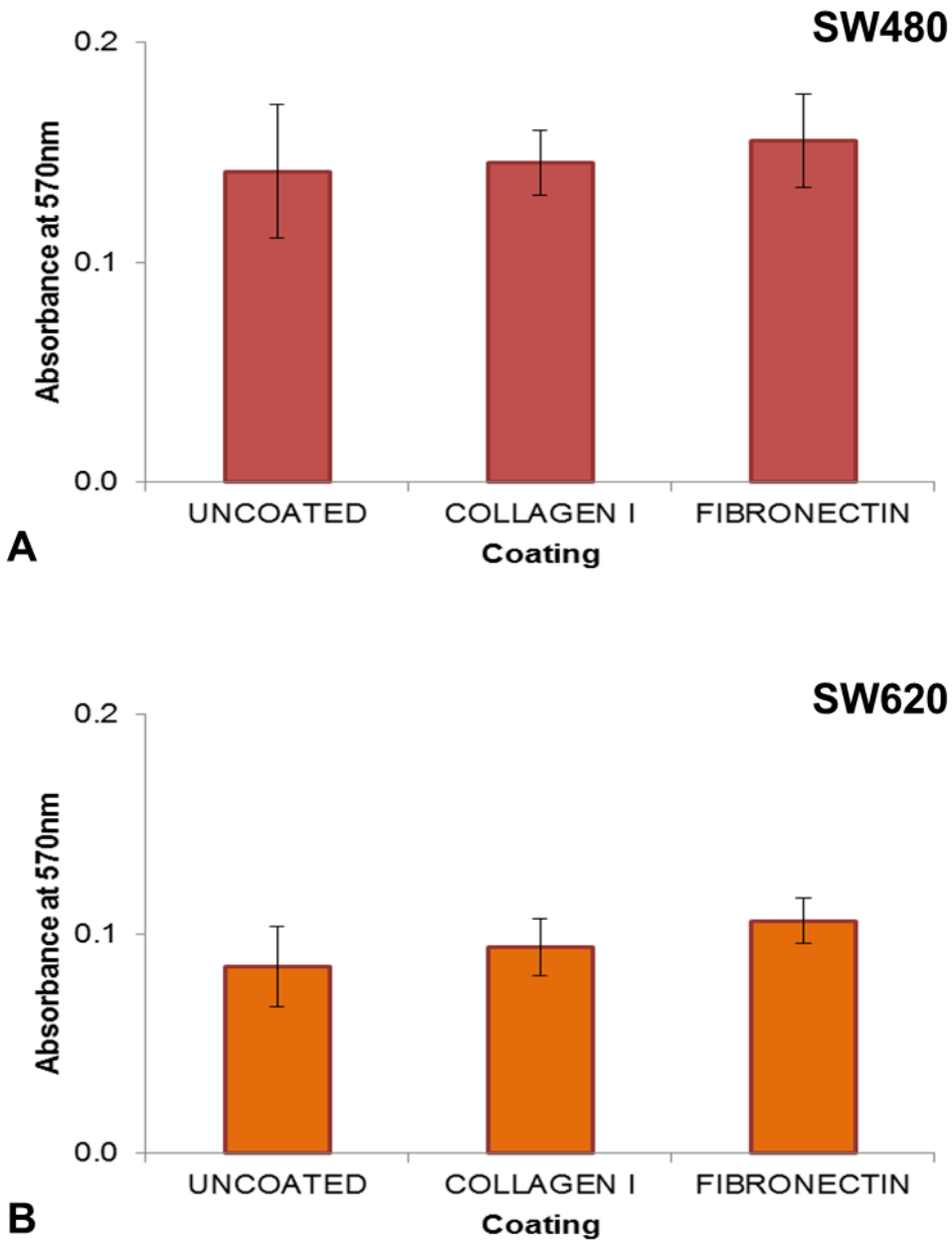

Figure 6.7: The 3D cell viability of both the SW480 and SW620 cell lines was unaffected by scaffold coating. Absorbance at 570nm of A: SW480 and B: SW620 cells after 24 hours of 3D culture, as determined by the MTT Cell Viability Assay. Data represent mean, n = 3, ±SEM for both graphs, no significance by a Dunnett's t-test.

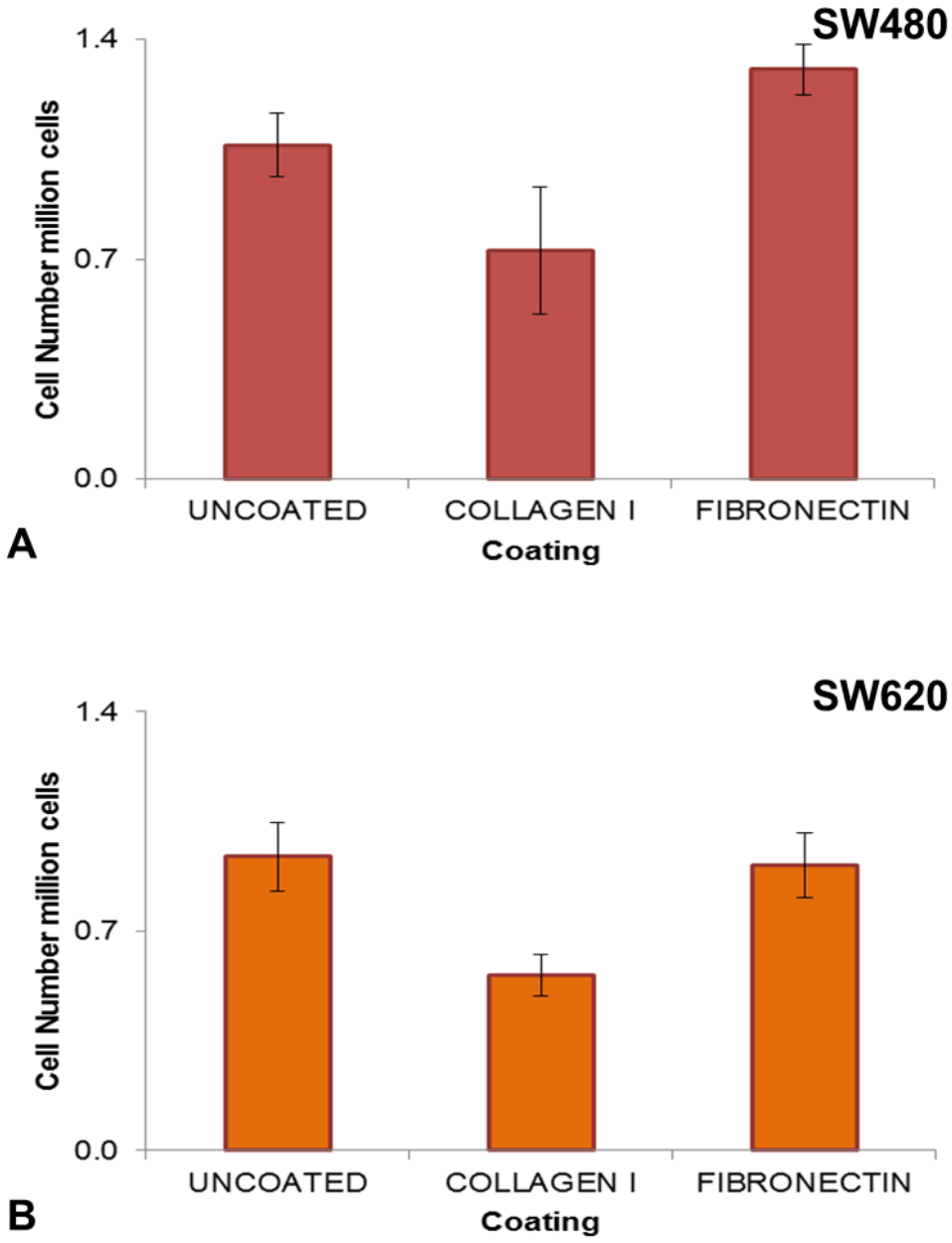

Figure 6.8: The number of SW480 and SW620 cells in the 3D material was unaffected by scaffold coating. Cell number in millions of cells of A: SW480 and B: SW620 cells after 24 hours of 3D culture, as determined by the Pico Green dsDNA Assay. Data represent mean, n = 3, ±SEM for both graphs, no significance by a Dunnett's t-test.

6.3.2 Characterisation of the growth of a stromal equivalent for the 3D model

Following the demonstration that this model can be adapted to incorporate an ECM-like component by pre-coating Alvetex® Scaffold with collagen I or fibronectin prior to culture of the SW480 or SW620 cell line, the potential of this model to incorporate a co-culture element will now be examined. As the seeding and culture of the murine embryonic fibroblast cell line NIH/3T3 on Alvetex® Scaffold has already been established [278], this cell line will be used to provide a stromal equivalent for the assessment of co-cultures on Alvetex® Scaffold.

6.3.2.1 Alvetex® Scaffold appeared to support the co-culture of colorectal cancer cell lines with NIH/3T3 fibroblasts

When cultured on Alvetex® Scaffold, the NIH/3T3 cell line adopts a cell distribution which differs greatly from the cell distribution observed with either the SW480 or SW620 cell lines. After 7 days of culture, the NIH/3T3 cells are seen to have a sparse distribution throughout the entire depth of the material, with the cells found at a higher density at the top and bottom surfaces of the material (Figure 6.9A) and this higher density of cells at the top and bottom surfaces does not appear to differ between the seeding and non-seeding surface. This distribution of cells is maintained across the diameter of the disc where the initial 100µl seeding dose was applied in a concentrated manner, with very few cells observed at the very edge of the material beyond the seeding area.

When the colorectal cancer cell lines were seeded on top of this fibroblast culture and maintained for a further 7 days, an altered cell distribution was observed (Figure 6.9B & C). In the case of both the SW480 and SW620 cell lines, there appears to be a denser layer of cell growth at the seeding surface of the material. In the case of the SW480 cell line this additional cell growth took the form of dense groups of cells with apparent areas between where fewer cells are growing on top of the fibroblast layer (Figure 6.9B), while the SW620 cell line appeared to grow as rounded cells in a continuous layer across the fibroblast culture (Figure 6.9C).

However, as this analysis was carried out on histologically stained samples, the distinction between the fibroblast and colorectal cancer cells was not clear and thus it was hard to determine the extent to which the cancer cell line had infiltrated into the stromal equivalent. To overcome the problem with identifying the colorectal cancer cell lines from the fibroblast cells, a commercially available variant of the NIH/3T3 cell line was obtained, the NIH3T3/GFP cell line, which has been transfected to stably express the GFP protein when cultured in media containing the selection antibiotic Blasticidin. These two cell lines were subsequently assessed to see if they retained comparable culturing properties in 2D and 3D culture with a view to culturing the NIH3T3/GFP cell line for culture on Alvetex® Scaffold in the same manner that the NIH/3T3 cell line is cultured.

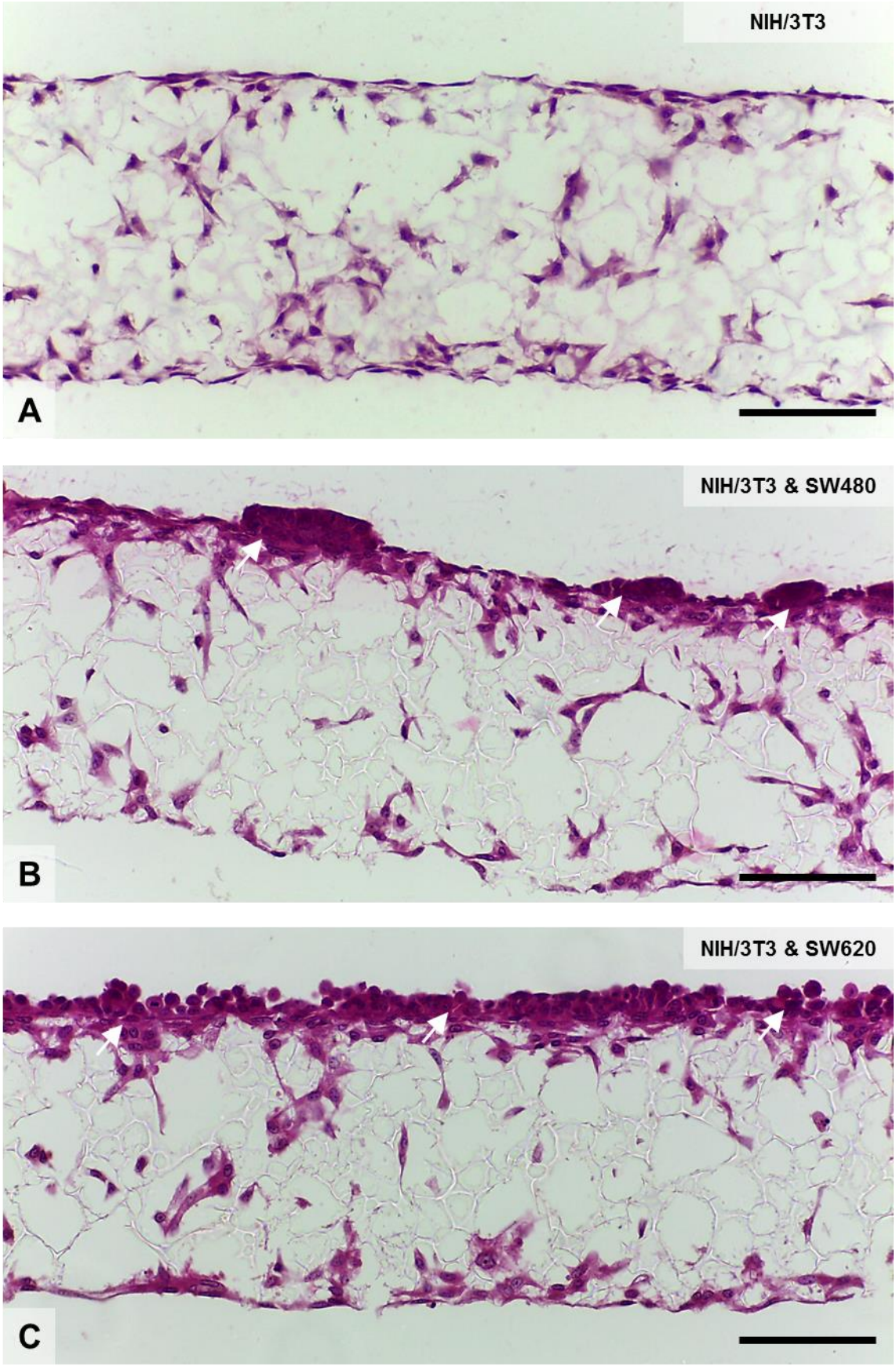

Figure 6.9: Alvetex® Scaffold could support co-cultures of NIH/3T3 cells with both the SW480 and SW620 cell lines. H&E stained images of scaffolds which had been cultured for 7 days with A: NIH/3T3 cells only or scaffolds which had been cultured for 7 days with NIH/3T3 cells and 7 days with B: SW480 and C: SW620 cells, with the probable location of cancer cells indicated by arrows. Scale bars = 100µm for both images.

6.3.2.2 Both the NIH/3T3 and NIH3T3/GFP cell lines have a similar 2D morphology

When maintained in standard 2D culture the NIH/3T3 cell line adopted the characteristic spindle-like morphology which is commonly associated with fibroblasts (Figure 6.10A & B). The NIH3T3/GFP also adopted this morphology in 2D culture (Figure 6.10C & D); although the individual cells of this cell line appeared to be slightly smaller than the NIH/3T3 cell line. When the monolayer cultures of the NIH3T3/GFP cell line was imaged using a filter for GFP fluorescence, the GFP protein was clearly visible throughout the cytoplasm of the NIH3T3/GFP cells and no cells in these cultures were observed to be present without expressing the GFP protein (Figure 6.10E & F).

In addition to the morphological similarities between these two cell lines, both exhibited contact inhibition of growth once the monolayer cultures reached a high level of confluency. However, while the NIH/3T3 cell line stopped proliferating at this point, the NIH3T3/GFP cell line lost adhesion to the culture flask and lifted off as a large sheet of cells into the culture media. This demonstrates that the NIH3T3/GFP cell line may be more sensitive to overgrowing in standard 2D cultures.

6.3.2.3 The NIH3T3/GFP cell line had a faster rate of proliferation in 2D culture than the NIH/3T3 cell line

The maintenance of the NIH/3T3 and NIH3T3/GFP cell lines in standard 2D culture for up to 7 days highlights further differences between these two cell lines. The counting of cells trypsinised from monolayer cultures demonstrated that the rate of proliferation is different for each of these cell lines. The NIH/3T3 cell line was seen to steadily increase in number from the initial 0.25×10^6 seeded into a T25 flask over the whole of the 7 day period, with an average of 6.73×10^6 cells found by day 7 (Figure 6.11A). However, the NIH3T3/GFP cell line was seen to increase in number at a faster rate, with the population peaking at 7.96×10^6 cells by day 5 of culture (Figure 6.11B). As this produced a monolayer culture which was nearly 100% confluent, these monolayers lifted off the culture plastic, such that very few cells were found remaining attached by 7 days of culture.

When the cell counts for the NIH/3T3 and NIH3T3/GFP cell lines at day 5 were compared and subjected to Hayflick's equations for calculating the rate of population doubling of cells in culture [217], the difference in proliferation rates is clearly seen. The NIH/3T3 cells were found to double once every 27 hours, whereas the NIH3T3/GFP cells were doubling once every 24 hours.

This difference in proliferation between the two cell lines also had an effect on the viability of the 2D cultures of NIH/3T3 and NIH3T3/GFP cells. The viability of NIH/3T3 cell line was seen to steadily increase over the whole 7 day culture period (Figure 6.12A), in line with the increasing cell number previously noted. In contrast, the NIH3T3/GFP cell line exhibited a crash in cell viability after 3 days of culture (Figure 6.12B), demonstrating that the monolayer culture was losing viability as the culture became 100% confluent in the culture flask.

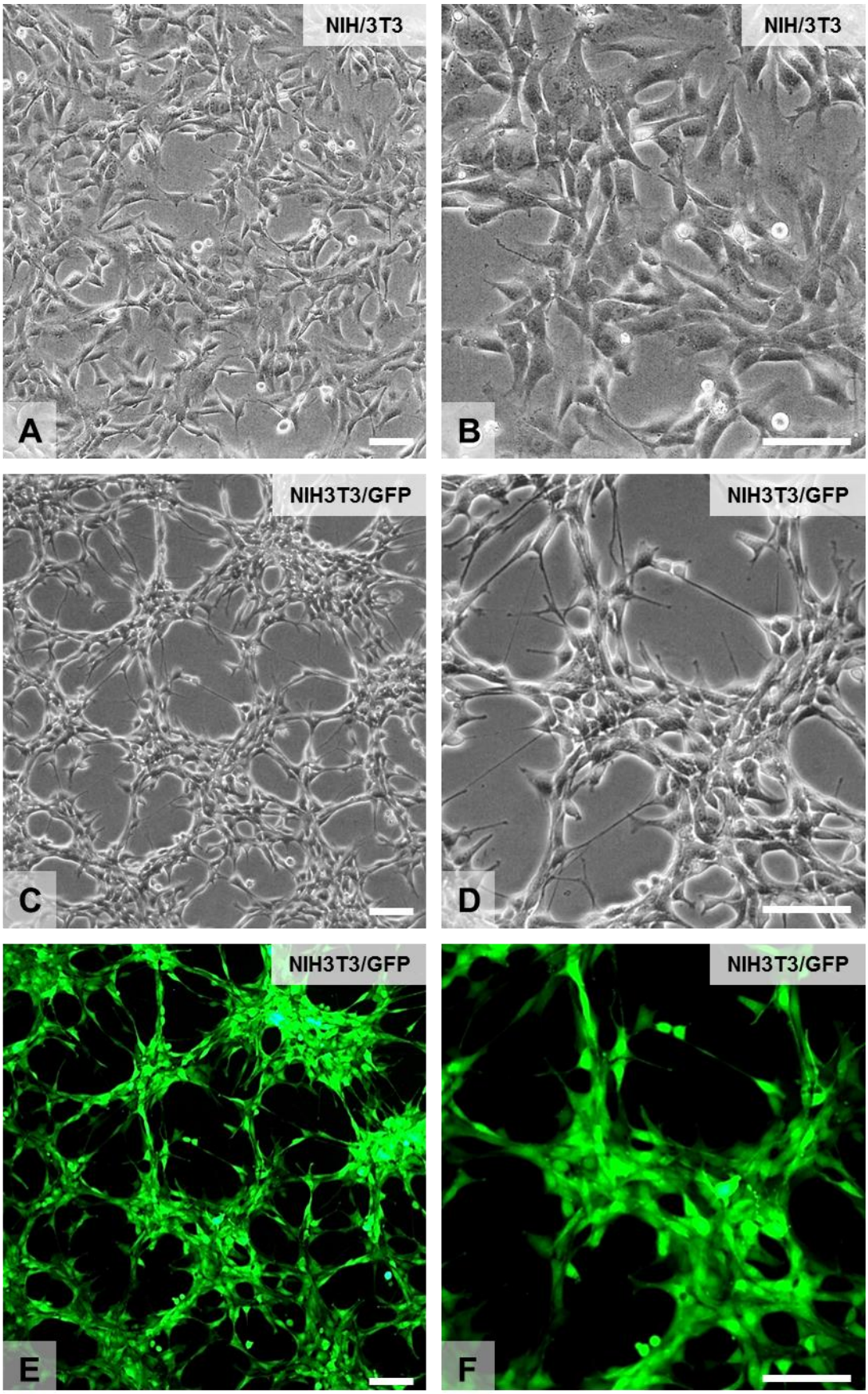

Figure 6.10: Phase contrast and fluorescence images of NIH/3T3 and NIH3T3/GFP cells in 2D culture. Both cell lines displayed similar characteristics in 2D culture. Phase images of A and B: NIH/3T3 and C and D: NIH3T3/GFP cell lines showing both have classic fibroblast morphologies. Fluorescence images of E and F: NIH3T3/GFP showing that all cells expressed GFP. Scale bars = 100µm for all images.

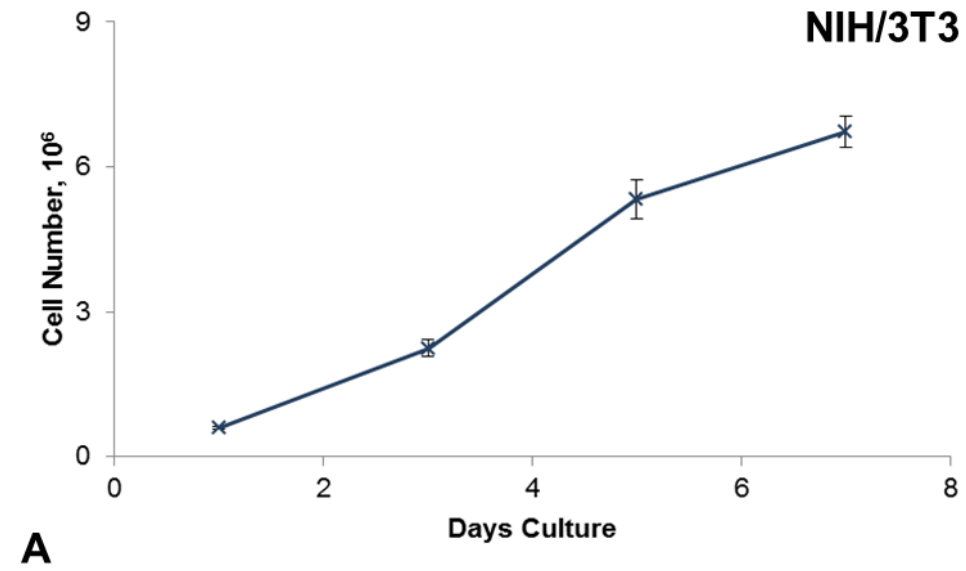

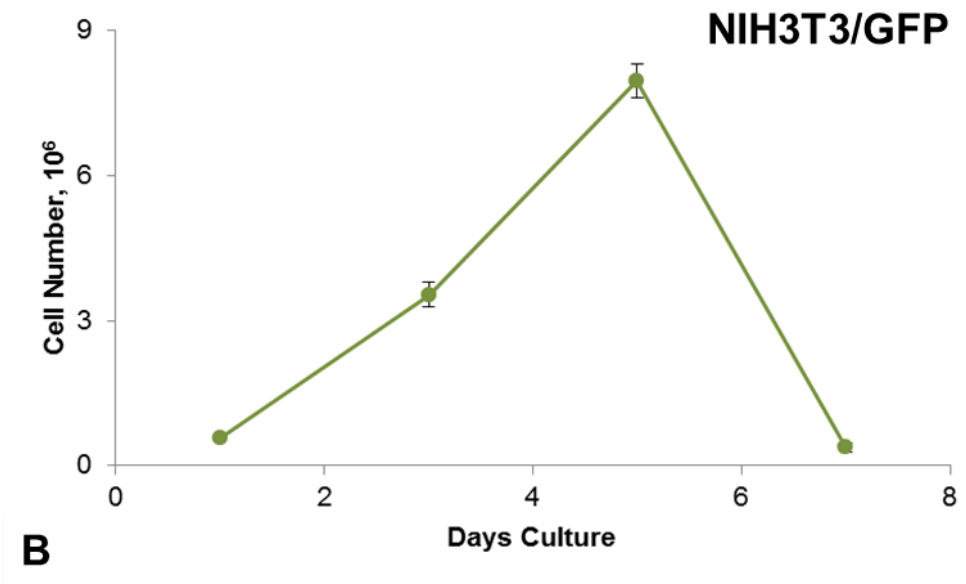

Figure 6.11: The NIH3T3/GFP cell line had a quicker proliferation rate than the standard NIH/3T3 cell line and experienced a population crash as it outgrew the plasticware. Cell counts for A: NIH/3T3 and B: NIH3T3/GFP cells. Data represent mean, n = 3, ±SEM for both graphs.

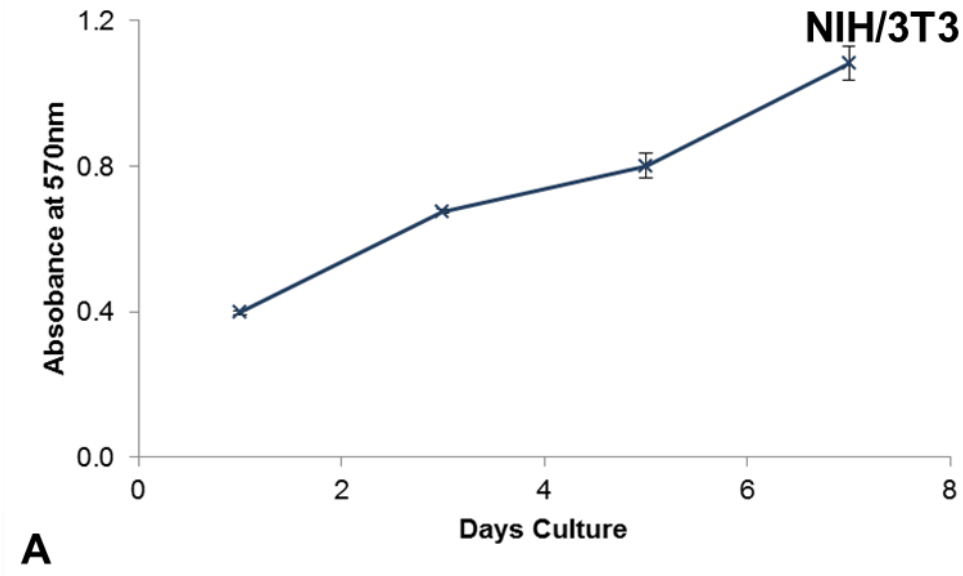

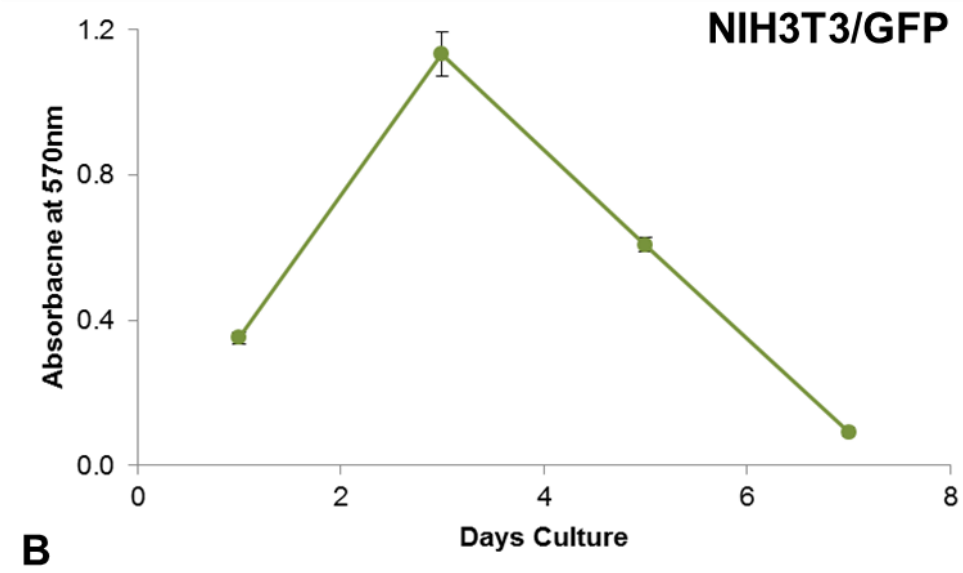

Figure 6.12: The NIH/3T3 cell line maintained an increasing level of cell viability when maintained in 2D culture over 7 days, while the NIH3T3/GFP cell line experienced a drop in viability before the cells overgrew the plasticware. Absorbance at 570nm of A: NIH/3T3 and B: NIH3T3/GFP cells as determined by the MTT Cell Viability Assay. Data represent mean, n = 3, ±SEM for both graphs.

6.3.2.4 The NIH3T3/GFP produced a more dense 3D culture than the NIH/3T3 cell line

With the NIH3T3/GFP cell line exhibiting a quicker rate of proliferation in 2D culture, it was expected that there were be a difference in the cell density of the 7 day 3D cultures of these two cell lines. As previously noted, the NIH/3T3 cell line was found to be sparsely distributed throughout the depth of the material after 7 days culture on Alvetex® Scaffold (Figure 6.13A). In comparison, while the NIH3T3/GFP cell line exhibited a similar pattern of cell distribution, the cell growth was more dense than the NIH/3T3 cultures (Figure 6.13B).

The 3D cultures were also assessed for GFP fluorescence to ensure that this was retained by all cells. Once fixed, embedded and sectioned samples of the NIH3T3/GFP cultures were stained with DAPI to highlight the cell nuclei, they were subjected to examination via fluorescence microscopy. The GFP (Figure 6.13C) and DAPI (Figure 6.13D) images obtained demonstrate that all cells within the 3D culture retained expression of GFP and therefore this tag is suitable for use to distinguish between the fibroblast and cancer compartments of any subsequent co-culture.

6.3.2.5 Both the NIH/3T3 and NIH3T3/GFP cell lines can be maintained in 3D culture for up to 7 days

As the 2D culture of the NIH3T3/GFP cell line demonstrated that the cells lost viability while still remaining attached to the culture flask, the viability of the 3D cultures of fibroblasts were compared to assess the suitability of the NIH3T3/GFP cell line.

When the viability of the cultures was assessed using the MTT Cell Viability Assay, the viability of the 3D cultures of both the NIH/3T3 and NIH3T3/GFP cell lines was seen to significantly increase between 4 days and 7 days culture (Figure 6.14). By 4 days, the NIH3T3/GFP cell line appeared to exhibit a greater level of viability than the NIH/3T3 cell line, whereas, by 7 days, the viability of the cultures was comparable between the two cell lines.

6.3.2.6 3D cultures of NIH3T3/GFP cells contained fewer cells than those of NIH/3T3 cells

As the viability of 3D fibroblast cultures on Alvetex® Scaffold was comparable by 7 days of culture, the amount of cell growth was assessed using the Bradford Assay to assess protein content and the Pico Green Assay to ascertain cell number. The 3D cultures of the NIH/3T3 did not significantly increase their protein content between 4 and 7 days of culture (Figure 6.15A), whereas the NIH3T3/GFP cultures did (Figure 6.15B). Additionally, it was observed that the NIH/3T3 cultures consistently had a higher protein content than the NIH3T3/GFP cultures for each time point assayed.

A similar trend was observed when the cell number was quantified, with the NIH/3T3 cultures containing a larger number of cells at each time point compared to the NIH3T3/GFP cultures (Figure 6.16). However, in this case, there was no significant increase in cell number observed for either cell line between day 4 and day 7 of 3D culture.

Together this data demonstrates that the NIH/3T3 and NIH3T3/GFP demonstrate broadly similar characteristics when maintained in 3D culture on Alvetex® Scaffold for 7 days after the concentrated seeding of 0.5×10^6 cells and could be used interchangeably in the protocols used here.

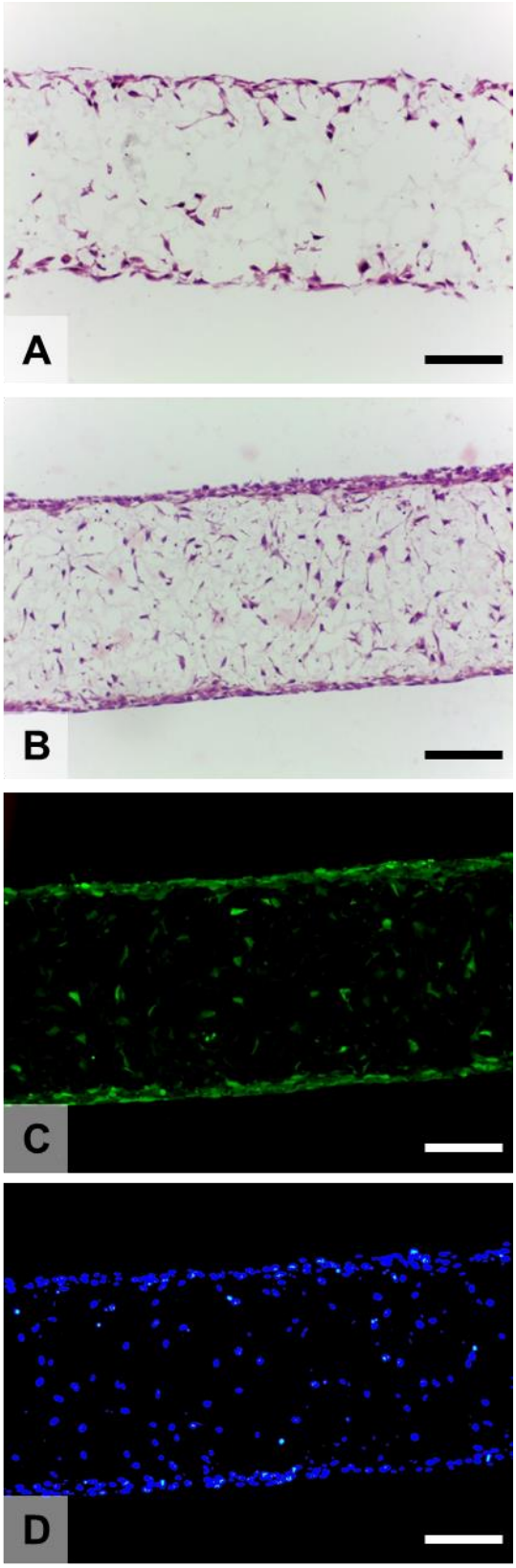

Figure 6.13: NIH3T3/GFP cells were more densely packed in Alvetex® Scaffold than standard NIH/3T3 cells. High magnification H&E images of scaffolds seeded with A: NIH/3T3 and B: NIH3T3/GFP cells and high magnification fluorescence images of NIH3T3/GFP cells showing C: GFP and D: DAPI. Scale bars = 100µm for all images.

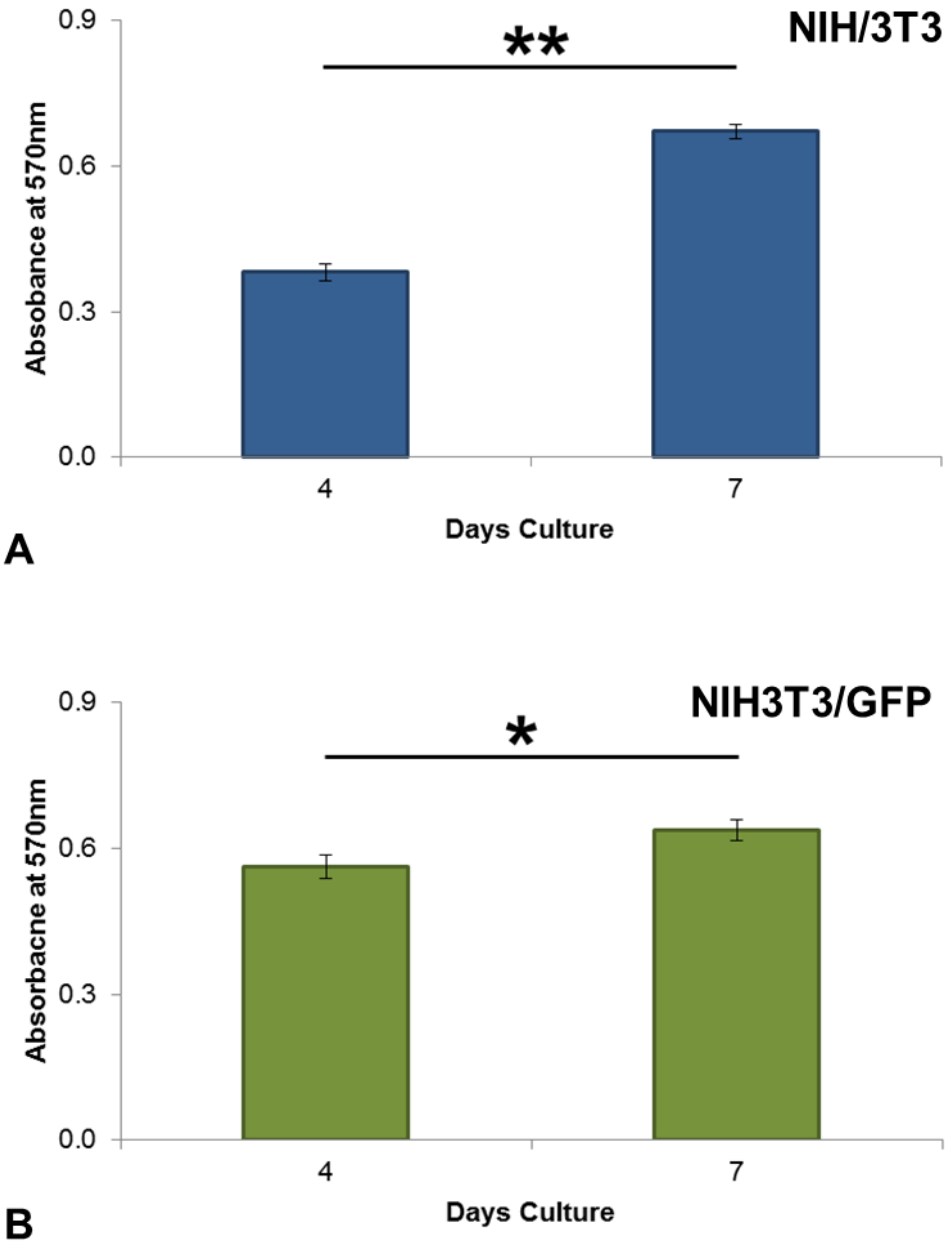

Figure 6.14: Both the NIH/3T3 and NIH3T3/GFP cell lines experienced an increase in viability from four to seven days in 3D culture. Absorbance at 570nm of A: NIH/3T3 and B: NIH3T3/GFP cells as determined by the MTT Cell Viability Assay. Data represent mean, n = 3, ±SEM for all graphs, * $p < 0.05$, ** $p < 0.01$ by a Student's t-test.

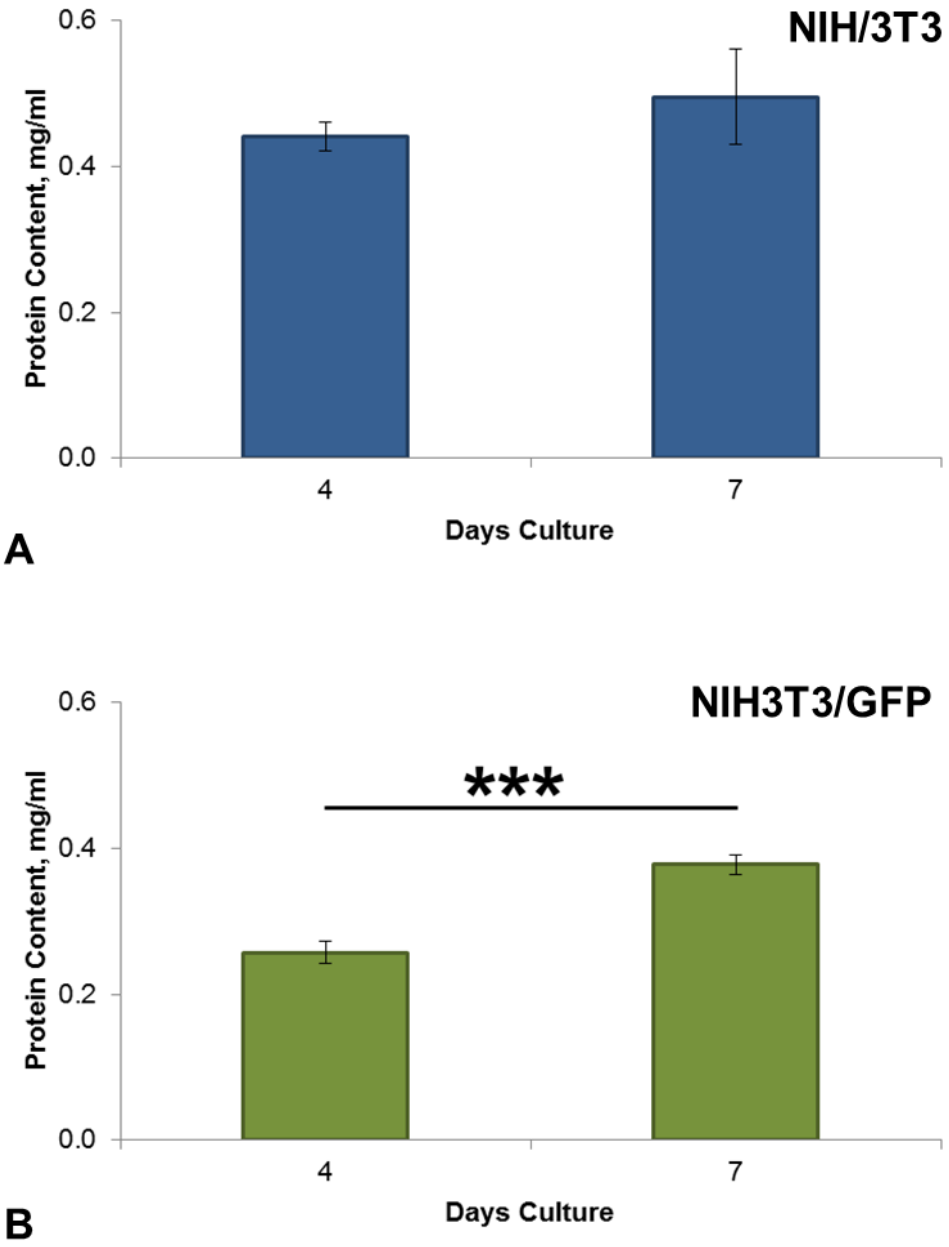

Figure 6.15: The NIH3T3/GFP cell line showed a significant increase in protein content over an extended culture period, whereas the NIH/3T3 cell line did not. Protein content in mg/ml of A: NIH/3T3 and B: NIH3T3/GFP cells as determined by the Bradford Assay. Data represent mean, n = 3, ±SEM for both graphs, *** $p < 0.005$ by a Student's t-test.

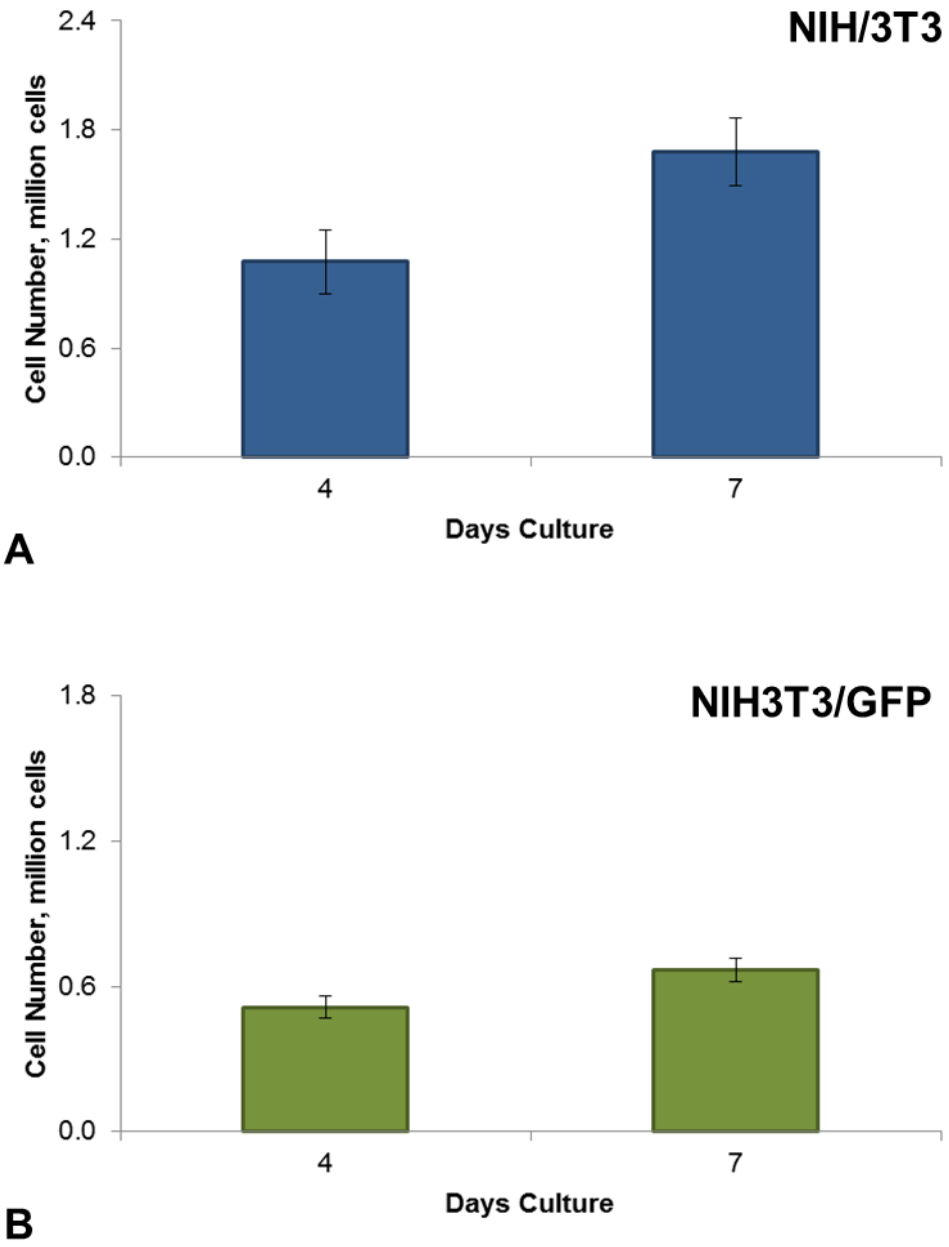

Figure 6.16: Neither the NIH/3T3 or NIH3T3/GFP cell lines displayed a significant increase in cell number over extended culture periods. Cell number in millions of cells of A: NIH/3T3 and B: NIH3T3/GFP cells as determined by the Pico Green dsDNA Assay. Data represent mean, n = 3, ±SEM for both graphs, no significance by a Student's t-test.

6.3.3 Co-culture provides the opportunity for a more biologically relevant model

With the NIH/3T3 and NIH3T3/GFP cell lines producing comparable 3D cultures after 7 days and with the NIH3T3/GFP able to maintain the GFP tag in 3D culture, it was concluded that the NIH3T3/GFP cell line could be used as a stromal equivalent in a co-culture model to provide a simple means of distinguishing between the fibroblast and cancer cells.

6.3.3.1 Alvetex® Scaffold could support co-cultures of colorectal cancer cell lines with the NIH3T3/GFP cell line

The co-culture of both the SW480 and SW620 cell lines for 10 days on top of 7 day old NIH3T3/GFP cultures produced samples which contained both cell types. Sample histological images for each co-culture (Figure 6.17A & B) display a deviation from the organisation of NIH3T3/GFP cells previously observed in 7 day cultures (Figure 6.13B). When these co-cultures were stained for cell nuclei and examined under fluorescent microscopy, distinct populations of cells were observed within the cultures which did not have a GFP tag but did contain the DAPI stain for nuclei, highlighted using an arrow for the SW480 co-cultures (Figure 6.17C & E) and an arrowhead for the SW620 co-cultures (Figure 6.17D & F). As it has already been demonstrated that all cells in the NIH3T3/GFP 3D cultures retained the GFP tag (Figure 6.13C & D), these populations of cells were assumed to be the colorectal cancer cell lines.

When higher magnification images of the co-cultures were examined (Figure 6.17G & H), the location of fibroblast and cancer cells is easily determined by the GFP tag. Cell nuclei seen in the absence of the GFP tag were assumed to be the cancer cells (closed-headed arrows, Figure 6.17G & H), while those seen with GFP expression were assumed to be the fibroblasts (open-headed arrows, Figure 6.17G & H). From these images, it was observed that while there was a build-up of cancer cells at the top of the scaffold, under a layer of fibroblast cells, there was also single infiltrating cell found within the scaffold which had migrated though the fibroblast cells found at the top of the scaffold.

These images suggest that Alvetex® Scaffold is capable of supporting the viable co-culture of the colorectal cancer cell lines SW480 and SW620 with the cell line NIH3T3/GFP acting as a stromal equivalent to ease cell type identification.

6.3.4 The expression of proteins in *in vitro* cultured samples is comparable to that seen in pathological samples

As the aim of this Chapter has been to assess the impact of the protein microenvironment on the migration of colorectal cancer cells and the feasibility of using the model developed here for co-culture with fibroblasts to generate a stromal equivalent, the impact of these alterations to the culture environment on the expression of proteins in the colorectal cancer cell lines was assessed.

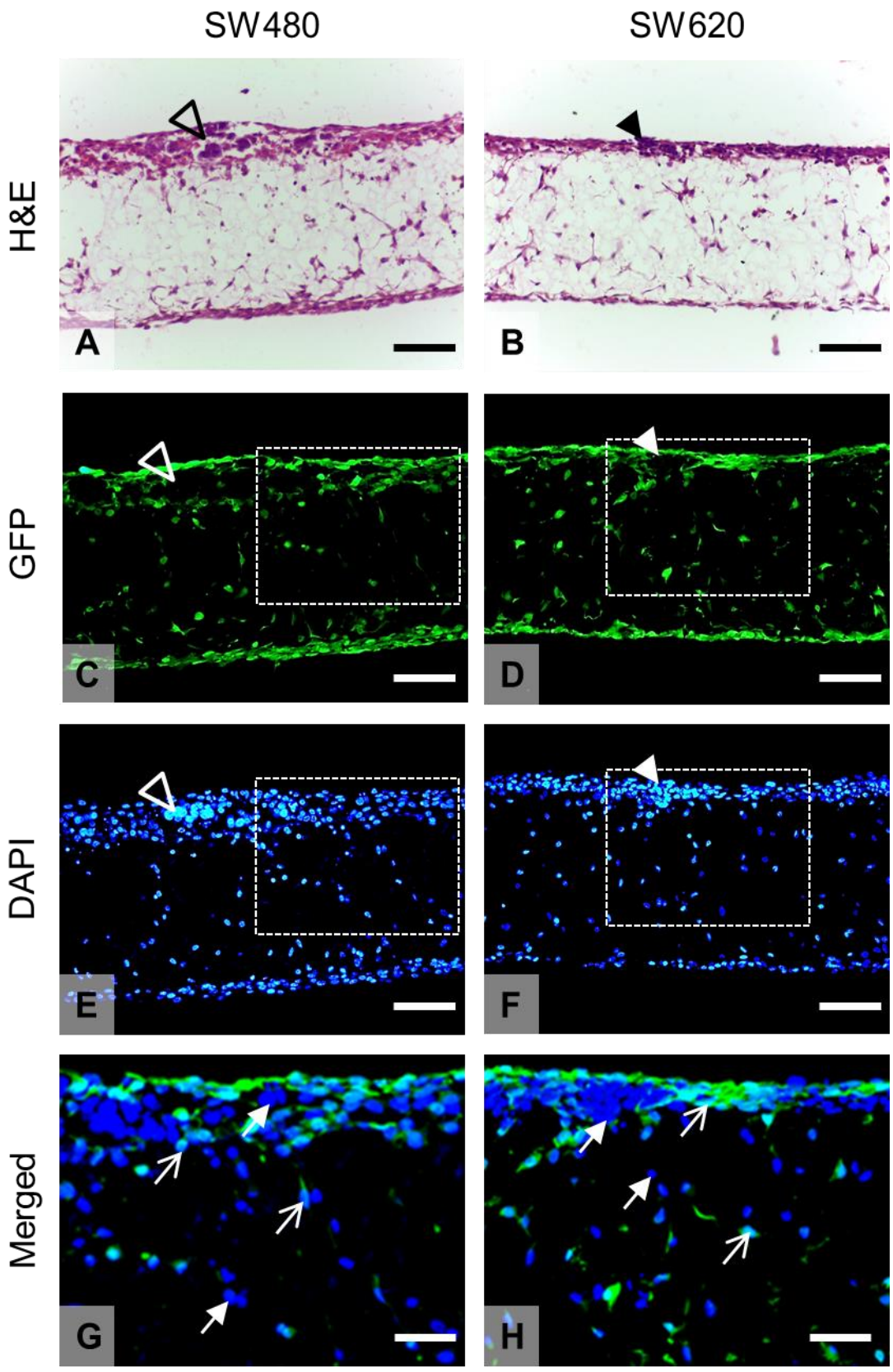

Figure 6.17: Alvetex® Scaffold could support co-culture of the NIH3T3/GFP cell line with both the SW480 and SW620 cell lines. H&E images of NIH3T3/GFP co-cultures with A: SW480 and B: SW620 cells, GFP images of NIH3T3/GFP co-cultures with C: SW480 and D: SW620 cells and DAPI images of NIH3T3/GFP co-cultures with E: SW480 and F: SW620 cells. The populations of colorectal cancer cells are highlighted by the open (SW480) and solid (SW620) arrow heads in images A-F. High magnification merged images NIH3T3/GFP co-cultures with G: SW480 and H: SW620 cells taken from the areas highlighted by dashed boxes in images C-F. Examples fibroblast nuclei, with associated GFP fluorescence, are shown by open-headed arrows and examples of cancer cell nuclei, lacking associated GFP fluorescence, are shown by closed-headed arrows in images G and H. Scale bars = 100μm for images A-F, 50μm for images G and H.

6.3.4.1 The inclusion of an ECM coating did not alter the expression of proteins in the SW480 and SW620 cell lines

When the expression of proteins in SW480 and SW620 cultures on uncoated and coated scaffolds was assessed, the inclusion of an ECM protein coating did not appear to effect the expression of proteins. All 3D SW480 cultures were found to be negative for E-cadherin (Figure 6.18A-C) and Slug (Figure 6.18J-L) expression, while positive for vimentin (Figure 6.18D-F) and β-catenin (Figure 6.18G-I) expression, although the vimentin staining observed here was lower than previously observed. Similarly, all 3D SW620 cultures were also found to be negative for E-cadherin (Figure 6.19A-C) and Slug (Figure 6.19J-L) expression, while positive for vimentin (Figure 6.19D-F) and β-catenin (Figure 6.19G-I) expression. With both cell lines, the pre-coating of Alvetex® Scaffold with either collagen I or fibronectin did not have an effect on the expression of these proteins.

6.3.4.2 Protein expression in co-cultures varied between the cell compartments

When the protein expression profiles of the 3D co-cultures were examined, a similar pattern of protein expression was seen between the co-cultures with the SW480 cell line and the SW620 cell line. In both cases, the cancer cells were seen to be negative for both E-cadherin (Figure 6.20A & B) and Slug (Figure 6.20G & H) and positive for vimentin (Figure 6.20C & D) and β-catenin (Figure 6.20E & F), although the amount of β-catenin staining observed was less than seen in previous cultures with cancer cells only (Figure 6.18D and Figure 6.19D). This suggests that the interaction between the cancer cells and the fibroblasts had altered the expression of key proteins that directs the behaviour of the cancer cells.

The co-cultures were also assessed for the expression of collagen I and collagen IV, with antibodies which detect both human and mouse proteins, to investigate the ECM environment that the fibroblasts were providing to the cancer cells. Collagen I expression was seen at low levels around both the cancer and fibroblast cells in the 3D culture (Figure 6.20I & J), whereas collagen IV expression was seen surrounding the fibroblast cells, not the cancer cells (Figure 6.20K & L). The E-cadherin and vimentin antibodies used were human specific and so did not react with the mouse fibroblasts (Figure 6.20A-D). The β-catenin and Slug antibodies used were able to detect both human and mouse proteins, but did not positive staining for these proteins was not seen in the fibroblast compartment of the co-cultures (Figure 6.20E-H). These data indicate that both cell types are capable of laying down ECM proteins on Alvetex® Scaffold to modify the growth environment to suit their needs. It also suggests that the ECM generated by the fibroblasts is different to that generated by the cancer cells and, therefore, adds to the more complex microenvironment provided by co-culture.

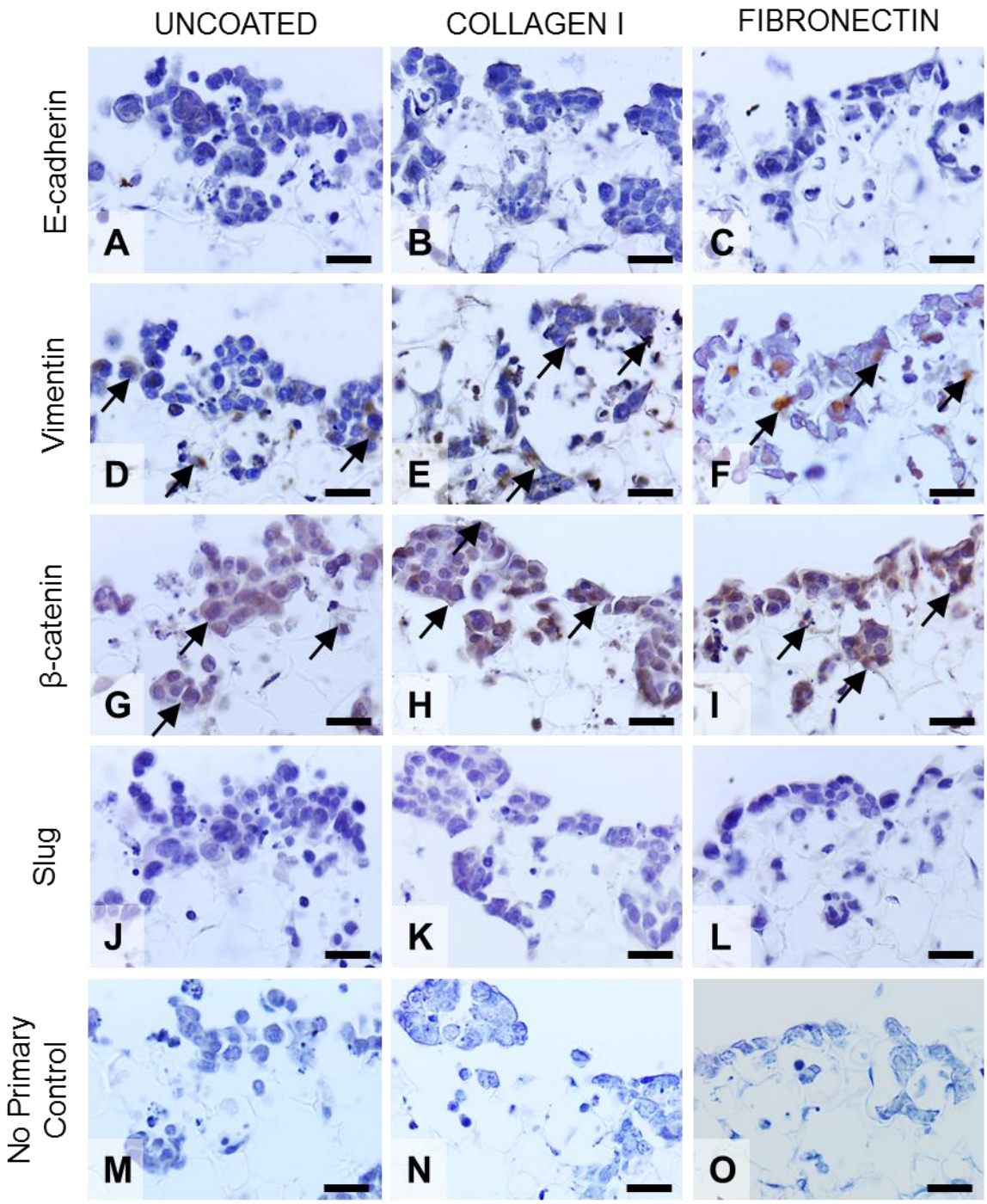

Figure 6.18: The pre-coating of scaffolds with collagen I or fibronectin did not affect protein expression in the SW480 cell line, with the cells expressing vimentin and β-catenin in all cultures. Immunohistochemical images of antibody staining for A, B and C: E-cadherin, D, E and F: Vimentin, G, H and I: β-catenin, J, K and L: Slug and M, N and O: no primary control on 10 day cultures of SW480 on uncoated, collagen I coated and fibronectin coated scaffolds, where the brown precipitate (arrows) indicates positive staining. Scale bars = 25μm for all images.

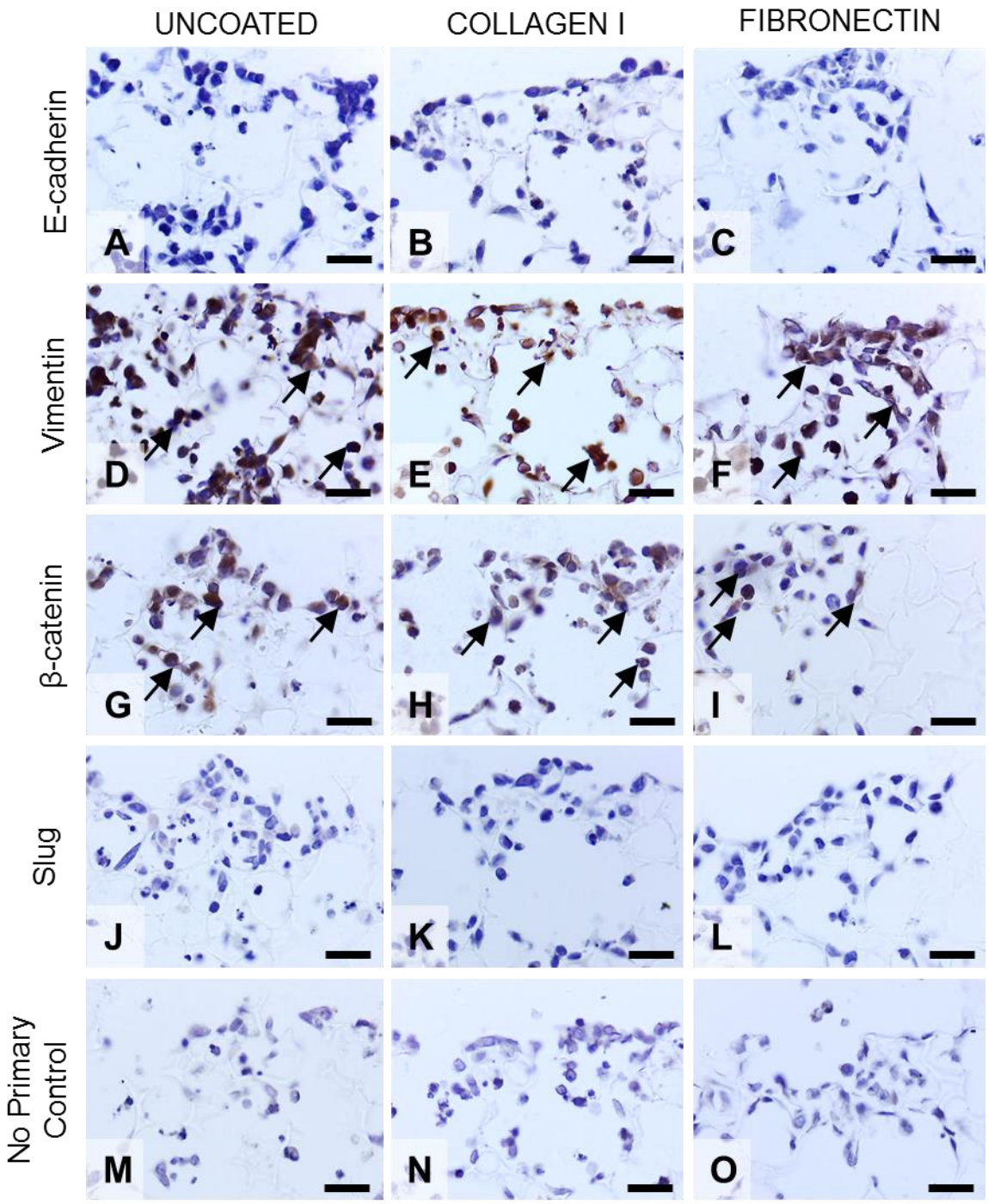

Figure 6.19: The pre-coating of scaffolds with collagen I or fibronectin did not affect protein expression in the SW620 cell line, with the cells expressing vimentin and β-catenin in all cultures. Immunohistochemical images of antibody staining for A, B and C: E-cadherin, D, E and F: Vimentin, G, H and I: β-catenin, J, K and L: Slug and M, N and O: no primary control on 10 day cultures of SW620 on uncoated, collagen I coated and fibronectin coated scaffolds, where the brown precipitate (arrows) indicates positive staining. Scale bars = 25μm for all images.

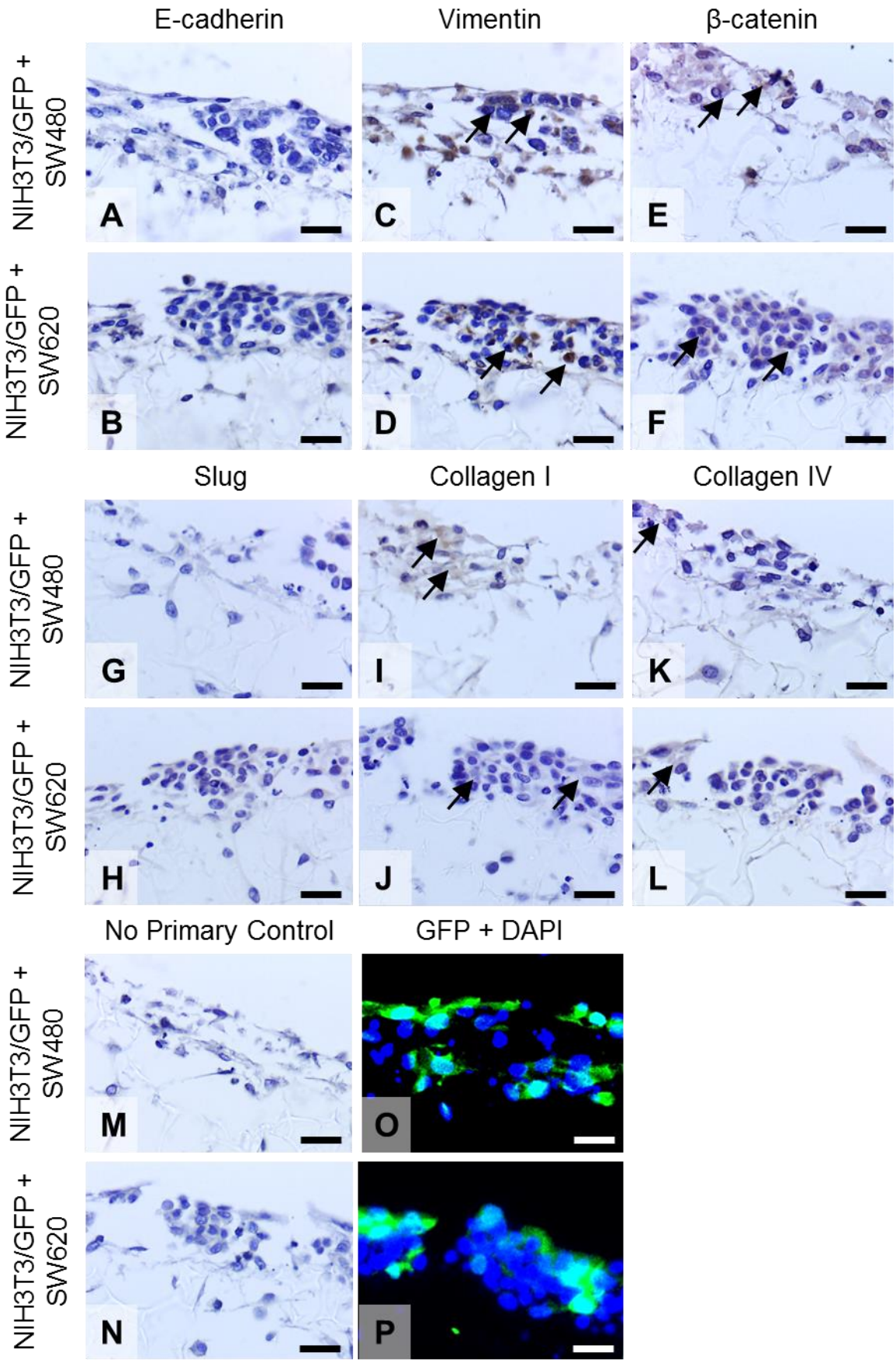

Figure 6.20: Co-culture of fibroblasts with colorectal cancer cells produces cultures which express a variety of proteins, with the cancer cells expressing vimentin, β-catenin and collagen I and the fibroblasts expressing collagen I and IV. Immunohistochemical images of antibody staining for A and B: E-cadherin, C and D: Vimentin, E and F: β-catenin, G and H: Slug and I and J: Collagen I, K and L: Collagen IV, M and N: no primary control and O and P: merged GFP and DAPI on 10 day 3D co-cultures of NIH3T3/GFP with SW480 and SW620 cells, where the brown precipitate (arrows) indicates positive staining. Scale bars = 25μm for all images.

6.3.4.3 The organised protein expression in healthy colonic tissue is disrupted in colorectal tumours

Immunohistochemical staining of pathological samples highlighted the expression of the six proteins under investigation here in both healthy colonic tissue and colorectal tumours. In the healthy tissue, the expression of proteins was found to be confined to specific cell types within the tissue which corresponds to their documented location in the literature. Both E-cadherin and β-catenin are localised to the colonic epithelium, with E-cadherin expression higher in cells which are exiting the crypts [437] and β-catenin in the cells at the base of the crypts [438], whereas vimentin is localised to the stromal compartment of healthy colonic tissue [439]. Collagen I is found to be expressed throughout colonic tissue, although staining was seen to be more intense in the stromal regions of the tissue, while collagen IV is found around the basement membrane and blood vessels of the colon [378]. Slug is expressed by adult colonic tissue [440], however no data could be found regarding the location of this protein in healthy tissue samples.

The expression of E-cadherin was largely absent from the tissue and was only present in the uppermost section of the colon epithelium, where the epithelial cells had exited the proliferative crypts (Figure 6.21A & B). In contrast, while absent from the epithelial cells, the expression of vimentin was found to be widespread through most of the tissue (Figure 6.21C & D).

The expression of β-catenin was seen to be confined to the nucleus of cells towards the base of the epithelial crypts (Figure 6.21E & F), while the expression of Slug was found to be absent in the samples analysed (Figure 6.21G & H). The common ECM component collagen I was found to be expressed at low levels throughout the tissue (Figure 6.21I & J), while the more specialised ECM protein collagen IV was found to be localised to the muscularis mucosa and to the walls of blood vessels within the tissue (Figure 6.21K & L).

In contrast, this clear pattern of staining is not seen in pathological samples taken from either Dukes' Stage B (Figure 6.22) or C (Figure 6.23) tumours. This data demonstrates the variability in the expression of proteins between separate tumours and between different regions of the same tumour. General trends are seen in the stained samples, with the upregulation of vimetin expression (Figure 6.22C & D and Figure 6.23C & D) in both the epithelial derived and stromal portion of the tumour, although the balance of this staining can vary from being more intense in the epithelial derived portion (Figure 6.22C) or the stromal portion (Figure 6.23D).

Any E-cadherin staining visible within the samples is confined to the epithelial derived portion of the tumours, with the expression of this protein varying across the tumour samples (Figure 6.23A & B). The expression of the other proteins examined is also seen to vary both between and within the tumours samples (Figure 6.22E-L and Figure 6.23E-L), with no clear trends in terms of expression in relation to cell or tumour type clearly visible.

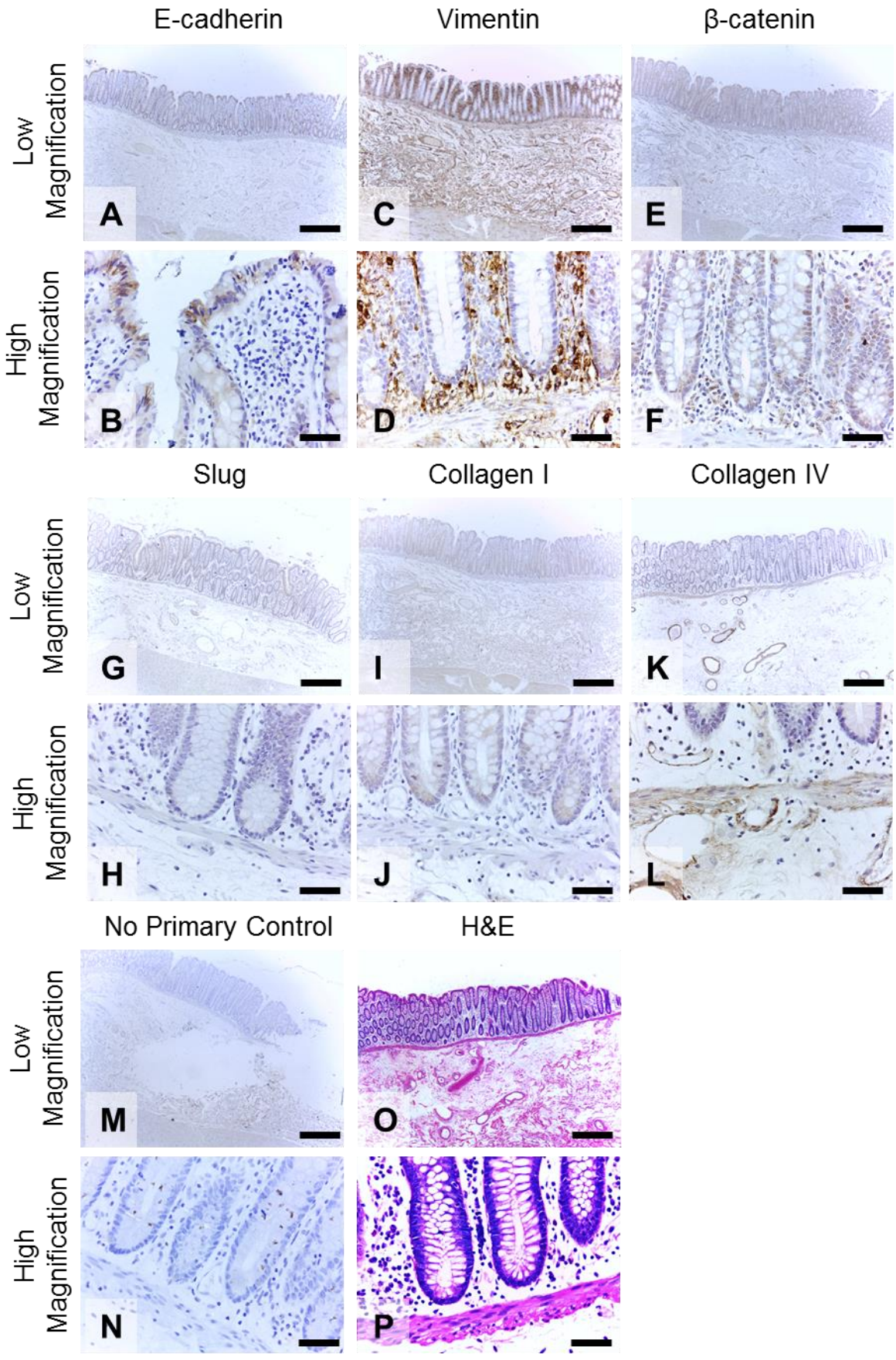

Figure 6.21: Proteins are expressed in specific compartments of healthy colonic tissue. Immunohistochemical images of antibody staining for A and B: E-cadherin, C and D: Vimentin, E and F: β-catenin, G and H: Slug and I and J: Collagen I, K and L: Collagen IV, M and N: no primary control and O and P: H&E on primary healthy human colon tissue at low and high magnification. Scale bars = 500µm for images A, C, E, G, I, K, M and O, 50µm for images B, D, F, H, J, L, N and P.

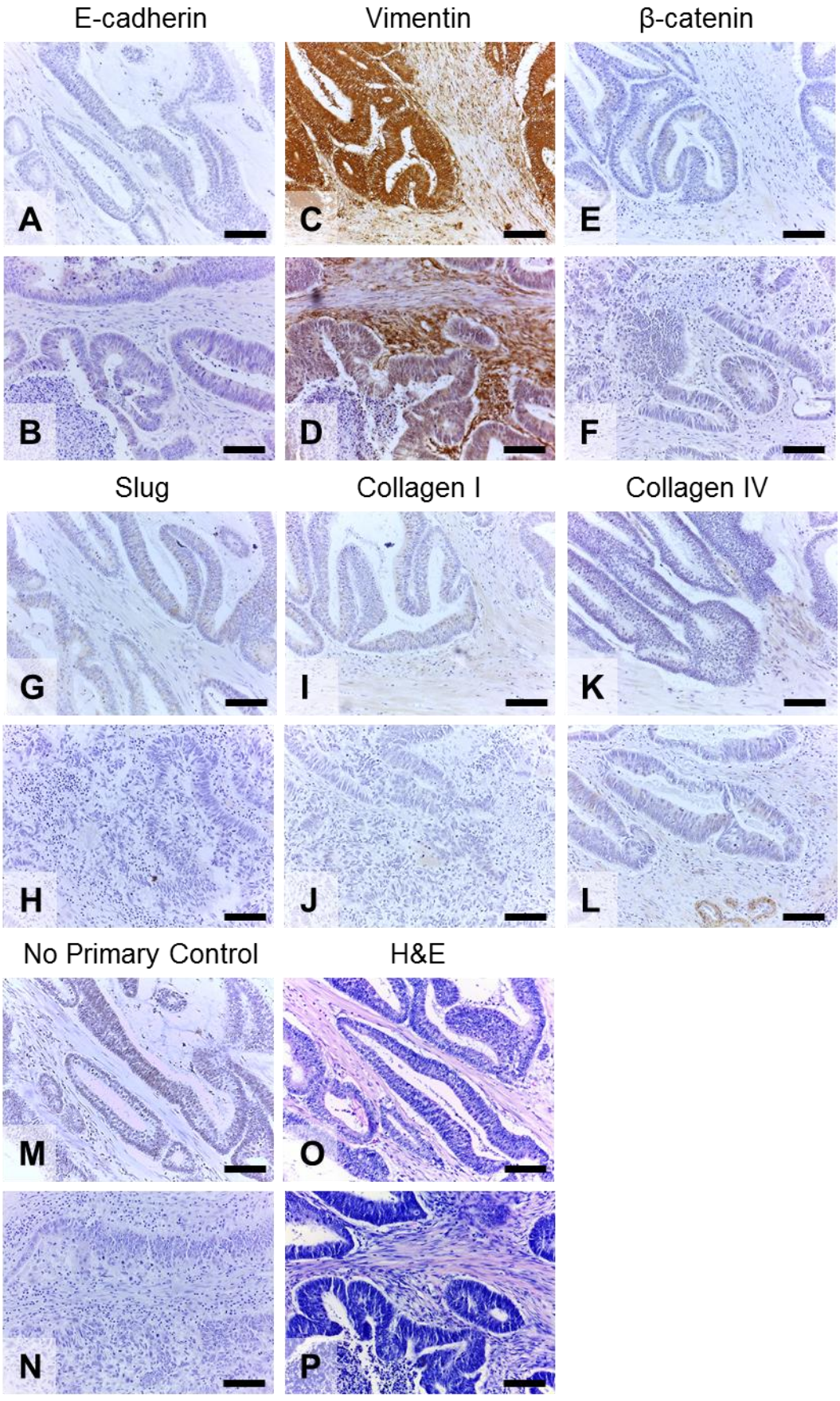

Figure 6.22: The expression of proteins varies between Dukes' Stage B tumours. Immunohistochemical images of antibody staining for A and B: E-cadherin, C and D: Vimentin, E and F: β-catenin, G and H: Slug and I and J: Collagen I, K and L: Collagen IV, M and N: no primary control and O and P: H&E on two examples of Dukes' Stage B colorectal carcinomas. Scale bars = 100μm for all images.

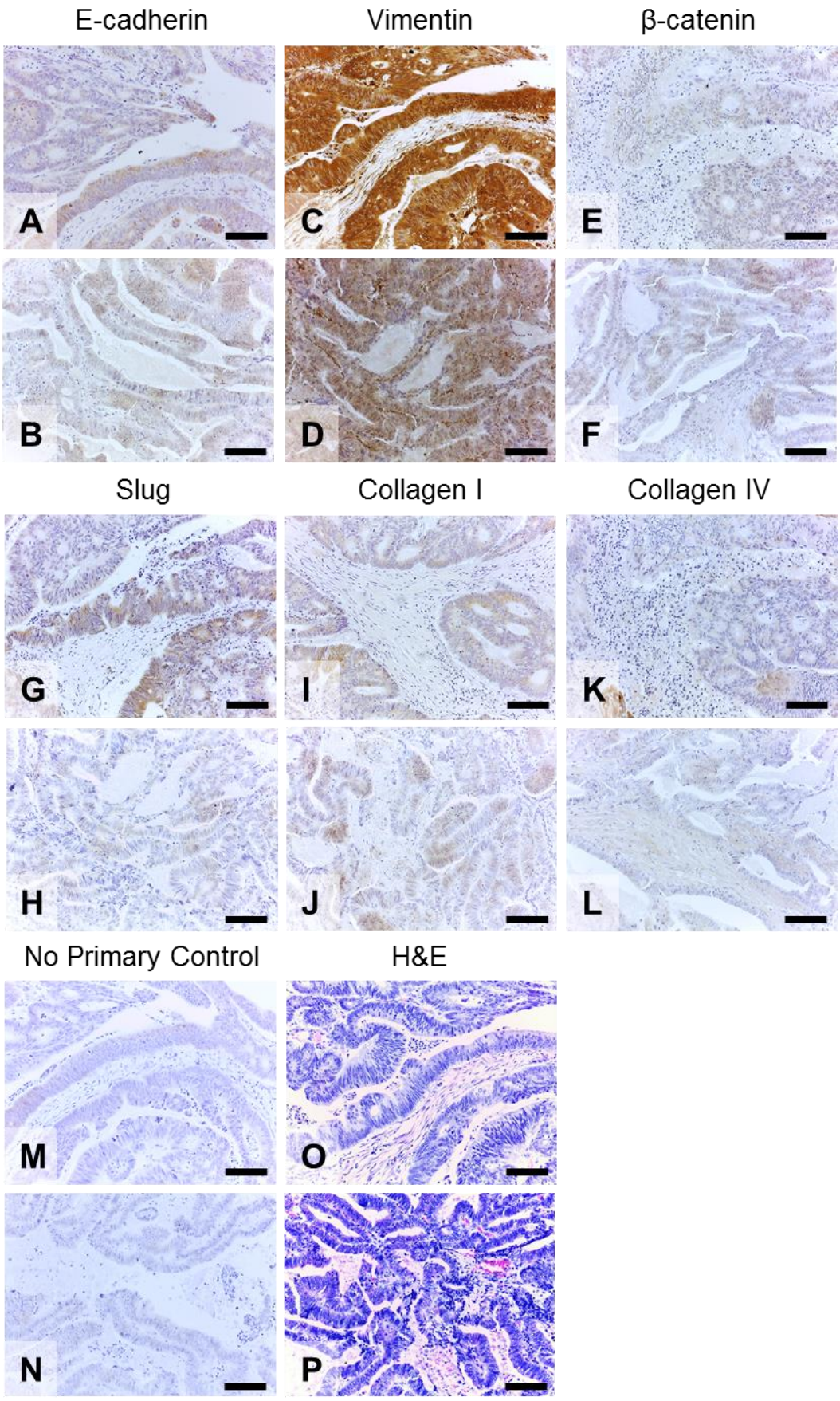

Figure 6.23: The expression of proteins varies between Dukes' Stage C tumours. Immunohistochemical images of antibody staining for A and B: E-cadherin, C and D: Vimentin, E and F: β-catenin, G and H: Slug and I and J: Collagen I, K and L: Collagen IV, M and N: no primary control and O and P: H&E on two examples of Dukes' Stage C colorectal carcinomas. Scale bars = 100μm for all images.

6.4 Discussion

The Chapter has aimed to assess the feasibility of including an ECM protein coating or co-culture element in the 3D migratory model under development here in order to provide a culture microenvironment which reflects the tumour environment seen in pathological samples (Figure 6.1A & B) better than standard 2D cultures (Figure 6.1C). While the use of a synthetic scaffold provides a 3D culturing environment, where the level of cell-cell interactions is increased over standard 2D monolayer cultures, which creates a culture environment which has an increased level of biological relevance, the format of this environment, a polystyrene scaffold, is still far removed from the protein rich multicellular tumour environment *in vivo*.

The inclusion of an appropriate ECM coating provides the cancer cells with an environment which directs cell attachment, proliferation and migration in a manner which more closely reflects cancer cell behaviour seen in tumours. The two ECM protein coatings selected to investigate the role of cell-protein interactions on cell behaviour in a 3D model were collagen I, due to the upregulation of this protein in colorectal cancer tissue at all stages of the disease [386], particularly in the stromal portion of the tumours [378, 387], and fibronectin, which is upregulated in primary colorectal tumours [79, 386]. The data presented here demonstrated that the inclusion of an ECM coating on Alvetex® Scaffold affected colorectal cancer cell migration, viability, proliferation and attachment in this 3D model and is summarised in Table 6.1.

Coating	SW480	SW620
Collagen I	− No significant effect on cell penetration − 33% decrease in cell viability − 43% decrease in cell number − Non-significant decrease in cell attachment after 24 hours − Increased population doubling time	− No significant effect on cell penetration, although more cells were confined to the seeding surface − 37% decrease in cell viability − No significant effect on cell number − Non-significant decrease in cell attachment after 24 hours − Decreased population doubling time
Fibronectin	− 27% increase in cell penetration − No significant effect on cell viability − 28% decrease in cell number − Non-significant increase in cell attachment after 24 hours − Increased population doubling time	− No significant effect on cell penetration − No significant effect on cell viability − No significant effect on cell number − No significant effect on cell attachment after 24 hours − Increased population doubling time

Table 6.1: Summary of the primary effect of ECM coatings cell culture in the 3D migration assay.

The cell penetration of the SW480 cell line, as a measure of cell migration, was found to be significantly increased when a fibronectin coating was present but not when a collagen I coating was present (Figure 6.3A). In contrast, the penetration of the SW620 cell line was unaffected (Figure 6.3B). Comparisons of this result to published data is difficult as many 3D migration models which utilise ECM gels are composed of either collagen I [209] or Matrigel [212], which may be supplemented with additional ECM components such as fibronectin [210], and these results are not

compared back to an uncoated 3D environment. However, the comparison of the invasion of the human fibrosarcoma cell line HT1080 into collagen I only and collagen I with fibronectin gels demonstrated that there was no difference observed when the gels were not mechanically stimulated [210].

The inclusion of a collagen I coating prior to 3D culture was also found to significantly decrease the viability of both the SW480 and SW620 cell lines (Figure 6.4). Again, no published data was found which compared the viability of SW480 or SW620 cultures on collagen I or fibronectin, either to each other or to tissue culture plasticware, for the data presented here to be compared to.

The data presented here also demonstrated that the pre-coating of Alvetex® Scaffold with either collagen I or fibronectin decreased the number of SW480 cells present after 10 days of culture (Figure 6.5A), a change which was assumed to be due to a decrease in cell proliferation. While there is no published data comparing the proliferation rate of SW480 cells cultured on ECM coatings to SW480 cells cultured on tissue culture plasticware, there is published data demonstrating that the proliferation rate of the SW480 cell line is comparable when the cells are cultured on thin ECM coatings of collagen I or fibronectin [441, 442]. This does not appear to be the case here; with the decreased number of SW480 cells present on the collagen I coated scaffolds after 10 days and the decreased generation time of 58 hours, as opposed to 68 hours, when compared to fibronectin coated scaffolds. However, as these experiments were carried out in a 3D culturing environment, this may account for the change in behaviour between collagen I coating and fibronectin coating which is not seen in 2D culture.

In terms of cell attachment to Alvetex® Scaffold over a 24 hour period, more SW480 cells were found to be attached than SW620 cells over the time period for all uncoated and coated scaffolds (Figure 6.8), and while there was no significant difference between uncoated and specific coated scaffolds, the inclusion of an ECM coating affected cell attachment overall. This correlates with some of the previously published data, as Del Buono *et al*. demonstrated that the SW480 cell line attached to thin collagen I or fibronectin gels than the SW620 cell line [443]. However, there is also published data demonstrating a lack of difference between the adhesion of the SW480 and SW620 cell lines to thin collagen I or fibronectin gels [444, 445], although this may be due to the difference in conditions during the adhesion assay, as Del Buono *et al*. assessed adhesion after 2 hours at room temperature and the other papers assessed adhesion after 1 hour at 37^{o}C.

As it has been demonstrated that the expression of both collagen I and fibronectin is increased in colorectal cancer tumours relative to normal mucosa [386], the inclusion of these ECM coatings in the 3D model under development here provided the colorectal cancer cell lines with an *in vitro* culturing environment which reflects the tumour microenvironment more closely. As the inclusion of these coatings affected multiple aspects of the behaviour of the cells in this model, the data presented here suggests the importance of providing this relevant microenvironment to obtain experimental data which truly reflects the behaviour of tumours *in vivo*.

As demonstrated in Figure 6.18 and Figure 6.19, the provision of an ECM coating does not affect the expression of E-cadherin, vimentin, β-catenin or Slug in either the SW480 or SW620 cell lines. This does not correlate with published data regarding the expression of E-cadherin and β-catenin in response to a thin ECM gel in 2D culture in a variety of cell types. It has been demonstrated that the expression of β-catenin is elevated in response to fibronectin as opposed to collagen I in both

pancreatic cancer cell lines [446] and primary dermal fibroblasts [447]. However, these papers disagree on how these levels relate to culture on standard tissue culture plasticware, with one demonstrating that the level of expression when cultured on fibronectin was comparable to expression when cultured on tissue culture plasticware [446], while the other demonstrated that the level of β-catenin expression was elevated in cells cultured on ECM coated plasticware, regardless of the ECM protein [447], although this difference may be due to the different cell types used by each study. Additionally, it was demonstrated that the expression of E-cadherin in pancreatic cell lines was decreased in cultures on collagen I when compared to cultures on uncoated or fibronectin coated plasticware [446]. The lack of alteration in protein expression seen in this model may be due to the increased dimensionality of the model or the use of different cell types.

Together, these data demonstrate that the inclusion of an ECM substrate in the 3D culture system does have an effect on many aspects of cell behaviour and highlight that the inclusion of ECM proteins provides a simple means of increasing the biological relevance of *in vitro* cancer models.

An alternative method to increase the biological relevance of *in vitro* cancer models is to introduce a secondary cell type to model the multicellular environment of the tumour microenvironment (Figure 6.1B). To achieve co-culture in the 3D migration model under development here, fibroblasts were selected as a secondary cell type as they have been shown to affect the migratory behaviour of cancer cells in *in vitro* models [273, 418]. The cell line NIH/3T3 was selected as the fibroblast cell line for use to achieve a co-culture as it has previously been used in co-culture with colorectal cancer cells [193] and decellularised ECM matrices generated from the culture of NIH/3T3 *in vitro* have been used as a 3D growth substrate for a variety of cancer types [184]. In addition, the NIH/3T3 cell line has previously been optimised for culture on Alvetex® Scaffold [278], which removed the need for an extensive optimisation process, as carried out in Chapter 3 for the colorectal cancer cell lines.

Initial experiments demonstrated that Alvetex® Scaffold appeared to be able to support co-cultures of NIH/3T3 fibroblasts and colorectal cancer cells (Figure 6.9); however, the identification of the location of the individual cell lines within the cultures was difficult to establish. In order to ease the process of cell type identification, a GFP-tagged variant of the NIH/3T3 cell line was obtained. While there is no published data for the NIH3T3/GFP cell line, with many papers utilising a GFP-tagged variant of the NIH/3T3 cell line relying on an in-house transfection which tags a specific protein of interest [448], which was not the aim in this study, as the use of GFP was to identify one cell type from another. Additionally, the use of a commercially available cell line allowed for the reduction of variability arising from transfections carried out by different research groups and to allow for the successful replication of results.

The successful demonstration of the co-culture of the NIH3T3/GFP cell line with both the SW480 and SW620 cell lines (Figure 6.17) illustrates that the 3D migration assay developed utilising Alvetex® Scaffold can be further adapted to incorporate a secondary cell type to increase the biological relevance of the model by modelling a multicellular microenvironment *in vitro*.

The utilisation of a co-culture model which relies on a synthetic scaffold base, as opposed to an ECM gel base, allows for the study of the effect that a secondary cell type has on the behaviour of cancer cells in the absence of signalling provided by the starting ECM gels. Many stratified organotypic migration models utilise fibroblasts encapsulated in collagen I gels to provide a stromal

equivalent to the cancer cells [76, 436], while others use fibroblast seeded decellularised tissue [216]. The use of decellularised tissue to provide the ECM architecture of a 3D model has the potential to provide an inappropriate microenvironment to the cancer cells, as the ECM organisation and characteristics of tissue is disrupted during cancer development [368, 386], and the provision of a 'healthy' microenvironment may alter the behaviour of the cancer cells from that seen if an 'unhealthy' microenvironment was provided. Additionally, the use of a collagen I gel as the ECM base of a 3D model may mask the protein environment produced by the fibroblasts, which alters with cancer progression [409], and provide a microenvironment which does not truly reflect the tumour microenvironment.

The expression of E-cadherin, vimentin, β-catenin and Slug in the SW480 and SW620 cell lines was not seen to alter with the addition of a secondary cell type (Figure 6.20). In these cultures, the expression of collagen I and collagen IV was also examined to assess the ECM environment that the fibroblasts were providing to the colorectal cancer cells. The expression of collagen I in both the cancer and fibroblast cells in these cultures correlates with the ubiquitous expression of collagen I seen in colorectal cancers [378, 386], whereas the limited expression of collagen IV in the fibroblast portion of the co-cultures also correlates with the expression of collagen IV previously noted in the stromal portion colorectal cancers [378, 449]

The co-culture work presented here is a proof of concept which demonstrates the feasibility of it when Alvetex® Scaffold is used to provide the 3D environment for *in vitro* cell culture and also demonstrates, by the examination of collagen expression, that it adds environmental complexity to the 3D model by producing biologically relevant ECM proteins. However, the role of incorporating fibroblasts into the 3D migration model in altering the migratory behaviour of colorectal cancer cells has not been examined here and would need to be assessed to fully validate co-culture on Alvetex® Scaffold as a viable 3D migration model to study the behaviour of colorectal cancer cells.

The staining of pathology samples demonstrated that the internal structure of colorectal cancers represents a disrupted form of the healthy colonic epithelium [38], both in terms of the organisation of cells and the localisation of protein expression. The staining of Dukes' Stage B and C tumours also highlights that the expression of proteins is highly variable both between patients and within the same sample, something that has been previously noted for E-cadherin [450, 451], vimentin [452, 453], β-catenin [451], Slug [450], collagen I [378] and collagen IV [378].

This high level of variability increases the difficulty of making an assessment about the accuracy of the protein expression achieved by the SW480 and SW620 cell lines in the 3D model developed here. While some comparisons can be drawn between the lack of E-cadherin expression in the cell lines (Figure 6.18A and Figure 6.18A) and some of the pathology samples (Figure 6.22A & B) and the high levels of vimentin in the cell lines (Figure 6.19D) and pathology samples (Figure 6.22C & D and Figure 6.23C & D), the lack of protein expression information of the original tumours from which the two cell lines were derived [48] allows for comparisons to unrelated tissue samples only, which limits the confidence in the interpretation of the data. The most accurate assessment of relationship the protein expression profile of colorectal cancer cells in 3D culture on Alvetex® Scaffold to the protein expression profile of the original tumour would be to use a cell line where expression information of the source tissue is available, or to use primary cells directly from the tumour taken for histological analysis.

7 Summary and General Discussion

7.1 Thesis Background

The tumour microenvironment, consisting of multiple cell types, ECM proteins and nutrient gradients, provides a complex signalling environment to direct the behaviour of the cancer cells [365, 366]. The interaction between the cancer cells and this tumour microenvironment can go on to impact patient survival, as seen by the correlation between the stromal content of tumours and survival rates [58]. The importance of these interactions is also seen when cancer cells metastasise to form secondary tumours, either in localised lymph nodes or more distant metastases in other organs. Paget's (1889) paper alludes to the need for a permissive microenvironment for the establishment of a secondary tumour [64]. Due to the severe impact that the formation of metastatic tumours has on patient survival, understanding the effect that the microenvironment has on acquisition of migratory behaviour prior to metastasis is important to be able to target it for therapeutic treatment.

While there have been numerous studies into the migratory behaviour of cancer cells using *in vitro* models, many of them are carried out using assays which enforce an unrealistic culturing microenvironment on the cells, such as scratch wound assays [199] and Transwell® inserts [206].These models can give rise to behaviours which do not reflect behaviour of cancers in patients. This discrepancy in behaviours can be problematic for drug discovery as it leads to many compounds which show promise in early *in vitro* screening failing in *in vivo* or clinical trials. This is reflected by the low rate of success in bringing antineoplastic agents through to a marketable therapy [454, 455]. Consequently, there has been a recent push within the scientific community to develop more accurate, 3D models of the tumour microenvironment in order to study the behaviour of the cells and identify compounds of therapeutic interest which are more likely to make it past *in vivo* screening. While many of these models have been documented in the literature, many of those that are a good reflection of the tumour microenvironment are unsuitable for widespread use due to variability between sample sets [177, 216] or the need for highly specialist equipment in order to establish the 3D culture [193].

One emerging area which may be well placed to provide a culturing solution which is both reproducible and reflects an accurate tumour microenvironment is the use of synthetic scaffold technologies to provide the 3D culturing environment. One such commercially available, technology is Alvetex®, a polystyrene based membrane which comes in two pore sizes. These have already been demonstrated to support the culture of a variety of cell lines [232, 261]. Therefore this material was selected to assess its feasibility for use in investigating the migration of cancer cells by recreating a more biologically relevant culture microenvironment.

The cancer type selected for this study was colorectal cancer, currently the fourth most diagnosed cancer type in England [9]. The importance of understanding the alteration in behaviour which gives rise to the formation of secondary tumours is of particular importance for this cancer because of the steep decline in patient survival seen between those patients diagnosed with and without

secondary tumours [59]. This is in addition to its overall poor prognosis rate in the UK relative to other Western countries [11, 12].

Further to the clear link between cancer progression and patient prognosis, the critical genetic mutations required for the initiation and progression of the disease are also well documented. First proposed by Fearon and Vogelstein [35], the adenoma-carcinoma progression of colorectal cancer demonstrates that the initial mutations required to change healthy colonic epithelium to an overproliferative pre-cursor and on to tumour formation rely on genetic mutations to key members of the Wnt signalling pathway as shown in Figure 1.1. These Wnt pathway mutations upset the usual control of proliferation vs differentiation seen in the healthy colonic epithelium [90] and can drive the cancer cells towards EMT resulting in an increase in the migratory behaviour of the cells [456].

In addition to the clear relationship between the Wnt signalling pathway and colorectal cancer, many other signalling pathways have been linked to promoting the migratory behaviour of colorectal cancer cells, including bone morphogenetic protein (BMP)-4 [457] and TGFβ [458]. One of these pathways which has been linked with the establishment of cancers in general is the IGF-I signalling pathway, which has known interactions with downstream mediators of Wnt signalling [138]. Inhibition of signalling within this pathway has been demonstrated to inhibit the migratory behaviour of colorectal cancer cell lines *in vitro* [334, 345], which suggests that targeting this pathway may be of some interest in the development of anti-migratory drugs.

7.2 Summary of Experimental Findings

7.2.1 Optimisation of a novel 3D *in vitro* migration model

Through the optimisation of cell culture protocols carried out in Chapter 3, a protocol for the 3D culture of both the SW480 and SW620 colorectal cancer cell lines on Alvetex® Scaffold was determined. This protocol was sufficient to allow for the growth of viable cultures of two cell lines with known differences in 2D culturing behaviour, in terms of cell morphology and cell proliferation rate [48], adding to the number of cell types that have successfully been cultured using this system [232, 260-263].

This optimisation process demonstrated the affect that the 3D culturing environment can have on the culture of cells, as the smaller void variant, Alvetex® Strata, was found to be unable to support 3D cultures of these cell lines due to poor adhesion to the material (Figure 3.19). As Alvetex® Scaffold and Alvetex® Strata are composed of the same material and it is the physical properties that vary (Figure 3.1), this demonstrates that the physical characteristics of the culture environment can have a large impact on experimental outcomes.

The assessment of protein expression in 3D cultures of different cell densities, obtained by different lengths of culturing, also demonstrated that the expression of the key EMT protein E-cadherin varied with culture density. The lack of E-cadherin expression, as detected via both immunohistochemical staining and Western blot analysis, in the lower density 7 day cultures, compared to the higher density 11 day cultures (Figure 3.21), correlates with the analysis of sparse

and dense 2D cultures of the SW480 cell line presented by Conacci-Sorrell *et al*. [223]. This suggests that under certain circumstances comparisons between 2D and 3D cultures can be made as they retain some similar culturing characteristics and this allows data obtained using this model to be compared to 2D counterpart studies.

7.2.2 Inhibition of the Wnt signalling pathway reduces cell migration in colorectal cancer

In Chapter 4, the effect of inhibiting Wnt signalling via small molecule inhibitors was assessed in 2D and 3D migration assays. This work highlighted two major results, firstly that the results obtained in the 2D and 3D models did not always correlate, with cardamonin causing a significant decrease in the amount of single cell migration of the SW620 cell line observed in a 2D scratch wound assay (Figure 4.25) but failing to significantly affect cell penetration in the 3D migration model (Figure 4.19).

Furthermore, this study highlighted a small molecule, IWR-1, with no previously published evidence supporting a role in the inhibition of cancer cell migration, which was found to decrease the cell penetration of the SW620 cell line in 3D (Figure 4.19) while having no observed affect in 2D (Figure 4.23 and Figure 4.25). This molecule was shown to be effective at the commonly used concentration of 10μM in addition to the lower concentration of 1μM, without affecting the proliferation of either of the two colorectal cancer cell lines, in contrast to data previously demonstrated for a variety of human and murine lung cancer cell lines [321].

The immunohistochemical analysis of 3D SW620 cultures in the absence and presence of 10μM IWR-1 demonstrated that application of this small molecule reduced the level of β-catenin seen within the cells (Figure 4.34). This finding correlates with the findings of Chen *et al*. [313], who demonstrated that the application of 10μM IWR-1 decreased the amount of β-catenin which was not bound to E-cadherin in the colorectal cancer cell line DLD-1.

7.2.3 Modulation of IGF-I signalling to alter the migration of colorectal cancer cells

The findings presented in Chapter 5 broadly correlate with the previously published data regarding the relationship between IGF-I signalling and the migratory behaviour of colorectal cancer cells. While failing to induce a change in the observed cell migration, either collective (Figure 5.8) or single cell (Figure 5.10), in 2D scratch wound assays, the addition of exogenous IGF-I into the culture media of the 3D migration assay induced an increase in the migration of the SW480 cell line (Figure 5.4). This correlates with data presented by Bauer *et al*. [334], where the migration and invasion of the colorectal cancer cell line KM12L4 was significantly increased in the presence of IGF-I in uncoated and Matrigel coated Transwell® assays, although IGF-I was used at a higher concentration in this study, 100ng/ml, than the effective concentration of 1ng/ml determined here. This data was not seen in conjunction with an increase in cell proliferation (Figure 5.6), which is not in agreement with previously published data showing that the injection of exogenous IGF-I into

mice with transplantation of colon 38 tissue resulted in a significant increase in tumour growth over a 6 week period compared to control mice [146].

Again, the data presented here for the work carried out using the IGF-IR inhibitor NVP-AEW541 broadly correlated with previously published data for its effect on the migratory behaviour of cancer cells, but not the proliferative behaviour. The inhibition of migration by NVP-AEW541 in the absence and presence of IGF-I has previously been demonstrated in Transwell® assays for Ewing's sarcoma [351] and pancreatic cancer [348] cell lines, whereas the inhibition of migration was only seen in the presence of IGF-I in the model used here (Figure 5.12 and Figure 5.20). As seen with the inclusion of IGF-I in the culture media, the inclusion of NVP-AEW541 was not seen to affect cell proliferation at concentrations where cell migration was affected (Figure 5.14 and Figure 5.22), whereas it has previously been shown to inhibit the proliferation of a variety of gastrointestinal tract cancer cell lines in the absence of IGF-I [345].

The mechanism of action for the IGF-I mediated increase in the cell migration of the SW480 cell line was determined to be via the action of PI3K leading into the Wnt signalling pathway, as opposed to via the action of Ras, as the application of the Wnt signalling inhibitor IWR-1, as identified in Chapter 4, was seen to return the IGF-I induced cell penetration levels back to control levels (Figure 5.28). As there is no published documentation of these compounds being used in conjunction to modulate the migratory behaviour of cancer cells, this result may provide an opportunity to target multiple signalling pathways simultaneously to reduce the migratory behaviour of cancers. This interaction between the Wnt and IGF-I pathways appears to be confirmed by the immunohistochemical staining of the 3D cultures, as the inclusion of IGF-I increased β-catenin expression (Figure 5.35 and Figure 5.38) whereas inclusion of either of the two inhibitors, NVP-AEW541 or IWR-1, decreased the expression of β-catenin (Figure 5.36, Figure 5.37 and Figure 5.38). The mechanism of action of the Wnt and IGF-I pathways and their inhibitors is demonstrated in Figure 7.1.

7.2.4 Improvement of the 3D migration model by utilising ECM coating and co-culture

In Chapter 6, the biological relevance of the model was increased by utilising ECM coating and co-culture to provide a culturing microenvironment which was a more accurate reflection of the tumour microenvironment. The data presented in this Chapter demonstrated that both protocols produce viable cultures with colorectal cancer cell lines (Figure 6.1 and Figure 6.17), with further analysis of the cultures on coated scaffolds demonstrating that the provision of an ECM substrate affected cancer cell migration (Figure 6.3), proliferation (Figure 6.5) and attachment (Figure 6.8).

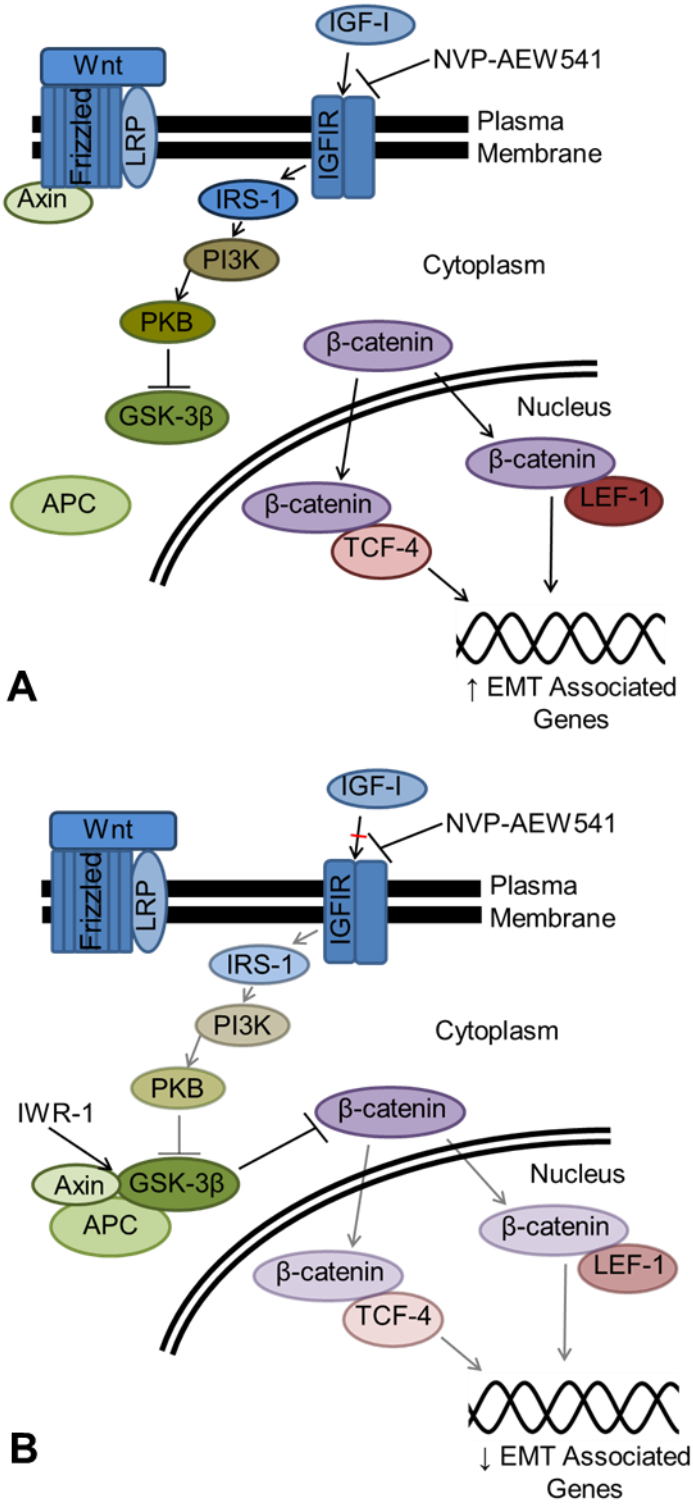

Figure 7.1: Schematic of the signalling interactions investigated by small molecule inhibitors in this thesis. In the control colorectal cancer cultures A: the Axin/APC/GSK-3β destruction complex is disrupted due to mutations to APC, leading to high levels of β-catenin, which translocates to the nucleus to mediate the transcription of EMT related genes. Additionally, IGF-I signalling can further inhibit the function of GSK-3β by the action of PI3K and PKB. In the presence of small molecules inhibitors B: IWR-1 stabilises the Axin/APC/GSK-3β destruction complex, even in the presence of a mutated APC protein, leading to the phosphorylation of β-catenin, targeting it for proteasomal degradation. Additionally, NVP-AEW541 binds to and blocks the IGF-IR, preventing the signalling cascade with inhibits GSK-3β function.

Immunohistochemical analysis of both *in vitro* 3D cultures and pathological samples demonstrated parallels between the protein expression profiles, with reduced E-cadherin expression and increased vimentin expression seen throughout (Figure 6.18, Figure 6.19, Figure 6.20, Figure 6.22 and Figure 6.23) and the expression of the basement membrane component collagen IV confined to the stromal portion of both co-cultures and pathological samples (Figure 6.20, Figure 6.22 and Figure 6.23). This demonstrates that while the organisation of the cells in the 3D cultures does not reflect that seen in pathological samples, the expression of proteins relating the EMT and migration are comparable.

For further detailed discussion of the findings generated in this thesis, refer to each of the primary results chapters.

7.3 Conclusions

In conclusion, the work presented in this thesis has demonstrated the application of modern cell culture technology to generate a 3D migration assay for colorectal cancer cells. While this model does not accurately replicate the tissue architecture of colorectal tumours, as seen from pathological samples, it provides the opportunity for a reproducible 3D model which does not rely on specialist equipment or protocols to provide insights into the behaviour of cancer cells *in vitro*, which allows it to be more accessible to a wider range of researchers.

Investigations into the effect of Wnt and IGF-I signalling on the migratory behaviour of colorectal cancer using the model generated in this thesis has highlighted IWR-1 as a compound of interest for the inhibition of the migration, which has not currently been shown in the literature. This demonstrates that data produced by this model can provide information regarding the signalling pathways involved in the change of migratory behaviour of cancer cells, even with the basic methods of analysis employed here and it is suggested that with the application of more complex assays, this model could yield further information regarding the events surrounding cancer cell migration.

7.4 Further Work

The results presented here in this thesis highlight several areas of further work for consideration. Firstly, as the co-culture work presented in in Chapter 6 was a proof of concept study to demonstrate the capacity of Alvetex® Scaffold to support the culture of colorectal cancer cells with a fibroblast-based stromal equivalent, the penetration of the two colorectal cancer cell lines should be quantified to assess the impact of co-culture on the migratory behaviour of these cells. While a limited amount of cell penetration would be expected relative to the amount seen in uncoated and coated assays, due to the physical barrier provided by the 3D fibroblast culture, there have been few examples in the literature of the changes in the behaviour of the SW480 and SW620 cell lines in response to fibroblasts, such as the demonstration of differing rates of proliferation in response to conditioned media from CAFs originating from either primary tumours or liver metastases [417].

Another area for further work which would follow on directly from data presented in this thesis should focus on investigation of the cumulative effect of media additives, as identified in Chapters 4

and 5, with the more biologically relevant 3D models utilising ECM coating and co-culture as presented in Chapter 6. While IWR-1, IGF-I and NVP-AEW541 have all been shown to be effective in modulating the migratory response of both the SW480 and SW620 cell lines in the uncoated 3D migration assay, inclusion of ECM coatings, which have also been shown to modulate cell behaviour in this model, or a secondary cell type may affect the efficacy of these additives in this model.

Additionally, the assessment of the impact of migration modulating media additives and ECM coatings on the expression of the EMT related proteins E-cadherin, vimentin, β-catenin and Slug was carried out using immunohistochemical staining, which provides qualitative data. Assessment of these protein levels via Western blots would provide quantitative data regarding protein expression, which would highlight any alterations to protein expression which are too small to be picked up by immunohistochemical staining. Also, while the proteins identified for analysis have been shown to be key proteins involved in EMT in colorectal cancer cells [79, 223], they are only a small selection of the proteins that have been identified as markers of EMT [80, 459] and a wider analysis of further EMT marker proteins may provide further clues to the mechanism of action by which the media additives and ECM coatings are modulating the migratory behaviour of colorectal cancer cells.

While the protein expression within the 3D migration model and pathological samples of colorectal cancer have been compared, there are problems with drawing conclusions between protein expression in cell lines and pathological samples, as discussed in Chapter 6. With the lack of pathological and protein expression information provided regarding the tumours from which the SW480 and SW620 cell lines were isolated [48], any alterations to protein expression may be artefacts of the extended period that these cells have been in *in vitro* culture and it is hard to determine if the protein expression pattern seen in the 3D model accurately reflects the protein expression in the original tumours. If pathological samples could be obtained such that part of the sample was histologically processed to determine the protein expression profile of the tumour and part of the tumour was processed for maintenance in both 2D and 3D *in vitro* cell culture, a comparison of protein expression profiles between the original tumour and *in vitro* cultures could be made to provide a more accurate assessment of the reliability of the 3D model in recreating a more accurate *in vivo*-like culturing environment.

Finally, an assessment of the applicability of the procedure carried out within this thesis to generate a 3D migration assay should be made on other cancer types. This would validate the model presented here as one which presents an easily accessible method for investigating the migration of a range of cancer cell types.

8 References

[1] ONS. Cancer Incidence and Mortality in the United Kingdom, 2008-10. 2012.

[2] ONS. Deaths Registered in England and Wales (Series DR), 2012. 2013.

[3] Strauli P. The spread of cancer in the organism. Facts and problems. Die Naturwissenschaften. 1977;64:403-9.

[4] Dvorak HF. Tumors: wounds that do not heal. Similarities between tumor stroma generation and wound healing. The New England journal of medicine. 1986;315:1650-9.

[5] Balmain A, Gray J, Ponder B. The genetics and genomics of cancer. Nat Genet. 2003;33 Suppl:238-44.

[6] Hanahan D, Weinberg RA. The hallmarks of cancer. Cell. 2000;100:57-70.

[7] Hanahan D, Weinberg RA. Hallmarks of cancer: the next generation. Cell. 2011;144:646-74.

[8] Floor SL, Dumont JE, Maenhaut C, Raspe E. Hallmarks of cancer: of all cancer cells, all the time? Trends Mol Med. 2012;18:509-15.

[9] ONS. Cancer Registration Statistics, England, 2011. 2013.

[10] ONS. Cancer Survival by NHS England Area Team: Patients diagnosed 1996-2011, followed up to 2012. 2013.

[11] Allemani C, Rachet B, Weir HK, Richardson LC, Lepage C, Faivre J, et al. Colorectal cancer survival in the USA and Europe: a CONCORD high-resolution study. BMJ open. 2013;3:e003055.

[12] Maringe C, Walters S, Rachet B, Butler J, Fields T, Finan P, et al. Stage at diagnosis and colorectal cancer survival in six high-income countries: a population-based study of patients diagnosed during 2000-2007. Acta Oncol. 2013;52:919-32.

[13] Crawford SM, Sauerzapf V, Haynes R, Forman D, Jones AP. Social and geographical factors affecting access to treatment of colorectal cancer: a cancer registry study. BMJ open. 2012;2:e000410.

[14] Downing A, Aravani A, Macleod U, Oliver S, Finan PJ, Thomas JD, et al. Early mortality from colorectal cancer in England: a retrospective observational study of the factors associated with death in the first year after diagnosis. Br J Cancer. 2013;108:681-5.

[15] Lichtenstein P, Holm NV, Verkasalo PK, Iliadou A, Kaprio J, Koskenvuo M, et al. Environmental and heritable factors in the causation of cancer--analyses of cohorts of twins from Sweden, Denmark, and Finland. The New England journal of medicine. 2000;343:78-85.

[16] Smyrk TC, Lynch HT. Microsatellite instability: impact on cancer progression in proximal and distal colorectal cancers. European journal of cancer. 1999;35:171-2.

[17] Berg M, Hagland HR, Soreide K. Comparison of CpG island methylator phenotype (CIMP) frequency in colon cancer using different probe- and gene-specific scoring alternatives on recommended multi-gene panels. PLoS One. 2014;9:e86657.

[18] Jass JR. Classification of colorectal cancer based on correlation of clinical, morphological and molecular features. Histopathology. 2007;50:113-30.

[19] Thibodeau SN, French AJ, Cunningham JM, Tester D, Burgart LJ, Roche PC, et al. Microsatellite instability in colorectal cancer: different mutator phenotypes and the principal involvement of hMLH1. Cancer Res. 1998;58:1713-8.

[20] Goel A, Arnold CN, Niedzwiecki D, Chang DK, Ricciardiello L, Carethers JM, et al. Characterization of sporadic colon cancer by patterns of genomic instability. Cancer Res. 2003;63:1608-14.
[21] Shimizu Y, Ikeda S, Fujimori M, Kodama S, Nakahara M, Okajima M, et al. Frequent alterations in the Wnt signaling pathway in colorectal cancer with microsatellite instability. Genes, chromosomes & cancer. 2002;33:73-81.
[22] Vasen HF, van der Meulen-de Jong AE, de Vos Tot Nederveen Cappel WH, Oliveira J, Group EGW. Familial colorectal cancer risk: ESMO clinical recommendations. Annals of oncology : official journal of the European Society for Medical Oncology / ESMO. 2009;20 Suppl 4:51-3.
[23] Jasperson KW, Tuohy TM, Neklason DW, Burt RW. Hereditary and familial colon cancer. Gastroenterology. 2010;138:2044-58.
[24] Nystrom-Lahti M, Parsons R, Sistonen P, Pylkkanen L, Aaltonen LA, Leach FS, et al. Mismatch repair genes on chromosomes 2p and 3p account for a major share of hereditary nonpolyposis colorectal cancer families evaluable by linkage. American journal of human genetics. 1994;55:659-65.
[25] Nicolaides NC, Papadopoulos N, Liu B, Wei YF, Carter KC, Ruben SM, et al. Mutations of two PMS homologues in hereditary nonpolyposis colon cancer. Nature. 1994;371:75-80.
[26] Kolodner RD, Tytell JD, Schmeits JL, Kane MF, Gupta RD, Weger J, et al. Germ-line msh6 mutations in colorectal cancer families. Cancer Res. 1999;59:5068-74.
[27] Lynch HT, de la Chapelle A. Genetic susceptibility to non-polyposis colorectal cancer. Journal of medical genetics. 1999;36:801-18.
[28] Lengauer C, Kinzler KW, Vogelstein B. Genetic instability in colorectal cancers. Nature. 1997;386:623-7.
[29] Bodmer WF, Bailey CJ, Bodmer J, Bussey HJ, Ellis A, Gorman P, et al. Localization of the gene for familial adenomatous polyposis on chromosome 5. Nature. 1987;328:614-6.
[30] Solomon E, Voss R, Hall V, Bodmer WF, Jass JR, Jeffreys AJ, et al. Chromosome 5 allele loss in human colorectal carcinomas. Nature. 1987;328:616-9.
[31] Groden J, Thliveris A, Samowitz W, Carlson M, Gelbert L, Albertsen H, et al. Identification and characterization of the familial adenomatous polyposis coli gene. Cell. 1991;66:589-600.
[32] Joslyn G, Carlson M, Thliveris A, Albertsen H, Gelbert L, Samowitz W, et al. Identification of deletion mutations and three new genes at the familial polyposis locus. Cell. 1991;66:601-13.
[33] Kinzler KW, Nilbert MC, Su LK, Vogelstein B, Bryan TM, Levy DB, et al. Identification of FAP locus genes from chromosome 5q21. Science. 1991;253:661-5.
[34] Nishisho I, Nakamura Y, Miyoshi Y, Miki Y, Ando H, Horii A, et al. Mutations of chromosome 5q21 genes in FAP and colorectal cancer patients. Science. 1991;253:665-9.
[35] Fearon ER, Vogelstein B. A genetic model for colorectal tumorigenesis. Cell. 1990;61:759-67.
[36] Fearon ER, Jones PA. Progressing toward a molecular description of colorectal cancer development. The FASEB journal : official publication of the Federation of American Societies for Experimental Biology. 1992;6:2783-90.
[37] Finlay GJ. Genetics, molecular biology and colorectal cancer. Mutation research. 1993;290:3-12.
[38] Kinzler KW, Vogelstein B. Lessons from hereditary colorectal cancer. Cell. 1996;87:159-70.

[39] Miyaki M, Seki M, Okamoto M, Yamanaka A, Maeda Y, Tanaka K, et al. Genetic changes and histopathological types in colorectal tumors from patients with familial adenomatous polyposis. Cancer Res. 1990;50:7166-73.
[40] Pinto D, Clevers H. Wnt, stem cells and cancer in the intestine. Biology of the cell / under the auspices of the European Cell Biology Organization. 2005;97:185-96.
[41] Yusof AS, Isa ZM, Shah SA. Dietary patterns and risk of colorectal cancer: a systematic review of cohort studies (2000-2011). Asian Pacific journal of cancer prevention : APJCP. 2012;13:4713-7.
[42] Renehan AG, Tyson M, Egger M, Heller RF, Zwahlen M. Body-mass index and incidence of cancer: a systematic review and meta-analysis of prospective observational studies. Lancet. 2008;371:569-78.
[43] Jiang Y, Ben Q, Shen H, Lu W, Zhang Y, Zhu J. Diabetes mellitus and incidence and mortality of colorectal cancer: a systematic review and meta-analysis of cohort studies. European journal of epidemiology. 2011;26:863-76.
[44] Giovannucci E. An updated review of the epidemiological evidence that cigarette smoking increases risk of colorectal cancer. Cancer epidemiology, biomarkers & prevention : a publication of the American Association for Cancer Research, cosponsored by the American Society of Preventive Oncology. 2001;10:725-31.
[45] Cho E, Smith-Warner SA, Ritz J, van den Brandt PA, Colditz GA, Folsom AR, et al. Alcohol intake and colorectal cancer: a pooled analysis of 8 cohort studies. Annals of internal medicine. 2004;140:603-13.
[46] Dukes CE. The Classification of Cancer of the Rectum. J PatholBacteriol. 1932;35:323-32.
[47] Edge SB, Byrd DR, Compton CC, Fritz AG, Greene FL, Trotti A. AJCC Cancer Staging Manual. 7th 2010 Edition ed: Springer; 2009.
[48] Leibovitz A, Stinson JC, McCombs WB, 3rd, McCoy CE, Mazur KC, Mabry ND. Classification of human colorectal adenocarcinoma cell lines. Cancer Res. 1976;36:4562-9.
[49] Chan CC, Menges M, Orzechowski HD, Orendain N, Pistorius G, Feifel G, et al. Increased matrix metalloproteinase 2 concentration and transcript expression in advanced colorectal carcinomas. International journal of colorectal disease. 2001;16:133-40.
[50] Kirklin JW, Dockerty MB, Waugh JM. The role of the peritoneal reflection in the prognosis of carcinoma of the rectum and sigmoid colon. Surgery, gynecology & obstetrics. 1949;88:326-31.
[51] Dukes CE. The Surgical Pathology of Rectal Cancer. Journal of clinical pathology. 1949;2:95-8.
[52] Astler VB, Coller FA. The prognostic significance of direct extension of carcinoma of the colon and rectum. Annals of surgery. 1954;139:846-52.
[53] Dukes CE, Bussey HJ. The spread of rectal cancer and its effect on prognosis. Br J Cancer. 1958;12:309-20.
[54] Ovalle WK, Nahirney PC. Netter's Essential Histology. 1st Edition ed: Saunders Elsevier; 2008.
[55] Turnbull RB, Jr., Kyle K, Watson FR, Spratt J. Cancer of the colon: the influence of the no-touch isolation technic on survival rates. Annals of surgery. 1967;166:420-7.
[56] Gunderson LL, Sosin H. Areas of failure found at reoperation (second or symptomatic look) following "curative surgery" for adenocarcinoma of the rectum. Clinicopathologic correlation and implications for adjuvant therapy. Cancer. 1974;34:1278-92.

[57] Newland RC, Chapuis PH, Pheils MT, MacPherson JG. The relationship of survival to staging and grading of colorectal carcinoma: a prospective study of 503 cases. Cancer. 1981;47:1424-9.
[58] Mesker WE, Junggeburt JM, Szuhai K, de Heer P, Morreau H, Tanke HJ, et al. The carcinoma-stromal ratio of colon carcinoma is an independent factor for survival compared to lymph node status and tumor stage. Cellular oncology : the official journal of the International Society for Cellular Oncology. 2007;29:387-98.
[59] NCIN. Colorectal Cancer Survival by Stage. 2009.
[60] Raraty MG, Winstanley JH. Variation in the staging of colorectal carcinomas: a survey of current practice. Annals of the Royal College of Surgeons of England. 1998;80:188-91.
[61] Compton CC. Key issues in reporting common cancer specimens: problems in pathologic staging of colon cancer. Archives of pathology & laboratory medicine. 2006;130:318-24.
[62] Gao P, Song YX, Wang ZN, Xu YY, Tong LL, Sun JX, et al. Is the prediction of prognosis not improved by the seventh edition of the TNM classification for colorectal cancer? Analysis of the surveillance, epidemiology, and end results (SEER) database. BMC Cancer. 2013;13:123.
[63] Hari DM, Leung AM, Lee JH, Sim MS, Vuong B, Chiu CG, et al. AJCC Cancer Staging Manual 7th edition criteria for colon cancer: do the complex modifications improve prognostic assessment? Journal of the American College of Surgeons. 2013;217:181-90.
[64] Paget S. The distribution of secondary growths in cancer of the breast. 1889. Cancer Metastasis Rev. 1989;8:98-101.
[65] Fidler IJ. The pathogenesis of cancer metastasis: the 'seed and soil' hypothesis revisited. Nature reviews Cancer. 2003;3:453-8.
[66] Friedl P, Brocker EB. The biology of cell locomotion within three-dimensional extracellular matrix. Cell Mol Life Sci. 2000;57:41-64.
[67] Price JT, Bonovich MT, Kohn EC. The biochemistry of cancer dissemination. Critical reviews in biochemistry and molecular biology. 1997;32:175-253.
[68] Sahai E. Mechanisms of cancer cell invasion. Curr Opin Genet Dev. 2005;15:87-96.
[69] Friedl P, Gilmour D. Collective cell migration in morphogenesis, regeneration and cancer. Nat Rev Mol Cell Biol. 2009;10:445-57.
[70] Friedl P, Wolf K. Plasticity of cell migration: a multiscale tuning model. J Cell Biol. 2010;188:11-9.
[71] Friedl P. Prespecification and plasticity: shifting mechanisms of cell migration. Curr Opin Cell Biol. 2004;16:14-23.
[72] Brahimi-Horn MC, Chiche J, Pouyssegur J. Hypoxia and cancer. Journal of molecular medicine. 2007;85:1301-7.
[73] Taddei ML, Giannoni E, Comito G, Chiarugi P. Microenvironment and tumor cell plasticity: an easy way out. Cancer letters. 2013;341:80-96.
[74] Erler JT, Weaver VM. Three-dimensional context regulation of metastasis. Clin Exp Metastasis. 2009;26:35-49.
[75] Nosho K, Baba Y, Tanaka N, Shima K, Hayashi M, Meyerhardt JA, et al. Tumour-infiltrating T-cell subsets, molecular changes in colorectal cancer, and prognosis: cohort study and literature review. J Pathol. 2010;222:350-66.

[76] Nystrom ML, Thomas GJ, Stone M, Mackenzie IC, Hart IR, Marshall JF. Development of a quantitative method to analyse tumour cell invasion in organotypic culture. J Pathol. 2005;205:468-75.
[77] Gaggioli C, Hooper S, Hidalgo-Carcedo C, Grosse R, Marshall JF, Harrington K, et al. Fibroblast-led collective invasion of carcinoma cells with differing roles for RhoGTPases in leading and following cells. Nat Cell Biol. 2007;9:1392-400.
[78] Thiery JP, Acloque H, Huang RY, Nieto MA. Epithelial-mesenchymal transitions in development and disease. Cell. 2009;139:871-90.
[79] Loboda A, Nebozhyn MV, Watters JW, Buser CA, Shaw PM, Huang PS, et al. EMT is the dominant program in human colon cancer. BMC medical genomics. 2011;4:9.
[80] Lee JM, Dedhar S, Kalluri R, Thompson EW. The epithelial-mesenchymal transition: new insights in signaling, development, and disease. J Cell Biol. 2006;172:973-81.
[81] Yilmaz M, Christofori G. EMT, the cytoskeleton, and cancer cell invasion. Cancer Metastasis Rev. 2009;28:15-33.
[82] Joyce T, Cantarella D, Isella C, Medico E, Pintzas A. A molecular signature for Epithelial to Mesenchymal transition in a human colon cancer cell system is revealed by large-scale microarray analysis. Clin Exp Metastasis. 2009;26:569-87.
[83] Paszek MJ, Zahir N, Johnson KR, Lakins JN, Rozenberg GI, Gefen A, et al. Tensional homeostasis and the malignant phenotype. Cancer cell. 2005;8:241-54.
[84] Cheng G, Tse J, Jain RK, Munn LL. Micro-environmental mechanical stress controls tumor spheroid size and morphology by suppressing proliferation and inducing apoptosis in cancer cells. PLoS One. 2009;4:e4632.
[85] Ingber DE. Can cancer be reversed by engineering the tumor microenvironment? Semin Cancer Biol. 2008;18:356-64.
[86] Clevers H. Wnt/beta-catenin signaling in development and disease. Cell. 2006;127:469-80.
[87] Hoppler S, Kavanagh CL. Wnt signalling: variety at the core. J Cell Sci. 2007;120:385-93.
[88] Debruyne D, Oliveira MJ, Bracke M, Mareel M, Leroy A. Colon cancer cells: pro-invasive signalling. Int J Biochem Cell Biol. 2006;38:1231-6.
[89] Geibel JP. Secretion and absorption by colonic crypts. Annu Rev Physiol. 2005;67:471-90.
[90] van der Flier LG, Clevers H. Stem cells, self-renewal, and differentiation in the intestinal epithelium. Annu Rev Physiol. 2009;71:241-60.
[91] Mao B, Wu W, Li Y, Hoppe D, Stannek P, Glinka A, et al. LDL-receptor-related protein 6 is a receptor for Dickkopf proteins. Nature. 2001;411:321-5.
[92] Pinto D, Gregorieff A, Begthel H, Clevers H. Canonical Wnt signals are essential for homeostasis of the intestinal epithelium. Genes Dev. 2003;17:1709-13.
[93] Korinek V, Barker N, Moerer P, van Donselaar E, Huls G, Peters PJ, et al. Depletion of epithelial stem-cell compartments in the small intestine of mice lacking Tcf-4. Nat Genet. 1998;19:379-83.
[94] van de Wetering M, Sancho E, Verweij C, de Lau W, Oving I, Hurlstone A, et al. The beta-catenin/TCF-4 complex imposes a crypt progenitor phenotype on colorectal cancer cells. Cell. 2002;111:241-50.

[95] Holmberg J, Genander M, Halford MM, Anneren C, Sondell M, Chumley MJ, et al. EphB receptors coordinate migration and proliferation in the intestinal stem cell niche. Cell. 2006;125:1151-63.
[96] Albuquerque C, Baltazar C, Filipe B, Penha F, Pereira T, Smits R, et al. Colorectal cancers show distinct mutation spectra in members of the canonical WNT signaling pathway according to their anatomical location and type of genetic instability. Genes, chromosomes & cancer. 2010;49:746-59.
[97] Homfray TF, Cottrell SE, Ilyas M, Rowan A, Talbot IC, Bodmer WF, et al. Defects in mismatch repair occur after APC mutations in the pathogenesis of sporadic colorectal tumours. Human mutation. 1998;11:114-20.
[98] Huang J, Papadopoulos N, McKinley AJ, Farrington SM, Curtis LJ, Wyllie AH, et al. APC mutations in colorectal tumors with mismatch repair deficiency. Proc Natl Acad Sci U S A. 1996;93:9049-54.
[99] Huang J, Zheng S, Jin SH, Zhang SZ. Somatic mutations of APC gene in carcinomas from hereditary non-polyposis colorectal cancer patients. World journal of gastroenterology : WJG. 2004;10:834-6.
[100] Johnson V, Volikos E, Halford SE, Eftekhar Sadat ET, Popat S, Talbot I, et al. Exon 3 beta-catenin mutations are specifically associated with colorectal carcinomas in hereditary non-polyposis colorectal cancer syndrome. Gut. 2005;54:264-7.
[101] Kitaeva MN, Grogan L, Williams JP, Dimond E, Nakahara K, Hausner P, et al. Mutations in beta-catenin are uncommon in colorectal cancer occurring in occasional replication error-positive tumors. Cancer Res. 1997;57:4478-81.
[102] Lovig T, Meling GI, Diep CB, Thorstensen L, Norheim Andersen S, Lothe RA, et al. APC and CTNNB1 mutations in a large series of sporadic colorectal carcinomas stratified by the microsatellite instability status. Scandinavian journal of gastroenterology. 2002;37:1184-93.
[103] Miyaki M, Iijima T, Kimura J, Yasuno M, Mori T, Hayashi Y, et al. Frequent mutation of beta-catenin and APC genes in primary colorectal tumors from patients with hereditary nonpolyposis colorectal cancer. Cancer Res. 1999;59:4506-9.
[104] Muller O, Nimmrich I, Finke U, Friedl W, Hoffmann I. A beta-catenin mutation in a sporadic colorectal tumor of the RER phenotype and absence of beta-catenin germline mutations in FAP patients. Genes, chromosomes & cancer. 1998;22:37-41.
[105] Salahshor S, Kressner U, Pahlman L, Glimelius B, Lindmark G, Lindblom A. Colorectal cancer with and without microsatellite instability involves different genes. Genes, chromosomes & cancer. 1999;26:247-52.
[106] Shitoh K, Furukawa T, Kojima M, Konishi F, Miyaki M, Tsukamoto T, et al. Frequent activation of the beta-catenin-Tcf signaling pathway in nonfamilial colorectal carcinomas with microsatellite instability. Genes, chromosomes & cancer. 2001;30:32-7.
[107] Suraweera N, Robinson J, Volikos E, Guenther T, Talbot I, Tomlinson I, et al. Mutations within Wnt pathway genes in sporadic colorectal cancers and cell lines. Int J Cancer. 2006;119:1837-42.
[108] Sjoblom T, Jones S, Wood LD, Parsons DW, Lin J, Barber TD, et al. The consensus coding sequences of human breast and colorectal cancers. Science. 2006;314:268-74.

[109] Ghosh D, Yu H, Tan XF, Lim TK, Zubaidah RM, Tan HT, et al. Identification of key players for colorectal cancer metastasis by iTRAQ quantitative proteomics profiling of isogenic SW480 and SW620 cell lines. Journal of proteome research. 2011;10:4373-87.
[110] El-Bahrawy M, Poulsom R, Rowan AJ, Tomlinson IT, Alison MR. Characterization of the E-cadherin/catenin complex in colorectal carcinoma cell lines. Int J Exp Pathol. 2004;85:65-74.
[111] Faux MC, Ross JL, Meeker C, Johns T, Ji H, Simpson RJ, et al. Restoration of full-length adenomatous polyposis coli (APC) protein in a colon cancer cell line enhances cell adhesion. J Cell Sci. 2004;117:427-39.
[112] Bandapalli OR, Dihlmann S, Helwa R, Macher-Goeppinger S, Weitz J, Schirmacher P, et al. Transcriptional activation of the beta-catenin gene at the invasion front of colorectal liver metastases. J Pathol. 2009;218:370-9.
[113] Rinderknecht E, Humbel RE. The amino acid sequence of human insulin-like growth factor I and its structural homology with proinsulin. J Biol Chem. 1978;253:2769-76.
[114] Ullrich A, Gray A, Tam AW, Yang-Feng T, Tsubokawa M, Collins C, et al. Insulin-like growth factor I receptor primary structure: comparison with insulin receptor suggests structural determinants that define functional specificity. EMBO J. 1986;5:2503-12.
[115] Kasuga M, Sasaki N, Kahn CR, Nissley SP, Rechler MM. Antireceptor antibodies as probes of insulinlike growth factor receptor structure. J Clin Invest. 1983;72:1459-69.
[116] Rinderknecht E, Humbel RE. Primary structure of human insulin-like growth factor II. FEBS Lett. 1978;89:283-6.
[117] Massague J, Czech MP. The subunit structures of two distinct receptors for insulin-like growth factors I and II and their relationship to the insulin receptor. J Biol Chem. 1982;257:5038-45.
[118] Steele-Perkins G, Turner J, Edman JC, Hari J, Pierce SB, Stover C, et al. Expression and characterization of a functional human insulin-like growth factor I receptor. J Biol Chem. 1988;263:11486-92.
[119] Olivecrona H, Hilding A, Ekstrom C, Barle H, Nyberg B, Moller C, et al. Acute and short-term effects of growth hormone on insulin-like growth factors and their binding proteins: serum levels and hepatic messenger ribonucleic acid responses in humans. The Journal of clinical endocrinology and metabolism. 1999;84:553-60.
[120] Johansson JO, Oscarsson J, Bjarnason R, Bengtsson BA. Two weeks of daily injections and continuous infusion of recombinant human growth hormone (GH) in GH-deficient adults: I. Effects on insulin-like growth factor-I (IGF-I), GH and IGF binding proteins, and glucose homeostasis. Metabolism: clinical and experimental. 1996;45:362-9.
[121] Lee PD, Durham SK, Martinez V, Vasconez O, Powell DR, Guevara-Aguirre J. Kinetics of insulin-like growth factor (IGF) and IGF-binding protein responses to a single dose of growth hormone. The Journal of clinical endocrinology and metabolism. 1997;82:2266-74.
[122] Han VK, D'Ercole AJ, Lund PK. Cellular localization of somatomedin (insulin-like growth factor) messenger RNA in the human fetus. Science. 1987;236:193-7.
[123] Lund PK, Moats-Staats BM, Hynes MA, Simmons JG, Jansen M, D'Ercole AJ, et al. Somatomedin-C/insulin-like growth factor-I and insulin-like growth factor-II mRNAs in rat fetal and adult tissues. J Biol Chem. 1986;261:14539-44.
[124] Friedrich N, Alte D, Volzke H, Spilcke-Liss E, Ludemann J, Lerch MM, et al. Reference ranges of serum IGF-1 and IGFBP-3 levels in a general adult population: results of the Study of

Health in Pomerania (SHIP). Growth hormone & IGF research : official journal of the Growth Hormone Research Society and the International IGF Research Society. 2008;18:228-37.
[125] Kong AP, Wong GW, Choi KC, Ho CS, Chan MH, Lam CW, et al. Reference values for serum levels of insulin-like growth factor (IGF-1) and IGF-binding protein 3 (IGFBP-3) and their ratio in Chinese adolescents. Clinical biochemistry. 2007;40:1093-9.
[126] Mattsson A, Svensson D, Schuett B, Osterziel KJ, Ranke MB. Multidimensional reference regions for IGF-I, IGFBP-2 and IGFBP-3 concentrations in serum of healthy adults. Growth hormone & IGF research : official journal of the Growth Hormone Research Society and the International IGF Research Society. 2008;18:506-16.
[127] Izumi T, White MF, Kadowaki T, Takaku F, Akanuma Y, Kasuga M. Insulin-like growth factor I rapidly stimulates tyrosine phosphorylation of a Mr 185,000 protein in intact cells. J Biol Chem. 1987;262:1282-7.
[128] Shemer J, Adamo M, Wilson GL, Heffez D, Zick Y, LeRoith D. Insulin and insulin-like growth factor-I stimulate a common endogenous phosphoprotein substrate (pp185) in intact neuroblastoma cells. J Biol Chem. 1987;262:15476-82.
[129] Sasaoka T, Rose DW, Jhun BH, Saltiel AR, Draznin B, Olefsky JM. Evidence for a functional role of Shc proteins in mitogenic signaling induced by insulin, insulin-like growth factor-1, and epidermal growth factor. J Biol Chem. 1994;269:13689-94.
[130] Myers MG, Jr., Backer JM, Sun XJ, Shoelson S, Hu P, Schlessinger J, et al. IRS-1 activates phosphatidylinositol 3'-kinase by associating with src homology 2 domains of p85. Proc Natl Acad Sci U S A. 1992;89:10350-4.
[131] Backer JM, Myers MG, Jr., Shoelson SE, Chin DJ, Sun XJ, Miralpeix M, et al. Phosphatidylinositol 3'-kinase is activated by association with IRS-1 during insulin stimulation. EMBO J. 1992;11:3469-79.
[132] Dufourny B, Alblas J, van Teeffelen HA, van Schaik FM, van der Burg B, Steenbergh PH, et al. Mitogenic signaling of insulin-like growth factor I in MCF-7 human breast cancer cells requires phosphatidylinositol 3-kinase and is independent of mitogen-activated protein kinase. J Biol Chem. 1997;272:31163-71.
[133] Tartare-Deckert S, Sawka-Verhelle D, Murdaca J, Van Obberghen E. Evidence for a differential interaction of SHC and the insulin receptor substrate-1 (IRS-1) with the insulin-like growth factor-I (IGF-I) receptor in the yeast two-hybrid system. J Biol Chem. 1995;270:23456-60.
[134] Craparo A, O'Neill TJ, Gustafson TA. Non-SH2 domains within insulin receptor substrate-1 and SHC mediate their phosphotyrosine-dependent interaction with the NPEY motif of the insulin-like growth factor I receptor. J Biol Chem. 1995;270:15639-43.
[135] Skolnik EY, Lee CH, Batzer A, Vicentini LM, Zhou M, Daly R, et al. The SH2/SH3 domain-containing protein GRB2 interacts with tyrosine-phosphorylated IRS1 and Shc: implications for insulin control of ras signalling. EMBO J. 1993;12:1929-36.
[136] Rozakis-Adcock M, McGlade J, Mbamalu G, Pelicci G, Daly R, Li W, et al. Association of the Shc and Grb2/Sem5 SH2-containing proteins is implicated in activation of the Ras pathway by tyrosine kinases. Nature. 1992;360:689-92.
[137] Jhun BH, Meinkoth JL, Leitner JW, Draznin B, Olefsky JM. Insulin and insulin-like growth factor-I signal transduction requires p21ras. J Biol Chem. 1994;269:5699-704.

[138] Cross DA, Alessi DR, Vandenheede JR, McDowell HE, Hundal HS, Cohen P. The inhibition of glycogen synthase kinase-3 by insulin or insulin-like growth factor 1 in the rat skeletal muscle cell line L6 is blocked by wortmannin, but not by rapamycin: evidence that wortmannin blocks activation of the mitogen-activated protein kinase pathway in L6 cells between Ras and Raf. The Biochemical journal. 1994;303 (Pt 1):21-6.
[139] Cross DA, Alessi DR, Cohen P, Andjelkovich M, Hemmings BA. Inhibition of glycogen synthase kinase-3 by insulin mediated by protein kinase B. Nature. 1995;378:785-9.
[140] van Weeren PC, de Bruyn KM, de Vries-Smits AM, van Lint J, Burgering BM. Essential role for protein kinase B (PKB) in insulin-induced glycogen synthase kinase 3 inactivation. Characterization of dominant-negative mutant of PKB. J Biol Chem. 1998;273:13150-6.
[141] Playford MP, Bicknell D, Bodmer WF, Macaulay VM. Insulin-like growth factor 1 regulates the location, stability, and transcriptional activity of beta-catenin. Proc Natl Acad Sci U S A. 2000;97:12103-8.
[142] Desbois-Mouthon C, Cadoret A, Blivet-Van Eggelpoel MJ, Bertrand F, Cherqui G, Perret C, et al. Insulin and IGF-1 stimulate the beta-catenin pathway through two signalling cascades involving GSK-3beta inhibition and Ras activation. Oncogene. 2001;20:252-9.
[143] Sell C, Rubini M, Rubin R, Liu JP, Efstratiadis A, Baserga R. Simian virus 40 large tumor antigen is unable to transform mouse embryonic fibroblasts lacking type 1 insulin-like growth factor receptor. Proc Natl Acad Sci U S A. 1993;90:11217-21.
[144] Sell C, Dumenil G, Deveaud C, Miura M, Coppola D, DeAngelis T, et al. Effect of a null mutation of the insulin-like growth factor I receptor gene on growth and transformation of mouse embryo fibroblasts. Molecular and cellular biology. 1994;14:3604-12.
[145] Ealey KN, Xuan W, Lu S, Archer MC. Colon carcinogenesis in liver-specific IGF-I-deficient (LID) mice. Int J Cancer. 2008;122:472-6.
[146] Wu Y, Yakar S, Zhao L, Hennighausen L, LeRoith D. Circulating insulin-like growth factor-I levels regulate colon cancer growth and metastasis. Cancer Res. 2002;62:1030-5.
[147] Manousos O, Souglakos J, Bosetti C, Tzonou A, Chatzidakis V, Trichopoulos D, et al. IGF-I and IGF-II in relation to colorectal cancer. Int J Cancer. 1999;83:15-7.
[148] Ma J, Pollak MN, Giovannucci E, Chan JM, Tao Y, Hennekens CH, et al. Prospective study of colorectal cancer risk in men and plasma levels of insulin-like growth factor (IGF)-I and IGF-binding protein-3. J Natl Cancer Inst. 1999;91:620-5.
[149] Probst-Hensch NM, Yuan JM, Stanczyk FZ, Gao YT, Ross RK, Yu MC. IGF-1, IGF-2 and IGFBP-3 in prediagnostic serum: association with colorectal cancer in a cohort of Chinese men in Shanghai. Br J Cancer. 2001;85:1695-9.
[150] Rinaldi S, Cleveland R, Norat T, Biessy C, Rohrmann S, Linseisen J, et al. Serum levels of IGF-I, IGFBP-3 and colorectal cancer risk: results from the EPIC cohort, plus a meta-analysis of prospective studies. Int J Cancer. 2010;126:1702-15.
[151] Palmqvist R, Hallmans G, Rinaldi S, Biessy C, Stenling R, Riboli E, et al. Plasma insulin-like growth factor 1, insulin-like growth factor binding protein 3, and risk of colorectal cancer: a prospective study in northern Sweden. Gut. 2002;50:642-6.
[152] Renehan AG, Zwahlen M, Minder C, O'Dwyer ST, Shalet SM, Egger M. Insulin-like growth factor (IGF)-I, IGF binding protein-3, and cancer risk: systematic review and meta-regression analysis. Lancet. 2004;363:1346-53.

[153] Major JM, Laughlin GA, Kritz-Silverstein D, Wingard DL, Barrett-Connor E. Insulin-like growth factor-I and cancer mortality in older men. The Journal of clinical endocrinology and metabolism. 2010;95:1054-9.
[154] Griffith LG, Swartz MA. Capturing complex 3D tissue physiology in vitro. Nat Rev Mol Cell Biol. 2006;7:211-24.
[155] Mueller-Klieser W. Three-dimensional cell cultures: from molecular mechanisms to clinical applications. The American journal of physiology. 1997;273:C1109-23.
[156] Kim JB. Three-dimensional tissue culture models in cancer biology. Semin Cancer Biol. 2005;15:365-77.
[157] Smalley KS, Lioni M, Herlyn M. Life isn't flat: taking cancer biology to the next dimension. In Vitro Cell Dev Biol Anim. 2006;42:242-7.
[158] Yamada KM, Cukierman E. Modeling tissue morphogenesis and cancer in 3D. Cell. 2007;130:601-10.
[159] Justice BA, Badr NA, Felder RA. 3D cell culture opens new dimensions in cell-based assays. Drug Discov Today. 2009;14:102-7.
[160] Dutta RC, Dutta AK. Cell-interactive 3D-scaffold; advances and applications. Biotechnol Adv. 2009;27:334-9.
[161] Ghajar CM, Bissell MJ. Tumor engineering: the other face of tissue engineering. Tissue engineering Part A. 2010;16:2153-6.
[162] Nyga A, Cheema U, Loizidou M. 3D tumour models: novel in vitro approaches to cancer studies. Journal of cell communication and signaling. 2011;5:239-48.
[163] Kimlin LC, Casagrande G, Virador VM. In vitro three-dimensional (3D) models in cancer research: An update. Molecular Carcinogenesis. 2013;52:167-82.
[164] Page H, Flood P, Reynaud EG. Three-dimensional tissue cultures: current trends and beyond. Cell and tissue research. 2013;352:123-31.
[165] Birgersdotter A, Sandberg R, Ernberg I. Gene expression perturbation in vitro--a growing case for three-dimensional (3D) culture systems. Semin Cancer Biol. 2005;15:405-12.
[166] Kenny PA, Lee GY, Myers CA, Neve RM, Semeiks JR, Spellman PT, et al. The morphologies of breast cancer cell lines in three-dimensional assays correlate with their profiles of gene expression. Mol Oncol. 2007;1:84-96.
[167] Wu YM, Tang J, Zhao P, Chen ZN, Jiang JL. Morphological changes and molecular expressions of hepatocellular carcinoma cells in three-dimensional culture model. Exp Mol Pathol. 2009;87:133-40.
[168] Yamada KM, Pankov R, Cukierman E. Dimensions and dynamics in integrin function. Braz J Med Biol Res. 2003;36:959-66.
[169] dit Faute MA, Laurent L, Ploton D, Poupon MF, Jardillier JC, Bobichon H. Distinctive alterations of invasiveness, drug resistance and cell-cell organization in 3D-cultures of MCF-7, a human breast cancer cell line, and its multidrug resistant variant. Clin Exp Metastasis. 2002;19:161-8.
[170] Rimann M, Graf-Hausner U. Synthetic 3D multicellular systems for drug development. Curr Opin Biotechnol. 2012;23:803-9.
[171] Quarles JM, Morris NG, Leibovitz A. Carcinoembryonic antigen production by human colorectal adenocarcinoma cells in matrix-perfusion culture. In vitro. 1980;16:113-8.

[172] Lee J, Cuddihy MJ, Kotov NA. Three-dimensional cell culture matrices: State of the art. Tissue Engineering Part B-Reviews. 2008;14:61-86.
[173] O'Keane JC, Kupchik HZ, Schroy PC, Andry CD, Collins E, O'Brien MJ. A three-dimensional system for long-term culture of human colorectal adenomas. Am J Pathol. 1990;137:1539-47.
[174] Breborowicz J, Easty GC, Birbeck M, Robertson D, Nery R, Neville AM. The monolayer and organ culture of human colorectal carcinomata and the associated "normal" colonic mucosa and their production of carcinoembryonic antigens. Br J Cancer. 1975;31:559-69.
[175] Brouquet A, Taleb P, Lot AS, Beauchet A, Julie C, Prevost G, et al. A model of primary culture of colorectal cancer and liver metastasis to predict chemosensitivity. J Surg Res. 2011;166:247-54.
[176] Sutherland RM. Cell and environment interactions in tumor microregions: the multicell spheroid model. Science. 1988;240:177-84.
[177] Kunz-Schughart LA. Multicellular tumor spheroids: intermediates between monolayer culture and in vivo tumor. Cell biology international. 1999;23:157-61.
[178] Hauptmann S, Zwadlo-Klarwasser G, Jansen M, Klosterhalfen B, Kirkpatrick CJ. Macrophages and multicellular tumor spheroids in co-culture: a three-dimensional model to study tumor-host interactions. Evidence for macrophage-mediated tumor cell proliferation and migration. Am J Pathol. 1993;143:1406-15.
[179] Dolznig H, Rupp C, Puri C, Haslinger C, Schweifer N, Wieser E, et al. Modeling colon adenocarcinomas in vitro a 3D co-culture system induces cancer-relevant pathways upon tumor cell and stromal fibroblast interaction. Am J Pathol. 2011;179:487-501.
[180] Tsunoda T, Takashima Y, Fujimoto T, Koyanagi M, Yoshida Y, Doi K, et al. Three-dimensionally specific inhibition of DNA repair-related genes by activated KRAS in colon crypt model. Neoplasia. 2010;12:397-404.
[181] Petersen OW, Ronnov-Jessen L, Howlett AR, Bissell MJ. Interaction with basement membrane serves to rapidly distinguish growth and differentiation pattern of normal and malignant human breast epithelial cells. Proc Natl Acad Sci U S A. 1992;89:9064-8.
[182] Kleinman HK, Martin GR. Matrigel: basement membrane matrix with biological activity. Semin Cancer Biol. 2005;15:378-86.
[183] Jongpaiboonkit L, King WJ, Lyons GE, Paguirigan AL, Warrick JW, Beebe DJ, et al. An adaptable hydrogel array format for 3-dimensional cell culture and analysis. Biomaterials. 2008;29:3346-56.
[184] Serebriiskii I, Castello-Cros R, Lamb A, Golemis EA, Cukierman E. Fibroblast-derived 3D matrix differentially regulates the growth and drug-responsiveness of human cancer cells. Matrix biology : journal of the International Society for Matrix Biology. 2008;27:573-85.
[185] Kobayashi H. Collagen gel droplet culture method to examine in vitro chemosensitivity. Methods in molecular medicine. 2005;110:59-67.
[186] Nakahara T, Sakaeda T, Nakamura T, Tamura T, Nishioka C, Aoyama N, et al. Chemosensitivity assessed by collagen gel droplet embedded culture drug sensitivity test, and MDR1, MRP1, and MRP2 mRNA expression in human colorectal adenocarcinomas. Pharmaceutical research. 2004;21:406-12.

[187] Derda R, Laromaine A, Mammoto A, Tang SK, Mammoto T, Ingber DE, et al. Paper-supported 3D cell culture for tissue-based bioassays. Proc Natl Acad Sci U S A. 2009;106:18457-62.
[188] Zhang M, Boughton P, Rose B, Lee CS, Hong AM. The use of porous scaffold as a tumor model. International journal of biomaterials. 2013;2013:396056.
[189] Leuhuber K, Klepal W, Hausott B, Marian B. Apoptosis in a tissue-like culture model of human colorectal adenoma cells. Tissue Cell. 2006;38:203-8.
[190] Roig AI, Hight SK, Shay JW. Two- and three-dimensional models for risk assessment of radiation-enhanced colorectal tumorigenesis. Radiat Res. 2009;171:33-40.
[191] Commandeur S, de Gruijl FR, Willemze R, Tensen CP, El Ghalbzouri A. An in vitro three-dimensional model of primary human cutaneous squamous cell carcinoma. Exp Dermatol. 2009;18:849-56.
[192] Nurmenniemi S, Sinikumpu T, Alahuhta I, Salo S, Sutinen M, Santala M, et al. A novel organotypic model mimics the tumor microenvironment. Am J Pathol. 2009;175:1281-91.
[193] Nyga A, Loizidou M, Emberton M, Cheema U. A novel tissue engineered three-dimensional in vitro colorectal cancer model. Acta Biomater. 2013;9:7917-26.
[194] Decaestecker C, Debeir O, Van Ham P, Kiss R. Can anti-migratory drugs be screened in vitro? A review of 2D and 3D assays for the quantitative analysis of cell migration. Med Res Rev. 2007;27:149-76.
[195] Kramer N, Walzl A, Unger C, Rosner M, Krupitza G, Hengstschlager M, et al. In vitro cell migration and invasion assays. Mutation research. 2013;752:10-24.
[196] Cimpean AM, Ribatti D, Raica M. The chick embryo chorioallantoic membrane as a model to study tumor metastasis. Angiogenesis. 2008;11:311-9.
[197] Jung J. Human tumor xenograft models for preclinical assessment of anticancer drug development. Toxicological research. 2014;30:1-5.
[198] Vaughan RB, Trinkaus JP. Movements of epithelial cell sheets in vitro. J Cell Sci. 1966;1:407-13.
[199] Rodriguez LG, Wu X, Guan JL. Wound-healing assay. Methods in molecular biology. 2005;294:23-9.
[200] Liang CC, Park AY, Guan JL. In vitro scratch assay: a convenient and inexpensive method for analysis of cell migration in vitro. Nature protocols. 2007;2:329-33.
[201] Horodyski J, Powell RJ. Effect of aprotinin on smooth muscle cell proliferation, migration, and extracellular matrix synthesis. J Surg Res. 1996;66:115-8.
[202] Ali IU, Hynes RO. Effects of LETS glycoprotein on cell motility. Cell. 1978;14:439-46.
[203] Artym VV, Yamada KM, Mueller SC. ECM degradation assays for analyzing local cell invasion. Methods in molecular biology. 2009;522:211-9.
[204] Zicha D, Dunn GA, Brown AF. A new direct-viewing chemotaxis chamber. J Cell Sci. 1991;99 (Pt 4):769-75.
[205] Albini A, Iwamoto Y, Kleinman HK, Martin GR, Aaronson SA, Kozlowski JM, et al. A rapid in vitro assay for quantitating the invasive potential of tumor cells. Cancer Res. 1987;47:3239-45.
[206] Marshall J. Transwell((R)) invasion assays. Methods in molecular biology. 2011;769:97-110.

[207] Hattermann K, Held-Feindt J, Mentlein R. Spheroid confrontation assay: a simple method to monitor the three-dimensional migration of different cell types in vitro. Annals of anatomy = Anatomischer Anzeiger : official organ of the Anatomische Gesellschaft. 2011;193:181-4.
[208] Wolf K, Alexander S, Schacht V, Coussens LM, von Andrian UH, van Rheenen J, et al. Collagen-based cell migration models in vitro and in vivo. Semin Cell Dev Biol. 2009;20:931-41.
[209] Bracke ME, Boterberg T, Bruyneel EA, Mareel MM. Collagen invasion assay. Methods in molecular medicine. 2001;58:81-9.
[210] Menon S, Beningo KA. Cancer cell invasion is enhanced by applied mechanical stimulation. PLoS One. 2011;6:e17277.
[211] Niggemann B, Drell TLt, Joseph J, Weidt C, Lang K, Zaenker KS, et al. Tumor cell locomotion: differential dynamics of spontaneous and induced migration in a 3D collagen matrix. Exp Cell Res. 2004;298:178-87.
[212] Zaman MH, Trapani LM, Sieminski AL, Mackellar D, Gong H, Kamm RD, et al. Migration of tumor cells in 3D matrices is governed by matrix stiffness along with cell-matrix adhesion and proteolysis. Proc Natl Acad Sci U S A. 2006;103:10889-94.
[213] Echeverria V, Meyvantsson I, Skoien A, Worzella T, Lamers C, Hayes S. An automated high-content assay for tumor cell migration through 3-dimensional matrices. J Biomol Screen. 2010;15:1144-51.
[214] Thevenot P, Nair A, Dey J, Yang J, Tang LP. Method to Analyze Three-Dimensional Cell Distribution and Infiltration in Degradable Scaffolds. Tissue Engineering Part C-Methods. 2008;14:319-31.
[215] Koehler BC, Scherr AL, Lorenz S, Urbanik T, Kautz N, Elssner C, et al. Beyond Cell Death - Antiapoptotic Bcl-2 Proteins Regulate Migration and Invasion of Colorectal Cancer Cells. PLoS One. 2013;8:e76446.
[216] Ridky TW, Chow JM, Wong DJ, Khavari PA. Invasive three-dimensional organotypic neoplasia from multiple normal human epithelia. Nat Med. 2010;16:1450-5.
[217] Hayflick L. Subculturing Human Diploid Fibroblast Cultures. In: Kruse PF, Patterson MK, editors. Tissue culture: methods and applications: Academic Press; 1973. p. 220-3.
[218] Knight E, Murray B, Carnachan R, Przyborski S. Alvetex (R): Polystyrene Scaffold Technology for Routine Three Dimensional Cell Culture. In: Haycock JW, editor. 3d Cell Culture: Methods and Protocols. Totowa: Humana Press Inc; 2011. p. 323-40.
[219] Calvo F, Sahai E. Cell communication networks in cancer invasion. Curr Opin Cell Biol. 2011;23:621-9.
[220] Otsubo T, Iwaya K, Mukai Y, Mizokami Y, Serizawa H, Matsuoka T, et al. Involvement of Arp2/3 complex in the process of colorectal carcinogenesis. Modern pathology : an official journal of the United States and Canadian Academy of Pathology, Inc. 2004;17:461-7.
[221] Etienne-Manneville S, Hall A. Integrin-mediated activation of Cdc42 controls cell polarity in migrating astrocytes through PKCzeta. Cell. 2001;106:489-98.
[222] Alt-Holland A, Shamis Y, Riley KN, DesRochers TM, Fusenig NE, Herman IM, et al. E-cadherin suppression directs cytoskeletal rearrangement and intraepithelial tumor cell migration in 3D human skin equivalents. J Invest Dermatol. 2008;128:2498-507.

[223] Conacci-Sorrell M, Simcha I, Ben-Yedidia T, Blechman J, Savagner P, Ben-Ze'ev A. Autoregulation of E-cadherin expression by cadherin-cadherin interactions: the roles of beta-catenin signaling, Slug, and MAPK. J Cell Biol. 2003;163:847-57.
[224] Arrondeau J, Gan HK, Razak AR, Paoletti X, Le Tourneau C. Development of anti-cancer drugs. Discov Med. 2010;10:355-62.
[225] Breslin S, O'Driscoll L. Three-dimensional cell culture: the missing link in drug discovery. Drug Discov Today. 2013;18:240-9.
[226] 3D Culture Cancer Search.
[227] 3D Culture Cancer Last 5 Years Search.
[228] Ben-Ze'ev A. The dual role of cytoskeletal anchor proteins in cell adhesion and signal transduction. Ann N Y Acad Sci. 1999;886:37-47.
[229] Stark HJ, Boehnke K, Mirancea N, Willhauck MJ, Pavesio A, Fusenig NE, et al. Epidermal homeostasis in long-term scaffold-enforced skin equivalents. The journal of investigative dermatology Symposium proceedings / the Society for Investigative Dermatology, Inc [and] European Society for Dermatological Research. 2006;11:93-105.
[230] Inanc B, Elcin AE, Elcin YM. Human embryonic stem cell differentiation on tissue engineering scaffolds: Effects of NGF and retinoic acid induction. Tissue Engineering Part A. 2008;14:955-64.
[231] Liao HT, Chen YY, Lai YT, Hsieh MF, Jiang CP. The osteogenesis of bone marrow stem cells on mPEG-PCL-mPEG/hydroxyapatite composite scaffold via solid freeform fabrication. BioMed research international. 2014;2014:321549.
[232] Stiles JM, Amaya C, Rains S, Diaz D, Pham R, Battiste J, et al. Targeting of beta adrenergic receptors results in therapeutic efficacy against models of hemangioendothelioma and angiosarcoma. PLoS One. 2013;8:e60021.
[233] Girard YK, Wang C, Ravi S, Howell MC, Mallela J, Alibrahim M, et al. A 3D fibrous scaffold inducing tumoroids: a platform for anticancer drug development. PLoS One. 2013;8:e75345.
[234] Chunhua L, Donglan L, Xiuqiong F, Lihua Z, Qin F, Yawei L, et al. Apigenin up-regulates transgelin and inhibits invasion and migration of colorectal cancer through decreased phosphorylation of AKT. The Journal of nutritional biochemistry. 2013;24:1766-75.
[235] Mele V, Muraro MG, Calabrese D, Pfaff D, Amatruda N, Amicarella F, et al. Mesenchymal stromal cells induce epithelial-to-mesenchymal transition in human colorectal cancer cells through the expression of surface-bound TGF-beta. Int J Cancer. 2013.
[236] Meacham CE, Morrison SJ. Tumour heterogeneity and cancer cell plasticity. Nature. 2013;501:328-37.
[237] Kirkland SC, Bailey IG. Establishment and characterisation of six human colorectal adenocarcinoma cell lines. Br J Cancer. 1986;53:779-85.
[238] Rutzky LP, Giovanella BC, Tom BH, Kaye CI, Noguchi PD, Kahan BD. Characterization of a human colonic adenocarcinoma cell line, LS123. In vitro. 1983;19:99-107.
[239] Tom BH, Rutzky LP, Jakstys MM, Oyasu R, Kaye CI, Kahan BD. Human colonic adenocarcinoma cells. I. Establishment and description of a new line. In vitro. 1976;12:180-91.
[240] Fujino H, Toyomura K, Chen XB, Regan JW, Murayama T. Prostaglandin E(2) regulates cellular migration via induction of vascular endothelial growth factor receptor-1 in HCA-7 human colon cancer cells. Biochemical pharmacology. 2011;81:379-87.

[241] Kirkland SC, Henderson K, Liu D, Pignatelli M. Organisation and gel contraction by human colonic carcinoma (HCA-7) sublines grown in 3-dimensional collagen gel. Int J Cancer. 1995;60:877-82.
[242] HCA-7 Migration Search.
[243] Hamada K, Monnai M, Kawai K, Nishime C, Kito C, Miyazaki N, et al. Liver metastasis models of colon cancer for evaluation of drug efficacy using NOD/Shi-scid IL2Rgammanull (NOG) mice. International journal of oncology. 2008;32:153-9.
[244] LS123 Search.
[245] LS123 Migration Search.
[246] Xia Y, Gil SG, Carter WG. Anchorage mediated by integrin alpha6beta4 to laminin 5 (epiligrin) regulates tyrosine phosphorylation of a membrane-associated 80-kD protein. J Cell Biol. 1996;132:727-40.
[247] Khurrum MR, Weerasinghe GR, Soriano ES, Riman R, Badali O, Gipson S, et al. Analysis of surface properties of human cancer cells using derivatized beads. Acta histochemica. 2002;104:217-23.
[248] LS174T Search.
[249] Jie JZ, Wang JW, Qu JG, Wang W, Hung T. Effects of adenoviral-mediated gene transduction of NK4 on proliferation, movement, and invasion of human colonic LS174T cancer cells in vitro. World journal of gastroenterology : WJG. 2006;12:3983-8.
[250] Zuo Y, Ren S, Wang M, Liu B, Yang J, Kuai X, et al. Novel roles of liver sinusoidal endothelial cell lectin in colon carcinoma cell adhesion, migration and in-vivo metastasis to the liver. Gut. 2013;62:1169-78.
[251] SW480 Search.
[252] SW480 Migration Search.
[253] McInroy L, Maatta A. Down-regulation of vimentin expression inhibits carcinoma cell migration and adhesion. Biochem Biophys Res Commun. 2007;360:109-14.
[254] Herrera A, Herrera M, Alba-Castellon L, Silva J, Garcia V, Loubat-Casanovas J, et al. Protumorigenic effects of Snail-expression fibroblasts on colon cancer cells. Int J Cancer. 2013.
[255] Witty JP, McDonnell S, Newell KJ, Cannon P, Navre M, Tressler RJ, et al. Modulation of matrilysin levels in colon carcinoma cell lines affects tumorigenicity in vivo. Cancer Res. 1994;54:4805-12.
[256] Hewitt RE, McMarlin A, Kleiner D, Wersto R, Martin P, Tsokos M, et al. Validation of a model of colon cancer progression. J Pathol. 2000;192:446-54.
[257] Fuller ES, Howell VM. Culture Models to Define Key Mediators of Cancer Matrix Remodeling. Frontiers in oncology. 2014;4:57.
[258] Gill BJ, West JL. Modeling the tumor extracellular matrix: Tissue engineering tools repurposed towards new frontiers in cancer biology. J Biomech. 2014;47:1969-78.
[259] Carnachan RJ, Bokhari M, Przyborski SA, Cameron NR. Tailoring the morphology of emulsion-templated porous polymers. Soft Matter. 2006;2:608-16.
[260] Bokhari M, Carnachan RJ, Przyborski SA, Cameron NR. Emulsion-templated porous polymers as scaffolds for three dimensional cell culture: effect of synthesis parameters on scaffold formation and homogeneity. Journal of Materials Chemistry. 2007;17:4088-94.

[261] Neofytou EA, Chang E, Patlola B, Joubert LM, Rajadas J, Gambhir SS, et al. Adipose tissue-derived stem cells display a proangiogenic phenotype on 3D scaffolds. J Biomed Mater Res A. 2011;98:383-93.
[262] Hayman MW, Smith KH, Cameron NR, Przyborski SA. Growth of human stem cell-derived neurons on solid three-dimensional polymers. Journal of Biochemical and Biophysical Methods. 2005;62:231-40.
[263] Bokhari M, Carnachan RJ, Cameron NR, Przyborski SA. Culture of HepG2 liver cells on three dimensional polystyrene scaffolds enhances cell structure and function during toxicological challenge. Journal of Anatomy. 2007;211:567-76.
[264] Mitchell SA, Davidson MR, Bradley RH. Glow discharge modified tissue culture polystyrene: role of surface chemistry in cellular attachment and proliferation. Surf Eng. 2006;22:337-44.
[265] Barker SL, Larocca PJ. Method of production and control of a commercial tissue culture surface. Journal of Tissue Culture Methods. 1994;16:151-3.
[266] Tamada Y, Ikada Y. Cell-adhesion to plasma-treated polymer surfaces. Polymer. 1993;34:2208-12.
[267] Xu LC, Siedlecki CA. Effects of surface wettability and contact time on protein adhesion to biomaterial surfaces. Biomaterials. 2007;28:3273-83.
[268] Zeyfert CM. Surface Functionalised Emulsion-Templated Porous Polymers for In-Vitro Cell Culture: University of Durham; 2010.
[269] Maa MC, Lee JC, Chen YJ, Chen YJ, Lee YC, Wang ST, et al. Eps8 facilitates cellular growth and motility of colon cancer cells by increasing the expression and activity of focal adhesion kinase. J Biol Chem. 2007;282:19399-409.
[270] Yang J, Balakrishnan A, Hamamoto S, Beattie CW, Das Gupta TK, Wellings SR, et al. Different mitogenic and phenotypic responses of human breast epithelial cells grown in two versus three dimensions. Exp Cell Res. 1986;167:563-9.
[271] Wolf K, Mazo I, Leung H, Engelke K, von Andrian UH, Deryugina EI, et al. Compensation mechanism in tumor cell migration: mesenchymal-amoeboid transition after blocking of pericellular proteolysis. J Cell Biol. 2003;160:267-77.
[272] Provenzano PP, Eliceiri KW, Campbell JM, Inman DR, White JG, Keely PJ. Collagen reorganization at the tumor-stromal interface facilitates local invasion. BMC medicine. 2006;4:38.
[273] Yu B, Chen X, Li J, Qu Y, Su L, Peng Y, et al. Stromal fibroblasts in the microenvironment of gastric carcinomas promote tumor metastasis via upregulating TAGLN expression. BMC cell biology. 2013;14:17.
[274] Mesker WE, Liefers GJ, Junggeburt JM, van Pelt GW, Alberici P, Kuppen PJ, et al. Presence of a high amount of stroma and downregulation of SMAD4 predict for worse survival for stage I-II colon cancer patients. Cellular oncology : the official journal of the International Society for Cellular Oncology. 2009;31:169-78.
[275] Jainchill JL, Aaronson SA, Todaro GJ. Murine sarcoma and leukemia viruses: assay using clonal lines of contact-inhibited mouse cells. Journal of virology. 1969;4:549-53.
[276] Albasri A, Seth R, Jackson D, Benhasouna A, Crook S, Nateri AS, et al. C-terminal Tensin-like (CTEN) is an oncogene which alters cell motility possibly through repression of E-cadherin in colorectal cancer. J Pathol. 2009;218:57-65.

[277] Elsaba TM, Martinez-Pomares L, Robins AR, Crook S, Seth R, Jackson D, et al. The stem cell marker CD133 associates with enhanced colony formation and cell motility in colorectal cancer. PLoS One. 2010;5:e10714.
[278] Knight EG. Influence of the microenvironment on the maintenance and differentiation of pluripotent stem cells. Durham: Durham University; 2013.
[279] Chaubey S, Ridley AJ, Wells CM. Using the Dunn chemotaxis chamber to analyze primary cell migration in real time. Methods in molecular biology. 2011;769:41-51.
[280] de Vries JE, Dinjens WN, De Bruyne GK, Verspaget HW, van der Linden EP, de Bruine AP, et al. In vivo and in vitro invasion in relation to phenotypic characteristics of human colorectal carcinoma cells. Br J Cancer. 1995;71:271-7.
[281] Frixen UH, Behrens J, Sachs M, Eberle G, Voss B, Warda A, et al. E-cadherin-mediated cell-cell adhesion prevents invasiveness of human carcinoma cells. J Cell Biol. 1991;113:173-85.
[282] Rye HS, Dabora JM, Quesada MA, Mathies RA, Glazer AN. Fluorometric assay using dimeric dyes for double-stranded and single-stranded-dna and rna with picogram sensitivity. Analytical Biochemistry. 1993;208:144-50.
[283] Galavotti S, Bartesaghi S, Faccenda D, Shaked-Rabi M, Sanzone S, McEvoy A, et al. The autophagy-associated factors DRAM1 and p62 regulate cell migration and invasion in glioblastoma stem cells. Oncogene. 2013;32:699-712.
[284] Sack U, Walther W, Scudiero D, Selby M, Kobelt D, Lemm M, et al. Novel effect of antihelminthic Niclosamide on S100A4-mediated metastatic progression in colon cancer. J Natl Cancer Inst. 2011;103:1018-36.
[285] Brown JD, Moon RT. Wnt signaling: why is everything so negative? Curr Opin Cell Biol. 1998;10:182-7.
[286] Dale TC. Signal transduction by the Wnt family of ligands. The Biochemical journal. 1998;329 (Pt 2):209-23.
[287] Willert K, Nusse R. Beta-catenin: a key mediator of Wnt signaling. Curr Opin Genet Dev. 1998;8:95-102.
[288] Munemitsu S, Albert I, Souza B, Rubinfeld B, Polakis P. Regulation of intracellular beta-catenin levels by the adenomatous polyposis coli (APC) tumor-suppressor protein. Proc Natl Acad Sci U S A. 1995;92:3046-50.
[289] Trakoontivakorn G, Nakahara K, Shinmoto H, Takenaka M, Onishi-Kameyama M, Ono H, et al. Structural analysis of a novel antimutagenic compound, 4-Hydroxypanduratin A, and the antimutagenic activity of flavonoids in a Thai spice, fingerroot (Boesenbergia pandurata Schult.) against mutagenic heterocyclic amines. Journal of agricultural and food chemistry. 2001;49:3046-50.
[290] Wang ZT, Lau CW, Chan FL, Yao X, Chen ZY, He ZD, et al. Vasorelaxant effects of cardamonin and alpinetin from Alpinia henryi K. Schum. Journal of cardiovascular pharmacology. 2001;37:596-606.
[291] Aggarwal B, Prasad S, Sung B, Krishnan S, Guha S. Prevention and Treatment of Colorectal Cancer by Natural Agents From Mother Nature. Current colorectal cancer reports. 2013;9:37-56.
[292] Sung B, Prasad S, Yadav VR, Aggarwal BB. Cancer cell signaling pathways targeted by spice-derived nutraceuticals. Nutr Cancer. 2012;64:173-97.

[293] Lee JH, Jung HS, Giang PM, Jin X, Lee S, Son PT, et al. Blockade of nuclear factor-kappaB signaling pathway and anti-inflammatory activity of cardamomin, a chalcone analog from Alpinia conchigera. The Journal of pharmacology and experimental therapeutics. 2006;316:271-8.
[294] Ahmad S, Israf DA, Lajis NH, Shaari K, Mohamed H, Wahab AA, et al. Cardamonin, inhibits pro-inflammatory mediators in activated RAW 264.7 cells and whole blood. European journal of pharmacology. 2006;538:188-94.
[295] Israf DA, Khaizurin TA, Syahida A, Lajis NH, Khozirah S. Cardamonin inhibits COX and iNOS expression via inhibition of p65NF-kappaB nuclear translocation and Ikappa-B phosphorylation in RAW 264.7 macrophage cells. Molecular immunology. 2007;44:673-9.
[296] Park MK, Jo SH, Lee HJ, Kang JH, Kim YR, Kim HJ, et al. Novel suppressive effects of cardamonin on the activity and expression of transglutaminase-2 lead to blocking the migration and invasion of cancer cells. Life sciences. 2013;92:154-60.
[297] Cho M, Ryu M, Jeong Y, Chung YH, Kim DE, Cho HS, et al. Cardamonin suppresses melanogenesis by inhibition of Wnt/beta-catenin signaling. Biochem Biophys Res Commun. 2009;390:500-5.
[298] Mureli S, Gans CP, Bare DJ, Geenen DL, Kumar NM, Banach K. Mesenchymal stem cells improve cardiac conduction by upregulation of connexin 43 through paracrine signaling. American journal of physiology Heart and circulatory physiology. 2013;304:H600-9.
[299] Park S, Gwak J, Han SJ, Oh S. Cardamonin suppresses the proliferation of colon cancer cells by promoting beta-catenin degradation. Biological & pharmaceutical bulletin. 2013;36:1040-4.
[300] Thakur R, Mishra DP. Pharmacological modulation of beta-catenin and its applications in cancer therapy. Journal of cellular and molecular medicine. 2013;17:449-56.
[301] Yadav VR, Prasad S, Aggarwal BB. Cardamonin sensitizes tumour cells to TRAIL through ROS- and CHOP-mediated up-regulation of death receptors and down-regulation of survival proteins. Br J Pharmacol. 2012;165:741-53.
[302] Emami KH, Nguyen C, Ma H, Kim DH, Jeong KW, Eguchi M, et al. A small molecule inhibitor of beta-catenin/CREB-binding protein transcription [corrected]. Proc Natl Acad Sci U S A. 2004;101:12682-7.
[303] Ma H, Nguyen C, Lee KS, Kahn M. Differential roles for the coactivators CBP and p300 on TCF/beta-catenin-mediated survivin gene expression. Oncogene. 2005;24:3619-31.
[304] Mavila N, James D, Utley S, Cu N, Coblens O, Mak K, et al. Fibroblast growth factor receptor-mediated activation of AKT-beta-catenin-CBP pathway regulates survival and proliferation of murine hepatoblasts and hepatic tumor initiating stem cells. PLoS One. 2012;7:e50401.
[305] Yan D, Avtanski D, Saxena NK, Sharma D. Leptin-induced epithelial-mesenchymal transition in breast cancer cells requires beta-catenin activation via Akt/GSK3- and MTA1/Wnt1 protein-dependent pathways. J Biol Chem. 2012;287:8598-612.
[306] Lazarova DL, Chiaro C, Wong T, Drago E, Rainey A, O'Malley S, et al. CBP Activity Mediates Effects of the Histone Deacetylase Inhibitor Butyrate on WNT Activity and Apoptosis in Colon Cancer Cells. Journal of Cancer. 2013;4:481-90.
[307] Lazarova DL, Wong T, Chiaro C, Drago E, Bordonaro M. p300 Influences Butyrate-Mediated WNT Hyperactivation In Colorectal Cancer Cells. Journal of Cancer. 2013;4:491-501.
[308] Ellerkamp V, Lieber J, Nagel C, Wenz J, Warmann SW, Fuchs J, et al. Pharmacological inhibition of beta-catenin in hepatoblastoma cells. Pediatric surgery international. 2013;29:141-9.

[309] Sasaki T, Hwang H, Nguyen C, Kloner RA, Kahn M. The Small Molecule Wnt Signaling Modulator ICG-001 Improves Contractile Function in Chronically Infarcted Rat Myocardium. PLoS One. 2013;8:e75010.
[310] Chung R, Wong D, Macsai C, Piergentili A, Del Bello F, Quaglia W, et al. Roles of Wnt/beta-catenin signalling pathway in the bony repair of injured growth plate cartilage in young rats. Bone. 2013;52:651-8.
[311] Kim H, Won S, Hwang DY, Lee JS, Kim M, Kim R, et al. Downregulation of Wnt/beta-catenin signaling causes degeneration of hippocampal neurons in vivo. Neurobiology of aging. 2011;32:2316 e1-15.
[312] Henderson WR, Jr., Chi EY, Ye X, Nguyen C, Tien YT, Zhou B, et al. Inhibition of Wnt/beta-catenin/CREB binding protein (CBP) signaling reverses pulmonary fibrosis. Proc Natl Acad Sci U S A. 2010;107:14309-14.
[313] Chen B, Dodge ME, Tang W, Lu J, Ma Z, Fan CW, et al. Small molecule-mediated disruption of Wnt-dependent signaling in tissue regeneration and cancer. Nat Chem Biol. 2009;5:100-7.
[314] Narwal M, Venkannagari H, Lehtio L. Structural basis of selective inhibition of human tankyrases. Journal of medicinal chemistry. 2012;55:1360-7.
[315] Yin A, Korzh S, Winata CL, Korzh V, Gong Z. Wnt signaling is required for early development of zebrafish swimbladder. PLoS One. 2011;6:e18431.
[316] Yin A, Korzh V, Gong Z. Perturbation of zebrafish swimbladder development by enhancing Wnt signaling in Wif1 morphants. Biochim Biophys Acta. 2012;1823:236-44.
[317] Myers CT, Appleby SC, Krieg PA. Use of small molecule inhibitors of the Wnt and Notch signaling pathways during Xenopus development. Methods. 2013.
[318] Koizumi Y, Kawashima N, Yamamoto M, Takimoto K, Zhou M, Suzuki N, et al. Wnt11 expression in rat dental pulp and promotional effects of Wnt signaling on odontoblast differentiation. Congenital anomalies. 2013;53:101-8.
[319] Ghaedi M, Calle EA, Mendez JJ, Gard AL, Balestrini J, Booth A, et al. Human iPS cell-derived alveolar epithelium repopulates lung extracellular matrix. J Clin Invest. 2013;123:4950-62.
[320] Hudson J, Titmarsh D, Hidalgo A, Wolvetang E, Cooper-White J. Primitive cardiac cells from human embryonic stem cells. Stem Cells Dev. 2012;21:1513-23.
[321] Busch AM, Johnson KC, Stan RV, Sanglikar A, Ahmed Y, Dmitrovsky E, et al. Evidence for tankyrases as antineoplastic targets in lung cancer. BMC Cancer. 2013;13:211.
[322] Huang SM, Mishina YM, Liu S, Cheung A, Stegmeier F, Michaud GA, et al. Tankyrase inhibition stabilizes axin and antagonizes Wnt signalling. Nature. 2009;461:614-20.
[323] Wang H, Hao J, Hong CC. Cardiac induction of embryonic stem cells by a small molecule inhibitor of Wnt/beta-catenin signaling. ACS Chem Biol. 2011;6:192-7.
[324] Vangipuram SD, Buck SA, Lyman WD. Wnt pathway activity confers chemoresistance to cancer stem-like cells in a neuroblastoma cell line. Tumour biology : the journal of the International Society for Oncodevelopmental Biology and Medicine. 2012;33:2173-83.
[325] Tenbaum SP, Ordonez-Moran P, Puig I, Chicote I, Arques O, Landolfi S, et al. beta-catenin confers resistance to PI3K and AKT inhibitors and subverts FOXO3a to promote metastasis in colon cancer. Nat Med. 2012;18:892-901.

[326] de Sousa EM, Vermeulen L, Richel D, Medema JP. Targeting Wnt signaling in colon cancer stem cells. Clinical cancer research : an official journal of the American Association for Cancer Research. 2011;17:647-53.
[327] Peterson RT. Drug discovery: Propping up a destructive regime. Nature. 2009;461:599-600.
[328] Yan Y, Lackner MR. FOXO3a and beta-catenin co-localization: double trouble in colon cancer? Nat Med. 2012;18:854-6.
[329] Bilir B, Kucuk O, Moreno CS. Wnt signaling blockage inhibits cell proliferation and migration, and induces apoptosis in triple-negative breast cancer cells. Journal of translational medicine. 2013;11:280.
[330] Zemans RL, McClendon J, Aschner Y, Briones N, Young SK, Lau LF, et al. Role of beta-catenin-regulated CCN matricellular proteins in epithelial repair after inflammatory lung injury. American journal of physiology Lung cellular and molecular physiology. 2013;304:L415-27.
[331] Hall-Jackson CA, Eyers PA, Cohen P, Goedert M, Boyle FT, Hewitt N, et al. Paradoxical activation of Raf by a novel Raf inhibitor. Chemistry & biology. 1999;6:559-68.
[332] Pampaloni F, Reynaud EG, Stelzer EH. The third dimension bridges the gap between cell culture and live tissue. Nat Rev Mol Cell Biol. 2007;8:839-45.
[333] Hongisto V, Jernstrom S, Fey V, Mpindi JP, Kleivi Sahlberg K, Kallioniemi O, et al. High-throughput 3D screening reveals differences in drug sensitivities between culture models of JIMT1 breast cancer cells. PLoS One. 2013;8:e77232.
[334] Bauer TW, Fan F, Liu W, Johnson M, Parikh NU, Parry GC, et al. Insulinlike growth factor-I-mediated migration and invasion of human colon carcinoma cells requires activation of c-Met and urokinase plasminogen activator receptor. Annals of surgery. 2005;241:748-56; discussion 56-8.
[335] Liu B, Fang M, Lu Y, Mendelsohn J, Fan Z. Fibroblast growth factor and insulin-like growth factor differentially modulate the apoptosis and G1 arrest induced by anti-epidermal growth factor receptor monoclonal antibody. Oncogene. 2001;20:1913-22.
[336] Weber MM, Fottner C, Liu SB, Jung MC, Engelhardt D, Baretton GB. Overexpression of the insulin-like growth factor I receptor in human colon carcinomas. Cancer. 2002;95:2086-95.
[337] Reinmuth N, Liu W, Fan F, Jung YD, Ahmad SA, Stoeltzing O, et al. Blockade of insulin-like growth factor I receptor function inhibits growth and angiogenesis of colon cancer. Clinical cancer research : an official journal of the American Association for Cancer Research. 2002;8:3259-69.
[338] Yavari K, Taghikhani M, Maragheh MG, Mesbah-Namin SA, Babaei MH. Knockdown of IGF-IR by RNAi inhibits SW480 colon cancer cells growth in vitro. Archives of medical research. 2009;40:235-40.
[339] Yavari K, Taghikhani M, Maragheh MG, Mesbah-Namin SA, Babaei MH, Arfaee AJ, et al. SiRNA-mediated IGF-1R inhibition sensitizes human colon cancer SW480 cells to radiation. Acta Oncol. 2010;49:70-5.
[340] Bauer TW, Fan F, Liu W, Camp ER, Yang A, Somcio RJ, et al. Targeting of insulin-like growth factor-I receptor with a monoclonal antibody inhibits growth of hepatic metastases from human colon carcinoma in mice. Annals of surgical oncology. 2007;14:2838-46.
[341] Ewing GP, Goff LW. The insulin-like growth factor signaling pathway as a target for treatment of colorectal carcinoma. Clinical colorectal cancer. 2010;9:219-23.
[342] Gao J, Chang YS, Jallal B, Viner J. Targeting the insulin-like growth factor axis for the development of novel therapeutics in oncology. Cancer Res. 2012;72:3-12.

[343] Garcia-Echeverria C, Pearson MA, Marti A, Meyer T, Mestan J, Zimmermann J, et al. In vivo antitumor activity of NVP-AEW541-A novel, potent, and selective inhibitor of the IGF-IR kinase. Cancer cell. 2004;5:231-9.
[344] Hopfner M, Huether A, Sutter AP, Baradari V, Schuppan D, Scherubl H. Blockade of IGF-1 receptor tyrosine kinase has antineoplastic effects in hepatocellular carcinoma cells. Biochemical pharmacology. 2006;71:1435-48.
[345] Piao W, Wang Y, Adachi Y, Yamamoto H, Li R, Imsumran A, et al. Insulin-like growth factor-I receptor blockade by a specific tyrosine kinase inhibitor for human gastrointestinal carcinomas. Molecular cancer therapeutics. 2008;7:1483-93.
[346] Cunningham MP, Thomas H, Marks C, Green M, Fan Z, Modjtahedi H. Co-targeting the EGFR and IGF-IR with anti-EGFR monoclonal antibody ICR62 and the IGF-IR tyrosine kinase inhibitor NVP-AEW541 in colorectal cancer cells. International journal of oncology. 2008;33:1107-13.
[347] Pennarun B, Kleibeuker JH, Oenema T, Stegehuis JH, de Vries EG, de Jong S. Inhibition of IGF-1R-dependent PI3K activation sensitizes colon cancer cells specifically to DR5-mediated apoptosis but not to rhTRAIL. Analytical cellular pathology. 2010;33:229-44.
[348] Moser C, Schachtschneider P, Lang SA, Gaumann A, Mori A, Zimmermann J, et al. Inhibition of insulin-like growth factor-I receptor (IGF-IR) using NVP-AEW541, a small molecule kinase inhibitor, reduces orthotopic pancreatic cancer growth and angiogenesis. European journal of cancer. 2008;44:1577-86.
[349] Adachi Y, Li R, Yamamoto H, Min Y, Piao W, Wang Y, et al. Insulin-like growth factor-I receptor blockade reduces the invasiveness of gastrointestinal cancers via blocking production of matrilysin. Carcinogenesis. 2009;30:1305-13.
[350] Scotlandi K, Manara MC, Nicoletti G, Lollini PL, Lukas S, Benini S, et al. Antitumor activity of the insulin-like growth factor-I receptor kinase inhibitor NVP-AEW541 in musculoskeletal tumors. Cancer Res. 2005;65:3868-76.
[351] Manara MC, Landuzzi L, Nanni P, Nicoletti G, Zambelli D, Lollini PL, et al. Preclinical in vivo study of new insulin-like growth factor-I receptor--specific inhibitor in Ewing's sarcoma. Clinical cancer research : an official journal of the American Association for Cancer Research. 2007;13:1322-30.
[352] Tanno B, Mancini C, Vitali R, Mancuso M, McDowell HP, Dominici C, et al. Down-regulation of insulin-like growth factor I receptor activity by NVP-AEW541 has an antitumor effect on neuroblastoma cells in vitro and in vivo. Clinical cancer research : an official journal of the American Association for Cancer Research. 2006;12:6772-80.
[353] Urbanska K, Trojanek J, Del Valle L, Eldeen MB, Hofmann F, Garcia-Echeverria C, et al. Inhibition of IGF-I receptor in anchorage-independence attenuates GSK-3beta constitutive phosphorylation and compromises growth and survival of medulloblastoma cell lines. Oncogene. 2007;26:2308-17.
[354] Gariboldi MB, Ravizza R, Monti E. The IGFR1 inhibitor NVP-AEW541 disrupts a pro-survival and pro-angiogenic IGF-STAT3-HIF1 pathway in human glioblastoma cells. Biochemical pharmacology. 2010;80:455-62.

[355] Hagerstrand D, Lindh MB, Pena C, Garcia-Echeverria C, Nister M, Hofmann F, et al. PI3K/PTEN/Akt pathway status affects the sensitivity of high-grade glioma cell cultures to the insulin-like growth factor-1 receptor inhibitor NVP-AEW541. Neuro-oncology. 2010;12:967-75.
[356] Tazzari PL, Tabellini G, Bortul R, Papa V, Evangelisti C, Grafone T, et al. The insulin-like growth factor-I receptor kinase inhibitor NVP-AEW541 induces apoptosis in acute myeloid leukemia cells exhibiting autocrine insulin-like growth factor-I secretion. Leukemia. 2007;21:886-96.
[357] Doepfner KT, Spertini O, Arcaro A. Autocrine insulin-like growth factor-I signaling promotes growth and survival of human acute myeloid leukemia cells via the phosphoinositide 3-kinase/Akt pathway. Leukemia. 2007;21:1921-30.
[358] Maiso P, Ocio EM, Garayoa M, Montero JC, Hofmann F, Garcia-Echeverria C, et al. The insulin-like growth factor-I receptor inhibitor NVP-AEW541 provokes cell cycle arrest and apoptosis in multiple myeloma cells. British journal of haematology. 2008;141:470-82.
[359] Wolf S, Lorenz J, Mossner J, Wiedmann M. Treatment of biliary tract cancer with NVP-AEW541: mechanisms of action and resistance. World journal of gastroenterology : WJG. 2010;16:156-66.
[360] Kaulfuss S, Burfeind P, Gaedcke J, Scharf JG. Dual silencing of insulin-like growth factor-I receptor and epidermal growth factor receptor in colorectal cancer cells is associated with decreased proliferation and enhanced apoptosis. Molecular cancer therapeutics. 2009;8:821-33.
[361] Slomiany MG, Black LA, Kibbey MM, Tingler MA, Day TA, Rosenzweig SA. Insulin-like growth factor-1 receptor and ligand targeting in head and neck squamous cell carcinoma. Cancer letters. 2007;248:269-79.
[362] Baserga R. The decline and fall of the IGF-I receptor. J Cell Physiol. 2013;228:675-9.
[363] Frystyk J, Skjaerbaek C, Dinesen B, Orskov H. Free insulin-like growth factors (IGF-I and IGF-II) in human serum. FEBS Lett. 1994;348:185-91.
[364] Andre F, Rigot V, Thimonier J, Montixi C, Parat F, Pommier G, et al. Integrins and E-cadherin cooperate with IGF-I to induce migration of epithelial colonic cells. Int J Cancer. 1999;83:497-505.
[365] Peddareddigari VG, Wang D, Dubois RN. The tumor microenvironment in colorectal carcinogenesis. Cancer microenvironment : official journal of the International Cancer Microenvironment Society. 2010;3:149-66.
[366] Lu P, Weaver VM, Werb Z. The extracellular matrix: a dynamic niche in cancer progression. J Cell Biol. 2012;196:395-406.
[367] Pelham RJ, Jr., Wang Y. Cell locomotion and focal adhesions are regulated by substrate flexibility. Proc Natl Acad Sci U S A. 1997;94:13661-5.
[368] Levental KR, Yu H, Kass L, Lakins JN, Egeblad M, Erler JT, et al. Matrix crosslinking forces tumor progression by enhancing integrin signaling. Cell. 2009;139:891-906.
[369] Baker AM, Bird D, Lang G, Cox TR, Erler JT. Lysyl oxidase enzymatic function increases stiffness to drive colorectal cancer progression through FAK. Oncogene. 2013;32:1863-8.
[370] Tilghman RW, Cowan CR, Mih JD, Koryakina Y, Gioeli D, Slack-Davis JK, et al. Matrix rigidity regulates cancer cell growth and cellular phenotype. PLoS One. 2010;5:e12905.
[371] Krndija D, Schmid H, Eismann JL, Lother U, Adler G, Oswald F, et al. Substrate stiffness and the receptor-type tyrosine-protein phosphatase alpha regulate spreading of colon cancer cells through cytoskeletal contractility. Oncogene. 2010;29:2724-38.

[372] Kaufman LJ, Brangwynne CP, Kasza KE, Filippidi E, Gordon VD, Deisboeck TS, et al. Glioma expansion in collagen I matrices: analyzing collagen concentration-dependent growth and motility patterns. Biophysical journal. 2005;89:635-50.
[373] Schor SL, Schor AM, Bazill GW. The effects of fibronectin on the adhesion and migration of chinese hamster ovary cells on collagen substrata. J Cell Sci. 1981;49:299-310.
[374] Neri A, Ruoslahti E, Nicolson GL. Distribution of fibronectin on clonal cell lines of a rat mammary adenocarcinoma growing in vitro and in vivo at primary and metastatic sites. Cancer Res. 1981;41:5082-95.
[375] Netti PA, Berk DA, Swartz MA, Grodzinsky AJ, Jain RK. Role of extracellular matrix assembly in interstitial transport in solid tumors. Cancer Res. 2000;60:2497-503.
[376] Seandel M, Noack-Kunnmann K, Zhu D, Aimes RT, Quigley JP. Growth factor-induced angiogenesis in vivo requires specific cleavage of fibrillar type I collagen. Blood. 2001;97:2323-32.
[377] Graham MF, Diegelmann RF, Elson CO, Lindblad WJ, Gotschalk N, Gay S, et al. Collagen content and types in the intestinal strictures of Crohn's disease. Gastroenterology. 1988;94:257-65.
[378] Hilska M, Collan Y, Peltonen J, Gullichsen R, Paajanen H, Laato M. The distribution of collagen types I, III, and IV in normal and malignant colorectal mucosa. The European journal of surgery = Acta chirurgica. 1998;164:457-64.
[379] Simon-Assmann P, Kedinger M, Haffen K. Immunocytochemical localization of extracellular-matrix proteins in relation to rat intestinal morphogenesis. Differentiation. 1986;32:59-66.
[380] Velculescu VE, Zhang L, Vogelstein B, Kinzler KW. Serial analysis of gene expression. Science. 1995;270:484-7.
[381] Zhang L, Zhou W, Velculescu VE, Kern SE, Hruban RH, Hamilton SR, et al. Gene expression profiles in normal and cancer cells. Science. 1997;276:1268-72.
[382] Ryu B, Jones J, Hollingsworth MA, Hruban RH, Kern SE. Invasion-specific genes in malignancy: serial analysis of gene expression comparisons of primary and passaged cancers. Cancer Res. 2001;61:1833-8.
[383] Porter DA, Krop IE, Nasser S, Sgroi D, Kaelin CM, Marks JR, et al. A SAGE (serial analysis of gene expression) view of breast tumor progression. Cancer Res. 2001;61:5697-702.
[384] Iacobuzio-Donahue CA, Argani P, Hempen PM, Jones J, Kern SE. The desmoplastic response to infiltrating breast carcinoma: gene expression at the site of primary invasion and implications for comparisons between tumor types. Cancer Res. 2002;62:5351-7.
[385] Ramaswamy S, Ross KN, Lander ES, Golub TR. A molecular signature of metastasis in primary solid tumors. Nat Genet. 2003;33:49-54.
[386] Zou X, Feng B, Dong T, Yan G, Tan B, Shen H, et al. Up-regulation of type I collagen during tumorigenesis of colorectal cancer revealed by quantitative proteomic analysis. Journal of proteomics. 2013;94:473-85.
[387] Nystrom H, Naredi P, Berglund A, Palmqvist R, Tavelin B, Sund M. Liver-metastatic potential of colorectal cancer is related to the stromal composition of the tumour. Anticancer research. 2012;32:5183-91.
[388] Vermeulen PB, Colpaert C, Salgado R, Royers R, Hellemans H, Van Den Heuvel E, et al. Liver metastases from colorectal adenocarcinomas grow in three patterns with different angiogenesis and desmoplasia. J Pathol. 2001;195:336-42.

[389] Yamada KM, Weston JA. Isolation of a major cell surface glycoprotein from fibroblasts. Proc Natl Acad Sci U S A. 1974;71:3492-6.
[390] Vaheri A, Ruoslahti E, Westermark B, Ponten J. A common cell-type specific surface antigen in cultured human glial cells and fibroblasts: loss in malignant cells. The Journal of experimental medicine. 1976;143:64-72.
[391] Vaheri A, Kurkinen M, Lehto VP, Linder E, Timpl R. Codistribution of pericellular matrix proteins in cultured fibroblasts and loss in transformation: fibronectin and procollagen. Proc Natl Acad Sci U S A. 1978;75:4944-8.
[392] Iacobuzio-Donahue CA, Maitra A, Shen-Ong GL, van Heek T, Ashfaq R, Meyer R, et al. Discovery of novel tumor markers of pancreatic cancer using global gene expression technology. Am J Pathol. 2002;160:1239-49.
[393] Smith HS, Riggs JL, Mosesson MW. Production of fibronectin by human epithelial cells in culture. Cancer Res. 1979;39:4138-44.
[394] Kornblihtt AR, Umezawa K, Vibe-Pedersen K, Baralle FE. Primary structure of human fibronectin: differential splicing may generate at least 10 polypeptides from a single gene. EMBO J. 1985;4:1755-9.
[395] Pujuguet P, Hammann A, Moutet M, Samuel JL, Martin F, Martin M. Expression of fibronectin ED-A+ and ED-B+ isoforms by human and experimental colorectal cancer. Contribution of cancer cells and tumor-associated myofibroblasts. Am J Pathol. 1996;148:579-92.
[396] Nagashima Y, Hasegawa S, Koshikawa N, Taki A, Ichikawa Y, Kitamura H, et al. Expression of matrilysin in vascular endothelial cells adjacent to matrilysin-producing tumors. Int J Cancer. 1997;72:441-5.
[397] Grondahl-Hansen J, Ralfkiaer E, Kirkeby LT, Kristensen P, Lund LR, Dano K. Localization of urokinase-type plasminogen activator in stromal cells in adenocarcinomas of the colon in humans. Am J Pathol. 1991;138:111-7.
[398] Santos AM, Jung J, Aziz N, Kissil JL, Pure E. Targeting fibroblast activation protein inhibits tumor stromagenesis and growth in mice. J Clin Invest. 2009;119:3613-25.
[399] Higashi N, Ishii H, Fujiwara T, Morimoto-Tomita M, Irimura T. Redistribution of fibroblasts and macrophages as micrometastases develop into established liver metastases. Clin Exp Metastasis. 2002;19:631-8.
[400] Ronnov-Jessen L, Petersen OW, Koteliansky VE, Bissell MJ. The origin of the myofibroblasts in breast cancer. Recapitulation of tumor environment in culture unravels diversity and implicates converted fibroblasts and recruited smooth muscle cells. J Clin Invest. 1995;95:859-73.
[401] Huijbers A, Tollenaar RA, v Pelt GW, Zeestraten EC, Dutton S, McConkey CC, et al. The proportion of tumor-stroma as a strong prognosticator for stage II and III colon cancer patients: validation in the VICTOR trial. Annals of oncology : official journal of the European Society for Medical Oncology / ESMO. 2013;24:179-85.
[402] Ngan CY, Yamamoto H, Seshimo I, Tsujino T, Man-i M, Ikeda JI, et al. Quantitative evaluation of vimentin expression in tumour stroma of colorectal cancer. Br J Cancer. 2007;96:986-92.
[403] Cammarota R, Bertolini V, Pennesi G, Bucci EO, Gottardi O, Garlanda C, et al. The tumor microenvironment of colorectal cancer: stromal TLR-4 expression as a potential prognostic marker. Journal of translational medicine. 2010;8:112.

[404] Wang D, Zhu T, Zhang FB, He C. Expression of ADAMTS12 in colorectal cancer-associated stroma prevents cancer development and is a good prognostic indicator of colorectal cancer. Digestive diseases and sciences. 2011;56:3281-7.
[405] Saigusa S, Toiyama Y, Tanaka K, Yokoe T, Okugawa Y, Fujikawa H, et al. Cancer-associated fibroblasts correlate with poor prognosis in rectal cancer after chemoradiotherapy. International journal of oncology. 2011;38:655-63.
[406] Kahlert C, Pecqueux M, Halama N, Dienemann H, Muley T, Pfannschmidt J, et al. Tumour-site-dependent expression profile of angiogenic factors in tumour-associated stroma of primary colorectal cancer and metastases. Br J Cancer. 2014;110:441-9.
[407] Kataoka H, DeCastro R, Zucker S, Biswas C. Tumor cell-derived collagenase-stimulatory factor increases expression of interstitial collagenase, stromelysin, and 72-kDa gelatinase. Cancer Res. 1993;53:3154-8.
[408] Zucker S, Vacirca J. Role of matrix metalloproteinases (MMPs) in colorectal cancer. Cancer Metastasis Rev. 2004;23:101-17.
[409] Ohtani H, Motohashi H, Sato H, Seiki M, Nagura H. Dual over-expression pattern of membrane-type metalloproteinase-1 in cancer and stromal cells in human gastrointestinal carcinoma revealed by in situ hybridization and immunoelectron microscopy. Int J Cancer. 1996;68:565-70.
[410] Adegboyega PA, Mifflin RC, DiMari JF, Saada JI, Powell DW. Immunohistochemical study of myofibroblasts in normal colonic mucosa, hyperplastic polyps, and adenomatous colorectal polyps. Archives of pathology & laboratory medicine. 2002;126:829-36.
[411] Nakagawa H, Liyanarachchi S, Davuluri RV, Auer H, Martin EW, Jr., de la Chapelle A, et al. Role of cancer-associated stromal fibroblasts in metastatic colon cancer to the liver and their expression profiles. Oncogene. 2004;23:7366-77.
[412] Gullotti L, Czerwitzki J, Kirfel J, Propping P, Rahner N, Steinke V, et al. FHL2 expression in peritumoural fibroblasts correlates with lymphatic metastasis in sporadic but not in HNPCC-associated colon cancer. Laboratory investigation; a journal of technical methods and pathology. 2011;91:1695-705.
[413] Hawinkels LJ, Paauwe M, Verspaget HW, Wiercinska E, van der Zon JM, van der Ploeg K, et al. Interaction with colon cancer cells hyperactivates TGF-beta signaling in cancer-associated fibroblasts. Oncogene. 2014;33:97-107.
[414] Wikberg ML, Edin S, Lundberg IV, Van Guelpen B, Dahlin AM, Rutegard J, et al. High intratumoral expression of fibroblast activation protein (FAP) in colon cancer is associated with poorer patient prognosis. Tumour biology : the journal of the International Society for Oncodevelopmental Biology and Medicine. 2013;34:1013-20.
[415] Yashiro M, Chung YS, Kubo T, Hato F, Sowa M. Differential responses of scirrhous and well-differentiated gastric cancer cells to orthotopic fibroblasts. Br J Cancer. 1996;74:1096-103.
[416] Fabra A, Nakajima M, Bucana CD, Fidler IJ. Modulation of the invasive phenotype of human colon carcinoma cells by organ specific fibroblasts of nude mice. Differentiation. 1992;52:101-10.
[417] Berdiel-Acer M, Bohem ME, Lopez-Doriga A, Vidal A, Salazar R, Martinez-Iniesta M, et al. Hepatic carcinoma-associated fibroblasts promote an adaptative response in colorectal cancer cells that inhibit proliferation and apoptosis: nonresistant cells die by nonapoptotic cell death. Neoplasia. 2011;13:931-46.

[418] Pena C, Cespedes MV, Lindh MB, Kiflemariam S, Mezheyeuski A, Edqvist PH, et al. STC1 expression by cancer-associated fibroblasts drives metastasis of colorectal cancer. Cancer Res. 2013;73:1287-97.
[419] Noel A, De Pauw-Gillet MC, Purnell G, Nusgens B, Lapiere CM, Foidart JM. Enhancement of tumorigenicity of human breast adenocarcinoma cells in nude mice by matrigel and fibroblasts. Br J Cancer. 1993;68:909-15.
[420] Krtolica A, Parrinello S, Lockett S, Desprez PY, Campisi J. Senescent fibroblasts promote epithelial cell growth and tumorigenesis: a link between cancer and aging. Proc Natl Acad Sci U S A. 2001;98:12072-7.
[421] Loeffler M, Kruger JA, Niethammer AG, Reisfeld RA. Targeting tumor-associated fibroblasts improves cancer chemotherapy by increasing intratumoral drug uptake. J Clin Invest. 2006;116:1955-62.
[422] Xu W, Liu H, Song J, Fu HX, Qiu L, Zhang BF, et al. The appearance of Tregs in cancer nest is a promising independent risk factor in colon cancer. J Cancer Res Clin Oncol. 2013;139:1845-52.
[423] Aharinejad S, Abraham D, Paulus P, Abri H, Hofmann M, Grossschmidt K, et al. Colony-stimulating factor-1 antisense treatment suppresses growth of human tumor xenografts in mice. Cancer Res. 2002;62:5317-24.
[424] Oosterling SJ, van der Bij GJ, Meijer GA, Tuk CW, van Garderen E, van Rooijen N, et al. Macrophages direct tumour histology and clinical outcome in a colon cancer model. J Pathol. 2005;207:147-55.
[425] Gulubova M, Ananiev J, Yovchev Y, Julianov A, Karashmalakov A, Vlaykova T. The density of macrophages in colorectal cancer is inversely correlated to TGF-beta1 expression and patients' survival. Journal of molecular histology. 2013;44:679-92.
[426] Yang W, Arii S, Gorrin-Rivas MJ, Mori A, Onodera H, Imamura M. Human macrophage metalloelastase gene expression in colorectal carcinoma and its clinicopathologic significance. Cancer. 2001;91:1277-83.
[427] Galon J, Mlecnik B, Bindea G, Angell HK, Berger A, Lagorce C, et al. Towards the introduction of the 'Immunoscore' in the classification of malignant tumours. J Pathol. 2014;232:199-209.
[428] Pages F, Berger A, Camus M, Sanchez-Cabo F, Costes A, Molidor R, et al. Effector memory T cells, early metastasis, and survival in colorectal cancer. The New England journal of medicine. 2005;353:2654-66.
[429] Galon J, Costes A, Sanchez-Cabo F, Kirilovsky A, Mlecnik B, Lagorce-Pages C, et al. Type, density, and location of immune cells within human colorectal tumors predict clinical outcome. Science. 2006;313:1960-4.
[430] Mlecnik B, Tosolini M, Kirilovsky A, Berger A, Bindea G, Meatchi T, et al. Histopathologic-based prognostic factors of colorectal cancers are associated with the state of the local immune reaction. Journal of clinical oncology : official journal of the American Society of Clinical Oncology. 2011;29:610-8.
[431] Dahlin AM, Henriksson ML, Van Guelpen B, Stenling R, Oberg A, Rutegard J, et al. Colorectal cancer prognosis depends on T-cell infiltration and molecular characteristics of the

tumor. Modern pathology : an official journal of the United States and Canadian Academy of Pathology, Inc. 2011;24:671-82.
[432] Hwang RF, Moore T, Arumugam T, Ramachandran V, Amos KD, Rivera A, et al. Cancer-associated stromal fibroblasts promote pancreatic tumor progression. Cancer Res. 2008;68:918-26.
[433] Ding S, Zhang W, Xu Z, Xing C, Xie H, Guo H, et al. Induction of an EMT-like transformation and MET in vitro. Journal of translational medicine. 2013;11:164.
[434] Koshida Y, Kuranami M, Watanabe M. Interaction between stromal fibroblasts and colorectal cancer cells in the expression of vascular endothelial growth factor. J Surg Res. 2006;134:270-7.
[435] Kunz-Schughart LA, Heyder P, Schroeder J, Knuechel R. A heterologous 3-D coculture model of breast tumor cells and fibroblasts to study tumor-associated fibroblast differentiation. Exp Cell Res. 2001;266:74-86.
[436] Che ZM, Jung TH, Choi JH, Yoon do J, Jeong HJ, Lee EJ, et al. Collagen-based co-culture for invasive study on cancer cells-fibroblasts interaction. Biochem Biophys Res Commun. 2006;346:268-75.
[437] Schneider MR, Dahlhoff M, Horst D, Hirschi B, Trulzsch K, Muller-Hocker J, et al. A key role for E-cadherin in intestinal homeostasis and Paneth cell maturation. PLoS One. 2010;5:e14325.
[438] Le NH, Franken P, Fodde R. Tumour-stroma interactions in colorectal cancer: converging on beta-catenin activation and cancer stemness. Br J Cancer. 2008;98:1886-93.
[439] Beppu H, Mwizerwa ON, Beppu Y, Dattwyler MP, Lauwers GY, Bloch KD, et al. Stromal inactivation of BMPRII leads to colorectal epithelial overgrowth and polyp formation. Oncogene. 2008;27:1063-70.
[440] Hemavathy K, Guru SC, Harris J, Chen JD, Ip YT. Human Slug is a repressor that localizes to sites of active transcription. Molecular and cellular biology. 2000;20:5087-95.
[441] Agrez M, Chen A, Cone RI, Pytela R, Sheppard D. The alpha v beta 6 integrin promotes proliferation of colon carcinoma cells through a unique region of the beta 6 cytoplasmic domain. J Cell Biol. 1994;127:547-56.
[442] Yokosaki Y, Monis H, Chen J, Sheppard D. Differential effects of the integrins alpha9beta1, alphavbeta3, and alphavbeta6 on cell proliferative responses to tenascin. Roles of the beta subunit extracellular and cytoplasmic domains. J Biol Chem. 1996;271:24144-50.
[443] Del Buono R, Pignatelli M, Bodmer WF, Wright NA. The role of the arginine-glycine-aspartic acid-directed cellular binding to type I collagen and rat mesenchymal cells in colorectal tumour differentiation. Differentiation. 1991;46:97-103.
[444] Laurich C, Wheeler MA, Iida J, Neudauer CL, McCarthy JB, Bullard KM. Hyaluronan mediates adhesion of metastatic colon carcinoma cells. J Surg Res. 2004;122:70-4.
[445] Wang JH, Manning BJ, Wu QD, Blankson S, Bouchier-Hayes D, Redmond HP. Endotoxin/lipopolysaccharide activates NF-kappa B and enhances tumor cell adhesion and invasion through a beta 1 integrin-dependent mechanism. Journal of immunology. 2003;170:795-804.
[446] Menke A, Philippi C, Vogelmann R, Seidel B, Lutz MP, Adler G, et al. Down-regulation of E-cadherin gene expression by collagen type I and type III in pancreatic cancer cell lines. Cancer Res. 2001;61:3508-17.

[447] Bielefeld KA, Amini-Nik S, Whetstone H, Poon R, Youn A, Wang J, et al. Fibronectin and beta-catenin act in a regulatory loop in dermal fibroblasts to modulate cutaneous healing. J Biol Chem. 2011;286:27687-97.
[448] Beningo KA, Dembo M, Wang YL. Responses of fibroblasts to anchorage of dorsal extracellular matrix receptors. Proc Natl Acad Sci U S A. 2004;101:18024-9.
[449] Jeziorska M, Haboubi NY, Schofield PF, Ogata Y, Nagase H, Woolley DE. Distribution of gelatinase B (MMP-9) and type IV collagen in colorectal carcinoma. International journal of colorectal disease. 1994;9:141-8.
[450] Shioiri M, Shida T, Koda K, Oda K, Seike K, Nishimura M, et al. Slug expression is an independent prognostic parameter for poor survival in colorectal carcinoma patients. Br J Cancer. 2006;94:1816-22.
[451] Kanczuga-Koda L, Wincewicz A, Fudala A, Abrycki T, Famulski W, Baltaziak M, et al. E-cadherin and beta-catenin adhesion proteins correlate positively with connexins in colorectal cancer. Oncology letters. 2014;7:1863-70.
[452] Deka J, Wiedemann N, Anderle P, Murphy-Seiler F, Bultinck J, Eyckerman S, et al. Bcl9/Bcl9l are critical for Wnt-mediated regulation of stem cell traits in colon epithelium and adenocarcinomas. Cancer Res. 2010;70:6619-28.
[453] Wang Q, Qian J, Wang F, Ma Z. Cellular prion protein accelerates colorectal cancer metastasis via the Fyn-SP1-SATB1 axis. Oncol Rep. 2012;28:2029-34.
[454] Kola I, Landis J. Can the pharmaceutical industry reduce attrition rates? Nature reviews Drug discovery. 2004;3:711-5.
[455] Pammolli F, Magazzini L, Riccaboni M. The productivity crisis in pharmaceutical R&D. Nature reviews Drug discovery. 2011;10:428-38.
[456] Medici D, Hay ED, Olsen BR. Snail and Slug promote epithelial-mesenchymal transition through beta-catenin-T-cell factor-4-dependent expression of transforming growth factor-beta3. Molecular biology of the cell. 2008;19:4875-87.
[457] Deng H, Makizumi R, Ravikumar TS, Dong H, Yang W, Yang WL. Bone morphogenetic protein-4 is overexpressed in colonic adenocarcinomas and promotes migration and invasion of HCT116 cells. Exp Cell Res. 2007;313:1033-44.
[458] Gatza CE, Holtzhausen A, Kirkbride KC, Morton A, Gatza ML, Datto MB, et al. Type III TGF-beta receptor enhances colon cancer cell migration and anchorage-independent growth. Neoplasia. 2011;13:758-70.
[459] De Wever O, Mareel M. Role of tissue stroma in cancer cell invasion. J Pathol. 2003;200:429-47.